Design of an Ultrasensitive Diagnostic Device for Point of Care Based on Thin Film Colour Interference

by

Natalie Anne Vankka

A thesis submitted in partial fulfillment of the requirements for the degree of

Doctor of Philosophy

in

Nanobiomaterials and Chemical Engineering

Departments of Biomedical Engineering and Chemical and Materials Engineering

University of Alberta

© Natalie Anne Vankka, 2022

Abstract

Point-of-care diagnostic testing offers many benefits compared to standard laboratory testing for biomarkers or diseases, including reducing the time and cost required to obtain a medical diagnosis. Most available point-of-care diagnostics are complex, expensive, or limited to high concentration, low volume samples. The aim of this work was to develop a highly sensitive, stand-alone, point-of-care medical diagnostic device that can quickly detect low concentrations of analyte (~ 4 pM) in high volume samples based on thin film colour interference. The device functions by immobilizing an antigen on a porous anodic aluminum oxide surface, then exposing the surface to a high-volume fluid sample containing the corresponding antibody at a low concentration. Transitional or turbulent fluid flow (up to a Reynolds number of ~ 10,000) over the device surface ensures that the fluid will be adequately mixed, exposing as much of the fluid to the surface as possible, increasing the chance of an antibody from the sample binding to the antigen coated surface. Binding leads to the formation of an antigen-antibody complex which causes a visible colour shift on the device surface, due to an increase in the optical path length. Substrate materials were coated with thin films of tantalum and aluminum, then anodized at 4 V to form the desired anodic alumina surface prior to protein immobilization. Several substrate materials were investigated including polycarbonate membranes, resin polymer discs, quartz frits discs, high purity tantalum discs, and silicon wafers. Two anodization methods were investigated for the high purity tantalum discs and pore size, surface morphology, and protein adsorption were analyzed and compared between the two methods. Several designs were considered including a filter and syringe design, a stirred tank with an impeller, and an airlift bioreactor design containing a draft tube. The limits of detection for a prothrombin and anti-prothrombin antigen-antibody prototype were determined for a stationary 20 μL fluid sample, a stationary 500

mL fluid sample, and a well-mixed 100 mL or 500 mL fluid sample in the stirred tank and the draft tube apparatus, based on a visible colour shift after exposure to the sample for 20 minutes. The use of a stationary 500 mL sample was able to reduce the limit of detection for anti-prothrombin to 0.0025 mg/mL (16.7 nM), a twenty-fold improvement in sensitivity compared to the stationary 20 µL drop, which had a limit of detection of 0.05 mg/mL (0.33 µM). Introducing turbulence by mixing the solution with an impeller above the coated surface further improved the sensitivity, and the limit of detection for the stirred tank set up was found to be 6.25×10^{-4} mg/mL (4.2 nM) – an 80-fold improvement compared to the stationary 20 µL drop. The final design was similar to an airlift bioreactor with a draft tube and allowed for the fluid flow to be recirculated and directed towards the coated surface. The introduction of directed transitional and turbulent flow in a 500 mL sample allowed for an 8,000-fold improvement in sensitivity compared to the 20 µL drop, with a limit of detection of 6.25×10^{-6} mg/mL (41.7 pM). Using a conical shape draft tube allowed for an 80,000-fold improvement in sensitivity compared to the 20 µL drop, with a limit of detection of 6.25×10^{-7} mg/mL (4.2 pM). Overall, the diagnostic device was able to detect anti-prothrombin in a high-volume sample, quantified by a colour shift, with improved sensitivity compared to the low volume sample after 20 minutes. Introducing directed transitional or turbulent flow and mixing into the high-volume sample improved the device sensitivity by a factor of 80,000.

Preface

This thesis is an original work by Natalie Vankka. No part of this thesis has been previously published at this time. A patent application for this work is being drafted ahead of any peer reviewed publications. The novelty of this work is an improvement in sensitivity due to increasing the sample volume and controlling the fluid flow in the transition and turbulent regimes.

Acknowledgements

I would like to thank the members of my supervisory and candidacy committees: Dr. Robert Burrell, Dr. Todd McMullen, Dr. Anthony Yeung, Dr. Xuehua Zhang and Dr. Hasan Uludag, for their support and guidance. I truly appreciate how willingly they shared their expertise and knowledge.

I would like to acknowledge and thank all the individuals who worked with me and helped me along the way: Ana Lopez-Campistrous (protein lab assistance), Jacob Damant (assistance with Fusion 360), Ben Damant (assistance with Fusion 360), Ciaran Terry (training and assistance with sputtering and anodization), Henry Forer (assistance with preparation of synthetic urine), Jordan Pitman (assistance with computational fluid dynamics), Len Bowlby (assistance with device preparation) and the other members and students of Dr. Burrell's lab. I would like to thank you all for your time, effort, and contributions.

This work was possible thanks to the generous funding from the University Hospital Foundation.

Lastly, I would like to thank my parents, Anne and Terry, my siblings, Michelle and Nicholas, and my partner, Ben, for their unconditional support and encouragement. Thank you for always believing in me.

Table of Contents

Chapter 1 – Purpose and Scope 1

1.1. Motivation 1

1.2. Aims & Objectives 2

1.3. Scope of Thesis 4

1.4. References 5

Chapter 2 – Introduction and Literature Review 6

2.1. Introduction – Review of High Sensitivity Diagnostic Tests 6

2.2. Device Colour Generation 10

2.3. Fluid Mechanics 16

2.4. Impeller Design 21

2.5. Airlift Bioreactors 23

2.6. Anodic Alumina 26

2.7. Protein Detection and Immobilization on Alumina Surfaces 28

2.8. References 33

Chapter 3 – General Materials and Methods 44

3.1. Introduction 44

3.2. Membrane Selection 45

3.3. Device Design 52

3.4. Sputtering 54

3.5. Electrochemical Oxidation 60
3.6. Protein Exposure and Adsorption 62
3.7. Analytical Techniques 66
3.7.1. Scanning Electron Microscopy 66
3.7.2. Ellipsometry 66
3.7.3. Colour Coordinates 66
3.7.4. Statistics 67
3.8. References 68
Chapter 4 – The Effect of Sputtering and Anodization Parameters on Membrane Performance 69
4.1. Introduction 69
4.2. Materials and Methods 70
4.3. Deposition and Anodization 70
4.3.1. Polymer-Tantalum Adhesion Test 71
4.3.2. Tantalum Disc-Aluminum Film Adhesion Test 74
4.4. Results 76
4.4.1. Polycarbonate Membrane Films 76
4.4.2. Quartz Frits Discs 77
4.4.3. 3D Printed Polymer Discs 87
4.4.4. Tantalum Discs 87
4.5. Conclusions 122

4.6. References 123

Chapter 5 – Adsorption of Biologics onto Porous Anodic Alumina on Quartz Frits Discs 124

5.1. Introduction 124

5.2. Materials and Methods 125

5.3. Device Preparation 125

5.4. Adsorption of Biologics 126

5.5. Discussion 126

5.6. Conclusions 132

5.7. References 133

Chapter 6 – Adsorption of Biologics onto Porous Anodic Alumina on Tantalum Discs 134

6.1. Introduction 134

6.2. Materials and Methods 135

6.3. Device Preparation 135

6.4. Adsorption of Biologics 136

6.5. Discussion 136

6.6. Conclusions 150

6.7. References 151

Chapter 7 – Design of Impeller Based Diagnostic Device 152

7.1. Introduction 152

7.2. Materials and Methods 154

7.3. Device Preparation 155
7.4. Impeller Design 155
7.5. Computational Fluid Dynamics 158
7.5.1. Governing Equations of Fluid Dynamics 158
7.5.2. Turbulence Modeling 161
7.5.3. Calculations 164
7.5.4. Base Case 165
7.5.5. Fusion 360 Filter Design Case 170
7.5.6. Stirred Tank Case 174
7.5.7. Future CFD Work 180
7.6. Discussion 181
7.7. Conclusions 183
7.8. References 184
Chapter 8 – Anti-Prothrombin Sensitivity on a Prothrombin-Coated Membrane Device 188
8.1. Introduction 188
8.2. Methods 189
8.3. Theoretical Calculations for Anti-Prothrombin Limit of Detection 190
8.4. Device Preparation 191
8.5. Prothrombin Immobilization and Complex Formation 191
8.6. Results 192

8.7. Discussion 355

8.8. Conclusions 359

8.9. References 360

Chapter 9 – A Model Urinary Antibody Detection Test Using an Ultrasensitive Thin Film Diagnostic Device 362

9.1. Introduction 362

9.2. Prothrombin-Anti-Prothrombin Model System 363

9.3. Materials and Methods 364

9.4. Device Preparation 365

9.5. Results 365

9.6. Limitations 372

9.7. Discussion 379

9.8. Future Work 380

9.9. Conclusions 381

9.10. References 383

Bibliography 385

Appendix 1 – Standard Operating Procedures (SOPs) 400

1.1. Bob Sputtering System SOP 400

1.2. Floyd Sputtering System SOP 404

1.3. Zeiss Sigma Field Emission Scanning Electron Microscope SOP 408

Appendix 2 – Quartz Frits Disc Holster Designs..... 415

Appendix 3 – Fusion 360 Impeller, Membrane Disc and Membrane Reinforcement Designs.. 417

Appendix 4 – Anodization Data 419

List of Tables

Table 3.1. Linear thermal expansion coefficients of materials considered for filter membrane of device. Low TEC is ideal to prevent expansion during sputtering [4]. 46

Table 6.1. MSE, Al_2O_3 layer thickness, and EMA% from ellipsometry of tantalum disc 1 anodized vertically at 4 V. 149

Table 6.2. MSE, Al_2O_3 layer thickness, and EMA% from ellipsometry of tantalum disc 3 anodized vertically at 4 V. 149

Table 6.3. MSE, Al_2O_3 layer thickness, and EMA% from ellipsometry of tantalum disc 4 anodized horizontally at 4 V. 149

Table 6.4. MSE, Al_2O_3 layer thickness, and EMA% from ellipsometry of tantalum disc 5 anodized horizontally at 4 V. 149

Table 8.1. MSE, Al_2O_3 layer thickness, and EMA% from ellipsometry of tantalum disc anodized vertically at 4 V that showed poor colour shifts from protein work (shown in Figure 8.3). 202

Table 8.2. MSE, Al_2O_3 layer thickness, and EMA% from ellipsometry of tantalum disc anodized vertically at 4 V that showed poor colour shifts from protein work (shown in Figure 8.5). 202

Table 8.3. MSE, Al_2O_3 layer thickness, and EMA % from ellipsometry of silicon wafer coated with tantalum and aluminum, then anodized at 4 V that showed strong colour shifts from protein work. 215

Table 8.4. MSE, Al_2O_3 layer thickness, and EMA % from ellipsometry of silicon wafer coated with 200 nm of tantalum and 106 nm of aluminum, then anodized at 4 V. 223

Table 8.5. Results of the independent T-test statistical analysis on the effect of 500 mL of 0.005 mg/mL of anti-prothrombin (AP) for 20 minutes with continuous stirring at ~ 195 RPM on the surface colour of the prothrombin-coated wafer based on x and y chromaticity coordinates compared to the prothrombin (II) only control, for the slides shown in Figure 8.33. Statistically significant results are in italics. (n = 3). 228

Table 8.6. Results of the ANOVA and Tukey post hoc statistical analysis tests on the effect of various anti-prothrombin concentrations on the surface colour using x and y chromaticity

coordinates compared to the prothrombin only control. Statistically significant results are in italics. (n = 3). 234

Table 8.7. MSE, Al_2O_3 layer thickness, and EMA % of silicon wafer coated with 200 nm of tantalum and 106 nm of aluminum, then anodized at 4 V shown in Figures 8.37 – 8.42. 239

Table 8.8. Results of the independent T-test statistical analysis tests on the effect of 500 mL of 5 × 10^{-4} mg/mL anti-prothrombin for 20 minutes followed by 450 mL of 0.005 mg/mL of anti-prothrombin for 10 minutes with continuous stirring on the surface colour of the prothrombin-coated wafer based on x and y chromaticity coordinates compared to the prothrombin only control. Statistically significant results are in italics. (n = 3)..... 247

Table 8.9. MSE, Al_2O_3 layer thickness, and EMA % from ellipsometry of silicon wafer coated with 200 nm of tantalum and 106 nm of aluminum, then anodized at 4 V used for protein work at an anti-prothrombin concentration of 0.005 mg/mL in following experiments. 248

Table 8.10. MSE, Al_2O_3 layer thickness, and EMA % from ellipsometry of silicon wafer coated with 200 nm of tantalum and 106 nm of aluminum, then anodized at 4 V used for protein work at an anti-prothrombin concentration of 0.0025 mg/mL in following experiments. 248

Table 8.11. MSE, Al_2O_3 layer thickness, and EMA % from ellipsometry of silicon wafer coated with 200 nm of tantalum and 107 nm of aluminum, then anodized at 4 V used for protein work at an anti-prothrombin concentration of 5 × 10^{-4} mg/mL in following experiments. 248

Table 8.12. RGB colour coordinates for three areas on each slide for three replicates prior to protein exposure, after exposure to 532 µL of 1 mg/mL prothrombin for 20 minutes, and after subsequent exposure to 500 mL of 0.005 mg/mL anti-prothrombin (AP) at concentrations. 256

Table 8.13. Results of the independent T-test statistical analysis tests on the effect of 500 mL of 0.005 mg/mL of anti-prothrombin for 20 minutes with continuous stirring on the surface colour of the prothrombin-coated wafer based on x and y chromaticity coordinates compared to the prothrombin only control. Statistically significant results are in italics. (n = 3). 258

Table 8.14. Results of the independent T-test statistical analysis tests on the effect of 500 mL of 0.0025 mg/mL of anti-prothrombin for 20 minutes with continuous stirring on the surface colour

of the prothrombin-coated wafer based on x and y chromaticity coordinates compared to the prothrombin only control. Statistically significant results are in italics. (n = 3). 258

Table 8.15. Results of the independent T-test statistical analysis tests on the effect of 500 mL of 5×10^{-4} mg/mL anti-prothrombin for 20 minutes with continuous stirring on the surface colour of the prothrombin-coated wafer based on x and y chromaticity coordinates compared to the prothrombin only control. Statistically significant results are in italics. (n = 3). 259

Table 8.16. MSE, Al_2O_3 layer thickness, and EMA % from ellipsometry of silicon wafer coated with 200 nm of tantalum and 105 nm of aluminum, then anodized at 4 V used for protein work at an anti-prothrombin concentration of 0.005 mg/mL in following repeat experiments..... 260

Table 8.17. Results of the independent T-test statistical analysis tests on the effect of 500 mL of 0.005 mg/mL of anti-prothrombin for 20 minutes with continuous stirring on the surface colour of the prothrombin-coated wafer based on x and y chromaticity coordinates compared to the prothrombin only control. Statistically significant results are in italics. (n = 3). 263

Table 8.18. Results of the independent T-test statistical analysis tests on the effect of 500 mL of 0.005 mg/mL of anti-prothrombin for 20 minutes with no stirring on the surface colour of the prothrombin-coated wafer based on x and y chromaticity coordinates compared to the prothrombin only control. Statistically significant results are in italics. (n = 3). 270

Table 8.19. Results of the independent T-test statistical analysis tests on the effect of 500 mL of 0.005 mg/mL of anti-prothrombin for 20 minutes with continuous stirring at ~ 195 RPM on the surface colour of the prothrombin-coated wafer based on x and y chromaticity coordinates compared to the prothrombin only control. Statistically significant results are in italics. (n = 3). 271

Table 8.20. Results of the independent T-test statistical analysis tests on the effect of 500 mL of 0.0025 mg/mL of anti-prothrombin for 20 minutes with no stirring on the surface colour of the prothrombin-coated wafer based on x and y chromaticity coordinates compared to the prothrombin only control. Statistically significant results are in italics. (n = 3). 271

Table 8.21. Results of the independent T-test statistical analysis tests on the effect of 500 mL of 0.0025 mg/mL of anti-prothrombin for 20 minutes with continuous stirring at ~ 195 RPM on the

surface colour of the prothrombin-coated wafer based on x and y chromaticity coordinates compared to the prothrombin only control. Statistically significant results are in italics. (n = 3). 272

Table 8.22. Results of the ANOVA and Tukey post hoc statistical analysis tests on the effect of various anti-prothrombin exposure times for a 250 mL volume at a concentration of 0.0025 mg/mL with no stirring on the surface colour using x and y chromaticity coordinates compared to the prothrombin only control. Statistically significant results are in italics. (n = 3). 276

Table 8.23. Results of the ANOVA and Tukey post hoc statistical analysis tests on the effect of various anti-prothrombin exposure times for a 250 mL volume at a concentration of 0.0025 mg/mL with continuous stirring at ~ 195 RPM on the surface colour using x and y chromaticity coordinates compared to the prothrombin only control. Statistically significant results are in italics. (n = 3). 277

Table 8.24. Methods table for subsequent experiments to assess impact of anti-prothrombin concentration, exposure time, sample volume, and shear/mixing. 279

Table 8.25. Results of the ANOVA and Tukey post hoc post hoc statistical analysis tests on the effect of various anti-prothrombin exposure times for a 100 mL volume at a concentration of 0.005 mg/mL with no stirring on the surface colour using x and y chromaticity coordinates compared to the prothrombin only control. Statistically significant results are in italics. (n = 3). 285

Table 8.26. Results of the ANOVA and Tukey post hoc statistical analysis tests on the effect of various anti-prothrombin exposure times for a 100 mL volume at a concentration of 0.0025 mg/mL with no stirring on the surface colour using x and y chromaticity coordinates compared to the prothrombin only control. Statistically significant results are in italics. (n = 3). 285

Table 8.27. Results of the ANOVA and Tukey post hoc statistical analysis tests on the effect of various anti-prothrombin exposure times for a 100 mL volume at a concentration of 0.00125 mg/mL with no stirring on the surface colour using x and y chromaticity coordinates compared to the prothrombin only control. Statistically significant results are in italics. (n = 3). 286

Table 8.28. Results of the ANOVA and Tukey post hoc statistical analysis tests on the effect of various anti-prothrombin exposure times for a 500 mL volume at a concentration of 0.005 mg/mL with no stirring on the surface colour using x and y chromaticity coordinates compared to the prothrombin only control. Statistically significant results are in italics. (n = 3). 286

Table 8.29. Results of the ANOVA and Tukey post hoc statistical analysis tests on the effect of various anti-prothrombin exposure times for a 500 mL volume at a concentration of 0.0025 mg/mL with no stirring on the surface colour using x and y chromaticity coordinates compared to the prothrombin only control. Statistically significant results are in italics. (n = 3). 287

Table 8.30. Results of the ANOVA and Tukey post hoc statistical analysis tests on the effect of various anti-prothrombin exposure times for a 500 mL volume at a concentration of 0.00125 mg/mL with no stirring on the surface colour using x and y chromaticity coordinates compared to the prothrombin only control. Statistically significant results are in italics. (n = 3). 287

Table 8.31. Results of the ANOVA and Tukey post hoc statistical analysis tests on the effect of various anti-prothrombin exposure times for a 100 mL volume at a concentration of 0.005 mg/mL with stirring at 195 RPM on the surface colour using x and y chromaticity coordinates compared to the prothrombin only control. Statistically significant results are in italics. (n = 3). 293

Table 8.32. Results of the ANOVA and Tukey post hoc statistical analysis tests on the effect of various anti-prothrombin exposure times for a 100 mL volume at a concentration of 0.0025 mg/mL with stirring at 195 RPM on the surface colour using x and y chromaticity coordinates compared to the prothrombin only control. Statistically significant results are in italics. (n = 3). 294

Table 8.33. Results of the Welch's t-test and Games-Howell post hoc statistical analysis tests on the effect of various anti-prothrombin exposure times for a 100 mL volume at a concentration of 0.00125 mg/mL with stirring at 195 RPM on the surface colour using x and y chromaticity coordinates compared to the prothrombin only control. Statistically significant results are in italics. (n = 3). 294

Table 8.34. Results of the ANOVA and Tukey post hoc statistical analysis tests on the effect of various anti-prothrombin exposure times for a 500 mL volume at a concentration of 0.005

mg/mL with stirring at 195 RPM on the surface colour using x and y chromaticity coordinates compared to the prothrombin only control. Statistically significant results are in italics. (n = 3). 295

Table 8.35. Results of the ANOVA and Tukey post hoc statistical analysis tests on the effect of various anti-prothrombin exposure times for a 500 mL volume at a concentration of 0.0025 mg/mL with stirring at 195 RPM on the surface colour using x and y chromaticity coordinates compared to the prothrombin only control. Statistically significant results are in italics. (n = 3). 295

Table 8.36. Results of the ANOVA and Tukey post hoc statistical analysis tests on the effect of various anti-prothrombin exposure times for a 500 mL volume at a concentration of 0.00125 mg/mL with stirring at 195 RPM on the surface colour using x and y chromaticity coordinates compared to the prothrombin only control. Statistically significant results are in italics. (n = 3). 296

Table 8.37. Results of the ANOVA and Tukey post hoc statistical analysis tests on the effect of various anti-prothrombin exposure times for a 100 mL volume at a concentration of 0.005 mg/mL with stirring at 360 RPM on the surface colour using x and y chromaticity coordinates compared to the prothrombin only control. Statistically significant results are in italics. (n = 3). 302

Table 8.38. Results of the Welch's t-test and Game-Howell post hoc statistical analysis tests on the effect of various anti-prothrombin exposure times for a 100 mL volume at a concentration of 0.0025 mg/mL with stirring at 360 RPM on the surface colour using x and y chromaticity coordinates compared to the prothrombin only control. Statistically significant results are in italics. (n = 3). 302

Table 8.39. Results of the ANOVA and Tukey post hoc statistical analysis tests on the effect of various anti-prothrombin exposure times for a 100 mL volume at a concentration of 0.00125 mg/mL with stirring at 360 RPM on the surface colour using x and y chromaticity coordinates compared to the prothrombin only control. Statistically significant results are in italics. (n = 3). 303

Table 8.40. Results of the ANOVA and Tukey post hoc statistical analysis tests on the effect of various anti-prothrombin exposure times for a 500 mL volume at a concentration of 0.005 mg/mL with stirring at 360 RPM on the surface colour using x and y chromaticity coordinates compared to the prothrombin only control. Statistically significant results are in italics. (n = 3). 303

Table 8.41. Results of the ANOVA and Tukey post hoc statistical analysis tests on the effect of various anti-prothrombin exposure times for a 500 mL volume at a concentration of 0.0025 mg/mL with stirring at 360 RPM on the surface colour using x and y chromaticity coordinates compared to the prothrombin only control. Statistically significant results are in italics. (n = 3). 304

Table 8.42. Results of the ANOVA and Tukey post hoc statistical analysis tests on the effect of various anti-prothrombin exposure times for a 500 mL volume at a concentration of 0.00125 mg/mL with stirring at 360 RPM on the surface colour using x and y chromaticity coordinates compared to the prothrombin only control. Statistically significant results are in italics. (n = 3). 304

Table 8.43. Results of the ANOVA and Tukey post hoc statistical analysis tests on the effect of various anti-prothrombin exposure times for a 100 mL volume at a concentration of 6.25×10^{-4} mg/mL with no stirring on the surface colour using x and y chromaticity coordinates compared to the prothrombin only control. Statistically significant results are in italics. (n = 3). 308

Table 8.44. Results of the ANOVA and Tukey post hoc statistical analysis tests on the effect of various anti-prothrombin exposure times for a 100 mL volume at a concentration of 6.25×10^{-4} mg/mL with stirring at 195 RPM on the surface colour using x and y chromaticity coordinates compared to the prothrombin only control. Statistically significant results are in italics. (n = 3). 309

Table 8.45. Results of the ANOVA and Tukey post hoc statistical analysis tests on the effect of various anti-prothrombin exposure times for a 100 mL volume at a concentration of 6.25×10^{-4} mg/mL with stirring at 360 RPM on the surface colour using x and y chromaticity coordinates compared to the prothrombin only control. Statistically significant results are in italics. (n = 3). 309

Table 8.46. Results of the ANOVA and Tukey post hoc statistical analysis tests on the effect of various anti-prothrombin exposure times for a 100 mL volume at a concentration of 5×10^{-4} mg/mL with no stirring on the surface colour using x and y chromaticity coordinates compared to the prothrombin only control. Statistically significant results are in italics. (n = 3). 313

Table 8.47. Results of the ANOVA and Tukey post hoc statistical analysis tests on the effect of various anti-prothrombin exposure times for a 100 mL volume at a concentration of 5×10^{-4} mg/mL with stirring at 195 RPM on the surface colour using x and y chromaticity coordinates compared to the prothrombin only control. Statistically significant results are in italics. (n = 3). 313

Table 8.48. Results of the ANOVA and Tukey post hoc statistical analysis tests on the effect of various anti-prothrombin exposure times for a 100 mL volume at a concentration of 5×10^{-4} mg/mL with stirring at 360 RPM on the surface colour using x and y chromaticity coordinates compared to the prothrombin only control. Statistically significant results are in italics. (n = 3). 314

Table 8.49. Results of the independent T-test statistical analysis on the effect of 500 mL of 0.005 mg/mL of anti-prothrombin (AP) in the syringe-filter device (replicate 1) without the impeller on the surface colour of the prothrombin-coated tantalum disc based on x and y chromaticity coordinates compared to the prothrombin (II) only control. Statistically significant results are in italics. (n = 3). 319

Table 8.50. Results of the independent T-test statistical analysis on the effect of 500 mL of 0.005 mg/mL of anti-prothrombin (AP) in the syringe-filter device (replicate 2) without the impeller on the surface colour of the prothrombin-coated tantalum disc based on x and y chromaticity coordinates compared to the prothrombin (II) only control. Statistically significant results are in italics. (n = 3). 319

Table 8.51. Results of the independent T-test statistical analysis on the effect of 500 mL of 0.005 mg/mL of anti-prothrombin (AP) in the syringe-filter device (replicate 3) without the impeller on the surface colour of the prothrombin-coated tantalum disc based on x and y chromaticity coordinates compared to the prothrombin (II) only control. Statistically significant results are in italics. (n = 3). 320

Table 8.52. Results of the independent T-test statistical analysis on the effect of 500 mL of 0.00125 mg/mL of anti-prothrombin (AP) in the syringe-filter device (replicate 1) without the impeller on the surface colour of the prothrombin-coated tantalum disc based on x and y chromaticity coordinates compared to the prothrombin (II) only control. Statistically significant results are in italics. (n = 3)..... 323

Table 8.53. Results of the independent T-test statistical analysis on the effect of 500 mL of 0.00125 mg/mL of anti-prothrombin (AP) in the syringe-filter device (replicate 2) without the impeller on the surface colour of the prothrombin-coated tantalum disc based on x and y chromaticity coordinates compared to the prothrombin (II) only control. Statistically significant results are in italics. (n = 3)..... 323

Table 8.54. Results of the independent T-test statistical analysis on the effect of 500 mL of 0.00125 mg/mL of anti-prothrombin (AP) in the syringe-filter device (replicate 3) without the impeller on the surface colour of the prothrombin-coated tantalum disc based on x and y chromaticity coordinates compared to the prothrombin (II) only control. Statistically significant results are in italics. (n = 3)..... 324

Table 8.55. Results of the ANOVA and Tukey post hoc statistical analysis tests on the effect of various anti-prothrombin exposure times for a 500 mL volume at a concentration of 6.25×10^{-4} mg/mL in the draft tube apparatus at a gas flow rate of ~ 3.5 lpm on the surface colour using x and y chromaticity coordinates compared to the prothrombin only control. Statistically significant results are in italics. (n = 3)..... 331

Table 8.56. Results of the ANOVA and Tukey post hoc statistical analysis tests on the effect of various anti-prothrombin exposure times for a 500 mL volume at a concentration of 6.25×10^{-4} mg/mL in the draft tube apparatus at a gas flow rate of ~ 9.5 lpm on the surface colour using x and y chromaticity coordinates compared to the prothrombin only control. Statistically significant results are in italics. (n = 3)..... 331

Table 8.57. Results of the independent T-test statistical analysis on the effect of 500 mL of 5×10^{-4} mg/mL of anti-prothrombin (AP) in the draft tube apparatus at a gas flow rate of ~ 3.5 lpm on the surface colour based on x and y chromaticity coordinates compared to the prothrombin (II) only control. Statistically significant results are in italics. (n = 3). 334

Table 8.58. Results of the independent T-test statistical analysis on the effect of 500 mL of 5 × 10^{-4} mg/mL of anti-prothrombin (AP) in the draft tube apparatus at a gas flow rate of ~ 9.5 lpm on the surface colour based on x and y chromaticity coordinates compared to the prothrombin (II) only control. Statistically significant results are in italics. (n = 3). 334

Table 8.59. Results of the ANOVA and Tukey post hoc statistical analysis tests on the effect of various anti-prothrombin exposure times for a 500 mL volume at a concentration of 6.25 × 10^{-5} mg/mL in the draft tube apparatus at a gas flow rate of ~ 3.5 lpm on the surface colour using x and y chromaticity coordinates compared to the prothrombin only control. Statistically significant results are in italics. (n = 3). 338

Table 8.60. Results of the ANOVA and Tukey post hoc statistical analysis tests on the effect of various anti-prothrombin exposure times for a 500 mL volume at a concentration of 6.25 × 10^{-5} mg/mL in the draft tube apparatus at a gas flow rate of ~ 9.5 lpm on the surface colour using x and y chromaticity coordinates compared to the prothrombin only control. Statistically significant results are in italics. (n = 3). 338

Table 8.61. Results of the ANOVA and Tukey post hoc statistical analysis tests on the effect of various anti-prothrombin exposure times for a 500 mL volume at a concentration of 6.25 × 10^{-6} mg/mL in the draft tube apparatus at a gas flow rate of ~ 3.5 lpm on the surface colour using x and y chromaticity coordinates compared to the prothrombin only control. Statistically significant results are in italics. (n = 3). 340

Table 8.62. Results of the ANOVA and Tukey post hoc statistical analysis tests on the effect of various anti-prothrombin exposure times for a 500 mL volume at a concentration of 6.25 × 10^{-6} mg/mL in the draft tube apparatus at a gas flow rate of ~ 9.5 lpm on the surface colour using x and y chromaticity coordinates compared to the prothrombin only control. Statistically significant results are in italics. (n = 3). 341

Table 8.63. Results of the independent T-test statistical analysis on the effect of 15 µL of rabbit anti-sheep IgG (H+L)-horseradish peroxidase (HRP) in the hydrophobic circles on the surface colour based on x and y chromaticity coordinates compared to the surface colour after exposure to 500 mL of 6.25 × 10^{-4} mg/mL anti-prothrombin for 10 minutes in the draft tube apparatus at a gas flow rate of ~ 3.5 lpm. Statistically significant results are in italics. (n = 3). 345

Table 8.64. Results of the independent T-test statistical analysis on the effect of 500 mL of MilliQ water containing no anti-prothrombin (AP) in the draft tube apparatus at a gas flow rate of ~ 9.5 lpm for 10 minutes on the surface colour based on x and y chromaticity coordinates compared to the prothrombin (II) only control. Statistically significant results are in italics. (n = 3). 347

Table 8.65. Results of the independent T-test statistical analysis on the effect of 500 mL of 6.25 × 10^{-6} mg/mL anti-prothrombin (AP) in the conical draft tube apparatus at a gas flow rate of ~ 3.5 lpm for 20 minutes on the surface colour based on x and y chromaticity coordinates compared to the prothrombin (II) only control. Statistically significant results are in italics. (n = 3). 350

Table 8.66. Results of the independent T-test statistical analysis on the effect of 500 mL of 6.25 × 10^{-7} mg/mL anti-prothrombin (AP) in the conical draft tube apparatus at a gas flow rate of ~ 3.5 lpm for 20 minutes on the surface colour based on x and y chromaticity coordinates compared to the prothrombin (II) only control. Statistically significant results are in italics. (n = 3). 353

Table 8.67. Results of the independent T-test statistical analysis on the effect of 15 µL of rabbit anti-sheep IgG (H+L)-horseradish peroxidase (HRP) in the hydrophobic circles on the surface colour based on x and y chromaticity coordinates compared to the surface colour after exposure to 500 mL of 6.25 × 10^{-7} mg/mL anti-prothrombin for 20 minutes in the conical draft tube apparatus at a gas flow rate of ~ 3.5 lpm. Statistically significant results are in italics. (n = 3). 354

Table 8.68. Summary table for each device design investigated and the discussed ELISA tests including the Reynolds number, limit of detection and the improvement in sensitivity compared to the small volume static test. 358

Table 9.1. Results of the independent T-test statistical analysis on the effect of 500 mL of synthetic urine containing anti-prothrombin (AP) at a concentration of 6.25 × 10^{-5} mg/mL in the draft tube apparatus at a gas flow rate of ~ 3.5 lpm for 20 minutes on the surface colour based on x and y chromaticity coordinates compared to the prothrombin (II) only control. Statistically significant results are in italics. (n = 3). 367

Table 9.2. Results of the ANOVA and Tukey post hoc statistical analysis tests on the effect of various synthetic urine exposure times for a 500 mL volume containing no anti-prothrombin (AP) in the draft tube apparatus at a gas flow rate of ~ 3.5 lpm on the surface colour using x and y chromaticity coordinates compared to the prothrombin only control. Statistically significant results are in italics. (n = 3)..... 370

Table 9.3. Results of the independent T-test statistical analysis on the effect 15 µL of 0.5 mg/mL anti-prothrombin (AP) for 20 minutes on the surface colour based on x and y chromaticity coordinates compared to the prothrombin (II) only control after exposure to 500 mL of synthetic urine in the draft tube apparatus at a gas flow rate of ~ 3.5 lpm for 20 minutes. Statistically significant results are in italics. (n = 3)..... 371

Table 9.4. Results of the ANOVA and Tukey post hoc statistical analysis tests on the effect of various bovine serum albumin (BSA) exposure times for a 500 mL volume at a concentration of 6.25×10^{-5} mg/mL in the draft tube apparatus at a gas flow rate of ~ 3.5 lpm on the surface colour using x and y chromaticity coordinates compared to the prothrombin only control. Statistically significant results are in italics. (n = 3)..... 374

Table 9.5. Results of the ANOVA and Tukey post hoc statistical analysis tests on the effect of various anti-prothrombin (AP) exposure times for a 500 mL volume at a concentration of 6.25×10^{-5} mg/mL in the draft tube apparatus at a gas flow rate of ~ 3.5 lpm on the surface colour using x and y chromaticity coordinates compared to the prothrombin and bovine serum albumin (BSA) coated surface. Statistically significant results are in italics. (n = 3)..... 377

List of Figures

Figure 2.1. The pregnancy test lateral flow immunoassay [9]. 7

Figure 2.2. Interference colours from an oil film on water [19]. 10

Figure 2.3. Path of reflected and refracted light rays through a thin film of oil [20]. 10

Figure 2.4. Pathway light travels through bound antibody, adsorbed protein, and aluminum oxide layers to produce a colour shift by interference. Binding of the antibody increases the OPL enough to produce a visible colour shift. Silicon wafers, polycarbonate membranes, porous quartz frits discs, and high purity tantalum discs were used as the substrate material in this work. The refractive index (η) of the adsorbed protein is equal to the refractive index of the aluminum oxide layer. 12

Figure 2.5. Revised Michel-Lévy interference colour chart displaying first, second, third and fourth order interference colours [30]. 15

Figure 2.6. CIE 1931 colour chromaticity diagram displaying MacAdam ellipses. Any two points within a single eclipse are indistinguishable to the human eye [31]. 15

Figure 2.7. Laminar, transitional, and turbulent flow regimes over the porous membrane device. Laminar flow is characterized by parallel layers of fluid flow sliding smoothly over one another that do not mix. Transition flow is a mixture of laminar and turbulent flow. Turbulent flow is characterized by random motion of the fluid elements and mixing [37]. 17

Figure 2.8. Laminar, transitional, and turbulent flow regimes characterized by dye. Turbulent flow is characterized by mixing of fluid elements and would allow for more fluid exposure to the surface [38]. 18

Figure 2.9. The four main types of impeller blades used. Airfoil (top left) [45], pitch blade (top right) [46], propeller blade (bottom left) [47] and radial blade (bottom right) [48]. 22

Figure 2.10. Schematic diagram of airlift reactor configurations: a) internal loop with riser section inside draft tube, b) internal loop with downcomer section inside draft tube, and c) external loop [57]. 24

Figure 2.11. Barrier-type anodic aluminum oxide (AAO) film (a) and porous-type aluminum oxide film (b) and the corresponding current density (j) vs. time (t) graphs [71]. 28

Figure 2.12. Structure of prothrombin ([96]) composed of the Gla domain (red), kringle-1 domain (orange), kringle-2 domain (yellow) and the protease domain (blue) with dimensions from Lim et al. ([95]) (A). Structures of glutamic acid and post translational gamma-carboxyglutamic acid residues with available carboxyl groups for immobilization on a positively charged alumina surface (B). Figure obtained from Sweet (2018) [72]. 31

Figure 3.1. 3D printed Vero Clear resin polymer membrane disc. 48

Figure 3.2. 3D printed Vero Clear resin polymer membrane reinforcement. 48

Figure 3.3. Top view and side view of the 3D printed Vero Clear resin polymer impeller to ensure turbulent flow and promote mixing of fluid elements at membrane surface. 49

Figure 3.4. Five- and nine-hole tantalum disc design, detailing the hole sizes and spacing. 50

Figure 3.5. Tantalum disc with a 26.6 mm diameter and no holes (left). Tantalum disc with a 26.6 mm diameter and one 1.18 mm hole for impeller attachment and four 1 mm holes to allow fluid flow through the disc (middle). Tantalum disc with a 26.6 mm diameter and one 1.18 mm hole for impeller attachment and eight 1 mm holes to allow fluid flow through the disc (right). 51

Figure 3.6. Diagnostic device stirred tank design. 52

Figure 3.7. Diagnostic device syringe/filter design. 53

Figure 3.8. Fluid flow arrows between the impeller and the tantalum disc in the diagnostic device syringe/filter design. The space between the impeller and the tantalum disc is exaggerated in this drawing to show the mixing above the surface induced by the impeller. 54

Figure 3.9. 3D printed quartz frits disc holsters epoxy glued to silicon wafers. Empty (top left), holding quartz frits discs prior to sputtering (top right), holding quartz frits discs after sputtering tantalum using the Bob sputtering system (bottom left) and holding quartz frits discs after sputtering aluminum (on top of tantalum layer) using the Floyd sputtering system (bottom right). 55

Figure 3.10. The planar magnetron sputtering system (Bob) at the University of Alberta nanoFAB used to deposit ~ 200 nm of tantalum on to polycarbonate membranes, polymer discs, silicon wafers, quartz frits and tantalum discs. 56

Figure 3.11. The Bob sputtering system at the University of Alberta nanoFAB, loaded, after sputtering. The silicon wafers are secured using clips and the quartz frits discs are held in place using the substrate holders. 57

Figure 3.12. The planar magnetron sputtering system (Floyd) at the University of Alberta nanoFAB used to deposit ~ 110 nm of aluminum on to the tantalum-coated silicon wafers, tantalum discs and quartz frits. 58

Figure 3.13. The six-shelf plate holder that holds the substrates and is loaded into the Floyd sputtering system's load lock chamber. 59

Figure 3.14. The eKLipse software computer screen displaying the user interface and control system for the Floyd sputtering system. 59

Figure 3.15. The electrochemical cell consisting of the cathode, anode, reference electrode and acid bath used for vertical anodization of substrates. The 3D printed substrate holder separates the cathode and anode by ~ 6 cm with the reference electrode centered between. 61

Figure 3.16. EG&G Princeton Applied Research Potentiostat/Galvanostat Model 273A used for anodization of substrates. 62

Figure 3.17. Design of tool used to cleave silicon wafers into rectangles of a consistent size. Image obtained from Sweet [1]. 64

Figure 3.18. 3D printed stencil tool used to cleave silicon wafers into rectangles of a consistent size. 64

Figure 4.1. The characteristic curve for anodization of aluminum and tantalum on a silicon wafer. The initial drop indicates aluminum oxide formation, followed by a steady current indicating pore formation, and a final drop in current indicating tantalum oxide formation. The final constant region indicates anodization is complete and the tantala dielectric layer has been formed. 71

Figure 4.2. Results of the tantalum-polymer disc adhesion test. Adherence of the thin tantalum film to the polymer substrate was poor as the tape was able to pull off a significant amount of tantalum metal. The tape (above) shows a significant amount of tantalum metal was pulled off of the polymer disc (below). 73

Figure 4.3. Results of two adhesion tests between tantalum discs and ~ 110 nm aluminum films before anodization. 74

Figure 4.4. Adhesion test between tantalum disc and 110 nm aluminum thin film after anodization. Poor adhesion likely due to poor anodization. 75

Figure 4.5. Polycarbonate membrane after sputtering ~ 200 nm of tantalum metal. The thin polycarbonate membrane curled and wrinkled during the sputtering process. 76

Figure 4.6. Current vs. time anodization plot for an unpolished quartz frits disc coated with 200 nm of tantalum and 110 nm of aluminum at 8 V. 78

Figure 4.7. Current vs. time anodization plot for an unpolished quartz frits disc coated with 200 nm of tantalum and 110 nm of aluminum at 4 V. 78

Figure 4.8. Current vs. time anodization plot for an unpolished quartz frits disc with no thin film coatings at 4 V. 79

Figure 4.9. Current vs. time anodization plot for a silicon wafer with no thin film coatings at 4 V. 79

Figure 4.10. Epoxy-dipped quartz frits disc drawing. Quartz frits discs were partially coated with epoxy to prevent the rise of the acid bath solution through the upper portion of the disc during anodization. Striped region is epoxy coated. 80

Figure 4.11. Epoxy-dipped quartz frits disc (40 – 100 μm porosity). 81

Figure 4.12. Current vs. time anodization plot for a polished quartz frits disc coated with 200 nm of tantalum and 110 nm of aluminum at 4 V (epoxy dipped). 82

Figure 4.13. Topographical SEM images of the 40 – 100 μm porosity polished quartz frits discs after sputtering ~ 200 nm of tantalum and ~ 110 nm of aluminum, followed by anodization at 4

V at magnifications of 50 X (top left), 500 X (top right), 10,000 X (bottom left) and 30,000 X (bottom right). 83

Figure 4.14. Topographical SEM images of the 100 – 160 μm porosity polished quartz frits discs after sputtering ~ 200 nm of tantalum and ~ 110 nm of aluminum, followed by anodization at 4 V at magnifications of 50 X (top left), 500 X (top right), 10,000 X (bottom left) and 30,000 X (bottom right). 84

Figure 4.15. Topographical SEM images of the silicon wafers after sputtering ~ 200 nm of tantalum and ~ 110 nm of aluminum, followed by anodization at 4 V at magnifications of 50 X (top left), 500 X (top right), 10,000 X (bottom left) and 30,000 X (bottom right). 85

Figure 4.16. Cross-sectional SEM image of a silicon wafer after sputtering ~ 200 nm of tantalum and ~ 110 nm of aluminum, followed by anodization at 4 V at a magnification of 30,000 X. 86

Figure 4.17. Cross-sectional SEM image of a silicon wafer after sputtering ~ 200 nm of tantalum and ~ 110 nm of aluminum, followed by anodization at 4 V at a magnification of 50,000 X. 86

Figure 4.18. Current vs. time anodization plot for first tantalum disc coated with 110 nm of aluminum at 4 V. Kapton tape was stuck on the face opposite to the aluminum coating to prevent anodization of the back tantalum face. 88

Figure 4.19. Current vs. time anodization plot for second tantalum disc coated with 110 nm of aluminum at 4 V. Kapton tape was stuck on the face opposite to the aluminum coating to prevent anodization of the back tantalum face. Anodization acid may have leaked through the Kapton tape to produce this curve. 88

Figure 4.20. Current vs. time anodization plot for third tantalum disc coated with 110 nm of aluminum at 4 V. Kapton tape was stuck on the face opposite to the aluminum coating to prevent anodization of the back tantalum face. Anodization acid may have leaked through the Kapton tape to produce this curve. 89

Figure 4.21. Current vs. time anodization plot for fourth tantalum disc coated with 110 nm of aluminum at 4 V. Kapton tape was stuck on the face opposite to the aluminum coating to prevent anodization of the back tantalum face. Anodization acid may have leaked through the Kapton tape to produce this curve. 89

Figure 4.22. Experimental set up for anodizing one face of tantalum disc. The electrochemical cell consisting of the cathode (aluminum foil), anode (tantalum disc), reference electrode and acid bath used for anodization of substrates. The cathode and anode clips are separated by ~ 10 cm with the reference electrode centered between. 91

Figure 4.23. Current vs. time anodization plot for a tantalum disc with no thin film coatings using the horizontal anodization method at 10 V. 92

Figure 4.24. Current vs. time anodization plot for a tantalum disc coated with 110 nm of aluminum using the horizontal anodization method to anodize the aluminum face at 4 V. 93

Figure 4.25. Current vs. time anodization plot for a piece of aluminum foil at 4 V..... 94

Figure 4.26. Topographical SEM images of anodized aluminum foil at magnification of 50,000 X (left) and 70,000 X (right). 95

Figure 4.27. Topographical SEM images of a tantalum disc that had the back tantalum face anodized at 10 V, then coated with ~ 110 nm of aluminum, followed by vertical anodization at 4 V that produced an unexpected curve at magnification of 50,000X (left) and 70,000X (right)... 96

Figure 4.28. Current vs. time anodization plot for a tantalum disc coated with 110 nm of aluminum at 4 V (vertical) with previous anodization of tantalum face at 10 V (SEM images shown in Figure 4.27). 96

Figure 4.29. Topographical SEM images of a tantalum disc after sputtering ~ 110 nm of aluminum, followed by horizontal anodization at 4 V that produced the expected curve at magnification of 50,000 X (left) and 70,000 X (right). 97

Figure 4.30. Current vs. time anodization plot for the tantalum disc coated with 110 nm of aluminum and anodized horizontally at 4 V (SEM images shown in Figure 4.29). 97

Figure 4.31. Current vs. time anodization plot for a silicon wafer coated with 125 nm of tantalum and 110 nm of aluminum at 4 V. 98

Figure 4.32. Current vs. time anodization plot for a silicon wafer coated with 250 nm of tantalum and 110 nm of aluminum at 4 V. 99

Figure 4.33. Current vs. time anodization plot for a silicon wafer coated with 500 nm of tantalum and 110 nm of aluminum at 4 V. 99

Figure 4.34. Current vs. time anodization plot for a silicon wafer coated with 1 μm of tantalum and 110 nm of aluminum at 4 V. 100

Figure 4.35. Topographical SEM image of a silicon wafer coated with ~ 125 nm of tantalum and ~ 110 nm of aluminum after anodization at 4 V at 10,000 X. 101

Figure 4.36. Topographical SEM image of a silicon wafer coated with ~ 125 nm of tantalum and ~ 110 nm of aluminum after anodization at 4 V at 30,000 X. 101

Figure 4.37. Topographical SEM image of a silicon wafer coated with ~ 125 nm of tantalum and ~ 110 nm of aluminum after anodization at 4 V at 50,000 X. 102

Figure 4.38. Topographical SEM image of a silicon wafer coated with ~ 250 nm of tantalum and ~ 110 nm of aluminum after anodization at 4 V at 10,000 X. 102

Figure 4.39. Topographical SEM image of a silicon wafer coated with ~ 250 nm of tantalum and ~ 110 nm of aluminum after anodization at 4 V at 30,000 X. 103

Figure 4.40. Topographical SEM image of a silicon wafer coated with ~ 250 nm of tantalum and ~ 110 nm of aluminum after anodization at 4 V at 50,520 X. 103

Figure 4.41. Topographical SEM image of a silicon wafer coated with ~ 1 μm of tantalum and ~ 110 nm of aluminum after anodization at 4 V at 10,000 X. 104

Figure 4.42. Topographical SEM image of a silicon wafer coated with ~ 1 μm of tantalum and ~ 110 nm of aluminum after anodization at 4 V at 30,000 X. 104

Figure 4.43. Topographical SEM image of a silicon wafer coated with ~ 1 μm of tantalum and ~ 110 nm of aluminum after anodization at 4 V at 50,000 X. 105

Figure 4.44. Two tantalum discs placed on aluminum foil on a cookie rack inside an oven prior to undergoing a self-cleaning cycle to remove organics from the surface. 105

Figure 4.45. Two tantalum discs after heat treatment in a self-cleaning oven cycle to remove organics from the surface. During the treatment, a layer of tantalum oxide appears to have formed on the surface..... 106

Figure 4.46. Current vs. time anodization curve of a tantalum disc after oven self-cleaning and deposition of 200 nm of tantalum and 110 nm of aluminum at 4 V. 107

Figure 4.47. Anodized tantalum disc coated with ~ 110 nm of aluminum after being cleaned with HPLC grade isopropanol (left) and anodized tantalum disc coated with ~ 200 nm tantalum and ~ 110 nm aluminum after being cleaned using a self-cleaning oven cycle. Adhesion appears much better for the disc that underwent the self-cleaning oven cycle cleaning method. 108

Figure 4.48. Current vs. time anodization curve of first tantalum disc after oven self-cleaning and deposition of 200 nm of tantalum and 110 nm of aluminum at 4 V. It is likely that the back side tantalum face and the aluminum coated face were both anodized. 109

Figure 4.49. Current vs. time anodization curve of second tantalum disc after oven self-cleaning and deposition of 200 nm of tantalum and 110 nm of aluminum at 4 V. It is likely that the back side tantalum face and the aluminum coated face were both anodized. 109

Figure 4.50. Topographical SEM image of the first oven cleaned tantalum disc with ~ 200 nm of tantalum and ~ 110 nm of aluminum after anodization at 4 V at 10,000 X. 110

Figure 4.51. Topographical SEM image of the first oven cleaned tantalum disc with ~ 200 nm of tantalum and ~ 110 nm of aluminum after anodization at 4 V at 30,000 X. 110

Figure 4.52. Topographical SEM image of the first oven cleaned tantalum disc with ~ 200 nm of tantalum and ~ 110 nm of aluminum after anodization at 4 V at 50,000 X. 111

Figure 4.53. Topographical SEM image of the second oven cleaned tantalum disc with ~ 200 nm of tantalum and ~ 110 nm of aluminum after anodization at 4 V at 10,000 X. 111

Figure 4.54. Topographical SEM image of the second oven cleaned tantalum disc with ~ 200 nm of tantalum and ~ 110 nm of aluminum after anodization at 4 V at 30,000 X. 112

Figure 4.55. Topographical SEM image of the second oven cleaned tantalum disc with ~ 200 nm of tantalum and ~ 110 nm of aluminum after anodization at 4 V at 50,000 X. 112

Figure 4.56. Current vs. time anodization curve of the back side of tantalum disc number 1 at 10 V after cleaning in a self-cleaning oven, prior to thin film sputtering. 113

Figure 4.57. Current vs. time anodization curve of the back side of tantalum disc number 2 at 10 V after cleaning in a self-cleaning oven, prior to thin film sputtering. 114

Figure 4.58. Current vs. time anodization curve of the back side of tantalum disc number 3 at 10 V after cleaning in a self-cleaning oven, prior to thin film sputtering. 114

Figure 4.59. Current vs. time anodization curve of tantalum disc 1 (vertical method) after coating with 200 nm of tantalum and 110 nm of aluminum at 4 V (back side previously anodized at 10 V). 115

Figure 4.60. Current vs. time anodization curve of tantalum disc 2 (vertical method) after coating with 200 nm of tantalum and 110 nm of aluminum at 4 V (back side previously anodized at 10 V). 116

Figure 4.61. Current vs. time anodization curve of tantalum disc 3 (vertical method) after coating with 200 nm of tantalum and 110 nm of aluminum at 4 V (back side previously anodized at 10 V). 116

Figure 4.62. Current vs. time anodization curve of tantalum disc 4 (horizontal method) after coating with 200 nm of tantalum and 110 nm of aluminum at 4 V (no previous anodization).. 117

Figure 4.63. Current vs. time anodization curve of tantalum disc 5 (horizontal method) after coating with 200 nm of tantalum and 110 nm of aluminum at 4 V (no previous anodization).. 117

Figure 4.64. Current vs. time anodization curve of tantalum disc 6 (horizontal method) after coating with 200 nm of tantalum and 110 nm of aluminum at 4 V (no previous anodization).. 118

Figure 4.65. Topographical SEM image of oven cleaned tantalum disc 2 that was anodized on the back side at 10 V then sputtered with ~ 200 nm of tantalum and ~ 110 nm of aluminum, then anodized vertically at 4 V at 10,000 X. 119

Figure 4.66. Topographical SEM image of oven cleaned tantalum disc 2 that was anodized on the back side at 10 V then sputtered with ~ 200 nm of tantalum and ~ 110 nm of aluminum, then anodized vertically at 4 V at 30,000 X. 119

Figure 4.67. Topographical SEM image of oven cleaned tantalum disc 2 that was anodized on the back side at 10 V then sputtered with ~ 200 nm of tantalum and ~ 110 nm of aluminum, then anodized vertically at 4 V at 50,000 X. 120

Figure 4.68. Topographical SEM image of oven cleaned tantalum disc 6 that was sputtered with ~ 200 nm of tantalum and ~ 110 nm of aluminum, then anodized horizontally at 4 V at 10,000 X. 120

Figure 4.69. Topographical SEM image of oven cleaned tantalum disc 6 that was sputtered with ~ 200 nm of tantalum and ~ 110 nm of aluminum, then anodized horizontally at 4 V at 30,000 X. 121

Figure 4.70. Topographical SEM image of oven cleaned tantalum disc 6 that was sputtered with ~ 200 nm of tantalum and ~ 110 nm of aluminum, then anodized horizontally at 4 V at 50,000 X. 121

Figure 5.1. Visual detection of protein on a silicon wafer coated with ~ 200 nm of tantalum, ~ 110 nm of aluminum after anodization at 4 V. Colour shifts occur due to the interaction of alumina and the protein exposed to the surface. 1 – control circle with no protein placed. 2 – prothrombin protein adsorbed. 3 – prothrombin adsorbed then anti-prothrombin adsorbed. 4 – prothrombin, anti-prothrombin and secondary antibody adsorbed. 127

Figure 5.2. Coated and anodized polished quartz frits disc (porosity = 40 – 100 μm) protein analysis. No visible colour shift occurred between the control surface with no exposure to prothrombin (left circle) and the surfaces that had been exposed to 20 μL of 1 mg/mL prothrombin (middle and right circles). 128

Figure 5.3. Coated and anodized polished quartz frits disc (porosity = 100 – 160 μm) protein analysis. No visible colour shift occurred between the control surface with no exposure to prothrombin (left circle) and the surfaces that had been exposed to 20 μL of 1 mg/mL prothrombin (middle and right circles). 129

Figure 5.4. Coated and anodized polished quartz frits disc (porosity = 100 – 160 μm) protein analysis at an alternate angle. No visible colour shift occurred between the control surface with

no exposure to prothrombin (left circle) and the surfaces that had been exposed to 20 µL of 1 mg/mL prothrombin (middle and right circles). 129

Figure 5.5. Control quartz frits disc with no exposure to protein (left) and polished quartz frits disc (porosity = 100 – 160 µm) that was entirely exposed to 1 mg/mL prothrombin (right). No visible colour shift can be detected between the control surface and the prothrombin exposed surface. 130

Figure 5.6. Control quartz frits disc with no exposure to protein (left) and polished quartz frits disc (porosity = 100 – 160 µm) that was entirely exposed to 1 mg/mL prothrombin (right) at an alternate angle. No visible colour shift can be detected between the control surface and the prothrombin exposed surface. 131

Figure 6.1. Visual detection of adsorbed protein on a tantalum disc coated with ~ 110 nm of aluminum then anodized at 4 V. Colour shifts indicate binding of prothrombin and anti-prothrombin to the surface. 1, 2 – prothrombin protein layer adsorbed followed by a layer of anti-prothrombin protein. 3 – prothrombin protein only adsorbed. 4 – control circle with no protein adsorbed. 137

Figure 6.2. Visual detection of protein on a tantalum disc coated with ~ 110 nm of aluminum then anodized at 4 V. Anodization of the aluminum surface was not successful and poor results were obtained for protein detection. Clear colour shifts are not observed between the circles. 1, 2 – exposed to prothrombin then anti-prothrombin. 3 – exposed to prothrombin only. 4 – control circle with no protein exposure. 138

Figure 6.3. Control circle with no adsorbed protein (circle 1), adsorption of prothrombin (circle 2), prothrombin + anti-prothrombin (circle 3), prothrombin + anti-prothrombin + secondary antibody (circle 4) on tantalum disc 1 using the vertical anodization method (back side anodized at 10 V prior to sputtering, aluminum face anodized vertically at 4 V after sputtering). 140

Figure 6.4. Control circle with no adsorbed protein (circle 1), adsorption of prothrombin (circle 2), prothrombin + anti-prothrombin (circle 3), prothrombin + anti-prothrombin + secondary antibody (circle 4) on tantalum disc 3 using the vertical anodization method (back side anodized at 10 V prior to sputtering, aluminum face anodized vertically at 4 V after sputtering). 141

Figure 6.5. Control circle with no adsorbed protein (circle 1), adsorption of prothrombin (circle 2), prothrombin + anti-prothrombin (circle 3), prothrombin + anti-prothrombin + secondary antibody (circle 4) on tantalum disc 4 using the horizontal anodization method (aluminum face anodized flat at 4 V). 141

Figure 6.6. Control circle with no adsorbed protein (circle 1), adsorption of prothrombin (circle 2), prothrombin + anti-prothrombin (circle 3), prothrombin + anti-prothrombin + secondary antibody (circle 4) on tantalum disc 5 using the horizontal anodization method (aluminum face anodized flat at 4 V). 142

Figure 6.7. Topographical SEM image of tantalum disc 1 shown in Figure 6.3 (vertical method, strong colour shifts) at magnification of 10,000 X. 144

Figure 6.8. Topographical SEM image of tantalum disc 1 shown in Figure 6.3 (vertical method, strong colour shifts) at magnification of 30,000 X. 145

Figure 6.9. Topographical SEM image of tantalum disc 1 shown in Figure 6.3 (vertical method, strong colour shifts) at magnification of 50,000 X. 145

Figure 6.10. Topographical SEM image of tantalum disc 1 shown in Figure 6.3 (vertical method, strong colour shifts) at magnification of 70,000 X. 146

Figure 6.11. Topographical SEM image of tantalum disc 4 shown in Figure 6.5 (horizontal method, strong colour shifts) at magnification of 10,000 X. 146

Figure 6.12. Topographical SEM image of tantalum disc 4 shown in Figure 6.5 (horizontal method, strong colour shifts) at magnification of 30,000 X. 147

Figure 6.13. Topographical SEM image of tantalum disc 4 shown in Figure 6.5 (horizontal method, strong colour shifts) at magnification of 50,000 X. 147

Figure 6.14. Topographical SEM image of tantalum disc 4 shown in Figure 6.5 (horizontal method, strong colour shifts) at magnification of 70,000 X. 148

Figure 7.1. Cross-sectional image showing the inside of the Fusion 360 filter design. 157

Figure 7.2. Impeller speed calculations. 165

Figure 7.3. Solution methods and controls for base case CFD simulation on ANSYS Fluent... 167

Figure 7.4. Residuals for continuity, x-velocity, y-velocity, z-velocity, k and omega as a function of iterations for the base case in ANSYS Fluent. 167

Figure 7.5. Screenshot of turbulent viscosity ratio contour during ANSYS Fluent base case simulation. 168

Figure 7.6. Screenshot of velocity vectors during ANSYS Fluent base case simulation. 168

Figure 7.7. Screenshot of velocity magnitude path lines during ANSYS Fluent base case simulation. 169

Figure 7.8. Residuals for continuity, x-velocity, y-velocity, z-velocity, k and epsilon as a function of iterations for the Fusion 360 filter design case in ANSYS Fluent. 171

Figure 7.9. Screenshot of turbulent viscosity ratio contour in the vertical plane surrounding the impeller during ANSYS Fluent Fusion 360 filter design case. The clear portion represents the location of the impeller. TVR > 10 indicates turbulent flow. 171

Figure 7.10. Screenshot of turbulent viscosity ratio just above the surface of the disc membrane, and just beneath the impeller, during ANSYS Fluent Fusion 360 filter design case. TVR > 10 indicates turbulent flow. 172

Figure 7.11. Screenshot of velocity vectors in the vertical plane surrounding the impeller during ANSYS Fluent Fusion 360 filter design case. The clear portion represents the location of the impeller. 172

Figure 7.12. Screenshot of velocity vectors just above the surface of the disc membrane and just beneath the impeller, during ANSYS Fluent Fusion 360 filter design case. 173

Figure 7.13. Fusion 360 stirred tank impeller design. 174

Figure 7.14. Solution method settings for the stirred tank case ANSYS Fluent simulation. 176

Figure 7.15. Residuals for continuity, x-velocity, y-velocity, z-velocity, k and omega as a function of iterations for the stirred tank case in ANSYS Fluent. 177

Figure 7.16. Screenshot of turbulent viscosity ratio (top view) in ANSYS Fluent stirred tank simulation. TVR > 10 indicates turbulent flow. 177

Figure 7.17. Screenshot of turbulent viscosity ratio (side view) in ANSYS Fluent stirred tank simulation. TVR > 10 indicates turbulent flow. 178

Figure 7.18. Screenshot of velocity vectors (top view) in ANSYS Fluent stirred tank simulation. 178

Figure 7.19. Screenshot of velocity vectors (side view) in ANSYS Fluent stirred tank simulation. 179

Figure 8.1. Tantalum disc coated with ~ 200 nm of tantalum then ~ 110 nm of aluminum and anodized at 4 V using the horizontal method after protein analysis. Each of the four circles was exposed to 20 µL of 1 mg/mL of prothrombin for 20 minutes. 194

Figure 8.2. Tantalum disc coated with ~ 200 nm of tantalum then ~ 110 nm of aluminum and anodized at 4 V using the horizontal method after protein analysis. Each of the four circles was exposed to 20 µL of 1 mg/mL of prothrombin for 20 minutes. 195

Figure 8.3. Tantalum disc coated with ~ 200 nm of tantalum then ~ 110 nm of aluminum and anodized at 4 V using the horizontal method after protein analysis. Each of the four circles was exposed to 20 µL of 1 mg/mL of prothrombin for 20 minutes. 195

Figure 8.4. Tantalum disc coated with ~ 200 nm of tantalum then ~ 110 nm of aluminum and anodized at 4 V using the horizontal method after protein analysis. Each of the four circles was exposed to 20 µL of 1 mg/mL of prothrombin for 20 minutes. 196

Figure 8.5. Tantalum disc coated with ~ 200 nm of tantalum then ~ 110 nm of aluminum and anodized at 4 V using the horizontal method after protein analysis. Each of the four circles was exposed to 20 µL of 1 mg/mL of prothrombin for 20 minutes. 196

Figure 8.6. Tantalum disc coated with ~ 200 nm of tantalum then ~ 110 nm of aluminum and anodized at 4 V using the horizontal method after protein analysis. Each of the four circles was exposed to 20 µL of 1 mg/mL of prothrombin for 20 minutes. 197

Figure 8.7. Tantalum disc coated with ~ 200 nm of tantalum then ~ 110 nm of aluminum and anodized at 4 V using the horizontal method after protein analysis. Each circle exposed to 20 µL of 1 mg/mL prothrombin for 20 minutes. Then one circle exposed to 0.5 mg/mL anti-prothrombin for 20 minutes (farthest left circle), one circle exposed to 0.05 mg/mL anti-

prothrombin for 20 minutes (middle left circle), one circle exposed to 0.005 mg/mL anti-prothrombin for 20 minutes (middle right circle). The farthest right circle was not exposed to any anti-prothrombin and used as a control with prothrombin only. 198

Figure 8.8. Topographical SEM image of tantalum disc shown in Figure 8.3 (horizontal method, poor colour shifts) at magnification of 10,000 X..... 200

Figure 8.9. Topographical SEM image of tantalum disc shown in Figure 8.3 (horizontal method, poor colour shifts) at magnification of 30,000 X..... 200

Figure 8.10. Topographical SEM image of tantalum disc shown in Figure 8.3 (horizontal method, poor colour shifts) at magnification of 50,000 X..... 201

Figure 8.11. Topographical SEM image of tantalum disc shown in Figure 8.3 (horizontal method, poor colour shifts) at magnification of 70,000 X..... 201

Figure 8.12. Top view (left) and side view (right) of conductive epoxy attachment to tantalum disc for direct attachment to alligator clip during anodization. 204

Figure 8.13. Horizontal anodization set up with conductive epoxy attachment to tantalum disc for direct attachment to alligator clip during anodization. 204

Figure 8.14. Current vs time anodization plot for oven cleaned tantalum disc A coated with ~ 200 nm tantalum and ~ 93 nm aluminum at 4 V, using the horizontal method with the conductive epoxy attachment. 205

Figure 8.15. Current vs time anodization plot for oven cleaned tantalum disc B coated with ~ 200 nm tantalum and ~ 93 nm aluminum at 4 V, using the horizontal method with the conductive epoxy attachment. 206

Figure 8.16. Current vs time anodization plot for oven cleaned tantalum disc C coated with ~ 200 nm tantalum and ~ 93 nm aluminum at 4 V, using the horizontal method with the conductive epoxy attachment. 206

Figure 8.17. Tantalum disc A coated with ~ 200 nm of tantalum then ~ 93 nm of aluminum and anodized at 4 V using the horizontal method with the conductive epoxy attachment after protein analysis. Each circle exposed to 20 μL of 1 mg/mL prothrombin for 20 minutes. Then one circle

exposed to 20 μL of 0.5 mg/mL anti-prothrombin for 20 minutes (middle left circle), one circle exposed to 20 μL of 0.05 mg/mL anti-prothrombin for 20 minutes (middle right circle), one circle exposed to 20 μL of 0.005 mg/mL anti-prothrombin for 20 minutes (farthest right circle). The farthest left circle was not exposed to any anti-prothrombin and used as a control with prothrombin only. 208

Figure 8.18. Tantalum disc B coated with ~ 200 nm of tantalum then ~ 93 nm of aluminum and anodized at 4 V using the horizontal method with the conductive epoxy attachment after protein analysis. Each circle exposed to 20 μL of 1 mg/mL prothrombin for 20 minutes. Then one circle exposed to 20 μL of 0.5 mg/mL anti-prothrombin for 20 minutes (middle left circle), one circle exposed to 20 μL of 0.05 mg/mL anti-prothrombin for 20 minutes (middle right circle), one circle exposed to 20 μL of 0.005 mg/mL anti-prothrombin for 20 minutes (farthest right circle). The farthest left circle was not exposed to any anti-prothrombin and used as a control with prothrombin only. 209

Figure 8.19. Tantalum disc C coated with ~ 200 nm of tantalum then ~ 93 nm of aluminum and anodized at 4 V using the horizontal method with the conductive epoxy attachment after protein analysis. Each circle exposed to 20 μL of 1 mg/mL prothrombin for 20 minutes. Then one circle exposed to 20 μL of 0.5 mg/mL anti-prothrombin for 20 minutes (middle left circle), one circle exposed to 20 μL of 0.05 mg/mL anti-prothrombin for 20 minutes (middle right circle), one circle exposed to 20 μL of 0.005 mg/mL anti-prothrombin for 20 minutes (farthest right circle). The farthest left circle was not exposed to any anti-prothrombin and used as a control with prothrombin only. 210

Figure 8.20. Silicon wafer coated with ~ 200 nm of tantalum then ~ 93 nm of aluminum and anodized at 4 V after protein analysis. The farthest left circle (1) was exposed to no protein (blank). The other six circles (2 – 7) exposed to 20 μL of 1 mg/mL prothrombin for 20 minutes. Circle 2 exposed to prothrombin only. Then circles 3 – 7 exposed to 20 μL of varying anti-prothrombin concentrations for 20 minutes: 0.5 mg/mL anti-prothrombin (3), 0.05 mg/mL anti-prothrombin (4), 0.005 mg/mL anti-prothrombin (5), 5×10^{-4} mg/mL anti-prothrombin (6), 5×10^{-5} mg/mL anti-prothrombin (7)..... 212

Figure 8.21. Silicon wafer coated with ~ 200 nm of tantalum then ~ 93 nm of aluminum and anodized at 4 V after protein analysis. The farthest left circle (1) was exposed to no protein

(blank). The other six circles (2 – 7) exposed to 20 µL of 1 mg/mL prothrombin for 20 minutes. Circle 2 exposed to prothrombin only. Then circles 3 – 7 exposed to 20 µL of varying anti-prothrombin concentrations for 20 minutes: 0.5 mg/mL anti-prothrombin (3), 0.05 mg/mL anti-prothrombin (4), 0.005 mg/mL anti-prothrombin (5), 5×10^{-4} mg/mL anti-prothrombin (6), 5×10^{-5} mg/mL anti-prothrombin (7)..... 213

Figure 8.22. Silicon wafer coated with ~ 200 nm of tantalum then ~ 93 nm of aluminum and anodized at 4 V after protein analysis. The farthest left circle (1) was exposed to no protein (blank). The other six circles (2 – 7) exposed to 20 µL of 1 mg/mL prothrombin for 20 minutes. Circle 2 exposed to prothrombin only. Then circles 3 – 7 exposed to 20 µL of varying anti-prothrombin concentrations for 20 minutes: 0.5 mg/mL anti-prothrombin (3), 0.05 mg/mL anti-prothrombin (4), 0.005 mg/mL anti-prothrombin (5), 5×10^{-4} mg/mL anti-prothrombin (6), 5×10^{-5} mg/mL anti-prothrombin (7)..... 214

Figure 8.23. Experimental set up for 500 mL volume anti-prothrombin sensitivity experiments. Set up consists of a 1 L beaker and a motorized impeller attached to a Tech II Railmaster 2400. Tantalum disc or silicon wafer that was previously exposed to 1 mg/mL of prothrombin is placed in the bottom of the beaker. 217

Figure 8.24. Tantalum disc (D) exposed to 20 µL of 1 mg/mL prothrombin in each of the four circles (left) compared to tantalum disc (F) that was exposed to 20 µL of 1 mg/mL prothrombin in each of the four circles then subsequently exposed to a 500 mL solution of 0.005 mg/mL anti-prothrombin with continuous stirring at ~ 195 RPM for 20 minutes (right). 218

Figure 8.25. Tantalum disc G after protein work. Left circle exposed to no protein and used as a blank control, middle circle exposed to 20 µL of 1 mg/mL prothrombin for 20 minutes, right circle exposed to 20 µL of 0.25 mg/mL anti-prothrombin for 20 minutes (no previous prothrombin exposure in right circle). 219

Figure 8.26. Tantalum disc (D) exposed to 20 µL of 1 mg/mL prothrombin in each of the four circles (left) compared to tantalum disc (F) that was exposed to 20 µL of 1 mg/mL prothrombin in each of the four circles then subsequently exposed to a 500 mL solution of 0.005 mg/mL anti-prothrombin with continuous stirring at ~ 195 RPM for 40 minutes (right). 220

Figure 8.27. Tantalum disc G after protein work. Left circle exposed to no protein and used as a blank control, middle circle exposed to 20 µL of 1 mg/mL prothrombin for 20 minutes then 20 µL of 0.5 mg/mL anti-prothrombin for 20 minutes, right circle exposed to 20 µL of 0.25 mg/mL anti-prothrombin for 20 minutes (no previous prothrombin exposure in right circle). 221

Figure 8.28. Tantalum disc G after protein work. Left circle exposed to no protein and used as a blank control, middle circle exposed to 20 µL of 1 mg/mL prothrombin for 20 minutes then 20 µL of 0.5 mg/mL anti-prothrombin for 20 minutes then 20 µL of 1 mg/mL secondary anti-body for 20 minutes, right circle exposed to 20 µL of 0.25 mg/mL anti-prothrombin for 20 minutes then 20 µL of 1 mg/mL secondary anti-body for 20 minutes (no previous prothrombin exposure in right circle)..... 222

Figure 8.29. Silicon wafer slide (~ 1.3 cm by ~ 6.2 cm) coated with ~ 200 nm of tantalum and ~ 106 nm of aluminum then anodized at 4 V prior to protein work. 225

Figure 8.30. Silicon wafer slide (~ 1.3 cm by ~ 6.2 cm) coated with ~ 200 nm of tantalum and ~ 106 nm of aluminum then anodized at 4 V after the entire surface was coated with 532 µL of 1 mg/mL prothrombin for 20 minutes. 225

Figure 8.31. Silicon wafer slide (~ 1.3 cm by ~ 6.2 cm) coated with ~ 200 nm of tantalum and ~ 106 nm of aluminum then anodized at 4 V after the entire surface was coated with 532 µL of 1 mg/mL prothrombin for 20 minutes. The hydrophobic circle was subsequently exposed to 20 µL of 0.5 mg/mL anti-prothrombin for 20 minutes..... 226

Figure 8.32. Silicon wafer slide (~ 1.3 cm by ~ 6.2 cm) coated with ~ 200 nm of tantalum and ~ 106 nm of aluminum then anodized at 4 V after the entire surface was coated with 532 µL of 1 mg/mL prothrombin for 20 minutes. The hydrophobic circle was subsequently exposed to 20 µL of 0.5 mg/mL anti-prothrombin for 20 minutes. The entire wafer was then exposed to 500 mL of 0.005 mg/mL anti-prothrombin with continuous stirring at ~ 195 RPM for 20 minutes. 226

Figure 8.33. Images in Figure 8.29, 8.30, and 8.32 cropped and lined up to better visualize the colour shifts. Silicon wafer slides (~ 1.3 cm by ~ 6.2 cm) coated with ~ 200 nm of tantalum and ~ 106 nm of aluminum then anodized at 4 V with no exposure to protein (top), after exposure of entire slide to 532 µL of 1 mg/mL prothrombin for 20 minutes (middle), after subsequent

exposure of entire slide to 500 mL of 0.005 mg/mL anti-prothrombin for 20 minutes with continuous stirring at ~ 195 RPM (bottom). 227

Figure 8.34. Silicon wafer (replicate 1) coated with ~ 200 nm of tantalum then ~ 106 nm of aluminum and anodized at 4 V after protein analysis. The farthest left circle (1) was exposed to no protein (blank). The other six circles (2 – 7) exposed to 20 µL of 1 mg/mL prothrombin for 20 minutes. Circle 2 exposed to prothrombin only. Then circles 3 – 7 exposed to 20 µL of varying anti-prothrombin concentrations for 20 minutes: 0.5 mg/mL anti-prothrombin (3), 0.05 mg/mL anti-prothrombin (4), 0.005 mg/mL anti-prothrombin (5), 5×10^{-4} mg/mL anti-prothrombin (6), 5×10^{-5} mg/mL anti-prothrombin (7). 230

Figure 8.35. Silicon wafer (replicate 2) coated with ~ 200 nm of tantalum then ~ 106 nm of aluminum and anodized at 4 V after protein analysis. The farthest left circle (1) was exposed to no protein (blank). The other six circles (2 – 7) exposed to 20 µL of 1 mg/mL prothrombin for 20 minutes. Circle 2 exposed to prothrombin only. Then circles 3 – 7 exposed to 20 µL of varying anti-prothrombin concentrations for 20 minutes: 0.5 mg/mL anti-prothrombin (3), 0.05 mg/mL anti-prothrombin (4), 0.005 mg/mL anti-prothrombin (5), 5×10^{-4} mg/mL anti-prothrombin (6), 5×10^{-5} mg/mL anti-prothrombin (7). 231

Figure 8.36. Silicon wafer (replicate 3) coated with ~ 200 nm of tantalum then ~ 106 nm of aluminum and anodized at 4 V after protein analysis. The farthest left circle (1) was exposed to no protein (blank). The other six circles (2 – 7) exposed to 20 µL of 1 mg/mL prothrombin for 20 minutes. Circle 2 exposed to prothrombin only. Then circles 3 – 7 exposed to 20 µL of varying anti-prothrombin concentrations for 20 minutes: 0.5 mg/mL anti-prothrombin (3), 0.05 mg/mL anti-prothrombin (4), 0.005 mg/mL anti-prothrombin (5), 5×10^{-4} mg/mL anti-prothrombin (6), 5×10^{-5} mg/mL anti-prothrombin (7). 232

Figure 8.37. Silicon wafer slide (replicate 1) (~ 1.3 cm by ~ 6.2 cm) coated with ~ 200 nm of tantalum and ~ 106 nm of aluminum then anodized at 4 V after the entire surface was coated with 532 µL of 1 mg/mL prothrombin for 20 minutes. The hydrophobic circle was subsequently exposed to 20 µL of 0.5 mg/mL anti-prothrombin for 20 minutes. 236

Figure 8.38. Silicon wafer slide (replicate 2) (~ 1.3 cm by ~ 6.2 cm) coated with ~ 200 nm of tantalum and ~ 106 nm of aluminum then anodized at 4 V after the entire surface was coated

with 532 µL of 1 mg/mL prothrombin for 20 minutes. The hydrophobic circle was subsequently exposed to 20 µL of 0.5 mg/mL anti-prothrombin for 20 minutes. 237

Figure 8.39. Silicon wafer slide (replicate 3) (~ 1.3 cm by ~ 6.2 cm) coated with ~ 200 nm of tantalum and ~ 106 nm of aluminum then anodized at 4 V after the entire surface was coated with 532 µL of 1 mg/mL prothrombin for 20 minutes. The hydrophobic circle was subsequently exposed to 20 µL of 0.5 mg/mL anti-prothrombin for 20 minutes. 237

Figure 8.40. Silicon wafer slide (replicate 1) (~ 1.3 cm by ~ 6.2 cm) coated with ~ 200 nm of tantalum and ~ 106 nm of aluminum then anodized at 4 V with no exposure to protein (top), after exposure of entire slide to 532 µL of 1 mg/mL prothrombin for 20 minutes (middle), after subsequent exposure of entire slide to 500 mL of 5×10^{-4} mg/mL anti-prothrombin for 20 minutes with continuous stirring at ~ 195 RPM (bottom). 238

Figure 8.41. Silicon wafer slide (replicate 2) (~ 1.3 cm by ~ 6.2 cm) coated with ~ 200 nm of tantalum and ~ 106 nm of aluminum then anodized at 4 V with no exposure to protein (top), after exposure of entire slide to 532 µL of 1 mg/mL prothrombin for 20 minutes (middle), after subsequent exposure of entire slide to 500 mL of 5×10^{-4} mg/mL anti-prothrombin for 20 minutes with continuous stirring at ~ 195 RPM (bottom). 238

Figure 8.42. Silicon wafer slide (replicate 3) (~ 1.3 cm by ~ 6.2 cm) coated with ~ 200 nm of tantalum and ~ 106 nm of aluminum then anodized at 4 V with no exposure to protein (top), after exposure of entire slide to 532 µL of 1 mg/mL prothrombin for 20 minutes (middle), after subsequent exposure of entire slide to 500 mL of 5×10^{-4} mg/mL anti-prothrombin for 20 minutes with continuous stirring at ~ 195 RPM (bottom). 239

Figure 8.43. Silicon wafer slide (~ 1.3 cm by ~ 6.2 cm) coated with ~ 200 nm of tantalum and ~ 106 nm of aluminum then anodized at 4 V after the entire surface was coated with 532 µL of 1 mg/mL prothrombin for 20 minutes. The hydrophobic circle was subsequently exposed to 20 µL of 0.5 mg/mL anti-prothrombin for 20 minutes. The entire wafer was then exposed to 500 mL of 5×10^{-4} mg/mL anti-prothrombin with continuous stirring at ~ 195 RPM for 5 minutes. 240

Figure 8.44. Silicon wafer slide (~ 1.3 cm by ~ 6.2 cm) coated with ~ 200 nm of tantalum and ~ 106 nm of aluminum then anodized at 4 V after the entire surface was coated with 532 µL of 1 mg/mL prothrombin for 20 minutes. The hydrophobic circle was subsequently exposed to 20 µL

of 0.5 mg/mL anti-prothrombin for 20 minutes. The entire wafer was then exposed to 500 mL of 5×10^{-4} mg/mL anti-prothrombin with continuous stirring at ~ 195 RPM for 10 minutes. 240

Figure 8.45. Silicon wafer slide (replicate 1) (~ 1.3 cm by ~ 6.2 cm) coated with ~ 200 nm of tantalum and ~ 106 nm of aluminum then anodized at 4 V after the entire surface was coated with 532 µL of 1 mg/mL prothrombin for 20 minutes. The hydrophobic circle was subsequently exposed to 20 µL of 0.5 mg/mL anti-prothrombin for 20 minutes. The entire slide was then exposed to 500 mL of 5×10^{-4} mg/mL anti-prothrombin with continuous stirring at ~ 195 RPM for 20 minutes. The entire slide was then exposed to 450 mL of 0.005 mg/mL anti-prothrombin with continuous stirring at ~ 195 RPM for 5 minutes. 241

Figure 8.46. Silicon wafer slide (replicate 2) (~ 1.3 cm by ~ 6.2 cm) coated with ~ 200 nm of tantalum and ~ 106 nm of aluminum then anodized at 4 V after the entire surface was coated with 532 µL of 1 mg/mL prothrombin for 20 minutes. The hydrophobic circle was subsequently exposed to 20 µL of 0.5 mg/mL anti-prothrombin for 20 minutes. The entire slide was then exposed to 500 mL of 5×10^{-4} mg/mL anti-prothrombin with continuous stirring at for 20 minutes. The entire slide was then exposed to 450 mL of 0.005 mg/mL anti-prothrombin with continuous stirring for 5 minutes. 242

Figure 8.47. Silicon wafer slide (replicate 3) (~ 1.3 cm by ~ 6.2 cm) coated with ~ 200 nm of tantalum and ~ 106 nm of aluminum then anodized at 4 V after the entire surface was coated with 532 µL of 1 mg/mL prothrombin for 20 minutes. The hydrophobic circle was subsequently exposed to 20 µL of 0.5 mg/mL anti-prothrombin for 20 minutes. The entire slide was then exposed to 500 mL of 5×10^{-4} mg/mL anti-prothrombin with continuous stirring for 20 minutes. The entire slide was then exposed to 450 mL of 0.005 mg/mL anti-prothrombin with continuous stirring for 5 minutes. 242

Figure 8.48. Silicon wafer slide (replicate 1) (~ 1.3 cm by ~ 6.2 cm) coated with ~ 200 nm of tantalum and ~ 106 nm of aluminum then anodized at 4 V after the entire surface was coated with 532 µL of 1 mg/mL prothrombin for 20 minutes. The hydrophobic circle was subsequently exposed to 20 µL of 0.5 mg/mL anti-prothrombin for 20 minutes. The entire slide was then exposed to 500 mL of 5×10^{-4} mg/mL anti-prothrombin with continuous stirring for 20 minutes. The entire slide was then exposed to 450 mL of 0.005 mg/mL anti-prothrombin with continuous stirring for 10 minutes. 243

Figure 8.49. Silicon wafer slide (replicate 2) (~ 1.3 cm by ~ 6.2 cm) coated with ~ 200 nm of tantalum and ~ 106 nm of aluminum then anodized at 4 V after the entire surface was coated with 532 µL of 1 mg/mL prothrombin for 20 minutes. The hydrophobic circle was subsequently exposed to 20 µL of 0.5 mg/mL anti-prothrombin for 20 minutes. The entire slide was then exposed to 500 mL of 5×10^{-4} mg/mL anti-prothrombin with continuous stirring for 20 minutes. The entire slide was then exposed to 450 mL of 0.005 mg/mL anti-prothrombin with continuous stirring for 10 minutes..... 243

Figure 8.50. Silicon wafer slide (replicate 3) (~ 1.3 cm by ~ 6.2 cm) coated with ~ 200 nm of tantalum and ~ 106 nm of aluminum then anodized at 4 V after the entire surface was coated with 532 µL of 1 mg/mL prothrombin for 20 minutes. The hydrophobic circle was subsequently exposed to 20 µL of 0.5 mg/mL anti-prothrombin for 20 minutes. The entire slide was then exposed to 500 mL of 5×10^{-4} mg/mL anti-prothrombin with continuous stirring for 20 minutes. The entire slide was then exposed to 450 mL of 0.005 mg/mL anti-prothrombin with continuous stirring for 10 minutes..... 244

Figure 8.51. Silicon wafer slide (replicate 1) (~ 1.3 cm by ~ 6.2 cm) coated with ~ 200 nm of tantalum and ~ 106 nm of aluminum then anodized at 4 V prior to protein work (top), after the entire surface was coated with 532 µL of 1 mg/mL prothrombin for 20 minutes (middle), and after the entire slide was exposed to 500 mL of 5×10^{-4} mg/mL anti-prothrombin with continuous stirring at ~ 195 RPM for 20 minutes and 450 mL of 0.005 mg/mL anti-prothrombin with continuous stirring at ~195 RPM for 10 minutes (bottom). 245

Figure 8.52. Silicon wafer slide (replicate 2) (~ 1.3 cm by ~ 6.2 cm) coated with ~ 200 nm of tantalum and ~ 106 nm of aluminum then anodized at 4 V prior to protein work (top), after the entire surface was coated with 532 µL of 1 mg/mL prothrombin for 20 minutes (middle), and after the entire slide was exposed to 500 mL of 5×10^{-4} mg/mL anti-prothrombin with continuous stirring at ~ 195 RPM for 20 minutes and 450 mL of 0.005 mg/mL anti-prothrombin with continuous stirring at ~ 195 RPM for 10 minutes (bottom). 245

Figure 8.53. Silicon wafer slide (replicate 3) (~ 1.3 cm by ~ 6.2 cm) coated with ~ 200 nm of tantalum and ~ 106 nm of aluminum then anodized at 4 V prior to protein work (top), after the entire surface was coated with 532 µL of 1 mg/mL prothrombin for 20 minutes (middle), and after the entire slide was exposed to 500 mL of 5×10^{-4} mg/mL anti-prothrombin with

continuous stirring at ~ 195 RPM for 20 minutes and 450 mL of 0.005 mg/mL anti-prothrombin with continuous stirring at ~ 195 RPM for 10 minutes (bottom). 246

Figure 8.54. Silicon wafer slide (replicate 1) (~ 1.3 cm by ~ 6.2 cm) coated with ~ 200 nm of tantalum and ~ 106 nm of aluminum then anodized at 4 V with no exposure to protein (top), after exposure of entire slide to 532 µL of 1 mg/mL prothrombin for 20 minutes (second from top), after subsequent exposure of hydrophobic circle to 20 µL of 0.5 mg/mL anti-prothrombin for 20 minutes (second from bottom), after subsequent exposure of entire slide to 500 mL of 0.005 mg/mL anti-prothrombin for 20 minutes with continuous stirring at ~ 195 RPM (bottom). 251

Figure 8.55. Silicon wafer slide (replicate 2) (~ 1.3 cm by ~ 6.2 cm) coated with ~ 200 nm of tantalum and ~ 106 nm of aluminum then anodized at 4 V with no exposure to protein (top), after exposure of entire slide to 532 µL of 1 mg/mL prothrombin for 20 minutes (second from top), after subsequent exposure of hydrophobic circle to 20 µL of 0.5 mg/mL anti-prothrombin for 20 minutes (second from bottom), after subsequent exposure of entire slide to 500 mL of 0.005 mg/mL anti-prothrombin for 20 minutes with continuous stirring at ~ 195 RPM (bottom). 251

Figure 8.56. Silicon wafer slide (replicate 3) (~ 1.3 cm by ~ 6.2 cm) coated with ~ 200 nm of tantalum and ~ 106 nm of aluminum then anodized at 4 V with no exposure to protein (top), after exposure of entire slide to 532 µL of 1 mg/mL prothrombin for 20 minutes (second from top), after subsequent exposure of hydrophobic circle to 20 µL of 0.5 mg/mL anti-prothrombin for 20 minutes (second from bottom), after subsequent exposure of entire slide to 500 mL of 0.005 mg/mL anti-prothrombin for 20 minutes with continuous stirring at ~ 195 RPM (bottom). 252

Figure 8.57. Silicon wafer slide (replicate 1) (~ 1.3 cm by ~ 6.2 cm) coated with ~ 200 nm of tantalum and ~ 106 nm of aluminum then anodized at 4 V with no exposure to protein (top), after exposure of entire slide to 532 µL of 1 mg/mL prothrombin for 20 minutes (second from top), after subsequent exposure of hydrophobic circle to 20 µL of 0.5 mg/mL anti-prothrombin for 20 minutes (second from bottom), after subsequent exposure of entire slide to 500 mL of 0.0025 mg/mL anti-prothrombin for 20 minutes with continuous stirring at ~ 195 RPM (bottom). 252

Figure 8.58. Silicon wafer slide (replicate 2) (~ 1.3 cm by ~ 6.2 cm) coated with ~ 200 nm of tantalum and ~ 106 nm of aluminum then anodized at 4 V with no exposure to protein (top), after exposure of entire slide to 532 µL of 1 mg/mL prothrombin for 20 minutes (second from top),

after subsequent exposure of hydrophobic circle to 20 μL of 0.5 mg/mL anti-prothrombin for 20 minutes (second from bottom), after subsequent exposure of entire slide to 500 mL of 0.0025 mg/mL anti-prothrombin for 20 minutes with continuous stirring at ~ 195 RPM (bottom). 253

Figure 8.59. Silicon wafer slide (replicate 3) (~ 1.3 cm by ~ 6.2 cm) coated with ~ 200 nm of tantalum and ~ 106 nm of aluminum then anodized at 4 V with no exposure to protein (top), after exposure of entire slide to 532 μL of 1 mg/mL prothrombin for 20 minutes (second from top), after subsequent exposure of hydrophobic circle to 20 μL of 0.5 mg/mL anti-prothrombin for 20 minutes (second from bottom), after subsequent exposure of entire slide to 500 mL of 0.0025 mg/mL anti-prothrombin for 20 minutes with continuous stirring at ~ 195 RPM (bottom). 253

Figure 8.60. Silicon wafer slide (replicate 1) (~ 1.3 cm by ~ 6.2 cm) coated with ~ 200 nm of tantalum and ~ 107 nm of aluminum then anodized at 4 V with no exposure to protein (top), after exposure of entire slide to 532 μL of 1 mg/mL prothrombin for 20 minutes (second from top), after subsequent exposure of hydrophobic circle to 20 μL of 0.5 mg/mL anti-prothrombin for 20 minutes (second from bottom), after subsequent exposure of entire slide to 500 mL of 5×10^{-4} mg/mL anti-prothrombin for 20 minutes with continuous stirring at ~ 195 RPM (bottom). 254

Figure 8.61. Silicon wafer slide (replicate 2) (~ 1.3 cm by ~ 6.2 cm) coated with ~ 200 nm of tantalum and ~ 107 nm of aluminum then anodized at 4 V with no exposure to protein (top), after exposure of entire slide to 532 μL of 1 mg/mL prothrombin for 20 minutes (second from top), after subsequent exposure of hydrophobic circle to 20 μL of 0.5 mg/mL anti-prothrombin for 20 minutes (second from bottom), after subsequent exposure of entire slide to 500 mL of 5×10^{-4} mg/mL anti-prothrombin for 20 minutes with continuous stirring at ~ 195 RPM (bottom). 254

Figure 8.62. Silicon wafer slide (replicate 3) (~ 1.3 cm by ~ 6.2 cm) coated with ~ 200 nm of tantalum and ~ 107 nm of aluminum then anodized at 4 V with no exposure to protein (top), after exposure of entire slide to 532 μL of 1 mg/mL prothrombin for 20 minutes (second from top), after subsequent exposure of hydrophobic circle to 20 μL of 0.5 mg/mL anti-prothrombin for 20 minutes (second from bottom), after subsequent exposure of entire slide to 500 mL of 5×10^{-4} mg/mL anti-prothrombin for 20 minutes with continuous stirring at ~ 195 RPM (bottom). 255

Figure 8.63. Silicon wafer slide (replicate 1) (~ 1.3 cm by ~ 6.2 cm) coated with ~ 200 nm of tantalum and ~ 105 nm of aluminum then anodized at 4 V with no exposure to protein (top), after

exposure of entire slide to 532 µL of 1 mg/mL prothrombin for 20 minutes (second from top), after subsequent exposure of hydrophobic circle to 20 µL of 0.5 mg/mL anti-prothrombin for 20 minutes (second from bottom), after subsequent exposure of entire slide to 500 mL of 0.005 mg/mL anti-prothrombin for 20 minutes with continuous stirring at ~ 195 RPM (bottom). 261

Figure 8.64. Silicon wafer slide (replicate 2) (~ 1.3 cm by ~ 6.2 cm) coated with ~ 200 nm of tantalum and ~ 105 nm of aluminum then anodized at 4 V with no exposure to protein (top), after exposure of entire slide to 532 µL of 1 mg/mL prothrombin for 20 minutes (second from top), after subsequent exposure of hydrophobic circle to 20 µL of 0.5 mg/mL anti-prothrombin for 20 minutes (second from bottom), after subsequent exposure of entire slide to 500 mL of 0.005 mg/mL anti-prothrombin for 20 minutes with continuous stirring at ~ 195 RPM (bottom). 261

Figure 8.65. Silicon wafer slide (replicate 3) (~ 1.3 cm by ~ 6.2 cm) coated with ~ 200 nm of tantalum and ~ 105 nm of aluminum then anodized at 4 V with no exposure to protein (top), after exposure of entire slide to 532 µL of 1 mg/mL prothrombin for 20 minutes (second from top), after subsequent exposure of hydrophobic circle to 20 µL of 0.5 mg/mL anti-prothrombin for 20 minutes (second from bottom), after subsequent exposure of entire slide to 500 mL of 0.005 mg/mL anti-prothrombin for 20 minutes with continuous stirring at ~ 195 RPM (bottom). 262

Figure 8.66. Silicon wafer rectangles (three replicates – ~ 1 cm by ~ 1.2 cm each) coated with ~ 200 nm of tantalum and ~ 108 nm of aluminum then anodized at 4 V with no exposure to protein (top), after exposure of each rectangle to 35 µL of 1 mg/mL prothrombin for 20 minutes (middle), after subsequent exposure of each rectangle to 500 mL of 0.005 mg/mL anti-prothrombin for 20 minutes with no stirring (bottom)..... 266

Figure 8.67. Silicon wafer rectangles (three replicates – ~ 1 cm by ~ 1.2 cm each) coated with ~ 200 nm of tantalum and ~ 108 nm of aluminum then anodized at 4 V with no exposure to protein (top), after exposure of each rectangle to 35 µL of 1 mg/mL prothrombin for 20 minutes (middle), after subsequent exposure of each rectangle to 500 mL of 0.005 mg/mL anti-prothrombin for 20 minutes with continuous stirring at ~ 195 RPM (bottom). 266

Figure 8.68. Silicon wafer rectangles (three replicates – ~ 1 cm by ~ 1.2 cm each) coated with ~ 200 nm of tantalum and ~ 108 nm of aluminum then anodized at 4 V with no exposure to protein (top), after exposure of each rectangle to 35 µL of 1 mg/mL prothrombin for 20 minutes

(middle), after subsequent exposure of each rectangle to 500 mL of 0.0025 mg/mL anti-prothrombin for 20 minutes with no stirring (bottom)..... 268

Figure 8.69. Silicon wafer rectangles (three replicates – ~ 1 cm by ~ 1.2 cm each) coated with ~ 200 nm of tantalum and ~ 108 nm of aluminum then anodized at 4 V with no exposure to protein (top), after exposure of each rectangle to 35 µL of 1 mg/mL prothrombin for 20 minutes (middle), after subsequent exposure of each rectangle to 500 mL of 0.0025 mg/mL anti-prothrombin for 20 minutes with continuous stirring at ~ 195 RPM (bottom). 268

Figure 8.70. Silicon wafer rectangles (three replicates – ~ 1 cm by ~ 1.2 cm each) coated with ~ 200 nm of tantalum and ~ 108 nm of aluminum then anodized at 4 V with no exposure to protein (row 1), after exposure of each rectangle to 35 µL of 1 mg/mL prothrombin for 20 minutes (row 2), after subsequent exposure of each rectangle to 250 mL of 0.0025 mg/mL anti-prothrombin for 5, 10, 20 and 40 minutes with no stirring (rows 3, 4, 5, 6). 274

Figure 8.71. Silicon wafer rectangles (three replicates – ~ 1 cm by ~ 1.2 cm each) coated with ~ 200 nm of tantalum and ~ 111 nm of aluminum then anodized at 4 V with no exposure to protein (row 1), after exposure of each rectangle to 35 µL of 1 mg/mL prothrombin for 20 minutes (row 2), after subsequent exposure of each rectangle to 250 mL of 0.0025 mg/mL anti-prothrombin for 5, 10, 20 and 40 minutes with continuous stirring at the regular impeller speed of ~ 195 RPM (rows 3, 4, 5, 6). 275

Figure 8.72. Silicon wafer rectangles (three replicates – ~ 1 cm by ~ 1.2 cm each) coated with ~ 200 nm of tantalum and ~ 108 nm of aluminum then anodized at 4 V with no exposure to protein (row 1), after exposure of each rectangle to 40 µL of 1 mg/mL prothrombin for 20 minutes (row 2), after subsequent exposure of each rectangle to 100 mL of 0.005 mg/mL anti-prothrombin for 5, 10, 20 and 40 minutes with no stirring (rows 3, 4, 5, 6). 282

Figure 8.73. Silicon wafer rectangles (three replicates – ~ 1 cm by ~ 1.2 cm each) coated with ~ 200 nm of tantalum and ~ 108 nm of aluminum then anodized at 4 V with no exposure to protein (row 1), after exposure of each rectangle to 35 µL of 1 mg/mL prothrombin for 20 minutes (row 2), after subsequent exposure of each rectangle to 100 mL of 0.0025 mg/mL anti-prothrombin for 5, 10, 20 and 40 minutes with no stirring (rows 3, 4, 5, 6). 282

Figure 8.74. Silicon wafer rectangles (three replicates – ~ 1 cm by ~ 1.2 cm each) coated with ~ 200 nm of tantalum and ~ 107 nm of aluminum then anodized at 4 V with no exposure to protein (row 1), after exposure of each rectangle to 35 µL of 1 mg/mL prothrombin for 20 minutes (row 2), after subsequent exposure of each rectangle to 100 mL of 0.00125 mg/mL anti-prothrombin for 5, 10, 20 and 40 minutes with no stirring (rows 3, 4, 5, 6). 283

Figure 8.75. Silicon wafer rectangles (three replicates – ~ 1 cm by ~ 1.2 cm each) coated with ~ 200 nm of tantalum and ~ 107 nm of aluminum then anodized at 4 V with no exposure to protein (row 1), after exposure of each rectangle to 35 µL of 1 mg/mL prothrombin for 20 minutes (row 2), after subsequent exposure of each rectangle to 500 mL of 0.005 mg/mL anti-prothrombin for 5, 10, 20 and 40 minutes with no stirring (rows 3, 4, 5, 6). 283

Figure 8.76. Silicon wafer rectangles (three replicates – ~ 1 cm by ~ 1.2 cm each) coated with ~ 200 nm of tantalum and ~ 108 nm of aluminum then anodized at 4 V with no exposure to protein (row 1), after exposure of each rectangle to 35 µL of 1 mg/mL prothrombin for 20 minutes (row 2), after subsequent exposure of each rectangle to 500 mL of 0.0025 mg/mL anti-prothrombin for 5, 10, 20 and 40 minutes with no stirring (rows 3, 4, 5, 6). 284

Figure 8.77. Silicon wafer rectangles (three replicates – ~ 1 cm by ~ 1.2 cm each) coated with ~ 200 nm of tantalum and ~ 107 nm of aluminum then anodized at 4 V with no exposure to protein (row 1), after exposure of each rectangle to 35 µL of 1 mg/mL prothrombin for 20 minutes (row 2), after subsequent exposure of each rectangle to 500 mL of 0.00125 mg/mL anti-prothrombin for 5, 10, 20 and 40 minutes with no stirring (rows 3, 4, 5, 6). 284

Figure 8.78. Silicon wafer rectangles (three replicates – ~ 1 cm by ~ 1.2 cm each) coated with ~ 200 nm of tantalum and ~ 107 nm of aluminum then anodized at 4 V with no exposure to protein (row 1), after exposure of each rectangle to 35 µL of 1 mg/mL prothrombin for 20 minutes (row 2), after subsequent exposure of each rectangle to 100 mL of 0.005 mg/mL anti-prothrombin for 5, 10, 20 and 40 minutes with continuous stirring at the regular impeller speed of 195 RPM (rows 3, 4, 5, 6). 290

Figure 8.79. Silicon wafer rectangles (three replicates – ~ 1 cm by ~ 1.2 cm each) coated with ~ 200 nm of tantalum and ~ 108 nm of aluminum then anodized at 4 V with no exposure to protein (row 1), after exposure of each rectangle to 35 µL of 1 mg/mL prothrombin for 20 minutes (row

2), after subsequent exposure of each rectangle to 100 mL of 0.0025 mg/mL anti-prothrombin for 5, 10, 20 and 40 minutes with continuous stirring at the regular impeller speed of 195 RPM (rows 3, 4, 5, 6). 291

Figure 8.80. Silicon wafer rectangles (three replicates – ~ 1 cm by ~ 1.2 cm each) coated with ~ 200 nm of tantalum and ~ 108 nm of aluminum then anodized at 4 V with no exposure to protein (row 1), after exposure of each rectangle to 40 μL of 1 mg/mL prothrombin for 20 minutes (row 2), after subsequent exposure of each rectangle to 100 mL of 0.00125 mg/mL anti-prothrombin for 5, 10, 20 and 40 minutes with continuous stirring at the regular impeller speed of 195 RPM (rows 3, 4, 5, 6). 291

Figure 8.81. Silicon wafer rectangles (three replicates – ~ 1 cm by ~ 1.2 cm each) coated with ~ 200 nm of tantalum and ~ 111 nm of aluminum then anodized at 4 V with no exposure to protein (row 1), after exposure of each rectangle to 35 μL of 1 mg/mL prothrombin for 20 minutes (row 2), after subsequent exposure of each rectangle to 500 mL of 0.005 mg/mL anti-prothrombin for 5, 10, 20 and 40 minutes with continuous stirring at the regular impeller speed of 195 RPM (rows 3, 4, 5, 6). 292

Figure 8.82. Silicon wafer rectangles (three replicates – ~ 1 cm by ~ 1.2 cm each) coated with ~ 200 nm of tantalum and ~ 109 nm of aluminum then anodized at 4 V with no exposure to protein (row 1), after exposure of each rectangle to 35 μL of 1 mg/mL prothrombin for 20 minutes (row 2), after subsequent exposure of each rectangle to 500 mL of 0.0025 mg/mL anti-prothrombin for 5, 10, 20 and 40 minutes with continuous stirring at the regular impeller speed of 195 RPM (rows 3, 4, 5, 6). 292

Figure 8.83. Silicon wafer rectangles (three replicates – ~ 1 cm by ~ 1.2 cm each) coated with ~ 200 nm of tantalum and ~ 111 nm of aluminum then anodized at 4 V with no exposure to protein (row 1), after exposure of each rectangle to 40 μL of 1 mg/mL prothrombin for 20 minutes (row 2), after subsequent exposure of each rectangle to 500 mL of 0.00125 mg/mL anti-prothrombin for 5, 10, 20 and 40 minutes with continuous stirring at the regular impeller speed of 195 RPM (rows 3, 4, 5, 6). 293

Figure 8.84. Silicon wafer rectangles (three replicates – ~ 1 cm by ~ 1.2 cm each) coated with ~ 200 nm of tantalum and ~ 108 nm of aluminum then anodized at 4 V with no exposure to protein

(row 1), after exposure of each rectangle to 40 µL of 1 mg/mL prothrombin for 20 minutes (row 2), after subsequent exposure of each rectangle to 100 mL of 0.005 mg/mL anti-prothrombin for 5, 10, and 20 minutes with continuous stirring at an increased impeller speed of 360 RPM (rows 3, 4, 5). 299

Figure 8.85. Silicon wafer rectangles (three replicates – ~ 1 cm by ~ 1.2 cm each) coated with ~ 200 nm of tantalum and ~ 111 nm of aluminum then anodized at 4 V with no exposure to protein (row 1), after exposure of each rectangle to 35 µL of 1 mg/mL prothrombin for 20 minutes (row 2), after subsequent exposure of each rectangle to 100 mL of 0.0025 mg/mL anti-prothrombin for 5, 10, and 20 minutes with continuous stirring at an increased impeller speed of 360 RPM (rows 3, 4, 5). 299

Figure 8.86. Silicon wafer rectangles (three replicates – ~ 1 cm by ~ 1.2 cm each) coated with ~ 200 nm of tantalum and ~ 111 nm of aluminum then anodized at 4 V with no exposure to protein (row 1), after exposure of each rectangle to 40 µL of 1 mg/mL prothrombin for 20 minutes (row 2), after subsequent exposure of each rectangle to 100 mL of 0.00125 mg/mL anti-prothrombin for 5, 10, and 20 minutes with continuous stirring at an increased impeller speed of 360 RPM (rows 3, 4, 5). 300

Figure 8.87. Silicon wafer rectangles (three replicates – ~ 1 cm by ~ 1.2 cm each) coated with ~ 200 nm of tantalum and ~ 111 nm of aluminum then anodized at 4 V with no exposure to protein (row 1), after exposure of each rectangle to 40 µL of 1 mg/mL prothrombin for 20 minutes (row 2), after subsequent exposure of each rectangle to 500 mL of 0.005 mg/mL anti-prothrombin for 5, 10, and 20 minutes with continuous stirring at an increased impeller speed of 360 RPM (rows 3, 4, 5). 300

Figure 8.88. Silicon wafer rectangles (three replicates – ~ 1 cm by ~ 1.2 cm each) coated with ~ 200 nm of tantalum and ~ 109 nm of aluminum then anodized at 4 V with no exposure to protein (row 1), after exposure of each rectangle to 35 µL of 1 mg/mL prothrombin for 20 minutes (row 2), after subsequent exposure of each rectangle to 500 mL of 0.0025 mg/mL anti-prothrombin for 5, 10, and 20 minutes with continuous stirring at an increased impeller speed of 360 RPM (rows 3, 4, 5). 301

Figure 8.89. Silicon wafer rectangles (three replicates – ~ 1 cm by ~ 1.2 cm each) coated with ~ 200 nm of tantalum and ~ 111 nm of aluminum then anodized at 4 V with no exposure to protein (row 1), after exposure of each rectangle to 40 µL of 1 mg/mL prothrombin for 20 minutes (row 2), after subsequent exposure of each rectangle to 500 mL of 0.00125 mg/mL anti-prothrombin for 5, 10, and 20 minutes with continuous stirring at an increased impeller speed of 360 RPM (rows 3, 4, 5). 301

Figure 8.90. Silicon wafer rectangles (three replicates – ~ 1 cm by ~ 1.2 cm each) coated with ~ 200 nm of tantalum and ~ 106 nm of aluminum then anodized at 4 V with no exposure to protein (row 1), after exposure of each rectangle to 40 µL of 1 mg/mL prothrombin for 20 minutes (row 2), after subsequent exposure of each rectangle to 100 mL of 6.25×10^{-4} mg/mL anti-prothrombin for 5, 10, 20 and 40 minutes with no stirring (rows 3, 4, 5, 6). 307

Figure 8.91. Silicon wafer rectangles (three replicates – ~ 1 cm by ~ 1.2 cm each) coated with ~ 200 nm of tantalum and ~ 106 nm of aluminum then anodized at 4 V with no exposure to protein (row 1), after exposure of each rectangle to 40 µL of 1 mg/mL prothrombin for 20 minutes (row 2), after subsequent exposure of each rectangle to 100 mL of 6.25×10^{-4} mg/mL anti-prothrombin for 5, 10, 20 and 40 minutes with continuous stirring at the regular impeller speed of 195 RPM (rows 3, 4, 5, 6). 307

Figure 8.92. Silicon wafer rectangles (three replicates – ~ 1 cm by ~ 1.2 cm each) coated with ~ 200 nm of tantalum and ~ 106 nm of aluminum then anodized at 4 V with no exposure to protein (row 1), after exposure of each rectangle to 40 µL of 1 mg/mL prothrombin for 20 minutes (row 2), after subsequent exposure of each rectangle to 100 mL of 6.25×10^{-4} mg/mL anti-prothrombin for 5, 10, and 20 minutes with continuous stirring at an increased impeller speed of 360 RPM (rows 3, 4, 5)..... 308

Figure 8.93. Silicon wafer rectangles (three replicates – ~ 1 cm by ~ 1.2 cm each) coated with ~ 200 nm of tantalum and ~ 106 nm of aluminum then anodized at 4 V with no exposure to protein (row 1), after exposure of each rectangle to 40 µL of 1 mg/mL prothrombin for 20 minutes (row 2), after subsequent exposure of each rectangle to 100 mL of 5×10^{-4} mg/mL anti-prothrombin for 5, 10, 20 and 40 minutes with no stirring (rows 3, 4, 5, 6). 311

Figure 8.94. Silicon wafer rectangles (three replicates – ~ 1 cm by ~ 1.2 cm each) coated with ~ 200 nm of tantalum and ~ 106 nm of aluminum then anodized at 4 V with no exposure to protein (row 1), after exposure of each rectangle to 40 μL of 1 mg/mL prothrombin for 20 minutes (row 2), after subsequent exposure of each rectangle to 100 mL of 5×10^{-4} mg/mL anti-prothrombin for 5, 10, 20 and 40 minutes with continuous stirring at the regular impeller speed of 195 RPM (rows 3, 4, 5, 6). 312

Figure 8.95. Silicon wafer rectangles (three replicates – ~ 1 cm by ~ 1.2 cm each) coated with ~ 200 nm of tantalum and ~ 106 nm of aluminum then anodized at 4 V with no exposure to protein (row 1), after exposure of each rectangle to 40 μL of 1 mg/mL prothrombin for 20 minutes (row 2), after subsequent exposure of each rectangle to 100 mL of 5×10^{-4} mg/mL anti-prothrombin for 5, 10, and 20 minutes with continuous stirring at an increased impeller speed of 360 RPM (rows 3, 4, 5). 312

Figure 8.96. 3D printed filter containing tantalum disc attached to 60 cc/mL Air-Tite syringe for filter-syringe experiments. 317

Figure 8.97. Tantalum disc (replicate 1 – 26.6 mm diameter) coated with ~ 200 nm of tantalum and ~ 110 nm of aluminum then anodized at 4 V prior to protein exposure (top), after exposure of entire surface to 80 μL of 1 mg/mL prothrombin for 20 minutes (middle), and after exposure to 500 mL of 0.005 mg/mL anti-prothrombin in the syringe-filter device without impeller (bottom)..... 317

Figure 8.98. Tantalum disc (replicate 2 – 26.6 mm diameter) coated with ~ 200 nm of tantalum and ~ 110 nm of aluminum then anodized at 4 V prior to protein exposure (top), after exposure of entire surface to 80 μL of 1 mg/mL prothrombin for 20 minutes (middle), and after exposure to 500 mL of 0.005 mg/mL anti-prothrombin in the syringe-filter device without impeller (bottom)..... 318

Figure 8.99. Tantalum disc (replicate 3 – 26.6 mm diameter) coated with ~ 200 nm of tantalum and ~ 110 nm of aluminum then anodized at 4 V prior to protein exposure (top), after exposure of entire surface to 80 μL of 1 mg/mL prothrombin for 20 minutes (middle), and after exposure to 500 mL of 0.005 mg/mL anti-prothrombin in the syringe-filter device without impeller (bottom)..... 318

Figure 8.100. Tantalum disc (replicate 1 – 26.6 mm diameter) coated with ~ 200 nm of tantalum and ~ 110 nm of aluminum then anodized at 4 V prior to protein exposure (top), after exposure of entire surface to 80 μL of 1 mg/mL prothrombin for 20 minutes (middle), and after exposure to 500 mL of 0.00125 mg/mL anti-prothrombin in the syringe-filter device without impeller (bottom)..... 321

Figure 8.101. Tantalum disc (replicate 2 – 26.6 mm diameter) coated with ~ 200 nm of tantalum and ~ 110 nm of aluminum then anodized at 4 V prior to protein exposure (top), after exposure of entire surface to 80 μL of 1 mg/mL prothrombin for 20 minutes (middle), and after exposure to 500 mL of 0.00125 mg/mL anti-prothrombin in the syringe-filter device without impeller (bottom)..... 322

Figure 8.102. Tantalum disc (replicate 3 – 26.6 mm diameter) coated with ~ 200 nm of tantalum and ~ 110 nm of aluminum then anodized at 4 V prior to protein exposure (top), after exposure of entire surface to 80 μL of 1 mg/mL prothrombin for 20 minutes (middle), and after exposure to 500 mL of 0.00125 mg/mL anti-prothrombin in the syringe-filter device without impeller (bottom)..... 322

Figure 8.103. Draft tube Fusion 360 design. 326

Figure 8.104. Porter Cable compressor used to introduce bubbling into the system (left) and rotameter used to measure gas flow rate (right)..... 327

Figure 8.105. 3D printed draft tube with screws attached (left), brass tube bubbler (middle), and 3D printed draft tube and bubbler placed in a graduated cylinder to form final draft tube apparatus (right). 327

Figure 8.106. Silicon wafer rectangles (three replicates – ~ 1 cm by ~ 1.2 cm each) coated with ~ 200 nm of tantalum and ~ 111 nm of aluminum then anodized at 4 V with no exposure to protein (row 1), after exposure of each rectangle to 40 μL of 1 mg/mL prothrombin for 20 minutes (row 2), after subsequent exposure of each rectangle to 500 mL of 6.25×10^{-4} mg/mL anti-prothrombin for 5 and 10 minutes in the draft tube apparatus at a gas flow rate of ~ 3.5 lpm (rows 3, 4). 330

Figure 8.107. Silicon wafer rectangles (three replicates – ~ 1 cm by ~ 1.2 cm each) coated with ~ 200 nm of tantalum and ~ 111 nm of aluminum then anodized at 4 V with no exposure to protein (row 1), after exposure of each rectangle to 40 μL of 1 mg/mL prothrombin for 20 minutes (row 2), after subsequent exposure of each rectangle to 500 mL of 6.25×10^{-4} mg/mL anti-prothrombin for 5 and 10 minutes in the draft tube apparatus at a gas flow rate of ~ 9.5 lpm (rows 3, 4). 330

Figure 8.108. Silicon wafer rectangles (three replicates – ~ 1 cm by ~ 1.2 cm each) coated with ~ 200 nm of tantalum and ~ 111 nm of aluminum then anodized at 4 V with no exposure to protein (row 1), after exposure of each rectangle to 40 μL of 1 mg/mL prothrombin for 20 minutes (row 2), after subsequent exposure of each rectangle to 500 mL of 5×10^{-4} mg/mL anti-prothrombin for 5 minutes in the draft tube apparatus at a gas flow rate of ~ 3.5 lpm (row 3). 333

Figure 8.109. Silicon wafer rectangles (three replicates – ~ 1 cm by ~ 1.2 cm each) coated with ~ 200 nm of tantalum and ~ 111 nm of aluminum then anodized at 4 V with no exposure to protein (row 1), after exposure of each rectangle to 40 μL of 1 mg/mL prothrombin for 20 minutes (row 2), after subsequent exposure of each rectangle to 500 mL of 5×10^{-4} mg/mL anti-prothrombin for 5 minutes in the draft tube apparatus at a gas flow rate of ~ 9.5 lpm (row 3). 333

Figure 8.110. Silicon wafer rectangles (three replicates – ~ 1 cm by ~ 1.2 cm each) coated with ~ 200 nm of tantalum and ~ 111 nm of aluminum then anodized at 4 V with no exposure to protein (row 1), after exposure of each rectangle to 40 μL of 1 mg/mL prothrombin for 20 minutes (row 2), after subsequent exposure of each rectangle to 500 mL of 6.25×10^{-5} mg/mL anti-prothrombin for 5, 10, 15 and 20 minutes in the draft tube apparatus at a gas flow rate of ~ 3.5 lpm (rows 3, 4, 5, 6). 336

Figure 8.111. Silicon wafer rectangles (three replicates – ~ 1 cm by ~ 1.2 cm each) coated with ~ 200 nm of tantalum and ~ 111 nm of aluminum then anodized at 4 V with no exposure to protein (row 1), after exposure of each rectangle to 40 μL of 1 mg/mL prothrombin for 20 minutes (row 2), after subsequent exposure of each rectangle to 500 mL of 6.25×10^{-5} mg/mL anti-prothrombin for 5, 10, 15 and 20 minutes in the draft tube apparatus at a gas flow rate of ~ 9.5 lpm (rows 3, 4, 5, 6). 337

Figure 8.112. Silicon wafer rectangles (three replicates – ~ 1 cm by ~ 1.2 cm each) coated with ~ 200 nm of tantalum and ~ 105 nm of aluminum then anodized at 4 V with no exposure to protein (row 1), after exposure of each rectangle to 40 µL of 1 mg/mL prothrombin for 20 minutes (row 2), after subsequent exposure of each rectangle to 500 mL of 6.25×10^{-6} mg/mL anti-prothrombin for 20 and 40 minutes in the draft tube apparatus at a gas flow rate of ~ 3.5 lpm (rows 3, 4). 340

Figure 8.113. Silicon wafer rectangles (three replicates – ~ 1 cm by ~ 1.2 cm each) coated with ~ 200 nm of tantalum and ~ 105 nm of aluminum then anodized at 4 V with no exposure to protein (row 1), after exposure of each rectangle to 40 µL of 1 mg/mL prothrombin for 20 minutes (row 2), after subsequent exposure of each rectangle to 500 mL of 6.25×10^{-6} mg/mL anti-prothrombin for 20 and 40 minutes in the draft tube apparatus at a gas flow rate of ~ 9.5 lpm (rows 3, 4). 341

Figure 8.114. Silicon wafer rectangles (three replicates – ~ 1 cm by ~ 1.2 cm each) coated with ~ 200 nm of tantalum and ~ 107 nm of aluminum then anodized at 4 V with no exposure to protein (row 1), after exposure of each rectangle to 40 µL of 1 mg/mL prothrombin for 20 minutes (row 2), after subsequent exposure of each rectangle to 500 mL of 6.25×10^{-4} mg/mL anti-prothrombin for 10 minutes in the draft tube apparatus at a gas flow rate of ~ 3.5 lpm (row 3), after subsequent exposure of hydrophobic circles to 15 µL of rabbit anti-sheep IgG (H+L)-horseradish peroxidase (HRP) conjugate for 20 minutes (row 4)..... 344

Figure 8.115. Silicon wafer rectangles (three replicates – ~ 1 cm by ~ 1.2 cm each) coated with ~ 200 nm of tantalum and ~ 110 nm of aluminum then anodized at 4 V with no exposure to protein (row 1), after exposure of each rectangle to 40 µL of 1 mg/mL prothrombin for 20 minutes (row 2), and after subsequent exposure of each rectangle to 500 mL of MilliQ water in the draft tube apparatus at a gas flow rate of ~ 9.5 lpm for 10 minutes (row 3). 346

Figure 8.116. Fusion 360 design of conical shaped draft tube. 348

Figure 8.117. Silicon wafer rectangles (three replicates – ~ 1 cm by ~ 0.6 cm each) coated with ~ 200 nm of tantalum and ~ 110 nm of aluminum then anodized at 4 V with no exposure to protein (row 1), after exposure of each rectangle to 20 µL of 1 mg/mL prothrombin for 20 minutes (row 2), and after subsequent exposure of each rectangle to 500 mL of 6.25×10^{-6} mg/mL anti-

prothrombin for 20 minutes in the conical draft tube apparatus at a gas flow rate of ~ 3.5 lpm (row 3). 350

Figure 8.118. Silicon wafer rectangles (three replicates – ~ 1 cm by ~ 0.6 cm each) coated with ~ 200 nm of tantalum and ~ 110 nm of aluminum then anodized at 4 V with no exposure to protein (row 1), after exposure of each rectangle to 20 μL of 1 mg/mL prothrombin for 20 minutes (row 2), after subsequent exposure of each rectangle to 500 mL of 6.25×10^{-7} mg/mL anti-prothrombin for 20 minutes in the conical draft tube apparatus at a gas flow rate of ~ 3.5 lpm (row 3), and after subsequent exposure of hydrophobic circles to 15 μL of rabbit anti-sheep IgG (H+L)-horseradish peroxidase (HRP) conjugate for 20 minutes (row 4). 352

Figure 9.1. Silicon wafer rectangles (three replicates – ~ 1 cm by ~ 1.2 cm each) coated with ~ 200 nm of tantalum and ~ 105 nm of aluminum then anodized at 4 V with no exposure to protein (row 1), after exposure of each rectangle to 40 μL of 1 mg/mL prothrombin for 20 minutes (row 2), after subsequent exposure of each rectangle to 500 mL of synthetic urine containing anti-prothrombin at a concentration of 6.25×10^{-5} mg/mL for 20 minutes in the draft tube apparatus at a gas flow rate of ~ 3.5 lpm (row 3). 367

Figure 9.2. Silicon wafer rectangles (three replicates – ~ 1 cm by ~ 1.2 cm each) coated with ~ 200 nm of tantalum and ~ 105 nm of aluminum then anodized at 4 V with no exposure to protein (row 1), after exposure of each rectangle to 40 μL of 1 mg/mL prothrombin for 20 minutes (row 2), after subsequent exposure of each rectangle to 500 mL of synthetic urine containing no anti-prothrombin for 10 and 20 minutes in the draft tube apparatus at a gas flow rate of ~ 3.5 lpm (rows 3, 4), and after exposure of the hydrophobic circles to 15 μL of 0.5 mg/mL anti-prothrombin for 20 minutes (row 5). 370

Figure 9.3. Silicon wafer rectangles (three replicates – ~ 1 cm by ~ 1.2 cm each) coated with ~ 200 nm of tantalum and ~ 110 nm of aluminum then anodized at 4 V with no exposure to protein (row 1), after exposure of each rectangle to 40 μL of 1 mg/mL prothrombin for 20 minutes (row 2), after subsequent exposure of each rectangle to 500 mL of 6.25×10^{-5} mg/mL lyophilized bovine serum albumin for 10 and 20 minutes in the draft tube apparatus at a gas flow rate of ~ 3.5 lpm (rows 3, 4) and after exposure of the hydrophobic circles to 15 μL of 0.5 mg/mL anti-prothrombin for 20 minutes (row 5). 374

Figure 9.4 Silicon wafer rectangles (three replicates – ~ 1 cm by ~ 1.2 cm each) coated with ~ 200 nm of tantalum and ~ 110 nm of aluminum then anodized at 4 V with no exposure to protein (row 1), after exposure of each rectangle to 40 μL of 1 mg/mL prothrombin for 20 minutes (row 2), after subsequent exposure of each rectangle to 40 μL of 1 mg/mL lyophilized bovine serum albumin for 20 minutes (row 3), and after subsequent exposure of each rectangle to 500 mL of 6.25×10^{-5} mg/mL anti-prothrombin for 10 and 20 minutes in the draft tube apparatus at a gas flow rate of ~ 3.5 lpm (rows 4, 5). 377

List of Symbols and Abbreviations

Abbreviation	Definition
3D	three dimensional
A	area
AAO	anodic aluminum oxide
Al	aluminum
Al_2O_3	aluminum oxide
ANOVA	analysis of variance
AP	anti-prothrombin
BSA	bovine serum albumin
C_μ	turbulence model constant
CFD	computational fluid dynamics
CIE	International Commission on Illumination or Commission Internationale de I'Eclairage
D	diameter
Da	Dalton
DC	direct current
DNA	deoxyribonucleic acid
e_t	total energy per unit mass
EBSD	electron backscattered detector
EDX	energy dispersive X-ray
EHT	electron high tension
EIA	enzyme immunoassay
ELISA	enzyme-linked immunosorbent assay
EMA	effective medium approximation
f	femto (10^{-15})
F_b	body force
FESEM	field emission scanning electron microscope
HEPES	4-(2-hydroxyethyl)-1-piperazineethanesulfonic acid
HIV	human immunodeficiency virus

HRP	horseradish peroxidase
IgG	immunoglobulin G
II	prothrombin
j	current density
k	turbulent kinetic energy
LED	light emitting diode
LFA	lateral flow assay
LoC	lab-on-a-chip
lpm	liters per minute
M	molar (moles per liter)
m	milli (10^{-3})
MSE	mean squared error
n	nano (10^{-9})
NaCl	sodium chloride
nanoFAB	nano fabrication and characterization facility
OPL	optical path length
p	pico (10^{-12})
p	pressure
PCR	polymerase chain reaction
PDMS	polydimethylsiloxane
PLA	poly(lactic acid)
POC	point-of-care
POCT	point-of-care testing
PVD	physical vapor deposition
r	radius
RANS	Reynolds-Averaged Navier-Stokes
Re	Reynolds number
RGB	red-green-blue
RPM	revolutions per minute
RPS	revolutions per second
SEM	scanning electron microscopy

SiMoA	single molecule array
SOP	standard operating procedure
SPR	surface plasmon resonance
SST	shear stress transport
t	time
Ta	tantalum
TEC	thermal expansion coefficient
TVR	turbulent viscosity ratio
U	applied potential
v	velocity
v/v	volume per volume
δ	boundary layer thickness
δ_{ij}	Kronecker delta
ε	turbulent dissipation rate
ε_{ij}	strain rate tensor
η	refractive index
μ	dynamic viscosity
μ_T	eddy viscosity
μ	micro (10^{-6})
μPAD	microfluidic paper-based analytical devices
ν	kinematic viscosity
ρ	density
τ	stress tensor
ω	angular velocity
ω	specific rate of dissipation

Chapter 1 – Purpose and Scope

1.1. Motivation

Testing of saliva, urine, blood, or other tissue for certain diseases is often done in a laboratory setting. Usually, the laboratories are at clinics separate from the hospital and it can take several days for test results to be delivered to the physician and then to the patient. Standard diagnostic tests, including enzyme-linked immunosorbent assay (ELISA) and polymerase chain reaction (PCR), are used in the laboratory to detect specific diseases, proteins, or biomarkers, with ELISA being considered the gold standard. The current testing procedures are expensive and result in delayed diagnosis and treatment. The development of a rapid, affordable, diagnostic test that can be used at the point of care and provide results in minutes would significantly improve patient care and reduce the costs and times associated with laboratory testing for diseases.

Thin film interference can be used in the development of a point-of-care (POC) diagnostic test that provides rapid results rather than sending a sample to a laboratory for testing. Commercially available POC tests are expensive and lack sensitivity due to the limited volumes (μL) that can be tested [1]. A POC test that can handle large sample volumes (100 – 2,000 mL) such as urine, ascites fluids, pleural fluids and purulent fluids offers the opportunity to detect low levels of analyte. For example, there is 25,000 times more analyte in a 500 mL sample than in a 20 μL sample of the same concentration. Further, the ability to test large samples offers benefits in the environmental sector, such as the ability to test wastewater. The device should be specific, easy to use and highly sensitive to detect the protein or biomarker of interest. By using a porous substrate, stirred tank, or draft tube, large volumes of a sample can be passed over the device surface allowing for detection of proteins at a low analyte concentration. Using a large sample

volume allows for detection at lower concentrations, improving the sensitivity of the diagnostic tool. The ability to detect a particular toxin or bacteria at the nanomolar level at the point-of-care can provide information to healthcare providers and patients about a diagnosis and potential treatment methods within minutes. The potential uses of thin films and colour shifts to detect a certain protein within 20 minutes in the healthcare field can range from alerting medical professionals of infectious diseases to selecting patient treatment based on certain biomarkers. Further, point-of-care diagnostics have the potential to be used by patients themselves to monitor certain conditions, such as diabetes or heart disease.

1.2. Aims & Objectives

The proposed research is the development of a stand-alone, point-of-care medical diagnostic device that can detect low concentrations of analyte in high volume samples based on a colour change due to thin film interference. Fluid flow through a membrane or stirring a fluid sample over the thin film substrate will allow for larger volumes of fluid to be tested. By using a high-volume system, the diagnostic should be able to indicate very low concentrations, down to the nanomolar or picomolar level, of a certain biomarker or protein of interest based on a visible colour shift on the thin film surface. The porous nature of the quartz frits discs and the 1 mm diameter holes in the tantalum discs allow for large fluid samples to pass through the device and interact with the adsorbed protein layer that lies above the thin films of alumina and tantalum, acting as a filter. Flow must be controlled to maximize exposure of the fluid to the surface protein layer to ensure binding occurs if the appropriate biomarker is present in the sample. Applications are for materials at a low concentration in which a large volume can be obtained including medical applications, food applications or water applications – such as looking for a particular toxin in water, urine, or blood. Rapid detection of biomarkers or pathogens at the

patient's side can potentially lead to quicker care decisions and improved patient outcomes. Research has been conducted on the detection of several biomarkers for certain diseases with high sensitivity including human immunodeficiency virus (HIV) [2], leukocytosis [2], Alzheimer's disease [3], and breast cancer [4].

The initial device was designed to function by passing large volumes of a fluid containing anti-prothrombin through a tantalum disc with either four or eight 1 mm diameter holes, coated with prothrombin and with thin films of aluminum oxide, tantalum oxide and tantalum and observing for a colour shift – indicating an antigen-antibody complex has formed. The subsequent design consisted of a stirred tank apparatus, in which a silicon wafer slide coated with protein and thin films of aluminum oxide, tantalum oxide and tantalum was placed in the bottom of a beaker and a large fluid volume was mixed above the membrane. The final design consisted of a draft tube apparatus, in which flow was continuously directed at the coated silicon wafer slide. In all cases, the substrate material (tantalum disc or silicon wafer) was coated with prothrombin prior to exposure to the large fluid sample, which contained a low concentration of anti-prothrombin. The formation of an antigen-antibody complex on the substrate surface occurred when anti-prothrombin from the fluid sample bound to prothrombin on the coated surface and was indicated by a colour shift on the substrate surface. Transitional or turbulent flow is required to ensure well-mixed flow and to expose as much of the fluid to the surface as possible. For experimental purposes, prothrombin will be placed on the surface of the membrane and the concentration of anti-prothrombin in solution will be continuously diluted and passed through the filter or placed in the stirred tank to determine the level of sensitivity that can be achieved. The prothrombin anti-prothrombin binding complex will produce a colour shift on the substrate surface, compared to prothrombin alone, indicating the presence of anti-prothrombin in

solution. It is proposed that a highly sensitive point-of-care diagnostic device based on thin film interference can be developed to detect low concentrations of a specific biomarker by using larger volumes of fluid and creating transitional or turbulent flow and mixing at the thin film membrane surface.

1.3. Scope of Thesis

Chapter 2 introduces the study with an introduction and a literature review of high sensitivity diagnostic tests as well as background on device colour generation, fluid mechanics, and alumina surfaces. Thin film technology, thin film deposition, electrochemical oxidation and fluid flow regimes will be reviewed. Chapter 3 provides materials and methods used for the work, including membrane selection, device design, sputtering, electrochemical oxidation, protein exposure and adsorption techniques, and analytical techniques to study samples. Chapter 4 discusses the effect of sputtering and anodization parameters on the performance of silicon wafers, polycarbonate membranes, polymer discs, quartz frits discs and tantalum discs. Chapter 5 explores the adsorption of biologics onto porous anodic alumina on porous, polished quartz frits. Chapter 6 explores the adsorption of biologics onto porous anodic alumina on high purity tantalum discs. Chapter 7 details the designs of the impeller based diagnostic device and computational fluid dynamics (CFD) simulations to visualize flow patterns and turbulence in the diagnostic device designs. Chapter 8 examines anti-prothrombin sensitivity on prothrombin-coated tantalum discs and silicon wafers for the diagnostic device by analyzing prothrombin immobilization and complex formation, as well as the limit of detection for anti-prothrombin on the thin film and prothrombin coated substrate. The device sensitivity will also be assessed in Chapter 8. The final chapter, Chapter 9, tests the thin film diagnostic device using the prothrombin-anti-prothrombin model in synthetic urine.

1.4. References

1. Chin, C.D., V. Linder, and S.K. Sia, *Commercialization of microfluidic point-of-care diagnostic devices.* LAB ON A CHIP, 2012. **12**(12): p. 2118-2134.

2. Ng, E., et al., *Magneto-nanosensor smartphone platform for the detection of HIV and leukocytosis at point-of-care.* Nanomedicine, 2019. **16**: p. 10-19.

3. Li, D. and M.M. Mielke, *An Update on Blood-Based Markers of Alzheimer's Disease Using the SiMoA Platform.* Neurol Ther, 2019. **8**(Suppl 2): p. 73-82.

4. Malecka, K., D. Pankratov, and E.E. Ferapontova, *Femtomolar electroanalysis of a breast cancer biomarker HER-2/neu protein in human serum by the cellulase-linked sandwich assay on magnetic beads.* Analytica Chimica Acta, 2019. **1077**: p. 140-149.

Chapter 2 – Introduction and Literature Review

2.1. Introduction – Review of High Sensitivity Diagnostic Tests

Standard diagnostic tests used today include enzyme immunoassays (EIAs) for proteins and polymerase chain reaction (PCR) for nucleic acids, with enzyme linked immunosorbent assay (ELISA) being considered the gold standard [1]. ELISA is used to detect and quantify antibodies, antigens, proteins, glycoproteins, and hormones with high sensitivity by creating antibody-antigen complexes [1]. Four types of ELISA are commonly used: direct, indirect, sandwich and competitive. All four types function the same way: a target macromolecule, such as an antigen, is immobilized and undergoes incubation with an enzyme-linked antibody to produce a measurable product [2]. ELISA uses several detection strategies including chromogenic, fluorescence and chemiluminescence, increasing substrate flexibility [2]. PCR is used to amplify small segments of deoxyribonucleic acid (DNA) to large enough concentrations to study. However, ELISA and PCR are time consuming, require expensive equipment, and high levels of training to be properly used [3]. These diagnostic tests often occur in a separate laboratory setting, are expensive, require large pieces of equipment, and have a significant time delay to receive the test result.

In recent years, point-of-care testing (POCT) has increased in popularity and extensive research has focused on the development of a low cost, specific and easy to use diagnostic that provides rapid results [4]. POCT can promptly detect analytes by performing laboratory tests at the patient's side, allowing for quicker diagnoses and medical decisions [5]. Lateral flow assays (LFAs) are the most common point-of-care devices currently used [6]. LFAs are paper-based platforms used to detect and quantify analytes in a mixture and display results within 5 – 30 minutes. In a LFA, a liquid containing the analyte of interest moves by capillary action along the

polymeric strips [6]. The polymeric strips contain molecules that the analyte can interact with. The analyte is initially exposed to buffer salts and surfactants as well as an area containing antibodies specific to the target analyte. These antibodies are conjugated to coloured or fluorescent particles, such as colloidal gold or latex microspheres. The test line contains an immobilized antibody or antigen designed to react with the analyte and conjugated antibody complex by fluorescence or a colour change. If the analyte of interest is present in the sample, the test line will become visible in the detection zone, indicating the analyte is bound to the conjugated antibody. LFAs are inexpensive, easy to use, fast-acting and applicable to standard and multiplex formats [7]. LFAs are limited to solutions with a high analyte concentration (µM to mM) [8]. Amplification techniques can be used when analyte concentration is low, but this increases complexity of the test [8]. The pregnancy test is the most well-known lateral flow assay used, shown in Figure 2.1.

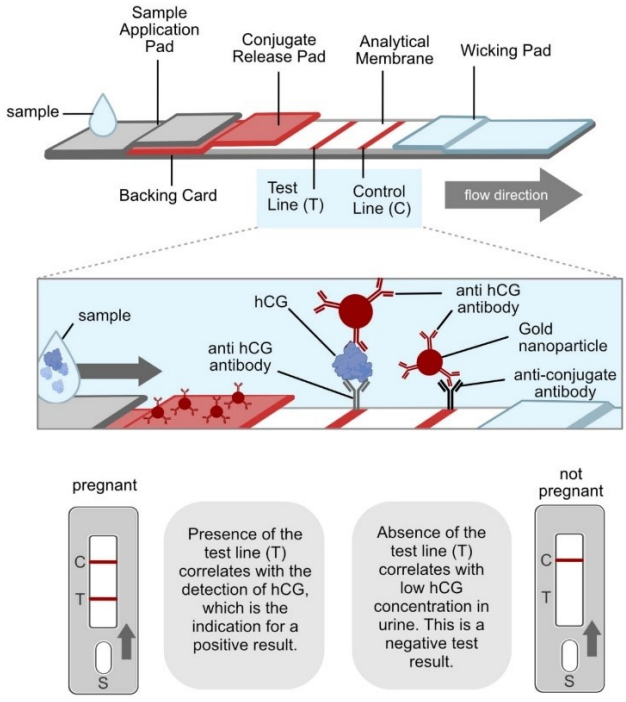


Figure 2.1. The pregnancy test lateral flow immunoassay [9].

Microfluidic devices are also commonly used for POCT [10]. Microfluidics is a technology used to manipulate and control the flow behavior of small volumes of fluid using micro channels and connections in a tiny chip [11]. Microfluidics are easy to use and allow for high sensitivity in a controlled environment [12]. The Lab-on-a-chip (LoC) technology uses microfluidic properties to detect biomolecules and can be assisted by magnetic nanoparticles [13]. Microfluidic paper-based analytical devices (μPADs) function by patterning a paper material with chemicals that will bind the analyte of interest and result in a colour change if analyte is present [12]. Polydimethylsiloxane (PDMS) is an example of a material used to create microfluidic devices that often require an external pressure source to induce fluid flow. However, PDMS devices require special training and equipment that can be costly. Alternate technologies use electronic sensors that may measure changes in conductance or resistance using carbon nanosensors or antibodies based on a certain concentration of biomolecules [12]. Further, detection chemicals such as antibodies can be placed on the chip to detect specific analytes. Commercial microfluidic devices are expensive and limited to low volumes.

Several other highly sensitive POCT diagnostics are used including electrochemical biosensors and surface plasmon resonance (SPR). Electrochemical biosensors are used to monitor certain biomolecules, for example, glucose monitoring in diabetics, by detection of a redox enzyme [14]. SPR is a label-free technique that monitors binding interactions by observing refractive index changes to a metal surface in real time [15]. Analyte binding to the immobilized surface molecule changes how light is absorbed and causes a shift in the minimum light intensity at the detector. This shift in intensity indicates that the analyte is present and bound. Drawbacks of SPR include its low sensitivity, expensive cost, and complexity.

Ng et al. (2019) [16] studied a mobile magneto-nanosensor POC platform for the detection of HIV in saliva and leukocytosis in plasma or whole blood at high sensitivities. The giant magnetoresistive nanosensor chip detects magnetic nanoparticles by generating an alternating magnetic field and measuring a change in electrical resistance. The changes in resistance correlate to analyte concentration and connection to a smartphone makes for a user interface [16]. Li and Mielke (2019) [17] studied single molecule array (SiMoA) to detect proteins in blood at sub-femtomolar concentrations. SiMoA involves confinement of a single magnetic bead coupled with enzyme and substrate to produce a fluorescent product in a femtoliter-well. Fluorescence can be measured in a short period of time; however, this application is limited to small volumes and is not currently applicable to patient care in the clinical setting [17]. Malecka, Pankratov and Ferapontova (2019) [18] explored a technique for the detection of breast cancer biomarkers at the femtomolar level using a cellulase-linked sandwich assay on magnetic beads based on changes in electrical properties. This ultrasensitive assay allows for high sensitivity detection but is not yet clinically available.

Available POCT devices are either expensive, lack sensitivity or complex to use. Further, most available devices are restricted to high concentration, low volume samples. Fluid passage through a porous membrane with adequate surface exposure or stirring a large fluid volume over a coated membrane allows a significantly larger amount of fluid to be tested for the analyte of interest, increasing the sensitivity of the test, and allowing detection at lower analyte concentrations. The development of a POC diagnostic device that is affordable, easy to use, highly sensitive, portable and can detect a specific analyte in large fluid volumes without amplification offers many benefits to healthcare.

2.2. Device Colour Generation

The fundamental concept behind the device colour generation is that of thin film interference. Just as gasoline on wet pavement generates interference colours producing a rainbow, as seen in Figure 2.2, thin layers of metal can be used to generate colour interference by altering the path of light. As shown in Figure 2.3, when light strikes the surface of the oil, a portion of this light is reflected and a portion enters the film via refraction, which is then reflected from the bottom surface, in this case water. The path difference between the two reflected rays combine to generate interference. The colour generated is dependent on the layer thickness, indicating that the oils thickness varies above the water.



Figure 2.2. Interference colours from an oil film on water [19].

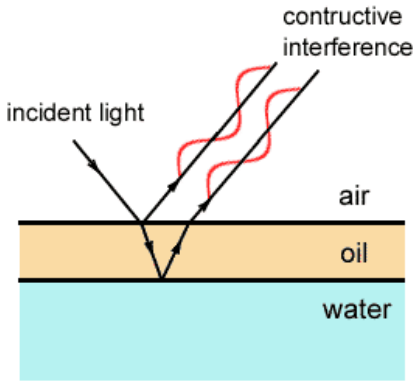


Figure 2.3. Path of reflected and refracted light rays through a thin film of oil [20].

Colour interference can be achieved in a laboratory setting by altering the material properties of a multi-layer surface to control the amount of light reflected at each layer's surface. The colours generated by thin film interference depend on the thickness of the film as well as the optical path length (OPL). The physical path length can be described as the distance light travels within the film before exiting. The OPL is the product of the physical path length and the refractive index of the medium through which light propagates. Colour interference occurs when different rays of reflected light have different OPLs. Constructive interference occurs when the light shift in the medium is an integral of a full wavelength and destructive interference occurs when the light shift in the medium is an integral of a half wavelength. For visible colour interference to occur, the optical path length travelled by the refracted light ray must be at least half a wavelength [21]. Constructive interference will occur if the thin film is half a wavelength thick, as the optical path length will be one full wavelength. If the thin film is a quarter of a wavelength thick, destructive interference will occur as the optical path length is half a wavelength. This information can be used to select the optimal alumina layer thickness based on the wavelength of visible light (~380 – 700 nm) [22]. By manipulating characteristics of different layers, multiple OPLs can be achieved, each forming a distinct colour. Anodizing metals such as tantalum or aluminum creates an oxide film on the metal's surface with a different refractive index than the metal. When light strikes, it is reflected from the oxide surface as well as the oxide-metal interface, creating interference. Changes in film thickness such as by adsorption of a protein monolayer, can lead to a different colour being observed. Alone, a thin protein monolayer may not be thick enough to generate a significant OPL difference and would fail to produce a visible colour interference shift. Pairing this thin layer to the layer beneath it, in this case aluminum oxide, by matching their refractive indices can create a path distance long

enough for a visible shift to occur. Immobilizing a specific antigen with the same refractive index as a porous, aluminum oxide layer on the surface allows for interference to occur between the antigen surface and the aluminum oxide/tantalum interface. If the antibody associated with the immobilized antigen is present in the fluid sample, an antigen-antibody complex will form on the surface of the thin film, increasing the optical path length resulting in a visible colour change, as seen in Figure 2.4.

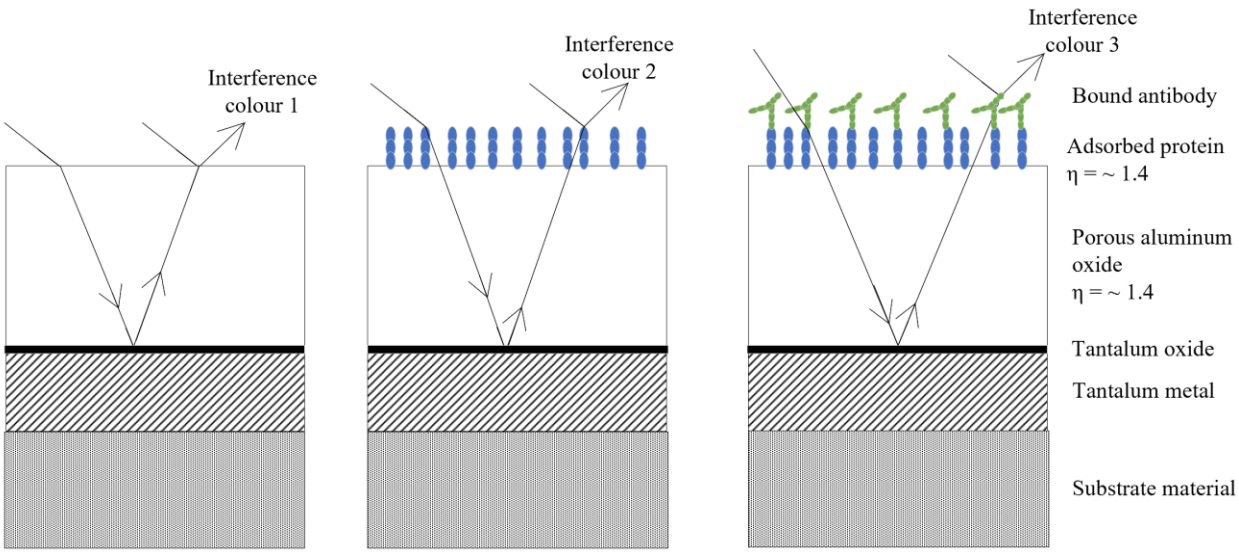


Figure 2.4. Pathway light travels through bound antibody, adsorbed protein, and aluminum oxide layers to produce a colour shift by interference. Binding of the antibody increases the OPL enough to produce a visible colour shift. Silicon wafers, polycarbonate membranes, porous quartz frits discs, and high purity tantalum discs were used as the substrate material in this work. The refractive index (η) of the adsorbed protein is equal to the refractive index of the aluminum oxide layer.

Thin films of aluminum and tantalum were deposited onto the polycarbonate membranes, porous, polished quartz frits discs, silicon wafers, and high purity tantalum discs using direct current (DC) planar magnetron sputtering systems – a form of physical vapor deposition (PVD).

The planar magnetron sputtering system consists of the cathode, which is the surface of the sputtering target, and the anode [23]. The cathode surface is bombarded with energetic ions formed from collisions between argon gas and electrons to release target atoms to be deposited onto the anode using a magnetic field. Electrons are trapped over the target material by a magnetic field to increase the number of collisions and increase the deposition rate.

Anodization is used to alter the structures and properties of metals by converting the metal surface into a metal oxide layer. Electrochemical oxidation occurs when a valve metal is immersed into an acid electrolyte bath and exposed to an electric current creating an oxide layer. After aluminum has been completely anodized into porous alumina, the tantalum layer is exposed to the current and undergoes electrochemical oxidation to form tantalum oxide. The applied potential determines the thickness of the tantalum oxide layer and the current declines to zero as the tantalum oxide layer reaches its maximum thickness [24]. The tantalum oxide layer thus forms a dielectric layer that limits the current flow and stops the dissolution of aluminum. Reproducing the thickness of the tantala layer can act as an internal control for the device by ensuring the colour generated by the tantala layer consistently contributes the same to the surface colour under different conditions [25]. Light is partially absorbed by the tantalum metal beneath, while between 40% and 60% is reflected as visible light [25].

The key to developing a visible, strong colour shift is to ensure the alumina layer has the same refractive index as the protein. The refractive index of an adsorbed protein in solution usually varies between 1.35 and 1.6 when measured by ellipsometry [26]. The variation is due to different protein properties and protein surface interactions. Failure to match the refractive indices of the alumina and protein can decrease sensitivity and increase noise due to an additional reflection. In the visible range, the refractive indices of alumina, water and air are 1.7,

1.33, 1.0003, respectively ([27], [28]). By altering anodization parameters, such as anodizing voltage or electrolyte, the amount of air in the aluminum oxide layer can be manipulated by adjusting the pore size and pore density of aluminum oxide to obtain an index of refraction similar to the protein of interest [29].

The range of interference colours produced by thin film interference is shown in Figure 2.5 on the Michel-Lévy interference colour chart with first and second orders producing the strongest visual intensity. The low-order colours are generated by thinner films and are more distinct, while the high-order colours have thicker films and are less distinct [30]. As thickness of the thin film increases, the colour order increases as more wavelengths can constructively and destructively interfere and the colours become less intense. Visible interference colours can be plotted on a Commission Internationale de l'éclairage (CIE) 1931 colour chromaticity chart to map human colour perception. Figure 2.6 displays the CIE 1931 colour chromaticity chart displaying MacAdam ellipses. MacAdam ellipses demonstrate how far apart two colours must be in order for the human eye to perceive a difference. Any two points in a single ellipse are indistinguishable to the human eye [31], therefore it is important to select a sensitive colour region when developing a diagnostic test that depends on a visual colour shift. Further, Sandström et al. (1985) [32] demonstrated that first order interference colours are the most sensitive to changes in thickness and the use of first order colours would allow for the most sensitive colour change in a thin film device.

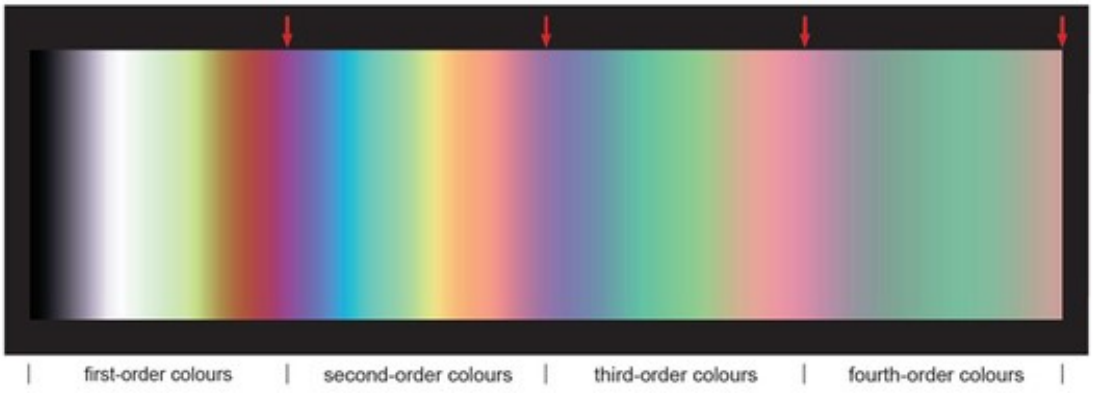


Figure 2.5. Revised Michel-Lévy interference colour chart displaying first, second, third and fourth order interference colours [30].

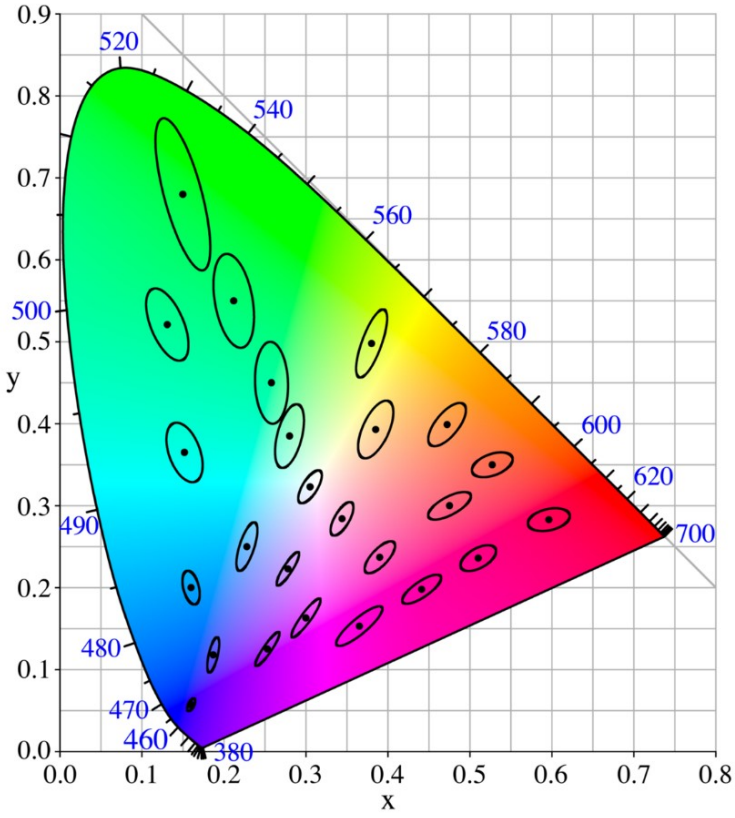


Figure 2.6. CIE 1931 colour chromaticity diagram displaying MacAdam ellipses. Any two points within a single eclipse are indistinguishable to the human eye [31].

2.3. Fluid Mechanics

The objective for the diagnostic device is to detect a specific analyte in a large volume of fluid by passing fluid through the porous membrane and over the thin film surface or stirring a large fluid volume above the thin film surface. Since large fluid volumes are tested in this application, the fluid mechanics of the system are important to consider. Fluid exposure to the thin film/protein surface should be maximized to allow for the formation of the antigen-antibody complex. The syringe used to pass fluid through the membrane, or the draft tube apparatus can be thought of as a miniature pipe. Pipe flow is classified into three flow regimes: laminar, transition and turbulent [33]. The type of flow is determined by a dimensionless parameter called Reynolds number. Reynolds number can be calculated using Equation 2-1 [33]:

$$Re = \frac{\rho v D}{\mu} \tag{2-1}$$

Where v is the average fluid velocity (m/s), D is the internal pipe diameter (m), ρ is the liquid density (kg/m^3) and μ is the dynamic viscosity of the fluid (Pa·s). Each flow regime can be classified based on the Reynolds number [33]:

Re < 2000: Laminar flow

2000 < Re < 4000: Critical/transition flow

Re > 4000: Turbulent flow

Laminar flow is characterized by smooth, regular fluid flow with little to no mixing [34]. Flow properties, such as velocity and pressure, remain constant at each point in the fluid while the fluid flows in parallel layers with no disruption. Transition flow is a mixture of both laminar and turbulent flow and exhibits characteristics of both flow types [35]. Turbulent flow is

characterized by irregular flow patterns, continuous mixing, and the presence of eddies [36]. Fluid speed is continuously changing in magnitude and direction, and no clear flow layers are present. In laminar flow, transport is driven only by diffusion as no mixing occurs. In transition and turbulent flow regimes, transport is driven by a combination of mixing and diffusion. The three flow regimes are displayed in Figure 2.7.

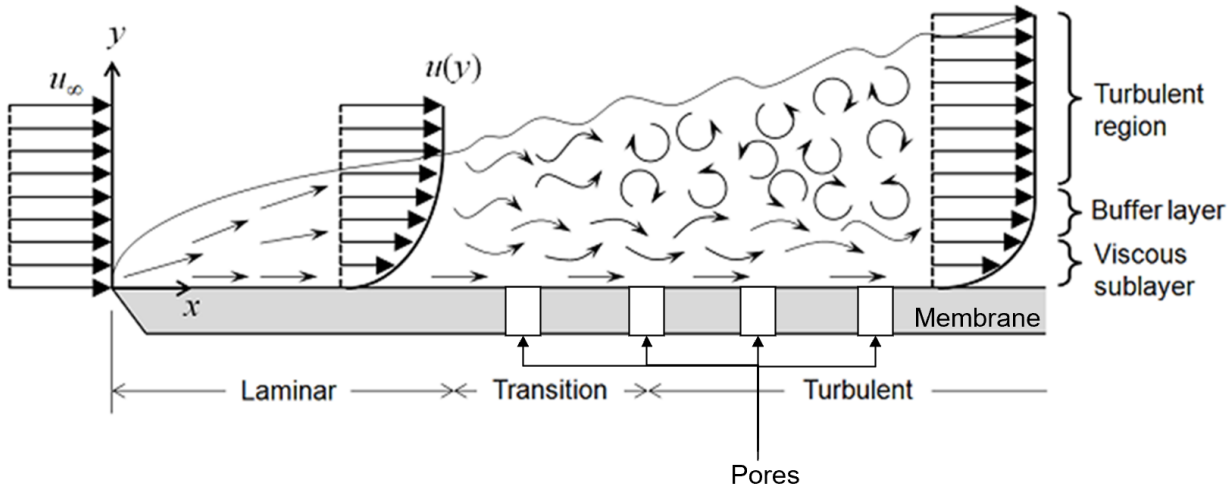


Figure 2.7. Laminar, transitional, and turbulent flow regimes over the porous membrane device. Laminar flow is characterized by parallel layers of fluid flow sliding smoothly over one another that do not mix. Transition flow is a mixture of laminar and turbulent flow. Turbulent flow is characterized by random motion of the fluid elements and mixing [37].

To achieve a colour change, antigen-antibody complex formation must occur through binding of the analyte to the surface protein at very low concentrations. Flow past the surface and through the membrane must be well-mixed and disordered to expose as much of the fluid as possible to the surface and to allow for the binding to occur. The flow pattern of each regime is demonstrated in Figure 2.8, by observing the behavior of a dye streak in flowing fluid in each regime. In the laminar regime, the dye travels in a straight line, indicating no mixing with other

fluid elements. All fluid molecules follow a regular, straight path, and the dye does not interact with fluid elements above or beneath it. In the turbulent region, all fluid molecules undergo speed and direction changes, leading to significant fluid mixing and the dye is mixed throughout the pipe. If significant mixing is occurring when the fluid reaches the membrane surface, more fluid elements will come into contact with the surface, increasing the chance of binding occurring.

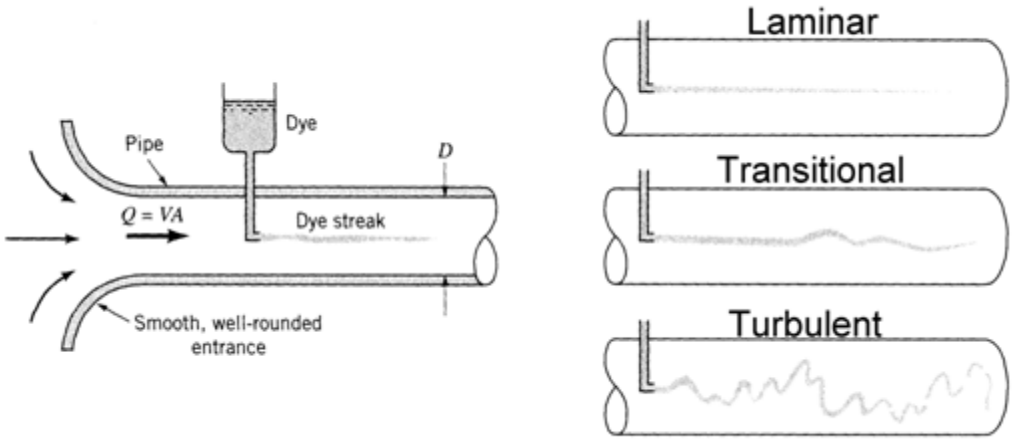


Figure 2.8. Laminar, transitional, and turbulent flow regimes characterized by dye. Turbulent flow is characterized by mixing of fluid elements and would allow for more fluid exposure to the surface [38].

The fluid elements will interact with the adsorbed protein layer on the surface prior to passing though the membrane filter or in the mixing tank apparatus allowing the antigen-antibody complex to form, which will cause a colour shift. The fluid can be passed through the membrane using gravity alone, or using pressure induced by a syringe. To obtain turbulent flow, the fluid's velocity needs to be greater than what would be produced by gravity, thus, the filtration in this device will be assisted by a syringe. The fluid flow profile created by the

diagnostic device will be similar to the flow profile of a pressure driven sand filter. The applied pressure by the syringe forces the fluid passed an impeller, which enhances fluid mixing just above the thin film surface, then through the porous membrane.

In the stirred tank or draft tube apparatus, a large fluid sample (500 mL) is continuously mixed above the coated membrane material. The coated membrane material is placed in the bottom of the apparatus near the boundary or wall. In turbulent flow, the viscous sublayer is a thin layer of flow near a surface or boundary in which viscous effects are dominant, as can be seen in Figure 2.7 [39]. The no-slip boundary condition at the wall of the viscous sublayer assumes that there is no movement of the layer of fluid in direct contact with the boundary or wall relative to the wall, meaning the velocity of the fluid layer is zero at the wall due to the fluid's viscosity or resistance to flow [40]. The viscous sublayer is very small, and is approximately equal to 0.1 – 1 % of the total boundary layer thickness [41]. Since the coated membrane sits on the bottom of the device against the wall, it would be in the viscous sublayer flow region where flow is considered laminar. Although the membrane surface is in this region, the flow regime of the rest of the 500 mL sample is important to consider as the transport mechanisms are different in different flow regimes. In stationary or laminar flow, no fluid mixing occurs at any point and transport is driven only by diffusion. In transitional or turbulent flow, transport is driven by diffusion and by mixing of fluid elements. Although the viscous sublayer is present at the walls in turbulent flow, mixing in the bulk fluid sample can bring individual fluid elements near the viscous sublayer. The mixing that occurs in turbulent flow can greatly reduce the distance required for a molecule to diffuse to come into contact with the surface. As a prothrombin-anti-prothrombin model is used in this work, consider a prothrombin coated membrane placed at the bottom of a tank containing a 500 mL fluid sample with a low

concentration of anti-prothrombin. In stationary or laminar flow, anti-prothrombin molecules must diffuse a great distance to come into contact with the prothrombin coated surface. In well-mixed or turbulent flow, the anti-prothrombin molecules may be brought to the edge of the viscous sublayer due to mixing of fluid elements, leaving only the thickness of the viscous sublayer as the distance to diffuse, greatly reducing the diffusion time required. At 20°C, the diffusion coefficient of human IgG in 10-times-diluted serum was found to be $(4.4 \pm 0.2) \times 10^{-7}$ cm^2/s [42]. In a stationary fluid sample, anti-prothrombin molecules rely on diffusion alone to travel through the entire 500 mL volume to reach the coated membrane. In turbulent flow, diffusion would only be required to travel the distance of the viscous sublayer, which is a thin layer in direct contact with the wall. By reducing the distance anti-prothrombin molecules must diffuse in solution to that of the viscous sublayer thickness only, the time required for anti-prothrombin to bind is greatly reduced. The thickness of the turbulent boundary layer on a smooth flat plate aligned parallel to a uniform stream can be calculated using Equation 2-2 [43]:

$$\frac{\delta}{x} \cong \frac{0.38}{(Re_x{}^{1/5})} \tag{2-2}$$

Where δ is the boundary layer thickness, x is the length of the plate, and Re_x is the Reynolds number over the plate [43]. For a flat plate length of 10 cm, and Reynolds numbers of 4000 and 6000, the boundary layer thicknesses are ~ 7.2 mm and ~ 6.7 mm. As the viscous sublayer is approximately equal to 0.1 – 1% of the total boundary layer [41], the viscous sublayer would fall in between 0.0072 mm and 0.072 mm for a Reynolds number of 4000 and between 0.0067 mm and 0.067 mm for Reynolds number of 6000. For a 500 mL fluid sample in a 1 L beaker, the distance from the top of the fluid sample to the bottom of the beaker is ~ 73 mm. Thus, inducing turbulence greatly reduces the distance an anti-prothrombin molecule must travel in solution by diffusion alone.

2.4. Impeller Design

To achieve turbulent flow on the membrane surface, an impeller was placed just above the surface to encourage mixing. As force is applied to the syringe, the fluid forces the impeller to rotate and maximizes the mixing of fluid elements. The impeller is used to increase the fluid velocity and increase fluid mixing, resulting in turbulent flow just above the membrane surface. Turbulent flow at the thin film surface is important to maximize surface exposure to the fluid elements and the impeller should be designed accordingly. The four main impeller blade types used, shown in Figure 2.9, include airfoil, pitch blade, propeller blade and radial blade [44]:

- Airfoil: Airfoil or dynaflow impeller blades are designed to produce maximum airflow with the lowest shear, making them suitable for low to medium viscosity mixtures.
- Pitch blade: The pitch blade impeller has a high mixing intensity and is suitable for mixtures of medium viscosity. The pitch blade is versatile and ideal for applications that require significant mixing.
- Propeller blade: The propeller blade or marine-type impeller blades provide medium to high mixing intensity with medium shear.
- Radial blade: Radial blade impellers produce high shear rates with low mixing intensity and flow. These blades are ideal when agitation is required near the bottom of the tank.



Figure 2.9. The four main types of *impeller blades used. Airfoil (top left) [45], pitch blade (top right) [46], propeller blade (bottom left) [47] and radial blade (bottom right) [48].*

The pitch blade impeller design is most suitable for the diagnostic device application due to the high amount of mixing required to create turbulent flow. Pitch blade impellers use flat blades that are set at an angle of 45°. The 45° angle of the blades allows for optimal overall mixing as it simultaneously produces axial and radial flow [49]. Rewatkar and Joshi (2010) studied the effect of impeller blade angle on liquid mixing by measuring the mixing time at various blade angles [50]. Blade angle was varied from 30° to 90° and mixing time was found to decrease as blade angle increased, indicating faster mixing, due to an increase in volumetric flow rate. At 90°, mixing time increased. It was found that a blade angle of 45° was the most energy

efficient [50]. The impeller clearance from the bottom wall was also an important factor in determining mixing time along with blade angle. As bottom clearance distance decreased (impeller placed closer to bottom of tank), a blade angle of 60° resulted in increased mixing time [50]. Li et al. (2021) also suggested the optimal impeller angle for mixing and power consumption is 45° [51]. The effect of impeller blade width on mixing time was also investigated and it was determined a blade with of 0.35 times the diameter of the impeller resulted in the lowest mixing time [50]. Another factor that is important to consider in impeller design is the number of blades. It has been shown that the number of blades and blade configuration has an impact on fluid mixing ([50], [52], [53]). It was found that as the number of blades increased from 4 to 6 to 8, the mixing time decreased, indicating that 8 blades produced the quickest mixing [50]. For stirred tanks, the Reynolds number is defined as the impeller Reynolds number, Re_i, as shown in Equation 2-3 [54]:

$$Re_i = \frac{N_i D_i^2 \rho}{\mu} \tag{2-3}$$

Where N_i is the stirrer speed (RPS), D_i is the impeller diameter, ρ is the fluid density, and μ is the fluid viscosity [54].

2.5. Airlift Bioreactors

One experimental design for the diagnostic device investigated the use of a draft tube and a bubbler to induce mixing, as an alternative to stirring with an impeller. The apparatus functions in the same way as an airlift bioreactor. Airlift bioreactors agitate the contents of the bioreactor pneumatically by injecting gas into a bubble column at the bottom of the reactor [55]. Mixing occurs as the bubbles rise to the top of the reactor. Airlift reactors usually contain an internal loop gas draft tube that directs the fluid circulation in a specific direction, and allows for more

defined liquid flow patterns ([56], [57]). Gas sparging at the bottom of the reactor induces liquid upflow as the bubbles rise [58]. The gas then escapes from the top of the reactor and the liquid is recirculated through the draft tube to the bottom of the reactor. Figure 2.10 shows a schematic diagram of three different airlift reactor configurations.

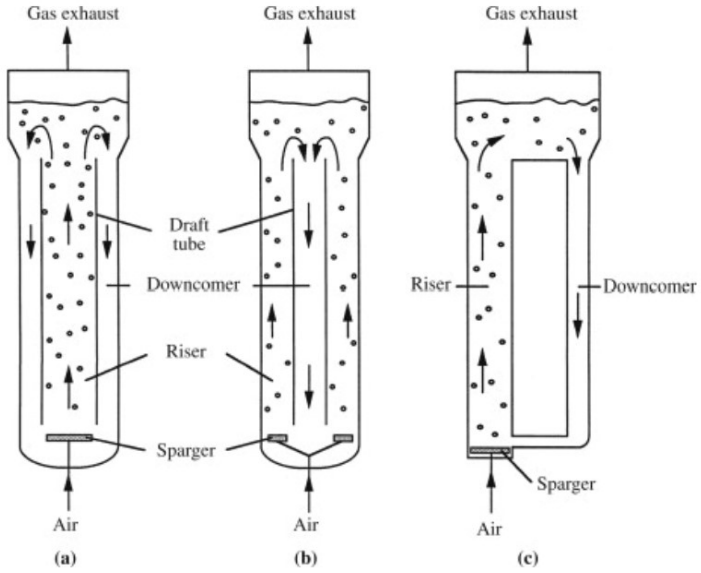


Figure 2.10. Schematic diagram of airlift reactor configurations: a) internal loop with riser section inside draft tube, b) internal loop with downcomer section inside draft tube, and c) external loop [57].

Each configuration shown in Figure 2.10 consists of a riser and a downcomer section. Gas is sparged only into the riser section of the vessel, decreasing the density of the fluid and causing the liquid in the riser to move upward with the gas bubbles [57]. Gas bubbles escape from the top of the vessel leaving behind more dense bubble-free liquid that recirculates through the downcomer. For the diagnostic device, a large volume sample with a low analyte concentration is studied. The use of an airlift reactor with an internal loop draft tube allows for the flow to be directed at the coated substrate material. Sparging gas on the outside of the draft

tube, as shown in Figure 2.10 b, causes recirculation of the fluid down the middle of the draft tube. Placing the thin film and antigen coated membrane material just beneath the bottom outlet of the draft tube ensures that the fluid sample is continuously recirculated and directed towards the surface, increasing the likelihood of antibodies in the sample binding to the antigen coated surface. Compared to a stirred tank in which fluid elements are randomly mixed throughout the tank, the airlift reactor draft tube set up continuously recirculates the fluid sample directly over the coated membrane, potentially improving the device sensitivity and allowing for analyte detection at lower concentrations.

Airlift bioreactors offer several advantages over a stirred tank with an impeller including improved energy efficiency, predictable flow patterns, and lower shear rates and shear stresses, while still providing rapid mixing of fluid elements ([56], [59], [60], [61], [62]). In a stirred tank, agitation of the fluid sample with an impeller generates heat in the system, which could potentially lead to protein denaturation [63]. Since airlift bioreactors are pneumatically agitated, the shear stress and heat generation are reduced compared to a mechanically agitated stirred tank with an impeller [64]. Airlift bioreactors containing draft tubes have been shown to produce efficient mixing and turbulent flow at increased gas flow rates ([55], [65], [66], [67]). The ability to direct flow towards the membrane surface with adequate mixing makes the airlift bioreactor design a suitable option for the diagnostic device design. For an airlift reactor, the bubble Reynolds number, Re_b, is calculated using Equation 2-4 [68]:

$$Re_b = \frac{V_z d_{10}}{\nu_L} \tag{2-4}$$

Where V_z is the bubble rising velocity (m/s), d_{10} is the bubble equivalent diameter (m), and ν_L is the kinematic viscosity of the liquid phase (m^2/s) [68].

2.6. Anodic Alumina

Anodization is an electrochemical process used to increase the thickness of the natural oxide layer on a metal surface by immersing the metal, such as aluminum, into an acid electrolyte bath and passing an electric current through it [69]. Anodization of aluminum metal leads to the formation of a porous alumina structure by increasing the thickness of the aluminum oxide layer on the surface. The aluminum oxide layer on the anode surface thickens during anodization due to the inward migration of O^{2-} ions and the outward migration of Al^{3+} ions under the electric field [70]. Two types of oxide films can be grown on aluminum depending mainly on the nature of the electrolyte used: barrier-type oxide films, where a uniformly thick oxide layer grows on the surface, and porous-type oxide films, where oxide growth occurs to develop a regular array of pores. Barrier-type films form when the anodic oxide is practically insoluble in the electrolyte, and forms in neutral electrolytes (pH 5 – 7) such as borate, oxalate, and citrate [71]. Porous-type films typically grow in acidic electrolytes in which the anodic oxide is slightly soluble, including oxalic acid, phosphoric acid, sulfuric acid, chromic acid, malic acid, and citric acid [71]. During porous-type anodization of aluminum, positive H^+ ions from the acidic electrolyte accelerate towards the cathode due to the applied electric field and turn into hydrogen gas. Negative ions from the acidic electrolyte (e.g. $X\text{-}O^-$ and $X\text{-}O^{2-}$) move towards the aluminum anode and convert the aluminum metal to a porous aluminum oxide film ([72], [73]). These reactions lead to the formation (Equation 2-5) and dissolution (Equation 2-6) of aluminum oxide [73]:

$$2\ Al^{3+} + 3\ O^{2-} \rightarrow Al_2O_3 \tag{2-5}$$

$$Al_2O_3 + 6H^+ \rightarrow 2\ Al_3^+\ (aq) + 3\ H_2O \tag{2-6}$$

Figure 2.11 shows the two types of anodic aluminum oxide (AAO) films and the corresponding current density (j) as a function of time (t) graphs under potentiostatic conditions in which the applied potential (U) is constant. For barrier-type anodization, there is a limit on the obtainable thickness of the film as the current density (j) and the film growth rate decrease almost exponentially with time (t) and the thickness of the barrier-type film is directly proportional to the applied potential (U) [71]. For porous-type anodization, the current density initially decreases as a resistant oxide barrier layer grows. As oxidation of this layer continues, the oxide layer grows, and individual paths propagate through the oxide film along high-energy grain boundaries forming micro cracks [72]. The complete formation of the micro cracks causes a reduction in the resistance, and an increase in current density, followed by the breakdown of the barrier film. As the barrier film breaks down, the formation of a porous layer begins from the micro cracks. The current density reaches a local maximum followed by a slight decrease, then remains relatively constant due to an equilibrium between O^{2-} and OH^{-} integration into the oxide film and metal ion dissolution ([71], [72]).

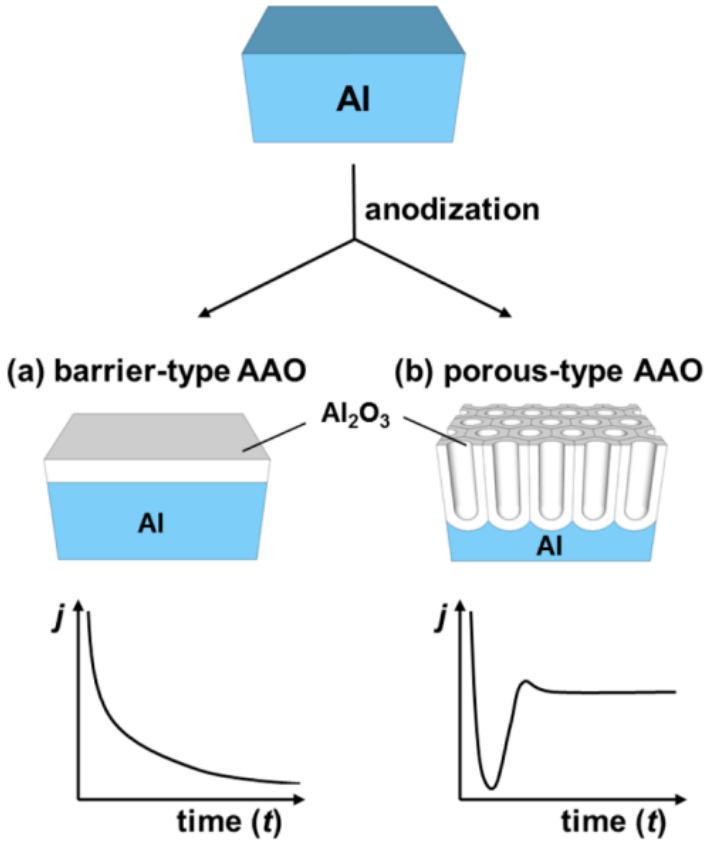


Figure 2.11. Barrier-type anodic aluminum oxide (AAO) film (a) and porous-type aluminum oxide film (b) and the corresponding current density (j) vs. time (t) graphs [71].

2.7. Protein Detection and Immobilization on Alumina Surfaces

Porous anodic alumina has many biomedical applications in recent years including drug delivery and release ([74], [75]), biosensing ([76], [77]) and tissue engineering [78]. Some biosensing applications involve detection of an immobilized protein on the porous anodic alumina surface [76]. In many cases, modifications are made to the porous anodic alumina surface such as coating with polymers, proteins, metals, or oxides, to improve the stability and biocompatibility of the surface [73]. Kumeria et al. (2012) used a gold-coated nanoporous anodic alumina immunosensor to detect cancer cells with concentrations between 1×10^3 and 1×10^5 cells/mL with a limit of detection of < 1000 cells/mL [79]. Rajeev et al. (2018) functionalized

nanoporous anodic alumina with 3-isocyanatopropyl triethoxy silane to detect tumor necrosis factor alpha with a limit of detection of 0.13 μg/mL [80]. Anodic aluminum oxide nanoporous membranes have been used to quantify parathyroid hormone-like hormone secretions from cultured human neuroblastoma and keratinocyte cell lines with limits of detection between 60 and 400 ng/mL [81]. Many other biosensor applications of anodic alumina have been demonstrated using optical and electrochemical sensing methods [82]. Alumina biosensor applications that use visual detection methods based on colour interference have also been demonstrated ([83], [84]). Micromolar sensitivity has been demonstrated for the detection of anti-prothrombin on a prothrombin coated alumina sensor, as a visible colour shift was detected after placing a 20 μL volume of 0.025 mg/mL anti-prothrombin (0.17 μM) on the alumina and prothrombin coated surface for 20 minutes [72].

In an aqueous environment, water chemisorption can occur at the aluminum surface by a reaction between an aluminum ion (Lewis acid) and a hydroxyl ion (Lewis base) [85]. The chemisorption of water leads to the formation of hydroxyl groups at the alumina surface which behave as Bronsted acid sites and act as a catalytic center of alumina [85]. Dehydration of two neighboring hydroxyl ions from the alumina surface leads to the formation of strained oxygen bridges which act as active Lewis acid sites which also act as a catalytic center of alumina [85].

Costa et al. (2016) conducted a review of the adsorption of amino acids and peptides on metal and oxide surfaces in an aqueous environment and found that adsorption often occurs by hydrogen bonding or by ligand exchange with a surface hydroxyl group ([86], [87]). Carboxyl groups have been shown to bind strongly to alumina surfaces [88]. The adsorption of carboxylic acids on alumina and other metal oxides is very strong due to their much higher adsorption energies compared to other organic compounds [85]. Kummert and Stumm (1980) explain the

adsorption of carboxyl groups to alumina surfaces based on the ligand exchange model, which suggests that anions of organic acids, such as carboxylic, phenolic-OH or amino groups, replace the surface hydroxyl groups of alumina [89]. Other models that have been proposed for carboxylic group binding to alumina include bridging ([90], [91]) and by the formation of esters with hydroxyl groups on the alumina surface [92].

Prothrombin is composed of 579 amino acids organized into four domains: the Gla domain (residues 1-46), kringle-1 (residues 65-143), kringle-2 (residues 170-248) and the protease domain (residues 285-579) and has a molecular weight of approximately 72,000 Da ([93], [94]). The total length of a bound prothrombin molecule is ~ 11 nm, composed of fragment 1 (3.8 nm), fragment 2 (3.0 nm) and thrombin (4.5 nm) [95]. The structure of prothrombin as well as the glutamic acid and post translational gamma-carboxyglutamic acid residues containing an available carboxyl group for immobilization on an alumina surface are shown in Figure 2.12 [72]:

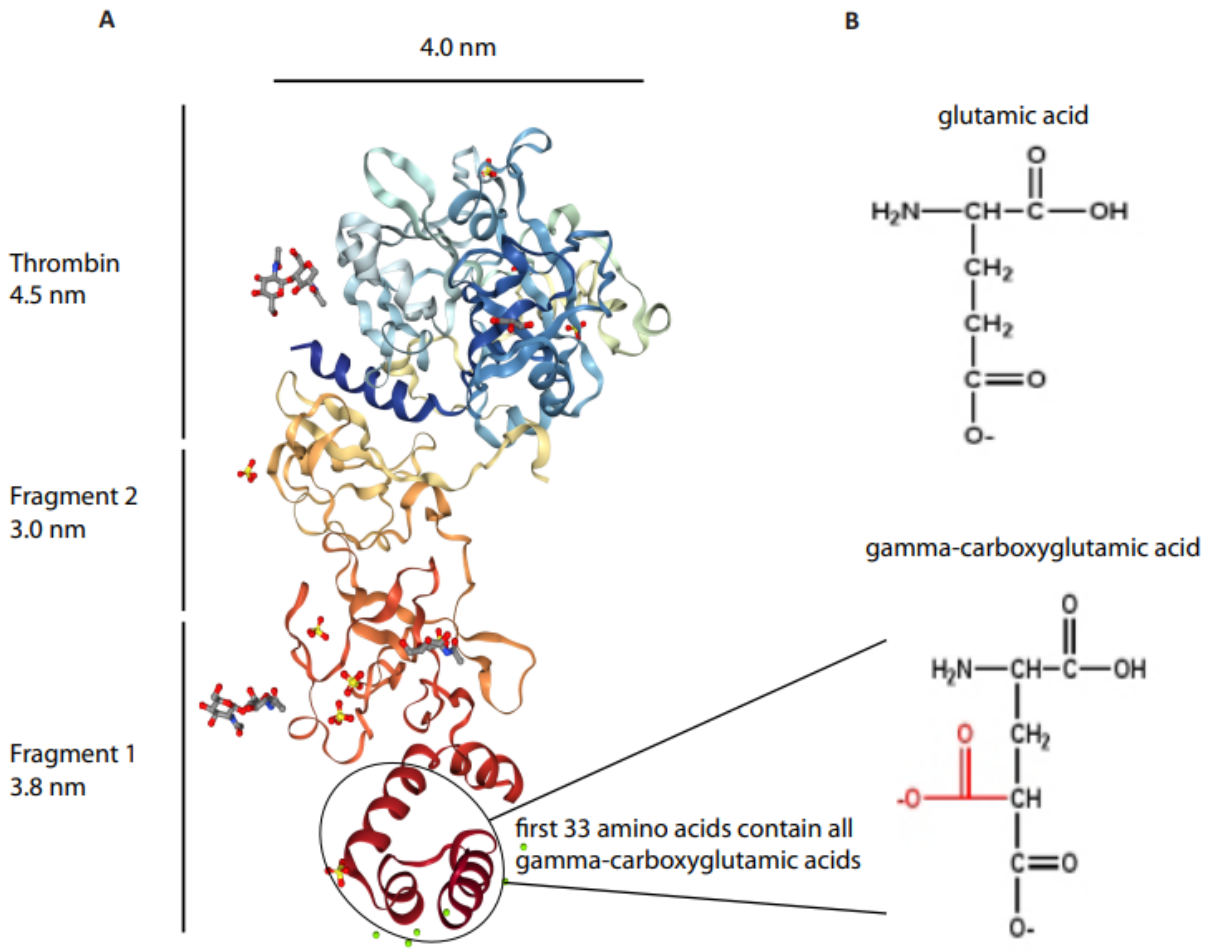


Figure 2.12. Structure of prothrombin ([96]) composed of the Gla domain (red), kringle-1 domain (orange), kringle-2 domain (yellow) and the protease domain (blue) with dimensions from Lim et al. ([95]) (A). Structures of glutamic acid and post translational gamma-carboxyglutamic acid residues with available carboxyl groups for immobilization on a positively charged alumina surface (B). Figure obtained from Sweet (2018) [72].

Vitamin K-dependent proteins, such as prothrombin, contain gamma-carboxyglutamic acid-rich (GLA) domains with a high density of anionic carboxyl groups, allowing them to securely bind to an alumina surface [97]. Prothrombin, also known as coagulation factor II, plays an important role in the blood coagulation cascade and contains ten carboxyglutamic acid

residues in the first 34 amino acids of fragment 1 [98]. These carboxyglutamic acid residues contain carboxyl groups that are available for binding to an alumina film. The ten residues concentrated in a small area on fragment 1 allow for strong binding in a consistent orientation leading to a consistent thickness of bound molecules allowing for detection by a visible colour shift ([72], [86]).

2.8. References

1. Alhajj, M. and A. Farhana, *Enzyme Linked Immunosorbent Assay*, in *StatPearls*. 2022: Treasure Island (FL).

2. ThermoFisher Scientific. *Overview of ELISA*. [cited 2022 March 16]; Available from: https://www.thermofisher.com/ca/en/home/life-science/protein-biology/protein-biology-learning-center/protein-biology-resource-library/pierce-protein-methods/overview-elisa.html.

3. Thiha, A. and F. Ibrahim, *A Colorimetric Enzyme-Linked Immunosorbent Assay (ELISA) Detection Platform for a Point-of-Care Dengue Detection System on a Lab-on-Compact-Disc.* Sensors (Basel), 2015. **15**(5): p. 11431-41.

4. Price, C.P., *Point of care testing.* BMJ, 2001. **322**(7297): p. 1285-8.

5. Vashist, S.K., *Point-of-Care Diagnostics: Recent Advances and Trends.* Biosensors (Basel), 2017. **7**(4).

6. Koczula, K.M. and A. Gallotta, *Lateral flow assays.* Essays Biochem, 2016. **60**(1): p. 111-20.

7. Andryukov, B.G., *Six decades of lateral flow immunoassay: from determining metabolic markers to diagnosing COVID-19.* AIMS Microbiol, 2020. **6**(3): p. 280-304.

8. Chin, C.D., V. Linder, and S.K. Sia, *Commercialization of microfluidic point-of-care diagnostic devices.* LAB ON A CHIP, 2012. **12**(12): p. 2118-2134.

9. Breitbach, A. *Milenia HybriDetect – A Universal Lateral Flow Development Platform*. 2021 [cited 2022 March 16]; Available from: https://www.milenia-biotec.com/en/universal-lateral-flow-development-tool/.

10. Nsamela, A. *Microfluidics for point of care diagnostic devices: a review*. 2020 [cited 2022 March 16]; Available from: https://www.elveflow.com/microfluidic-

reviews/general-microfluidics/microfluidics-for-point-of-care-diagnostic-devices-a-review/.

11. Mejia-Salazar, J.R., et al., *Microfluidic Point-of-Care Devices: New Trends and Future Prospects for eHealth Diagnostics.* Sensors (Basel), 2020. **20**(7).

12. Campbell, J.M., et al., *Microfluidic and Paper-Based Devices for Disease Detection and Diagnostic Research.* Int J Mol Sci, 2018. **19**(9).

13. Arshavsky-Graham, S. and E. Segal, *Lab-on-a-Chip Devices for Point-of-Care Medical Diagnostics*. Springer Berlin Heidelberg: Berlin, Heidelberg. p. 1-19.

14. Medical Design Briefs. *Biosensors: Bringing Diagnosis to the Point of Care*. 2019 March 16, 2022; Available from: https://www.medicaldesignbriefs.com/component/content/article/mdb/features/articles/33568.

15. Thoren, K. *The Role of Surface Plasmon Resonance in Clinical Laboratories*. 2019 [cited 2022 March 16]; Available from: https://www.aacc.org/cln/articles/2019/may/the-role-of-surface-plasmon-resonance-in-clinical-laboratories.

16. Ng, E., et al., *Magneto-nanosensor smartphone platform for the detection of HIV and leukocytosis at point-of-care.* Nanomedicine, 2019. **16**: p. 10-19.

17. Li, D. and M.M. Mielke, *An Update on Blood-Based Markers of Alzheimer's Disease Using the SiMoA Platform.* Neurol Ther, 2019. **8**(Suppl 2): p. 73-82.

18. Malecka, K., D. Pankratov, and E.E. Ferapontova, *Femtomolar electroanalysis of a breast cancer biomarker HER-2/neu protein in human serum by the cellulase-linked sandwich assay on magnetic beads.* Analytica Chimica Acta, 2019. **1077**: p. 140-149.

19. HyperPhysics. *Oil Film Interference*. [cited 2022 March 16]; Available from: http://hyperphysics.phy-astr.gsu.edu/hbase/phyopt/oilfilm.html.

20. Physics World. *Rainbow on the oil*. [cited 2022 March 16]; Available from: http://www.hk-phy.org/iq/oil_rainbow/oil_rainbow_e.html.

21. Lumen. *Thin Film Interference*. [cited 2022 March 16]; Available from: https://courses.lumenlearning.com/physics/chapter/27-7-thin-film-interference/.

22. National Aeronautics and Space Administration Science Mission Directorate. *Visible Light*. 2010 [cited 2022 March 16]; Available from: http://science.nasa.gov/ems/09_visiblelight.

23. Frey, H., *Cathode Sputtering*, in *Handbook of Thin-Film Technology*, H. Frey and H.R. Khan, Editors. 2015, Springer Berlin Heidelberg: Berlin, Heidelberg. p. 133-165.

24. Macagno, V. and J.W. Schultze, *The growth and properties of thin oxide layers on tantalum electrodes.* Journal of Electroanalytical Chemistry and Interfacial Electrochemistry, 1984. **180**(1): p. 157-170.

25. Charlesby, A. and J.J. Polling, *The Optical Properties of Thin Oxide Films on Tantalum.* Proceedings of the Royal Society of London. Series A, Mathematical and Physical Sciences, 1955. **227**(1171): p. 434-447.

26. Voros, J., *The density and refractive index of adsorbing protein layers.* Biophys J, 2004. **87**(1): p. 553-61.

27. Wypych, G., *Handbook of Fillers (3rd Edition)*. ChemTec Publishing.

28. Engineering ToolBox. *Refractive Index common Liquids, Solids and Gases*. 2008 [cited 2022 April 4]; Available from: https://www.engineeringtoolbox.com/refractive-index-d_1264.html.

29. Ono, S. and N. Masuko, *Evaluation of pore diameter of anodic porous films formed on aluminum.* Surface and Coatings Technology, 2003. **169-170**: p. 139-142.

30. Open Learn. *Interference Colours*. [cited 2022 March 16]; Available from: https://www.open.edu/openlearn/science-maths-technology/introduction-minerals-and-rocks-under-the-microscope/content-section-2.2.5.

31. LEC Expert. *White and LEDs binning*. 2015 [cited 2022 March 16]; Available from: https://www.lec-expert.com/topics/white-and-leds-binning.

32. Sandström, T., M. Stenberg, and H. Nygren, *Visual detection of organic monomolecular films by interference colors.* Applied Optics, 1985. **24**(4): p. 472-479.

33. Shashi Menon, E., *Chapter Five - Fluid Flow in Pipes*, in *Transmission Pipeline Calculations and Simulations Manual*, E. Shashi Menon, Editor. 2015, Gulf Professional Publishing: Boston. p. 149-234.

34. The Editors of Encyclopaedia Britannica. *"laminar flow"*. 2018 [cited 2022 March 16]; Available from: https://www.britannica.com/science/laminar-flow.

35. Engineering ToolBox. *Laminar, Transitional and Turbulent Flow*. 2004 [cited 2022 March 16]; Available from: https://www.engineeringtoolbox.com/laminar-transitional-turbulent-flow-d_577.html.

36. The Editors of Encyclopaedia Britannica. *"turbulent flow"*. 2020 [cited 2022 March 16]; Available from: https://www.britannica.com/science/turbulent-flow

37. SU2. *Transitional Flat Plate*. 2020 [cited 2022 March 16]; Available from: https://su2code.github.io/tutorials/Transitional_Flat_Plate/

38. The Pillars Curriculum. *ITP: Laminar vs Turbulent*. 2008 [cited 2022 March 16]; Available from: http://pillars.che.pitt.edu/student/slide.cgi?course_id=10&slide_id=14.0

39. Kumar, S.S., et al., *Three dimensional flow motions in the viscous sublayer.* Theoretical and Applied Mechanics Letters, 2021. **11**(2): p. 100239.

40. Rapp, B.E., *Chapter 9 - Fluids*, in *Microfluidics: Modelling, Mechanics and Mathematics*, B.E. Rapp, Editor. 2017, Elsevier: Oxford. p. 243-263.

41. Cebeci, T., *Chapter 4 - General Behavior of Turbulent Boundary Layers*, in *Analysis of Turbulent Flows with Computer Programs (Third Edition)*, T. Cebeci, Editor. 2013, Butterworth-Heinemann: Oxford. p. 89-153.

42. Pokrić, B. and Z. Pučar, *The two-cross immunodiffusion technique: Diffusion coefficients and precipitating titers of IgG in human serum and rabbit serum antibodies.* Analytical Biochemistry, 1979. **93**: p. 103-114.

43. Çengel, Y.A. and J.M. Cimbala, *Fluid Mechanics: Fundamentals and Applications*. 1st ed. 2006, New York: McGraw-Hill.

44. Norstone Inc. *Four Main Types of Mixing Blades and Dispersing Impellers*. [cited 2022 March 16]; Available from: https://www.norstoneinc.com/four-main-types-of-mixing-blades-and-dispersing-impellers/#:~:text=There%20are%20four%20main%20impeller,propeller%20blade%2C%20or%20radial%20blade.

45. CFM. *ELTA Axial Airfoil Impellers 16-A150P05*. 2022 [cited 2022 March 16]; Available from: https://select.cfmfans.com/catalog/axial-impellers/elta-axial-airfoil-impellers/16-A150P05.

46. Caframo LabSolutions. *4 Blade Pitched Only*. 2022 [cited 2022 March 16]; Available from: https://www.caframolabsolutions.com/products/impellers-shafts/pitched-turbine-a561/.

47. Mixer Direct. *3 Blade Propeller, LH, Sq, 3" Dia, 3/4" Bore*. 2022 [cited 2022 March 16]; Available from: https://www.mixerdirect.com/products/3-blade-propeller-lh-sq-3-dia-3-4-bore.

48. Indco. *6" Dia. 4-Blade Radial Flow Turbine - Mill Finish*. 2021 [cited 2022 March 16]; Available from: https://www.indco.com/shop/product/rti-6/6-dia-4-blade-radial-flow-turbine-mill-finish.

49. Mirro, R. and K. Voll. *Which Impeller Is Right for Your Cell Line?* 2009 [cited 2022 March 16]; Available from: https://bioprocessintl.com/analytical/cell-line-

development/which-impeller-is-right-for-your-cell-line-183538/#:~:text=The%20blades%20on%20pitched%2Dblade,of%20unidirectional%20marine%20blade%20impellers.

50. Rewatkar, V.B. and J.B. Joshi, *EFFECT OF IMPELLER DESIGN ON LIQUID PHASE MIXING IN MECHANICALLY AGITATED REACTORS.* Chemical Engineering Communications, 1991. **102**(1): p. 1-33.

51. Li, X., et al., *Numerical optimization for blades of Intermig impeller in solid–liquid stirred tank.* Chinese Journal of Chemical Engineering, 2021. **29**: p. 57-66.

52. Boonkanokwong, V., et al., *The effect of the number of impeller blades on granular flow in a bladed mixer.* Powder Technology, 2016. **302**: p. 333-349.

53. Djerroud, M., G. Dituba Ngoma, and W. Ghie, *Numerical Identification of Key Design Parameters Enhancing the Centrifugal Pump Performance: Impeller, Impeller-Volute, and Impeller-Diffuser.* ISRN Mechanical Engineering, 2011. **2011**: p. 794341.

54. Doran, P.M., *Chapter 7 - Fluid Flow*, in *Bioprocess Engineering Principles (Second Edition)*, P.M. Doran, Editor. 2013, Academic Press: London. p. 201-254.

55. *Airlift Bioreactors: Hydrodynamics and Rheology Application to Secondary Metabolites Production*. 2013, IntechOpen 2013-07-24.

56. Wang, S.-J. and J.-J. Zhong, *Chapter 6 - Bioreactor Engineering*, in *Bioprocessing for Value-Added Products from Renewable Resources*, S.-T. Yang, Editor. 2007, Elsevier: Amsterdam. p. 131-161.

57. Doran, P.M., *Chapter 14 - Reactor Engineering*, in *Bioprocess Engineering Principles (Second Edition)*, P.M. Doran, Editor. 2013, Academic Press: London. p. 761-852.

58. Zhu, Y., *Chapter 14 - Immobilized Cell Fermentation for Production of Chemicals and Fuels*, in *Bioprocessing for Value-Added Products from Renewable Resources*, S.-T. Yang, Editor. 2007, Elsevier: Amsterdam. p. 373-396.

59. Chisti, Y. and M. Moo-Young, *Bioreactors*, in *Encyclopedia of Physical Science and Technology (Third Edition)*, R.A. Meyers, Editor. 2003, Academic Press: New York. p. 247-271.

60. de Jesus, S.S., et al., *Influence of impeller type on hydrodynamics and gas-liquid mass-transfer in stirred airlift bioreactor.* AIChE Journal, 2015. **61**(10): p. 3159-3171.

61. Khan, S., M. Siddiqui, and K. Osama, *Bioreactors for Hairy Roots Culture: A Review.* 2019.

62. Luo, H.-P. and M.H. Al-Dahhan, *Local characteristics of hydrodynamics in draft tube airlift bioreactor.* Chemical Engineering Science, 2008. **63**(11): p. 3057-3068.

63. Kim, T.D., et al., *Thermal behavior of proteins: Heat-resistant proteins and their heat-induced secondary structural changes.* Biochemistry, 2000. **39**(48): p. 14839-14846.

64. BioReactor Sciences. *Airlift (AL) Bioreactor Systems*. [cited 2022 May 13]; Available from: https://www.bioreactorsciences.com/air-lift-bioreactor-system#:~:text=AirLift%20(or%20GasLift)%20bioreactors%20are,as%20animal%20and%20plant%20cells.

65. Molina Grima, E., Y. Chisti, and M. Moo-Young, *Characterization of shear rates in airlift bioreactors for animal cell culture.* Journal of Biotechnology, 1997. **54**(3): p. 195-210.

66. Mehmia, M.R., et al., *Design and operational aspects of airlift bioreactors for petroleum biodesulfurization.* ENVIRONMENTAL PROGRESS, 2004. **23**(3): p. 206-214.

67. Lübbert, A., *Bubble Columns and Airlift Bioreactors*, in *Encyclopedia of Life Support Systems (EOLSS)*. 2017.

68. Colombet, D., et al., *Experiments and modelling of a draft tube airlift reactor operated at high gas throughputs.* Chemical Engineering Science, 2013. **104**: p. 32-43.

69. Aluminum Anodizers Council. *What is Anodizing?* [cited 2022 March 16]; Available from: https://www.anodizing.org/general/custom.asp?page=what-is-anodizing.

70. Mohamed, A.K., *Growth Mechanism of Porous Anodic Films Formed on Aluminium in Sulphuric Acid*, in *Faculty of Engineering and Physical Sciences* 2010, University of Manchester.

71. Lee, W. and S.-J. Park, *Porous Anodic Aluminum Oxide: Anodization and Templated Synthesis of Functional Nanostructures.* Chemical Reviews, 2014. **114**(15): p. 7487-7556.

72. Sweet, H.M., *Development of a Nanostructured Thin Film Device and Optics System for Protein Detection*, in *Materials Engineering*. 2018, University of Alberta.

73. Aramesh, M. and J. Cervenka, *Surface Modification of Porous Anodic Alumina for Medical and Biological Applications*. 2014. p. 439-467.

74. Kapruwan, P., J. Ferré-Borrull, and L.F. Marsal, *Nanoporous Anodic Alumina Platforms for Drug Delivery Applications: Recent Advances and Perspective.* Advanced Materials Interfaces, 2020. **7**(22): p. 2001133.

75. Porta-i-Batalla, M., et al., *3D Nanoporous Anodic Alumina Structures for Sustained Drug Release.* Nanomaterials, 2017. **7**(8): p. 227.

76. Santos, A., et al., *Photoluminescent Enzymatic Sensor Based on Nanoporous Anodic Alumina.* ACS Applied Materials & Interfaces, 2012. **4**(7): p. 3584-3588.

77. Pol, L., et al., *Real-Time Monitoring of Biotinylated Molecules Detection Dynamics in Nanoporous Anodic Alumina for Bio-Sensing.* Nanomaterials, 2019. **9**(3): p. 478.

78. Davoodi, E., et al., *Nano-porous anodic alumina: fundamentals and applications in tissue engineering.* Journal of Materials Science: Materials in Medicine, 2020. **31**(7): p. 60.

79. Kumeria, T., et al., *Label-free reflectometric interference microchip biosensor based on nanoporous alumina for detection of circulating tumour cells.* Biosens Bioelectron, 2012. **35**(1): p. 167-173.

80. Rajeev, G., et al., *A label-free optical biosensor based on nanoporous anodic alumina for tumour necrosis factor-alpha detection in chronic wounds.* Sensors and Actuators, B: Chemical, 2018. **257**: p. 116-123.

81. de la Escosura-Muñiz, A., et al., *In situ monitoring of PTHLH secretion in neuroblastoma cells cultured onto nanoporous membranes.* Biosensors and Bioelectronics, 2018. **107**: p. 62-68.

82. Amouzadeh Tabrizi, M., J. Ferre-Borrull, and L.F. Marsal, *Advances in Optical Biosensors and Sensors Using Nanoporous Anodic Alumina.* Sensors (Basel), 2020. **20**(18).

83. Liu, Y., et al., *A colorimetric sensor based on anodized aluminum oxide (AAO) substrate for the detection of nitroaromatics.* Sensors and Actuators B: Chemical, 2011. **160**(1): p. 1149-1158.

84. Ayas, S., et al., *Colorimetric detection of ultrathin dielectrics on strong interference coatings.* Optics Letters, 2018. **43**(6): p. 1379-1382.

85. Kasprzyk-Hordern, B., *Chemistry of alumina, reactions in aqueous solution and its application in water treatment.* Adv Colloid Interface Sci, 2004. **110**(1-2): p. 19-48.

86. Nickel, M.R., *Physical and Optical Characterization of Anodized Aluminum-Tantalum Thin Films for use in Thin Film Diagnostics*, in *Materials Engineering*. 2018, University of Alberta.

87. Costa, D., L. Savio, and C.M. Pradier, *Adsorption of Amino Acids and Peptides on Metal and Oxide Surfaces in Water Environment: A Synthetic and Prospective Review.* The Journal of Physical Chemistry B, 2016. **120**(29): p. 7039-7052.

88. van den Brand, J., et al., *Interaction of Anhydride and Carboxylic Acid Compounds with Aluminum Oxide Surfaces Studied Using Infrared Reflection Absorption Spectroscopy.* Langmuir, 2004. **20**(15): p. 6308-6317.

89. Kummert, R. and W. Stumm, *The surface complexation of organic acids on hydrous γ-Al2O3.* Journal of Colloid And Interface Science, 1980. **75**(2): p. 373-385.

90. Evans, H.E. and W.H. Weinberg, *A comparison of the vibrational structures of ethanol, acetic acid, and acetaldehyde adsorbed on alumina.* The Journal of Chemical Physics, 1979. **71**(12): p. 4789-4798.

91. Barron, A.R., *The interaction of carboxylic acids with aluminium oxides: journeying from a basic understanding of alumina nanoparticles to water treatment for industrial and humanitarian applications.* DALTON TRANSACTIONS, 2014. **43**(22): p. 8127-8143.

92. Karaman, M.E., D.A. Antelmi, and R.M. Pashley, *The production of stable hydrophobic surfaces by the adsorption of hydrocarbon and fluorocarbon carboxylic acids onto alumina substrates.* Colloids and Surfaces A: Physicochemical and Engineering Aspects, 2001. **182**(1-3): p. 285-298.

93. Chinnaraj, M., et al., *Structure of prothrombin in the closed form reveals new details on the mechanism of activation.* Scientific Reports, 2018. **8**(1): p. 2945.

94. Austen, D.E.G., *29 - Clinical Biochemistry of Blood Coagulation*, in *Scientific Foundations of Biochemistry in Clinical Practice (Second Edition)*, D.L. Williams and V. Marks, Editors. 1994, Butterworth-Heinemann. p. 495-513.

95. Lim, T.K., V.A. Bloomfield, and G.L. Nelsestuen, *Structure of the prothrombin- and blood clotting factor X-membrane complexes.* Biochemistry, 1977. **16**(19): p. 4177-81.

96. Pozzi, N., Z. Chen, and E. Di Cera, *How the Linker Connecting the Two Kringles Influences Activation and Conformational Plasticity of Prothrombin.* J Biol Chem, 2016. **291**(12): p. 6071-82.

97. InterPro. *Gamma-carboxyglutamic acid-rich (GLA) domain*. [cited 2022 March 16]; Available from: https://www.ebi.ac.uk/interpro/entry/InterPro/IPR000294/.

98. Walz, D.A., D. Hewett-Emmett, and W.H. Seegers, *Amino Acid Sequence of Human Prothrombin Fragments 1 and 2.* Proceedings of the National Academy of Sciences of the United States of America, 1977. **74**(5): p. 1969-1972.

Chapter 3 – General Materials and Methods

3.1. Introduction

The diagnostic device functions based on a visible colour shift due to thin film interference on the multilayered surface. Thin layers of tantalum and aluminum were placed on the polycarbonate membranes, polymer discs, silicon wafers, porous quartz frits discs and the high purity tantalum discs using DC magnetron sputtering and were anodized to formulate the AAO thin films. Several materials were considered including polycarbonate membranes and Vero Clear resin polymer discs, but quartz frits were initially selected based on the low thermal expansion coefficient (TEC) and porosity. The rough surface of the quartz frits led to issues during anodization, and ultimately, high purity tantalum discs with either four or eight 1 mm holes and silicon wafers were chosen as the substrate materials. Membrane porosity is important to consider to ensure smooth flow through the device while maximizing exposure to the surface. The pores or holes should be large enough to obtain turbulent flow through the membrane, but they should be small enough to prevent fluid flow only through the pores in order to expose the entire surface to the fluid. Protein immobilization, adsorption and sensitivity were studied based on visible colour shifts after large volumes of fluid containing the protein of interest were passed over the membrane surface and interacted with the protein bound to the alumina surface. Analytical techniques were used to study various characteristics and optical properties of the surface including scanning electron microscopy (SEM) and ellipsometry. These techniques were also used to assess changes to the surface structure due to metal deposition and protein adsorption. Statistical analysis was completed. Standard operating procedures (SOPs) for the Bob Sputtering System, the Floyd Sputtering System and the Zeiss Sigma (Gemie) Field

Emission Scanning Electron Microscope (FESEM) with energy dispersive X-ray (EDX)/electron backscattered detector (EBSD) can be found in Appendix 1.

3.2. Membrane Selection

Several substrate types for the membrane were considered in the development of the diagnostic device. Membrane porosity must be high enough to allow fluid to pass through at an appropriate rate, but low enough to ensure enough time for the fluid elements to interact with and mix at the surface, allowing an antigen-antibody complex to form. Polycarbonate membranes, porous quartz frits discs with two different porosities, porous 3D-printed Vero Clear Resin discs, and porous, high purity tantalum discs were considered. Further, the selected material should adhere well to the deposited metal films to prevent the device from falling apart. Silicon wafers were used as a control, as this substrate has been previously studied in similar experiments ([1], [2]). Test grade silicon wafer substrates with a diameter of 100 mm were used in this work (University Wafer). Initially, 25 mm diameter Whatman ® Nucleopore Track-Etch Polycarbonate Membranes with a porosity of 5 μm (GE Healthcare Life Sciences) were tested, however, sputtering of tantalum and aluminum onto the polycarbonate membrane caused the membrane to curl and wrinkle. The wrinkling of the membrane was thought to be due to the mismatch in thermal expansion coefficient between polycarbonate and the sputtered metal, tantalum. Thermal expansion coefficient (TEC) is defined as a material property that indicates the extent a material expands upon heating [3]. The higher the thermal expansion coefficient, the more the material will expand when heated. Thermal expansion coefficient is an important factor to consider when selecting the membrane material as the material must undergo sputtering of tantalum and aluminum metal, which occurs at high temperatures. If the substrate material and the metal to be sputtered have a large difference in thermal expansion coefficient, the substrate may morph, curl

or wrinkle during sputtering, as occurred with the polycarbonate membrane shown in Figure 4.5 in Chapter 4 – The Effect of Sputtering and Anodization Parameters on Membrane Performance. The thermal expansion coefficients of several materials considered are shown in Table 3.1 [4]. The high thermal expansion coefficient of polycarbonate and the difference in thermal expansion coefficients between tantalum metal and polycarbonate helps explain why the membranes deformed during the high temperature sputtering process. Thermal expansion coefficients can also help explain why some materials may be more suitable for sputtering than others. Initially, quartz fritz was selected to be the filter material due to its low thermal expansion coefficient. After further consideration, tantalum metal itself and silicon wafers were chosen as the substrate materials.

Table 3.1. Linear thermal expansion coefficients of materials considered for filter membrane of device. Low TEC is ideal to prevent expansion during sputtering [4].

Material	**Thermal Expansion Coefficient**
Alumina	8.1
Al	21-24
Nylon	72-80
Polycarbonate	70
Polycarbonate glass fiber, reinforced	22
Glass	4-6
Tantalum	6.5
Porcelain	7
Quartz	0.7-1

Smooth surfaces generally provide better results when studying the optical properties of a surface. However, rough surfaces were of interest for this diagnostic device due to the larger surface area they provide. An increased surface area provides more area for the antigen and antibody to interact, possibly increasing the device sensitivity even further. Unpolished and polished porous quartz frits discs were analyzed. The unpolished quartz frits had a rough surface, limiting the ability to directly measure optical properties, but were of interest due to the larger surface area they provide. The unpolished quartz frits used were the Quartz Fritted Porous Discs from GM Quartz with a 25 mm diameter, 4 mm thickness and pore sizes of 16 – 40 μm (F) and 40 – 100 μm (M) [5]. Quartz Porous Glass Filter Discs from Micquartz were used for analysis of polished quartz frits [6]. The discs have an outer diameter of 25 – 27 mm, a thickness of 3 mm, and porosities of either 100 – 160 microns (G1) or 40 – 100 microns (G2). The material of the discs is high fused quartz (99.998% SiO_2) and the discs were fire polished prior to use.

The next membrane material considered was a 3D printed polymer (Vero Clear Resin) disc, as shown in Figure 3.1. The tab at the bottom of the disc was printed to ensure the entire disc could be submerged in electrolyte during anodization and was to be removed prior to use in the device. Membrane reinforcements, as shown in Figure 3.2, were also printed to support the disc while exposed to turbulent flow. To increase the turbulent flow at the membrane surface, Vero Clear Resin polymer impellers were also 3D printed and are shown in Figure 3.3. The Vero Clear Resin polymer impellers were used in the diagnostic device design to encourage mixing above the multilayer surface. The polymer membrane, membrane reinforcements, and impellers were drafted in Fusion 360 by Jacob Damant and 3D printed at the University of Alberta Engineering Garage.

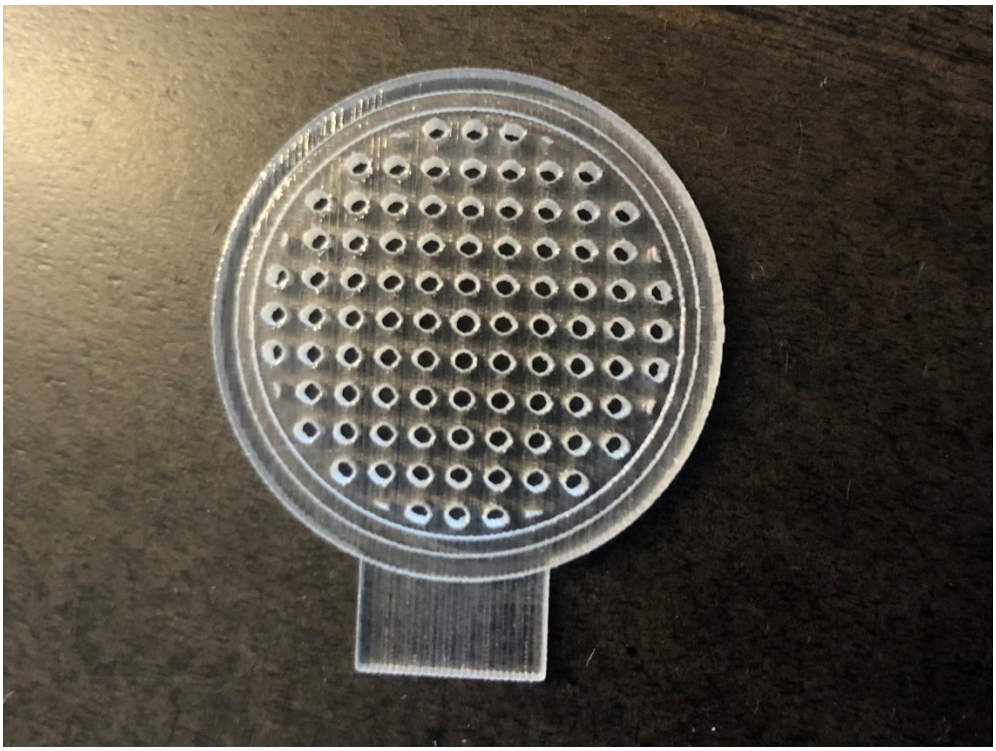


Figure 3.1. 3D printed Vero Clear resin polymer membrane disc.

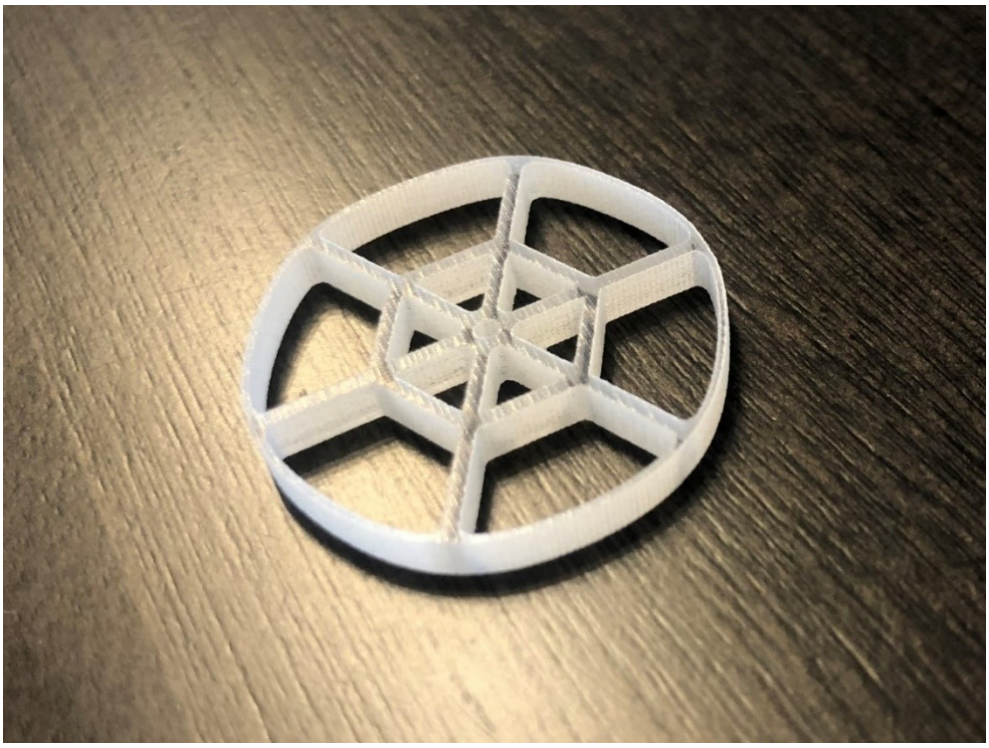


Figure 3.2. 3D printed Vero Clear resin polymer membrane reinforcement.

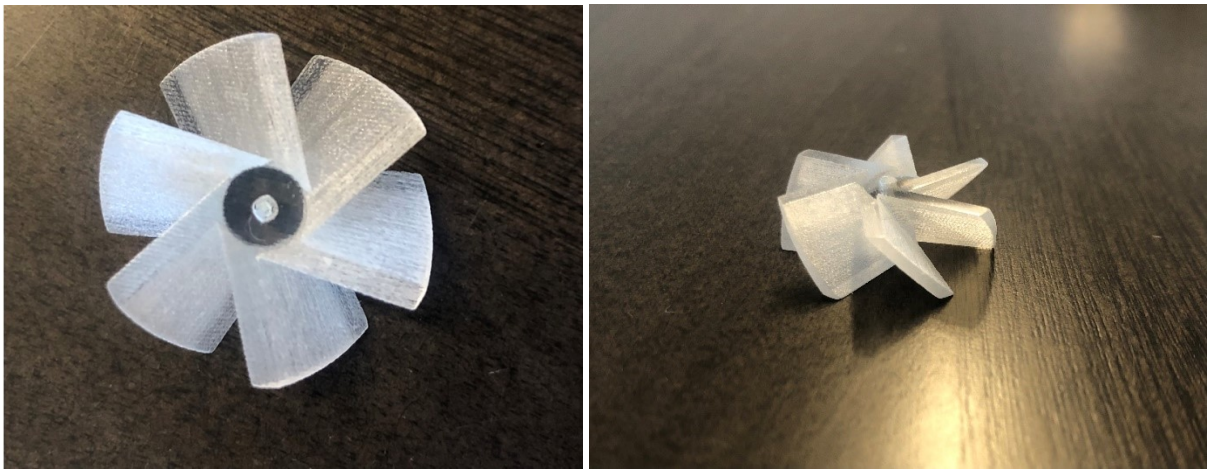


Figure 3.3. Top view and side view of the 3D printed Vero Clear resin polymer impeller to ensure turbulent flow and promote mixing of fluid elements at membrane surface.

Adhesion tests were conducted after sputtering ~ 200 nm of tantalum on to the polymer discs to investigate adherence of the tantalum metal layer to the polymer disc (see Section 4.3.1-Polymer-Tantalum Adhesion Test). Polymer discs were submerged in either 30% hydrogen peroxide, ACS or 2-propanol (isopropanol) HPLC grade for 1 hour prior to sputtering to remove residues from the surface. Even with these cleaning methods, adhesion between the polymer surface and the thin tantalum film was poor after sputtering. Due to the poor adhesion between the polymer and tantalum metal, other materials for the membrane were considered.

Tantalum discs were investigated for their use as a membrane material. High purity tantalum discs with a diameter of 26.6 mm were purchased from Stanford Advanced Materials. Tantalum discs with no holes, tantalum discs with five holes, and tantalum discs with nine holes were all purchased. The discs with no holes were used to study adhesion between the sputtered aluminum and tantalum disc surface as well as prothrombin-anti-prothrombin interactions on the sputtered surface. Discs with five holes and nine holes were to be used to study high volume flow through the discs. The center holes in both discs were to be used to attach the impeller and

had a diameter of 1.18 mm. Flow through four and eight 1 mm holes was to be investigated. Figure 3.4 details the design of the tantalum discs with five holes and nine holes.

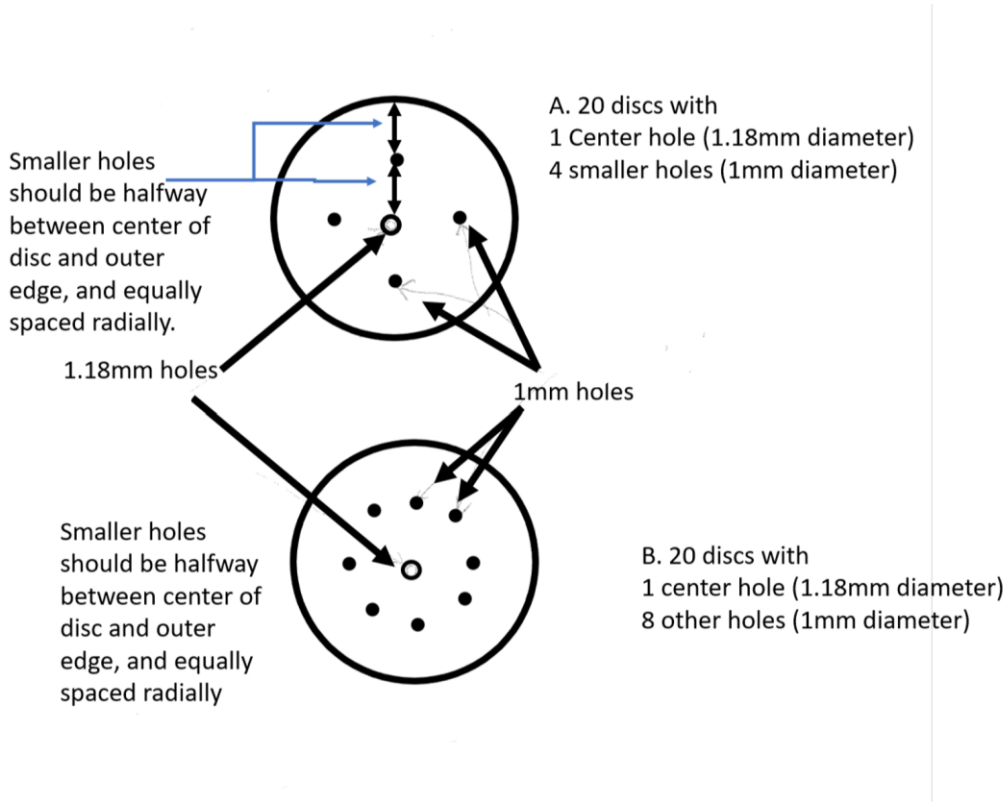


Figure 3.4. Five- and nine-hole tantalum disc design, detailing the hole sizes and spacing.

Tantalum metal discs were an ideal substrate as there would be no issue with mismatches in thermal expansion coefficient due to sputtering tantalum metal. As the discs were composed of tantalum, the tantalum sputtering step could potentially be skipped and the discs could be sputtered with only aluminum and then anodized. Experiments were conducted on the tantalum discs in which only ~ 110 nm of aluminum was sputtered, and in which ~ 200 nm of tantalum and ~ 110 nm of aluminum were sputtered onto the surface to determine which method produced better results. Sputtering the tantalum layer onto the high purity tantalum disc prior to the aluminum layer produced better results during anodization as the sputtered tantalum formed the

dielectric layer, rather than the tantalum disc. Therefore ~ 200 nm of tantalum was sputtered on to the discs prior to sputtering aluminum in the protein adsorption and diagnostic device applications. Several methods were used to clean the tantalum discs prior to sputtering tantalum and aluminum. One method involved submerging the discs in acetone for one hour to clean off any organic residues from the surface. Adhesion issues occurred and another cleaning method was attempted. Tantalum discs were placed in the oven and ran through a self-cleaning oven cycle at 700 °F to clean the surface and remove organics. The self-cleaning oven cycle provided much better results for adhesion of the tantalum film and produced a smoother surface after anodization. The self-cleaning oven cleaning method was used to clean the discs for the rest of the work. Figure 3.5 shows the high purity tantalum discs prior to cleaning and sputtering with no holes (left), five holes (middle), and nine holes (right).

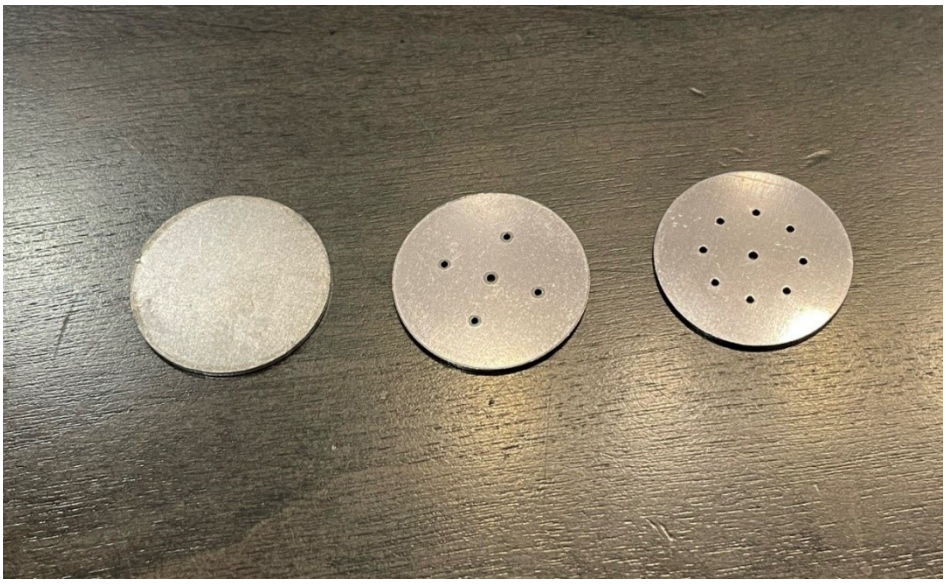


Figure 3.5. Tantalum disc with a 26.6 mm diameter and no holes (left). Tantalum disc with a 26.6 mm diameter and one 1.18 mm hole for impeller attachment and four 1 mm holes to allow fluid flow through the disc (middle). Tantalum disc with a 26.6 mm diameter and one 1.18 mm hole for impeller attachment and eight 1 mm holes to allow fluid flow through the disc (right).

3.3. Device Design

Two device designs were considered to improve the sensitivity by using larger fluid volumes. One of the designs was a stirred tank consisting of a 1 L beaker filled with 500 mL of fluid, with an impeller submerged just beneath the surface of the fluid. The impeller was connected to a Tech II Railmaster 2400 that provides power. The substrate material coated with the thin films of tantalum, anodic aluminum oxide, and prothrombin was placed in the bottom of the beaker and the Tech II Railmaster 2400 was turned on to spin the impeller and encourage mixing above the surface of the substrate. Figure 3.6 shows the design of the stirred tank set up.

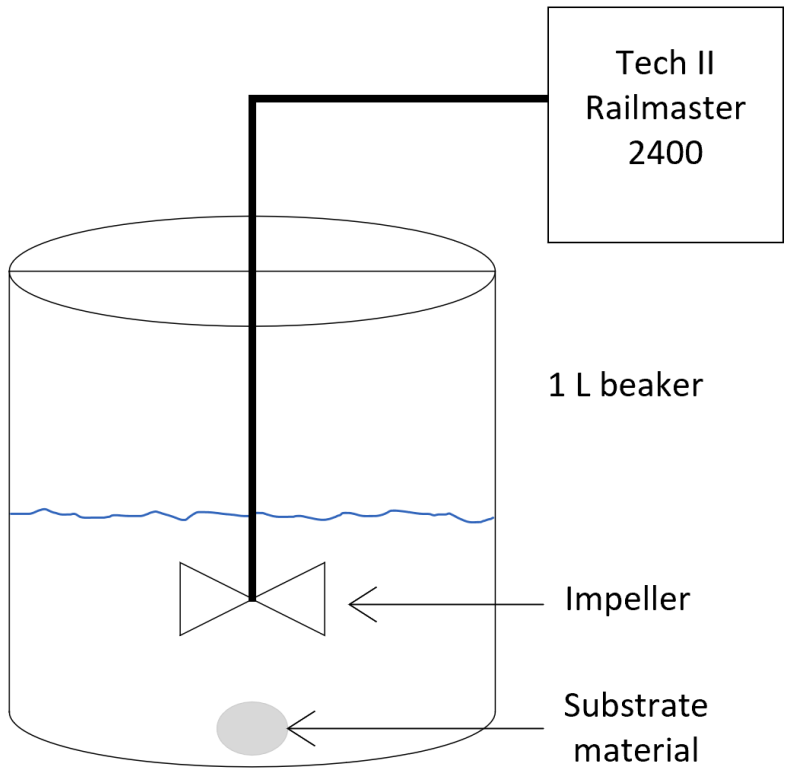


Figure 3.6. Diagnostic device stirred tank design.

The other device design involved using a syringe to increase fluid velocity and achieve turbulent flow at the surface of the membrane. The syringe was connected to a filter that is

designed so that the fluid sample being pushed through the syringe will contact the outer side of the impeller as shown in Figure 3.7. The high velocity fluid should cause the impeller to spin, encouraging mixing of fluid elements just above the coated membrane with the adsorbed prothrombin layer, as shown in Figure 3.8. Together, the high velocity and the impeller should promote mixing and turbulent flow at the membrane surface, maximizing the exposure of fluid elements to the coated surface prior to passing through the pores. Since the concentration of anti-prothrombin in the fluid sample is very low, mixing at the surface is important to increase the likelihood of binding between prothrombin and anti-prothrombin on the surface.

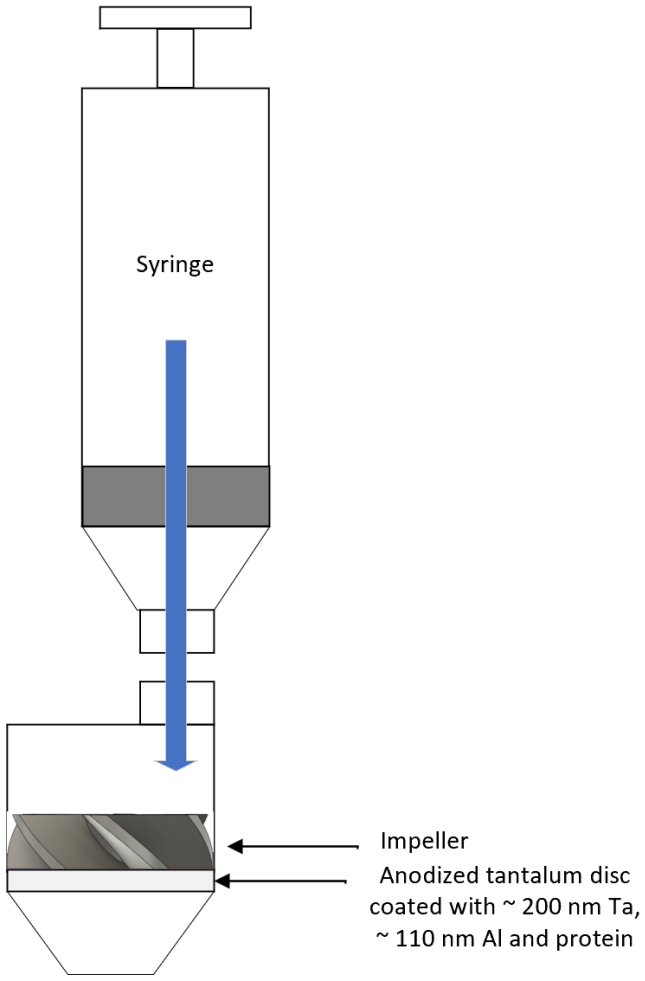


Figure 3.7. Diagnostic device syringe/filter design.

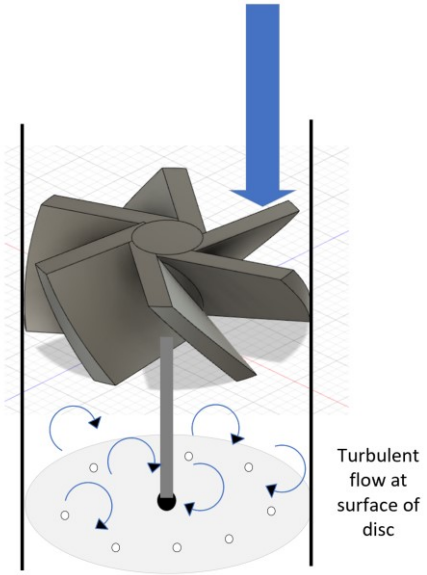


Figure 3.8. Fluid flow arrows between the impeller and the tantalum disc in the diagnostic device syringe/filter design. The space between the impeller and the tantalum disc is exaggerated in this drawing to show the mixing above the surface induced by the impeller.

3.4. Sputtering

Thin films of tantalum and aluminum were deposited onto silicon wafers, 3 mm thick porous, polished quartz frits discs, 4 mm thick porous, unpolished quartz frits discs and 26.6 mm diameter high purity tantalum discs for analysis. Sputtering was conducted at the University of Alberta nanoFAB facility. Sputtering System #1 (Bob) was used to deposit ~ 200 nm of tantalum onto the substrate. Sputtering System #3 (Floyd) was used to deposit ~ 110 nm of aluminum onto the substrate. Both Bob and Floyd are planar DC magnetron sputtering systems. The Bob system is manually operated, and the Floyd system is computer controlled. The aluminum and tantalum sputtering targets used had diameters of 7.62 cm (3") and purities of 99.9995% and 99.95% (Angstrom Engineering), respectively (Kurt J. Lesker Company, Jefferson Hills, PA). In order to sputter the quartz frits discs, quartz frits disc holsters were designed using Fusion 360, 3D printed, and epoxy glued (JB Weld, ClearWeld Quick Setting Epoxy) to silicon wafers. Each

silicon wafer held four quartz frits discs. The holders are composed of a plastic material and were 3D printed using the Stratasys J750 3D printer, then glued to the silicon wafer using epoxy glue. Appendix 2 shows the quartz frits disc holder and design, and Figure 3.9 displays the empty holders, the holders containing quartz frits before sputtering, and the holders containing quartz frits after sputtering tantalum and aluminum.



Figure 3.9. 3D printed quartz frits disc holsters epoxy glued to silicon wafers. Empty (top left), holding quartz frits discs prior to sputtering (top right), holding quartz frits discs after sputtering tantalum using the Bob sputtering system (bottom left) and holding quartz frits discs after sputtering aluminum (on top of tantalum layer) using the Floyd sputtering system (bottom right).

The Bob sputtering system, a sputter-up planar DC magnetron sputtering system, was used to deposit a thin layer (~ 200 nm) of tantalum onto the polycarbonate membranes, polymer discs, quartz frits, tantalum discs and silicon wafers. The tantalum target was loaded into Gun 1 and a base pressure of 2×10^{-6} Torr was achieved. The cryopump was opened to allow argon gas to enter the chamber until a working pressure of 7 mTorr was reached. Power was supplied at 300 W and a voltage of ~ 330 – 340 V was reached. Substrates were rotated at 20 RPM with a working distance of 12 cm. Tantalum was sputtered onto the substrate for 25 minutes with the goal of attaining a ~ 200 nm thick film, with a deposition rate of ~ 8 nm/min. Substrates were secured in place using small clips. The Bob sputtering system is shown in Figure 3.10 and the substrate placement is shown in Figure 3.11. The Bob sputtering system SOP can be found in Appendix 1.

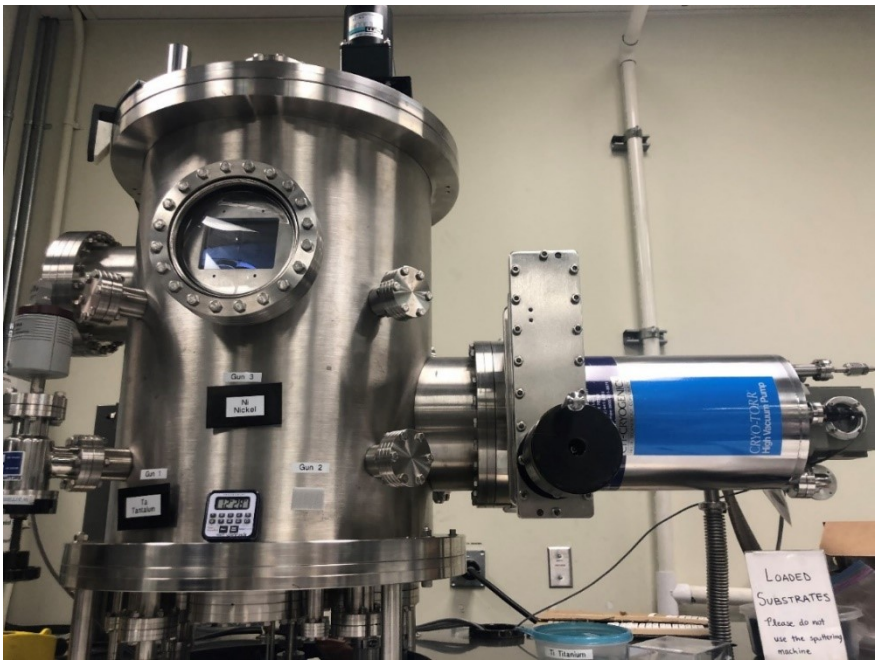


Figure 3.10. The planar magnetron sputtering system (Bob) at the University of Alberta nanoFAB used to deposit ~ 200 nm of tantalum on to polycarbonate membranes, polymer discs, silicon wafers, quartz frits and tantalum discs.

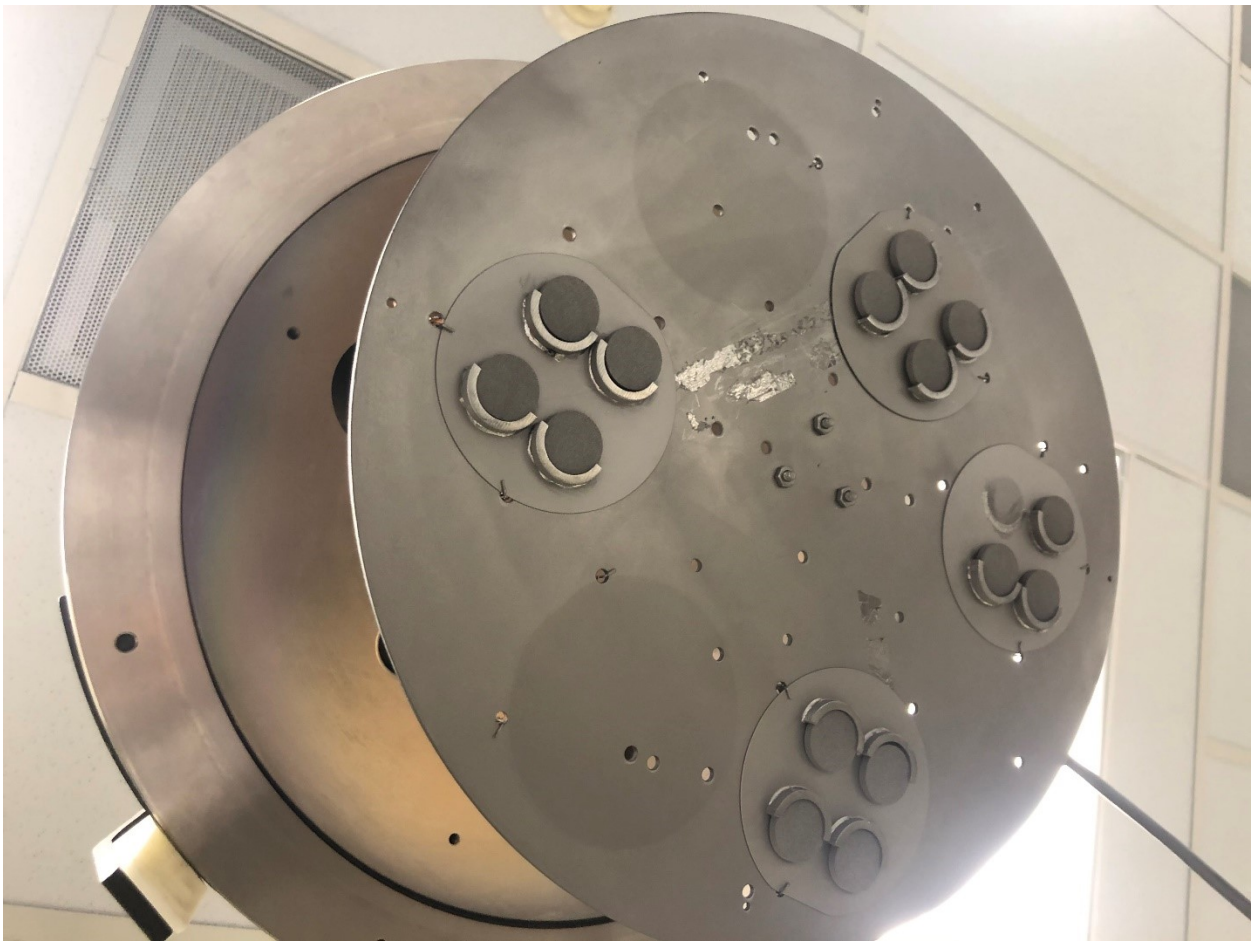


Figure 3.11. The Bob sputtering system at the University of Alberta nanoFAB, loaded, after sputtering. The silicon wafers are secured using clips and the quartz frits discs are held in place using the substrate holders.

The Floyd system, a sputter-down planar DC magnetron sputtering system, was used to deposit a thin layer (~ 110 nm) of aluminum on top of the tantalum layer on the silicon wafers, tantalum discs and quartz frits. The Floyd system is controlled using the eKLipse software (Kurt J. Lesker Company). Substrates were rotated at 20 RPM with a working distance of 12.5 cm. The tantalum coated quartz frits held by the silicon wafers were placed into the load-lock chamber containing six shelves. A base pressure of 10^{-7} Torr was reached and the cryopump was opened to allow argon gas to enter the chamber until a working pressure of 7 mTorr was reached. The

default burn-in time of 30 s was used, followed by a deposition time between 550 and 750 s with the goal of depositing ~ 110 nm of aluminum, depending on the current deposition rate. The aluminum deposition rate of the Floyd sputtering system varied over time depending on target usage. The Floyd sputtering system is shown in Figure 3.12 and the six-shelf load-lock chamber is shown in Figure 3.13. Figure 3.14 displays the eKLipse software from which the Floyd sputtering system is controlled. The Floyd sputtering system SOP can be found in Appendix 1.

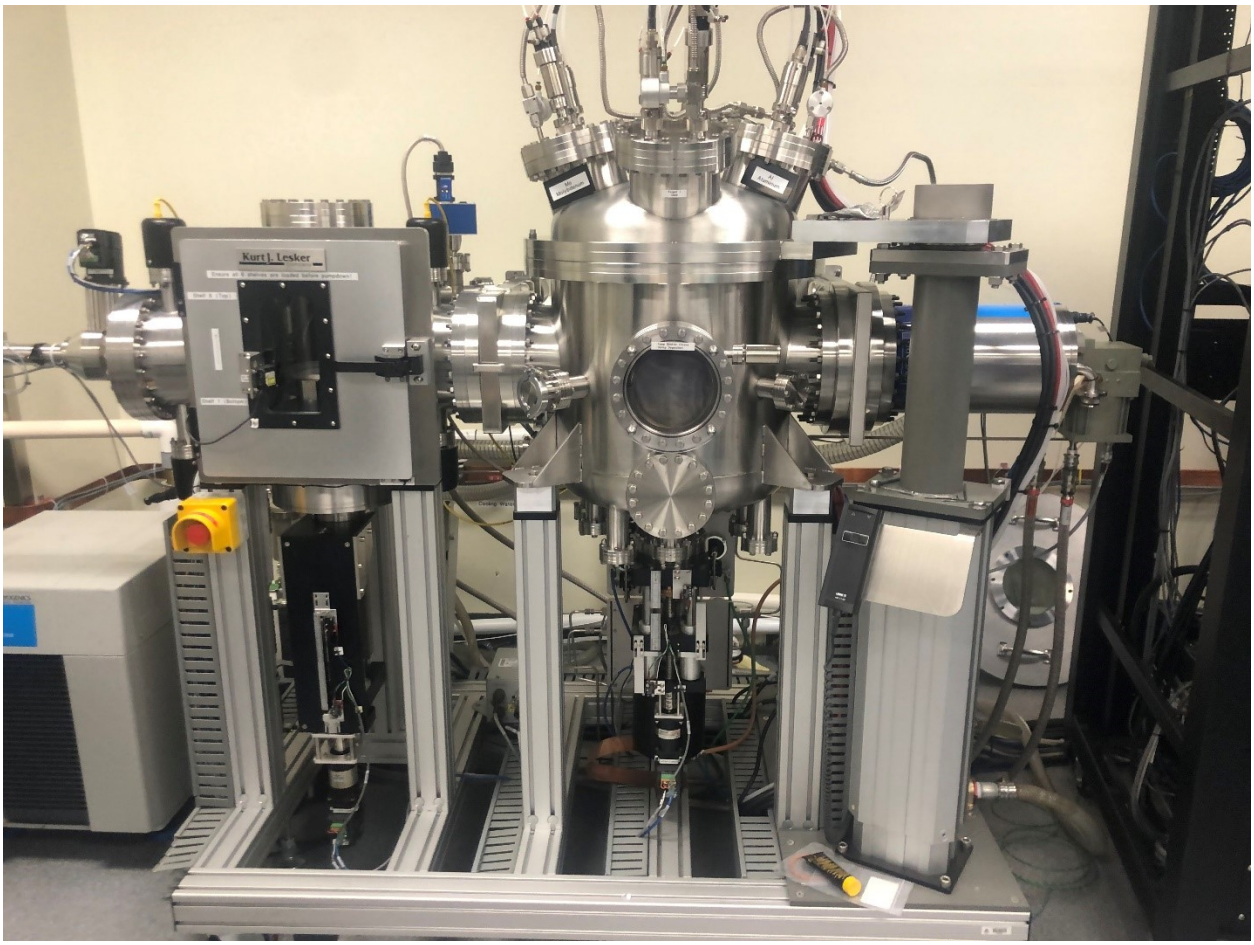


Figure 3.12. The planar magnetron sputtering system (Floyd) at the University of Alberta nanoFAB used to deposit ~ 110 nm of aluminum on to the tantalum-coated silicon wafers, tantalum discs and quartz frits.



Figure 3.13. The six-shelf plate holder that holds the substrates and is loaded into the Floyd sputtering system's load lock chamber.

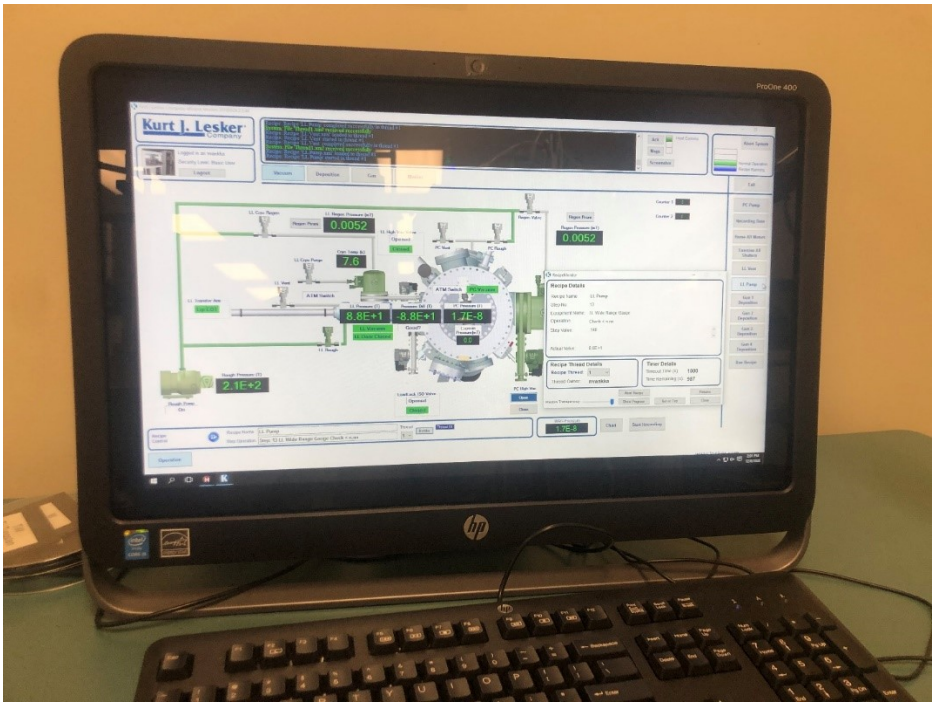


Figure 3.14. The eKLipse software computer screen displaying the user interface and control system for the Floyd sputtering system.

3.5. Electrochemical Oxidation

Electrochemical oxidation experiments were conducted in the Research Transition Facility at the University of Alberta. Experiments were conducted at voltages of 4 V, 8 V and 10 V, depending on the application. For training and control purposes, anodization was conducted on a silicon wafer coated with ~ 200 nm of tantalum and ~ 110 nm of aluminum. Polished, porous quartz frits discs, silicon wafers and high purity tantalum discs coated with ~ 200 nm of tantalum and ~110 nm of aluminum were anodized for analysis. A 0.4/0.1 M phosphoric acid/oxalic acid bath was prepared as follows: 22.693 g of 0.1 M oxalic acid was added to 500 mL deionized water and allowed to dissolve for one minute with a stir bar and magnetic stir plate set to 320 RPM. The oxalic acid solution was filled to 1500 mL with deionized water. 49.265 mL of 0.4 H_3PO_4 was added to the solution. Deionized water was added until a total volume of ~ 1800 mL was reached. The 1800 mL solution was used for anodization of the silicon wafers. To anodize the smaller quartz frits discs and tantalum discs, ~ 700 mL out of the 1800 mL was poured into a smaller beaker.

Before anodization, the thin film samples were rinsed with deionized water and dried to ensure debris was removed from the surface. The magnetic stir plate and stir bar were set to 200 RPM (1800 mL solution) and 110 RPM (700 mL solution) for the duration of the experiment. The cathode consisted of a glass substrate that was the same size as the anode covered in aluminum foil and the anode was the thin film sample. The aluminum metal coated side of the anode faced the cathode, and the electrodes were separated by ~ 4 cm for silicon wafers and ~ 6 cm for tantalum and quartz discs. The anode was placed such that the entire surface was parallel within the area of the cathode. Anodization time and voltages were inputted into the PowerSuite software (T1 = 3000s, Potential E0 = 3.9 V, Potential E1 = 4.0 V). The cathode/anode holder

was lowered into the acid bath with the accumet™ saturated potassium chloride calomel reference electrode (Thermo Fisher, Waltham, MA) centered between the cathode and anode. Data was recorded and analyzed using the PowerSuite software (Ametek® Scientific Instruments, Berwyn, Pennsylvania). Once complete, the electrodes were removed from the acid bath. The sample was rinsed with deionized water and allowed to air dry, assisted by gravity. The 3D printed substrate holder, magnetic stir plate and the electrochemical cell containing the cathode, anode, reference electrode and acid bath for the vertical anodization method is shown in Figure 3.15. Figure 3.16 shows the EG&G Princeton Applied Research Potentiostat/Galvanostat Model 273A (Ametek® Scientific Instruments, Berwyn, Pennsylvania) used for anodization.

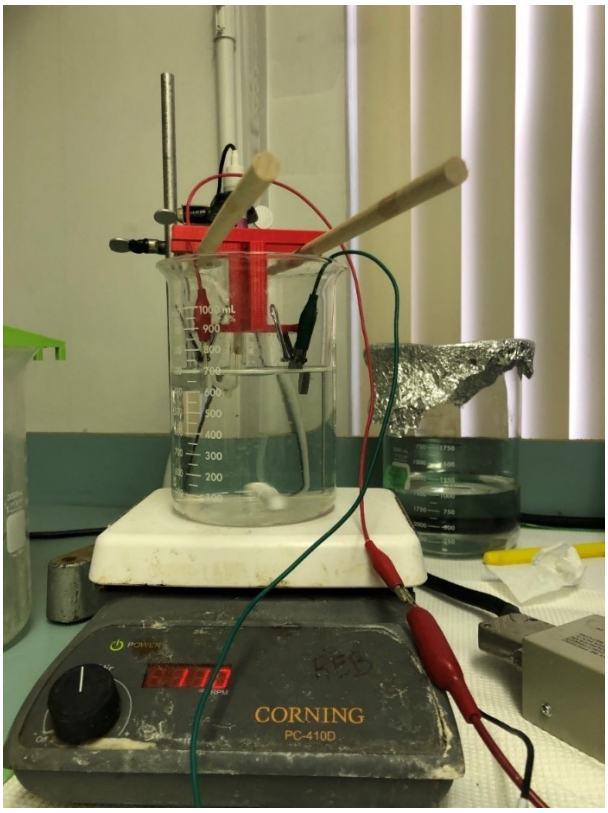


Figure 3.15. The electrochemical cell consisting of the cathode, anode, reference electrode and acid bath used for vertical anodization of substrates. The 3D printed substrate holder separates the cathode and anode by ~ 6 cm with the reference electrode centered between.



Figure 3.16. EG&G Princeton Applied Research Potentiostat/Galvanostat Model 273A used for anodization of substrates.

3.6. Protein Exposure and Adsorption

Hyphen BioMed highly purified human prothrombin from citrated human plasma from Aniara was reconstituted in distilled water and used for experiments. The concentration of prothrombin used was 1 mg/mL. The antibody used was an affinity purified IgG sheep anti-human prothrombin in a 10 mM 4-(2-hydroxyethyl)-1-piperazineethanesulfonic acid (HEPES), 150 mM NaCl, 50% (v/v) glycerol buffer at a pH of 7.4 from Affinity Biologicals with a concentration of 0.5 mg/mL. The secondary antibody used was a 1 mg/mL rabbit anti-sheep IgG (H+L)-horseradish peroxidase (HRP) conjugate supplied by Bio-Rad.

Protein exposure and adsorption were studied on silicon wafers for training, analysis and control purposes and onto 3 mm thick, porous, polished quartz frits discs, 4 mm thick porous, unpolished quartz frits discs, silicon wafers, and high purity tantalum discs for analysis. The silicon wafers, quartz frits, and tantalum discs were coated with ~ 200 nm of tantalum and ~ 110 nm of aluminum and anodized at 4 V to convert the aluminum layer into porous anodic alumina and to form a dielectric tantala layer prior to protein exposure.

Silicon wafers were cleaved into small rectangles after thin film sputtering and anodization. To ensure the wafers were cleaved consistently, a 3D printed tool was used for cleavage. The tool design is shown in Figure 3.17 [1]. The 3D printed stencil tool is shown in Figure 3.18. The 3D printed stencil was placed on top of the wafer face coated with the thin metal films, and a diamond scribe was run through the slots in the 3D printed tool to create lines on the surface of the wafer. The tool was then removed, and the diamond scribe was run from the lines to the edge of the wafer. The wafer was then held on either side of the lines and cleaved using a small amount of pressure to form rectangular slides with dimensions of ~ 1.3 × 6.2 cm that were used for protein work. In some cases, the diamond scribe was used to cleave the wafer slides again, into rectangles with dimensions of ~ 1 cm by ~ 1.2 cm. Tantalum discs and quartz frits discs were not cleaved prior to protein work.

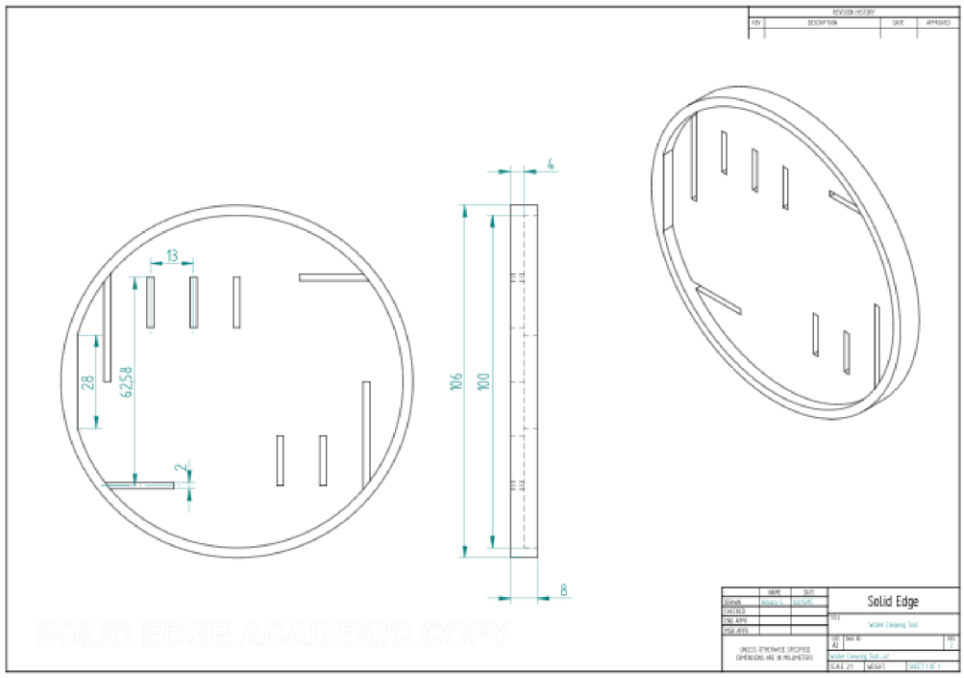


Figure 3.17. Design of tool used to cleave silicon wafers into rectangles of a consistent size. Image obtained from Sweet [1].

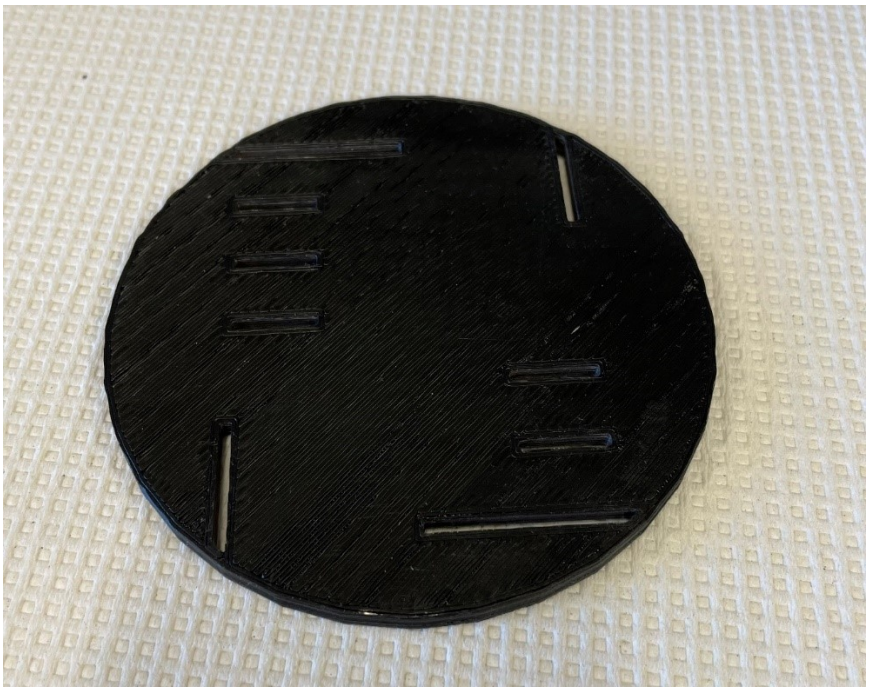


Figure 3.18. 3D printed stencil tool used to cleave silicon wafers into rectangles of a consistent size.

A Sharpie marker was used to draw hydrophobic circles with diameters of 0.7 cm – 1 cm on the coated silicon wafer slides and tantalum discs to control the surface area exposed to protein. A pipette was used to place 20 µL of protein solution into each circle and the pipette tip was used to spread the solution to the edges of the circle. Samples were then placed on a wet paper towel in a Petri dish for 20 minutes to prevent evaporation during the experiment. A pipette was used to remove the solution from the substrate and the substrate was rinsed with deionized water and dried with oil free compressed air. This process was initially completed using a prothrombin solution to immobilize prothrombin on the surface of the substrate. To form the antibody-antigen complex, the same process was completed by placing anti-prothrombin into the circles where prothrombin had previously been immobilized. Finally, a layer of a secondary antibody was placed in some circles after anti-prothrombin immobilization. The substrates were viewed using the Logitech BRIO 4K web camera and the Logitech Capture software, with the incident light from a light emitting diode (LED) source of 4350 LUX. The pictures were taken through a polarizing filter at 75° from normal, to obtain a digital image of at least 1280 × 720 pixels, 96 dpi.

To test the ability of quartz frits discs to adsorb and immobilize protein, the same process was used. Quartz frits discs coated with ~ 200 nm of tantalum and ~ 110 nm of aluminum were anodized and exposed to protein. In one experiment, three circles were drawn on the quartz frits disc to control the surface area exposed to protein. For the high purity tantalum discs, four 7 mm circles were drawn on the disc to control the surface area exposed to protein. This method was also used to determine the minimum concentration of anti-prothrombin required to produce a colour shift on stationary tantalum disc and silicon wafer surfaces. Additionally, protein was placed over the entire anodized surface of the silicon wafer slides, quartz frits and tantalum discs.

3.7. Analytical Techniques

3.7.1. Scanning Electron Microscopy

The Zeiss Sigma Field Emission Scanning Electron Microscope (FESEM) with energy dispersive X-ray spectroscopy (EDX) and electron backscatter diffraction (EBSD) at the University of Alberta nanoFAB was used to capture topographical and cross-sectional images to observe surface morphology and layer thickness of samples. An electron high tension (EHT) range of 3.0 to 10.0 kV and working distances from 5.0 mm to 10.4 mm were used for imaging. A diamond pen was used to cleave the silicon wafers prior to SEM imaging.

3.7.2. Ellipsometry

The variable-angle spectroscopic ellipsometer (J.A. Woollam M-2000V) at the University of Alberta nanoFAB was used to collect data on the thickness, optical constant (refractive index and extinction coefficient), percent void/effective medium approximation % (EMA %) and standard error values for the thin film layers on the tantalum discs and silicon wafers. The data was analyzed using the J. A. Woollam CompleteEASE software. A model developed by Nickel to represent the aluminum oxide porous film was used for data collection [2]. Data was recorded at angles of 55°, 65° and 75° from the surface normal over the visible light range, with wavelengths of 370 to 700 nm.

3.7.3. Colour Coordinates

Images of the visible surface colours were taken using the Logitech BRIO 4K web camera and the Logitech Capture software, with the incident light from an LED source of 4350 LUX. The pictures were taken through a polarizing filter at 75° from normal, to obtain a digital image of at least 1280 × 720 pixels, 96 dpi. All analyzed images were taken using the same camera and lighting conditions to ensure consistency throughout the experiments. The ImageJ

software from National Institutes of Health, Bethesda, MD (https://imagej.nih.gov/ij/) was used to collect the red-green-blue (RGB) colour coordinates. Areas between 3,000 pixels and 900,000 pixels were selected, depending on the size of the wafer or disc sample, and the mean and standard deviations for RGB colour coordinates were recorded for each area. RGB colour coordinates were converted to Yxy coordinates using the ColorMine website (http://colormine.org/convert/rgb-to-yxy) to compare colour shifts and complete statistical analysis.

3.7.4. Statistics

IBM SPSS Statistics, Version 28.0 (IBM Corporation, released 2021, Armonk, NY) was used to complete statistical analysis, compare results, and determine statistically significant differences in results. An independent T-test was used for comparisons of two independent groups. A Levene's homogeneity of variance test was used to assess if variances were equal between groups. When variances were equal, one-way analysis of variance (ANOVA) and Tukey post hoc tests were used when analyzing more than two groups ($n > 2$). When variances were unequal, a Welch's t-test and Games-Howell post hoc test was used. For all tests, a 5% level of significance was used.

3.8. References

1. Sweet, H.M., *Development of a Nanostructured Thin Film Device and Optics System for Protein Detection*, in *Materials Engineering*. 2018, University of Alberta.

2. Nickel, M.R., *Physical and Optical Characterization of Anodized Aluminum-Tantalum Thin Films for use in Thin Film Diagnostics*, in *Materials Engineering*. 2018, University of Alberta.

3. C-therm. *What is Coefficient of Thermal Expansion (CTE)? How Do I Measure It?* 2018 [cited 2022 March 17]; Available from: https://ctherm.com/resources/newsroom/blog/coefficient-of-thermal-expansion/.

4. Engineering ToolBox. *Thermal Expansion - Linear Expansion Coefficients*. 2003 [cited 2022 March 17]; Available from: https://www.engineeringtoolbox.com/linear-expansion-coefficients-d_95.html.

5. GM Quartz. *Quartz Fritted Porous Discs*. [cited March 17 2022]; Available from: https://gm-quartz.com/products/quartz-fritted-discs.

6. MicQuartz. *Custom Quartz Frits Porous Glass Filter Disc Quartz Sand Filter in Different Porosity*. [cited 2022 March 17]; Available from: https://www.micquartz.com/quartz-glass-products/quartz-plates/custom-different-porosity-of-quartz-porous-glass-filter-disc-quartz-sand-filter/.

Chapter 4 – The Effect of Sputtering and Anodization Parameters on Membrane Performance

4.1. Introduction

Various parameters can be changed while sputtering and anodizing to obtain the metal and metal oxide film properties, surface morphology and structure desired. While sputtering, the main parameters affecting deposition are working pressure (mTorr), DC power (W), sputtering time (s) and substrate temperature (°C) [1]. Changing these properties can result in different film thicknesses and adherence of metal to the substrate surface. Anodization parameters that can be altered include electrolyte composition and anodization voltage [2]. Alumina pore size was found to increase in direct proportion with the applied voltage and inversely with electrolyte concentration [2]. It was also found that the interpore distance increases linearly with applied voltage [2]. By altering voltage and electrolyte composition, the desired alumina properties can be obtained.

Hilary Sweet [3] and Matthew Nickel [4] showed the effects various sputtering and anodization parameters have on the surface morphology and structure of aluminum and tantalum deposited on a silicon wafer. Knowing the optimal parameters for deposition and anodization of aluminum and tantalum provided a starting point for selection of parameters in these experiments. The silicon wafers were used as a control to determine whether quartz frits and tantalum discs were acceptable materials for sputtering of aluminum and tantalum metal as well as electrochemical oxidation prior to adsorption of protein. This chapter explores the optimal anodization and deposition parameters for silicon wafers applied to quartz frits discs and tantalum discs to determine the impact of these parameters on a new substrate. The microstructural and optical changes that occur as a result of metal deposition and anodization

will be observed and compared to a control substrate with known, expected behavior, silicon wafers.

4.2. Materials and Methods

Detailed materials and methods can be found in Chapter 3 – General Materials and Methods. Unless otherwise stated, a 0.4/0.1 M phosphoric acid/oxalic acid bath was used as the electrolyte and anodization was conducted until the dielectric tantala layer was formed, indicated by a steady, low current after a drop.

4.3. Deposition and Anodization

Deposition and anodization parameters for a device containing thin films of tantalum, tantala and alumina have been determined for optimal membrane performance on a silicon wafer ([3], [4]). The optimal thin film thicknesses to be deposited on a silicon wafer to yield strong visual colour shifts due to the adsorption of prothrombin and anti-prothrombin were ~ 200 nm of tantalum and ~ 110 nm of aluminum. These thicknesses were selected as a starting point to determine membrane performance on porous quartz frits discs and tantalum discs as the metal films are in direct contact with biologics.

Anodization of aluminum and tantalum on silicon wafers has been shown to produce porous alumina and a tantala barrier suitable for visible protein deposition ([3], [4]). The techniques used to anodize aluminum and tantalum on silicon wafers were applied to unpolished and polished porous, quartz frits as well as high purity tantalum discs and compared to a silicon wafer control to observe if similar behavior occurred. The anodization of aluminum and tantalum on a silicon wafer at a constant voltage produces a characteristic graph of current as a function of time, shown in Figure 4.1. The initial drop in current density is due to the formation of the aluminum oxide barrier layer. The slight increase followed by a constant current indicates the

formation of pores in the aluminum oxide. The final drop in current indicates the tantalum oxide dielectric layer formation. Once the current is constant, the tantala dielectric layer has been formed.

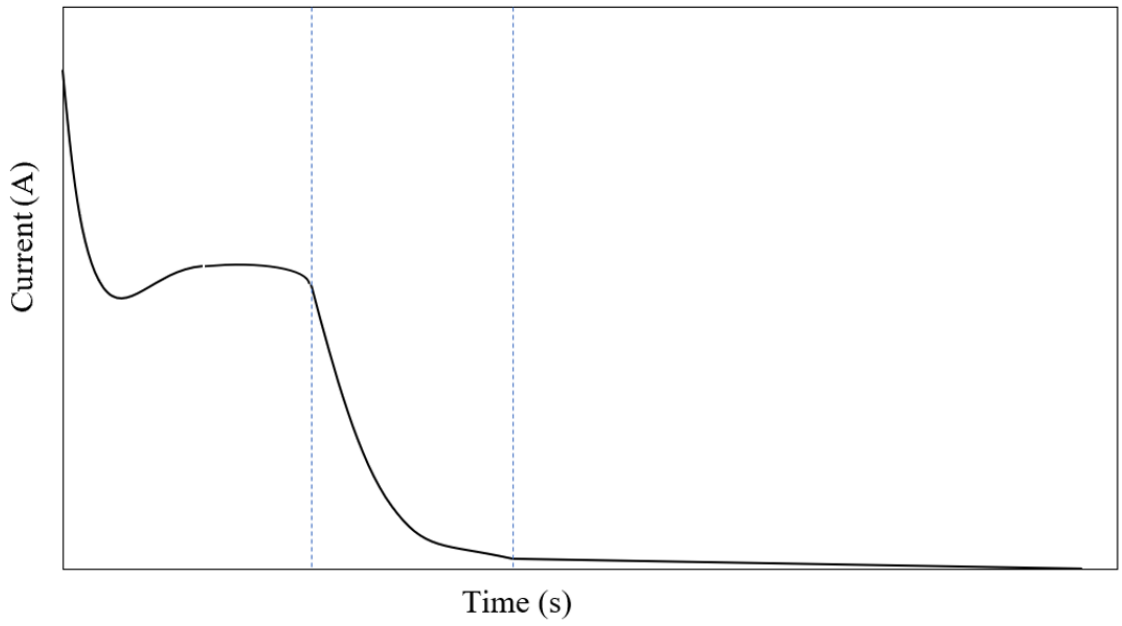


Figure 4.1. The characteristic curve for anodization of aluminum and tantalum on a silicon wafer. The initial drop indicates aluminum oxide formation, followed by a steady current indicating pore formation, and a final drop in current indicating tantalum oxide formation. The final constant region indicates anodization is complete and the tantala dielectric layer has been formed.

4.3.1. Polymer-Tantalum Adhesion Test

After sputtering ~ 200 nm of tantalum onto the 3D printed polymer discs, an adhesion test was conducted to determine how well the tantalum film adhered to the polymer disc. An adaptation of the ASTM adhesion test method by Rezaee et al. (2019) [5] was followed. Adhesion tests were conducted using 3M Scotch Magic 810 tape and the tantalum-coated

polymer disc surface. Faster peel rates have been shown to produce larger peel forces [5]. The adhesion tests were conducted on thin films four hours after tantalum deposition with a peel rate of 10 mm/sec and at an angle of 90° [5]. The tape was left in place on the substrate for four minutes prior to peeling. The pull rate was measured by cutting a 7 cm piece of tape and sticking 5 cm to a desk, leaving a 2 cm tab to pull. The tape was pulled at an angle of 90° and the time taken to peel the adhered 5 cm was measured. This process was repeated until a consistent rate of 10 mm/sec was achieved. Once the peel rate was consistently obtained, the same force was used to peel tape off of the tantalum-coated polymer disc. To improve adhesion between the polymer disc and the tantalum layer, the polymer discs were cleaned prior to sputtering tantalum and the adhesion test was conducted after sputtering. For cleaning, polymer discs were submerged into 100 mL of either 30% hydrogen peroxide, ACS or 2-propanol (isopropanol), HPLC grade for 1 hour. After cleaning, ~ 200 nm of tantalum was sputtered onto the substrates and adhesion tests were conducted as described. Figure 4.2 shows the results of the adhesion test conducted on the 3D printed polymer disc. Adhesion between the tantalum film and the polymer disc was poor as the tape was able to pull off a significant amount of tantalum metal.



Figure 4.2. Results of the tantalum-polymer disc adhesion test. Adherence of the thin tantalum film to the polymer substrate was poor as the tape was able to pull off a significant amount of tantalum metal. The tape (above) shows a significant amount of tantalum metal was pulled off of the polymer disc (below).

4.3.2. Tantalum Disc-Aluminum Film Adhesion Test

Tantalum discs were cleaned by submerging in acetone for 1 hour prior to sputtering ~ 110 nm of aluminum onto the surfaces. Four hours after sputtering, adhesion tests following the same procedure described in Section 4.3.1. Polymer-Tantalum Adhesion Test were conducted to study the adhesion between the tantalum disc surface and the sputtered aluminum. Figure 4.3 displays the results from two adhesion tests between the aluminum thin film and the tantalum disc surface.

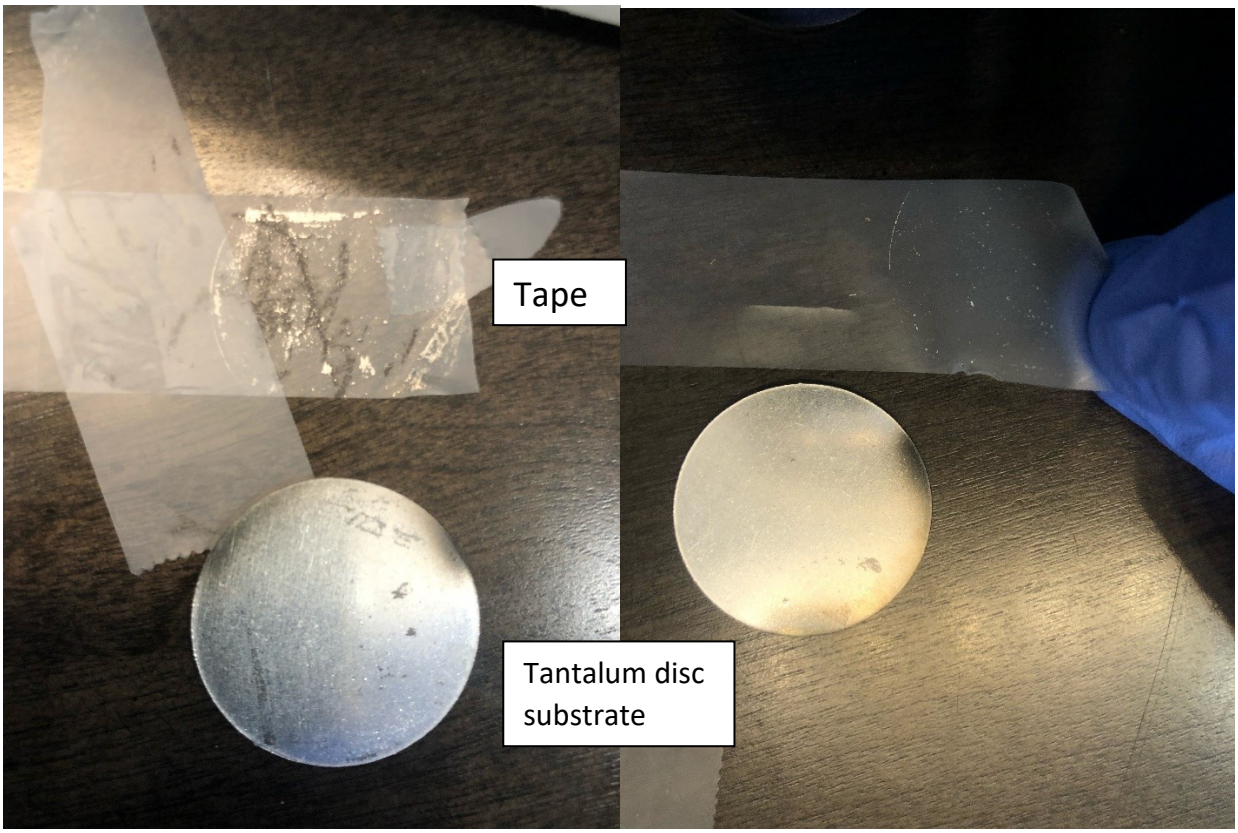


Figure 4.3. Results of two adhesion tests between tantalum discs and ~ 110 nm aluminum films before anodization.

Adhesion tests were also conducted after anodization to determine whether anodizing improved adhesion. Figure 4.4 displays the results from the adhesion test between the aluminum

thin film and the tantalum disc surface after anodization. To ensure only the aluminum coated face of the tantalum disc was anodized, Kapton tape was placed on the opposite face of the tantalum disc. Anodization of the tantalum disc did not produce the typical aluminum anodization curve. It was suspected that this was due to anodization acid leaking between the Kapton tape and the tantalum face, causing the tantalum face to be anodized. As a result, the adhesion was poor after anodization.

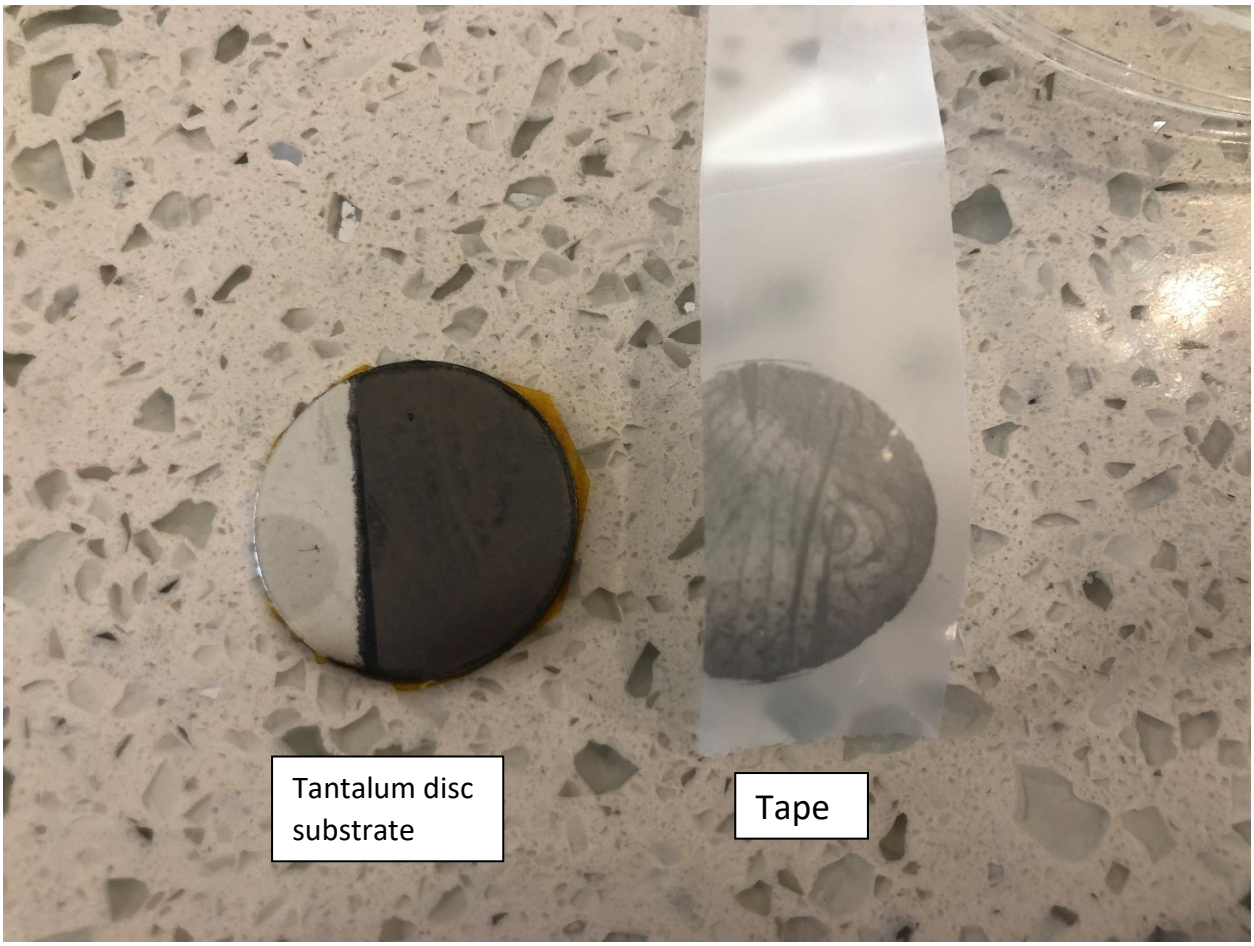


Figure 4.4. Adhesion test between tantalum disc and 110 nm aluminum thin film after anodization. Poor adhesion likely due to poor anodization.

4.4. Results

4.4.1. Polycarbonate Membrane Films

Initially, thin polycarbonate membrane films with a diameter of 25 mm were coated with ~ 200 nm of tantalum by sputtering. During the sputtering process, the polycarbonate films became curled and wrinkled, as shown in Figure 4.5, making them unsuitable for anodization and future research. It was thought that the polycarbonate films deformed due to the mismatch in thermal expansion coefficients of polycarbonate and tantalum, and the high sputtering temperature (refer to Table 3.1 for thermal expansion coefficients). Due to membrane wrinkling, thin polycarbonate films were deemed unsuitable for the diagnostic device application and alternative materials were investigated.



Figure 4.5. Polycarbonate membrane after sputtering ~ 200 nm of tantalum metal. The thin polycarbonate membrane curled and wrinkled during the sputtering process.

4.4.2. Quartz Frits Discs

Unpolished quartz frits discs with a 25 mm diameter, 4 mm thickness and a pore size of 16 – 40 μm coated with ~ 200 nm of tantalum and ~ 110 nm of aluminum were anodized and compared to the control, silicon wafers coated with ~ 200 nm of tantalum and ~ 110 nm of aluminum. Silicon wafers were selected as the control material because previous work displayed the optimal conditions and expected anodization results for silicon wafer substrates ([3], [4]). The unpolished quartz frits discs were investigated to determine whether rough surfaces can be used in anodization and protein adsorption for potential use in the diagnostic device. Rough surfaces offer a larger surface area and different properties than smooth, polished surfaces that were of interest. Initially, an anodization voltage of 8 V was used for the unpolished quartz frits with the stir plate set to 110 RPM. The resulting graph did not follow the expected trend and was sharp and jagged, rather than smooth. Figure 4.6 displays the graph generated at 8 V for the unpolished quartz frits disc with a porosity of 16 – 40 μm, coated with 200 nm of tantalum and 110 nm of aluminum. Next, a lower anodization voltage of 4 V was used to anodize an unpolished quartz frits disc of the same porosity, coated with 200 nm of tantalum and 110 nm of aluminum. Similar results were obtained, as shown in Figure 4.7. The resulting graphs did not display the expected characteristics for anodization of a multilayered aluminum/tantalum surface. To determine whether the issue was with the thin film coatings or the quartz frits disc material, anodization was conducted on an uncoated quartz frits disc with the same properties at 4 V, with the resulting graph shown in Figure 4.8. Under these conditions, it was expected that the current would smoothly drop to zero, as seen with the uncoated silicon wafer anodized at 4 V, shown in Figure 4.9. However, the uncoated, rough quartz disc displayed sharp, jagged

current changes that did not follow a smooth trend to zero amperes. This suggests that the anodization issue was due to the quartz frits disc itself.

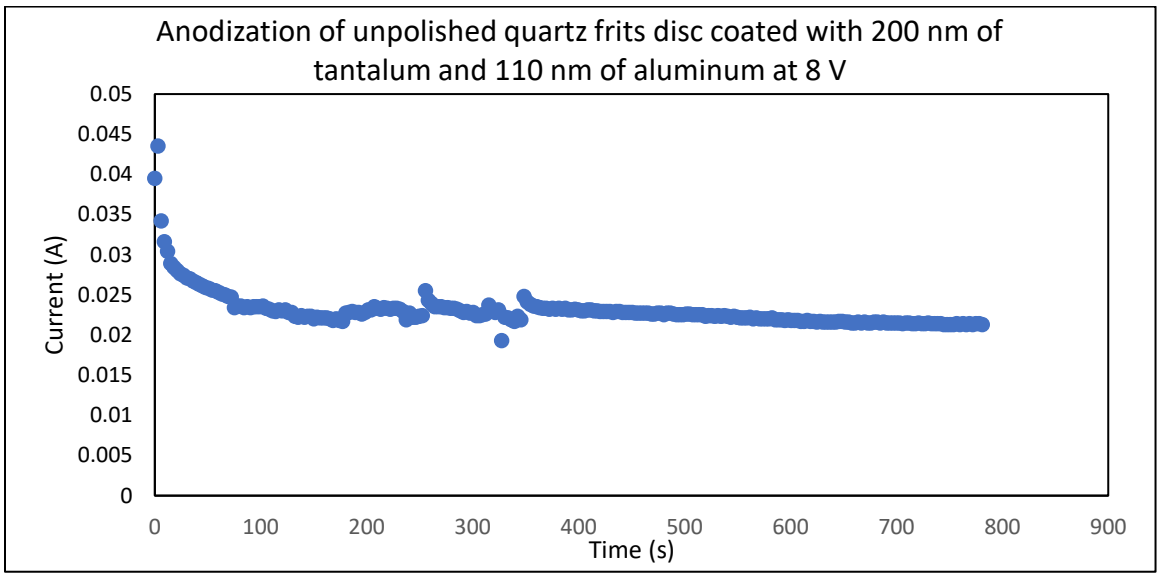


Figure 4.6. Current vs. time anodization plot for an unpolished quartz frits disc coated with 200 nm of tantalum and 110 nm of aluminum at 8 V.

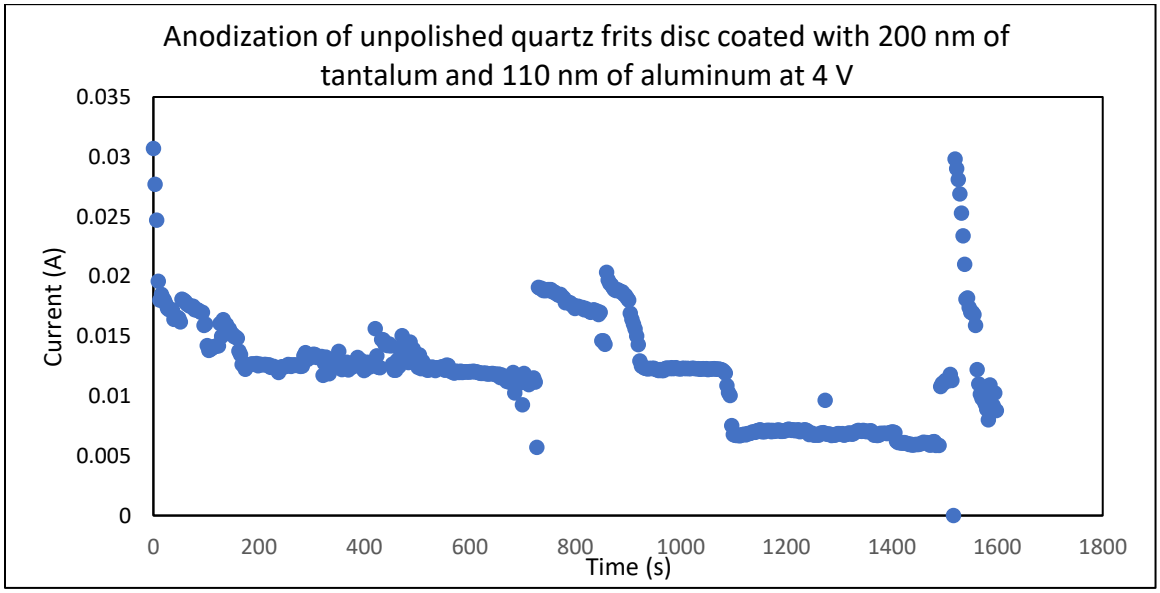


Figure 4.7. Current vs. time anodization plot for an unpolished quartz frits disc coated with 200 nm of tantalum and 110 nm of aluminum at 4 V.

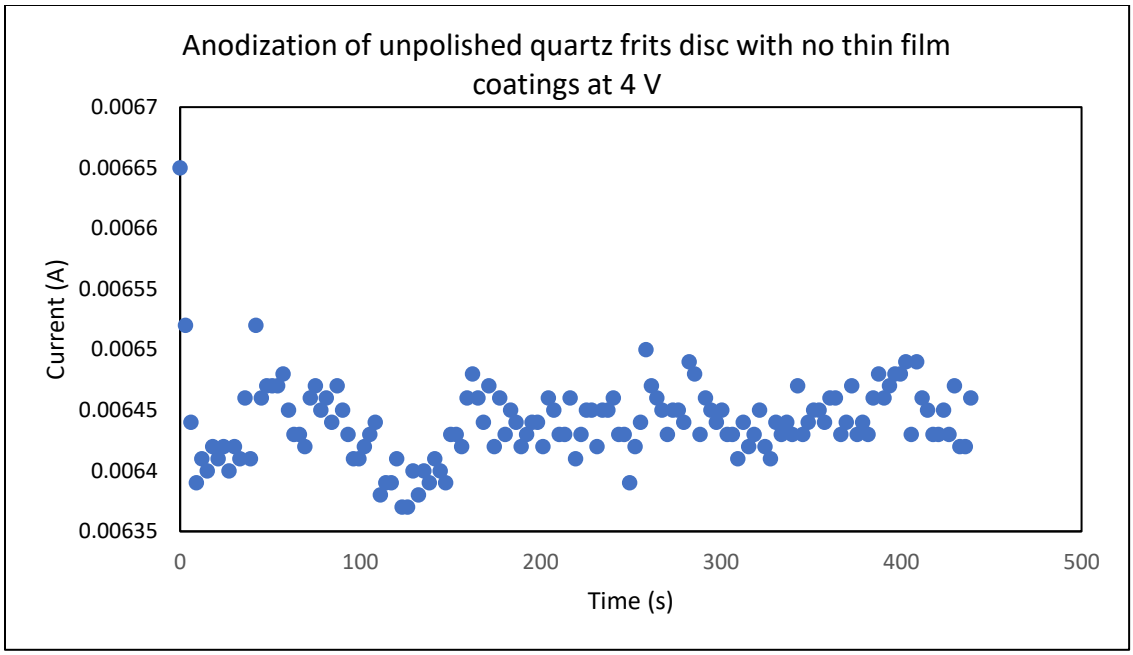


Figure 4.8. Current vs. time anodization plot for an unpolished quartz frits disc with no thin film coatings at 4 V.

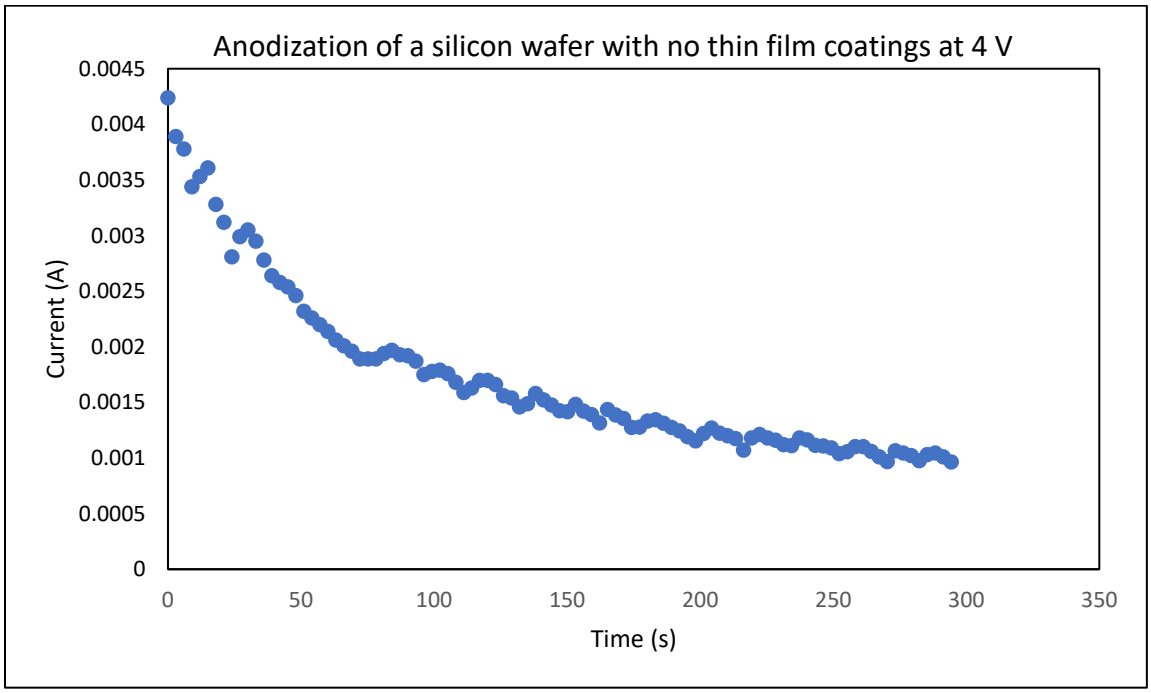


Figure 4.9. Current vs. time anodization plot for a silicon wafer with no thin film coatings at 4 V.

It was thought that the poor anodization and jagged curve could be due to the quartz frits discs absorbing the acid bath solution and capillary action carrying the fluid up the disc, causing the entire quartz frits disc to become soaked with acid. As a result, the clip holding the disc in the acid bath contacted the acid bath solution and became wet. In order for anodization to properly occur, the clip must stay dry throughout the process. To prevent fluid from rising up the quartz frits disc and contacting the anodization clip, future discs were dipped into epoxy to coat ¼ to 1/3 of the substrate prior to sputtering. This would ensure that the sputtered metal would still be present to conduct electricity during anodization, but the epoxy would prevent fluid from rising to the upper portion of the disc and contacting the clip. Figure 4.10 displays a drawing of the quartz frits discs after being dipped in epoxy and Figure 4.11 shows an image of a polished quartz frits disc after being dipped in epoxy.

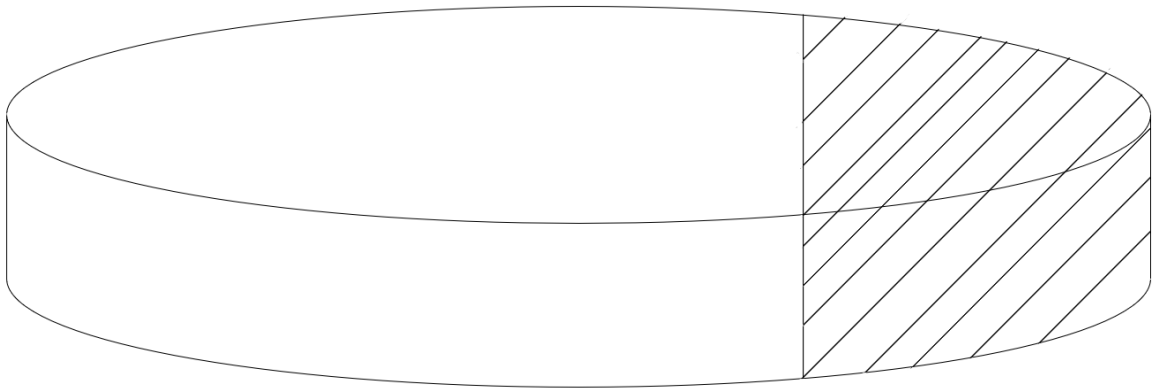


Figure 4.10. Epoxy-dipped quartz frits disc drawing. Quartz frits discs were partially coated with epoxy to prevent the rise of the acid bath solution through the upper portion of the disc during anodization. Striped region is epoxy coated.



Figure 4.11. Epoxy-dipped quartz frits disc (40 – 100 µm porosity).

Polished quartz frits coated with ~ 200 nm of tantalum and ~ 110 nm of aluminum were anodized and compared to the control, silicon wafers coated with ~ 200 nm of tantalum and ~ 110 nm of aluminum. Prior to sputtering, the quartz frits discs were dipped in epoxy, as shown in Figure 4.11. Although the quartz frits were fire polished, the surface still appeared rough. Polished quartz frits discs were anodized at 4 V. The epoxy layer appeared to stop the rise of acid and prevented short circuiting during anodization, however, the polished quartz frits discs still failed to produce the proper anodization curve indicating the formation of alumina and the tantala dielectric layer, as shown in Figure 4.12. The curves appeared smooth, but it could not be confirmed whether the alumina and tantala dielectric layer had properly formed as the profile

shown in Figure 4.1 was not obtained. It is possible that anodization on the quartz frits failed due to the rough surface, or due to acid being absorbed by the substrate.

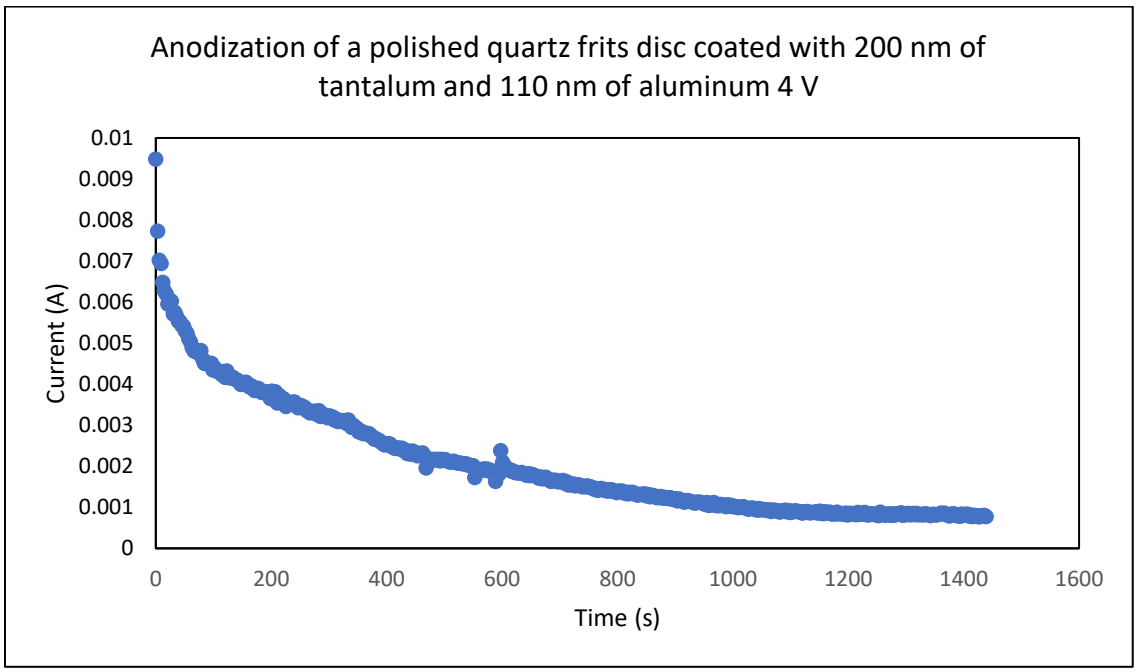


Figure 4.12. Current vs. time anodization plot for a polished quartz frits disc coated with 200 nm of tantalum and 110 nm of aluminum at 4 V (epoxy dipped).

SEM images were taken of the coated and anodized silicon wafers and quartz frits discs to visualize the morphology and thickness of the thin films. All SEM images were taken using the InLens mode with an EHT range of 3.0 – 10.0 kV. The working distance varied between 5.0 mm and 10.4 mm. Figures 4.13, 4.14 and 4.15 show the topographical profiles of the 40 – 100 µm porosity polished quartz frits, the 100 – 160 µm porosity polished quartz frits and the silicon wafer after sputtering ~ 200 nm of tantalum and ~ 110 nm of aluminum and anodization, respectively, at magnifications of 50 X (top left), 500 X (top right), 10,000 X (bottom left) and 30,000 X (bottom right). On the silicon wafer, the porous alumina layer can be seen. On the quartz frits discs, the porous alumina layer is not as visible, suggesting a failure to properly

anodize, as previously discussed. The large pores and cracks in the quartz frits discs likely allowed for acid to be drawn up into the material during anodization, wetting the disc and interfering with the electrical circuit. Points on the anodization graph where the current randomly drops to zero amperes indicate an incomplete electrical circuit. Further, the uneven quartz surfaces, as seen at a magnification of 50 X, was likely not suitable for alumina formation or protein adsorption.

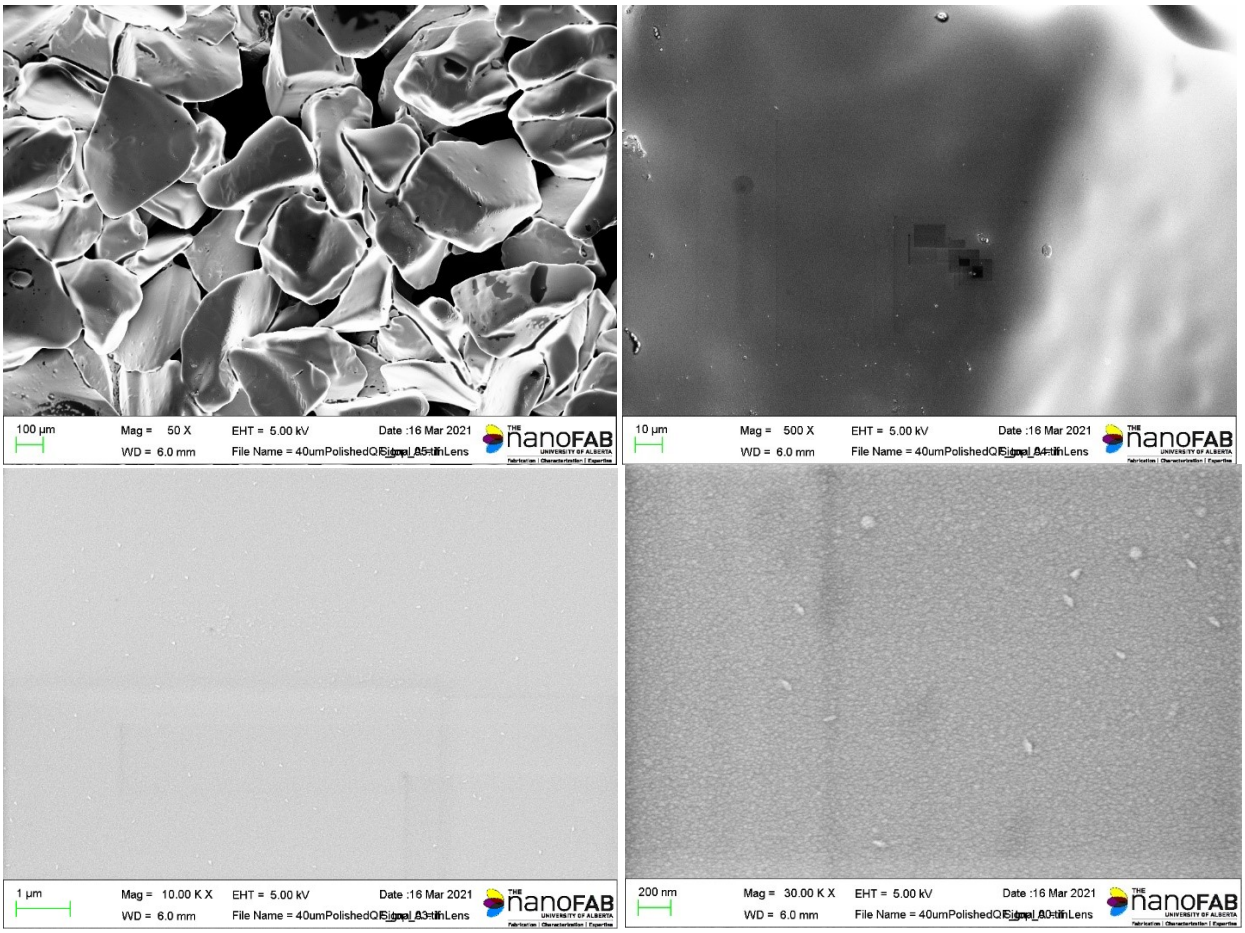


Figure 4.13. Topographical SEM images of the 40 – 100 µm porosity polished quartz frits discs after sputtering ~ 200 nm of tantalum and ~ 110 nm of aluminum, followed by anodization at 4 V at magnifications of 50 X (top left), 500 X (top right), 10,000 X (bottom left) and 30,000 X (bottom right).

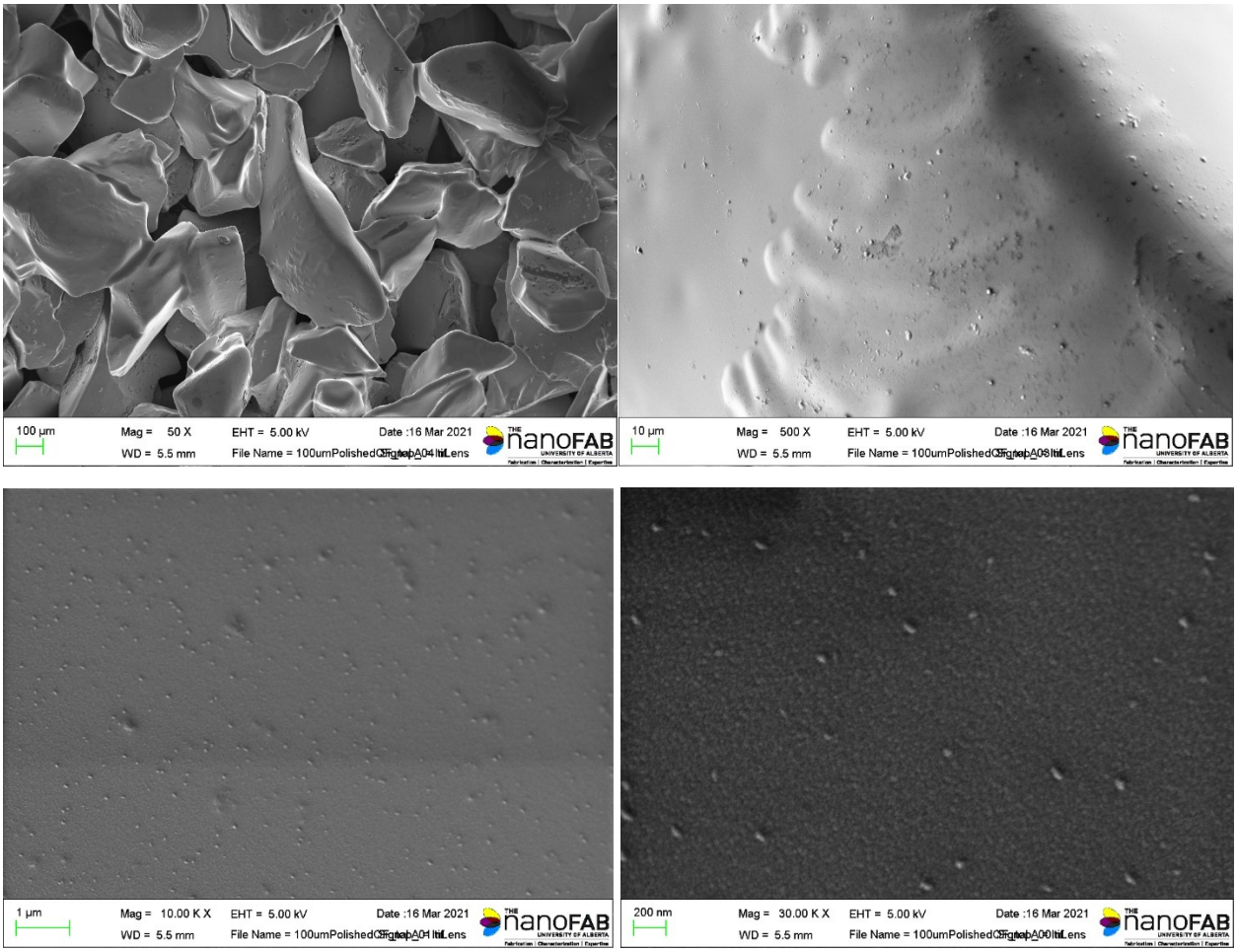


Figure 4.14. Topographical SEM images of the 100 – 160 µm porosity polished quartz frits discs after sputtering ~ 200 nm of tantalum and ~ 110 nm of aluminum, followed by anodization at 4 V at magnifications of 50 X (top left), 500 X (top right), 10,000 X (bottom left) and 30,000 X (bottom right).

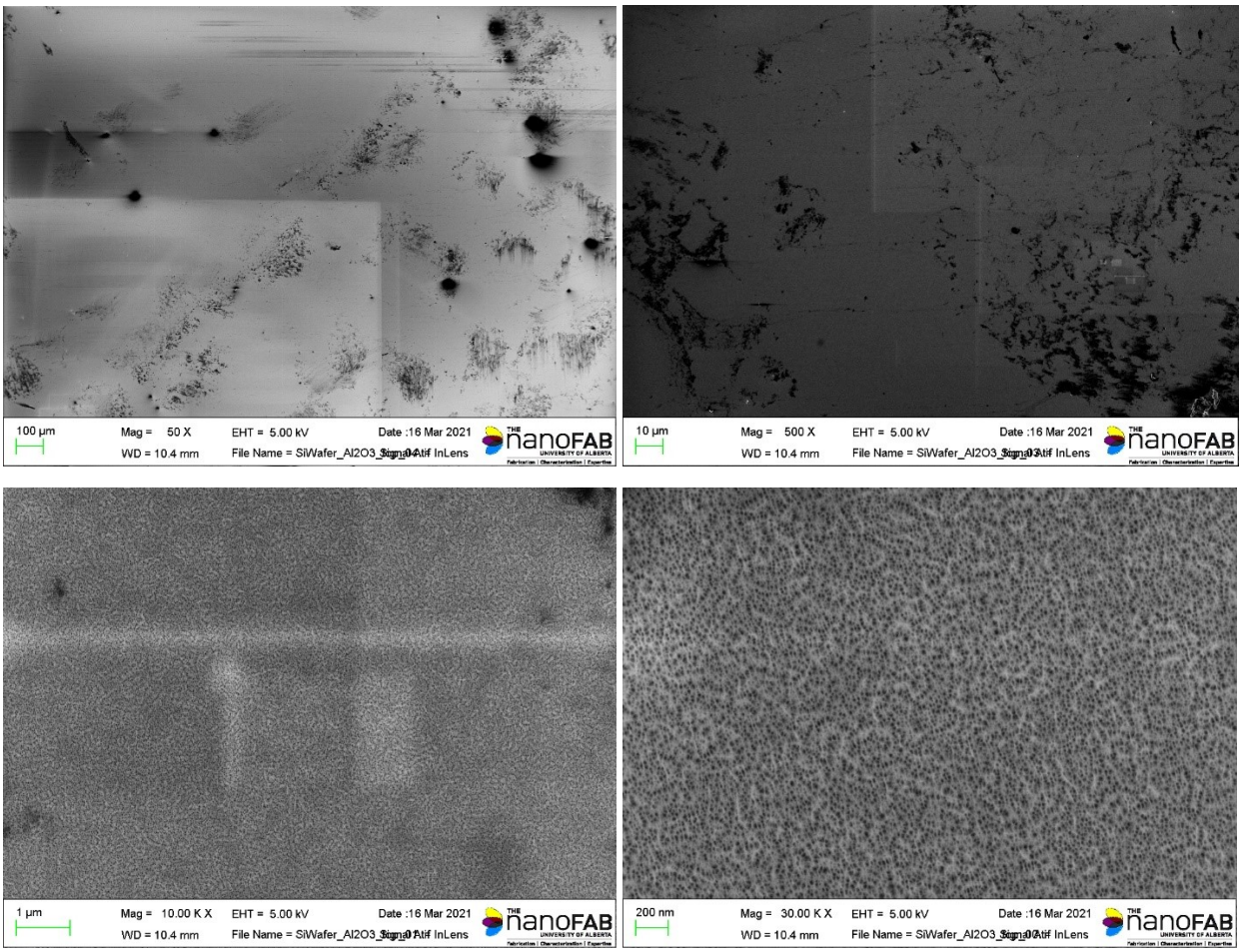


Figure 4.15. Topographical SEM images of the silicon wafers after sputtering ~ 200 nm of tantalum and ~ 110 nm of aluminum, followed by anodization at 4 V at magnifications of 50 X (top left), 500 X (top right), 10,000 X (bottom left) and 30,000 X (bottom right).

Figures 4.16 and 4.17 display cross-sectional SEM images of the silicon wafer and the thin film layers after sputtering ~ 200 nm of tantalum and ~ 110 nm of aluminum after anodization at 4 V at magnifications of 30,000 X and 50,000 X, respectively. Side images were expected to show the thin layers of alumina, tantala, and tantalum metal, however, the thin films appeared disrupted. It is likely that during the cleaving of the wafers, the top alumina layer was disrupted. Both Figure 4.16 and Figure 4.17 show the top layer appearing pushed back and uneven along the surface. It is likely that breakage of the wafers disrupted the thin film. The thin

films could be seen; however, thickness was difficult to measure due to the uneven surface. Future images should be taken along an edge of the wafer that was not cleaved to avoid layer disruption due to cleavage with the diamond pen.

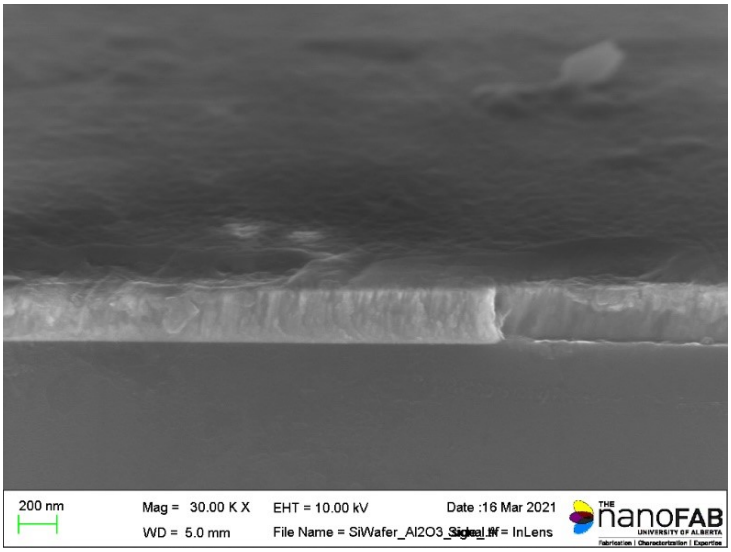


Figure 4.16. Cross-sectional SEM image of a *silicon wafer after sputtering ~ 200 nm of tantalum and ~ 110 nm of aluminum, followed by anodization at 4 V at a magnification of 30,000 X.*

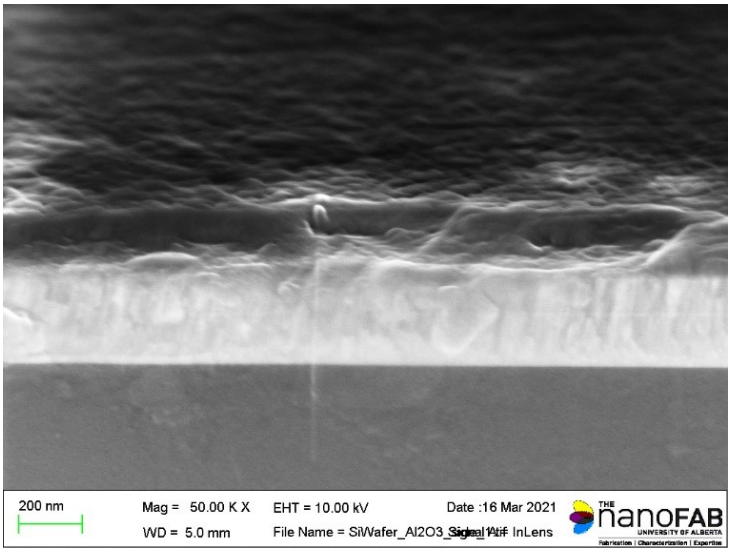


Figure 4.17. Cross-sectional SEM image of a *silicon wafer after sputtering ~ 200 nm of tantalum and ~ 110 nm of aluminum, followed by anodization at 4 V at a magnification of 50,000 X.*

4.4.3. 3D Printed Polymer Discs

The poor adhesion between the polymer disc surface and the sputtered tantalum layer after cleaning the substrate suggested that the polymer discs were unsuitable for the diagnostic device application as the poor adhesion would be an issue during anodization (see Section 4.3.1. Polymer-Tantalum Adhesion Test). Other substrate materials were investigated instead.

4.4.4. Tantalum Discs

After sputtering ~ 110 nm of aluminum onto the tantalum disc, the discs were prepared for anodization by sticking Uline Kapton Tape to the face opposite the aluminum thin film. The Kapton tape was used to prevent anodization of the back tantalum face while the thin aluminum layer was anodized. Four discs were anodized. One anodization curve resembled the characteristic aluminum anodization curve, while the other three did not. For the three that did not produce the characteristic curve, it was suspected that the anodization acid leaked through the Kapton tape and the tantalum face opposite to the aluminum film face was anodized. Figure 4.18 shows the first tantalum disc that was anodized – following a similar trend to the expected aluminum anodization curve. Figures 4.19, 4.20 and 4.21 displays the curves generated by the second, third, and fourth discs, respectively, in which the characteristic aluminum anodization curve was not generated. The curves for the second, third, and fourth tantalum discs appear to follow the expected curve for the anodization of tantalum, suggesting that anodization acid may have leaked through the Kapton tape, causing the back side tantalum face of these discs to be anodized instead of the aluminum coated face.

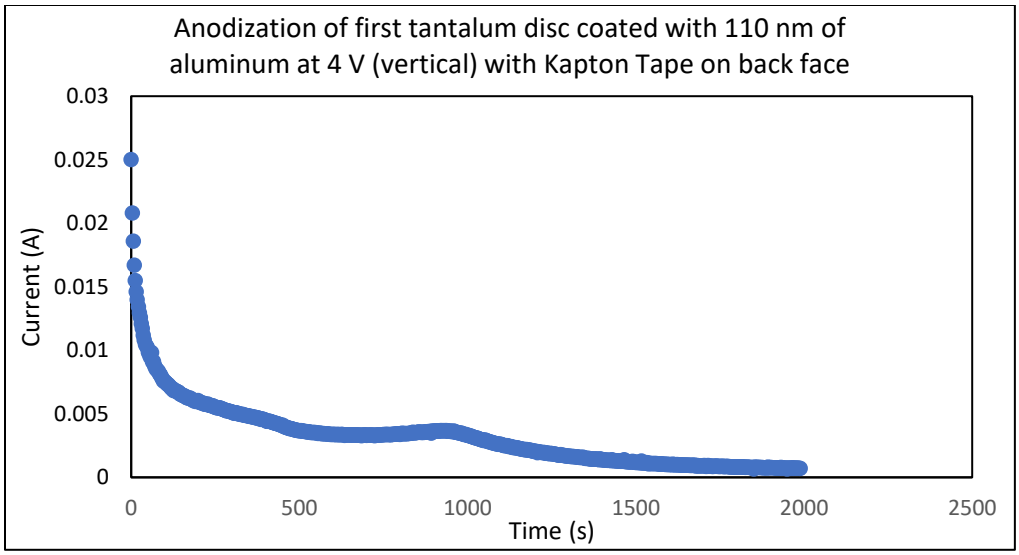


Figure 4.18. Current vs. time anodization plot for first tantalum disc coated with 110 nm of aluminum at 4 V. Kapton tape was stuck on the face opposite to the aluminum coating to prevent anodization of the back tantalum face.

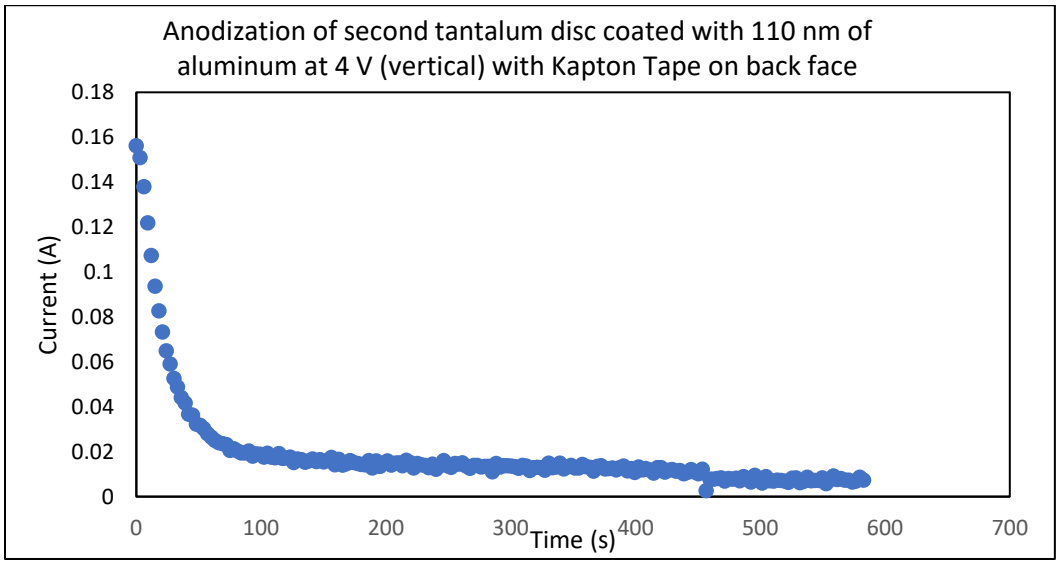


Figure 4.19. Current vs. time anodization plot for second tantalum disc coated with 110 nm of aluminum at 4 V. Kapton tape was stuck on the face opposite to the aluminum coating to prevent anodization of the back tantalum face. Anodization acid may have leaked through the Kapton tape to produce this curve.

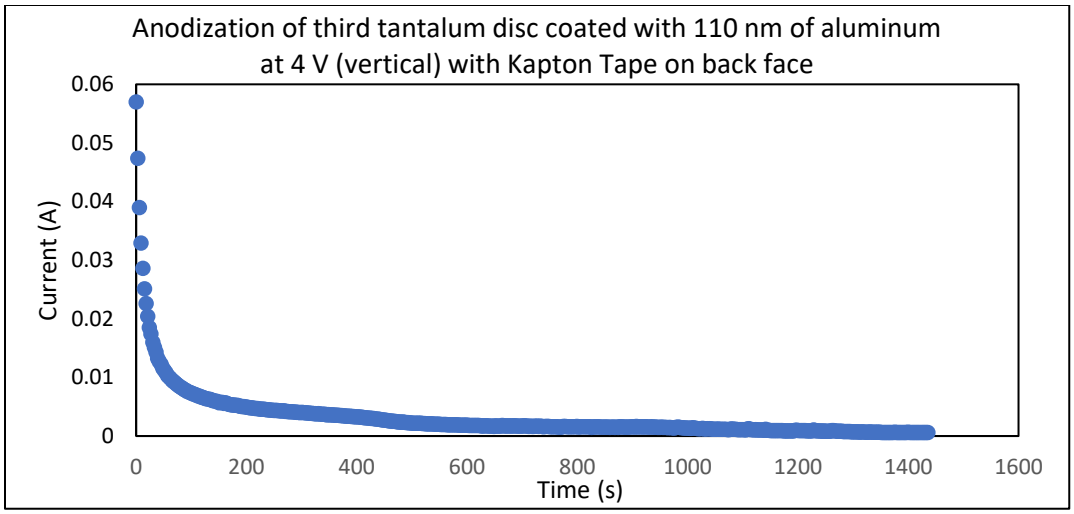


Figure 4.20. Current vs. time anodization plot for third tantalum disc coated with 110 nm of aluminum at 4 V. Kapton tape was stuck on the face opposite to the aluminum coating to prevent anodization of the back tantalum face. Anodization acid may have leaked through the Kapton tape to produce this curve.

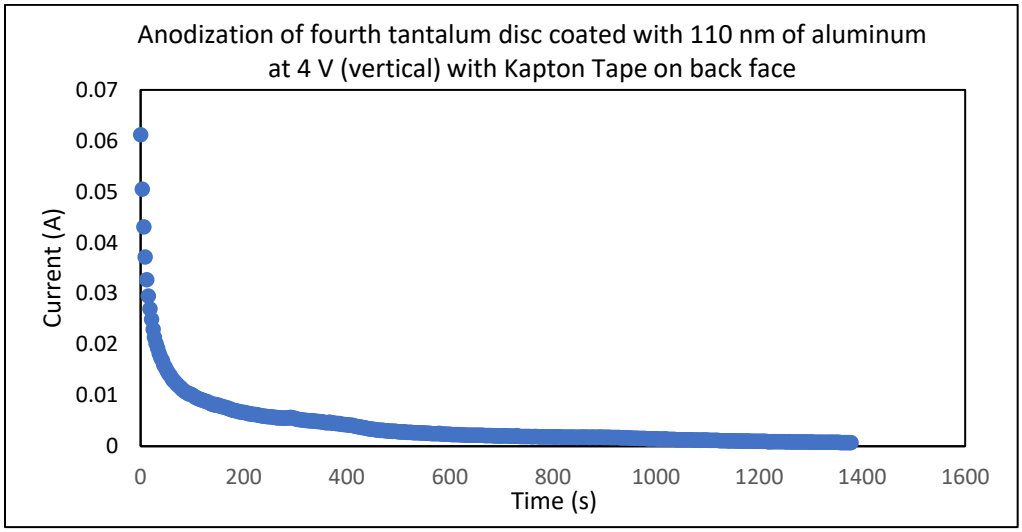


Figure 4.21. Current vs. time anodization plot for fourth tantalum disc coated with 110 nm of aluminum at 4 V. Kapton tape was stuck on the face opposite to the aluminum coating to prevent anodization of the back tantalum face. Anodization acid may have leaked through the Kapton tape to produce this curve.

Since the Kapton tape anodization method produced inconsistent results, two other methods were considered for anodization. In the first method, one face of the tantalum disc was anodized at 10 V prior to sputtering aluminum on the opposite face. For each volt used in tantalum anodization, about 1.6 nm of tantalum oxide is formed. Therefore, anodizing at 10 V would create a ~ 16 nm layer of tantalum oxide and form a dielectric layer. The prior anodization of one tantalum face would ensure that when anodizing aluminum at 4 V following sputtering, the opposite tantalum face would not interfere. The set up used to completely anodize one tantalum face while ensuring the other side was not anodized is shown in Figure 4.22. A glass Anchor Hocking dish was used instead of a beaker so the substrate could be placed horizontally and to ensure only one face of the disc contacted the acid bath. The aluminum foil cathode was bent into shape such that the entire face of the disc to be anodized was directly over top of the foil. Two test tubes taped together were placed on top of the aluminum foil for the tantalum disc anode to sit on, and the acid was pipetted into the dish until the bottom face of the disc was completely immersed in acid, while the top face remained dry. The tip of a metal compass was placed on the dry surface of the anode and the alligator clip was attached to the compass to create the electrical circuit.



Figure 4.22. Experimental set up for anodizing one face of tantalum disc. The electrochemical cell consisting of the cathode (aluminum foil), anode (tantalum disc), reference electrode and acid bath used for anodization of substrates. The cathode and anode clips are separated by ~ 10 cm with the reference electrode centered between.

The above set up produced the characteristic curve for anodization of tantalum, shown in Figure 4.23, suggesting that the submerged face was anodized successfully. In addition to this disc, six other discs were anodized on the tantalum face horizontally at 10 V using the same method. The anodization curves for the additional six discs can be found in Appendix 4 (Figure A4.1 – A4.6). The face that had not been anodized was then sputtered with ~ 110 nm of aluminum and anodized vertically as described in Chapter 3 – General Materials and Methods, using the set up shown in Figure 3.15.

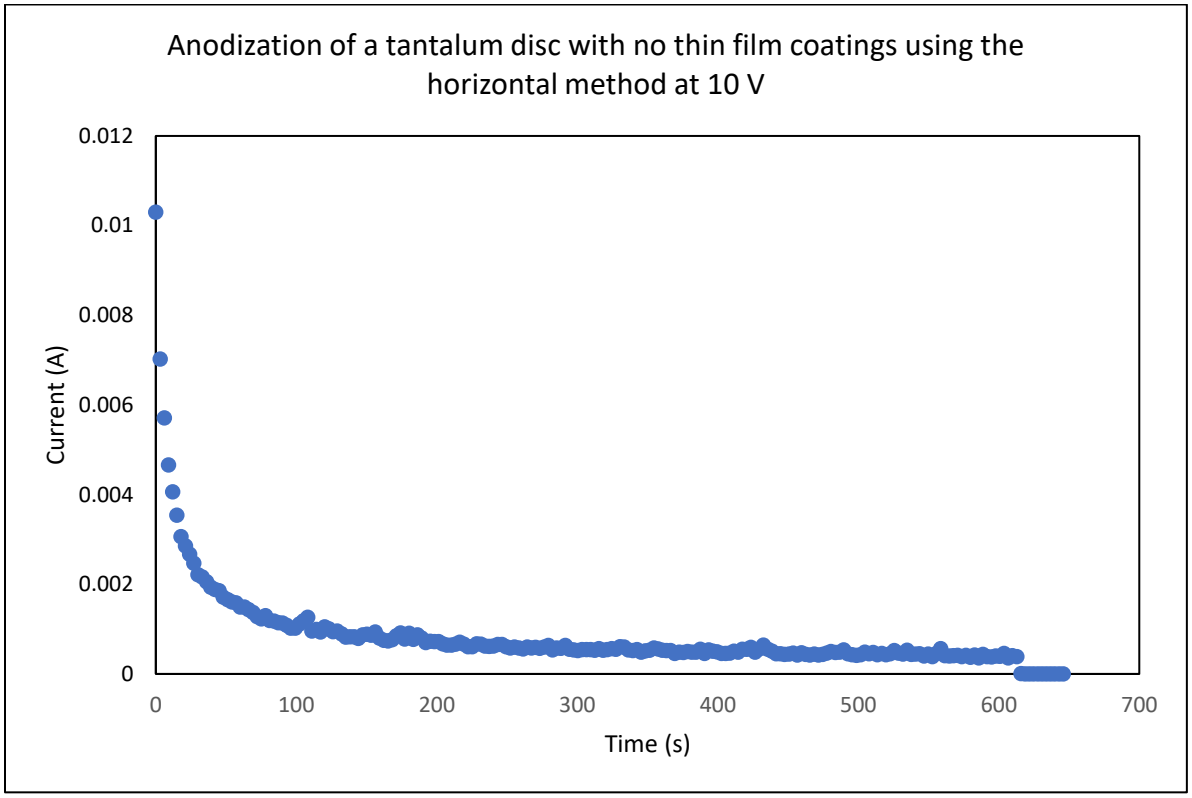


Figure 4.23. Current vs. time anodization plot for a tantalum disc with no thin film coatings using the horizontal anodization method at 10 V.

The second method involved sputtering ~ 110 nm of aluminum onto the tantalum disc, and following the same procedure described above and shown in Figure 4.22, except anodization

of the aluminum face was done at 4 V. There was no previous horizontal anodization of the back tantalum face at 10 V, as the back tantalum face did not contact the acid in this method. The face coated with the thin aluminum film was submerged in the acid horizontally, ensuring only the aluminum face was anodized. This method allowed for the entire surface to be anodized as the disc did not have to be partially outside of the acid for clip attachment. Figure 4.24 shows the anodization plot of a tantalum disc coated with ~ 110 nm of aluminum anodizing the aluminum face at 4 V using this horizontal method. In addition to this disc, five other tantalum discs were prepared and anodized under the same conditions (110 nm of aluminum anodized horizontally at 4 V). The anodization curves for the five additional discs can be found in Appendix 4 (Figures A4.7 – A4.11).

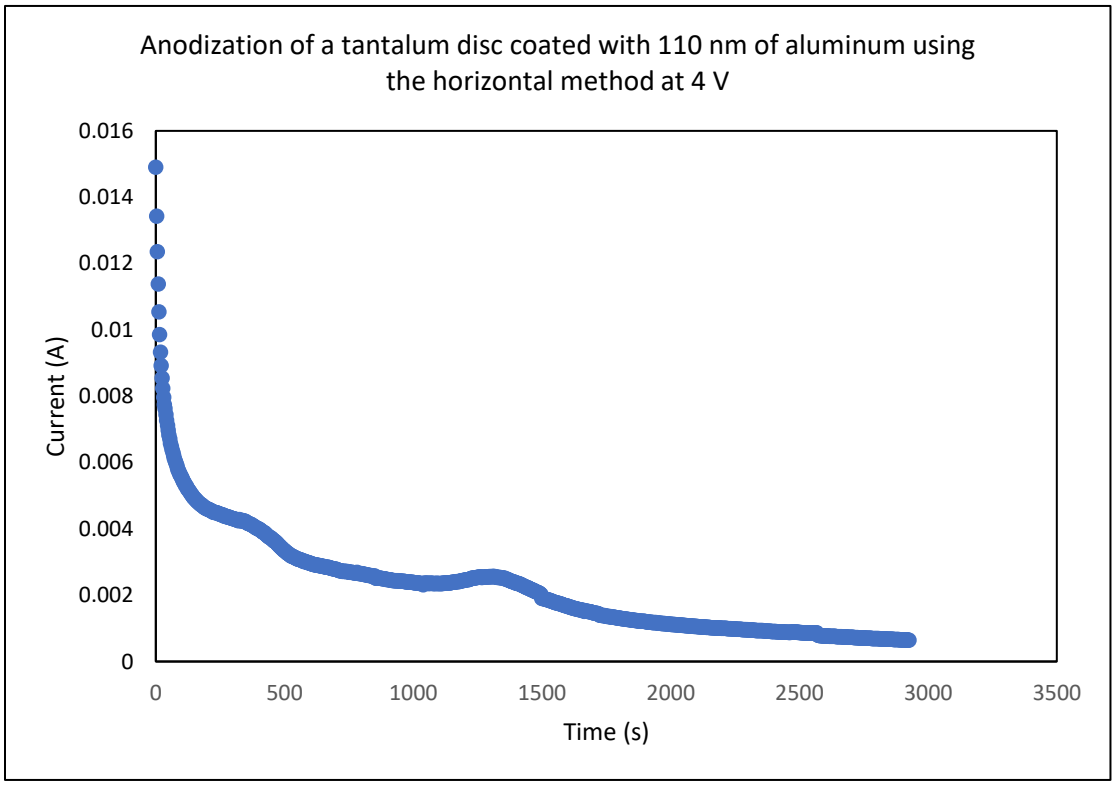


Figure 4.24. Current vs. time anodization plot for a tantalum disc coated with 110 nm of aluminum using the horizontal anodization method to anodize the aluminum face at 4 V.

Figure 4.25 shows the anodization curve produced when a thin piece of aluminum foil was anodized under the same conditions as the aluminum coated tantalum discs. The discrepancy between the aluminum foil curve and the tantalum disc curve suggests an issue with the anodization of the thin aluminum film on the tantalum disc. The aluminum foil anodization curve (Figure 4.25) follows a more obvious pore formation curve compared to the aluminum coated tantalum disc curve (Figure 4.24). To further investigate pore formation on the aluminum coated tantalum disc, SEM images were taken. SEM images were also taken of the anodized aluminum foil to verify and compare pore formation.

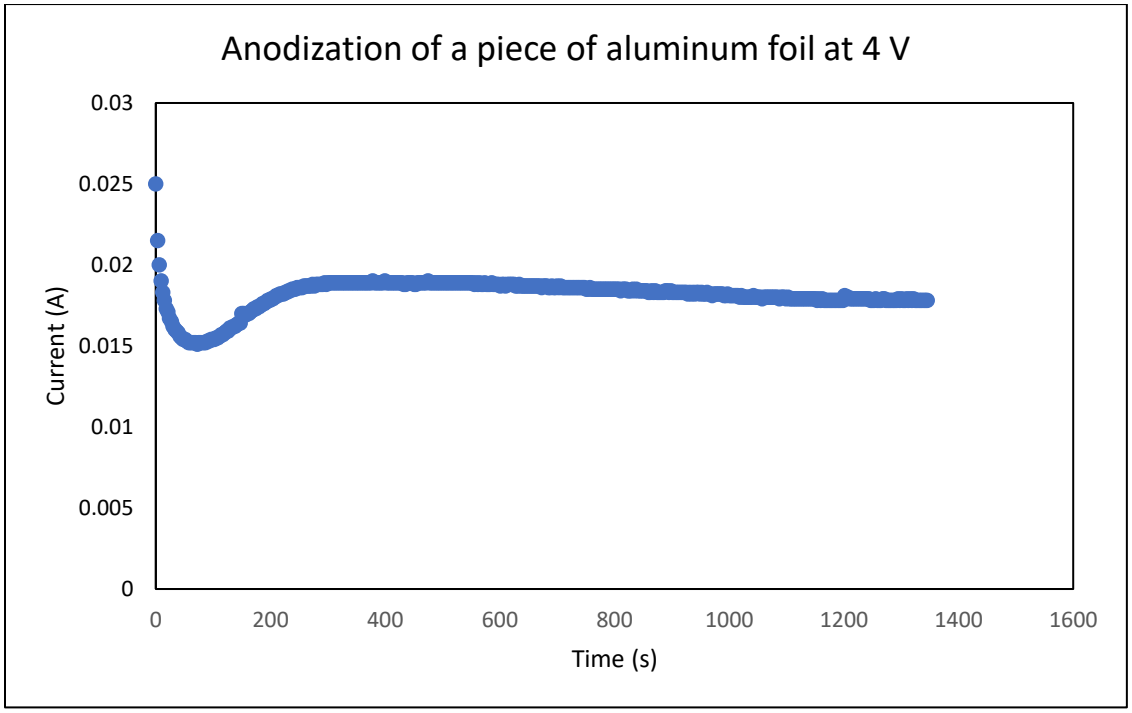


Figure 4.25. Current vs. time anodization plot for a piece of aluminum foil at 4 V.

SEM images were taken of the coated and anodized tantalum discs to visualize the morphology of the thin films, as well as to visualize pore formation. All SEM images were taken using the InLens mode with an EHT range of 3.0 to 10.0 kV. The working distance varied between 5.0 mm and 10.4 mm. Figure 4.26 shows the topographical profile of anodized

aluminum foil at magnifications of 50,000 X (left) and 70,000 X (right). Pores can be seen indicating that the porous, alumina layer was formed. Figure 4.27 shows the topographical profile of a tantalum disc that was anodized vertically after sputtering ~ 110 nm of aluminum onto the surface at 50,000 X (left) and 70,000 X (right). During anodization, the curve produced for this disc did not follow the expected aluminum anodization curve. Rather than rising and falling, the curve continuously dropped as shown in Figure 4.28. However, it appears that pores were formed on the surface by observing the SEM images. The anodization curves for six additional tantalum discs that were anodized horizontally at 10 V, then sputtered with 110 nm of aluminum, then anodized vertically at 4 V are shown in Appendix 4 (Figures A4.12 – A4.17). Figure 4.29 shows the topographical profile of a tantalum disc that was anodized horizontally at 4 V after sputtering ~ 110 nm of aluminum onto the surface at 50,000 X (left) and 70,000 X (right). For this disc, the anodization curve showed a minor rise and fall as shown in Figure 4.30 prior to dropping to 0 amperes. SEM images indicate that a porous alumina layer was formed on the surface.

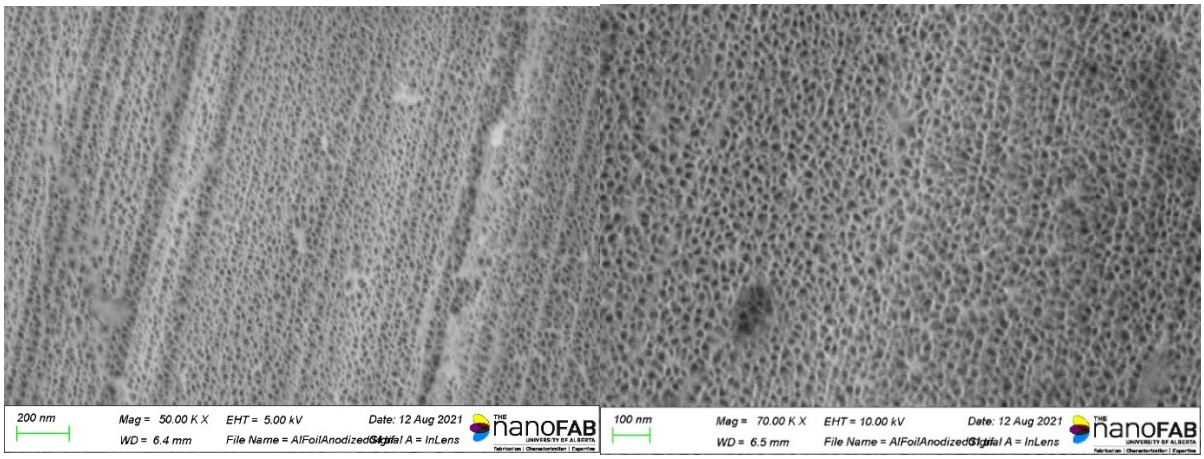


Figure 4.26. Topographical SEM images of anodized aluminum foil at magnification of 50,000 X (left) and 70,000 X (right).

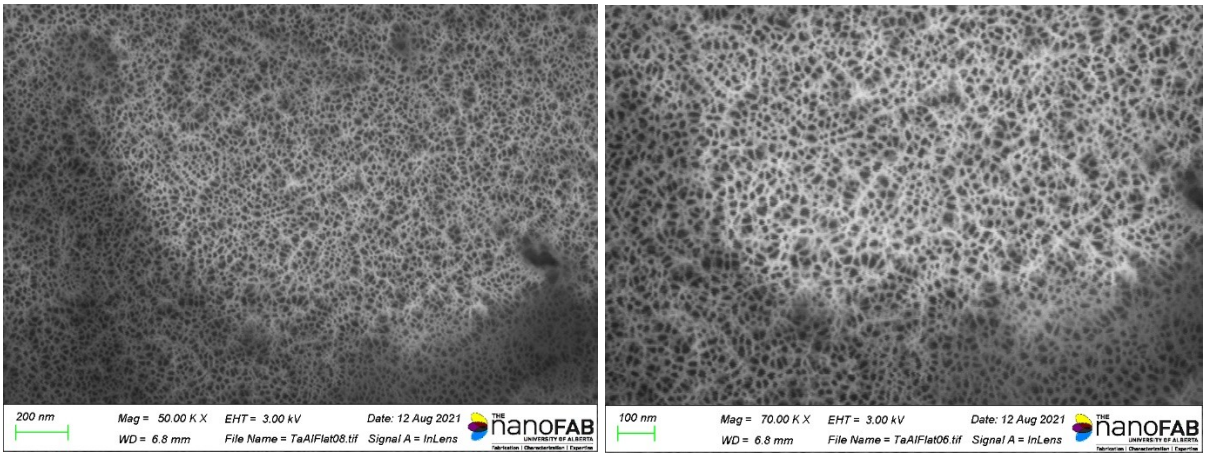


Figure 4.27. Topographical SEM images of a tantalum disc that had the back tantalum face anodized at 10 V, then coated with ~ 110 nm of aluminum, followed by vertical anodization at 4 V that produced an unexpected curve at magnification of 50,000X (left) and 70,000X (right).

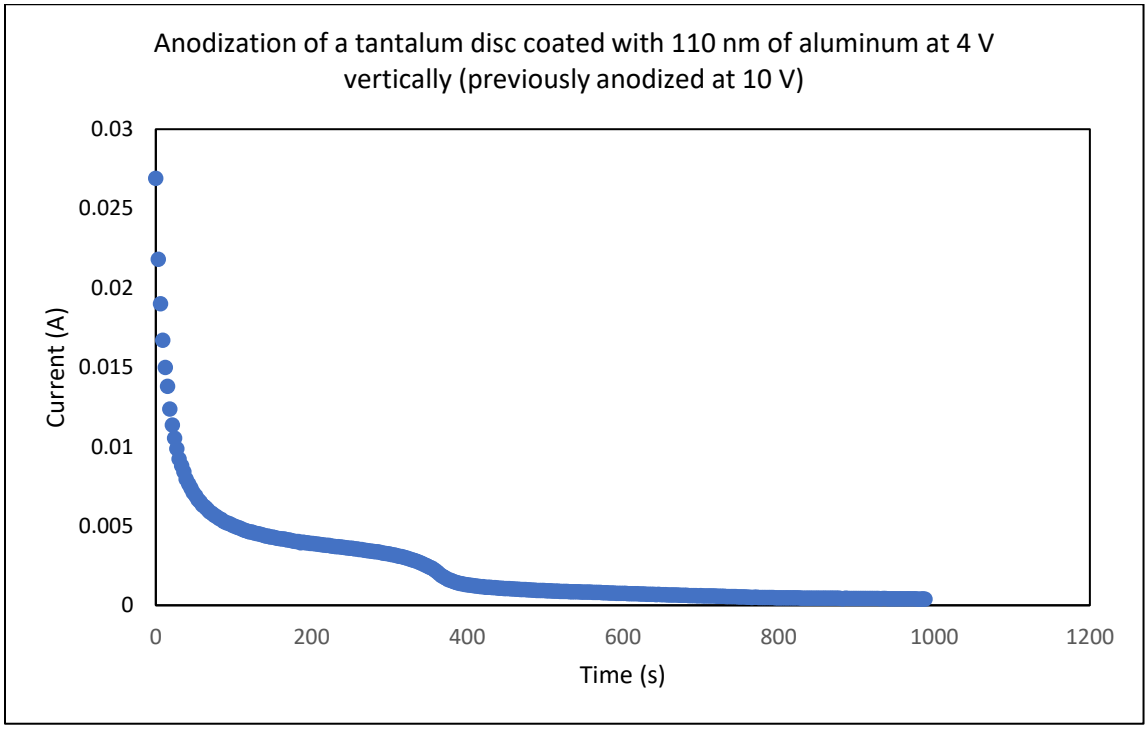


Figure 4.28. Current vs. time anodization plot for a tantalum disc coated with 110 nm of aluminum at 4 V (vertical) with previous anodization of tantalum face at 10 V (SEM images shown in Figure 4.27).

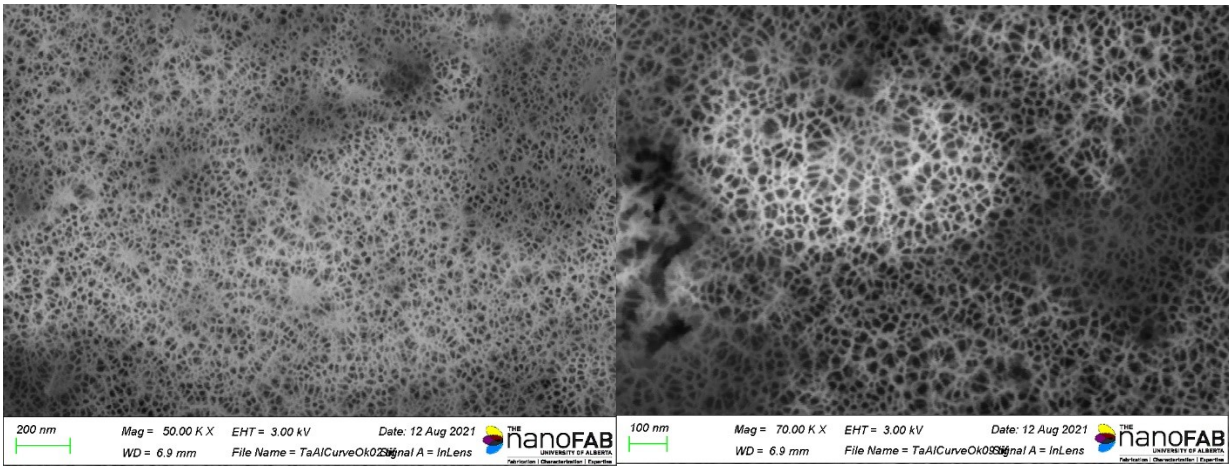


Figure 4.29. Topographical SEM images of a tantalum disc after sputtering ~ 110 nm of aluminum, followed by horizontal anodization at 4 V that produced the expected curve at magnification of 50,000 X (left) and 70,000 X (right).

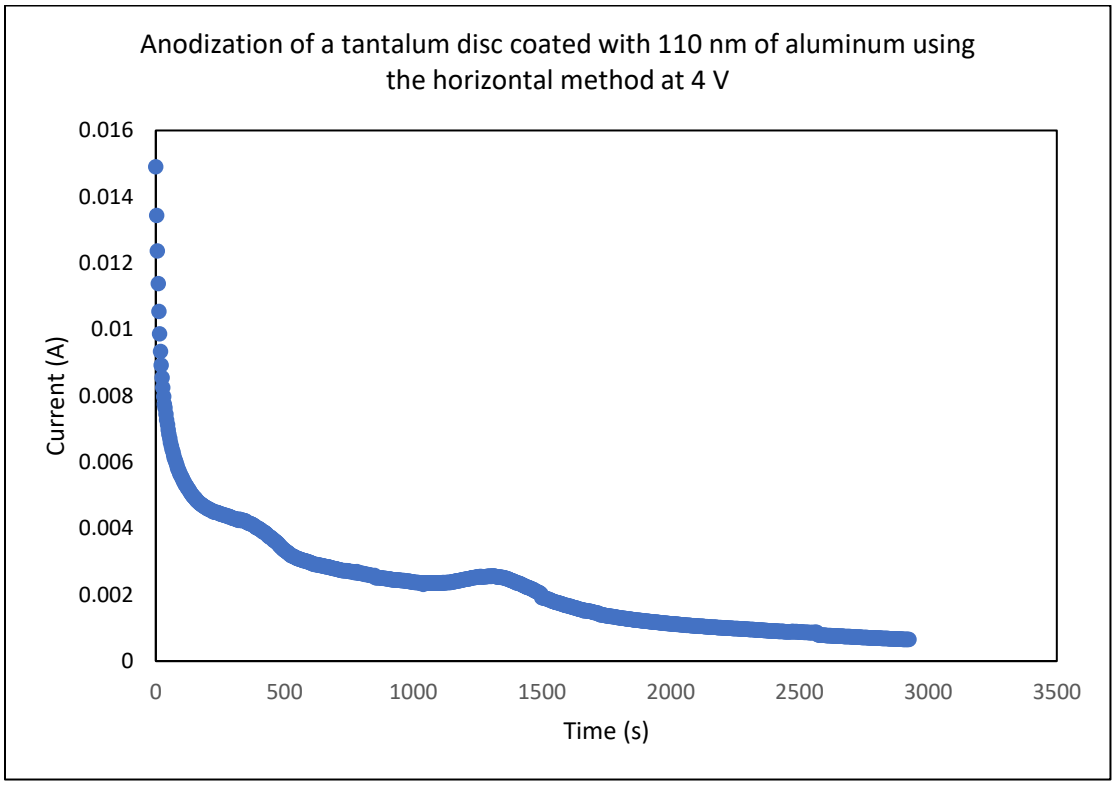


Figure 4.30. Current vs. time anodization plot for the tantalum disc coated with 110 nm of aluminum and anodized horizontally at 4 V (SEM images shown in Figure 4.29).

The pores were two times larger than expected when compared to work done by Matthew Nickel on silicon wafers coated with tantalum and aluminum [4]. To investigate whether the thickness of tantalum has any effect on the alumina structure or porosity, 125 nm, 250 nm, 500 nm and 1000 nm of tantalum were deposited onto silicon wafers. The wafers were then coated with ~ 110 nm of aluminum and anodized, then viewed by SEM. Figure 4.31, 4.32, 4.33, and 4.34 display the current vs. time anodization graphs at 4 V for the silicon wafers coated with 125 nm, 250 nm, 500 nm and 1 μm of tantalum, then 110 nm of aluminum, respectively.

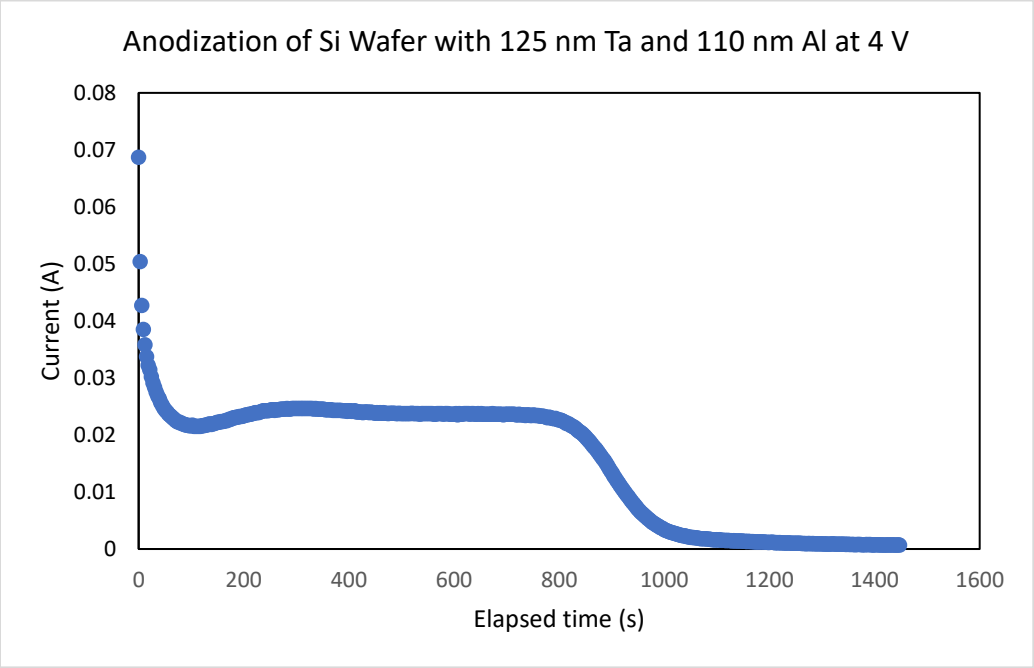


Figure 4.31. Current vs. time anodization plot for a silicon wafer coated with 125 nm of tantalum and 110 nm of aluminum at 4 V.

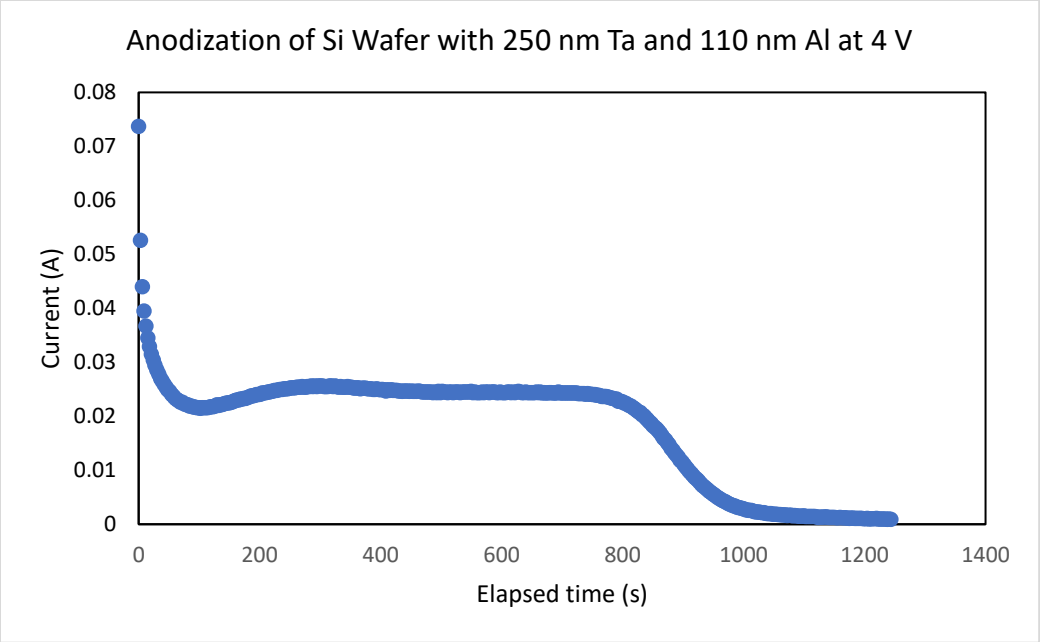


Figure 4.32. Current vs. time anodization plot for a silicon wafer coated with 250 nm of tantalum and 110 nm of aluminum at 4 V.

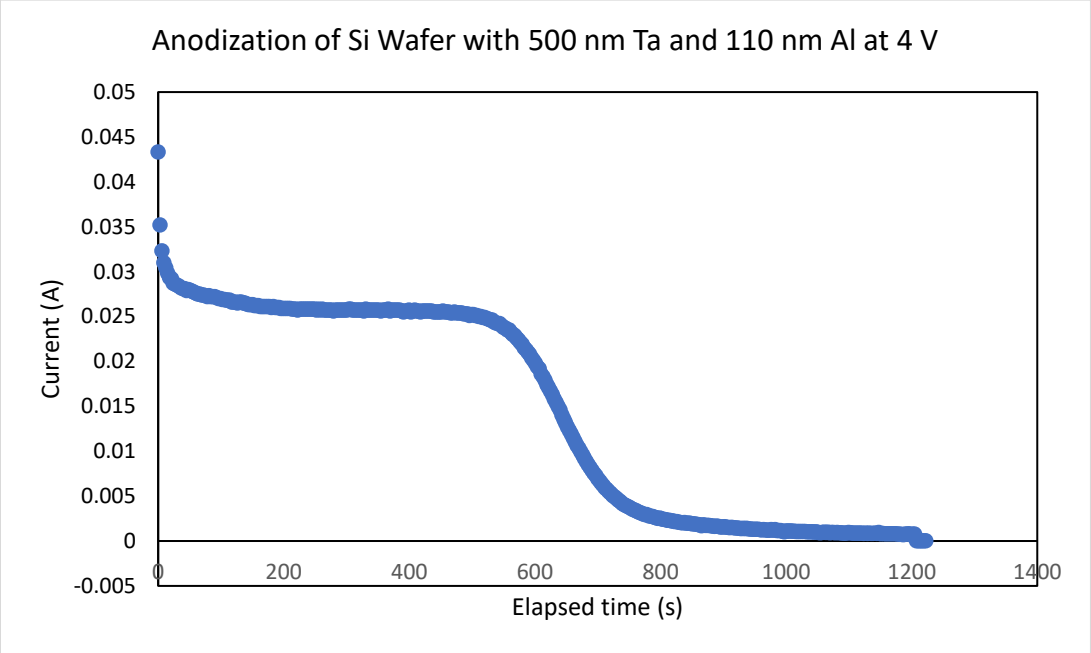


Figure 4.33. Current vs. time anodization plot for a silicon wafer coated with 500 nm of tantalum and 110 nm of aluminum at 4 V.

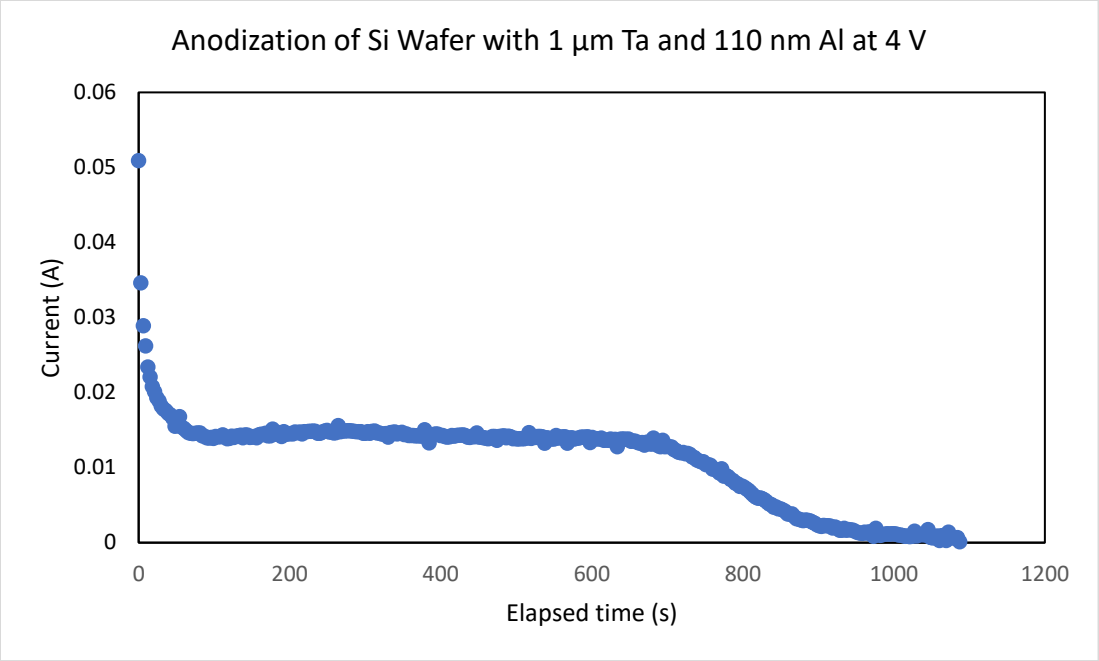


Figure 4.34. Current vs. time anodization plot for a silicon wafer coated with 1 µm of tantalum and 110 nm of aluminum at 4 V.

Figures 4.35, 4.36 and 4.37 show the topographical SEM images of the silicon wafers coated with ~ 125 nm of tantalum and ~ 110 nm of aluminum after anodization at 4 V at magnifications of 10,000 X, 30,000 X and 50,000 X, respectively. Figures 4.38, 4.39 and 4.40 show the topographical SEM images of the silicon wafer coated with ~ 250 nm of tantalum and ~ 110 nm of aluminum after anodization at 4 V at magnifications of 10,000 X, 30,000 X and 50,020 X, respectively. Figures 4.41, 4.42 and 4.43 show the topographical SEM images of the silicon wafer coated with ~ 1 µm of tantalum and ~ 110 nm of aluminum after anodization at 4 V at magnifications of 10,000 X, 30,000 X and 50,000 X, respectively. In each case, pores were visible on the surface, indicating that the thickness of the tantalum layer does not affect the alumina microstructure or porosity.

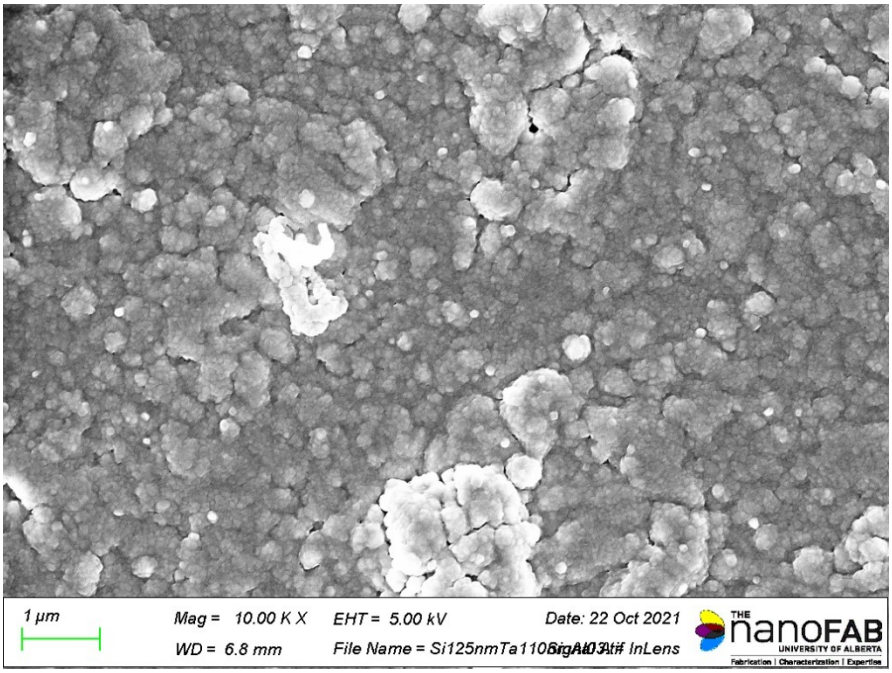


Figure 4.35. Topographical SEM image of a silicon wafer coated with ~ 125 nm of tantalum and ~ 110 nm of aluminum after anodization at 4 V at 10,000 X.

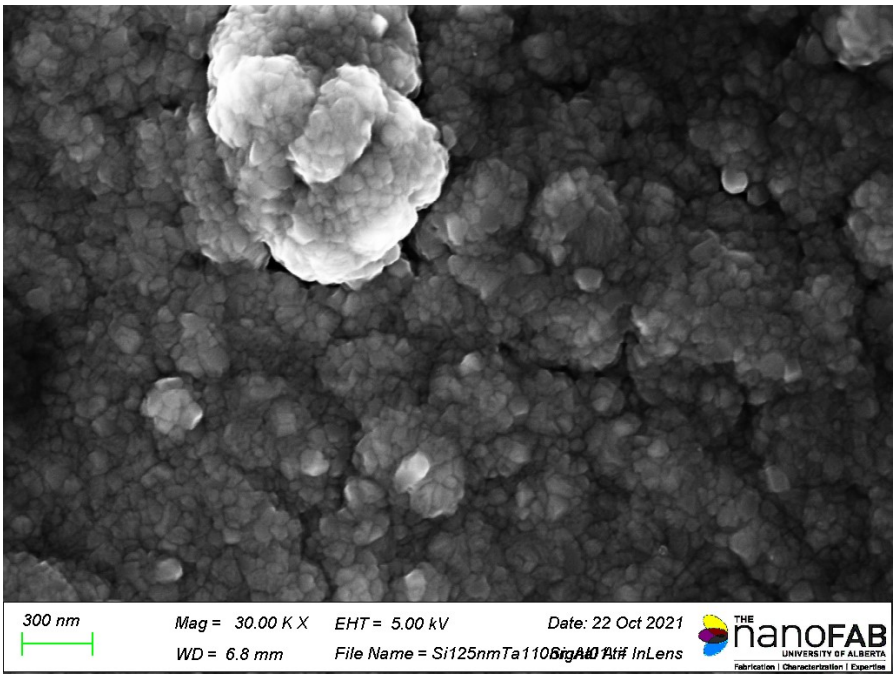


Figure 4.36. Topographical SEM image of a silicon wafer coated with ~ 125 nm of tantalum and ~ 110 nm of aluminum after anodization at 4 V at 30,000 X.

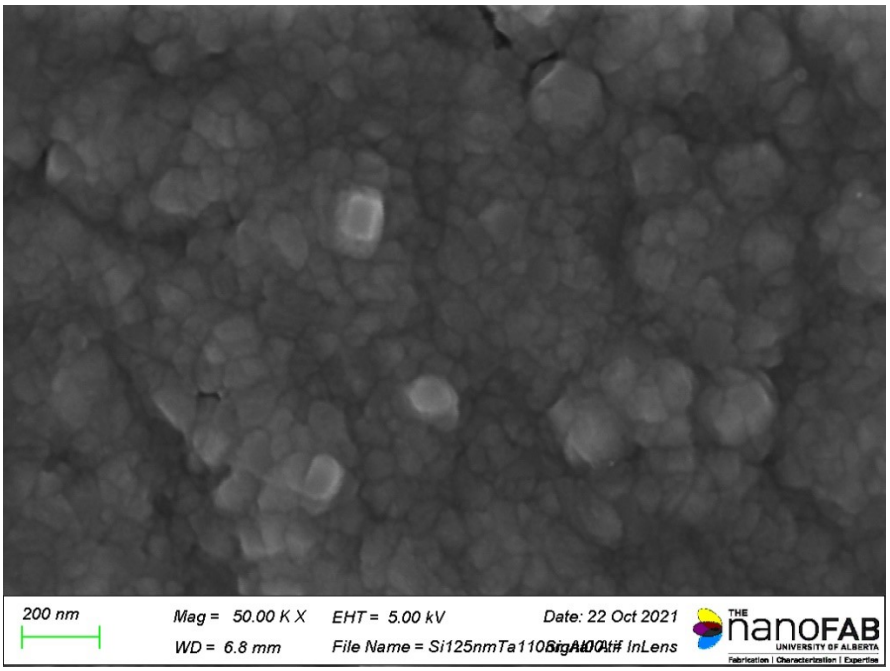


Figure 4.37. Topographical SEM image of a silicon wafer coated with ~ 125 nm of tantalum and ~ 110 nm of aluminum after anodization at 4 V at 50,000 X.

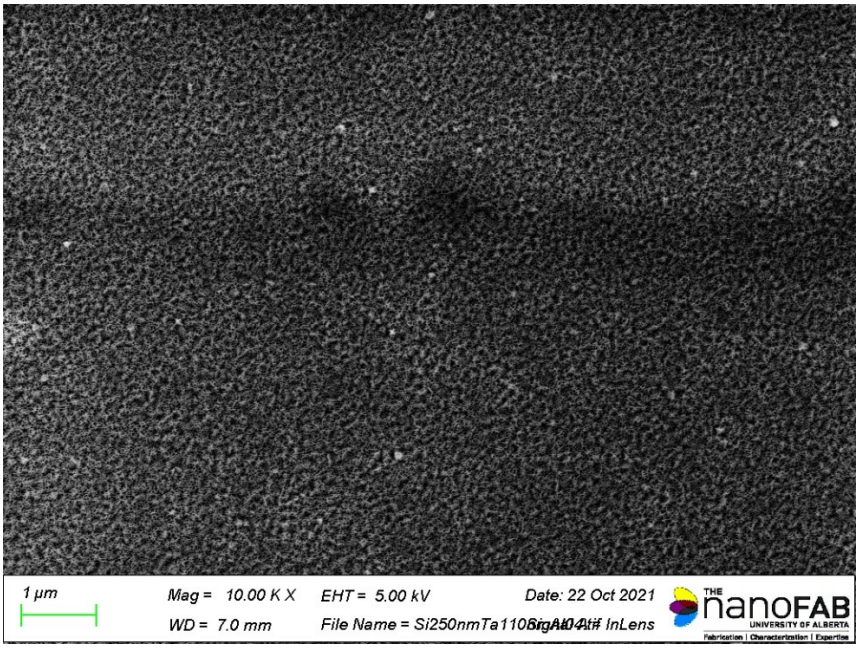


Figure 4.38. Topographical SEM image of a silicon wafer coated with ~ 250 nm of tantalum and ~ 110 nm of aluminum after anodization at 4 V at 10,000 X.

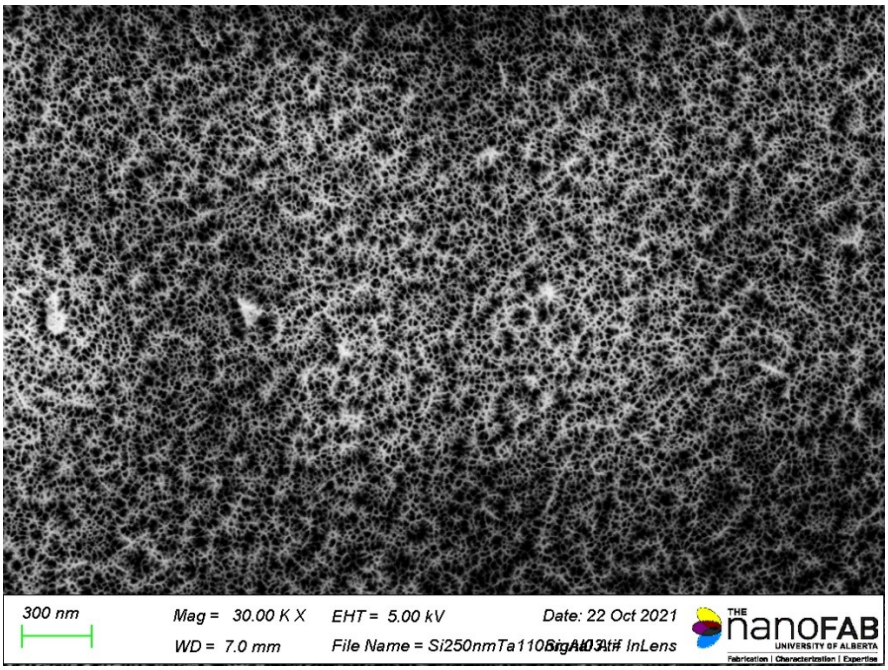


Figure 4.39. Topographical SEM image of a silicon wafer coated with ~ 250 nm of tantalum and ~ 110 nm of aluminum after anodization at 4 V at 30,000 X.

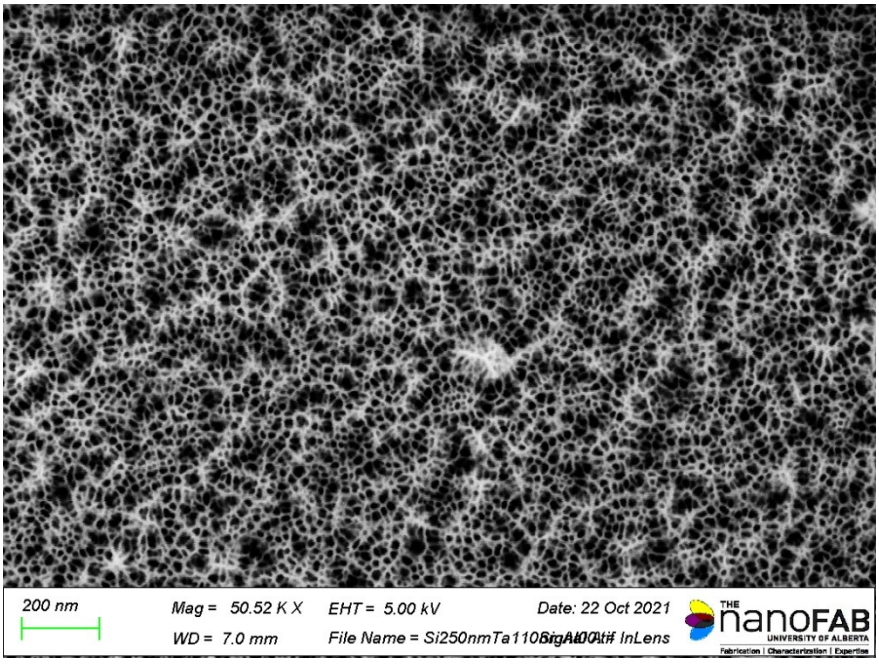


Figure 4.40. Topographical SEM image of a silicon wafer coated with ~ 250 nm of tantalum and ~ 110 nm of aluminum after anodization at 4 V at 50,520 X.

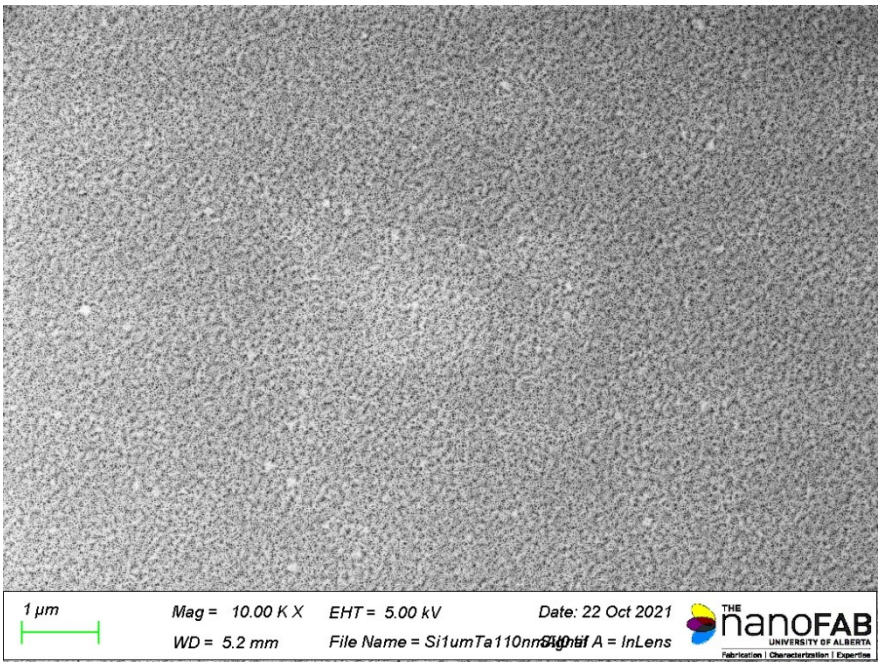


Figure 4.41. Topographical SEM image of a silicon wafer coated with ~ 1 µm of tantalum and ~ 110 nm of aluminum after anodization at 4 V at 10,000 X.

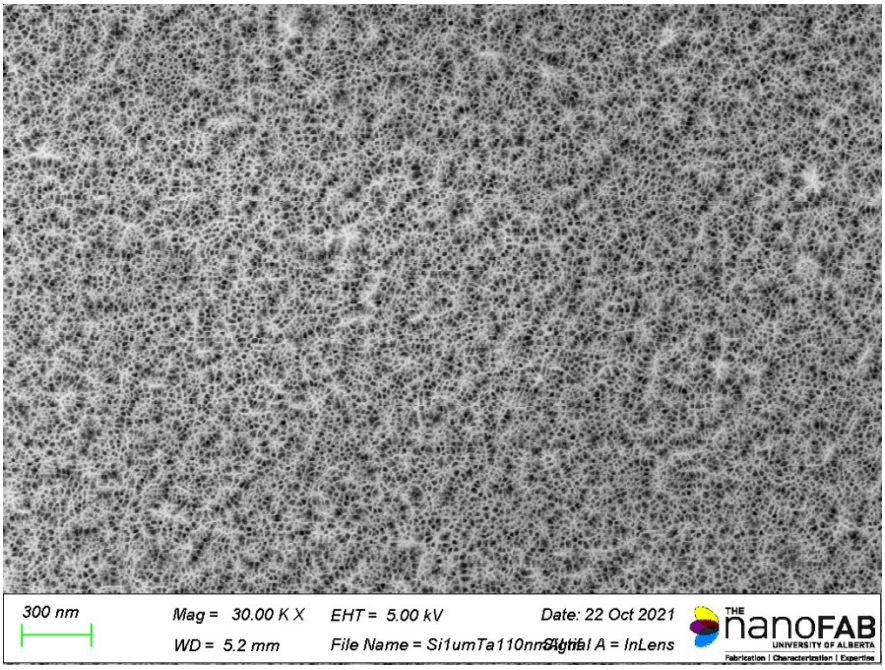


Figure 4.42. Topographical SEM image of a silicon wafer coated with ~ 1 µm of tantalum and ~ 110 nm of aluminum after anodization at 4 V at 30,000 X.

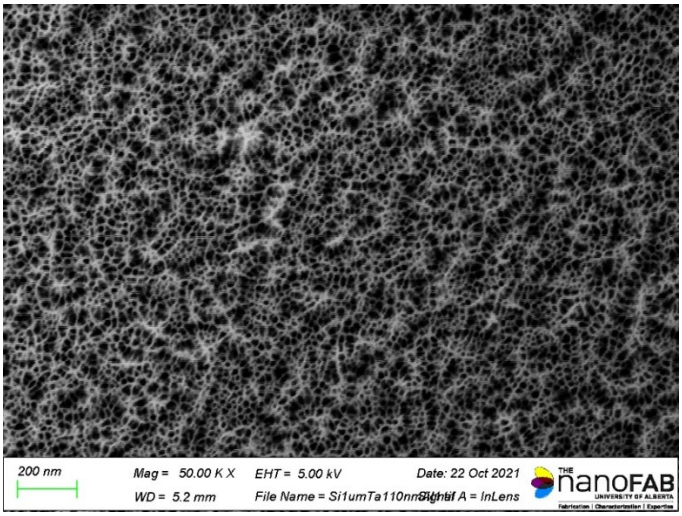


Figure 4.43. Topographical SEM image of a silicon wafer coated with ~ 1 µm of tantalum and ~ 110 nm of aluminum after anodization at 4 V at 50,000 X.

To clean and remove all organics from the tantalum disc surfaces prior to sputtering, two tantalum discs with five holes each were placed in a Jenn-Air JJW9527DDS 27" Electric Wall Oven and ran through a self-cleaning oven cycle, as shown in Figure 4.44. During the self-cleaning cycle, the oven reaches a temperature upwards of 700 °F [6].



Figure 4.44. Two tantalum discs placed on aluminum foil on a cookie rack inside an oven prior to undergoing a self-cleaning cycle to remove organics from the surface.

Figure 4.45 displays the two tantalum discs after the self-cleaning oven cycle was completed. Observing the discs visually suggests that a layer of tantalum oxide formed on the surface of the discs during the heating process. The conductivity of the heat-treated discs at the anodizing voltage was measured to determine if the thickness of the oxide layer generated in the cleaning process was greater than the thickness that would be generated by the anodizing voltage. Three silicon wafers coated with ~ 200 nm tantalum were anodized at 2 V, 4 V and 10 V to be used as controls and a voltmeter was used to measure the resistance across the anodized section and compared to the resistance across the heat-treated tantalum discs. Conducting a continuity test on the heat-treated tantalum discs using a voltmeter indicated an open loop, suggesting that a thick oxide layer formed on the discs during the self-cleaning oven cycle. Therefore a ~ 200 nm tantalum layer was sputtered onto the tantalum discs that underwent the self-cleaning oven cycle prior to sputtering aluminum in order to have a conductive tantalum layer available for anodization.

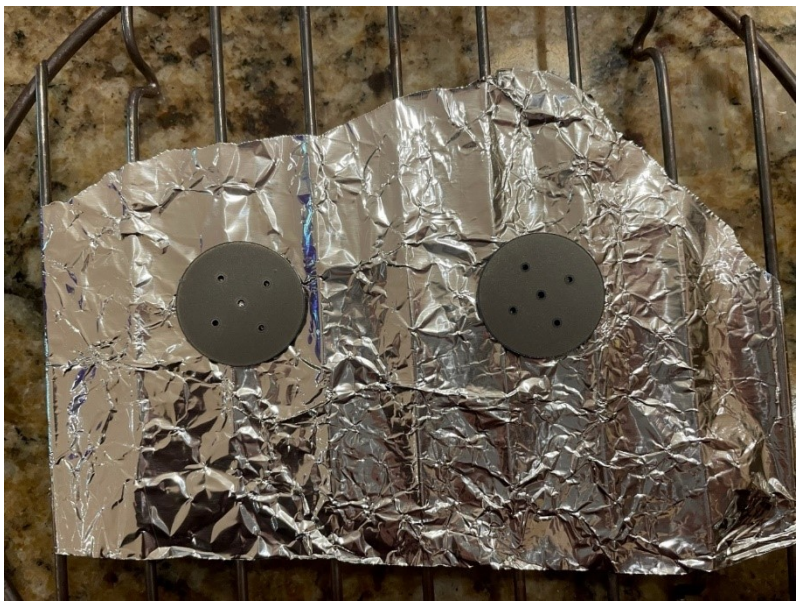


Figure 4.45. Two tantalum discs after heat treatment in a self-cleaning oven cycle to remove organics from the surface. During the treatment, a layer of tantalum oxide appears to have formed on the surface.

Figure 4.46 shows the anodization curve of a tantalum disc that was coated with ~ 200 nm of tantalum and ~ 110 nm of aluminum and anodized at 4 V after undergoing a self-cleaning oven cycle.

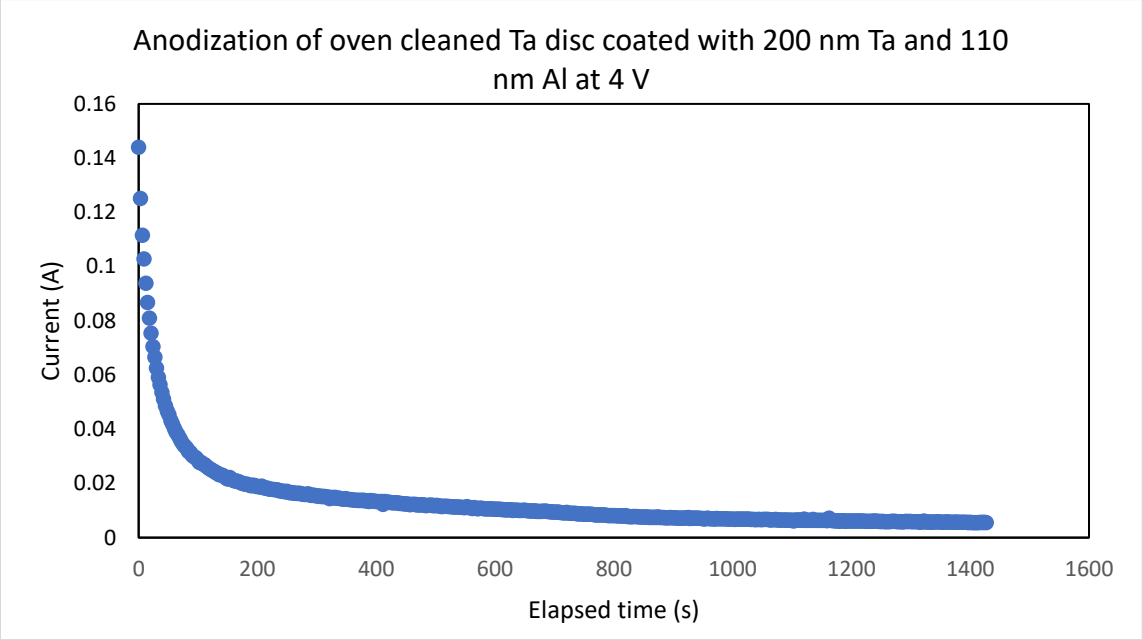


Figure 4.46. Current vs. time anodization curve of a tantalum disc after oven self-cleaning and deposition of 200 nm of tantalum and 110 nm of aluminum at 4 V.

Figure 4.47 shows one tantalum disc after anodization that had been cleaned by isopropanol HPLC grade prior to sputtering ~ 110 nm of aluminum (left) and one tantalum disc that had been cleaned using a self-cleaning oven cycle prior to sputtering ~ 200 nm of tantalum and ~ 110 nm of aluminum and anodizing (right). Visual observation indicates much better adhesion and a smoother surface for the aluminum film to the tantalum disc that had undergone a self-cleaning oven cycle compared to the disc that was cleaned with isopropanol HPLC grade prior to sputtering.

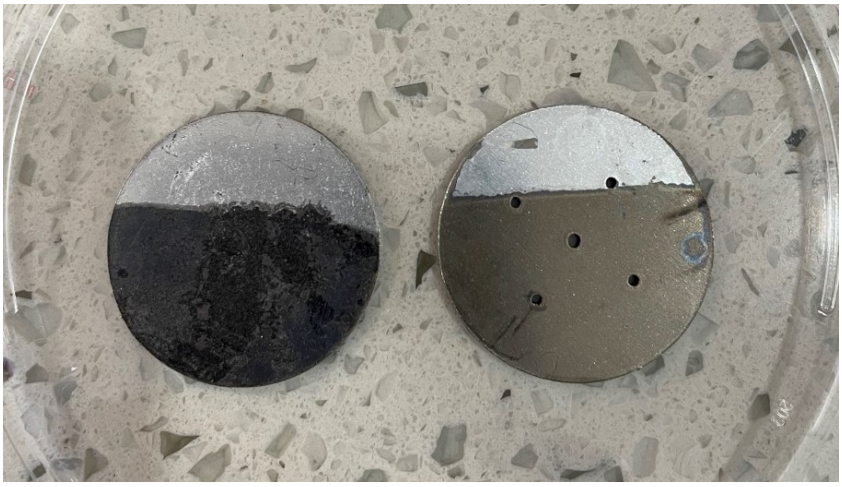


Figure 4.47. Anodized tantalum disc coated with ~ 110 nm of aluminum after being cleaned with HPLC grade isopropanol (left) and anodized tantalum disc coated with ~ 200 nm tantalum and ~ 110 nm aluminum after being cleaned using a self-cleaning oven cycle. Adhesion appears much better for the disc that underwent the self-cleaning oven cycle cleaning method.

Two oven-cleaned tantalum discs were coated with ~ 200 nm of tantalum and ~ 110 nm of aluminum, then the aluminum face was anodized at 4 V using the vertical anodization method. The anodization curves for these discs, shown in Figure 4.48 and 4.49, suggest that the back tantalum side of the disc was anodized, rather than the desired face with the thin layer of aluminum. As the back sides of the discs were not previously anodized at 10 V, it is expected that the back tantalum face was anodized. SEM images were taken of the aluminum face for both discs. Figures 4.50, 4.51, and 4.52 show topographical images of the first tantalum disc (corresponding anodization curve in Figure 4.48) after being run through a self-cleaning oven cycle and coated with thin films of ~ 200 nm of tantalum and ~ 110 nm of aluminum after anodization at 4 V at 10,000 X, 30,000 X and 50,000 X, respectively. Figures 4.53, 4.54, and 4.55 show the second tantalum disc (corresponding anodization curve in Figure 4.49) prepared under the same conditions at 10,000 X, 30,000 X and 50,000 X, respectively. In both cases, it is

likely that both the aluminum coated face and the opposite tantalum face were anodized, as pores can be seen on the aluminum coated side of the disc.

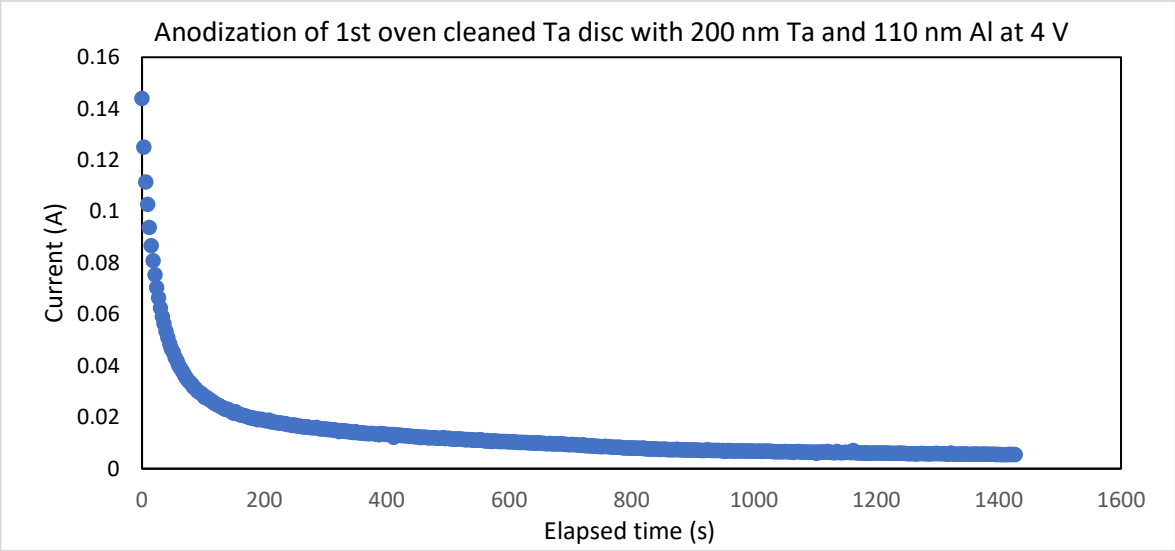


Figure 4.48. Current vs. time anodization curve of first tantalum disc after oven self-cleaning and deposition of 200 nm of tantalum and 110 nm of aluminum at 4 V. It is likely that the back side tantalum face and the aluminum coated face were both anodized.

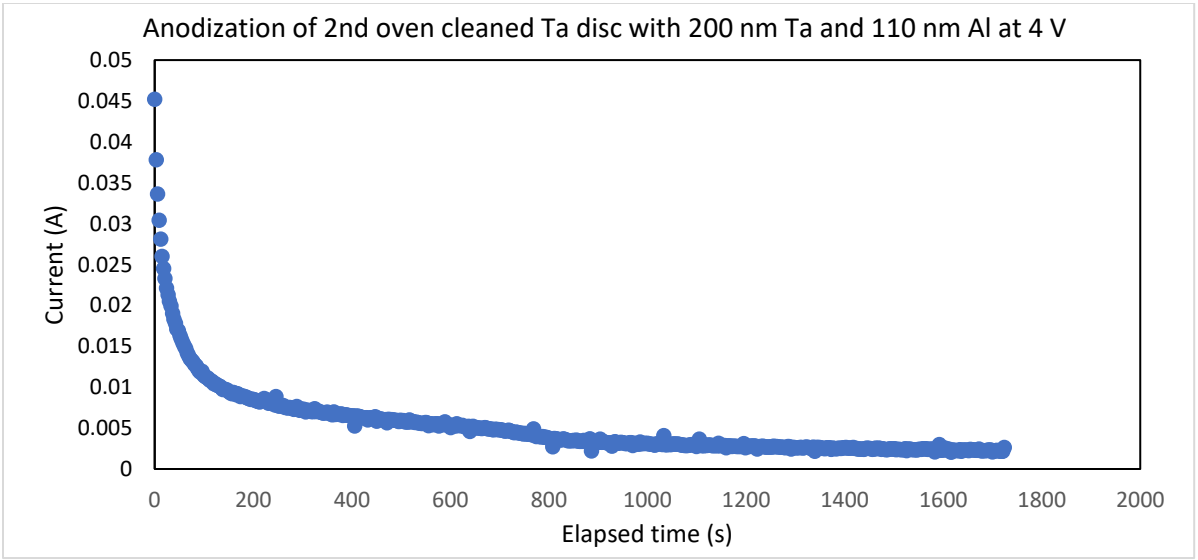


Figure 4.49. Current vs. time anodization curve of second tantalum disc after oven self-cleaning and deposition of 200 nm of tantalum and 110 nm of aluminum at 4 V. It is likely that the back side tantalum face and the aluminum coated face were both anodized.

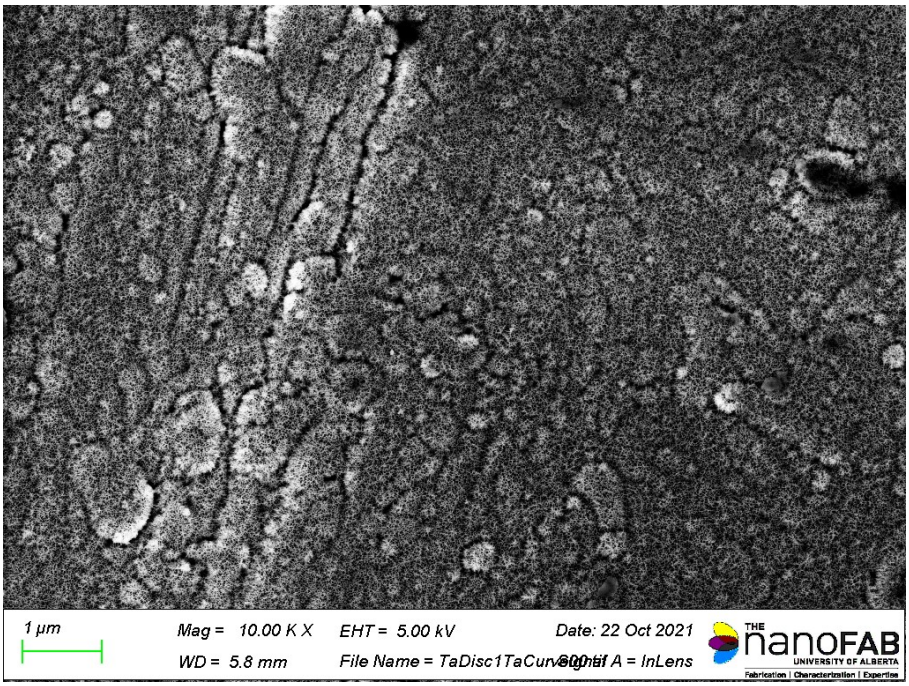


Figure 4.50. Topographical SEM image of the first oven cleaned tantalum disc with ~ 200 nm of tantalum and ~ 110 nm of aluminum after anodization at 4 V at 10,000 X.

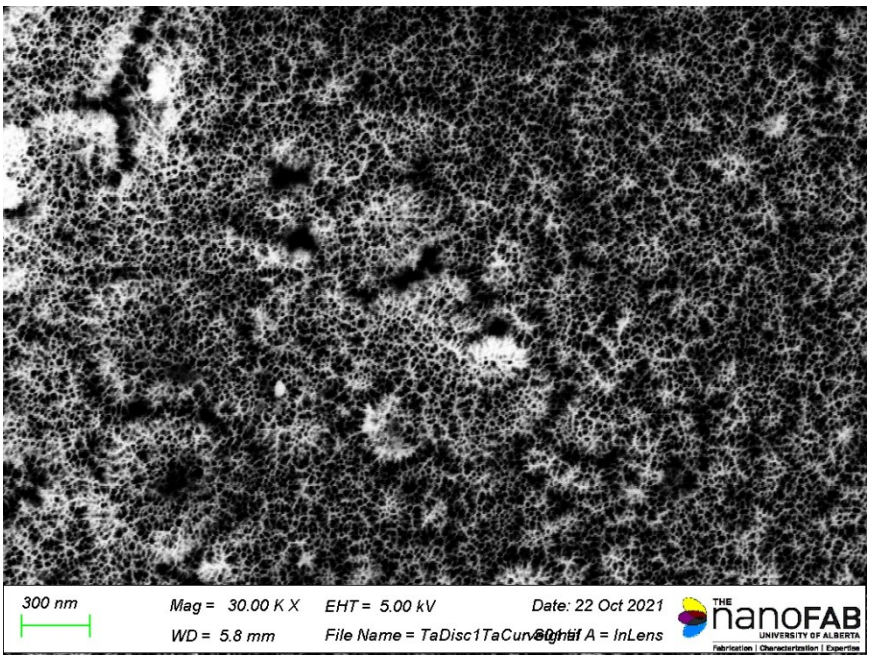


Figure 4.51. Topographical SEM image of the first oven cleaned tantalum disc with ~ 200 nm of tantalum and ~ 110 nm of aluminum after anodization at 4 V at 30,000 X.

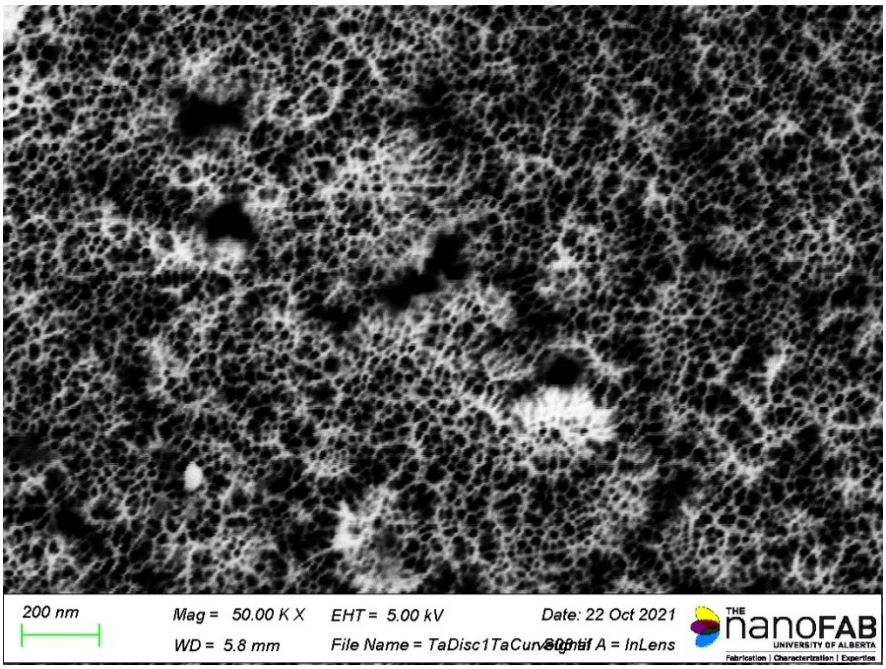


Figure 4.52. Topographical SEM image of the first oven cleaned tantalum disc with ~ 200 nm of tantalum and ~ 110 nm of aluminum after anodization at 4 V at 50,000 X.

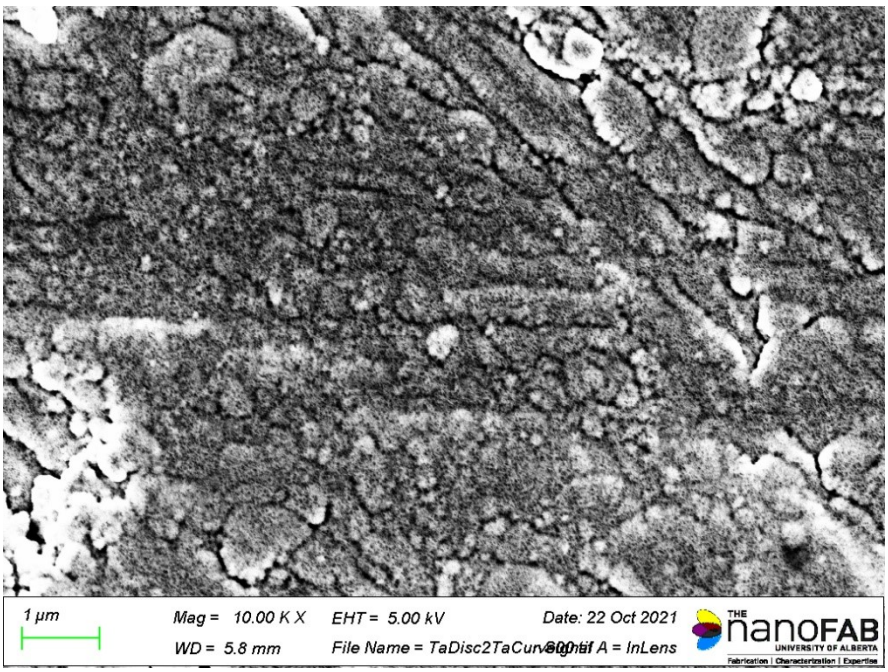


Figure 4.53. Topographical SEM image of the second oven cleaned tantalum disc with ~ 200 nm of tantalum and ~ 110 nm of aluminum after anodization at 4 V at 10,000 X.

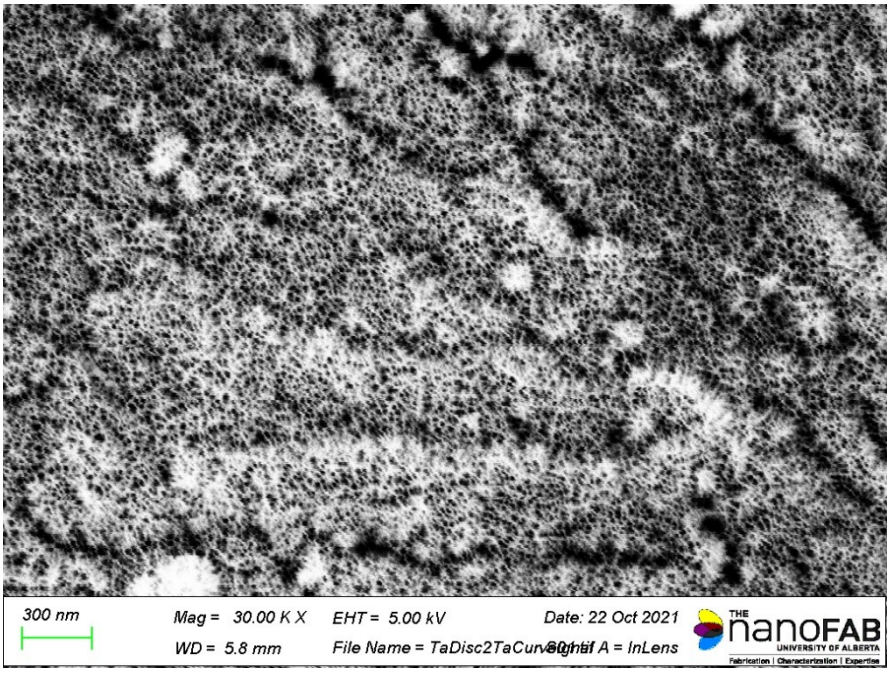


Figure 4.54. Topographical SEM image of the second oven cleaned tantalum disc with ~ 200 nm of tantalum and ~ 110 nm of aluminum after anodization at 4 V at 30,000 X.

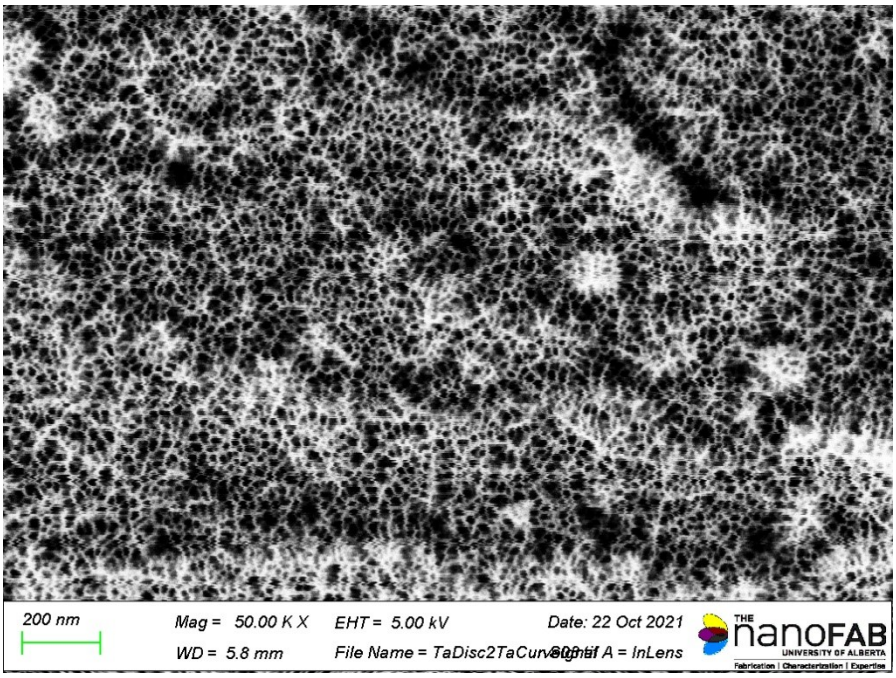


Figure 4.55. Topographical SEM image of the second oven cleaned tantalum disc with ~ 200 nm of tantalum and ~ 110 nm of aluminum after anodization at 4 V at 50,000 X.

Six more tantalum discs with five holes each were placed in the oven for a self-cleaning cycle to remove any organic residues. The back sides of three discs were anodized horizontally at 10 V to ensure that after sputtering of tantalum and aluminum, the front face coated with aluminum would be anodized instead of the back. The anodization curves of the back sides of the three tantalum discs are shown in Figure 4.56 (tantalum disc 1), 4.57 (tantalum disc 2) and 4.58 (tantalum disc 3).

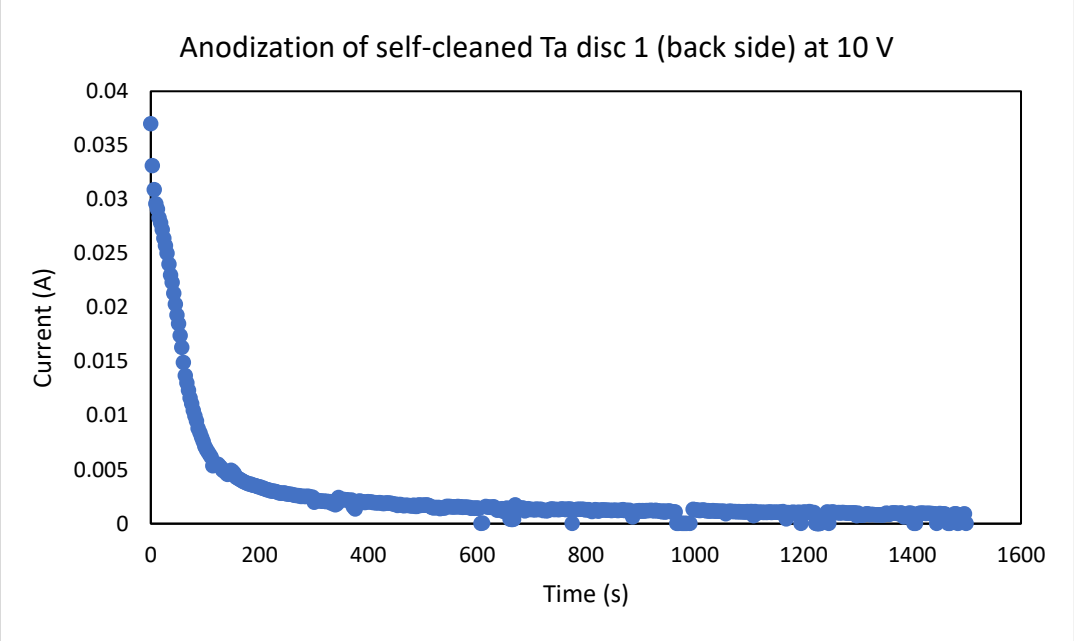


Figure 4.56. Current vs. time anodization curve of the back side of tantalum disc number 1 at 10 V after cleaning in a self-cleaning oven, prior to thin film sputtering.

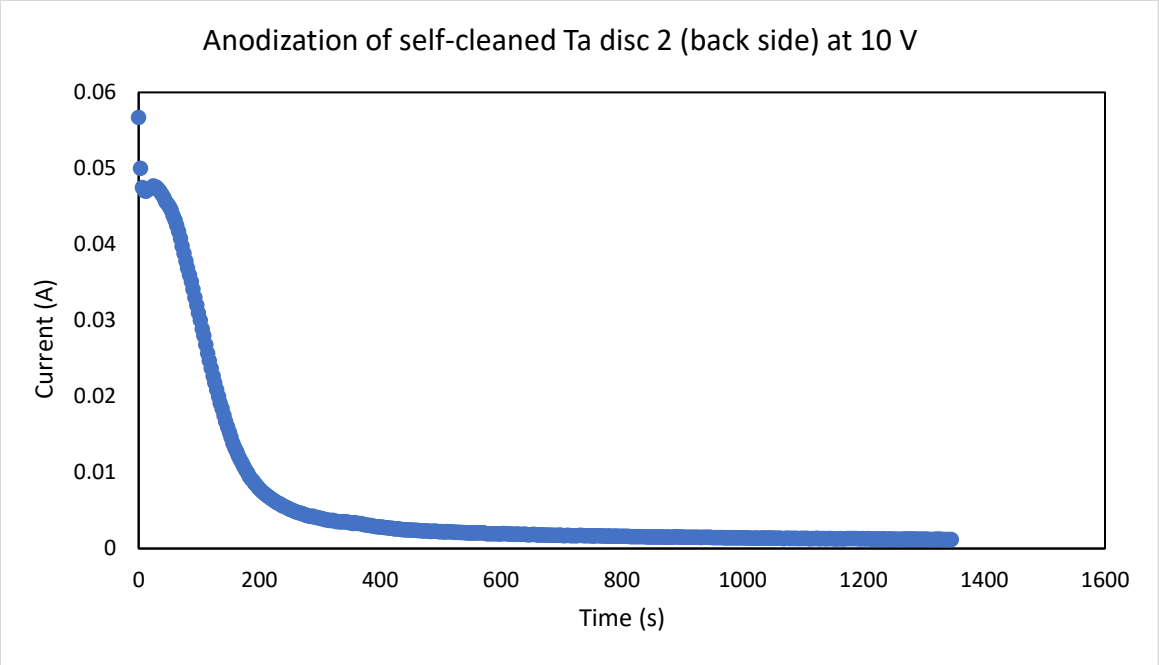


Figure 4.57. Current vs. time anodization curve of the back side of tantalum disc number 2 at 10 V after cleaning in a self-cleaning oven, prior to thin film sputtering.

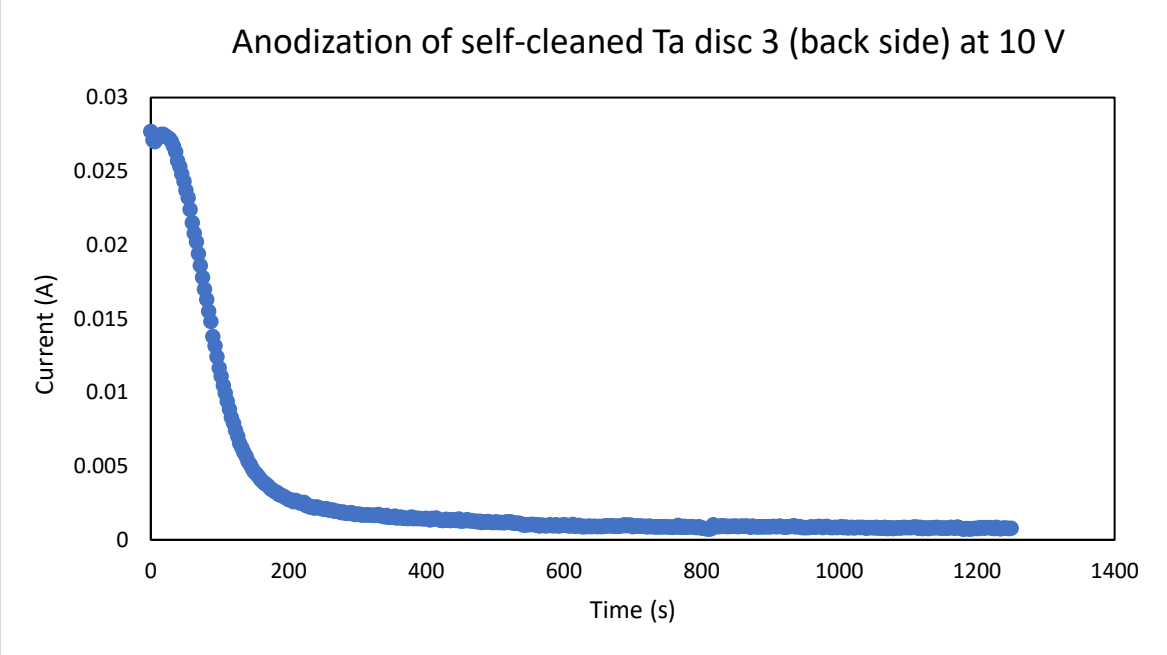


Figure 4.58. Current vs. time anodization curve of the back side of tantalum disc number 3 at 10 V after cleaning in a self-cleaning oven, prior to thin film sputtering.

After anodization of the back side, ~ 200 nm of tantalum was sputtered onto the front face of the tantalum discs, followed by ~ 110 nm of aluminum. Additionally, three other discs were sputtered with tantalum and aluminum under the same conditions. The three discs that were previously anodized at 10 V were then anodized vertically at 4 V to anodize the aluminum layer (tantalum disc 1, tantalum disc 2, tantalum disc 3). The other three discs that were not previously anodized underwent horizontal anodization at 4 V to anodize the aluminum layer (tantalum disc 4, tantalum disc 5, tantalum disc 6). The anodization curves of the three discs that were additionally anodized at 10 V are shown in Figures 4.59 (tantalum disc 1), 4.60 (tantalum disc 2) and 4.61 (tantalum disc 3). The anodization curves of the three discs that were only anodized horizontally at 4 V after thin film deposition are shown in Figures 4.62 (tantalum disc 4), 4.63 (tantalum disc 5), and 4.64 (tantalum disc 6).

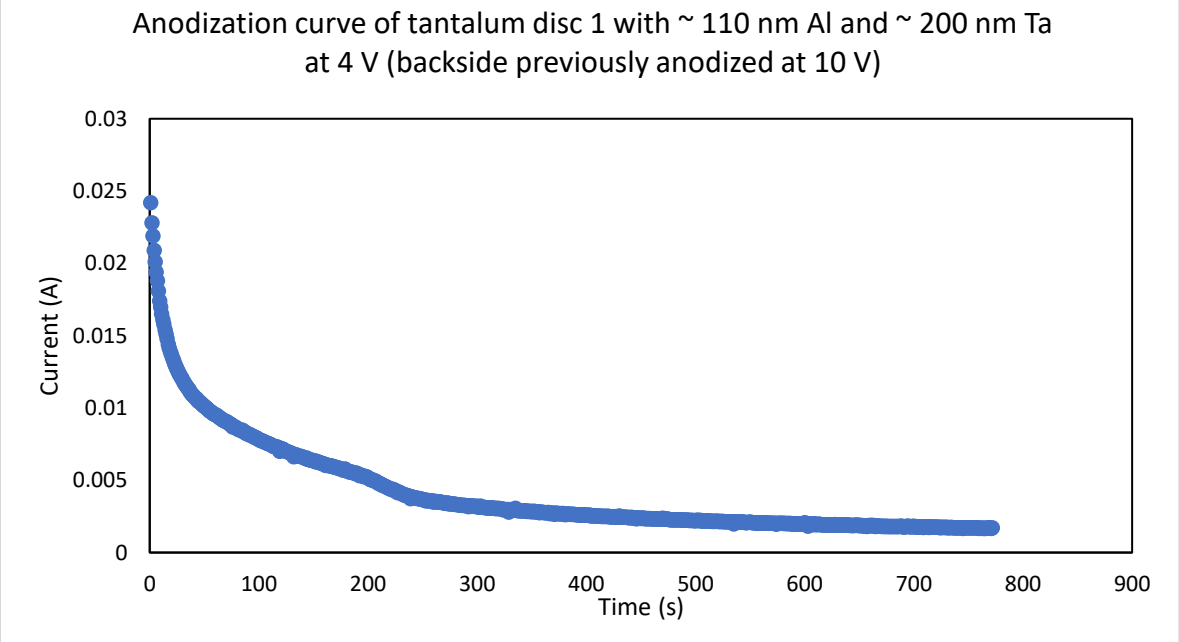


Figure 4.59. Current vs. time anodization curve of tantalum disc 1 (vertical method) after coating with 200 nm of tantalum and 110 nm of aluminum at 4 V (back side previously anodized at 10 V).

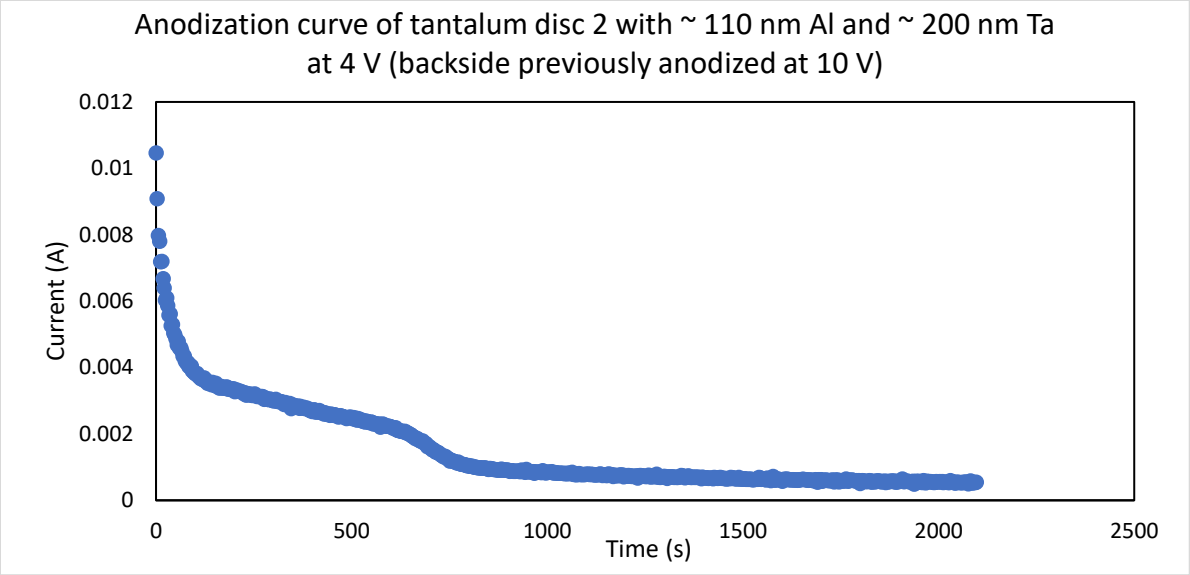


Figure 4.60. Current vs. time anodization curve of tantalum disc 2 (vertical method) after coating with 200 nm of tantalum and 110 nm of aluminum at 4 V (back side previously anodized at 10 V).

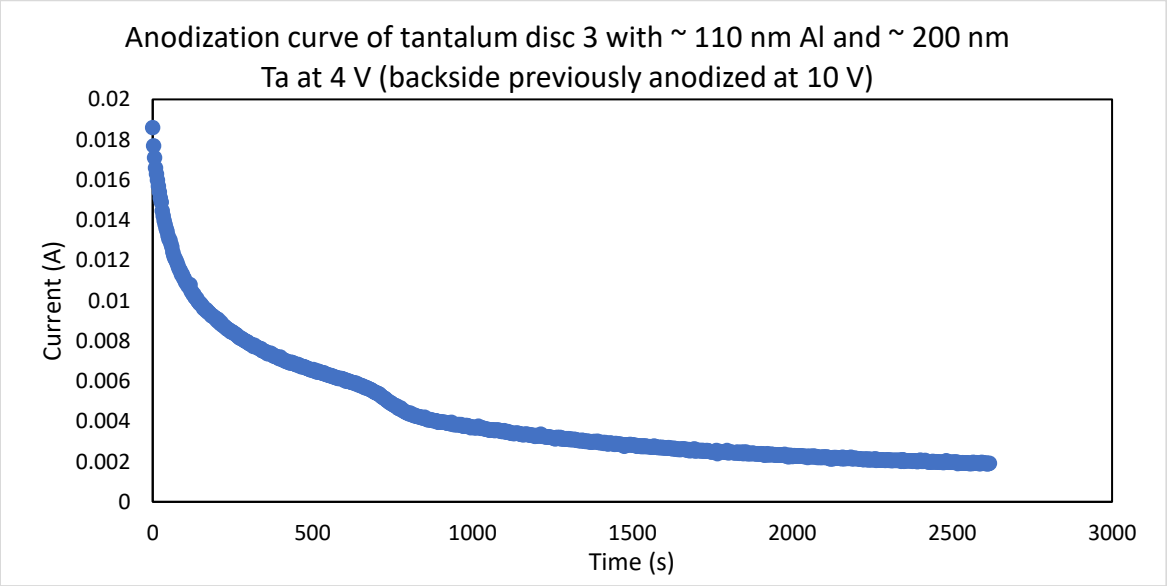


Figure 4.61. Current vs. time anodization curve of tantalum disc 3 (vertical method) after coating with 200 nm of tantalum and 110 nm of aluminum at 4 V (back side previously anodized at 10 V).

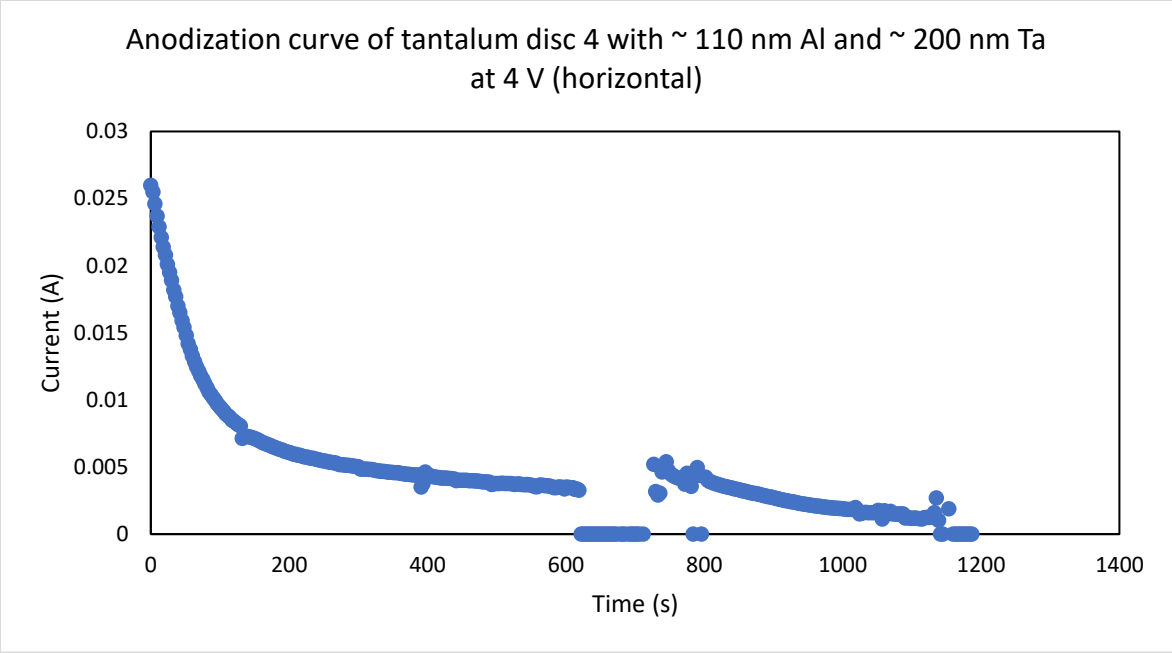


Figure 4.62. Current vs. time anodization curve of tantalum disc 4 (horizontal method) after coating with 200 nm of tantalum and 110 nm of aluminum at 4 V (no previous anodization).

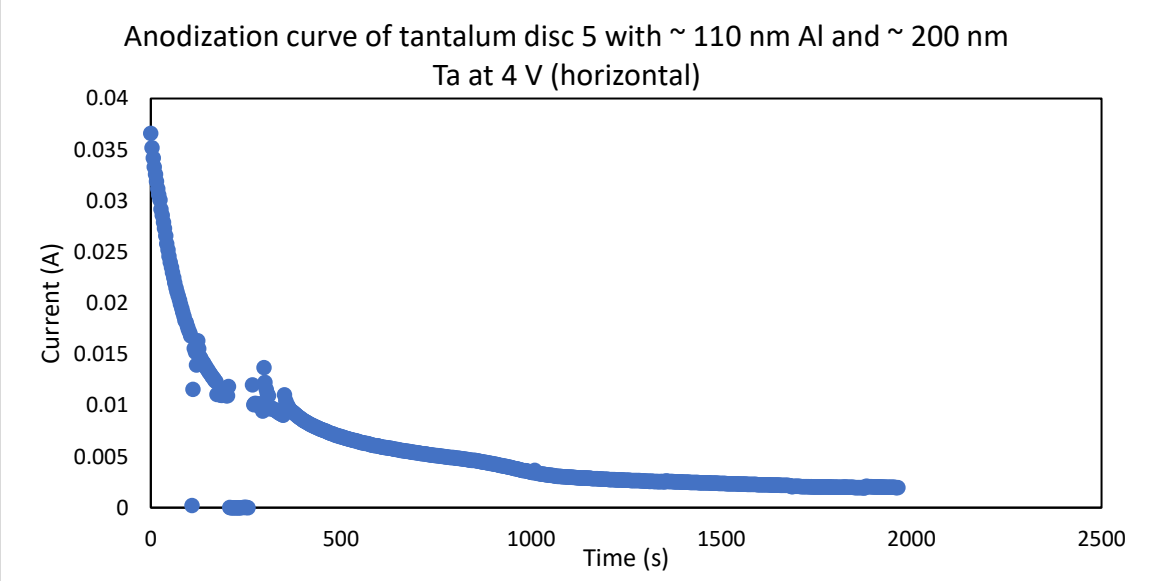


Figure 4.63. Current vs. time anodization curve of tantalum disc 5 (horizontal method) after coating with 200 nm of tantalum and 110 nm of aluminum at 4 V (no previous anodization).

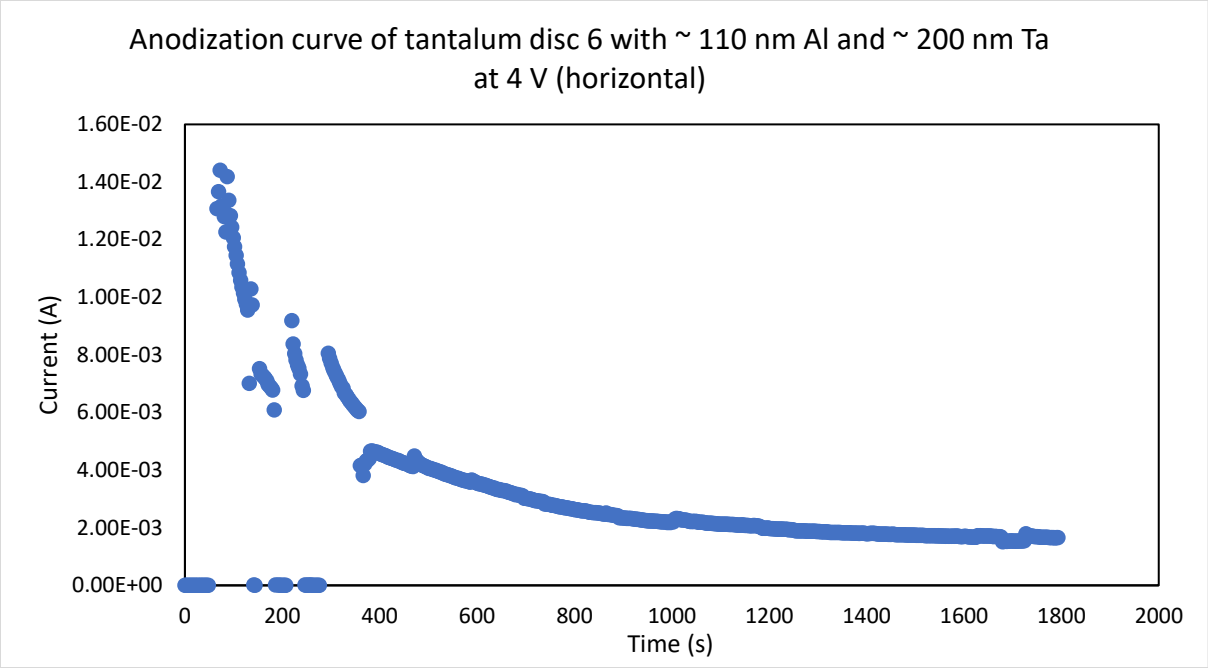


Figure 4.64. Current vs. time anodization curve of tantalum disc 6 (horizontal method) after coating with 200 nm of tantalum and 110 nm of aluminum at 4 V (no previous anodization).

SEM was used to view the discs and to determine which anodization method produced better results. Figure 4.65, 4.66 and 4.67 show SEM images of tantalum disc 2 that was anodized at 10 V (backside) then sputtered with ~ 200 nm tantalum and ~ 110 nm aluminum and then anodized at 4 V at magnifications of 10,000 X, 30,000 X and 50,000 X, respectively. Figure 4.68, 4.69 and 4.70 show SEM images of tantalum disc 6 that was sputtered with ~ 200 nm tantalum and ~ 110 nm aluminum and anodized at 4 V (no prior anodization) at magnifications of 10,000 X, 30,000 X and 50,000 X, respectively.

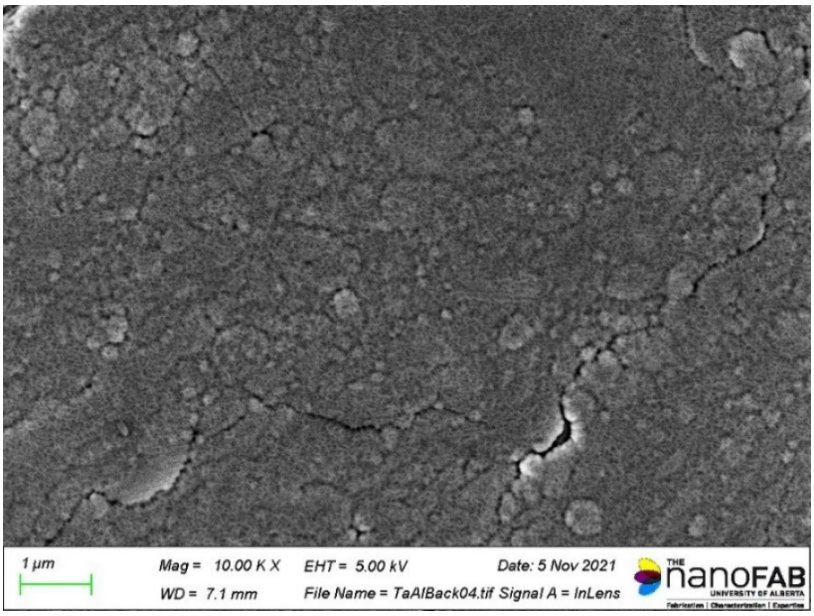


Figure 4.65. Topographical SEM image of oven cleaned tantalum disc 2 that was anodized on the back side at 10 V then sputtered with ~ 200 nm of tantalum and ~ 110 nm of aluminum, then anodized vertically at 4 V at 10,000 X.

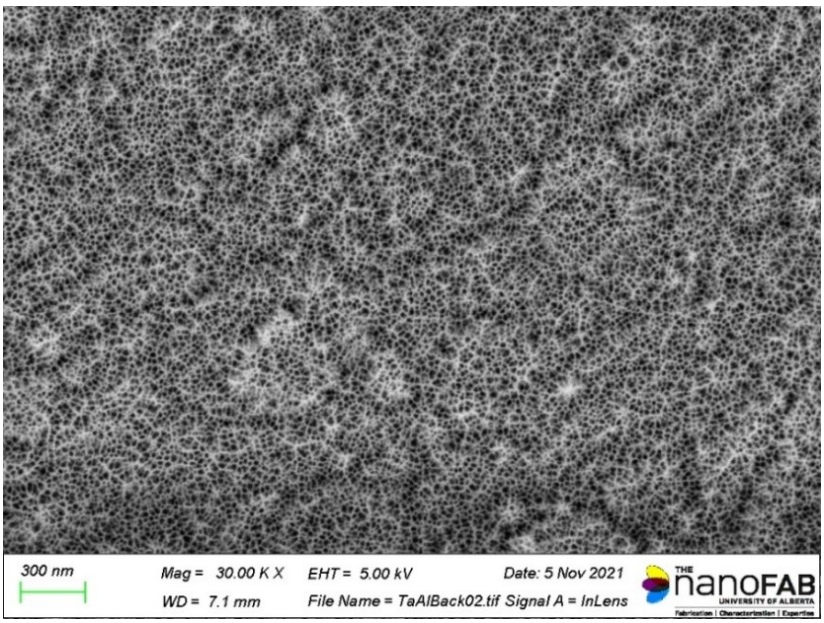


Figure 4.66. Topographical SEM image of oven cleaned tantalum disc 2 that was anodized on the back side at 10 V then sputtered with ~ 200 nm of tantalum and ~ 110 nm of aluminum, then anodized vertically at 4 V at 30,000 X.

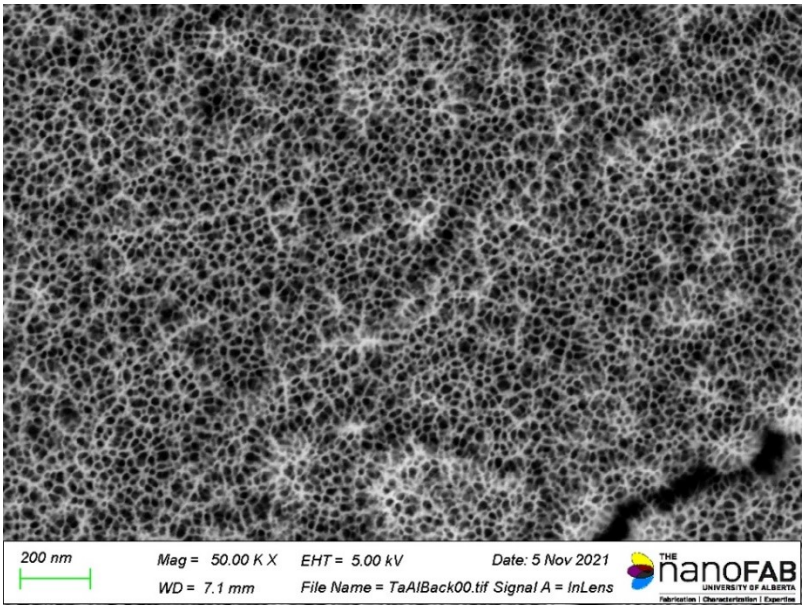


Figure 4.67. Topographical SEM image of oven cleaned tantalum disc 2 *that was anodized on the back side at 10 V then sputtered with ~ 200 nm of tantalum and ~ 110 nm of aluminum, then anodized vertically at 4 V at 50,000 X.*

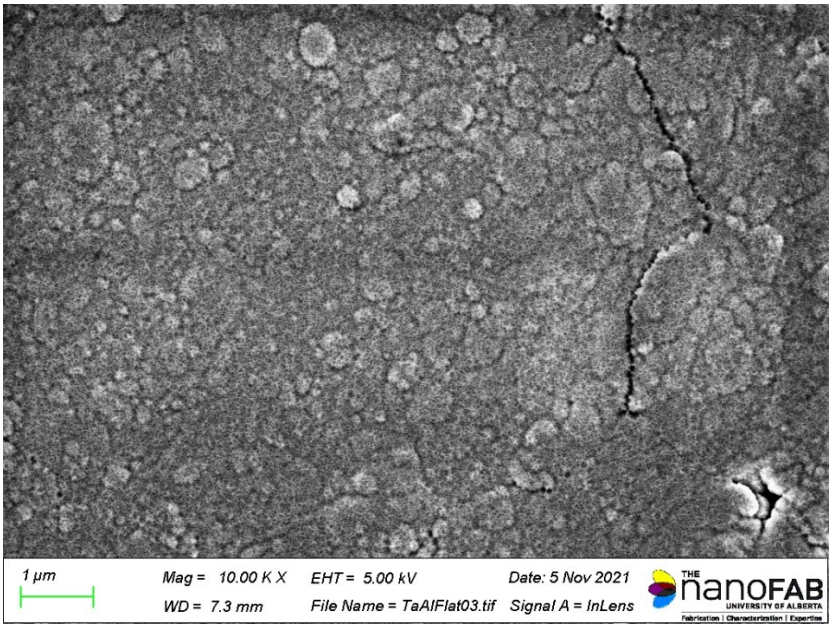


Figure 4.68. Topographical SEM image of oven cleaned tantalum disc 6 that was sputtered with ~ 200 nm of tantalum and ~ 110 nm of aluminum, then anodized horizontally at 4 V at 10,000 X.

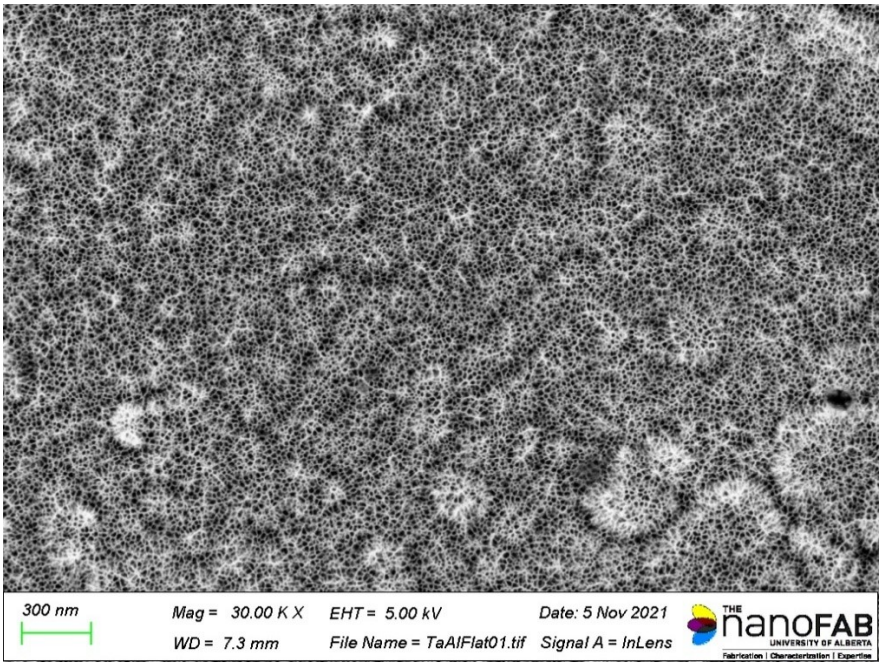


Figure 4.69. Topographical SEM image of oven cleaned tantalum disc 6 that was sputtered with ~ 200 nm of tantalum and ~ 110 nm of aluminum, then anodized horizontally at 4 V at 30,000 X.

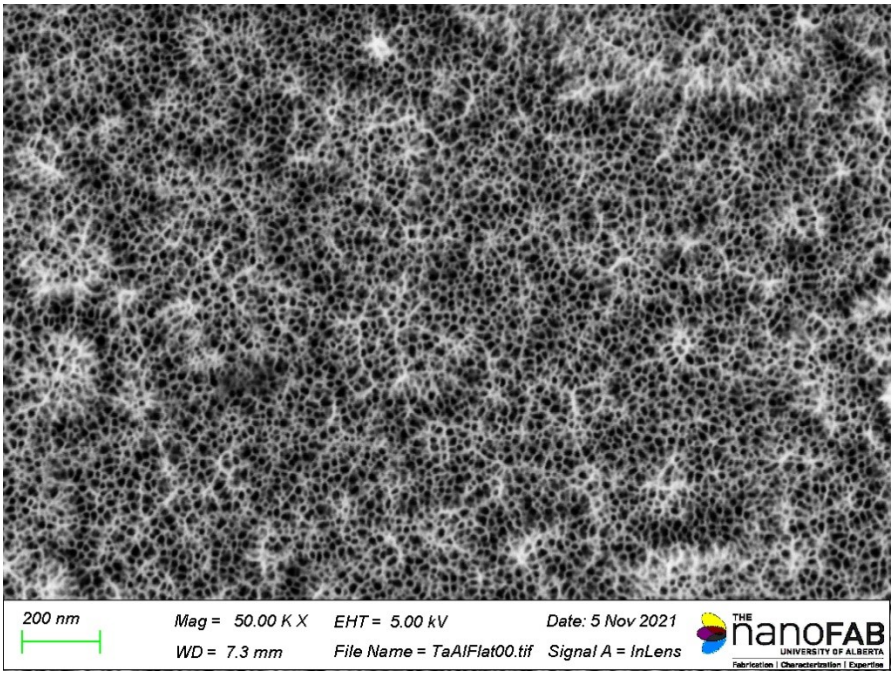


Figure 4.70. Topographical SEM image of oven cleaned tantalum disc 6 that was sputtered with ~ 200 nm of tantalum and ~ 110 nm of aluminum, then anodized horizontally at 4 V at 50,000 X.

Figures 4.67 – 4.72 all show the desired porous alumina structure, suggesting that both methods of tantalum disc anodization were successful. Protein adsorption will be tested on tantalum discs that were anodized using both methods to determine if one method produces better visual detection results than the other. Anodization data for work in subsequent chapters can be found in Appendix 4.

4.5. Conclusions

Thin polycarbonate films were not suitable for the diagnostic device membrane as they deformed during sputtering, likely due to a mismatch in thermal expansion coefficients and the high temperature sputtering conditions. Anodization could not be completed on the wrinkled membranes and therefore other materials were investigated for this application. 3D printed Vero Clear resin polymer membranes were also investigated, but poor adhesion between the polymer disc and tantalum thin film after sputtering deemed this material to be unsuitable. Sputtering of aluminum and tantalum metal onto unpolished and polished quartz frits discs was possible, however, the rough surfaces and nature of the quartz frits caused issues with anodization. Unpolished and polished quartz frits discs were not suitable for aluminum and tantalum thin film anodization, before and after coating the upper portion of the frits with epoxy. Anodization of quartz frits did not produce the characteristic anodization curve that indicates formation of the porous alumina layer and the dielectric tantala layer. SEM images of the coated quartz frits discs indicated that the desired porous alumina structure was not formed on the surface. High purity tantalum discs were sputtered and anodized using two different methods and compared to see which method produced better results. Both anodization methods produced the desired porous alumina structure, and both methods will be studied for protein adsorption applications in future chapters.

4.6. References

1. Huang, P.-c., et al., *The Effect of Sputtering Parameters on the Film Properties of Molybdenum Back Contact for CIGS Solar Cells.* International Journal of Photoenergy, 2013. **2013**: p. 390824.

2. Belwalkar, A., et al., *Effect of Processing Parameters on Pore Structure and Thickness of Anodic Aluminum Oxide (AAO) Tubular Membranes.* J Memb Sci, 2008. **319**(1-2): p. 192-198.

3. Sweet, H.M., *Development of a Nanostructured Thin Film Device and Optics System for Protein Detection*, in *Materials Engineering*. 2018, University of Alberta.

4. Nickel, M.R., *Physical and Optical Characterization of Anodized Aluminum-Tantalum Thin Films for use in Thin Film Diagnostics*, in *Materials Engineering*. 2018, University of Alberta.

5. Rezaee, M., et al., *Quantitative peel test for thin films/layers based on a coupled parametric and statistical study.* Scientific Reports, 2019. **9**(1): p. 19805.

6. ManualsLib. *Jenn-Air JJW9527DDS Manuals*. [cited 2022 March 17]; Available from: https://www.manualslib.com/products/Jenn-Air-Jjw9527dds-2860632.html.

Chapter 5 – Adsorption of Biologics onto Porous Anodic Alumina on Quartz Frits Discs

5.1. Introduction

Porous anodic alumina for biological or biomedical applications has been studied extensively in recent years [1]. One potential application is the adsorption of biologics onto porous anodic alumina. Protein adsorption and penetration into porous anodic alumina has been studied on a silicon wafer coated with thin films of alumina, tantala, and tantalum ([2], [3]). The aim of this work is to study protein adsorption on a porous anodic alumina surface in a high-volume fluid sample to achieve a higher sensitivity, using porous quartz frits discs, silicon wafers and high purity tantalum discs coated with thin films of alumina, tantala, and tantalum as substrate materials.

The porous quartz frits discs, high purity tantalum discs, and silicon wafers were coated with thin films of tantalum and aluminum, then anodized to produce a porous, anodic alumina surface. An antigen-antibody prototype consisting of prothrombin and anti-prothrombin was used to form the two protein layers for adsorption. Prothrombin was immobilized on the porous anodic alumina layer and an antigen-antibody complex was formed by exposing anti-prothrombin to the prothrombin coated surface. The formation of the prothrombin-anti-prothrombin complex on top of the porous anodic alumina increased the optical path length, leading to a visible colour shift on the surface. Ideally, the protein would not penetrate the porous anodic alumina layer and the change in optical path length was the result of anti-prothrombin binding. Protein penetration into the porous anodic alumina would alter the optical properties of alumina. The change in optical path length due to anti-prothrombin binding to prothrombin on the surface generated visible interference and result in a colour shift, indicating the adsorption of anti-prothrombin.

Prothrombin is a vitamin K-dependent protein that contains a carboxyglutamic domain [4]. Carboxyglutamic acid residues, such as those in prothrombin, have been shown to bind to alumina with high affinity, demonstrated by the patent "Aluminum oxide surfaces and interface molecules" by Dr. Robert E. Burrell [5]. The high binding affinity of prothrombin to alumina allows prothrombin to be immobilized on the surface in a consistent manner, making it a suitable surface for interaction and binding to anti-prothrombin in fluid.

5.2. Materials and Methods

Detailed materials and methods used for device preparation and the adsorption of biologics can be found in Chapter 3 – General Materials and Methods. A prothrombin/anti-prothrombin model as well as a secondary antibody were used to study protein adsorption and detection. Hyphen BioMed highly purified human prothrombin from citrated human plasma from Aniara was reconstituted in distilled water at a concentration of 1 mg/mL and used for experiments. The antibody used was an affinity purified IgG sheep anti-human prothrombin in a 10 mM 4-(2-hydroxyethyl)-1-piperazineethanesulfonic acid (HEPES), 150 mM NaCL, 50% (v/v) glycerol buffer at a pH of 7.4 from Affinity Biologicals with a concentration of 0.5 mg/mL. The secondary antibody used was a rabbit anti-sheep IgG (H+L)-horseradish peroxidase (HRP) conjugate with a concentration of 1 mg/mL supplied by Bio-Rad.

5.3. Device Preparation

Thin films of tantalum (~ 200 nm) and aluminum (~ 110 nm) were deposited onto the porous quartz frits discs and silicon wafer control substrates using the Bob and Floyd DC-planar magnetron sputtering systems, respectively, at the University of Alberta nanoFAB. Prior to protein adsorption, the aluminum coated faces of the substrates were anodized at 4 V in an aqueous 0.4/0.1 M phosphoric acid/oxalic acid bath to create the porous aluminum oxide layer

and the tantala dielectric layer. Further details on thin film deposition and anodization can be found in Chapter 3 – Materials and Methods. Prior to protein adsorption, silicon wafers were cleaved into ~ 1.3 cm by ~ 6.2 cm slides using a diamond scribe.

5.4. Adsorption of Biologics

Initially, the ability of the alumina, tantala and tantalum-coated porous quartz frits discs to adsorb prothrombin and anti-prothrombin was studied and compared to the performance of coated silicon wafers. A Sharpie marker was used to control the surface area exposed to protein on the silicon wafers, high purity tantalum discs, and quartz frits discs. To form the first protein layer, 20 µL of prothrombin with a concentration of 1 mg/mL was pipetted onto the surface and spread to cover the whole area inside the hydrophobic circles with diameters of 0.7 – 1 cm. The sample was left for 20 minutes on a wet paper towel inside a Petri dish to prevent evaporation. After 20 minutes, the protein solution was removed from the surface by pipetting and the substrates were rinsed with deionized water, then dried with oil free compressed air. For the second protein layer, a 20 µL solution of anti-prothrombin with a concentration of 0.5 mg/mL was pipetted on top of the prothrombin coated layer and the solution was spread to the edges of the hydrophobic circles. The substrates were placed on a wet paper towel in a Petri dish for 20 minutes, then rinsed with deionized water and dried. Finally, a secondary antibody (rabbit anti-sheep IgG (H+L)-horseradish peroxidase (HRP) conjugate) was placed on top of the anti-prothrombin layer, spread within the hydrophobic circles, placed on a wet cloth in a Petri dish for 20 minutes, then rinsed and dried.

5.5. Discussion

The silicon wafer control adsorbed, and immobilized proteins as expected and an observable colour shift occurred for each additional protein layer, as seen in Figure 5.1. The first

circle was used as a control, in which no protein was placed. The second circle was exposed to only 20 µL of 1 mg/mL prothrombin for 20 minutes. The light purple colour shift indicates that prothrombin adsorbed onto the surface. The third circle was exposed to prothrombin, then to 20 µL of 0.5 mg/mL anti-prothrombin for 20 minutes after rinsing and drying. The darker purple surface indicates the binding of anti-prothrombin to the prothrombin layer. The fourth circle was exposed to prothrombin, then anti-prothrombin, then 20 µL of a secondary antibody (1 mg/mL rabbit anti-sheep IgG (H+L)-horseradish peroxidase (HRP) conjugate) which resulted in the blue colour appearing in the fourth circle. The coated silicon wafer substrate clearly demonstrates visible colour shifts due to changes in optical path length from protein binding.

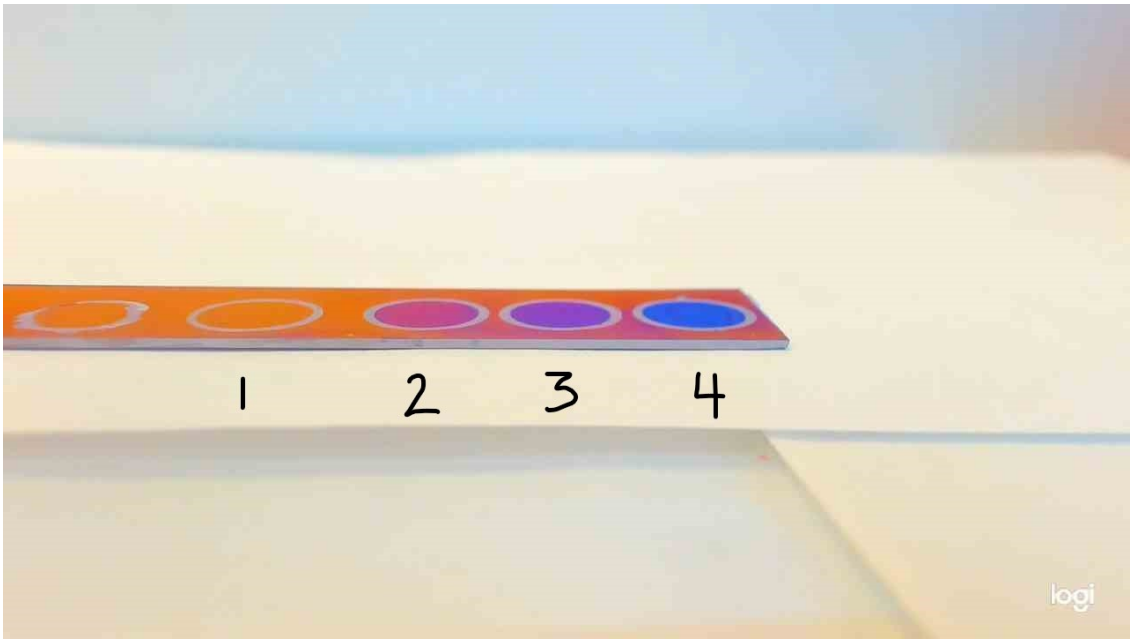


Figure 5.1. Visual detection of protein on a silicon wafer coated with ~ 200 nm of tantalum, ~ 110 nm of aluminum after anodization at 4 V. Colour shifts occur due to the interaction of alumina and the protein exposed to the surface. 1 – control circle with no protein placed. 2 – prothrombin protein adsorbed. 3 – prothrombin adsorbed then anti-prothrombin adsorbed. 4 – prothrombin, anti-prothrombin and secondary antibody adsorbed.

Figures 5.2 and 5.3 display the coated and anodized polished quartz frits discs with porosities of 40 – 100 µm and porosities of 100 – 160 µm, respectively, after 20 µL of 1 mg/mL prothrombin had been placed on the middle and right circles. Immediately after pipetting the protein solution on to the circle, the protein solution was absorbed into the quartz frits material. Figure 5.4 also displays the polished quartz frits disc with a porosity of 100 – 160 µm at an upright angle. No colour shift is visible between the control (left circle) and the portion of the disc that was exposed to prothrombin (center and right circles) for either porosity. Since exposure to prothrombin failed to produce a colour shift on the quartz frits discs, anti-prothrombin and the secondary antibody were not used.



Figure 5.2. Coated and anodized polished quartz frits disc (porosity = 40 – 100 µm) protein analysis. No visible colour shift occurred between the control surface with no exposure to prothrombin (left circle) and the surfaces that had been exposed to 20 µL of 1 mg/mL prothrombin (middle and right circles).



Figure 5.3. Coated and anodized polished quartz frits disc (porosity = 100 – 160 µm) protein analysis. No visible colour shift occurred between the control surface with no exposure to prothrombin (left circle) and the surfaces that had been exposed to 20 µL of 1 mg/mL prothrombin (middle and right circles).



Figure 5.4. Coated and anodized polished quartz frits disc (porosity = 100 – 160 µm) protein analysis at an alternate angle. No visible colour shift occurred between the control surface with no exposure to prothrombin (left circle) and the surfaces that had been exposed to 20 µL of 1 mg/mL prothrombin (middle and right circles).

To further investigate protein adsorption on the coated quartz frits discs, the entire surface of a polished quartz frits disc (porosity = 100 – 160 µm) was exposed to 1 mg/mL prothrombin and compared to a control quartz frits disc that was not exposed to any protein. Figure 5.5 and Figure 5.6 show the control quartz frits disc that had no exposure to protein (left) and the quartz frits disc that had been exposed to 1 mg/mL prothrombin (right). No visible colour shift was detected between the control quartz frits disc and the quartz frits disc that was exposed to prothrombin.



Figure 5.5. Control quartz frits disc with no exposure to protein (left) and polished quartz frits disc (porosity = 100 – 160 µm) that was entirely exposed to 1 mg/mL prothrombin (right). No visible colour shift can be detected between the control surface and the prothrombin exposed surface.

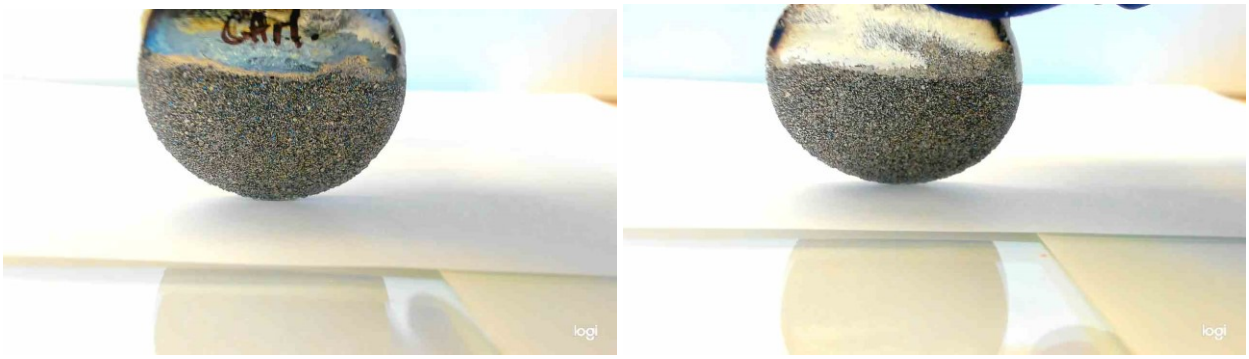


Figure 5.6. Control quartz frits disc with no exposure to protein (left) and polished quartz frits disc (porosity = 100 – 160 µm) that was entirely exposed to 1 mg/mL prothrombin (right) at an alternate angle. No visible colour shift can be detected between the control surface and the prothrombin exposed surface.

No colour shift occurred on the surface of the quartz frits disc when exposed to prothrombin, as had occurred on the silicon wafer substrate. A potential explanation for this issue may be the poor anodization of the quartz frits discs. Anodization of tantalum and aluminum coated quartz frits discs did not produce the expected characteristic anodization curve for anodization of aluminum. SEM images of the quartz frits discs after anodization did not show the porous anodic alumina surface that is desired for protein adsorption and detection. Another potential explanation may be due to the immediate uptake of the prothrombin solution by the quartz frits. The drop of protein solution was absorbed into the quartz frits disc immediately after pipetting, disappearing from the surface and allowing little time for the prothrombin to interact with the surface. In comparison, the prothrombin solution sat on top of the silicon wafer substrate for the entire 20 minutes and was then removed by a pipette. Further, the hydrophobic Sharpie circle failed to contain the solution and the exposure area was not well controlled, due to absorption of the solution by the quartz frits. Since no colour shift occurred after exposure to prothrombin, no further protein experiments were conducted on the quartz frits discs. These

results indicate that the quartz frits discs were unable to properly adsorb the proteins and produce a visible colour shift and should not be selected as the material for the diagnostic device.

5.6. Conclusions

The quartz frits discs coated with tantalum, tantala and alumina failed to properly adsorb and immobilize prothrombin on the surface. The quartz frits material itself, rather than sputtering or anodization conditions, was likely the reason for failure as the silicon wafers were prepared under the same conditions and produced visible colour shifts after exposure to protein. From these experiments, it was determined that porous quartz frits discs are not suitable for detecting protein adsorption by a visual colour shift and should not be further considered in the development of the diagnostic device.

5.7. References

1. Toccafondi, C., et al., *Biomedical Applications of Anodic Porous Alumina.* Current Nanoscience, 2015. **11**.

2. Sweet, H.M., *Development of a Nanostructured Thin Film Device and Optics System for Protein Detection*, in *Materials Engineering*. 2018, University of Alberta.

3. Nickel, M.R., *Physical and Optical Characterization of Anodized Aluminum-Tantalum Thin Films for use in Thin Film Diagnostics*, in *Materials Engineering*. 2018, University of Alberta.

4. Pozzi, N. and E. Di Cera, *Prothrombin structure: unanticipated features and opportunities.* Expert Rev Proteomics, 2014. **11**(6): p. 653-5.

5. Burrell, R.E., *Aluminum oxide surfaces and interface molecules*. 2019.

Chapter 6 – Adsorption of Biologics onto Porous Anodic Alumina on Tantalum Discs

6.1. Introduction

The next substrate that was investigated for the membrane of the diagnostic device was a high purity tantalum disc. The tantalum discs have a smooth surface and do not absorb fluid, mitigating several of the issues that were encountered with the porous quartz frits discs. The tantalum discs had one 1.18 mm hole for impeller attachment, and either four or eight 1 mm holes for fluid flow. Cleaning tantalum discs in a self-cleaning oven and depositing thin films of tantalum (~ 200 nm) and aluminum (~ 110 nm), then anodizing at 4 V produced the desired porous alumina structure on the surface as viewed by SEM and discussed in Chapter 4. The anodization results and SEM images suggest tantalum discs may be more suitable for protein adsorption and detection than the quartz frits discs.

The tantalum discs were coated with thin films of tantalum and aluminum, then anodized at 4 V to create the anodic aluminum oxide layer. An antigen-antibody prototype consisting of prothrombin and anti-prothrombin was used to form the two protein layers for adsorption. Prothrombin was immobilized on the porous anodic alumina layer and an antigen-antibody complex was formed by exposing anti-prothrombin to the prothrombin coated surface. The formation of the prothrombin-anti-prothrombin complex on top of the porous anodic alumina layer increased the optical path length and generated a visible colour shift. Ideally, the protein would not penetrate the porous anodic alumina layer and the change in optical path length was the result of anti-prothrombin binding. Protein penetration into the porous anodic alumina would alter the optical properties of alumina. The change in optical path length due to anti-prothrombin binding would generate visible interference and result in a colour shift, indicating the adsorption of anti-prothrombin.

Prothrombin is a vitamin K-dependent protein that contains a carboxyglutamic domain [1]. Carboxyglutamic acid residues, such as those in prothrombin, have been shown to bind to alumina with high affinity, as seen in the patent “Aluminum oxide surfaces and interface molecules” by Dr. Robert E. Burrell [2]. The high affinity of prothrombin to alumina allows prothrombin to be immobilized on the surface in a consistent manner, making it suitable for interaction with anti-prothrombin in fluid.

6.2. Materials and Methods

Detailed materials and methods regarding the adsorption of biologics can be found in Chapter 3 – General Materials and Methods. A prothrombin/anti-prothrombin model as well as a secondary antibody were used to study protein adsorption and detection. Hyphen BioMed highly purified human prothrombin from citrated human plasma from Aniara was reconstituted in distilled water at a concentration of 1 mg/mL and used for experiments. The antibody used was an affinity purified IgG sheep anti-human prothrombin in a 10 mM 4-(2-hydroxyethyl)-1-piperazineethanesulfonic acid (HEPES), 150 mM NaCL, 50% (v/v) glycerol buffer at a pH of 7.4 from Affinity Biologicals with a concentration of 0.5 mg/mL. The secondary antibody used was a 1 mg/mL rabbit anti-sheep IgG (H+L)-horseradish peroxidase (HRP) conjugate supplied by Bio-Rad.

6.3. Device Preparation

Thin films of tantalum (~ 200 nm) and aluminum (~ 110 nm) were sputtered onto the high purity tantalum discs using the Bob and Floyd DC-planar magnetron sputtering systems, respectively, at the University of Alberta nanoFAB, after cleaning the discs by a self-cleaning oven cycle. Prior to protein adsorption, the aluminum faces of the substrates were anodized at 4

V to create the porous aluminum oxide layer and the dielectric tantala layer. Further details on sputtering and anodization can be found in Chapter 3 – Materials and Methods.

6.4. Adsorption of Biologics

Initially, the ability of the alumina, tantala and tantalum-coated tantalum discs to adsorb prothrombin and anti-prothrombin was studied and compared to the performance of coated silicon wafers. A Sharpie marker was used to draw 0.7 cm – 1 cm diameter hydrophobic circles on the silicon wafers and tantalum discs to control the exposure surface area. To form the first protein layer, 20 μL of prothrombin at 1 mg/mL was pipetted onto the surface and spread within the hydrophobic circle. The sample was then left for 20 minutes on a wet paper towel inside a Petri dish. After 20 minutes, the solution was pipetted off of each surface to remove as much solution as possible and the substrates were rinsed with deionized water, then dried with oil free compressed air. To create the second protein layer, a 20 μL solution of anti-prothrombin at 0.5 mg/mL was pipetted on top of the prothrombin coated layer. The substrates were placed on a wet paper towel in a Petri dish for 20 minutes, then rinsed with deionized water and dried. Finally, a secondary antibody (rabbit anti-sheep IgG (H+L)-horseradish peroxidase (HRP) conjugate) was placed on top of the anti-prothrombin layer for some substrates, placed on a wet paper towel in a Petri dish for 20 minutes, rinsed and dried.

6.5. Discussion

Initially, ~ 110 nm of aluminum was sputtered onto the tantalum discs then anodized at 4 V. During anodization, the opposite tantalum face was covered with Kapton tape to prevent anodization of the tantalum surface. One of four discs with Kapton tape produced the expected aluminum anodization curve, while the other three did not. Figure 6.1 shows the tantalum disc that produced the characteristic aluminum anodization curve after exposure to protein on the

anodized alumina face. Circle 4 was the control circle and had no exposure to protein. Circle 3 was only exposed to prothrombin. Circles 1 and 2 were exposed to prothrombin, followed by anti-prothrombin. A visible colour difference can be observed between the no protein exposure control (4) and the prothrombin only circle (3). There is also a visible colour shift between the prothrombin only circle (3) and the prothrombin + anti-prothrombin circles (1, 2). The circle that was exposed to prothrombin only (3) is a dark purple whereas the circles that were exposed to prothrombin and anti-prothrombin (1, 2) are a bluer tone. The colour shifts on the surface indicate that prothrombin was able to bind to the alumina surface, and that anti-prothrombin was able to bind to prothrombin.

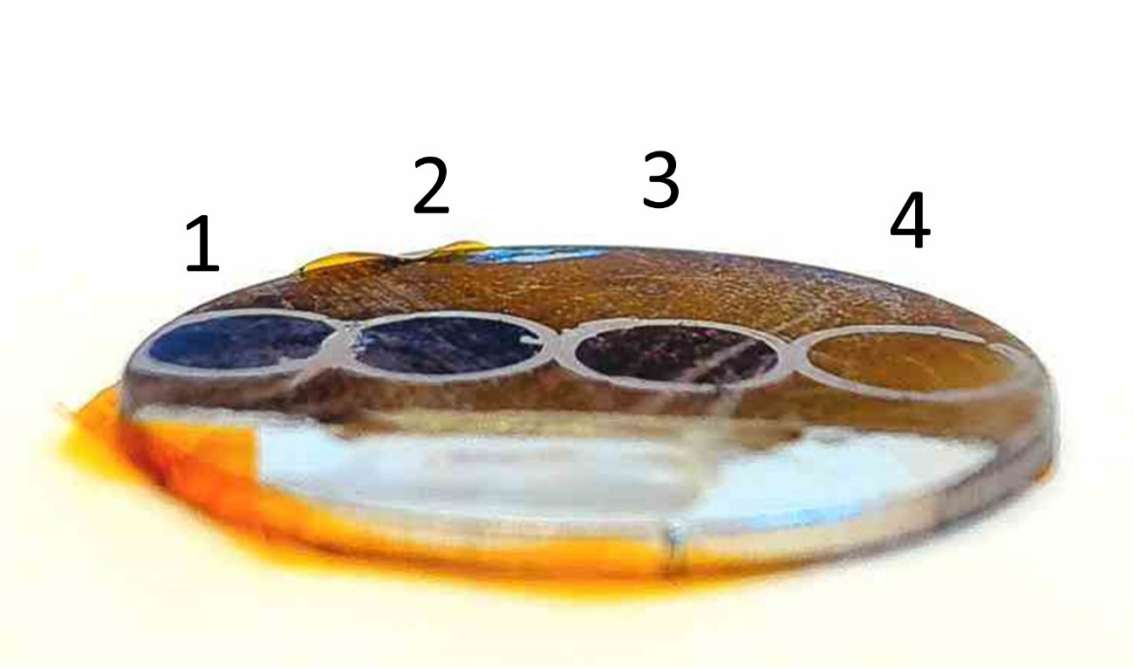


Figure 6.1. Visual detection of adsorbed protein on a tantalum disc coated with ~ 110 nm of aluminum then anodized at 4 V. Colour shifts indicate binding of prothrombin and anti-prothrombin to the surface. 1, 2 – prothrombin protein layer adsorbed followed by a layer of anti-prothrombin protein. 3 – prothrombin protein only adsorbed. 4 – control circle with no protein adsorbed.

Figure 6.2 shows the tantalum disc that failed to produce the characteristic aluminum anodization curve, after conducting protein experiments. It was suspected that the anodization acid leaked in between the Kapton tape and the tantalum surface, causing the opposite tantalum face to be anodized in addition to the aluminum coated face. Circle 4 was the control circle and had no exposure to protein. Circle 3 was only exposed to prothrombin. Circles 1 and 2 were exposed to prothrombin, followed by anti-prothrombin. Visible colour shifts are not as clear on this disc and the adsorption of prothrombin and anti-prothrombin cannot be confirmed. The inconsistent patterns on the surface and the appearance of random blue spots may be linked to protein adsorption on the surface, but it is not clear.

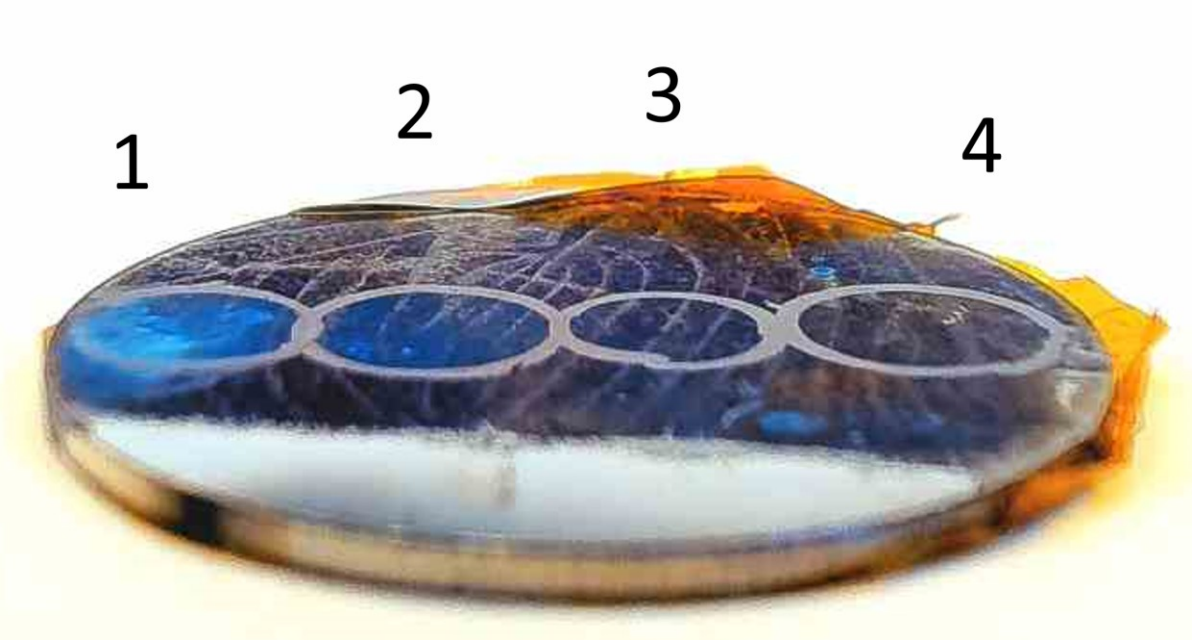


Figure 6.2. Visual detection of protein on a tantalum disc coated with ~ 110 nm of aluminum then anodized at 4 V. Anodization of the aluminum surface was not successful and poor results were obtained for protein detection. Clear colour shifts are not observed between the circles. 1, 2 – exposed to prothrombin then anti-prothrombin. 3 – exposed to prothrombin only. 4 – control circle with no protein exposure.

Three out of four tantalum discs with Kapton tape did not produce the characteristic aluminum anodization curve, and it appeared that anodization acid could still contact the opposite tantalum face. The use of Kapton tape alone is not a reliable method to ensure only the aluminum coated face of the tantalum disc is anodized.

Two alternative methods to anodize only the aluminum surface prior to protein deposition were conducted and the protein experiment results are shown below. Tantalum discs were placed in an oven for a self-cleaning cycle to clean and remove organics from the surface prior to sputtering. Two methods of anodization were used after cleaning in the oven. In the first method, tantalum discs were anodized at 10 V on the backside, using the horizontal method, to produce the tantala dielectric layer to prevent subsequent anodization of the back face at 4 V. The formation of this layer would ensure that the front side aluminum face was anodized at 4 V after sputtering rather than the back side of the tantalum disc. After anodization of the back face at 10 V, ~ 200 nm of tantalum and ~ 110 nm of aluminum were deposited on the front face that was not previously anodized. After sputtering, the aluminum faces of these discs were anodized vertically at 4 V. In the second method, ~ 200 nm of tantalum and ~ 110 nm of aluminum were deposited on to the tantalum discs and then the aluminum face was anodized horizontally at 4 V. Figures 6.3 and 6.4 show the adsorption of 20 μL of prothrombin (1 mg/mL), anti-prothrombin (0.5 mg/mL) and a secondary antibody on the alumina surface of discs that were anodized using the vertical method (back side previously anodized at 10 V). The anodization curves for the discs shown in Figures 6.3 and 6.4 are shown in Figures 4.59 (t = 800 s) and 4.61 (t = 2500 s), respectively. Figures 6.5 and 6.6 show the adsorption of prothrombin, anti-prothrombin and a secondary antibody on the surface of the disc that was anodized using the horizontal method (anodized horizontally on aluminum face with no previous anodization). The anodization curves

for the discs shown in Figures 6.5 and 6.6 are shown in Figures 4.62 (t = 1200 s) and 4.63 (t = 2000 s), respectively.

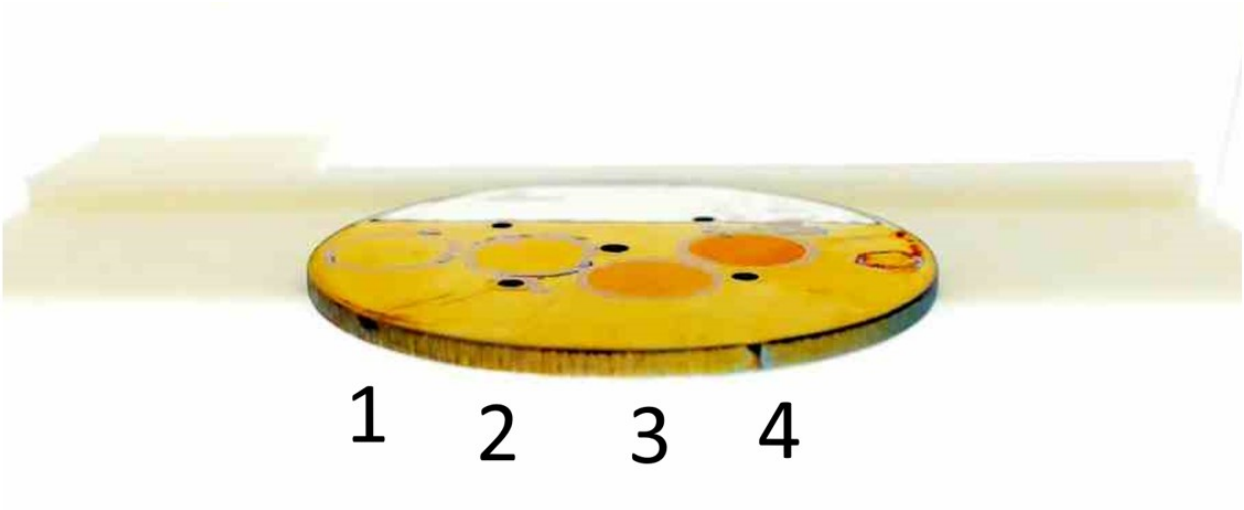


Figure 6.3. Control circle with no adsorbed protein (circle 1), adsorption of prothrombin (circle 2), prothrombin + anti-prothrombin (circle 3), prothrombin + anti-prothrombin + secondary antibody (circle 4) on tantalum disc 1 using the vertical anodization method (back side anodized at 10 V prior to sputtering, aluminum face anodized vertically at 4 V after sputtering).

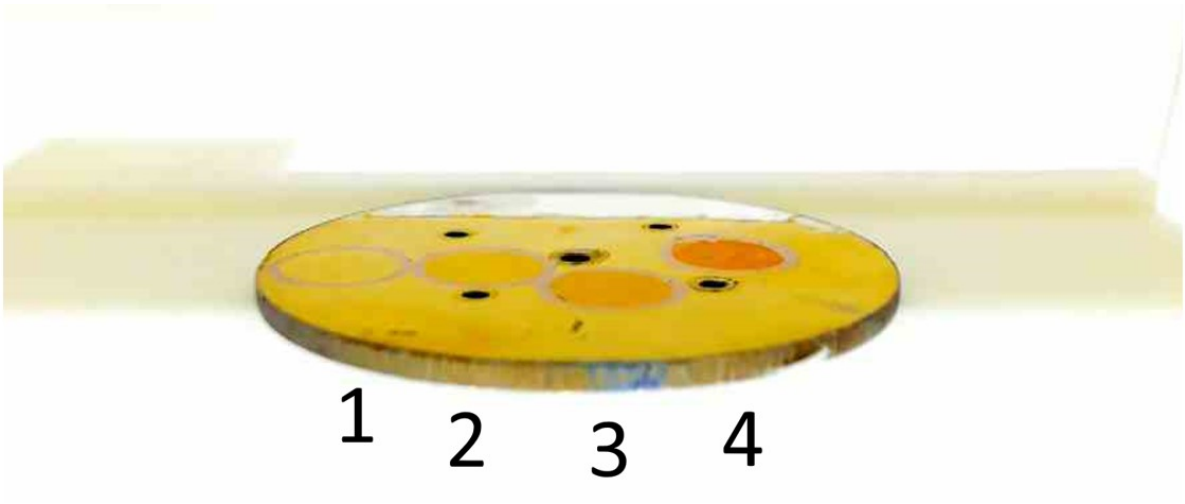


Figure 6.4. Control circle with no adsorbed protein (circle 1), adsorption of prothrombin (circle 2), prothrombin + anti-prothrombin (circle 3), prothrombin + anti-prothrombin + secondary antibody (circle 4) on tantalum disc 3 using the vertical anodization method (back side anodized at 10 V prior to sputtering, aluminum face anodized vertically at 4 V after sputtering).

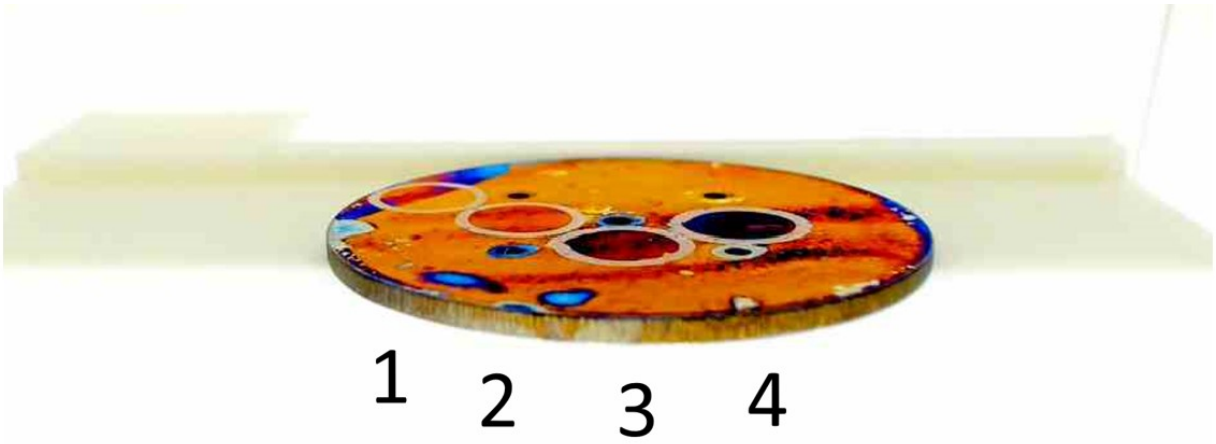


Figure 6.5. Control circle with no adsorbed protein (circle 1), adsorption of prothrombin (circle 2), prothrombin + anti-prothrombin (circle 3), prothrombin + anti-prothrombin + secondary antibody (circle 4) on tantalum disc 4 using the horizontal anodization method (aluminum face anodized flat at 4 V).

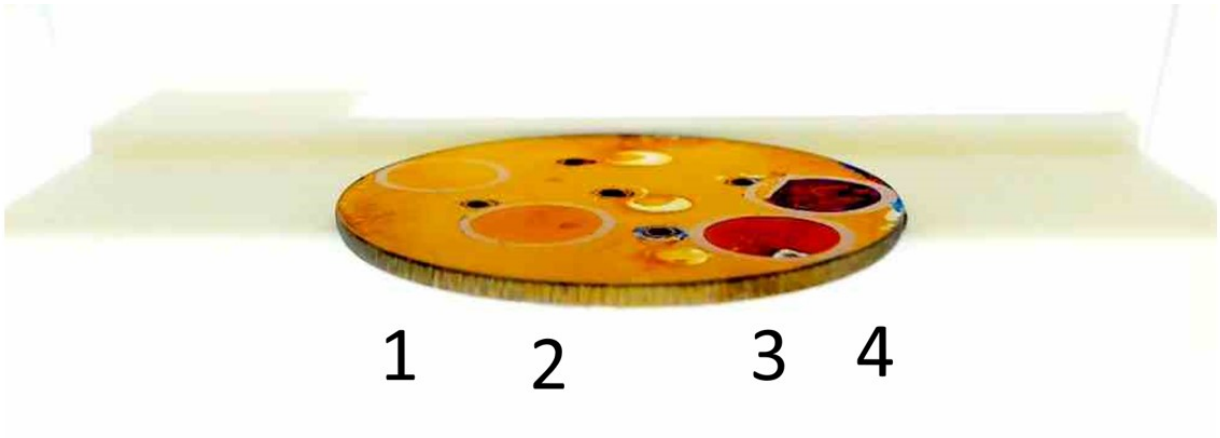


Figure 6.6. Control circle with no adsorbed protein (circle 1), adsorption of prothrombin (circle 2), prothrombin + anti-prothrombin (circle 3), prothrombin + anti-prothrombin + secondary antibody (circle 4) on tantalum disc 5 using the horizontal anodization method (aluminum face anodized flat at 4 V).

As seen in Figures 6.3 – 6.6, both anodization methods produced visible colour shifts when exposed to prothrombin, anti-prothrombin, and the secondary antibody. The vertical anodization method, in which the backside tantalum face was anodized at 10 V horizontally prior to sputtering then the aluminum face was anodized at 4 V vertically after sputtering, produced visible colour shifts from light yellow (prothrombin only) to light orange (prothrombin and anti-prothrombin) to dark orange (prothrombin, anti-prothrombin and the secondary antibody) after exposure to protein, seen in Figures 6.3 and 6.4. The horizontal anodization method, in which only the aluminum face was anodized at 4 V horizontally after sputtering, produced even stronger visible colour shifts from orange (prothrombin only) to red (prothrombin and anti-prothrombin) to dark red/purple (prothrombin, anti-prothrombin and the secondary antibody) after exposure to protein, seen in Figures 6.5 and 6.6.

The significant difference in colour shifts between the discs prepared using the vertical anodization method and the horizontal anodization method was an interesting result as the discs were prepared under the same sputtering conditions, and as a result, the thickness of the thin films should have been the same on both discs. The fact that the surface colours were quite different suggests that the optical path lengths were different for the discs prepared using each method. As the OPL is the product of the physical path length and the refractive index of the medium through which light propagates, and the physical path length should be the same in both cases, it was thought that there was a difference in refractive index of the two surfaces. The horizontal method produced stronger colour shifts than the vertical method, suggesting a greater optical path length for the discs anodized horizontally, meaning that the refractive index was likely greater for these discs. As the pore size is increased, the volume of air (refractive index = 1) increases while the influence of the alumina refractive index (1.7) is lowered. Intuitively, one might think that increasing pore size would lead to a smaller refractive index, and a smaller optical path length. However, as the pore size is increased, the density of pores is decreased. Although the volume of air in pores is greater, there is less pores available for air to fill. As a result, the surface contains more alumina, which has a higher refractive index than air, and the refractive index of the surface goes up. In this case, it was expected that the optical path length of the discs prepared using the horizontal method was greater than the discs prepared using the vertical method, due to increased pore size and decreased pore density. To study the pore size on each of the surfaces, SEM images were taken, and it was expected that the discs prepared using the horizontal anodization method would have slightly larger pores than the discs prepared using the vertical method. Figures 6.7, 6.8, 6.9 and 6.10 show SEM images of tantalum disc 1, prepared using the vertical anodization method and shown in Figure 6.3, at magnifications of

10,000 X, 30,000 X, 50,000 X and 70,000 X, respectively. Figures 6.11, 6.12, 6.13 and 6.14 show SEM images of tantalum disc 4, prepared using the horizontal anodization method and shown in Figure 6.5, at magnifications of 10,000 X, 30,000 X, 50,000 X and 70,000 X, respectively.

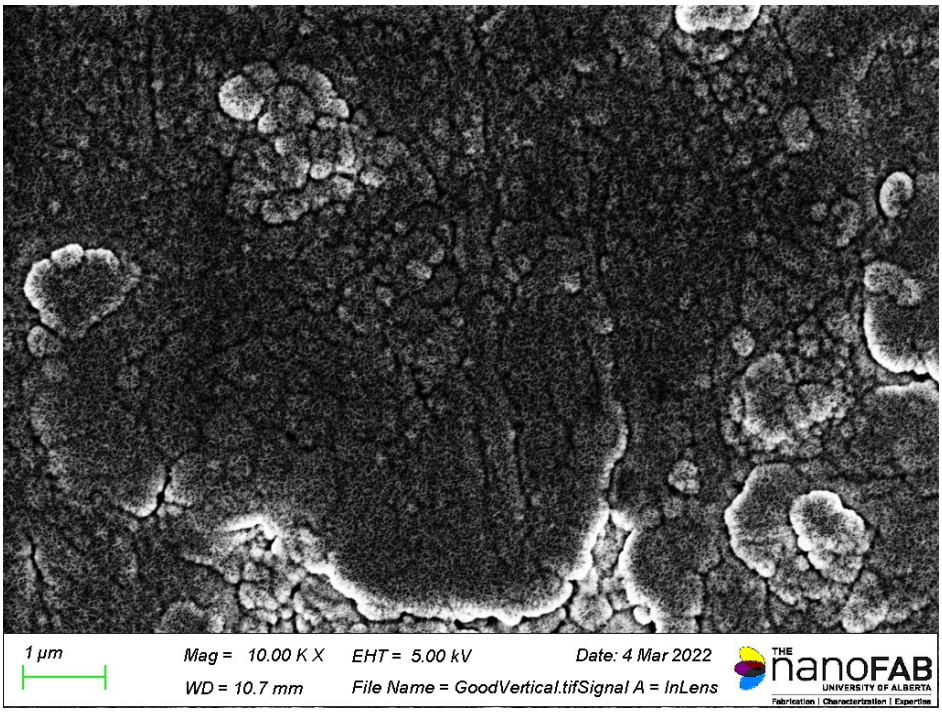


Figure 6.7. Topographical SEM image of tantalum disc 1 shown in Figure 6.3 (vertical method, strong colour shifts) at magnification of 10,000 X.

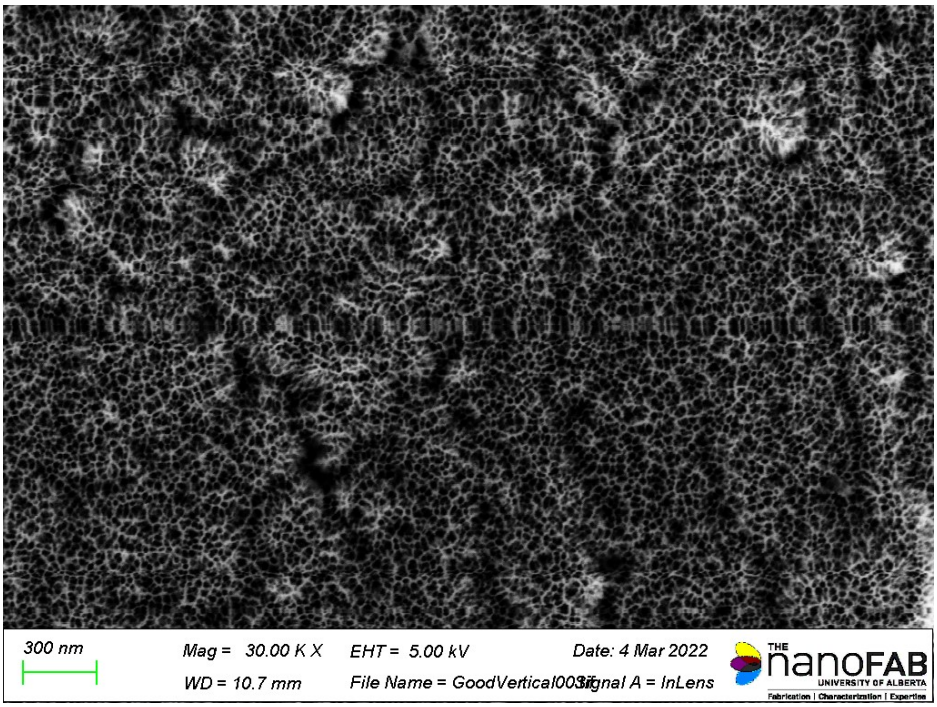


Figure 6.8. Topographical SEM image of tantalum disc 1 shown in Figure 6.3 (vertical method, strong colour shifts) at magnification of 30,000 X.

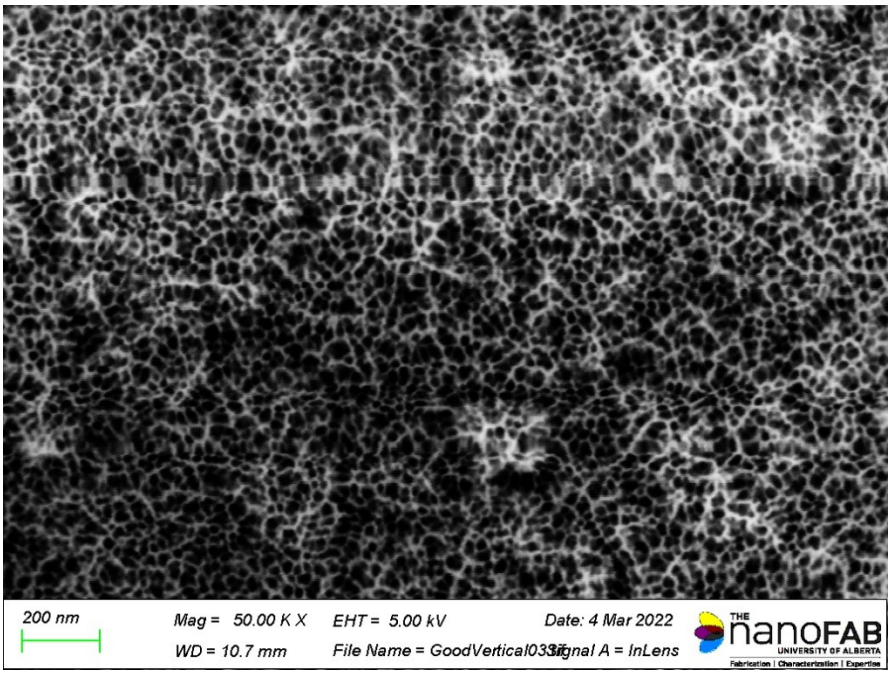


Figure 6.9. Topographical SEM image of tantalum disc 1 shown in Figure 6.3 (vertical method, strong colour shifts) at magnification of 50,000 X.

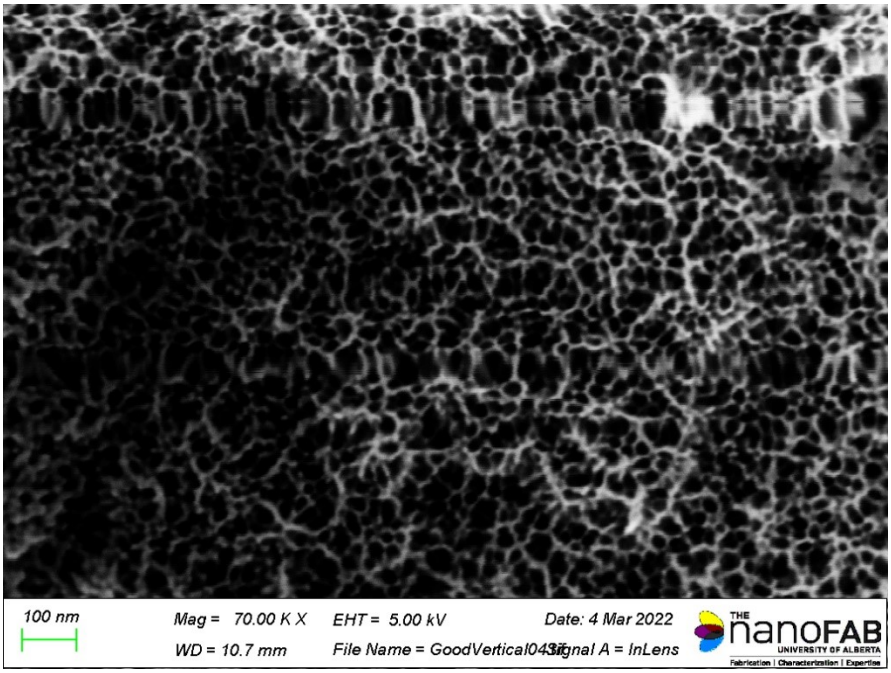


Figure 6.10. Topographical SEM image of tantalum disc 1 shown in Figure 6.3 (vertical method, strong colour shifts) at magnification of 70,000 X.

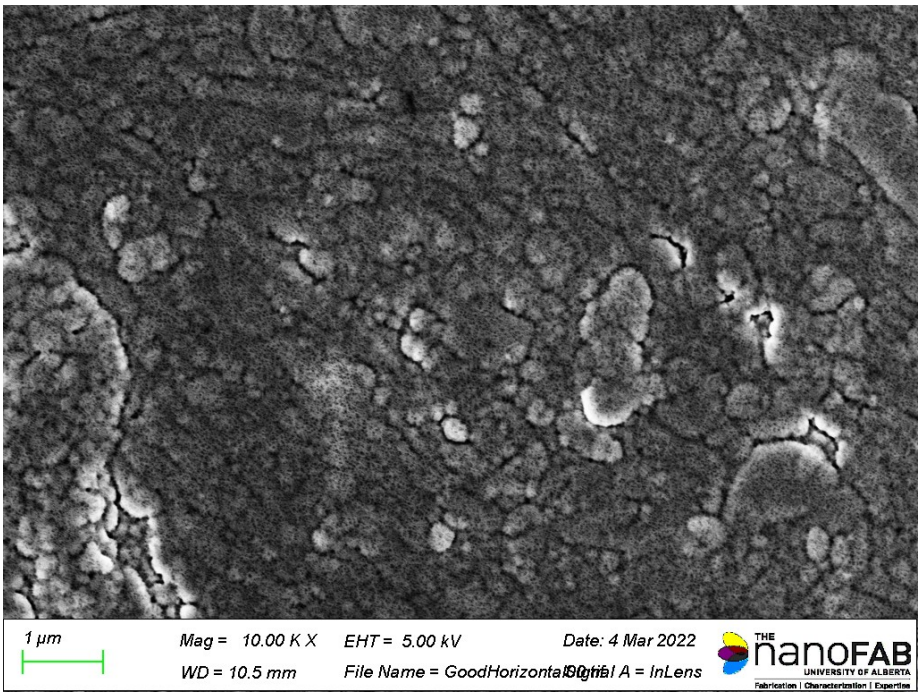


Figure 6.11. Topographical SEM image of tantalum disc 4 shown in Figure 6.5 (horizontal method, strong colour shifts) at magnification of 10,000 X.

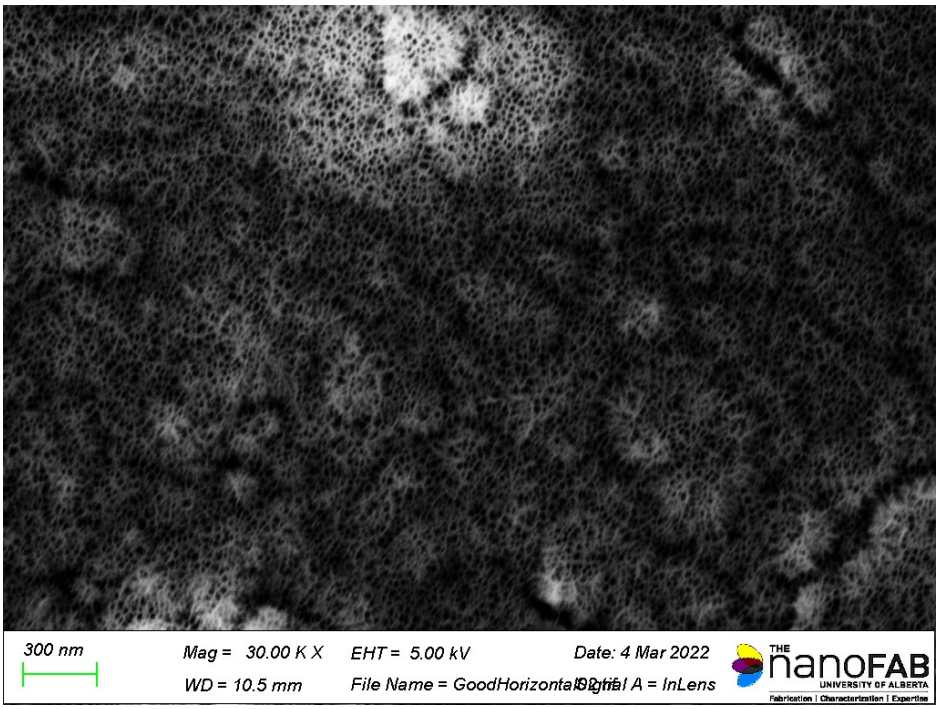


Figure 6.12. Topographical SEM image of tantalum disc 4 shown in Figure 6.5 (horizontal method, strong colour shifts) at magnification of 30,000 X.

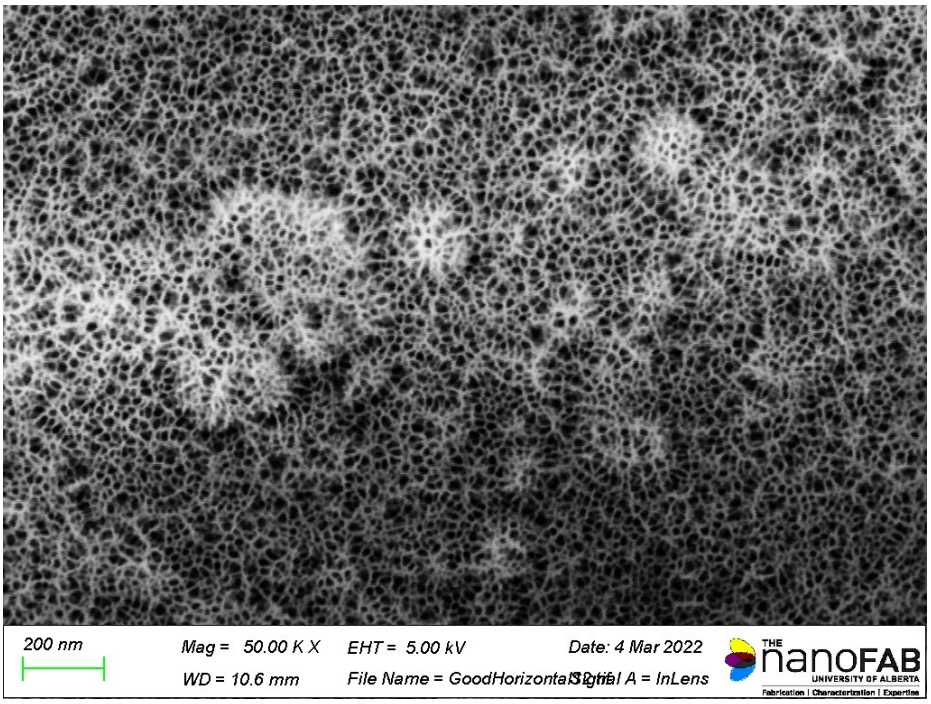


Figure 6.13. Topographical SEM image of tantalum disc 4 shown in Figure 6.5 (horizontal method, strong colour shifts) at magnification of 50,000 X.

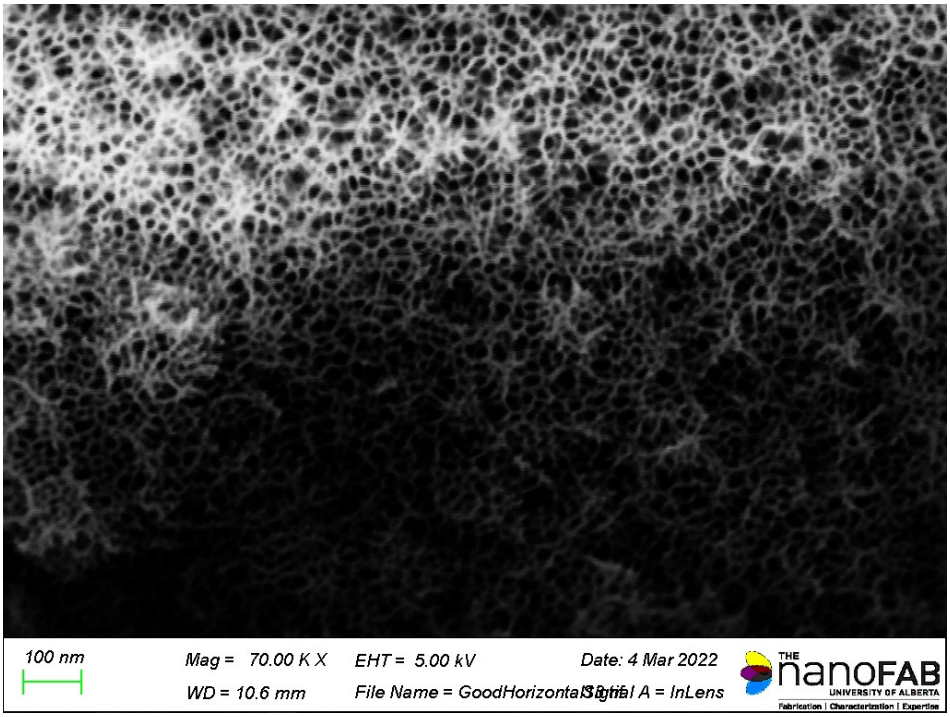


Figure 6.14. Topographical SEM image of tantalum disc 4 shown in Figure 6.5 (horizontal method, strong colour shifts) at magnification of 70,000 X.

Observing the SEM images, the pores are slightly smaller for the discs prepared using the vertical anodization method (Figures 6.7 – 6.10), compared to the pores produced from the horizontal anodization method (Figures 6.11 – 6.14). Although the horizontal anodization method produced larger pores, the pore density was decreased compared to the vertical anodization method. As a result, the refractive index was likely higher (closer to the refractive index of alumina than air), increasing the optical path length and leading to a stronger colour shift for the discs prepared using the horizontal method.

To further investigate the reason for the difference in colours, ellipsometry was conducted on the surfaces to measure the thickness, percent void and standard error values. It was expected that the refractive index of the discs prepared using the horizontal anodization method would be greater than the disc prepared using the vertical method as the colour shifts

suggested that the horizontal anodization method produced a greater optical path length, and the physical path lengths should have been the same in both cases. Tables 6.1, 6.2, 6.3 and 6.4 show the mean squared error (MSE), Al_2O_3 layer thickness, and EMA% values obtained from ellipsometry for the tantalum discs shown in Figures 6.3, 6.4, 6.5 and 6.6, respectively.

Table 6.1. MSE, Al_2O_3 layer thickness, and EMA% from ellipsometry of tantalum disc 1 anodized vertically at 4 V.

MSE	33.458
Al_2O_3 layer thickness (nm)	78.00 ± 0.255
EMA%	62.8 ± 0.18

Table 6.2. MSE, Al_2O_3 layer thickness, and EMA% from ellipsometry of tantalum disc 3 anodized vertically at 4 V.

MSE	32.507
Al_2O_3 layer thickness (nm)	78.06 ± 0.251
EMA%	63.2 ± 0.45

Table 6.3. MSE, Al_2O_3 layer thickness, and EMA% from ellipsometry of tantalum disc 4 anodized horizontally at 4 V.

MSE	37.473
Al_2O_3 layer thickness (nm)	95.40 ± 0.207
EMA%	54.3 ± 0.14

Table 6.4. MSE, Al_2O_3 layer thickness, and EMA% from ellipsometry of tantalum disc 5 anodized horizontally at 4 V.

MSE	50.374
Al_2O_3 layer thickness (nm)	90.03 ± 0.261
EMA%	50.7 ± 0.19

Interestingly, the Al_2O_3 layer thickness was significantly different for the discs prepared using the vertical anodization method (78.00 ± 0.255 and 78.06 ± 0.251) than those prepared using the horizontal anodization method (95.40 ± 0.207 and 90.03 ± 0.261). All four discs were sputtered with aluminum during the same session; therefore, it would be expected that the thickness of the Al_2O_3 layer would be the same for each disc. The vertical anodization method likely caused more dissolution of the aluminum layer, resulting in a decreased thickness compared to the horizontal anodization method. The time to anodize for the two discs prepared using the vertical method were 800 s and 2500 s, and the time to anodize for the two discs prepared using the horizontal method were 1200 s and 2000 s.

6.6. Conclusions

High purity tantalum discs coated with thin films of tantalum and aluminum after cleaning in a self-cleaning oven cycle proved to be suitable substrates for detection of protein by a visible colour shift when exposed to the prothrombin/anti-prothrombin model. Tantalum discs that were cleaned in a self-cleaning oven cycle then sputtered with ~ 200 nm of tantalum and ~ 110 nm of aluminum, then anodized at 4 V on the aluminum face using the horizontal anodization method showed stronger visible colour shifts than the vertical anodization method in which the backside of the tantalum disc was anodized at 10 V prior to sputtering. Strong colour signals were observed for both anodization methods, however, the horizontal anodization method in which only the aluminum face was anodized horizontally at 4 V allows for the entire disc face to be utilized in future experiments and produced stronger colour shifts compared to the first anodization method. Therefore, the horizontal anodization method in which the aluminum face is anodized horizontally at 4 V after sputtering was used for the rest of this work.

6.7. References

1. Pozzi, N. and E. Di Cera, *Prothrombin structure: unanticipated features and opportunities.* Expert Rev Proteomics, 2014. **11**(6): p. 653-5.

2. Burrell, R.E., *Aluminum oxide surfaces and interface molecules*. 2019.

Chapter 7 – Design of Impeller Based Diagnostic Device

7.1. Introduction

The aim of this work is to develop an ultrasensitive point-of-care diagnostic device, that can detect low analyte concentrations within 20 minutes. ELISAs have been shown to have a limit of detection in the femtomolar range for sample volumes of 2 – 5 μL and incubation times between 2 and 4 hours [1]. Increasing the sample volume could allow for increased device sensitivity and earlier detection. The CRISPR/Cas13 signal amplification linked immunosorbent assay achieved limits of detection in the femtomolar range, however, this process requires amplification steps. Other applications have limits of detection in the picomolar range, such as the graphene field-effect transistor biosensors that achieved a limit of detection as low as 2.6 pM for measuring thrombin [2]. In previous work by Matthew Nickel [3] and Hilary Sweet [4], protein in a stationary 20 μL drop of fluid was detected on a silicon wafer substrate coated with thin films of anodized tantalum and aluminum, using a prothrombin/anti-prothrombin model. The experimental limit of detection for anti-prothrombin on a prothrombin coated surface was shown to be 0.025 mg/mL by Sweet [4] and 0.02 mg/mL by Nickel [3].

To create a more sensitive device that can detect lower concentrations of analyte, larger volumes of fluid can be used. Using a sample volume of 500 mL has the potential to be 25,000 times more sensitive than using a sample volume of 20 μL. Even if the device is only 20% efficient, the sensitivity is still increased by a factor of 5,000 which would allow for detection at much lower concentrations. When using larger sample volumes, it is important to ensure that as many fluid elements as possible have the chance to interact with the prothrombin coated surface to allow for binding to occur if anti-prothrombin is present in the sample. For a 20 μL sample, the protein solution can be entirely exposed to the surface by placing a stationary drop on the

surface. A 500 mL sample cannot be placed on a small handheld surface. Instead, the fluid may be passed over the thin film surface and interact with the surface prior to passing through the pores or stirred above the thin film surface. Passing the sample over the surface of the device allows for larger fluid volumes to be tested, if there is adequate exposure of the sample to the surface. There must be turbulent flow and mixing of the sample just above the coated surface to enhance exposure of the fluid elements to the coated surface and increase the chances of binding. Enhanced mixing at the surface increases the likelihood of a fluid element containing an anti-prothrombin molecule coming into contact with the prothrombin coated surface, allowing for binding and the formation of an antigen-antibody complex on the surface that would subsequently lead to a visible colour shift. An impeller is placed just above the coated surface to encourage fluid mixing and develop turbulent flow above the surface.

Various factors including temperature, pH, surfactants, and hydrodynamic shear can lead to structural perturbation of protein molecules, which may cause loss of biological function or activity [5]. An important consideration for this diagnostic device is the effect of turbulent flow and enhanced mixing on protein structure and function. Damage to proteins by mechanical force, fluid shear, or related phenomena could cause protein denaturation or unfolding, which can lead to loss of enzymatic activity or reduced binding efficacy [6]. High shear rates have been shown to lead to aggregation or denaturation of proteins, but the susceptibility of proteins to shear damage varies due to the diversity of molecular sizes, conformations, and intramolecular interactions across different protein species [5]. Exposure of protein to fluid shear is common and seen in many bioprocessing steps, such as centrifugation or fractionation, and occurs naturally during circulation throughout the body (peak Reynolds number in normally functioning aortic valves ranges between 5,700 and 10,000) [7]. Thomas and Geer (2011) reviewed the

literature concerning shear damage to proteins and suggested interfacial effects are predominant compared to mechanical fluid shear [6]. Fluid mechanical shear alone is unlikely to significantly denature proteins ([6], [8], [9], [10], [11], [12], [13]). Biddlecombe et al. (2009) studied the effect of interfacial shear on the structural integrity of human monoclonal antibodies (IgG4 isotype) using a rotating disk shear device and found that pH and the nanometer-scale surface roughness associated with the solid-liquid interface were the primary factors affecting the rate of monomer loss [9]. Cardiopulmonary bypass machines are used to replace the function of the heart and provide a bloodless field for cardiac surgeries [14]. These machines function by draining venous blood to a reservoir, oxygenating the blood, and returning the blood to the body using a pump. Prolonged use of heart-lung machines can lead to post-operative difficulties for the patients, and several studies suggest this is due to the denaturation of blood proteins at blood-gas interfaces in the heart-lung machine ([15], [16]). Protein denaturation by cardiopulmonary bypasses occurs primarily because of gas-liquid interfacial effects, rather than shear forces on the protein produced by the pump [17]. Oxygenators are used to expose blood to oxygen and remove carbon dioxide from the blood before returning it to the body. Bubble oxygenators use a direct blood-gas interface by bubbling oxygen directly into deoxygenated blood, allowing the gas exchange to occur on the surface of the bubble in the blood [18]. The contact between blood and gas bubbles in a bubble oxygenator is the cause of protein denaturation [17]. Shear forces resulting from turbulence may lead to destruction of red blood cells in an oxygenator, but protein denaturation is primarily due to interfacial effects [17].

7.2. Materials and Methods

Detailed materials and methods regarding the impeller device design and selection can be found in Chapter 3 – General Materials and Methods. Fusion 360 designs were drafted, and 3D

printed at the University of Alberta Engineering Garage by Jacob Damant and Ben Damant. Available literature reviewing different impeller types and the effect of various features on mixing is reviewed in Chapter 2 – Introduction and Literature Review and assisted in selecting the impeller design.

7.3. Device Preparation

Thin films of tantalum (~ 200 nm) and aluminum (~ 110 nm) were sputtered onto the tantalum discs and silicon wafers using the Bob and Floyd DC-planar magnetron sputtering systems, respectively, at the University of Alberta nanoFAB. Prior to protein adsorption, the aluminum faces of the substrates were anodized at 4 V to create the porous aluminum oxide layer and the dielectric tantala layer. Further details on sputtering and anodization can be found in Chapter 3 – Materials and Methods. The coated and anodized tantalum discs and silicon wafers were exposed to prothrombin with a concentration of 1 mg/mL for 20 minutes to allow prothrombin to bind to the alumina surface prior to exposure to the fluid sample. The impeller was designed using Fusion 360 and Vero Clear Resin polymer was used to 3D print the impeller. The filter device that holds the impeller and the tantalum disc was designed using Fusion 360 and 3D printed at the University of Alberta Engineering Garage using a resin material. The filter device was designed to screw into the end of the Air-Tite 60 cc/mL Disposable Syringe, through which the fluid samples would be passed through.

7.4. Impeller Design

The diagnostic device filter and impeller were drafted in Fusion 360 by Jacob Damant for the syringe model design. Figure 3.7 shows the design of the diagnostic device and Figure 3.8 shows a close up drawing of the filter portion of the device, found in Chapter 3 – General Materials and Methods. Figure 7.1 shows a cross-sectional image of the Fusion 360 filter design.

The 3D printed filter was designed to screw into the Air-Tite 60 cc/mL Disposable Syringe such that as fluid left the syringe, it would enter the filter and contact the side of the impeller. The filter was designed to screw into the syringe on the side, rather in the center, so that as the fluid is pushed through the syringe, it will directly contact the side of the impeller and initiate rotation. Force is used to push the fluid through the syringe and into the filter. The force applied to the fluid would increase the fluid velocity. Targeting an impeller blade on the side, rather than the center of the impeller, with the high velocity fluid stream would lead to rotation of the impeller and mixing of the fluid as it passes by the impeller. Once initiated, the impeller would continue to rotate as the remaining fluid from the sample enters the filter portion of the device. The rapid spinning of the impeller, initiated by the force of the incoming fluid, causes enhanced mixing and turbulent flow at the surface just above the tantalum disc, as shown in Figure 3.8. The fluid arriving in the filter from the syringe contacts the impeller on the blade to initiate rotation of the impeller and fluid mixing. The space between the impeller and the tantalum disc in Figure 3.8 is exaggerated to include flow arrows that show mixing above the surface. The actual space between the diagnostic device and the impeller is minimal (less than 1 mm) to ensure mixing occurs as close to the prothrombin coated surface as possible. A pitch blade impeller type with a blade angle of 45° was selected for the diagnostic device application as a blade angle of 45° simultaneously produces axial and radial flow, allowing for optimal overall mixing ([19], [20]). The impeller was placed as close to the coated tantalum disc substrate as possible to ensure mixing of fluid elements occurred just prior to meeting the protein-coated surface. The impeller was designed with six blades, as six blades have been shown to produce quicker mixing compared to four blades [21].

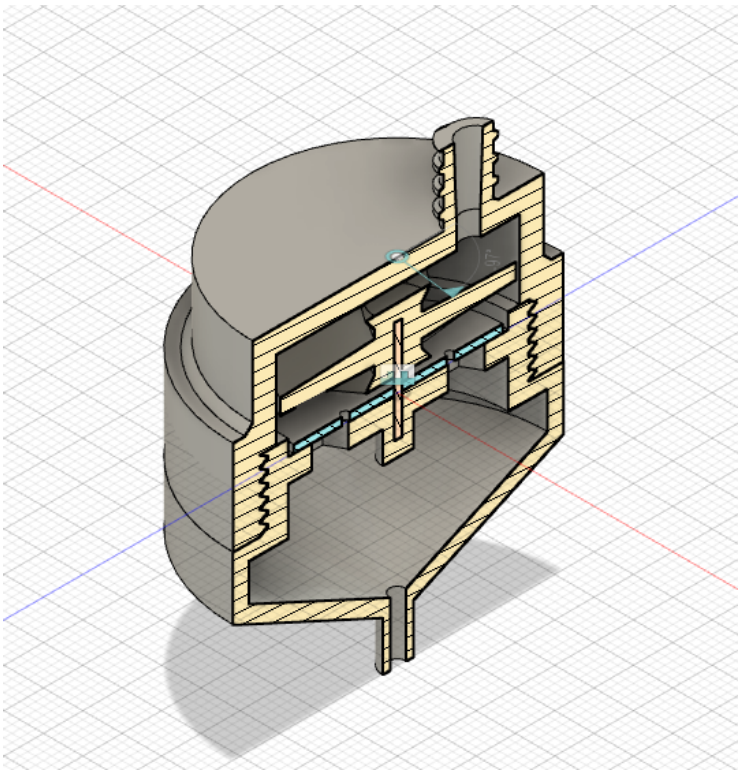


Figure 7.1. Cross-sectional image showing the inside of the Fusion 360 filter design.

The stirred tank design involved filling a 1 L beaker with 500 mL of fluid and placing an impeller just below the fluid surface and is shown in Figure 3.6. The impeller was connected to and powered by a Tech II Railmaster 2400 and set to a power of ~ 13. The impeller blade design was drafted in Fusion 360 by Ben Damant, as shown in Figure 7.13, for simulation purposes. For this design, the silicon wafer and tantalum disc substrates were coated with tantalum and aluminum, then anodized at 4 V. The entire surface was exposed to 1 mg/mL of prothrombin for 20 minutes, then rinsed and dried with deionized water. The silicon wafer slide or tantalum disc was then placed in the bottom of the beaker and the 500 mL fluid sample containing the anti-prothrombin concentration of interest was placed in the beaker, and the impeller was turned on. The impeller mixed the fluid and created turbulent flow in the beaker above the coated substrate, allowing for the mixing of fluid elements above the surface for 20 minutes.

7.5. Computational Fluid Dynamics

Computational fluid dynamics (CFD) involves mathematical modeling and numerical analysis of a specific fluid flow problem and generates quantitative predictions of fluid flow phenomena based on the conservation of mass, momentum, and energy [22]. ANSYS Design Modeler, Fusion 360, ANSYS Meshing, and ANSYS Fluent 2021 R1 (Academic Version) were used to complete CFD simulations. Fluid flow was simulated through the impeller and the diagnostic device designs to assess impeller performance, mixing, turbulence and flow patterns. Turbulence, velocity, pressure, strain rate, and fluid path lines were analyzed. Turbulence was assessed using the turbulent viscosity ratio (TVR), which is the ratio of the turbulent viscosity (or eddy viscosity) to the molecular viscosity. The eddy viscosity is not a fluid property, but rather a function of space and time that is computed using the Boussinesq hypothesis [23]. The Boussinesq hypothesis relates the Reynolds stresses to the mean velocity gradients using the eddy viscosity [23]. As a rule of thumb, TVR values of 10 or greater indicate turbulent flow [24]. The impeller and filter device designs were imported to ANSYS from Fusion 360 and used for the simulation geometry. The geometry was meshed using ANSYS Workbench and ANSYS Meshing prior to simulation. The base case simulation was used to assess the ability of the impeller designed in Fusion 360 to produce mixing and turbulent flow. Subsequent simulations involved assessing fluid behavior directly within the filter device and the stirred tank device, as per the Fusion 360 and experimental diagnostic device designs.

7.5.1. Governing Equations of Fluid Dynamics

The governing differential equations of fluid dynamics form the basis of computational fluid dynamics, and are called the Navier-Stokes Equations [25]. The conservation of mass states that mass is neither created nor destroyed in the moving fluid parcel. The conservation of

momentum states that the rate of change in momentum is equal to the sum of forces acting on the fluid, including the surface forces (pressure and viscous stresses), and the body forces (gravity, centrifugal, etc.) ([25], [26]). The conservation of energy states that the change in total energy is equal to the net rate of work done by the fluid subtracted from the net heat transfer [25]. For this CFD work, only the conservations of mass and momentum are solved, as temperature effects are not considered. The conservation of mass and the conservation of momentum are shown in Eulerian form in Equations 7-1 and 7-2, respectively [25]:

$$\frac{\partial \rho}{\partial t} + \nabla \cdot \rho \, \vec{V} = 0 \qquad \text{(Equation 7-1)}$$

$$\frac{\partial (\rho \vec{V})}{\partial t} + \vec{V} \cdot \nabla \left(\rho \, \vec{V} \right) = -\nabla p + \nabla \cdot \bar{\bar{\tau}} + \overrightarrow{F_b'} \qquad \text{(Equation 7-2)}$$

Where ρ is the fluid density (kg/m^3), $\vec{V}$ is the fluid velocity (m/s), p is the pressure, $\bar{\bar{\tau}}$ is the viscous stress tensor, and $\overrightarrow{F_b'}$ is the generic body force per unit volume. The conservation of momentum is a vector equation, and is therefore made up of three equations in Cartesian coordinates: one for the x direction, one for the y direction, and one for the z direction [25]. In a three-dimensional field, the stress tensor, $\bar{\bar{\tau}}$, is a 3 × 3 matrix composed of 9 unknown components. To make the problem well-defined, the viscous stress tensor components are expressed in terms of the flow variables, specifically velocity components, resulting in the Navier Stokes Equations. When deriving the viscous stress tensor components, several fundamental assumptions were made by Navier and Stokes: no viscous stresses are generated by pure translation or rigid body rotation, fluid flow is isotropic, the fluid is Newtonian (viscous stress is linearly proportional to strain rate), and the viscous stress force acts only tangentially to the surface of the fluid element (normal component of viscous stress force is zero) [25]. Under

these assumptions, the final expression of the viscous stress tensor in the Cartesian coordinate system is shown in Equation 7-3 [25]:

$$\bar{\bar{\tau}}_{ij} = 2\mu[\varepsilon_{ij} - \frac{1}{3}\nabla \cdot \vec{V}\delta_{ij}] \qquad \text{(Equation 7-3)}$$

Where μ is the dynamic viscosity, ε_{ij} is the strain rate tensor that describes the rate of change of the fluid element and δ_{ij} is the Kronecker delta (δ_{ij} = 1 if $i = j$ and δ_{ij} = 0 otherwise) ([25], [26]). Substituting the expression of viscous stress tensor (Equation 7-3) into the conservation of momentum (Equation 7-2) yields the final non-conservative form of the conservation of momentum, shown in Equation 7-4 [25]:

$$\rho[\frac{\partial \vec{V}}{\partial t} + \vec{V} \cdot \nabla\vec{V}] = -\nabla p + \mu\nabla^2\vec{V} + \frac{1}{3}\mu\nabla(\nabla \cdot \vec{V}) + \overrightarrow{F_b} \qquad \text{(Equation 7-4)}$$

Equation 7-4 can be expanded into the 3D form, composed of the x, y, and z components. The conservation of momentum equations in the conservative form are shown in Equations 7-5, 7-6 and 7-7 [25]:

$$\frac{\partial(\rho u)}{\partial t} + \nabla \cdot \left(\rho\vec{V}u\right) = -\frac{\partial p}{\partial x} + \nabla \cdot [\mu\left(\frac{\partial \vec{V}}{\partial x} + \nabla u\right) - \frac{2}{3}\mu(\nabla \cdot \vec{V})\hat{\imath}] + F_{b,x} \qquad \text{(Equation 7-5)}$$

$$\frac{\partial(\rho v)}{\partial t} + \nabla \cdot \left(\rho\vec{V}v\right) = -\frac{\partial p}{\partial y} + \nabla \cdot [\mu\left(\frac{\partial \vec{V}}{\partial y} + \nabla v\right) - \frac{2}{3}\mu(\nabla \cdot \vec{V})\hat{\jmath}] + F_{b,y} \qquad \text{(Equation 7-6)}$$

$$\frac{\partial(\rho w)}{\partial t} + \nabla \cdot \left(\rho\vec{V}w\right) = -\frac{\partial p}{\partial z} + \nabla \cdot [\mu\left(\frac{\partial \vec{V}}{\partial z} + \nabla w\right) - \frac{2}{3}\mu(\nabla \cdot \vec{V})\hat{k}] + F_{b,z} \qquad \text{(Equation 7-7)}$$

Where ρ is the fluid density (kg/m^3), $\vec{V}$ is the fluid velocity (m/s), p is the pressure, μ is the dynamic viscosity, F_b is the body force (in the x, y, and z directions), and u, v, and w are the x, y and z components of velocity, respectively. The conservation of energy, shown in Equation 7-8, is required for problems involving heat transfer and compressible flows [25]:

$$\frac{\partial(\rho e_t)}{\partial t} + \nabla \cdot [\vec{V}(\rho e_t + p)] = \nabla \cdot [k\nabla \mathrm{T} + (\bar{\bar{\tau}} \cdot \vec{V})] + \dot{S}_g \qquad \text{(Equation 7-8)}$$

Where ρ is the fluid density (kg/m^3), e_t is the total energy per unit mass, $\vec{V}$ is the fluid velocity (m/s), p is the pressure, k is the thermal conductivity of the fluid, T is the temperature, $\bar{\bar{\tau}}$ is the viscous stress tensor, and $\dot{S}_g$ is a generation source term of energy [25]. Since the density and viscosity are assumed to be constant in this CFD work, the conservation of energy equation is not required. Assuming constant density (incompressible flow) and constant viscosity, the conservations of mass and momentum yield a complete set of equations, and a mathematical model can be solved given initial and boundary conditions [25]. The five non-linear partial differential equations for the conservation of mass (Equation 7-1), the conservation of momentum (Equations 7-5, 7-6, 7-7), and the conservation of energy (Equation 7-8) are referred to as the Navier-Stokes Equations.

7.5.2. Turbulence Modeling

Turbulent fluid flow is characterized by unsteady, irregular flow patterns in which the transported quantities, such as mass and momentum, experience chaotic fluctuations in time and space [23]. These fluctuations lead to rapid mixing and increased transport of momentum and heat, resulting in a high rate of diffusivity for turbulent flows ([23], [27]). At any instant, turbulent flow is random and unpredictable. To model turbulence, statistical time averages in the flow field are examined. One major feature of turbulent flows is the presence of different scales of motion, and the scales of turbulent flows increase with increasing Reynolds number [23]. It is not practical to resolve every scale of flow in an industrial turbulent application using the Navier-Stokes Equations. For turbulence modeling, simplifications must be made to the Navier-Stokes Equations by time averaging, resulting in the Reynolds-Averaged Navier-Stokes (RANS)

Equations that solve for the mean flow field. Time averaging involves separating flow variables into mean flow and turbulent fluctuating components, and averaging these values over a sampling period long enough such that the random fluctuations average to zero [23]. For incompressible flows with no body forces, the Reynolds-Averaged conservation of mass is shown in Equation 7-9 [23]:

$$\nabla \cdot \overrightarrow{V} = 0 \qquad \text{(Equation 7-9)}$$

Where $\overrightarrow{V}$ is the mean velocity vector. The Reynolds-Averaged Momentum Equations for incompressible flows with no body forces are shown in Equations 7-10 and 7-11 [23]:

$$\rho\left[\frac{\partial \vec{V}}{\partial t} + \vec{V} \cdot \nabla \vec{V}\right] = -\nabla \bar{p} + \nabla \cdot \tau_{ij} \qquad \text{(Equation 7-10)}$$

Where

$$\tau_{ij} = \mu\left(\frac{\partial \bar{u}_i}{\partial x_j} + \frac{\partial \bar{u}_j}{\partial x_i}\right) - \rho\overline{u_i' u_j'} \qquad \text{(Equation 7-11)}$$

In Equations 7-10 and 7-11, ρ is the fluid density (kg/m^3), $\vec{V}$ is the fluid velocity (m/s), p is the pressure, μ is the dynamic viscosity, τ_{ij} is the total stress tensor, which is the sum of the laminar stresses, represented by $\mu\left(\frac{\partial \bar{u}_i}{\partial x_j} + \frac{\partial \bar{u}_j}{\partial x_i}\right)$ and the turbulent stresses, represented by $\rho\overline{u_i' u_j'}$ [23]. A bar over the variable indicates the mean component of the variable, and a prime (') symbol indicates a fluctuating component. The turbulent stress tensor, also known as the Reynolds stress tensor, is composed of nine terms that were created as a result of time averaging, and can be written in a tensor matrix form in (x, y, z) as [23]:

$$\begin{bmatrix} \rho\overline{u'u'} & \rho\overline{u'v'} & \rho\overline{u'w'} \\ \rho\overline{v'u'} & \rho\overline{v'v'} & \rho\overline{v'w'} \\ \rho\overline{w'u'} & \rho\overline{w'v'} & \rho\overline{w'w'} \end{bmatrix}$$

Due to the symmetric nature of the stress tensor, six additional unknowns have been introduced into the governing equations by the time averaging process, and the number of unknowns is greater than the number of equations. To make the problem well-defined, either six additional governing equations must be defined for the Reynolds stresses, or the Reynolds stress tensor components must be expressed in terms of the mean flow variables. The need to close the RANS equations is referred to as the RANS Closure Problem and can be addressed by turbulence modeling.

The most common approach to closing the RANS system is the use of turbulence models based on the Boussinesq Hypothesis [23]. The Boussinesq Hypothesis assumes turbulence is isotropic and relates the Reynolds stresses to the mean flow velocity gradients using an eddy viscosity, μ_T. For incompressible flows, the relation formulated by Boussinesq for the Reynolds stresses (R_{ij}) is shown in Equations 7-12 and 7-13 [23]:

$$R_{ij} = -\rho\overline{u_i'u_j'} = \mu_T\left(\frac{\partial \bar{u}_i}{\partial x_j} + \frac{\partial \bar{u}_j}{\partial x_i}\right) - \frac{2}{3}\delta_{ij}k \qquad \text{(Equation 7-12)}$$

Where

$$k = \frac{1}{2}\overline{u_i'u_i'} \qquad \text{(Equation 7-13)}$$

Where ρ is the fluid density (kg/m^3) and k is the turbulent kinetic energy. From this relation, the number of unknowns is reduced from nine to two: the eddy viscosity (μ_T) and the turbulent kinetic energy (k). The turbulent kinetic energy term in Equation 7-12 is often neglected, as shear turbulent stresses are dominant to normal stresses [23]. From the Boussinesq hypothesis, Equation 7-11 can be written as shown in Equation 7-14, and substituted into the incompressible Reynolds-Averaged Momentum Equation (Equation 7-10) [23]:

$$\tau_{ij} = (\mu + \mu_T)\left(\frac{\partial \bar{u}_i}{\partial x_j} + \frac{\partial \bar{u}_j}{\partial x_i}\right) \qquad \text{(Equation 7-14)}$$

Where μ is the dynamic viscosity. Numerous models have been developed to model the eddy viscosity and close the RANS problem, with the k-epsilon and k-omega two equation models being the most popular [23]. In the k-epsilon model, transport equations for the turbulent kinetic energy (k) and the turbulent dissipation rate (ε) are solved and the eddy viscosity (μ_T) is calculated using Equation 7-15 [23]:

$$\mu_T = \rho C_\mu \frac{k^2}{\varepsilon} \quad \text{(Equation 7-15)}$$

In the k-omega model, transport equations for the turbulent kinetic energy (k) and the specific rate of dissipation (ω) are solved. The turbulent dissipation rate (ε) is calculated using Equation 7-16, then the eddy viscosity (μ_T) is calculated using Equation 7-15 shown above [23]:

$$\varepsilon = C_\mu k \omega \quad \text{(Equation 7-16)}$$

In Equations 7-15 and 7-16, ρ is the fluid density (kg/m^3) and C_μ is the turbulence model constant, which usually has a value of 0.09 ([26], [28]). Once the eddy viscosity is obtained, it can be substituted into the RANS momentum equations (Equations 7-14 and 7-10), closing the system and allowing the RANS equations to be solved.

7.5.3. Calculations

The fluid velocity as it exits the syringe and contacts the impeller was calculated using the continuity equation (Equation 7-17) and the area of a circle (Equation 7-18) assuming the syringe was pushed at a constant velocity of 100 mm/s (v_1). As the fluid is pushed from the syringe with a radius 13.5 mm (r_1), through the syringe exit with a radius of 2.15 mm (r_2) and into the filter device, the fluid velocity was calculated to be 3.94 m/s (v_2) as it enters the device.

$$A_1 v_1 = A_2 v_2 \quad \text{(Equation 7-17)}$$

$$A = \pi r^2 \qquad \text{(Equation 7-18)}$$

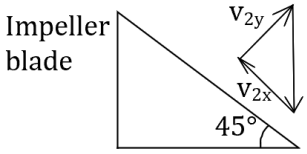
For the base case, the estimated impeller speed was calculated in radians per second (rad/s) using trigonometry and the inlet fluid velocity at which the fluid contacts the impeller, assuming no losses to friction, as shown in Figure 7.2 below.

Impeller Speed Calculations (base case)

$r_1 = 13.5$ mm (syringe radius)
$r_2 = 2.15$ mm (syringe outlet)
$v_1 = 100$ mm/s (speed in syringe)
v_2 = fluid speed exiting syringe
Impeller radius = 12 mm

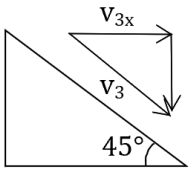
Continuity equation: $A_1 v_1 = A_2 v_2$

$$v_2 = \frac{A_1 v_1}{A_2} = \frac{\pi r_1^2 v_1}{\pi r_2^2} = \frac{\pi(13.5\ mm)^2(100\frac{mm}{s})}{\pi(2.15\ mm)^2} = 3942.67\frac{mm}{s}$$ (fluid speed that contacts impeller)



$v_2 = 3942.67$ mm/s

$v_{2x} = 3942.67\ \text{mm/s}\cos 45° = 2787.89\ \text{mm/s} = v_3$



$v_{3x} = 2787.89\ \text{mm/s}\cos 45° = 1971\ \text{mm/s}$ = impeller speed
Impeller angular velocity $\omega = v/r$
$\omega = (1.971\ \text{m/s})/(0.012\ \text{m}) =$ **164.3 rad/s**

Figure 7.2. Impeller speed calculations.

7.5.4. Base Case

Initially, a base case simulation was conducted to assess the impeller performance inside the syringe alone. ANSYS Workbench and ANSYS Fluent 2021 R1 (Academic Version) were used to complete CFD simulations. For this case, the speed of the impeller was calculated as discussed in Section 7.5.3. Calculations, and simulations assumed the impeller was already

spinning, rather than starting from rest. The base case was used to assess the performance of the impeller designed in Fusion 360, prior to being simulated in the device.

For the base case, the simulation was set up using the Standard k-omega (2 equation) Viscous Model with Shear Flow Corrections and Production Limiter selected. The k-omega turbulence model is well suited for simulating flow near a wall in the viscous sub-layer, while the k-epsilon turbulence model is better suited for simulating flow in regions away from the wall [29]. Water was selected as the fluid with a constant density of 1000 kg/m^3 and a constant viscosity of 0.001 kg/ms, as the initial experiments study low concentrations of anti-prothrombin in water. The impeller zone was defined as a rotating domain with a rotation-axis direction of (0, -1, 0) and a speed of 164.3 rad/s, as estimated in Section 7.5.3. Calculations. The inlet and outlets were described as having a turbulent intensity of 5%, hydraulic diameter of 0.032 m (syringe diameter) and a velocity magnitude of 0.1 m/s as initial guess values. The solution methods and controls are displayed in Figure 7.3. Animation solutions were completed for the following properties: turbulence viscosity ratio (contour), strain rate (contour), pressure (contour), velocity (vector) and velocity (path lines). The calculation was completed using 2000 times steps with a time step size of 0.025 s with 20 maximum iterations/time step to visualize impeller rotation. Figure 7.4 displays the residuals as a function of iterations for the base case simulation.

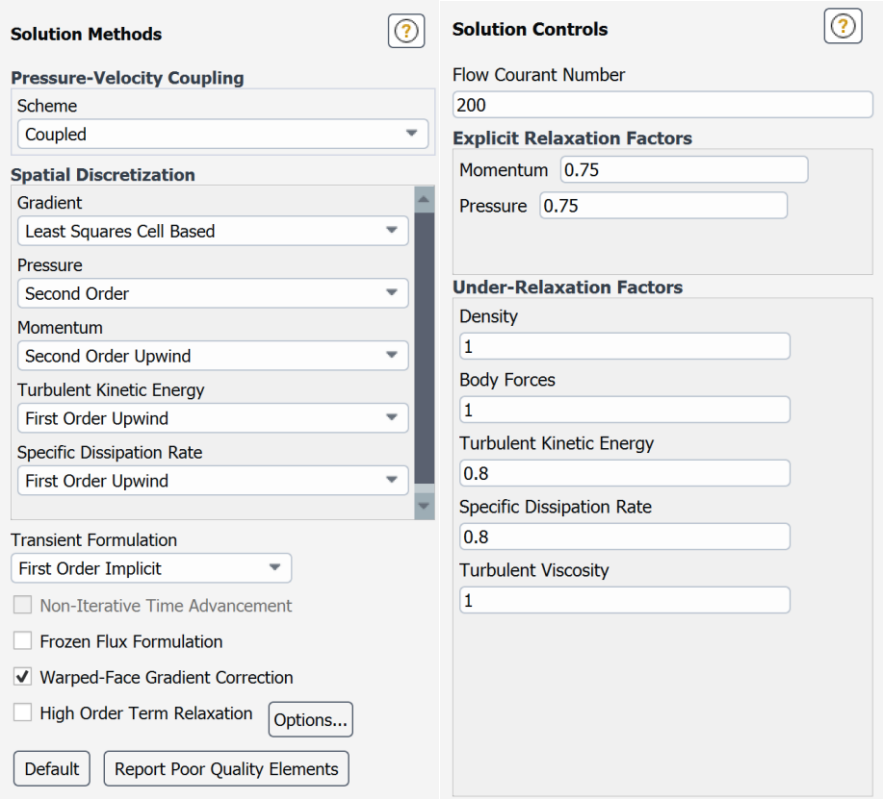


Figure 7.3. Solution methods and controls for base case CFD simulation on ANSYS Fluent.

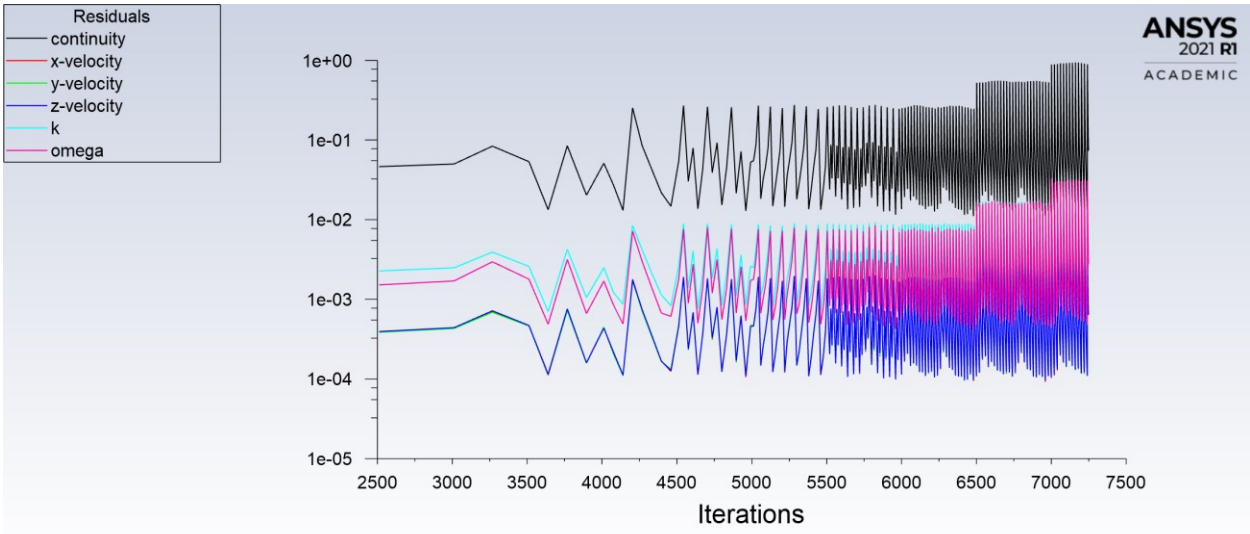


Figure 7.4. Residuals for continuity, x-velocity, y-velocity, z-velocity, k and omega as a function of iterations for the base case in ANSYS Fluent.

Figures 7.5, 7.6 and 7.7 show screenshots taken from the simulation animations of the turbulent viscosity ratio contour, the velocity vectors, and the velocity magnitude path lines, respectively.

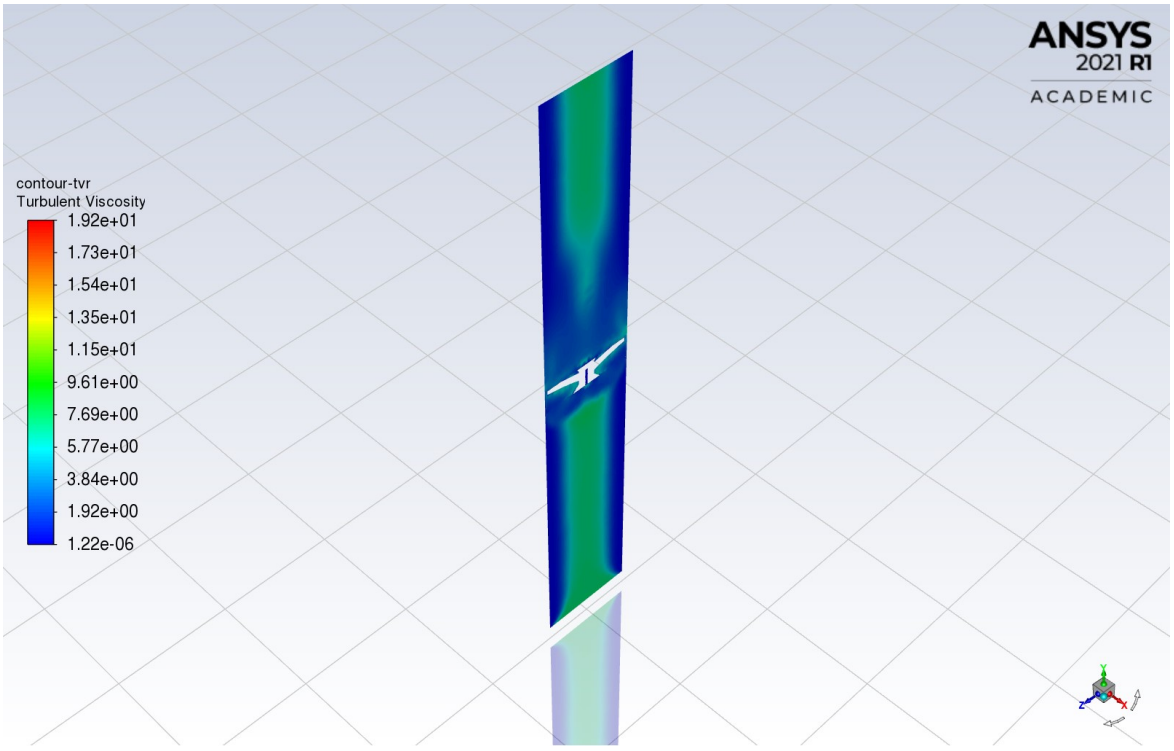


Figure 7.5. Screenshot of turbulent viscosity ratio contour during ANSYS Fluent base case simulation.

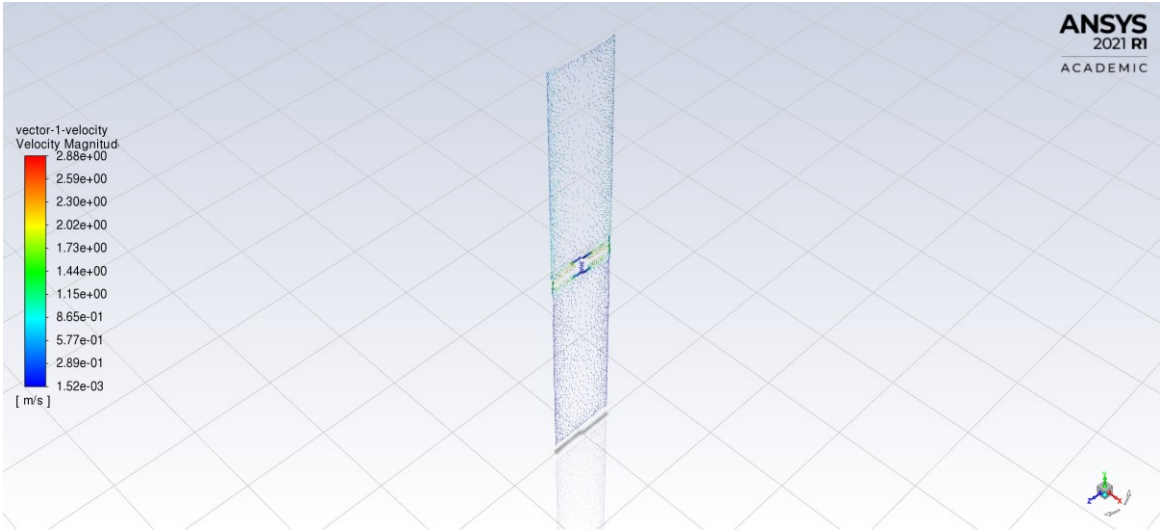


Figure 7.6. Screenshot of velocity vectors during ANSYS Fluent base case simulation.

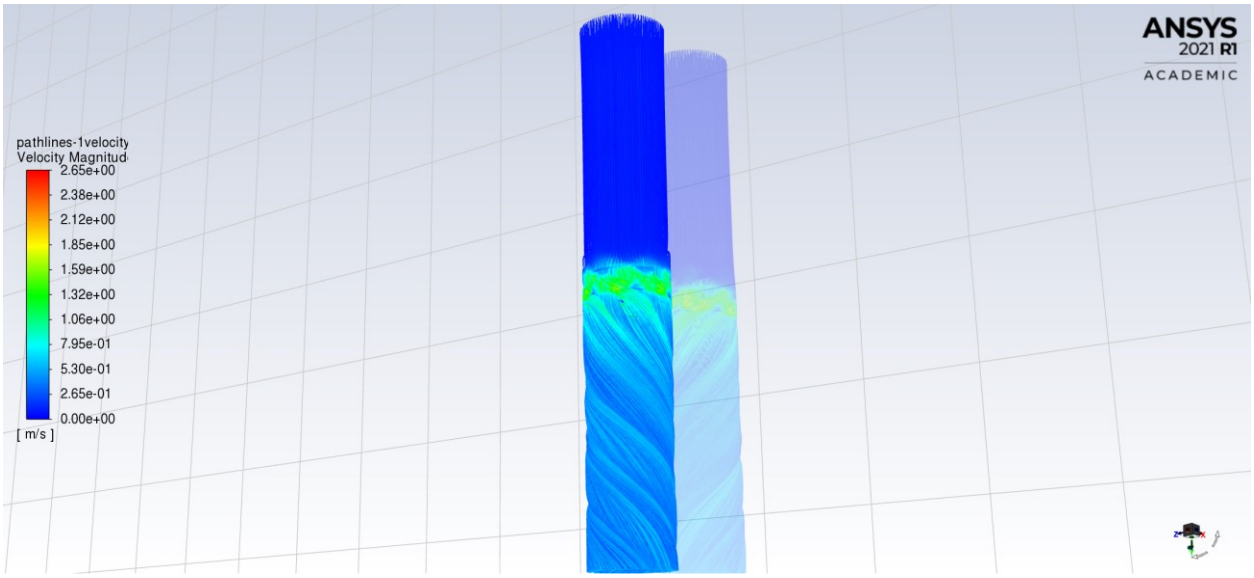


Figure 7.7. Screenshot of velocity magnitude path lines during ANSYS Fluent base case simulation.

The base case simulation was completed to assess the ability of the impeller designed in Fusion 360 to generate fluid mixing and does not represent either of the designs to be used for the diagnostic device. Several uncertainties existed in the base case simulation including the impeller rotation speed, as this was estimated in the calculations section, rather than measured experimentally, and the time step, as no time step refinements were completed. To verify the results of the base case simulation, time step refinements should be completed in which the simulation is conducted at different time step sizes, and a mesh convergence study should be completed. Mesh convergence studies involve repeating the simulation at decreased mesh element sizes and assessing the impact of this on the solution [30]. Further, all CFD simulations in this section should undergo experimental validation to be considered complete. Validation involves using experimental data to evaluate uncertainties in predictions made by CFD simulations. If experimental results match the predictions made by CFD, the simulation is considered valid and complete.

7.5.5. Fusion 360 Filter Design Case

The filter drafted by Jacob Damant in Fusion 360 (shown in Figure 7.1) was imported into ANSYS Fluent to assess flow behavior from the entrance point of the filter, past the impeller and over the membrane. The simulation was set up using the Standard k-epsilon (2 equation) Viscous Model. Water was selected as the fluid with a constant density of 1000 kg/m^3 and a constant viscosity of 0.001 kg/ms, as the initial experiments study low concentrations of anti-prothrombin in water. The rotation speed of the impeller was not specified, as rotation was initiated by the entering fluid contacting an impeller blade. The simulation was designed such that water entering the filter at a velocity of 0.1 m/s initiated impeller rotation, starting from stationary using the dynamic mesh and six degrees of freedom solver.

Animation solutions were completed for the following properties: turbulent viscosity ratio (contour), velocity (vector) and velocity (path lines). The calculation was completed using 2000 times steps with a time step size of 0.025 s with 20 maximum iterations/time step. The time step was chosen to minimize the rotation of the impeller at each time step, as the impeller should rotate 2° to 3° per time step ([31], [32], [33]). A time step even smaller than 0.025 s would have been selected for this simulation, but the computational resources and power required to complete the CFD simulation with a smaller time step were not available. Figure 7.8 displays the residuals as a function of iterations for the Fusion 360 filter simulation. Figures 7.9 and 7.10 show screenshots taken from the simulation animations of the turbulent viscosity ratio contour in the vertical plane surrounding the impeller, and in the plane just above the surface of the coated membrane and just below the impeller, respectively. Figures 7.11 and 7.12 show screenshots taken from the simulation animations of the velocity vectors in the vertical plane surrounding the impeller, and just above the surface of the coated membrane, respectively.

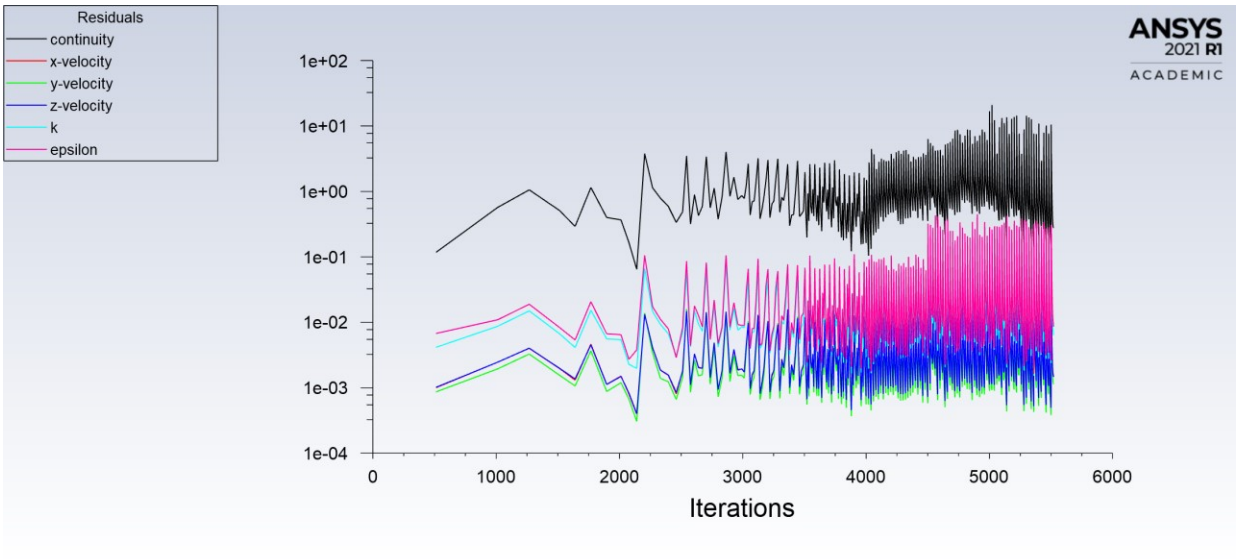


Figure 7.8. Residuals for continuity, x-velocity, y-velocity, z-velocity, k and epsilon as a function of iterations for the Fusion 360 filter design case in ANSYS Fluent.

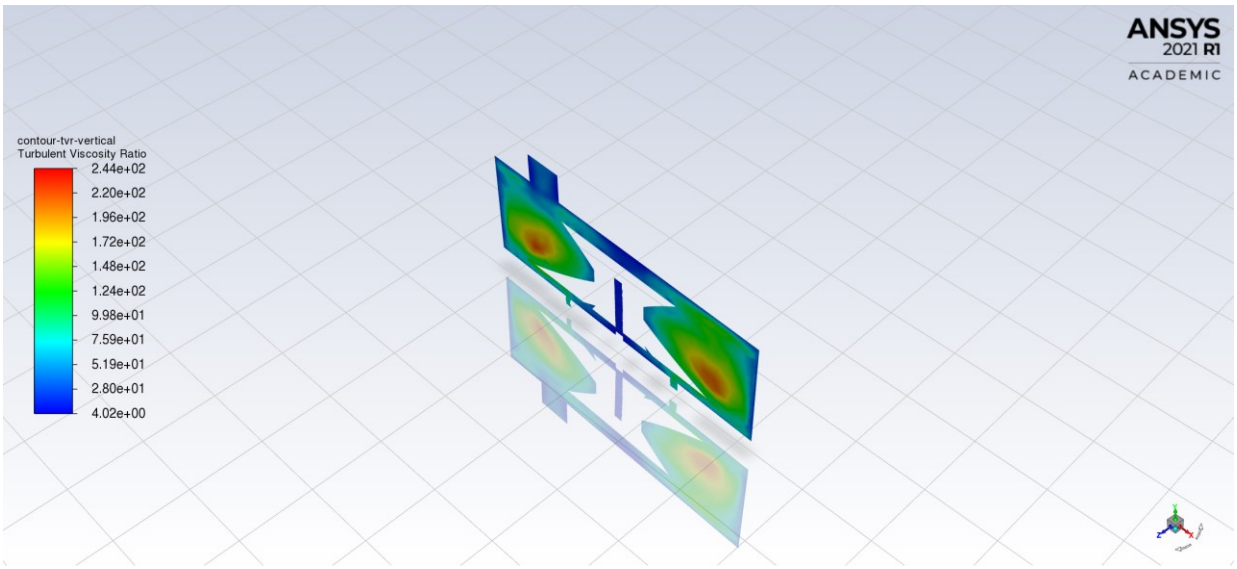


Figure 7.9. Screenshot of turbulent viscosity ratio contour in the vertical plane surrounding the impeller during ANSYS Fluent Fusion 360 filter design case. The clear portion represents the location of the impeller. TVR > 10 indicates turbulent flow.

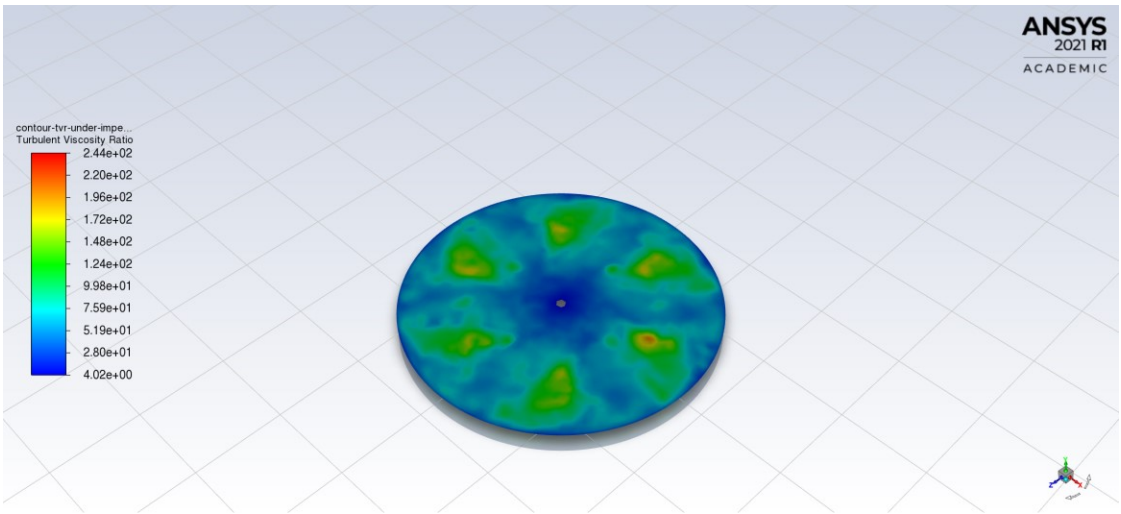


Figure 7.10. Screenshot of turbulent viscosity ratio just above the surface of the disc membrane, and just beneath the impeller, during ANSYS Fluent Fusion 360 filter design case. TVR > 10 indicates turbulent flow.

Observing Figures 7.9 and 7.10, the yellow, red and portions of the green regions are expected to experience turbulent flow, as the turbulent viscosity ratio is greater than 10 in these regions.

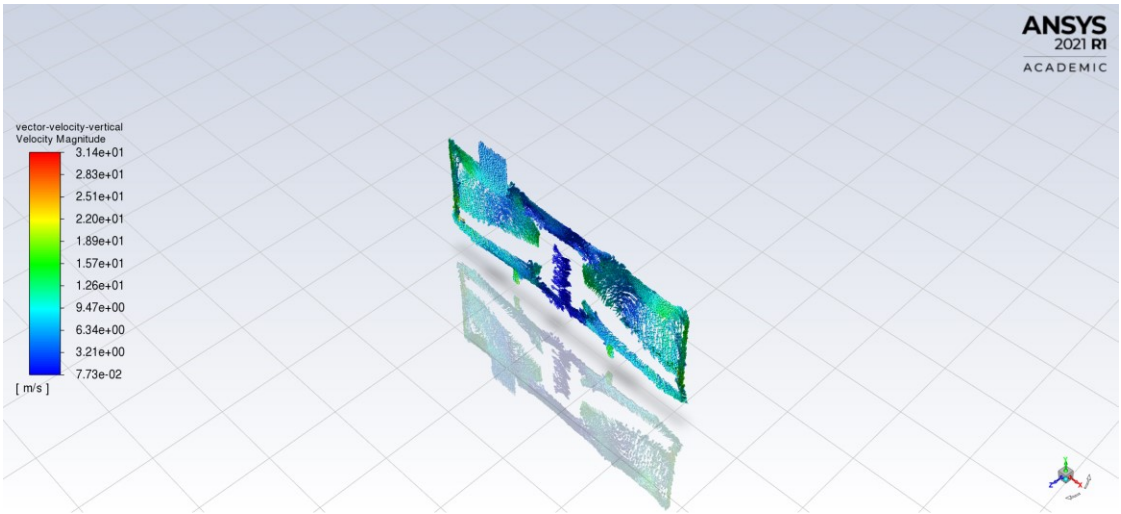


Figure 7.11. Screenshot of velocity vectors in the vertical plane surrounding the impeller during ANSYS Fluent Fusion 360 filter design case. The clear portion represents the location of the impeller.

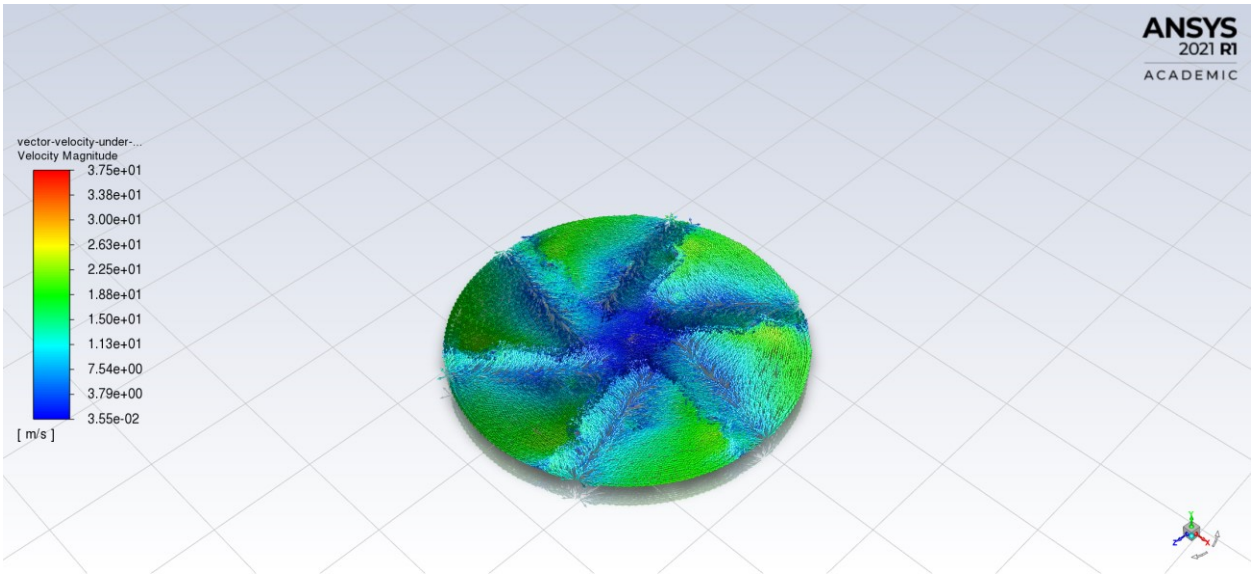


Figure 7.12. Screenshot of velocity vectors just above the surface of the disc membrane and just beneath the impeller, during ANSYS Fluent Fusion 360 filter design case.

Preliminary simulations in ANSYS Fluent of the Fusion 360 filter design suggest that turbulence should occur, and the system should be well-mixed based on the TVR and velocity vectors, however, more analysis is required for confirmation. Several assumptions were made during this simulation that should be investigated further in the future: the simulation was completed as a single-phase simulation, assuming that the fluid was already inside of the filter when the simulation started. In reality, the fluid domain inside the filter would fully consist of air at the beginning (t = 0) and would be filled with fluid as the syringe was pushed. Further, the center of gravity and torque parameters of the impeller were estimated based off an estimated impeller weight, and these parameters should be confirmed to produce a more accurate simulation in the future. As the final experimental design selected was the stirred tank, the CFD simulation for the filter design was not further explored. Future simulation work for this geometry should include time step refinements and a mesh convergence study, in which the simulation is repeated at decreased mesh element sizes and the impact of this on the solution is

analyzed [30]. Lastly, experimental data for this design should be obtained and compared to CFD predictions in order to validate and complete the simulation.

7.5.6. Stirred Tank Case

As several of the sensitivity experiments discussed in Chapter 8 were completed using a stirred tank set up, the physical impeller used in these experiments was drafted into a Fusion 360 model by Ben Damant and imported into ANSYS Fluent for fluid simulation. The Fusion 360 impeller is shown in Figure 7.13.

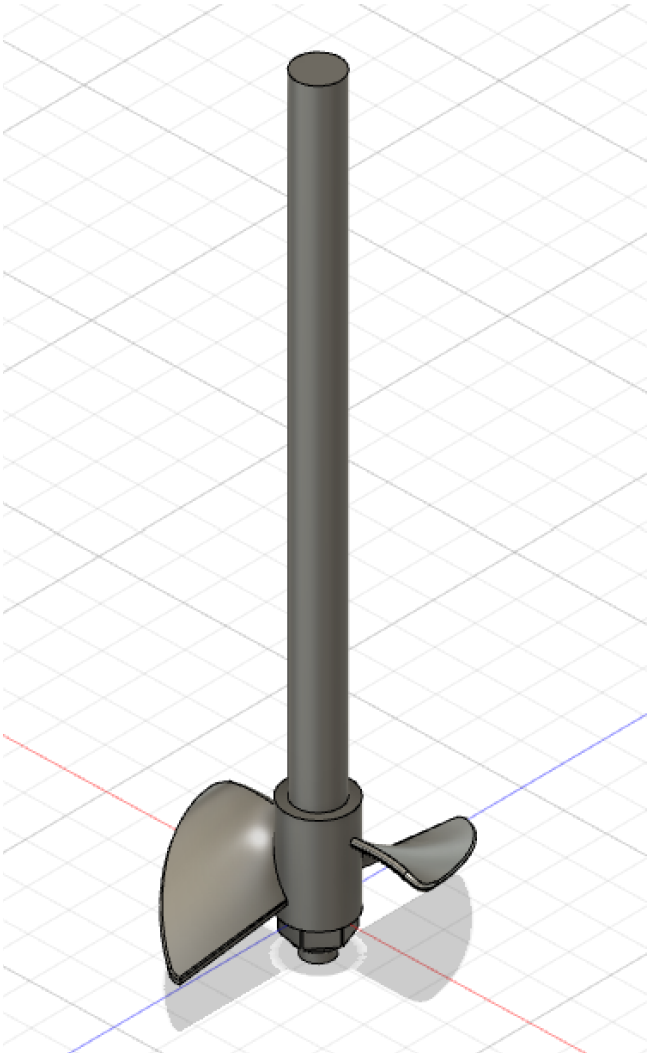


Figure 7.13. Fusion 360 stirred tank impeller design.

To calculate the speed of the impeller used in the stirred tank experiments in RPM, a one second video was taken of the impeller blade from above while the Tech II Railmaster 2400 was turned on and sent to a power of ~ 13, as this is the power used during experiments. The one second video was slowed down to visualize how many turns were made by the impeller in one second. The impeller rotated ~ 3.25 times in one second. Multiplying this value by 60 yields a value of 195 RPM. For stirred tank simulations, a value of 195 RPM or 20.4 rad/s was used for the impeller. The beaker measurements were measured approximately during experiments and used to design the beaker geometry in ANSYS. The beaker had a diameter of 10.5 cm, and the distances from the bottom of the beaker to the impeller and from the bottom of the beaker to the air-liquid interface were 5.3 cm and 7.3 cm, respectively. For simulation purposes, the beaker was assumed to be a perfect cylinder, and the slight curvature at the bottom was not considered. The coated membrane was designed as a 15 mm × 15 mm × 2 mm box and was placed in the bottom of the beaker. The membrane was subtracted from the cylindrical fluid domain using a Boolean operation. The set up was composed of a rotational zone (the impeller) and a stationary zone (the rest of the fluid domain). The moving reference frame model was used for the simulation as it predicts a good steady state approximation of fluid behavior if there are no secondary flows (e.g., due to interaction with baffles). To create the rotating zone, a cylinder was created to encompass the entire impeller, and the impeller geometry was subtracted from the cylinder by performing a Boolean operation. The mesh was generated in ANSYS Meshing as a tetrahedral mesh, then converted to polyhedral in ANSYS Fluent. A 4 mm Polyhedral mesh with 292,687 cells was used for the first simulation. The Shear Stress Transport (SST) k-omega turbulence model was selected as the SST k-omega model has been shown to work well for modeling turbulent flow in a stirred tank [34]. The pressure-based type solver was used, and a

steady state simulation was performed. Gravity was assumed to be negligible, and water was selected as the fluid with a constant density 997.7 kg/m^3 (room temperature), and a constant viscosity of 0.001 kg/ms [35]. The solution methods used (coupled solver, standard model coefficients) are shown in Figure 7.14.

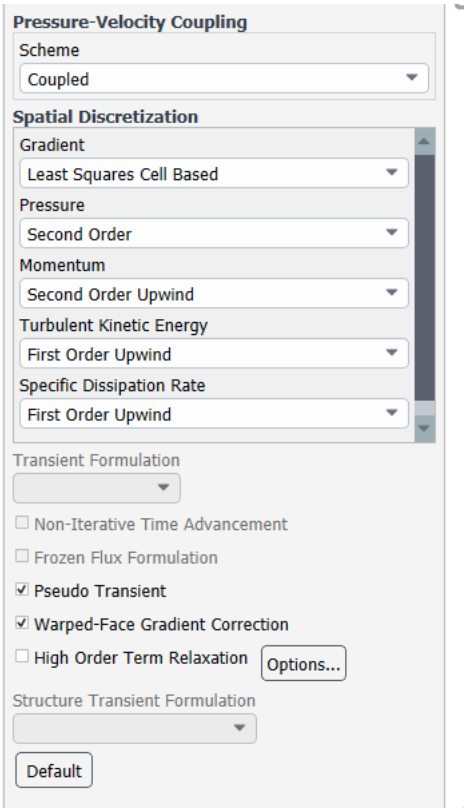


Figure 7.14. Solution method settings for the stirred tank case ANSYS Fluent simulation.

Animation solutions were completed for the following properties: turbulent viscosity ratio (contour), velocity (vector) and velocity (path lines). A steady state simulation was completed with 300 iterations. Figure 7.15 displays the residuals as a function of iterations for the stirred tank simulation.

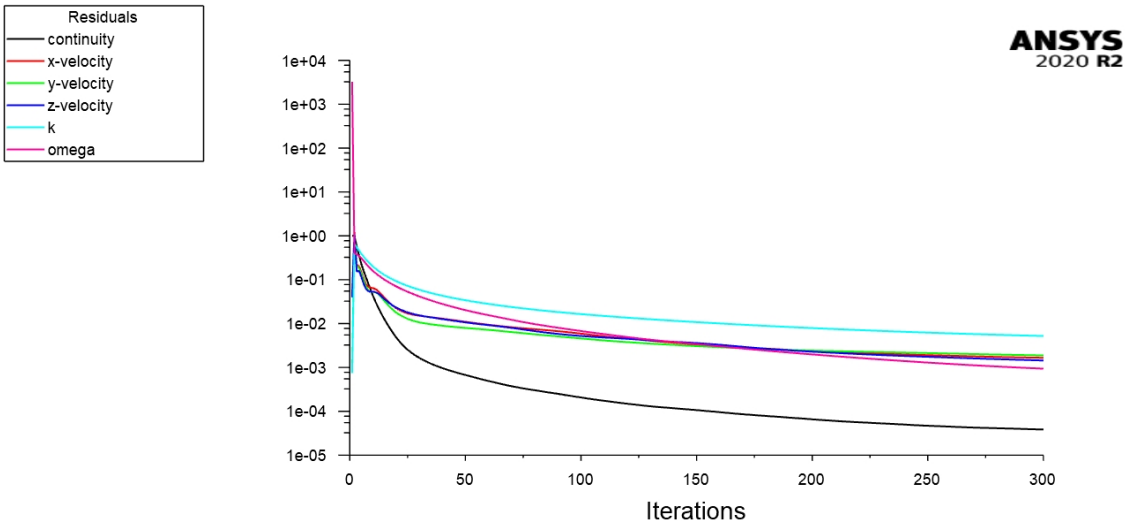


Figure 7.15. Residuals for continuity, x-velocity, y-velocity, z-velocity, k and omega as a function of iterations for the stirred tank case in ANSYS Fluent.

Figures 7.16 and 7.17 show screenshots taken from the simulation animations of the turbulent viscosity ratio contour from a top view and side view of the beaker, respectively. As a rule of thumb, a turbulent viscosity ratio greater than 10 indicates turbulent flow [24].

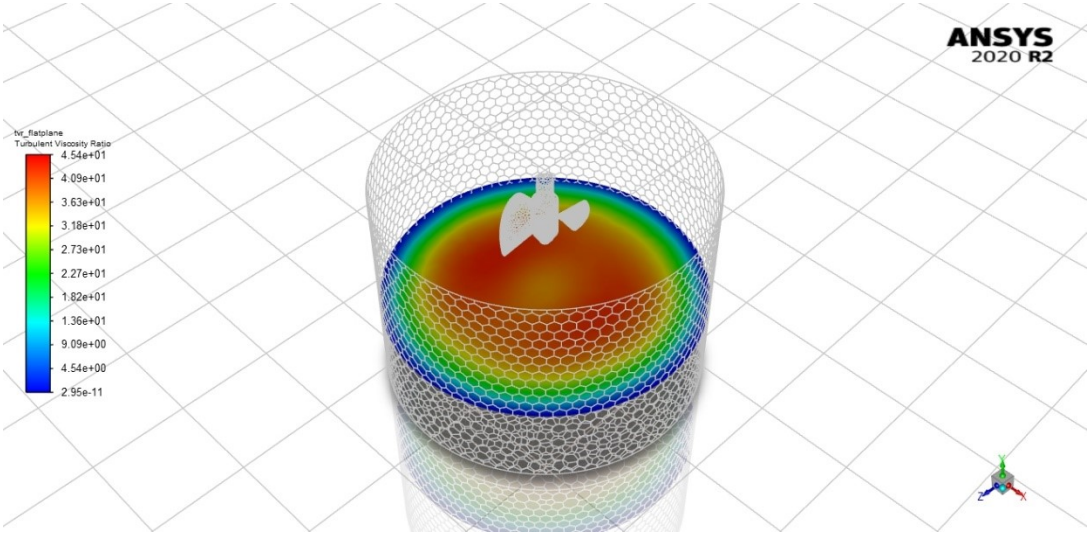


Figure 7.16. Screenshot of turbulent viscosity ratio (top view) in ANSYS Fluent stirred tank simulation. TVR > 10 indicates turbulent flow.

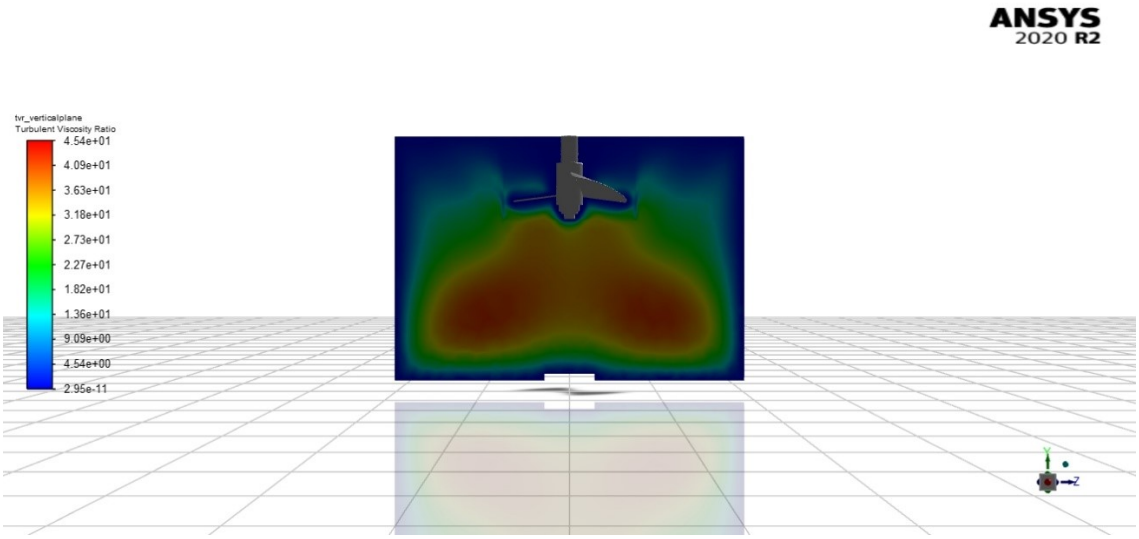


Figure 7.17. Screenshot of turbulent viscosity ratio (side view) in ANSYS Fluent stirred tank simulation. TVR > 10 indicates turbulent flow.

Observing Figures 7.16 and 7.17, turbulent flow should occur in the stirred tank as the turbulent viscosity ratio is greater than 10 in the green, yellow, and red regions. Figures 7.18 and 7.19 show screenshots taken from the simulation animations of the velocity vectors from a top view and side view of the beaker, respectively.

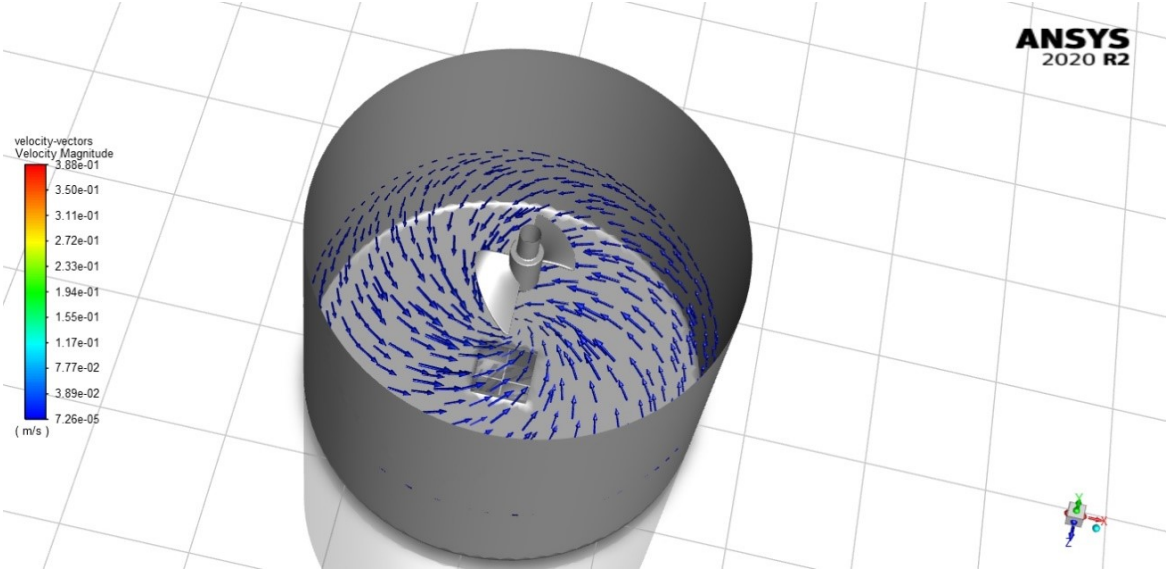


Figure 7.18. Screenshot of velocity vectors (top view) in ANSYS Fluent stirred tank simulation.

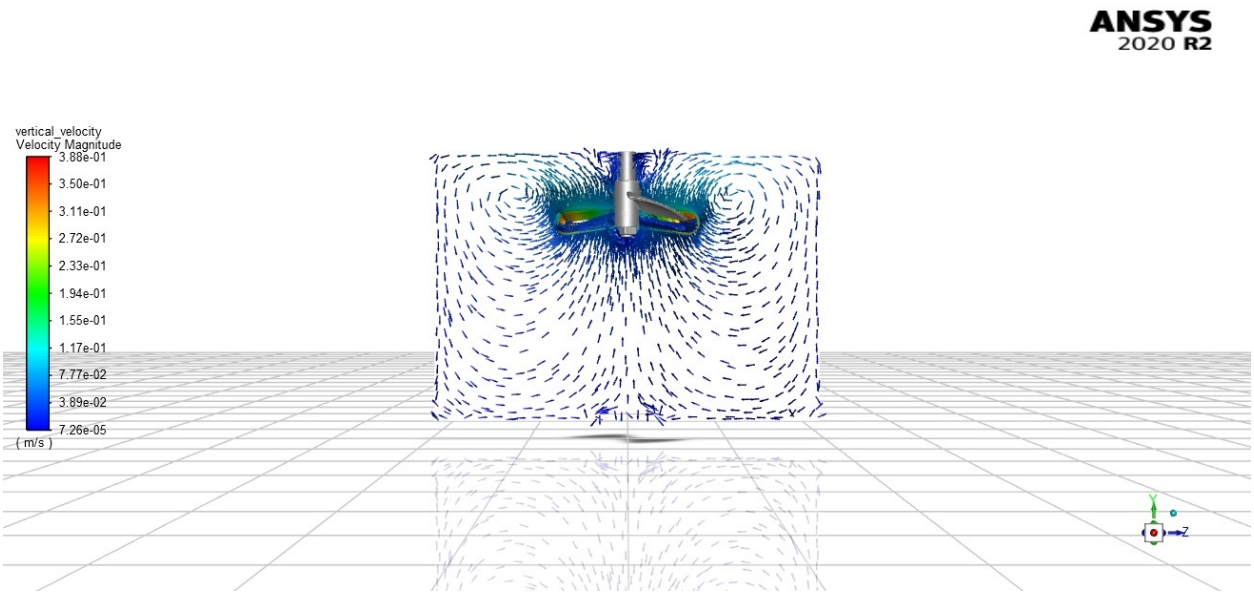


Figure 7.19. Screenshot of velocity vectors (side view) in ANSYS Fluent stirred tank simulation.

The results of the initial simulation suggest the fluid inside the beaker experiences turbulent flow and undergoes mixing above the membrane surface. To ensure that the simulation did not contain a significant amount of discretization error, a mesh convergence study was completed by decreasing the base cell mesh size from 4 mm to 2 mm in ANSYS Meshing. A new tetrahedral mesh was generated then converted to polyhedral in ANSYS Fluent. The 2 mm mesh contained 332,802 cells. The total number of cells did not increase by a large amount considering that the base cell mesh size was halved, likely because mesh refinement was performed near the walls of the impeller and walls of the cylindrical tank. In future work, the mesh should be further refined near the solid surfaces in the fluid domain so that the cell count is increased significantly. Results between the 4 mm mesh case and the 2 mm mesh case were compared and both simulations indicated similar amounts of turbulence (by observing TVR) and mixing (by observing velocity vectors) within the fluid domain. Quantitatively, the area weighted average wall shear converged to values that agreed from a computational error perspective for

both mesh sizes. As the purpose of this CFD investigation was to determine if the experimental setup would induce well mixed flow and turbulence, this brief mesh convergence study was considered satisfactory, and suggests that the experimental setup will generate turbulent and well-mixed flow in the real experimental studies. In the future, the stirred tank simulation should be validated by comparing CFD predictions to experimental data, such as experimental local velocity measurements. The simulation could be further verified in the future by completing a transient simulation, in which the average values over the entire period should agree with the values shown in the steady state simulation that was completed.

7.5.7. Future CFD Work

As previously mentioned, experimental validation is required for all CFD simulations to ensure the CFD simulations are reasonable at predicting the fluid behavior in reality. For the base case and Fusion 360 filter design case simulations, mesh refinements and time step refinements should be completed to verify the results of the simulation. Although the stirred tank case showed sufficient mixing and turbulence and mesh refinements were completed, several assumptions were made, and further simulation work should be completed in the future to account for these assumptions. First, the beaker was assumed to be a perfect cylinder, when in reality, there is curvature at the bottom of the beaker. In future simulations, more refined geometry with the exact beaker measurements and appropriate curvature should be used to assess the impact of this geometry on flow patterns and turbulence. Another limitation of the stirred tank simulation was that the top of the fluid volume was assumed to be a flat surface, when in reality, a small vortex is created at the surface due to the impeller spinning. Future simulations should investigate the effects of the vortex at the surface on flow patterns and turbulence.

Additionally, CFD simulations can be used in the future to investigate other geometries or experimental set ups to optimize turbulence and mixing. Baffles are often attached to the side of stirred tanks to enhance mixing and increase turbulence levels, so it may be of interest to study the effect of incorporating baffles or a draft tube into the experimental design ([36], [37]). Using CFD, multiple design geometries, such as incorporating the use of baffles or a draft tube, and the resulting flow patterns can be analyzed and compared to obtain optimal turbulence and mixing levels that can potentially allow for improved sensitivity.

As the CFD simulations were not verified or validated experimentally, it cannot be confirmed that the results in this section will accurately predict fluid behavior in reality. The CFD simulations completed in this work only offer the first steps into the investigation of fluid behavior through numerical and computational methods, and more work is required to confidently state that the simulation results accurately represent the fluid behavior.

7.6. Discussion

For small volume samples, anti-prothrombin molecules diffuse through the solution then bind to the prothrombin coated surface. In a 20 μL drop, diffusion occurs fast enough that a visual colour shift from anti-prothrombin binding can be detected after 20 minutes of exposure. For larger volume samples (500 mL), diffusion to the surface would take much longer, and the time required to see results would be significantly increased. To create a diagnostic device that tests larger volumes and can provide results within 20 minutes, another method must be used to ensure the anti-prothrombin molecules in solution come into contact with the prothrombin coated surface, rather than relying on diffusion alone. Sweet calculated the diffusion coefficient and the diffusion time for prothrombin in water at 21°C to move from the outermost surface of a 20 μL droplet to the alumina surface assuming momentum transfer was the underlying mechanism [4].

The calculated diffusion coefficient for prothrombin was 5.22×10^{-7} cm^2/s and the diffusion time was 51 minutes [4]. The diffusion time of 51 minutes was calculated based on the maximum distance that the protein would travel, from the air-surface interface of the droplet to the alumina surface, which was ~ 0.8 mm for a 20 μL droplet [4]. For a larger volume, the diffusion time would increase significantly, and the device would no longer be able to provide rapid results relying on diffusion alone. For a 500 mL volume, the distance from the air-solution interface at the top of the fluid volume in the 1 L beaker to the coated tantalum disc or silicon wafer surface is 7.3 cm. Based on the assumption that the diffusion time is 51 minutes for prothrombin to travel 0.8 mm in solution, it would take 4654 minutes (~ 77.6 hours) to travel 73 mm from the top of the 500 mL fluid volume to the bottom of the beaker, where the substrate material is placed. It is important to consider that not all protein molecules are found at the air-liquid interface, and they are spread out within the fluid volume. It is possible that some protein molecules may be found closer to the substrate than to the air-liquid interface, and diffusion of these molecules to the surface could be possible in a shorter amount of time. The purpose of the impeller is to increase fluid mixing and generate turbulent flow just above the surface to encourage anti-prothrombin molecules to contact the prothrombin coated surface in a shorter period of time, combining the effects of turbulence and diffusion. Enhanced mixing above the coated membrane causes many fluid elements to be exposed to the prothrombin coated surface, increasing the probability of an anti-prothrombin molecule binding. Mixing of fluid elements by the impeller reduces the need to rely on diffusion of anti-prothrombin alone, allowing larger volumes to be tested while still achieving rapid results. High diffusivity is a characteristic of turbulent flow due to the velocity fluctuations and turbulent transport is significantly more effective than molecular diffusion alone [27].

7.7. Conclusions

Using larger volume fluid samples has the potential to increase sensitivity of the diagnostic device and detect analytes in solution at lower concentrations. In order to improve sensitivity, the large fluid samples should experience turbulent flow and undergo adequate mixing to ensure that all fluid elements have a high chance of encountering the coated membrane, allowing for antigen-antibody binding at the surface. Two different large volume fluid set ups were considered to achieve increased sensitivity, and fluid behavior was simulated using ANSYS Fluent for each case. For the Fusion 360 filter design, preliminary simulations suggested that turbulent flow and mixing should occur above the membrane, but mesh refinements and time step refinements should be completed in the future to verify simulation results. For the stirred tank design, mesh refinement studies were completed, and preliminary results suggest that the fluid in this set up will experience significant mixing and turbulent flow as per the ANSYS Fluent simulation. CFD simulations suggest that both designs have the potential to produce sufficient turbulence and mixing in large volume samples to allow for a more sensitive device to be developed, but further verification and experimental validation is required for confirmation and completion of the simulations.

7.8. References

1. ThermoFisher Scientific. *Immunoassays*. [cited 2022 March 17]; Available from: https://www.thermofisher.com/ca/en/home/life-science/antibodies/immunoassays.html.

2. Khan, N.I., et al., *An integrated microfluidic platform for selective and real-time detection of thrombin biomarkers using a graphene FET.* Analyst, 2020. **145**(13): p. 4494-4503.

3. Nickel, M.R., *Physical and Optical Characterization of Anodized Aluminum-Tantalum Thin Films for use in Thin Film Diagnostics*, in *Materials Engineering*. 2018, University of Alberta.

4. Sweet, H.M., *Development of a Nanostructured Thin Film Device and Optics System for Protein Detection*, in *Materials Engineering*. 2018, University of Alberta.

5. Bekard, I.B., et al., *The effects of shear flow on protein structure and function.* Biopolymers, 2011. **95**(11): p. 733-745.

6. Thomas, C.R. and D. Geer, *Effects of shear on proteins in solution.* Biotechnol Lett, 2011. **33**(3): p. 443-56.

7. Stein, P.D. and H.N. Sabbah, *Turbulent blood flow in the ascending aorta of humans with normal and diseased aortic valves.* Circulation Research, 1976. **39**(1): p. 58-65.

8. Maa, Y.-F. and C.C. Hsu, *Effect of high shear on proteins.* Biotechnology and Bioengineering, 1996. **51**(4): p. 458-465.

9. Biddlecombe, J.G., et al., *Factors influencing antibody stability at solid–liquid interfaces in a high shear environment.* Biotechnology Progress, 2009. **25**(5): p. 1499-1507.

10. Kim, M.H., et al., *Surface deactivation of cellulase and its prevention.* Enzyme and Microbial Technology, 1982. **4**(2): p. 99-103.

11. Thomas, C.R., A.W. Nienow, and P. Dunnill, *Action of shear on enzymes: Studies with alcohol dehydrogenase.* Biotechnology and Bioengineering, 1979. **21**(12): p. 2263-2278.

12. Thomas, C.R. and P. Dunnill, *Action of shear on enzymes: Studies with catalase and urease.* Biotechnology and Bioengineering, 1979. **21**(12): p. 2279-2302.

13. Maa, Y.F. and C.C. Hsu, *Protein denaturation by combined effect of shear and air-liquid interface.* Biotechnol Bioeng, 1997. **54**(6): p. 503-12.

14. Sarkar, M. and V. Prabhu, *Basics of cardiopulmonary bypass.* Indian J Anaesth, 2017. **61**(9): p. 760-767.

15. Pruitt, K.M., R.M. Stroud, and J.W. Scott, *Blood Damage in the Heart-Lung Machine.* Proceedings of the Society for Experimental Biology and Medicine, 1971. **137**(2): p. 714-718.

16. *Plasma Protein Denaturation during Cardiopulmonary Bypass and the Influence of the Reticuloendothelial System upon these Changes*. [cited 2022 March 17]; Available from: https://www.osti.gov/opennet/servlets/purl/16011725.pdf.

17. Lumb, A.B., *Chapter 31 - Respiratory Support and Artificial Ventilation*, in *Nunn's Applied Respiratory Physiology (Eighth Edition)*, A.B. Lumb, Editor. 2017, Elsevier. p. 451-478.e3.

18. Brillman, J., *Chapter 185 - Neurologic Complications of Cardiac Surgery*, in *Office Practice of Neurology (Second Edition)*, M.A. Samuels and S.K. Feske, Editors. 2003, Churchill Livingstone: Philadelphia. p. 1188-1195.

19. Mirro, R. and K. Voll. *Which Impeller Is Right for Your Cell Line?* 2009 [cited 2022 March 16]; Available from: https://bioprocessintl.com/analytical/cell-line-development/which-impeller-is-right-for-your-cell-line-183538/#:~:text=The%20blades%20on%20pitched%2Dblade,of%20unidirectional%20marine%20blade%20impellers.

20. Li, X., et al., *Numerical optimization for blades of Intermig impeller in solid–liquid stirred tank.* Chinese Journal of Chemical Engineering, 2021. **29**: p. 57-66.

21. Rewatkar, V.B. and J.B. Joshi, *EFFECT OF IMPELLER DESIGN ON LIQUID PHASE MIXING IN MECHANICALLY AGITATED REACTORS.* Chemical Engineering Communications, 1991. **102**(1): p. 1-33.

22. Hu, H.H., *Chapter 10 - Computational Fluid Dynamics*, in *Fluid Mechanics (Fifth Edition)*, P.K. Kundu, I.M. Cohen, and D.R. Dowling, Editors. 2012, Academic Press: Boston. p. 421-472.

23. ANSYS, I. *ANSYS Innovation Courses: Basics of Turbulent Flows*. 2020 [cited 2022 April 14]; Available from: https://courses.ansys.com/index.php/courses/basics-of-turbulent-flows/.

24. Datawave Marine Solutions. *Practical CFD Modeling: Turbulence*. 2021 [cited 2022 April 14]; Available from: https://dmsonline.us/practical-cfd-modeling-turbulence/.

25. ANSYS, I. *ANSYS Innovation Courses: Governing Equations of Fluid Dynamics*. 2021 [cited 2022 April 27]; Available from: https://courses.ansys.com/index.php/courses/governing-equations-of-fluid-dynamics/.

26. Ferziger, J.H., M. Perić, and R.L. Street, *Computational methods for fluid dynamics*. Fourth edition. ed. 2020: Springer.

27. Roberts, P.J. and D.R. Webster. *TURBULENT DIFFUSION*. 2002.

28. SimScale. *K-Omega and K-Omega SST*. 2021 [cited 2022 April 29]; Available from: https://www.simscale.com/docs/simulation-setup/global-settings/k-omega-sst/.

29. Autodesk. *SST K-Omega Turbulence Models*. 2018 [cited 2022 April 18]; Available from: https://knowledge.autodesk.com/fr/support/cfd/learn-explore/caas/CloudHelp/cloudhelp/2019/FRA/SimCFD-Learning/files/GUID-0F5C4828-9F91-46B6-A16A-2578D72DCFCC-htm.html.

30. *Mesh Convergence*. [cited 2022 April 5]; Available from: https://abaqus-docs.mit.edu/2017/English/SIMACAEGSARefMap/simagsa-c-ctmmeshconverg.htm.

31. Zhao, F., et al., *Optimization design of the impeller based on orthogonal test in an ultra-low specific speed magnetic drive pump.* Energies, 2019. **12**(24).

32. Šškerlavaj, A. and R. Pavlin. *Effect of vortical structures on cavitation on impeller blades in pumps with suction chambers*. 2014. Institute of Physics Publishing.

33. Xu, J., *Fluid machinery and fluid mechanics : 4th International Symposium (4th ISFMFE)*. 2009: Springer.

34. Riquelme, M.C.S., *CFD Modelling of Bioprocesses: Integrating Mechanical Mixing, Aeration and Dynamic Rheology*, in *Chemical and Materials Engineering*. 2021, University of Alberta.

35. Engineering ToolBox. *Water - Density, Specific Weight and Thermal Expansion Coefficients*. 2003 [cited 2022 April 6]; Available from: https://www.engineeringtoolbox.com/water-density-specific-weight-d_595.html.

36. Demartini, L.C., H.A. Vielmo, and S.V. Möller, *Numeric and experimental analysis of the turbulent flow through a channel with baffle plates.* Journal of the Brazilian Society of Mechanical Sciences and Engineering, 2004. **26**(2): p. 153-159.

37. Kamla, Y., et al., *Effect of the Inclination of Baffles on the Power Consumption and Fluid Flows in a Vessel Stirred by a Rushton Turbine.* Chinese Journal of Mechanical Engineering, 2017. **30**(4): p. 1008-1016.

Chapter 8 – Anti-Prothrombin Sensitivity on a Prothrombin-Coated Membrane Device

8.1. Introduction

Antibody-antigen interactions are one of the most important ways in which the human immune system can identify and destroy foreign pathogens inside the body. Antibody-antigen binding is very specific and occurs when the antigenic epitope and the antibody paratope attractive forces overcome hydration forces of the two molecules [1]. For this to occur, the antigen and antibody must come within several nanometers of each other. Antibody-antigen reactions are influenced by many factors, including but not limited to temperature, pH, ionic strength, antigen and antibody concentrations, and incubation time [1].

Most immunoassay-based systems for protein detection depend on the immobilization of an antigen or antibody on a solid surface [2]. Antibody-antigen interactions on the assay surface are greatly affected by the immobilization method and characteristics. Factors affecting the antibody interactions with an immobilized antigen include the orientation and spacing of the immobilized protein to allow for optimal binding and incubation conditions [2]. ELISAs are one of the most sensitive immunoassays available to detect antigen-antibody pairs by immobilizing a molecule, forming an antigen-antibody complex, and amplifying the signal ([3], [4]). ELISA and the thin film diagnostic device in this study both depend on the antigen-antibody complex forming on a surface, rather than in a solution. ELISA sensitivities are dependent on the characteristics of the antibody-antigen interaction of interest but have a typical detection range of 0.1 to 1 fmole or 0.01 ng to 0.1 ng [3]. The sensitivity of ELISA is limited by the small sample volume, typically in the microliter range [4]. By increasing the volume of the sample, binding can occur at lower antibody concentrations. It has been previously shown that immobilized prothrombin is capable of binding to anti-prothrombin in solution on a porous anodic alumina

surface in small volumes [5]. The use of a porous membrane or a stirred tank and turbulent flow allows for a larger volume of fluid to be analyzed, as more fluid elements can be exposed to the surface of the coated membrane.

The goal of this work is to determine the limit of detection for anti-prothrombin in solution by binding to immobilized prothrombin on the device surface. It was expected that by increasing the sample volume, lower concentrations of the antibody in solution could be detected compared to currently available methods that utilize smaller volume samples. Passing the antibody containing fluid through a porous membrane or stirring the fluid above a coated membrane allows larger volumes of fluid to be exposed to the immobilized protein surface, decreasing the concentration required for detection. A series of experiments were conducted in which a solution of anti-prothrombin was continuously diluted until there was no visual colour shift on the surface to determine the experimental limit of detection on a stationary surface and for larger fluid volumes in the device. The ability to increase device sensitivity by using larger sample volumes has many applications in healthcare and the future of diagnostics.

8.2. Methods

Hyphen BioMed highly purified human prothrombin from citrated human plasma from Aniara was reconstituted in distilled water at a concentration of 1 mg/mL and used for experiments. The antibody used was an affinity purified IgG sheep anti-human prothrombin in a 10 mM 4-(2-hydroxyethyl)-1-piperazineethanesulfonic acid (HEPES), 150 mM NaCL, 50% (v/v) glycerol buffer at a pH of 7.4 from Affinity Biologicals with a concentration of 0.5 mg/mL. The secondary antibody used was a rabbit anti-sheep IgG (H+L)-horseradish peroxidase (HRP) conjugate supplied by Bio-Rad. Detailed materials and methods can be found in Chapter 3 – General Materials and Methods.

8.3. Theoretical Calculations for Anti-Prothrombin Limit of Detection

Sweet calculated the anti-prothrombin limit of detection using the prothrombin limit of detection, radiolabelled data, and the dimensions of prothrombin and anti-prothrombin [5]. The prothrombin limit of detection for a visible colour shift to occur was found to be 5.5 pmols of prothrombin bound with surface coverage of 34 – 38% for a 1 cm diameter circle (surface area of 0.7854 cm^2) [5]. Based on prothrombin dimensions of ~ 11 × 4 × 5 nm [6] and anti-prothrombin IgG dimensions of ~ 14.5 × 8.5 × 4 nm ([7], [8]), it was assumed that the anti-prothrombin limit of detection results when one anti-prothrombin molecule has bound for every two prothrombin molecules required to achieve 34 – 38% surface coverage, resulting in a theoretical limit of detection for anti-prothrombin of 2.7 pmols to generate a visible colour shift for a 1 cm diameter circle surface area [5]. In this application, an entire silicon wafer slide with dimensions of ~ 1.3 cm by ~ 6.2 cm and a surface area of ~ 8.06 cm^2 will be exposed to 532 µL of 1 mg/mL of prothrombin for 20 minutes prior to adsorption of anti-prothrombin. The theoretical limit of detection for a visible colour shift to occur for a surface area of 0.7854 cm^2 was found to be 5.5 pmols of prothrombin [5], so for a surface area of 8.06 cm^2, 56.4 pmols of prothrombin would be required to bind to generate a visible colour shift. For anti-prothrombin, the theoretical limit of detection for a visible colour shift to occur for a surface area of 0.7854 cm^2 was found to be 2.7 pmols [5]. For a surface area of 8.06 cm^2, 27.7 pmols of anti-prothrombin would be required to bind to generate a visible colour shift. Silicon wafer slides were also cut into smaller rectangles with dimensions of ~ 1.2 cm by ~ 1 cm, with a surface area of ~ 1.2 cm^2. For a surface area of 1.2 cm^2, the theoretical limit of detection for a visible colour shift to occur would be 8.4 pmols of prothrombin and 4.13 pmols of anti-prothrombin, based on the theoretical limit of detection found by Sweet [5].

8.4. Device Preparation

Thin films of tantalum that were ~ 200 nm thick and aluminum thin films with thicknesses between 90 nm and 110 nm were sputtered onto the tantalum discs and the silicon wafers using the Bob and Floyd DC-planar magnetron sputtering systems, respectively, at the University of Alberta nanoFAB. The aluminum faces of the substrates were anodized at 4 V until the end of pore formation to create the porous aluminum oxide layer and the dielectric tantala layer. Further details on sputtering and anodization can be found in Chapter 3 – Materials and Methods.

8.5. Prothrombin Immobilization and Complex Formation

For initial experiments to determine whether quartz frits and tantalum disc substrates were able to adsorb prothrombin and generate a visible colour shift, 20 μL drops of prothrombin with a concentration of 1 mg/mL were exposed to the surface for 20 minutes on a wet paper towel in a Petri dish. Hydrophobic Sharpie circles with a diameter of 0.7 cm were used to control the exposure area and the 20 μL solution was spread completely within the circle using the pipette tip. After 20 minutes, the solution was removed from the surface using a pipette and the substrates were rinsed with deionized water and dried with oil free compressed air. The anti-prothrombin solution with a concentration of either 0.5 mg/mL, 0.05 mg/mL, 0.005 mg/mL, 5×10^{-4} mg/mL or 5×10^{-5} mg/mL was then placed on to the hydrophobic circles that had previously been exposed to the prothrombin solution, using the same method. The same process was applied for a secondary antibody (rabbit anti-sheep IgG (H+L)-horseradish peroxidase (HRP) conjugate with a concentration of 1 mg/mL supplied by Bio-Rad) on the surface previously coated with prothrombin and anti-prothrombin in some cases. Visible colour shifts on the surface after each layer of protein exposure indicated protein binding.

To determine the minimum concentration for a visible colour shift to occur on the tantalum disc surface for stationary protein solutions, the same process was applied but the concentration of anti-prothrombin in solution was varied using a dilution series as described previously. For larger volume stirred tank fluid experiments, a hydrophobic Sharpie rectangle was drawn along the edges of the ~ 1.3 cm by ~ 6.2 cm silicon wafer slide. A volume of 532 µL of 1 mg/mL prothrombin was placed within the hydrophobic rectangle on the coated silicon wafer surface and spread to the edges of the circle using a pipette tip, then placed in a Petri dish with a wet paper towel for 20 minutes. The 532 µL solutions were removed off the surface using a pipette, then the silicon wafer was rinsed with deionized water and dried with oil free compressed air prior to anti-prothrombin exposure. Silicon wafer rectangles with dimensions of ~ 1.2 cm by ~ 1 cm were also studied, in which 1 mg/mL prothrombin solutions of 35 µL were used. After exposure to prothrombin, the silicon wafer slides and rectangles were placed in a stirred tank set up consisting of a 1 L beaker and an impeller attached to a motor. The impeller speed was controlled by a Tech II Railmaster 2400, and 500 mL of water containing anti-prothrombin at various concentrations (0.005 mg/mL, 0.0025 mg/mL and 5×10^{-4} mg/mL) was placed in the beaker. The solution was stirred above the coated membrane for 20 minutes with the Tech II Railmaster 2400 set to a power of ~ 13 – 14, and the slides were then imaged and analyzed to determine if a colour shift occurred compared to the prothrombin only coated surface.

8.6. Results

First, a dilution series experiment was conducted to determine the minimum amount of anti-prothrombin that could be detected on the coated tantalum disc when stationary. A stock solution of anti-prothrombin was made by placing 1 µL of the 10 mg/mL anti-prothrombin

solution into 199 µL of UltraPure distilled water to yield a concentration of 0.05 mg/mL. Invitrogen UltraPure Distilled Water was used for all dilutions. Four discs were used with the concentration of anti-prothrombin being different for each disc. Each disc had 4 circles drawn with Sharpie. One circle was used as a control and was exposed to only prothrombin for 20 minutes. The other three spots were exposed to prothrombin for 20 minutes and then the specific concentration of anti-prothrombin for 20 minutes. The first disc was to be exposed to the stock solution with an anti-prothrombin concentration of 0.05 mg/mL (stock solution for dilution series). For the second disc, 50 µL of the stock solution was placed into 450 µL of water to dilute the concentration of anti-prothrombin in solution by a factor of 10 (1 in 100 dilution of initial anti-prothrombin concentration), giving an anti-prothrombin concentration of 5×10^{-3} mg/mL. For the third disc, 50 µL of the solution used for the second disc was placed in 450 µL of water to further dilute the concentration of anti-prothrombin in solution by another factor of 10, giving an anti-prothrombin concentration of 5×10^{-4} mg/mL. For the fourth disc, 50 µL of the solution used for the third disc was placed in 450 µL of water to dilute the concentration of anti-prothrombin in solution by a factor of 10 again, giving an anti-prothrombin concentration of 5×10^{-5} mg/mL. Water was used to dilute the anti-prothrombin solutions as opposed to phosphate buffer as water is the typical laboratory standard used.

The results of this initial experiment were different than expected. In Chapter 6 – Adsorption of Biologics onto Porous Anodic Alumina on Tantalum Discs, two discs anodized using the horizontal method produced strong and consistent colour shift results (Figure 6.5 and Figure 6.6), which was not the case for five out of the six discs studied in this experiment. Figures 8.1 – 8.6 display the results from adsorption of 20 µL of 1 mg/mL prothrombin placed in each of the four circles on the surface of the discs for 20 minutes. As exposure to prothrombin

produced inconsistent results on the surfaces, anti-prothrombin was not placed on the surfaces as previously described. Each disc was prepared the same way – cleaned using the same self-cleaning oven cycle, then coated with ~ 200 nm of tantalum followed by ~ 110 nm of aluminum and anodized at 4 V using the horizontal method. The discs with strong results in Figure 6.5 and Figure 6.6 were also prepared this way.



Figure 8.1. Tantalum disc coated with ~ 200 nm of tantalum then ~ 110 nm of aluminum and anodized at 4 V using the horizontal method after protein analysis. Each of the four circles was exposed to 20 µL of 1 mg/mL of prothrombin for 20 minutes.



Figure 8.2. Tantalum disc coated with ~ 200 nm of tantalum then ~ 110 nm of aluminum and anodized at 4 V using the horizontal method after protein analysis. Each of the four circles was exposed to 20 µL of 1 mg/mL of prothrombin for 20 minutes.



Figure 8.3. Tantalum disc coated with ~ 200 nm of tantalum then ~ 110 nm of aluminum and anodized at 4 V using the horizontal method after protein analysis. Each of the four circles was exposed to 20 µL of 1 mg/mL of prothrombin for 20 minutes.



Figure 8.4. Tantalum disc coated with ~ 200 nm of tantalum then ~ 110 nm of aluminum and anodized at 4 V using the horizontal method after protein analysis. Each of the four circles was exposed to 20 µL of 1 mg/mL of prothrombin for 20 minutes.



Figure 8.5. Tantalum disc coated with ~ 200 nm of tantalum then ~ 110 nm of aluminum and anodized at 4 V using the horizontal method after protein analysis. Each of the four circles was exposed to 20 µL of 1 mg/mL of prothrombin for 20 minutes.



Figure 8.6. Tantalum disc coated with ~ 200 nm of tantalum then ~ 110 nm of aluminum and anodized at 4 V using the horizontal method after protein analysis. Each of the four circles was exposed to 20 µL of 1 mg/mL of prothrombin for 20 minutes.

Observing Figures 8.1 – 8.6, there is no consistent pattern of protein binding (indicated by a colour shift) in the hydrophobic circles drawn on the surface. Figures 8.1, 8.2, 8.3, 8.4 and 8.5 show random patches of dark red or orange among the yellow surface that do not correspond to where the protein was placed, which was unexpected after the clear results obtained in Chapter 6. Figure 8.6 was the only disc to reveal acceptable results and one can see a darker yellow colour within the circles compared to the light yellow on the rest of the disc surface. Since the surface only appeared to be consistent for the disc in Figure 8.6, only this disc was exposed to anti-prothrombin solutions to determine the minimum concentration of anti-prothrombin detectable on the surface. Figure 8.7 shows the same disc as in Figure 8.6 after placing 20 µL of varying anti-prothrombin concentrations on top of the prothrombin layer for 20 minutes. In Figure 8.7, the farthest left circle was exposed to 0.5 mg/mL of anti-prothrombin, the middle-left circle was exposed to 0.05 mg/mL of anti-prothrombin, and the middle right circle was exposed

to 0.005 mg/mL of anti-prothrombin, all for 20 minutes. The farthest right circle was not exposed to any anti-prothrombin and was used as a control with prothrombin only. The disc was then washed with deionized water and dried with oil free compressed air prior to visualizing.



Figure 8.7. Tantalum disc coated with ~ 200 nm of tantalum then ~ 110 nm of aluminum and anodized at 4 V using the horizontal method after protein analysis. Each circle exposed to 20 µL of 1 mg/mL prothrombin for 20 minutes. Then one circle exposed to 0.5 mg/mL anti-prothrombin for 20 minutes (farthest left circle), one circle exposed to 0.05 mg/mL anti-prothrombin for 20 minutes (middle left circle), one circle exposed to 0.005 mg/mL anti-prothrombin for 20 minutes (middle right circle). The farthest right circle was not exposed to any anti-prothrombin and used as a control with prothrombin only.

Observing Figure 8.7, anti-prothrombin concentrations of 0.5 mg/mL and 0.05 mg/mL produced a visible colour shift on the surface compared to the prothrombin only control. For an anti-prothrombin concentration of 0.005 mg/mL, it is difficult to tell if a colour shift occurred on

the surface. The unexpected results of this experiment in five out of six cases led to an investigation of why the results were different compared to the results in Chapter 6, as substrates were prepared the same way in both cases. As discussed in Chapter 6, the results from the vertical anodization method were different than the horizontal anodization method, with the horizontal method producing stronger colour shifts on the surface. The reason for this was thought to be due to an increased optical path length for the discs anodized horizontally compared to vertically. SEM and ellipsometry was completed on the discs studied in Chapter 6 and the results suggested this to be the case, as the pore size was larger but the pore density was decreased for discs prepared horizontally, resulting in a greater refractive index (see Chapter 6 – Adsorption of Biologics onto Porous Anodic Alumina on Tantalum Discs). SEM and ellipsometry were also conducted on the discs shown in Figure 8.1 – 8.6 to compare the alumina surface and help determine the reason for the discrepancy in results.

SEM images were taken of the tantalum disc shown in Figure 8.3 to view the surface of a disc that produced poor colour shifts during protein work. The first section of the disc was difficult to image, and clear images were not obtained, likely due to the uneven surface. Another section of the disc was imaged and displayed results similar to a tantalum disc prepared using the horizontal method that produced strong colour shifts during protein work. As the porosity and surface morphology of a disc producing strong colour shifts and a disc producing poor colour shifts were quite similar, it is likely that the uneven and non-uniform nature of the surface after anodization was responsible for the discrepancy in protein results. Figures 8.8, 8.9, 8.10 and 8.11 show SEM images of the tantalum disc shown in Figure 8.3, prepared using the horizontal method that had poor colour shifts during protein work, at magnifications of 10,000 X, 30,000 X, 50,000 X and 70,000 X, respectively.

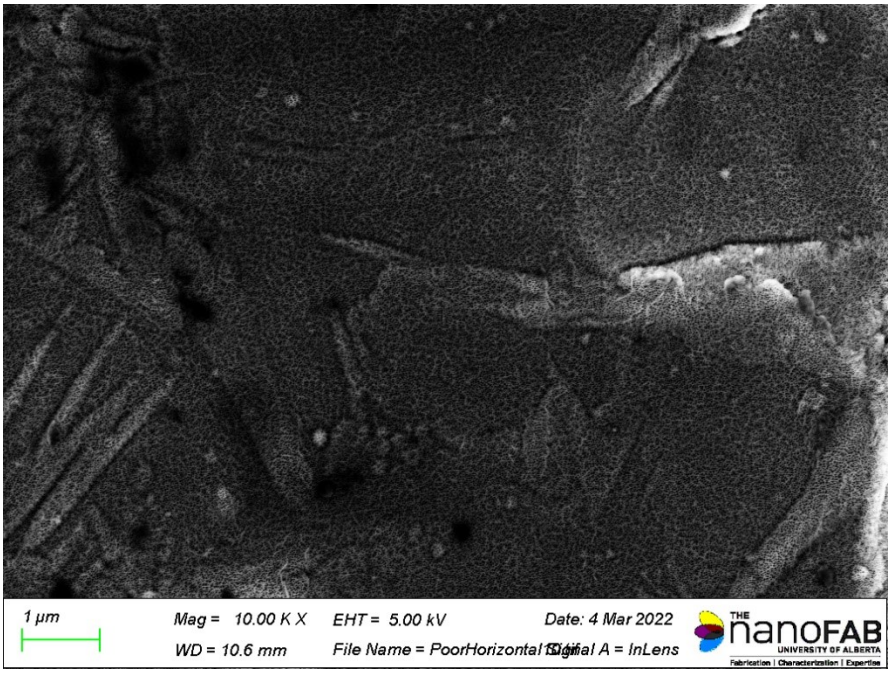


Figure 8.8. Topographical SEM image of tantalum disc shown in Figure 8.3 (horizontal method, poor colour shifts) at magnification of 10,000 X.

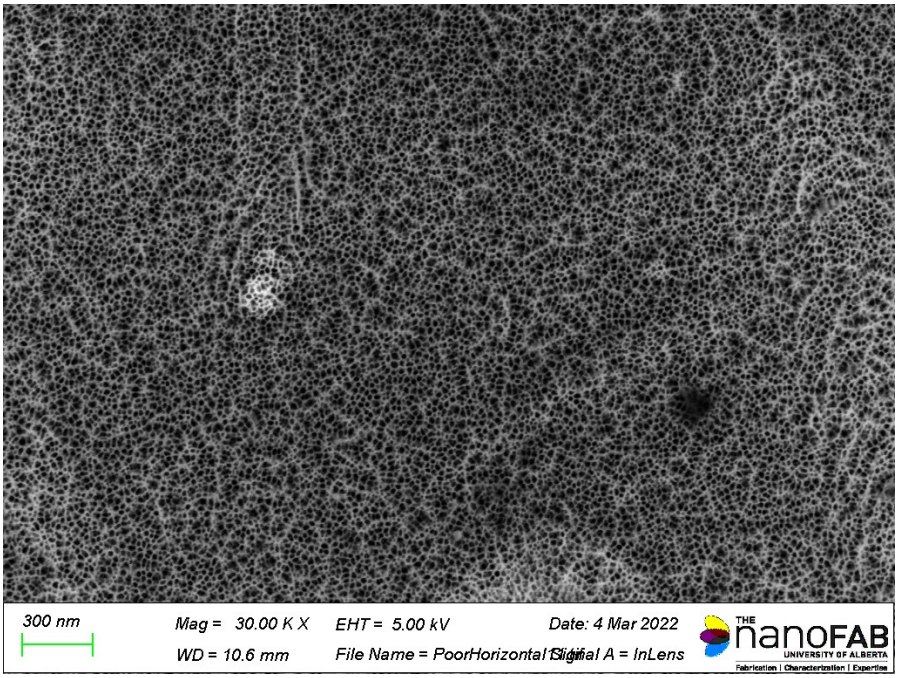


Figure 8.9. Topographical SEM image of tantalum disc shown in Figure 8.3 (horizontal method, poor colour shifts) at magnification of 30,000 X.

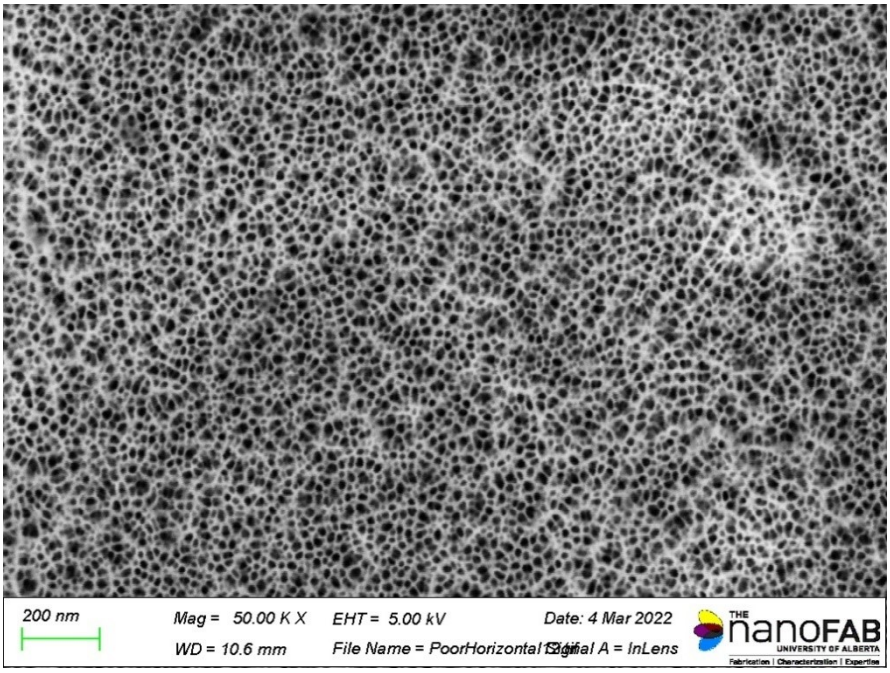


Figure 8.10. Topographical SEM image of tantalum disc shown in Figure 8.3 (horizontal method, poor colour shifts) at magnification of 50,000 X.

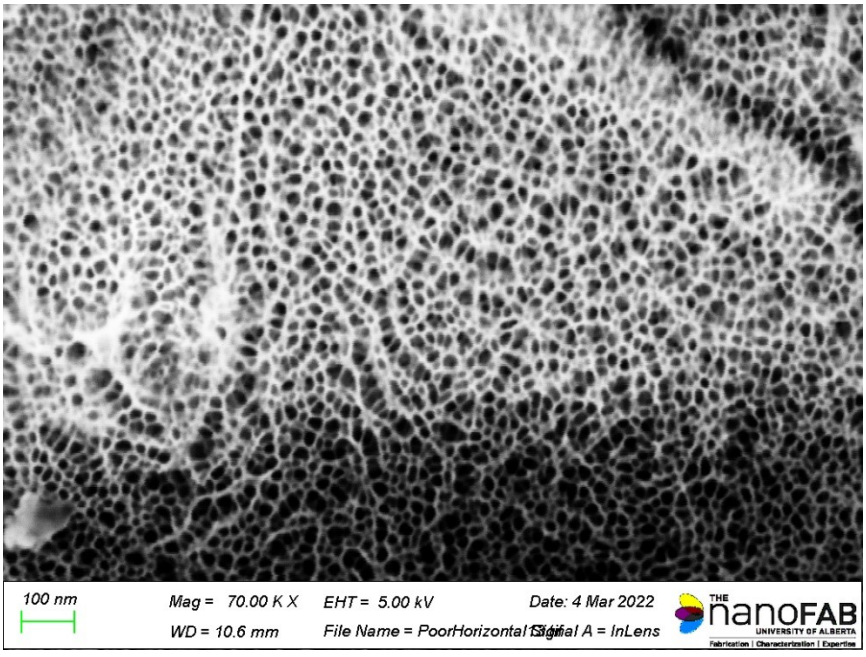


Figure 8.11. Topographical SEM image of tantalum disc shown in Figure 8.3 (horizontal method, poor colour shifts) at magnification of 70,000 X.

Ellipsometry was conducted on two of the discs above that yielded poor protein results. Tables 8.1 and 8.2 show the MSE, Al_2O_3 layer thickness, and EMA% values obtained from ellipsometry for the tantalum discs shown in Figures 8.3 and 8.5, respectively.

Table 8.1. MSE, Al_2O_3 layer thickness, and EMA% from ellipsometry of tantalum disc anodized vertically at 4 V that showed poor colour shifts from protein work (shown in Figure 8.3).

MSE	33.041
Al_2O_3 layer thickness (nm)	84.73 ± 0.190
EMA%	55.9 ± 0.14

Table 8.2. MSE, Al_2O_3 layer thickness, and EMA% from ellipsometry of tantalum disc anodized vertically at 4 V that showed poor colour shifts from protein work (shown in Figure 8.5).

MSE	54.917
Al_2O_3 layer thickness (nm)	58.81 ± 1.209
EMA%	77.9 ± 0.45

The discs were sputtered with aluminum at the same time under the same conditions and therefore it would be expected that the thickness of the Al_2O_3 layer would be the same for each disc. After horizontal anodization, the surface of the discs appeared very uneven and non-uniform, which may explain the poor protein results and the wide range of Al_2O_3 layer thickness. It is possible that the horizontal anodization method produced inconsistent results and surface uniformity due to poor conductivity during anodization.

Another possible reason for the discrepancy is that the discs prepared in Figures 8.1 – 8.6 were anodized on the tantalum edges in addition to the aluminum face, changing the pore size and alumina surface morphology. Another factor that could influence the anodization process is the room temperature at the time of anodization. Due to the horizontal anodization method set

up, stirring has not occurred during the anodization process. It is possible that the discs from Chapter 6 were anodized at a slightly warmer room temperature than those anodized in Chapter 8. An increase in room temperature would increase the movement of the acid bath molecules, increasing diffusion and allowing for better anodization results. If the temperature were different for the Chapter 8 discs, it is possible that the acid molecules were not moving as much, leading to different results.

Observing the anodization graphs for tantalum discs anodized previously using the horizontal method, another possible issue with anodization was conductivity. Several of the current as a function of time graphs showed sudden drops to zero amperes for brief time periods. It is possible that the contact between the compass and the tantalum disc was poor, leading to poor conductivity and an incomplete electrical circuit during anodization. To determine if conductivity issues were the reason for inconsistent protein results after anodization, a conductive epoxy was used to attach a metal stub to the back side of the discs for secure attachment of the anode alligator clip. Figure 8.12 shows a side view and a top view of the conductive epoxy attachment on the back of a tantalum disc. Figure 8.13 shows the anodization set up using this attachment. The anodization was set up the same as previously for horizontal anodization, however, the anode alligator clip was attached directly to the conductive epoxy metal attachment on the tantalum discs rather than to the metal compass that was in contact with the disc surface.



Figure 8.12. Top view (left) and side view (right) of conductive epoxy attachment to tantalum disc for direct attachment to alligator clip during anodization.

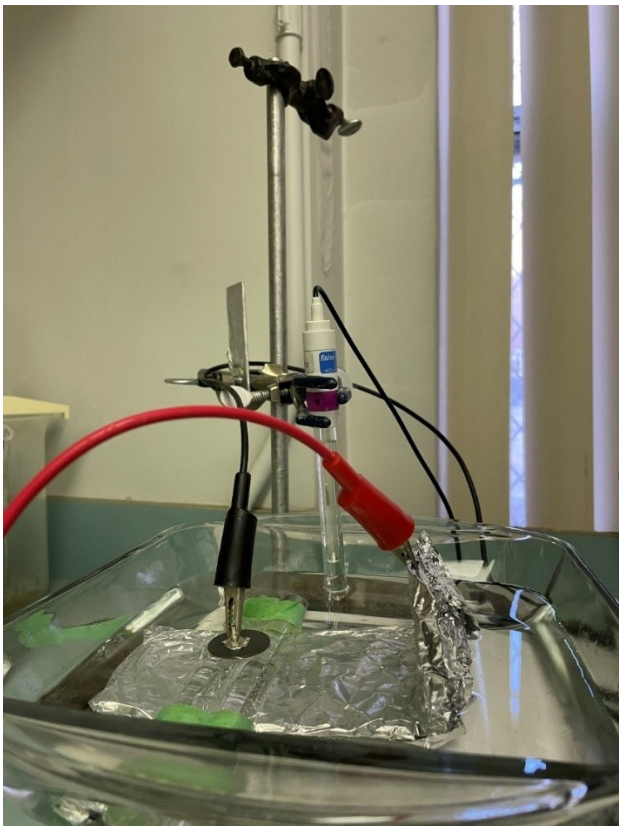


Figure 8.13. Horizontal anodization set up with conductive epoxy attachment to tantalum disc for direct attachment to alligator clip during anodization.

During anodization with the conductive epoxy attachment, no random drops to zero amperes were observed, suggesting that this was able to fix the conductivity issue. The anodization graphs for tantalum disc A, tantalum disc B, and tantalum disc C anodized horizontally with the conductive epoxy attachment are shown in Figures 8.14, 8.15 and 8.16, respectively. After anodization, the surfaces of the disc appeared uniform.

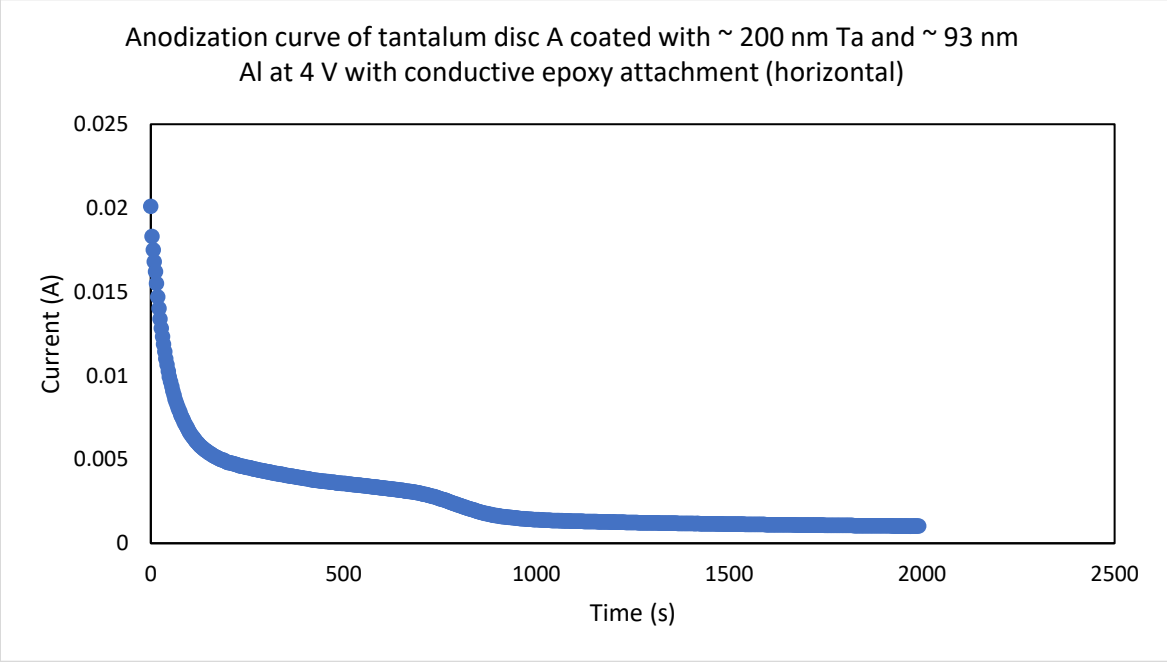


Figure 8.14. Current vs time anodization plot for oven cleaned tantalum disc A coated with ~ 200 nm tantalum and ~ 93 nm aluminum at 4 V, using the horizontal method with the conductive epoxy attachment.

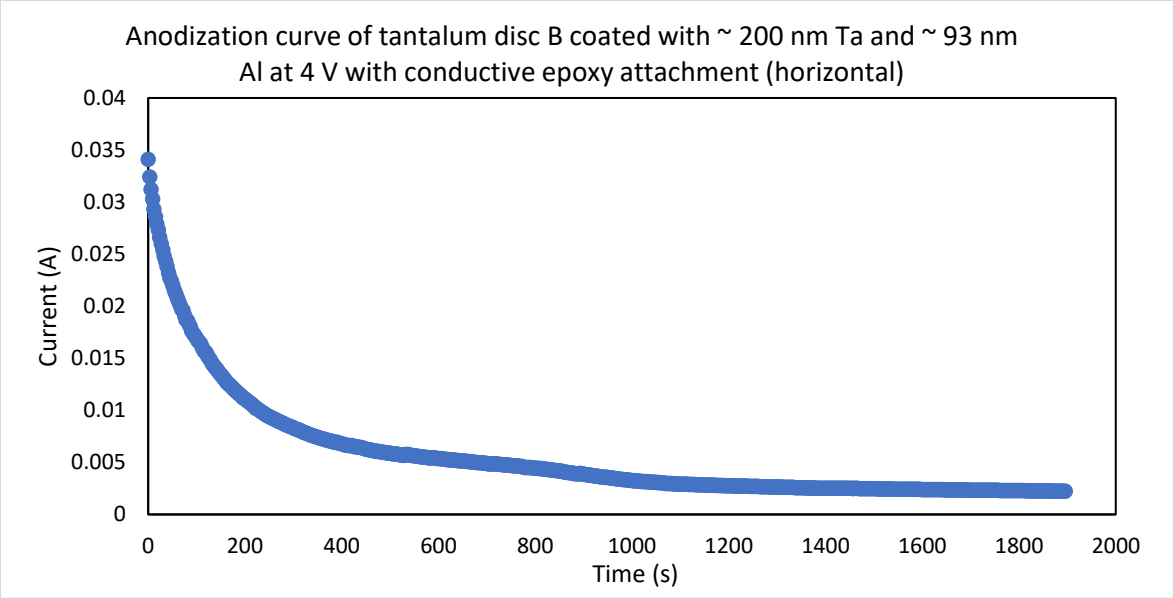


Figure 8.15. Current vs time anodization plot for oven cleaned tantalum disc B coated with ~ 200 nm tantalum and ~ 93 nm aluminum at 4 V, using the horizontal method with the conductive epoxy attachment.

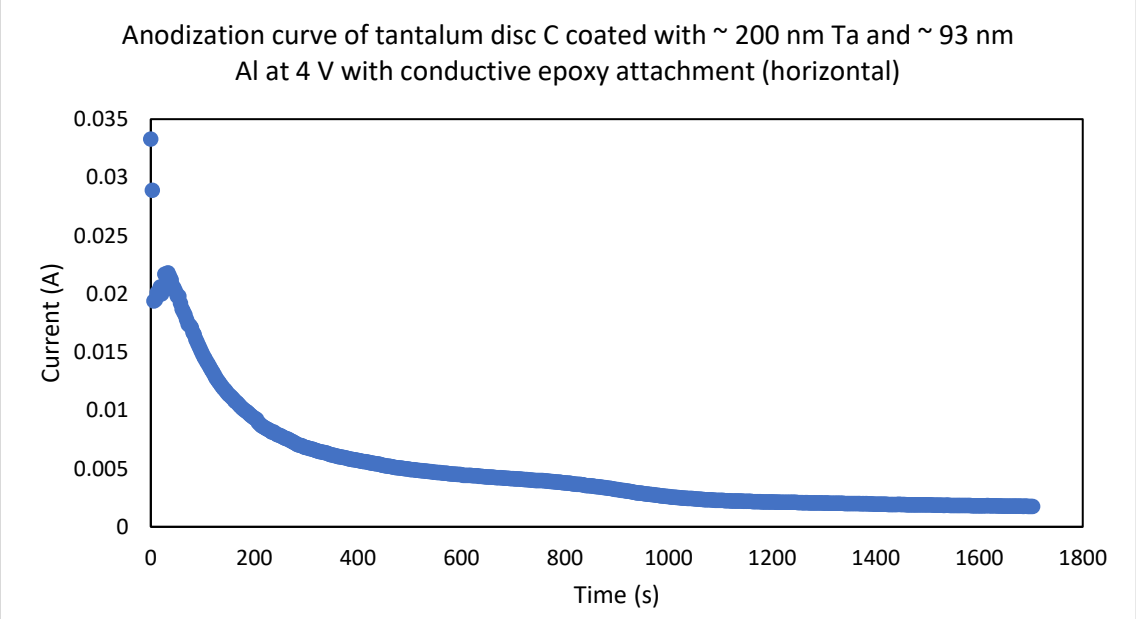


Figure 8.16. Current vs time anodization plot for oven cleaned tantalum disc C coated with ~ 200 nm tantalum and ~ 93 nm aluminum at 4 V, using the horizontal method with the conductive epoxy attachment.

The same protein dilution series experiment on stationary tantalum discs coated with ~ 200 nm of tantalum and ~ 93 nm of aluminum after anodizing horizontally at 4 V, using the conductive epoxy attachment were conducted to determine if the poor protein results were resolved by fixing the conductivity issue. Three tantalum discs (A, B, C) were studied to determine the minimum amount of anti-prothrombin visibly detectable on a stationary surface. In each case, four 0.7 cm hydrophobic circles were drawn with Sharpie and all circles were exposed to 20 μL of 1 mg/mL of prothrombin for 20 minutes, then rinsed with deionized water and dried with oil free compressed air. On each disc, the middle-left circle was exposed to 20 μL of 0.5 mg/mL of anti-prothrombin, the middle-right circle was exposed to 20 μL of 0.05 mg/mL of anti-prothrombin, and the farthest right circle was exposed to 20 μL of 0.005 mg/mL of anti-prothrombin, all for 20 minutes. The farthest left circle was not exposed to any anti-prothrombin and was used as a control with prothrombin only. The discs were then washed with deionized water and dried with oil free compressed air prior to visualizing. Figures 8.17, 8.18 and 8.19 show the results of the protein experiments for tantalum disc A, tantalum disc B, and tantalum disc C, respectively.

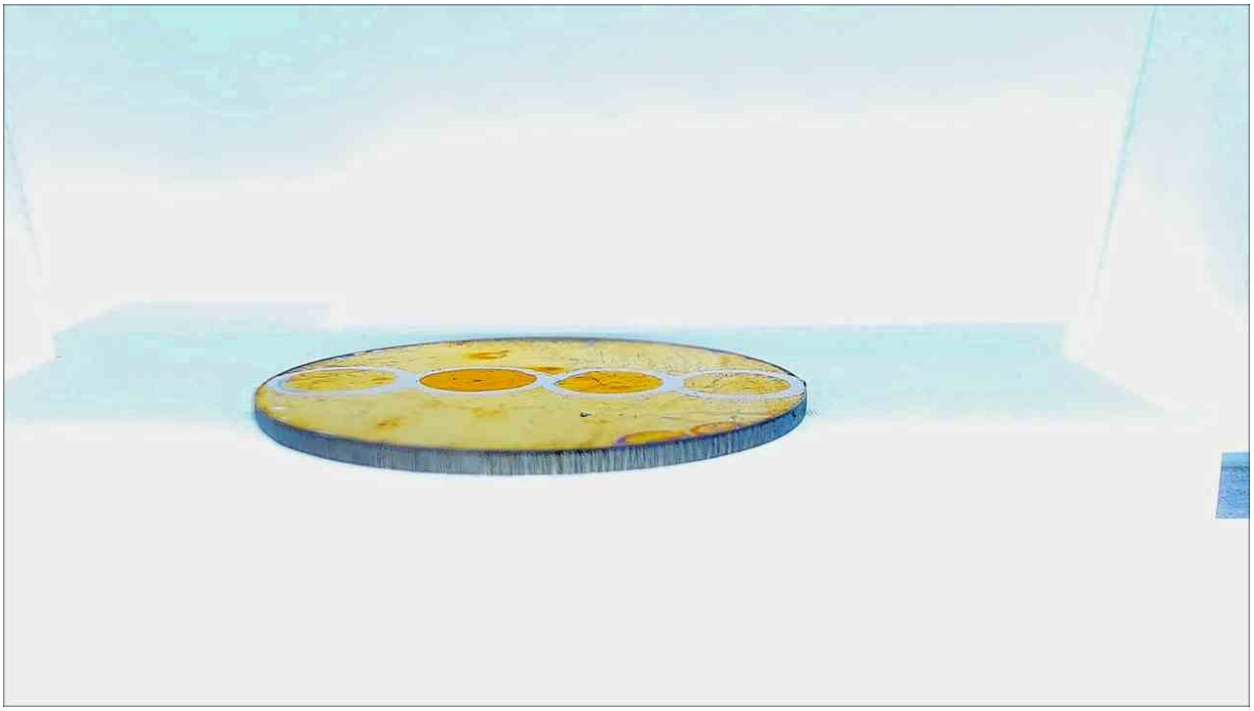


Figure 8.17. Tantalum disc A coated with ~ 200 nm of tantalum then ~ 93 nm of aluminum and anodized at 4 V using the horizontal method with the conductive epoxy attachment after protein analysis. Each circle exposed to 20 µL of 1 mg/mL prothrombin for 20 minutes. Then one circle exposed to 20 µL of 0.5 mg/mL anti-prothrombin for 20 minutes (middle left circle), one circle exposed to 20 µL of 0.05 mg/mL anti-prothrombin for 20 minutes (middle right circle), one circle exposed to 20 µL of 0.005 mg/mL anti-prothrombin for 20 minutes (farthest right circle). The farthest left circle was not exposed to any anti-prothrombin and used as a control with prothrombin only.



Figure 8.18. Tantalum disc B coated with ~ 200 nm of tantalum then ~ 93 nm of aluminum and anodized at 4 V using the horizontal method with the conductive epoxy attachment after protein analysis. Each circle exposed to 20 µL of 1 mg/mL prothrombin for 20 minutes. Then one circle exposed to 20 µL of 0.5 mg/mL anti-prothrombin for 20 minutes (middle left circle), one circle exposed to 20 µL of 0.05 mg/mL anti-prothrombin for 20 minutes (middle right circle), one circle exposed to 20 µL of 0.005 mg/mL anti-prothrombin for 20 minutes (farthest right circle). The farthest left circle was not exposed to any anti-prothrombin and used as a control with prothrombin only.



Figure 8.19. Tantalum disc C coated with ~ 200 nm of tantalum then ~ 93 nm of aluminum and anodized at 4 V using the horizontal method with the conductive epoxy attachment after protein analysis. Each circle exposed to 20 µL of 1 mg/mL prothrombin for 20 minutes. Then one circle exposed to 20 µL of 0.5 mg/mL anti-prothrombin for 20 minutes (middle left circle), one circle exposed to 20 µL of 0.05 mg/mL anti-prothrombin for 20 minutes (middle right circle), one circle exposed to 20 µL of 0.005 mg/mL anti-prothrombin for 20 minutes (farthest right circle). The farthest left circle was not exposed to any anti-prothrombin and used as a control with prothrombin only.

Observing Figures 8.17 – 8.19, anti-prothrombin concentrations of 0.5 mg/mL and 0.05 mg/mL produced colour shifts on the surface compared to the prothrombin only coated surface. For an anti-prothrombin concentration of 0.005 mg/mL, no visible colour shift is detectable compared to the prothrombin only surface. As silicon wafers have previously been shown to produce strong and consistent colour shifts in similar experiments, analysis was also completed

on silicon wafers coated with tantalum and aluminum, then anodized at 4 V ([5], [9]). The minimum amount of anti-prothrombin visibly detectable on a stationary silicon wafer was determined, using a similar protein dilution series experiment to the one detailed above. Silicon wafers were coated with ~ 200 nm of tantalum then ~ 93 nm of aluminum and anodized at 4 V prior to protein work. A silicon wafer was cut into ~ 1.3 cm × ~ 6.2 cm slides using a stencil and a diamond scribe, and seven 0.7 cm hydrophobic Sharpie circles were drawn on each slide. Six of the circles were exposed to 1 mg/mL of prothrombin for 20 minutes, then rinsed with deionized water and dried with oil free compressed air. One circle was left as a blank (1). On each slide, each circle was subsequently exposed to a 20 μL volume of anti-prothrombin at different concentrations. From left to right, the concentrations of protein placed on the surface for 20 minutes were as follows: blank/no protein (1), 1 mg/mL prothrombin only (2), 1 mg/mL prothrombin + 0.5 mg/mL anti-prothrombin (3), 1 mg/mL prothrombin + 0.05 mg/mL anti-prothrombin (4), 1 mg/mL prothrombin + 0.005 mg/mL anti-prothrombin (5), 1 mg/mL prothrombin + 5×10^{-4} mg/mL anti-prothrombin (6), 1 mg/mL prothrombin + 5×10^{-5} mg/mL anti-prothrombin (7). The wafers were then washed with deionized water and dried with oil free compressed air prior to visualizing. Figures 8.20, 8.21 and 8.22 show the results of the protein experiments for three silicon wafer slides.

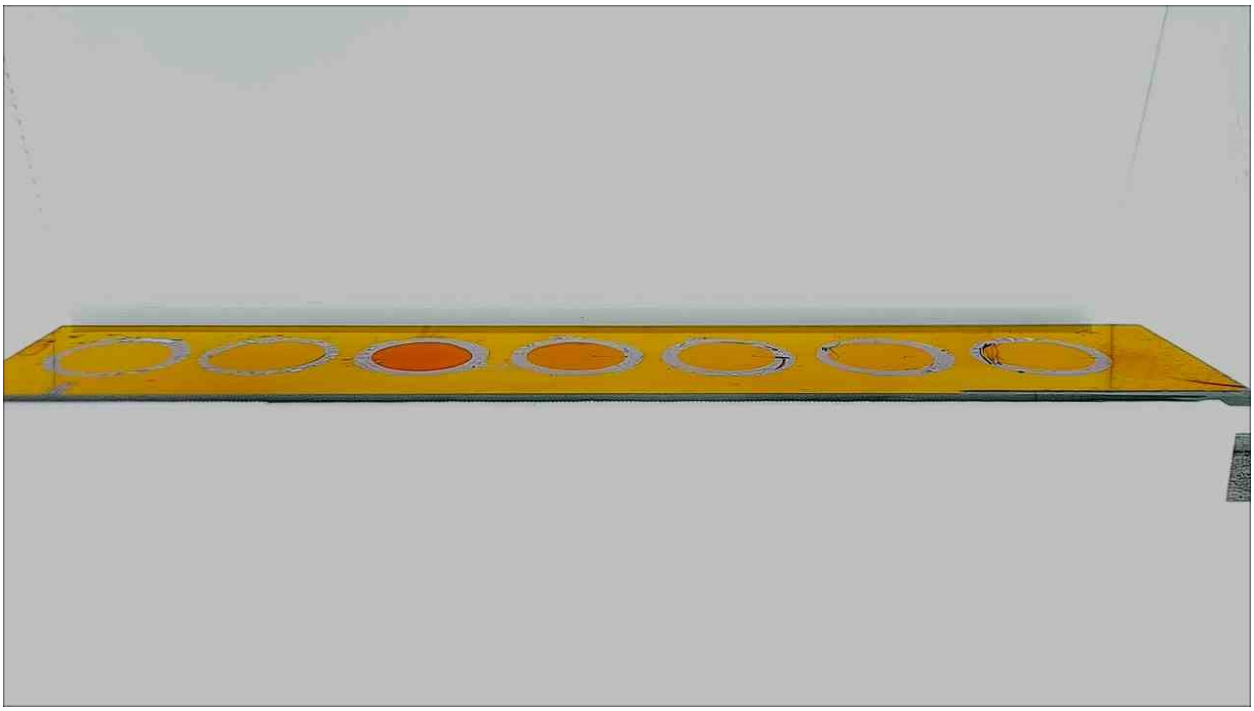


Figure 8.20. Silicon wafer coated with ~ 200 nm of tantalum then ~ 93 nm of aluminum and anodized at 4 V after protein analysis. The farthest left circle (1) was exposed to no protein (blank). The other six circles (2 – 7) exposed to 20 μL of 1 mg/mL prothrombin for 20 minutes. Circle 2 exposed to prothrombin only. Then circles 3 – 7 exposed to 20 μL of varying anti-prothrombin concentrations for 20 minutes: 0.5 mg/mL anti-prothrombin (3), 0.05 mg/mL anti-prothrombin (4), 0.005 mg/mL anti-prothrombin (5), 5×10^{-4} mg/mL anti-prothrombin (6), 5×10^{-5} mg/mL anti-prothrombin (7).

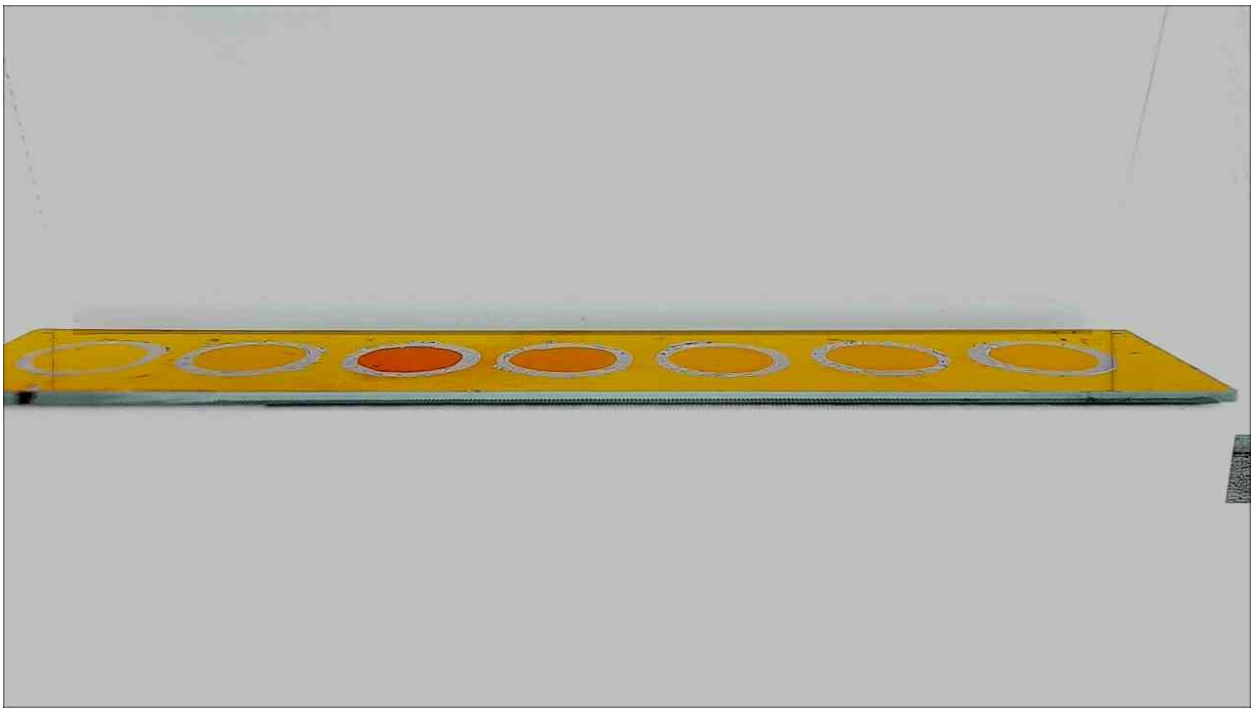


Figure 8.21. Silicon wafer coated with ~ 200 nm of tantalum then ~ 93 nm of aluminum and anodized at 4 V after protein analysis. The farthest left circle (1) was exposed to no protein (blank). The other six circles (2 – 7) exposed to 20 μL of 1 mg/mL prothrombin for 20 minutes. Circle 2 exposed to prothrombin only. Then circles 3 – 7 exposed to 20 μL of varying anti-prothrombin concentrations for 20 minutes: 0.5 mg/mL anti-prothrombin (3), 0.05 mg/mL anti-prothrombin (4), 0.005 mg/mL anti-prothrombin (5), 5×10^{-4} mg/mL anti-prothrombin (6), 5×10^{-5} mg/mL anti-prothrombin (7).

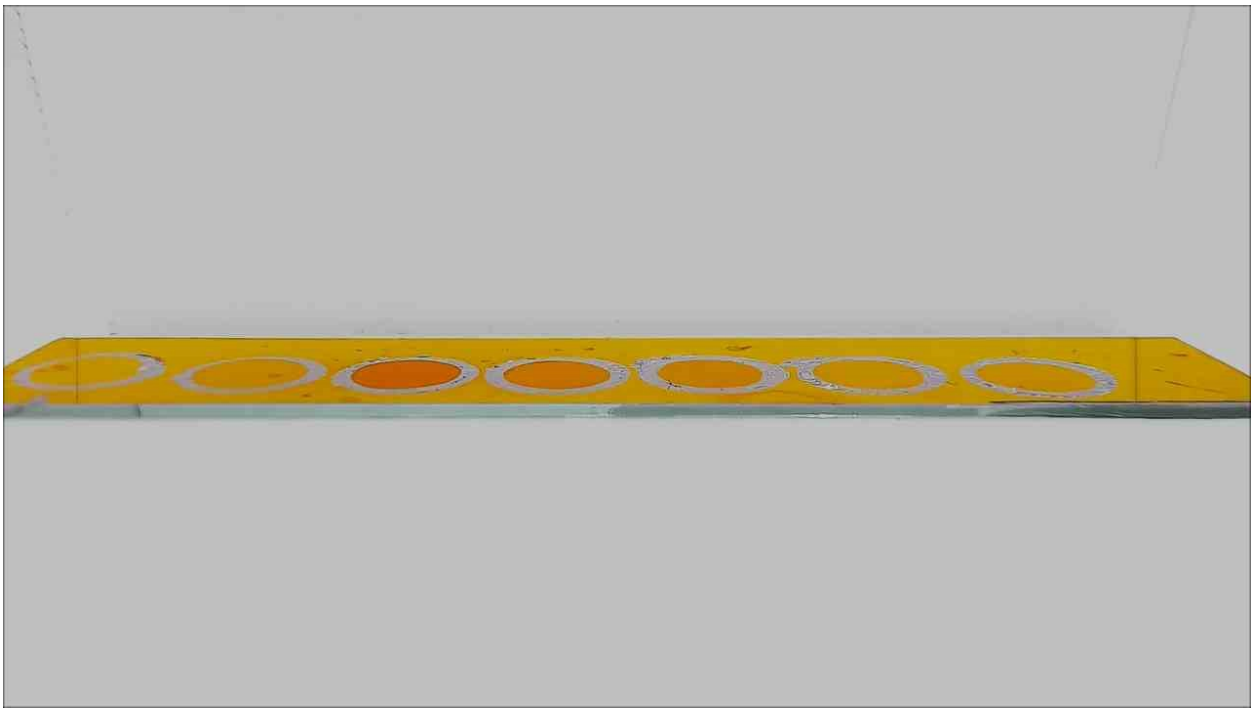


Figure 8.22. Silicon wafer coated with ~ 200 nm of tantalum then ~ 93 nm of aluminum and anodized at 4 V after protein analysis. The farthest left circle (1) was exposed to no protein (blank). The other six circles (2 – 7) exposed to 20 μL of 1 mg/mL prothrombin for 20 minutes. Circle 2 exposed to prothrombin only. Then circles 3 – 7 exposed to 20 μL of varying anti-prothrombin concentrations for 20 minutes: 0.5 mg/mL anti-prothrombin (3), 0.05 mg/mL anti-prothrombin (4), 0.005 mg/mL anti-prothrombin (5), 5×10^{-4} mg/mL anti-prothrombin (6), 5×10^{-5} mg/mL anti-prothrombin (7).

For each silicon wafer slide, anti-prothrombin concentrations of 0.5 mg/mL and 0.05 mg/mL resulted in visibly detectable colour shifts compared to the prothrombin only control circle. Anti-prothrombin concentration of 0.005 mg/mL, 5×10^{-4} mg/mL, and 5×10^{-5} mg/mL did not yield a visible colour shift on the surface compared to the prothrombin only control. Ellipsometry was conducted on the silicon wafer shown in Figures 8.20 – 8.22 to determine the thickness and the EMA % of the aluminum oxide layer on the silicon wafers that yielded strong

colour shifts shown above. Table 8.3 shows the MSE, Al_2O_3 layer thickness, and EMA% values obtained from ellipsometry for the silicon wafer coated with thin films of tantalum and aluminum, and anodized at 4 V.

Table 8.3. MSE, Al_2O_3 layer thickness, and EMA % from ellipsometry of silicon wafer coated with tantalum and aluminum, then anodized at 4 V that showed strong colour shifts from protein work.

MSE	20.339
Al_2O_3 layer thickness (nm)	93.05 ± 0.125 nm
EMA%	59.9 ± 0.08

The strong colour shifts and consistent surface morphology shown on the tantalum discs due to protein binding suggest that the conductive epoxy attachment to the tantalum discs fixed the conductivity issue during anodization, and as a result, produced consistent results after exposure to protein. The next experiment conducted involved using larger volumes of fluid to improve the sensitivity of the device. Four tantalum discs were prepared the same way as the discs shown in Figures 8.17 – 8.19 for the larger volume experiments. The discs were cleaned in a self-cleaning oven cycle, then sputtered with ~ 200 nm of tantalum then ~ 93 nm of aluminum. After sputtering, the conductive epoxy attachment was attached to the back of the discs, and the discs were anodized using the horizontal anodization method shown in Figure 8.13 at 4 V. The anodization curves of these four discs are shown in Figures A4.17 (tantalum disc D), A4.18 (tantalum disc E), A4.19 (tantalum disc F) and A4.20 (tantalum disc G) in Appendix 4. For the larger volume experiments, four Sharpie circles with diameters of 0.7 cm were drawn on each of the tantalum discs. Images were taken prior to prothrombin exposure for comparison to a blank control. In each of the four circles on tantalum disc D, E, and F, 20 µL of 1 mg/mL of

prothrombin was pipetted onto the surface and left in a Petri dish with a wet paper towel for 20 minutes. After 20 minutes, the prothrombin was pipetted off the surface and the discs were rinsed with deionized water and dried with oil free compressed air. Tantalum disc D was used as a control with only prothrombin exposure in each of the four circles. Tantalum disc F was used to test the sensitivity of anti-prothrombin in a larger volume. The conductive epoxy attachments were removed from the back of the tantalum disc using scissors prior to the large volume experiments.

Figure 8.23 shows the set up used for the larger volume experiments. The set-up consists of a 1 L beaker and an impeller attached to a motor. The impeller was clamped and lowered into the beaker, so the impeller blades were placed just beneath the surface of the fluid. The speed of the impeller was controlled by a Tech II Railmaster 2400 that was set to a power of ~ 13 – 14 (~ 195 RPM) for the experiments, as this setting produced stirring of the mixture while avoiding the formation of a large vortex at the air-liquid interface. The tantalum discs and silicon wafer substrates were placed in the bottom of the glass and the impeller was positioned above the disc to encourage mixing of the fluid above the surface of the disc. Using a fluid volume of 500 mL has the potential to be 25,000 times more sensitive than using a volume of 20 μL. As the limit of detection on a stationary tantalum disc surface likely fell between 0.05 mg/mL and 0.005 mg/mL of anti-prothrombin for a 20 μL drop placed on the surface for 20 minutes, a concentration of 0.005 mg/mL of anti-prothrombin was used as the starting point for the 500 mL volume experiments. As the volume used is significantly larger, the sensitivity would be expected to improve.

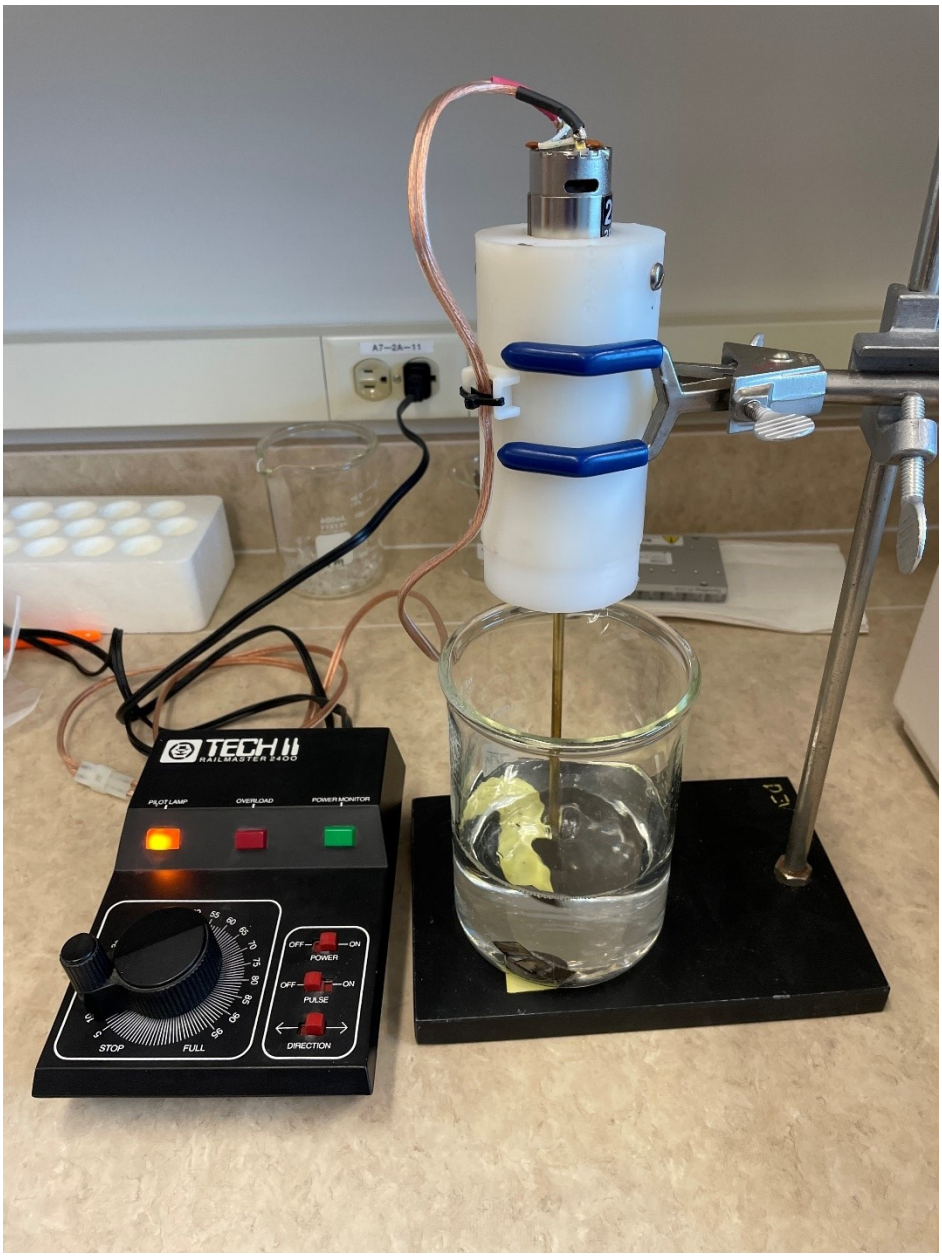


Figure 8.23. Experimental set up for 500 mL volume anti-prothrombin sensitivity experiments. Set up consists of a 1 L beaker and a motorized impeller attached to a Tech II Railmaster 2400. Tantalum disc or silicon wafer that was previously exposed to 1 mg/mL of prothrombin is placed in the bottom of the beaker.

Tantalum disc F was placed in the bottom of the beaker and 500 mL of a 0.005 mg/mL solution of anti-prothrombin was placed in the beaker. The solution was prepared by placing 250 µL of a 10 mg/mL anti-prothrombin stock solution into 499.75 mL of water. The Tech II Railmaster 2400 was turned on and set to an impeller power of ~ 13 – 14 (~195 RPM). The solution was stirred for 20 minutes while the tantalum disc remained in the bottom of the bottle. After 20 minutes, the impeller was stopped, and the tantalum disc (F) was removed from the solution. The disc was rinsed with deionized water and dried with oil free compressed air. Figure 8.24 shows the tantalum disc that was exposed to a 500 mL solution of 0.005 mg/mL anti-prothrombin after 20 minutes of stirring at ~ 195 RPM (tantalum disc F, right), next to a tantalum disc that was only exposed to 20 µL of 1 mg/mL prothrombin in each of the circles for 20 minutes (tantalum disc D, left).



Figure 8.24. Tantalum disc (D) exposed to 20 µL of 1 mg/mL prothrombin in each of the four circles (left) compared to tantalum disc (F) that was exposed to 20 µL of 1 mg/mL prothrombin in each of the four circles then subsequently exposed to a 500 mL solution of 0.005 mg/mL anti-prothrombin with continuous stirring at ~ 195 RPM for 20 minutes (right).

Observing Figure 8.24, it is difficult to tell whether a colour shift occurred due to anti-prothrombin binding after 20 minutes. Although the prothrombin only disc (D) appeared slightly lighter in colour compared to the prothrombin + 0.005 mg/mL anti-prothrombin disc (F), it is possible that anti-prothrombin bound to the entire surface of tantalum disc F after exposure to the 500 mL volume for 20 minutes. To discern whether anti-prothrombin binding occurred on the alumina layer, three 0.8 cm circles were drawn on tantalum disc G. The left circle was left as a blank, the middle circle was exposed to 1 mg/mL of prothrombin for 20 minutes, and the right circle was exposed to 0.25 mg/mL of anti-prothrombin for 20 minutes with no prior exposure to prothrombin, and the results are shown in Figure 8.25.



Figure 8.25. Tantalum disc G after protein work. Left circle exposed to no protein and used as a blank control, middle circle exposed to 20 µL of 1 mg/mL prothrombin for 20 minutes, right circle exposed to 20 µL of 0.25 mg/mL anti-prothrombin for 20 minutes (no previous prothrombin exposure in right circle).

In the meantime, tantalum disc F was placed back in the bottle and exposed to the 500 mL solution of 0.005 mg/mL prothrombin for an additional 20 minutes (total exposure time: 40 minutes) to determine whether a longer time period produced better results. Figure 8.26 shows the prothrombin only disc (D) next to tantalum disc F that was exposed to a 500 mL solution of 0.005 mg/mL anti-prothrombin for 40 minutes.

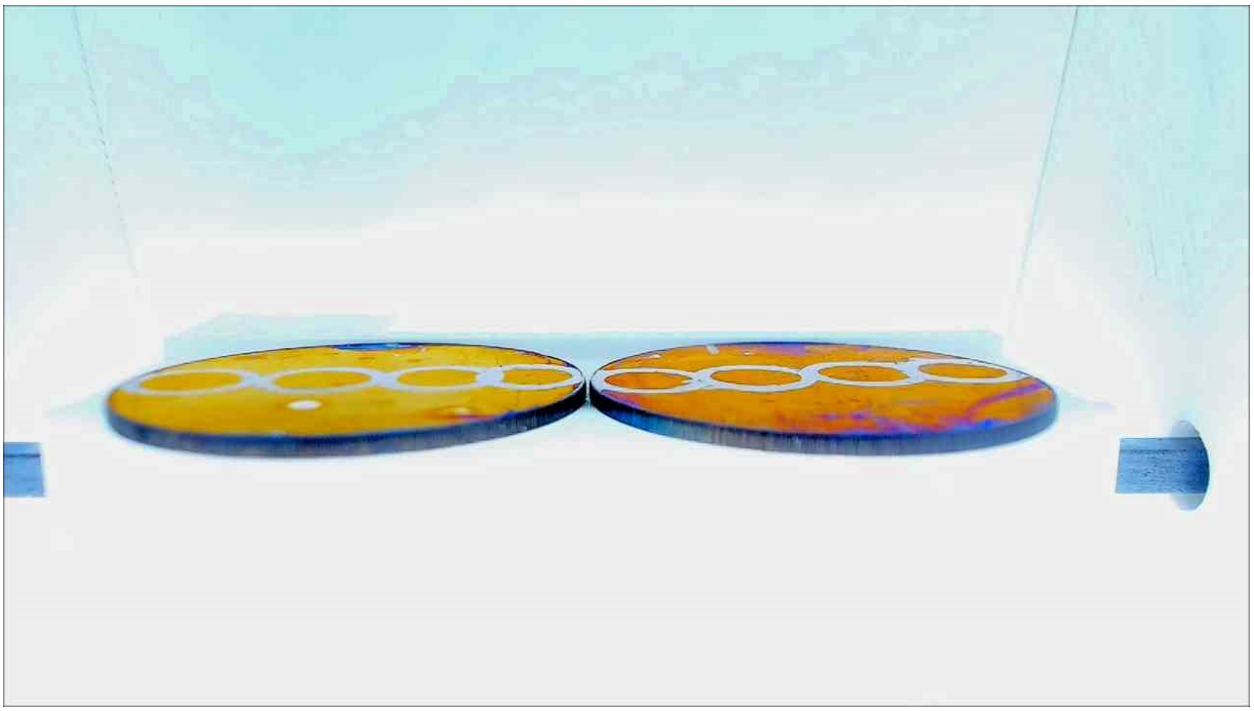


Figure 8.26. Tantalum disc (D) exposed to 20 µL of 1 mg/mL prothrombin in each of the four circles (left) compared to tantalum disc (F) that was exposed to 20 µL of 1 mg/mL prothrombin in each of the four circles then subsequently exposed to a 500 mL solution of 0.005 mg/mL anti-prothrombin with continuous stirring at ~ 195 RPM for 40 minutes (right).

Comparing Figures 8.24 and 8.26, it looks as if the entire tantalum disc (F) that was exposed to 0.005 mg/mL anti-prothrombin is a darker orange colour than tantalum disc D that was exposed to prothrombin only. It also appears that the entire disc is a darker orange after 40 minutes compared to after 20 minutes. It is possible that the entire disc bound anti-prothrombin

to the alumina layer, not only the areas that had been previously exposed to prothrombin in the four hydrophobic circles. Observing Figure 8.25 also suggests that it is possible that anti-prothrombin binds directly to the alumina layer, even in the absence of prothrombin.

Figure 8.25 also suggests that the alumina layer is too thin at 93 nm to see a strong colour shift between the blank circle and the prothrombin only circle. The same disc that is shown in Figure 8.25 was exposed to additional protein to assess the strength of colour shifts. The middle circle, that was previously exposed to only 20 µL of 1 mg/mL prothrombin for 20 minutes, was exposed to 20 µL of 0.25 mg/mL of anti-prothrombin for 20 minutes and is shown in Figure 8.27. Afterwards, the middle and right circles were both exposed to 20 µL of 1 mg/mL Rabbit Anti-Sheep IgG (H+L)-HRP Conjugate (Bio-Rad) secondary anti-body for 20 minutes, and the results are shown in Figure 8.28.



Figure 8.27. Tantalum disc G after protein work. Left circle exposed to no protein and used as a blank control, middle circle exposed to 20 µL of 1 mg/mL prothrombin for 20 minutes then 20 µL of 0.5 mg/mL anti-prothrombin for 20 minutes, right circle exposed to 20 µL of 0.25 mg/mL anti-prothrombin for 20 minutes (no previous prothrombin exposure in right circle).



Figure 8.28. Tantalum disc G after protein work. Left circle exposed to no protein and used as a blank control, middle circle exposed to 20 µL of 1 mg/mL prothrombin for 20 minutes then 20 µL of 0.5 mg/mL anti-prothrombin for 20 minutes then 20 µL of 1 mg/mL secondary anti-body for 20 minutes, right circle exposed to 20 µL of 0.25 mg/mL anti-prothrombin for 20 minutes then 20 µL of 1 mg/mL secondary anti-body for 20 minutes (no previous prothrombin exposure in right circle).

For subsequent experiments, silicon wafers and tantalum discs were prepared with an alumina layer thickness of closer to 110 nm, as the thicker layer would produce stronger colour shifts due to the increased optical path length. A silicon wafer was prepared by sputtering ~ 200 nm of tantalum then ~ 106 nm of aluminum and was anodized at 4 V. Ellipsometry was conducted on the silicon wafer used in the following experiments to determine the thickness and the EMA % of the aluminum oxide layer on the silicon wafer. Table 8.4 shows the MSE, Al_2O_3 layer thickness, and EMA% values obtained from ellipsometry for the silicon wafer coated with thin films of tantalum and aluminum, and anodized at 4 V.

Table 8.4. MSE, Al_2O_3 layer thickness, and EMA % from ellipsometry of silicon wafer coated with 200 nm of tantalum and 106 nm of aluminum, then anodized at 4 V.

MSE	19.928
Al_2O_3 layer thickness (nm)	106.42 ± 0.115 nm
EMA%	55.4 ± 0.07

The wafer was cut into slides using the 3D printed stencil tool and an image was taken of the wafer before protein work for comparison purposes. The wafer prior to protein work is shown in Figure 8.29 and appears a yellow/tan colour. A Sharpie pen was used to draw a hydrophobic outline along the edges of the rectangular slide. The entire rectangular slide was then coated with prothrombin by pipetting 532 µL volume of 1 mg/mL prothrombin onto the surface and spreading it to the edges and was left in a Petri dish with a wet paper towel for 20 minutes. The wafer was then rinsed with deionized water and dried with oil free compressed air. An image was taken of the slide after coating with prothrombin to compare to the wafer with no protein and the wafer after exposure to anti-prothrombin. Figure 8.30 shows the wafer after the entire surface was exposed to prothrombin and appears orange. Next, a 0.7 cm hydrophobic circle was drawn on the wafer and a 20 µL solution of 0.5 mg/mL anti-prothrombin was pipetted into the circle and left in a Petri dish with a wet paper towel for 20 minutes. After 20 minutes, the anti-prothrombin solution was removed, and the wafer slide was rinsed with deionized water and dried with oil free compressed air. Figure 8.31 shows an image of the wafer that is completely coated in prothrombin, with the circle containing an additional anti-prothrombin layer. The circle that was exposed to anti-prothrombin appears bright pink, while the rest of the slide remains an orange colour. The anti-prothrombin circle was to be used as an internal control for the larger volume experiments, as a strong colour shift should occur in the circle due to the higher

concentration of anti-prothrombin used. The colour of the slide after the large volume experiments could be compared to the colour produced by the higher anti-prothrombin concentration seen in the hydrophobic circle. The wafer slide was then attached to an old tantalum disc using double sided Scotch 3M tape and placed in the bottom of the stirring apparatus. The wafer slide was taped to a tantalum disc in order for the wafer to stay in place at the bottom of the beaker for the duration of the experiment. The wafer slide alone would not be heavy enough to remain in place throughout the experiment, so attachment to the tantalum disc weighs the wafer down and ensure it remains in place when the impeller is turned on and for the duration of the stirring experiment. A 500 mL solution of 0.005 mg/mL anti-prothrombin was then placed into the beaker and the impeller was attached and lowered into the beaker. The Tech II Railmaster 2400 was turned on and set to an impeller power of ~ 13 – 14 (stirring at ~ 195 RPM), and the solution was stirred for 20 minutes while the wafer slide attached to the tantalum disc remained at the bottom. After 20 minutes, the impeller was stopped, and the substrate was removed from the solution. The wafer slide was removed from the tantalum disc and rinsed with deionized water and dried with oil free compressed air. Figure 8.32 shows an image of the wafer slide taken after exposure to 500 mL of 0.005 mg/mL anti-prothrombin with continuous stirring for 20 minutes in the large volume experiment. Figure 8.33 shows the images prior to protein work (top), after exposure to 532 μL of 1 mg/mL prothrombin for 20 minutes (middle), and after subsequent exposure to 500 mL of 0.005 mg/mL anti-prothrombin for 20 minutes with continuous stirring (bottom) cropped and lined up to better visualize the colour shifts.

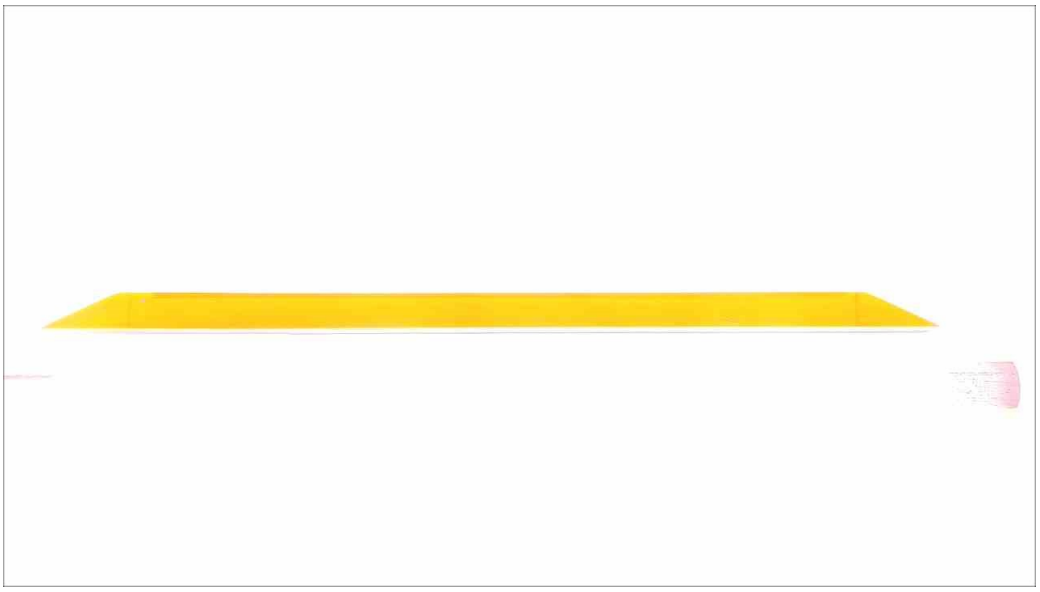


Figure 8.29. Silicon wafer slide (~ 1.3 cm by ~ 6.2 cm) coated with ~ 200 nm of tantalum and ~ 106 nm of aluminum then anodized at 4 V prior to protein work.



Figure 8.30. Silicon wafer slide (~ 1.3 cm by ~ 6.2 cm) coated with ~ 200 nm of tantalum and ~ 106 nm of aluminum then anodized at 4 V after the entire surface was coated with 532 µL of 1 mg/mL prothrombin for 20 minutes.



Figure 8.31. Silicon wafer slide (~ 1.3 cm by ~ 6.2 cm) coated with ~ 200 nm of tantalum and ~ 106 nm of aluminum then anodized at 4 V after the entire surface was coated with 532 µL of 1 mg/mL prothrombin for 20 minutes. The hydrophobic circle was subsequently exposed to 20 µL of 0.5 mg/mL anti-prothrombin for 20 minutes.

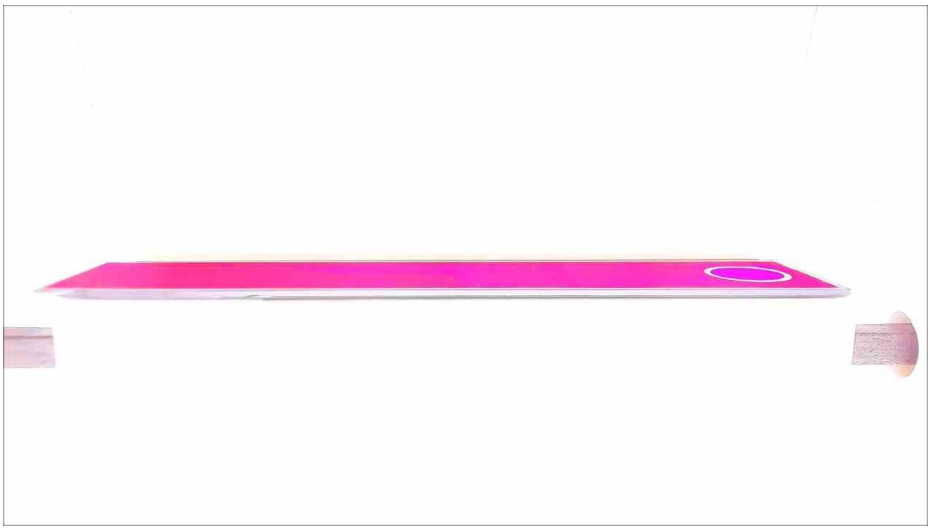


Figure 8.32. Silicon wafer slide (~ 1.3 cm by ~ 6.2 cm) coated with ~ 200 nm of tantalum and ~ 106 nm of aluminum then anodized at 4 V after the entire surface was coated with 532 µL of 1 mg/mL prothrombin for 20 minutes. The hydrophobic circle was subsequently exposed to 20 µL of 0.5 mg/mL anti-prothrombin for 20 minutes. The entire wafer was then exposed to 500 mL of 0.005 mg/mL anti-prothrombin with continuous stirring at ~ 195 RPM for 20 minutes.

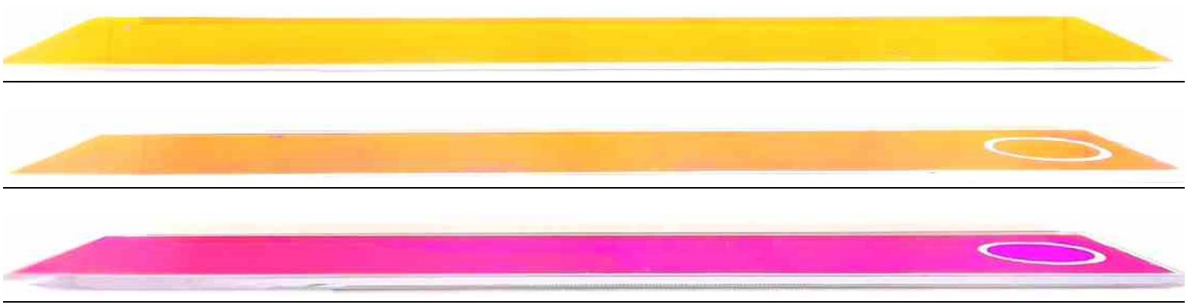


Figure 8.33. Images in Figure 8.29, 8.30, and 8.32 cropped and lined up to better visualize the colour shifts. Silicon wafer slides (~ 1.3 cm by ~ 6.2 cm) coated with ~ 200 nm of tantalum and ~ 106 nm of aluminum then anodized at 4 V with no exposure to protein (top), after exposure of entire slide to 532 µL of 1 mg/mL prothrombin for 20 minutes (middle), after subsequent exposure of entire slide to 500 mL of 0.005 mg/mL anti-prothrombin for 20 minutes with continuous stirring at ~ 195 RPM (bottom).

Observing Figure 8.33, the initial colour of the silicon wafer coated with 200 nm of tantalum and 106.42 ± 0.115 nm of aluminum after anodization was a yellowish colour. After exposure of the entire surface to 532 µL of 1 mg/mL prothrombin for 20 minutes and the formation of a prothrombin monolayer on the surface, the surface colour shifted to orange. The shift to bright pink after exposing the surface to 500 mL of 0.005 mg/mL of anti-prothrombin with continuous stirring for 20 minutes indicates the formation of the antigen-antibody complex on the surface. Statistical analysis was conducted by selecting three separate areas on the prothrombin only coated slide and the prothrombin + anti-prothrombin coated slide in Figure 8.33 to determine if there was a statistically significant difference in the x and y chromaticity coordinates for the prothrombin only coated surface compared to the prothrombin + anti-prothrombin coated surface. For each slide, three separate rectangular areas on the prothrombin

slide and three separate rectangular areas on the prothrombin + anti-prothrombin slide were selected and analyzed using ImageJ to determine the RGB coordinates (n = 3). The average RGB coordinates for each area were converted to Yxy colour coordinates using the ColorMine website (http://colormine.org/convert/rgb-to-yxy). The x and y coordinates were analyzed separately using independent T-tests. Table 8.5 shows the results of the statistical analysis on the effect of 500 mL of 0.005 mg/mL anti-prothrombin for 20 minutes on the surface colour of the prothrombin-coated wafer based on x and y chromaticity coordinates. The x and y coordinates after exposure to anti-prothrombin (AP) were compared to the prothrombin (II) control, and a p value less than 0.05 indicates statistical significance.

Table 8.5. Results of the independent T-test statistical analysis on the effect of 500 mL of 0.005 mg/mL of anti-prothrombin (AP) for 20 minutes with continuous stirring at ~ 195 RPM on the surface colour of the prothrombin-coated wafer based on x and y chromaticity coordinates compared to the prothrombin (II) only control, for the slides shown in Figure 8.33. Statistically significant results are in italics. (n = 3).

Prothrombin (II) control	**Vs. II + AP (mg/mL)**	**Difference detectable by eye vs. control?**	**x coordinate + p values**	**y coordinate + p values**
1 mg/mL II control x = 0.45 ± 0.01 y = 0.42 ± 0.01	0.005 mg/mL with continuous stirring at ~ 195 RPM for 20 minutes	Yes	x = 0.41 ± 0.02 *p < 0.05*	y = 0.22 ± 0.02 *p < 0.001*

Both the x and y chromaticity coordinates were statistically different between the prothrombin only coated surface and the prothrombin + 0.005 mg/mL anti-prothrombin coated

surface. Since the colour shifts were significantly stronger on the 106 nm aluminum film, the stationary dilution series was conducted in triplicate on a silicon wafer sputtered with ~ 200 nm of tantalum and ~ 106 nm of aluminum that was anodized at 4 V. The minimum amount of anti-prothrombin visibly detectable on a stationary silicon wafer with an alumina thickness of 106 nm was determined. The silicon wafer was cut into ~ 1.3 cm × 6.2 cm rectangular slides using the stencil and a diamond pen, and seven hydrophobic Sharpie circles were drawn on each rectangle. Six of the circles were exposed to 1 mg/mL of prothrombin for 20 minutes, then rinsed with deionized water and dried with oil free compressed air. One circle was left as a blank (1). On each slide, each circle was exposed to a 20 μL volume anti-prothrombin at a different concentration. From left to right, the concentrations of protein placed on the surface for 20 minutes were as follows: blank/no protein (1), 1 mg/mL prothrombin only (2), 1 mg/mL prothrombin + 0.5 mg/mL anti-prothrombin (3), 1 mg/mL prothrombin + 0.05 mg/mL anti-prothrombin (4), 1 mg/mL prothrombin + 0.005 mg/mL anti-prothrombin (5), 1 mg/mL prothrombin + 5×10^{-4} mg/mL anti-prothrombin (6), 1 mg/mL prothrombin + 5×10^{-5} mg/mL anti-prothrombin (7). The wafers were then rinsed with deionized water and dried with oil free compressed air prior to visualizing and imaging. Figures 8.34, 8.35 and 8.36 show the results of the protein experiments for three silicon wafer rectangle replicates.

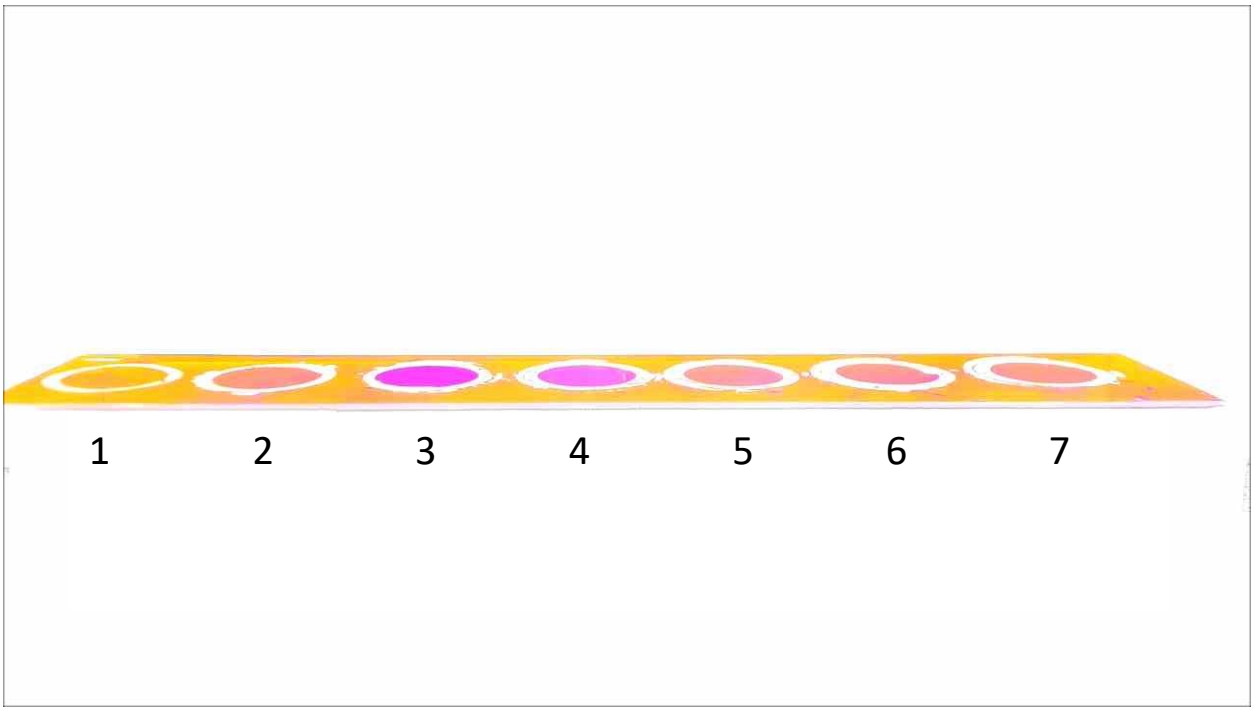


Figure 8.34. Silicon wafer (replicate 1) coated with ~ 200 nm of tantalum then ~ 106 nm of aluminum and anodized at 4 V after protein analysis. The farthest left circle (1) was exposed to no protein (blank). The other six circles (2 – 7) exposed to 20 µL of 1 mg/mL prothrombin for 20 minutes. Circle 2 exposed to prothrombin only. Then circles 3 – 7 exposed to 20 µL of varying anti-prothrombin concentrations for 20 minutes: 0.5 mg/mL anti-prothrombin (3), 0.05 mg/mL anti-prothrombin (4), 0.005 mg/mL anti-prothrombin (5), 5×10^{-4} mg/mL anti-prothrombin (6), 5×10^{-5} mg/mL anti-prothrombin (7).

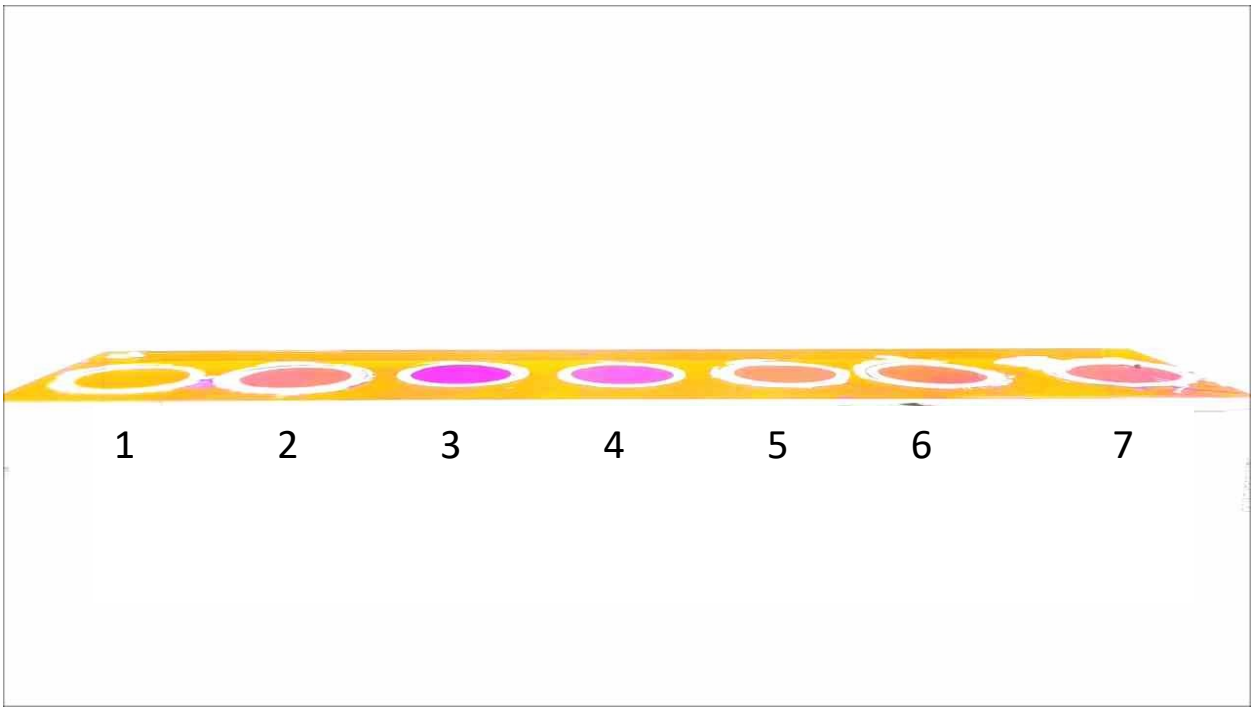


Figure 8.35. Silicon wafer (replicate 2) coated with ~ 200 nm of tantalum then ~ 106 nm of aluminum and anodized at 4 V after protein analysis. The farthest left circle (1) was exposed to no protein (blank). The other six circles (2 – 7) exposed to 20 µL of 1 mg/mL prothrombin for 20 minutes. Circle 2 exposed to prothrombin only. Then circles 3 – 7 exposed to 20 µL of varying anti-prothrombin concentrations for 20 minutes: 0.5 mg/mL anti-prothrombin (3), 0.05 mg/mL anti-prothrombin (4), 0.005 mg/mL anti-prothrombin (5), 5×10^{-4} mg/mL anti-prothrombin (6), 5×10^{-5} mg/mL anti-prothrombin (7).

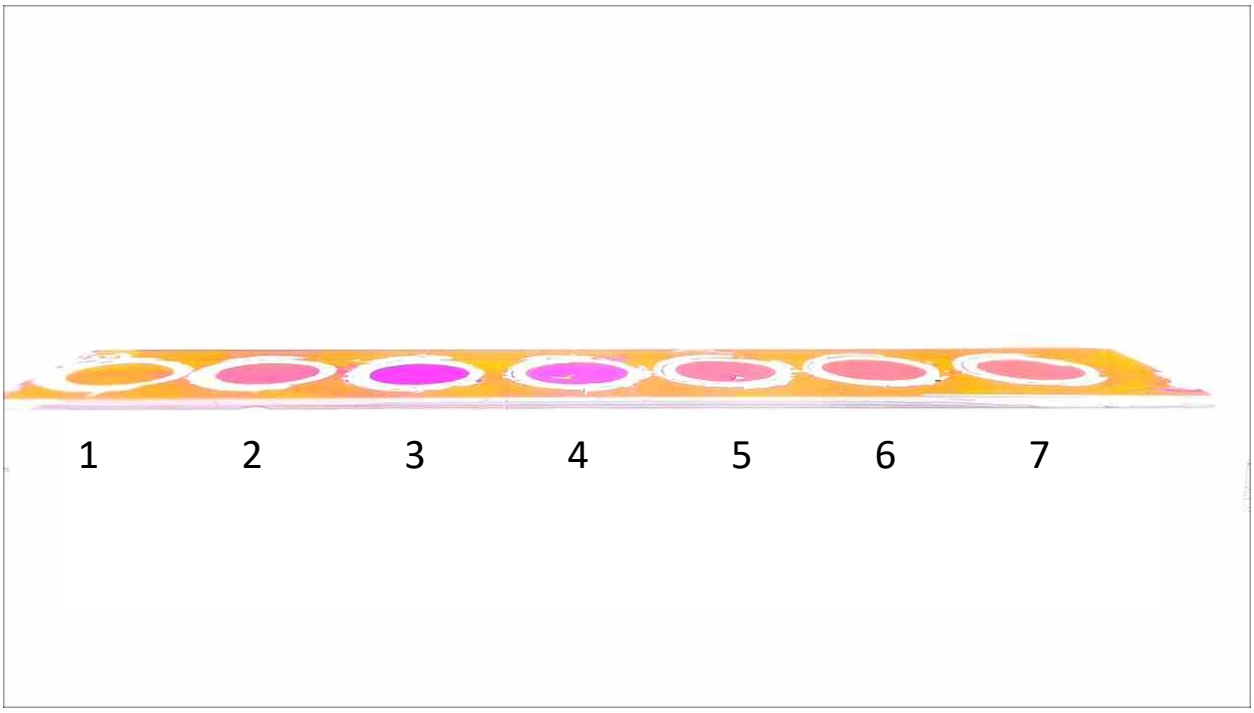


Figure 8.36. Silicon wafer (replicate 3) coated with ~ 200 nm of tantalum then ~ 106 nm of aluminum and anodized at 4 V after protein analysis. The farthest left circle (1) was exposed to no protein (blank). The other six circles (2 – 7) exposed to 20 µL of 1 mg/mL prothrombin for 20 minutes. Circle 2 exposed to prothrombin only. Then circles 3 – 7 exposed to 20 µL of varying anti-prothrombin concentrations for 20 minutes: 0.5 mg/mL anti-prothrombin (3), 0.05 mg/mL anti-prothrombin (4), 0.005 mg/mL anti-prothrombin (5), 5×10^{-4} mg/mL anti-prothrombin (6), 5×10^{-5} mg/mL anti-prothrombin (7).

In all three replicates, the base colour of the silicon wafer slide after sputtering 200 nm of tantalum and 106.01 ± 0.109 nm is an orange-tan colour. A shift to orange-pink occurred after exposure to 20 µL of 1 mg/mL prothrombin for 20 minutes, indicating the formation of a prothrombin layer on the surface. In the third circle, a strong colour shift to bright pink occurred after exposure to 20 µL of 0.5 mg/mL anti-prothrombin for 20 minutes. In the fourth circle, a noticeable colour shift occurred to pink after exposure to 20 µL of 0.05 mg/mL of anti-

prothrombin for 20 minutes. For all three replicates, the fifth, sixth and seventh circles appear a similar light orange-pink color as the second circle, which was only exposed to prothrombin. The fifth, sixth, and seventh circles were exposed to 20 µL of anti-prothrombin at concentrations of 0.005 mg/mL, 5×10^{-4} mg/mL and 5×10^{-5} mg/mL, respectively. As no visible colour shift occurred at these concentrations compared to the prothrombin only circle, the limit of detection on a stationary silicon wafer surface was determined to be 0.05 mg/mL of anti-prothrombin.

Statistical analysis was completed on the three replicates shown in Figures 8.34, 8.35 and 8.36 (n = 3). For each concentration, an area in the coloured circle was selected and analyzed using ImageJ to determine the RGB coordinates. The average RGB coordinates were taken for each of the three samples for the prothrombin only circle and for each anti-prothrombin concentration. The RGB coordinates were converted to Yxy colour coordinates using the ColorMine website (http://colormine.org/convert/rgb-to-yxy). The x and y coordinates were analyzed using one-way ANOVA and Tukey post hoc tests. Table 8.6 shows the results of the statistical analysis on the effect of various anti-prothrombin concentrations on the surface colour of the prothrombin-coated wafer based on x and y chromaticity coordinates. The x and y coordinates at each anti-prothrombin (AP) concentration were compared to the prothrombin (II) control, and a p value less than 0.05 indicates statistical significance.

Table 8.6. Results of the ANOVA and Tukey post hoc statistical analysis tests on the effect of various anti-prothrombin concentrations on the surface colour using x and y chromaticity coordinates compared to the prothrombin only control. Statistically significant results are in italics. (n = 3).

Prothrombin (II) control	**Vs. II + AP (mg/mL)**	**Difference detectable by eye vs. control?**	**x coordinate + p values**	**y coordinate + p values**
1 mg/mL II control x = 0.42 ± 0.02 y = 0.32 ± 0.04	0.5	Yes	x = 0.32 ± 0.00 *p = 0.001*	y = 0.17 ± 0.00 *p = 0.001*
	0.05	Yes	x = 0.32 ± 0.00 *p < 0.001*	y = 0.20 ± 0.01 *p = 0.006*
	0.005	No	x = 0.41 ± 0.03 p > 0.9	y = 0.33 ± 0.05 p > 0.9
	5×10^{-4}	No	x = 0.43 ± 0.04 p > 0.9	y = 0.34 ± 0.04 p > 0.9
	5×10^{-5}	No	x = 0.42 ± 0.00 p = 1	y = 0.33 ± 0.02 p > 0.9

The results of the statistical analysis indicate statistical significance only for anti-prothrombin concentrations of 0.5 mg/mL and 0.05 mg/mL, indicating a statistical difference in x and y chromaticity coordinates for these concentrations compared to the prothrombin only control surface colour. The x and y chromaticity coordinates obtained from the surface colour at anti-prothrombin concentrations of 0.005 mg/mL, 5×10^{-4} mg/mL and 5×10^{-5} mg/mL are not statistically different from the prothrombin only control surface colour, and no visible colour shift occurred at these concentrations.

The faintest anti-prothrombin concentration that underwent a visibly detectable colour shift compared to the 1 mg/mL prothrombin control on the silicon wafers above was an anti-prothrombin concentration of 0.05 mg/mL. As it was previously shown that a detectable colour shift occurred after 20 minutes for an anti-prothrombin concentration of 0.005 mg/mL in the 500 mL stirred experiments (Figure 8.33), the next stirred experiments were conducted with an anti-prothrombin concentration of 5×10^{-4} mg/mL. The 5×10^{-4} mg/mL anti-prothrombin solution was prepared by diluting the 500 mL 0.005 mg/mL anti-prothrombin solution. To obtain an anti-prothrombin concentration of 5×10^{-4} mg/mL, 50 mL of the 0.005 mg/mL anti-prothrombin solution was placed in 450 mL of MilliQ water. The wafer was cut into slides using the 3D printed tool and a diamond scribe, and a Sharpie pen was used to draw a hydrophobic outline along the edges of the rectangular slide. The entire rectangular slide was coated with prothrombin by pipetting 532 µL of 1 mg/mL prothrombin onto the surface and spreading it to the edges and was then left in a Petri dish with a wet paper towel for 20 minutes. The wafer slide was then rinsed with deionized water and dried with oil free compressed air. An image was taken of the slide after coating with prothrombin to compare to the wafer with no protein and the wafer after exposure to anti-prothrombin. Next, a 0.7 cm hydrophobic circle was drawn on the wafer and a 20 µL solution of 0.5 mg/mL anti-prothrombin was pipetted into the circle and left in a Petri dish with a wet paper towel for 20 minutes. After 20 minutes, the wafer slide was rinsed with deionized water and dried with oil free compressed air. Figures 8.38, 8.39, and 8.40 show the three silicon wafer replicates after the entire surface after exposure to 532 µL of 1 mg/mL prothrombin for 20 minutes, then subsequent exposure to 20 µL of 0.5 mg/mL anti-prothrombin in the hydrophobic circle. The wafer slide was then attached to an old tantalum disc using double sided Scotch 3M tape and placed in the bottom of the stirring apparatus. A 500 mL solution of 5

$\times 10^{-4}$ mg/mL anti-prothrombin was then placed into the beaker and the impeller was attached. The Tech II Railmaster 2400 was turned on and set to an impeller power of ~ 13 – 14 (~ 195 RPM), and the solution was stirred for 20 minutes while the wafer slide and tantalum disc remained at the bottom of the beaker. After 20 minutes, the impeller was stopped, and the substrate was removed from the solution. The wafer slide was rinsed with deionized water and dried with oil free compressed air. Figures 8.41, 8.42, and 8.43 show the images of the silicon wafer coated with ~ 200 nm of tantalum and ~ 106 nm of aluminum then anodized at 4 V prior to protein work (top), after exposure to 532 µL of 1 mg/mL prothrombin for 20 minutes (middle), and after subsequent exposure to 500 mL of 5×10^{-4} mg/mL anti-prothrombin for 20 minutes with continuous stirring at ~ 195 RPM (bottom) cropped and lined up to visualize the colour shifts of replicates 1, 2 and 3, respectively.

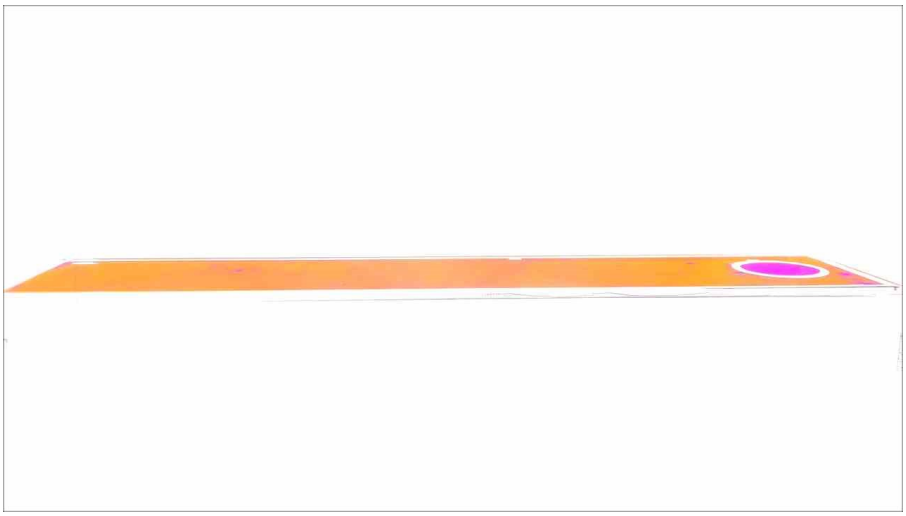


Figure 8.37. Silicon wafer slide (replicate 1) (~ 1.3 cm by ~ 6.2 cm) coated with ~ 200 nm of tantalum and ~ 106 nm of aluminum then anodized at 4 V after the entire surface was coated with 532 µL of 1 mg/mL prothrombin for 20 minutes. The hydrophobic circle was subsequently exposed to 20 µL of 0.5 mg/mL anti-prothrombin for 20 minutes.

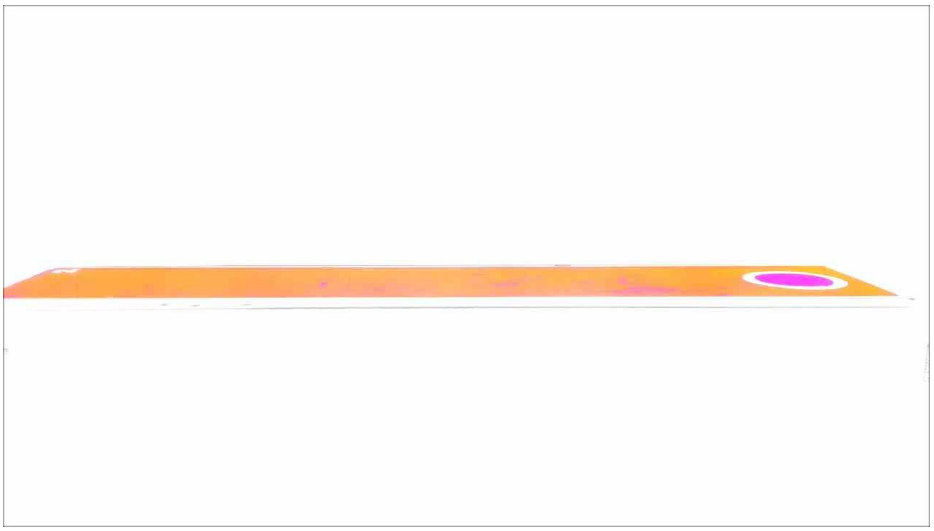


Figure 8.38. Silicon wafer slide (replicate 2) (~ 1.3 cm by ~ 6.2 cm) coated with ~ 200 nm of tantalum and ~ 106 nm of aluminum then anodized at 4 V after the entire surface was coated with 532 µL of 1 mg/mL prothrombin for 20 minutes. The hydrophobic circle was subsequently exposed to 20 µL of 0.5 mg/mL anti-prothrombin for 20 minutes.

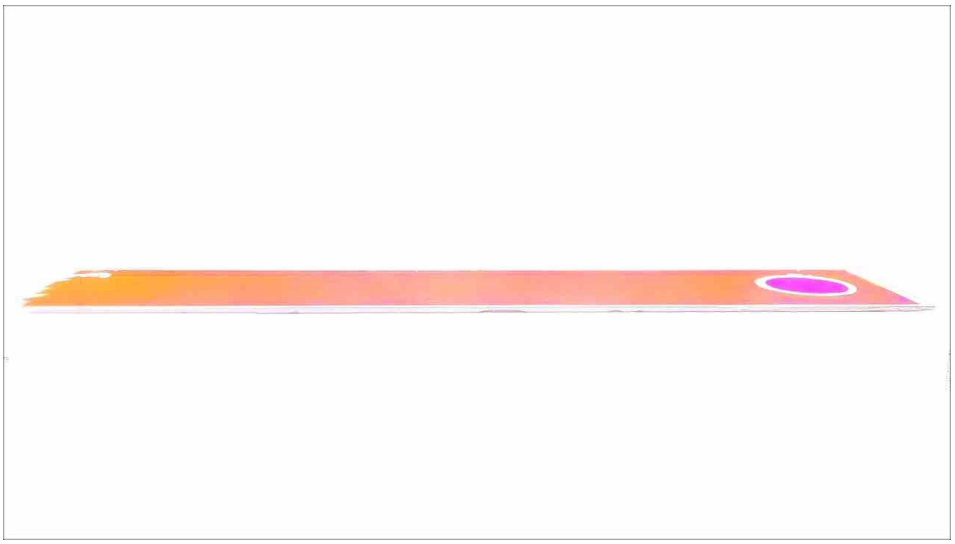


Figure 8.39. Silicon wafer slide (replicate 3) (~ 1.3 cm by ~ 6.2 cm) coated with ~ 200 nm of tantalum and ~ 106 nm of aluminum then anodized at 4 V after the entire surface was coated with 532 µL of 1 mg/mL prothrombin for 20 minutes. The hydrophobic circle was subsequently exposed to 20 µL of 0.5 mg/mL anti-prothrombin for 20 minutes.

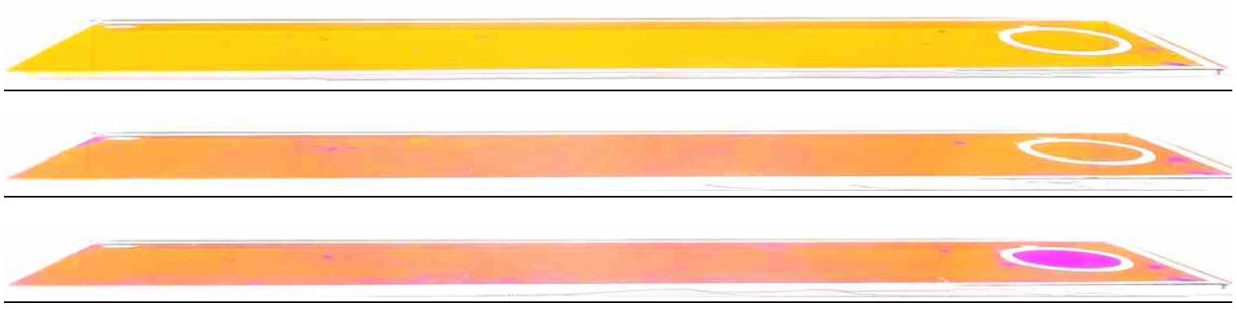


Figure 8.40. Silicon wafer slide (replicate 1) (~ 1.3 cm by ~ 6.2 cm) coated with ~ 200 nm of tantalum and ~ 106 nm of aluminum then anodized at 4 V with no exposure to protein (top), after exposure of entire slide to 532 μL of 1 mg/mL prothrombin for 20 minutes (middle), after subsequent exposure of entire slide to 500 mL of 5 × 10^{-4} mg/mL anti-prothrombin for 20 minutes with continuous stirring at ~ 195 RPM (bottom).

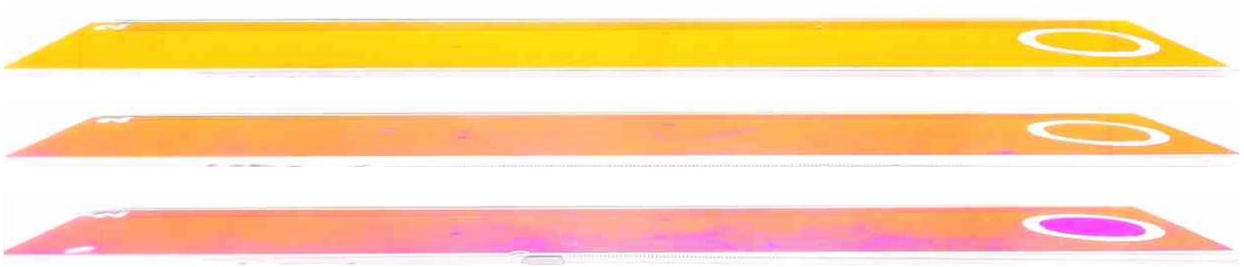


Figure 8.41. Silicon wafer slide (replicate 2) (~ 1.3 cm by ~ 6.2 cm) coated with ~ 200 nm of tantalum and ~ 106 nm of aluminum then anodized at 4 V with no exposure to protein (top), after exposure of entire slide to 532 μL of 1 mg/mL prothrombin for 20 minutes (middle), after subsequent exposure of entire slide to 500 mL of 5 × 10^{-4} mg/mL anti-prothrombin for 20 minutes with continuous stirring at ~ 195 RPM (bottom).

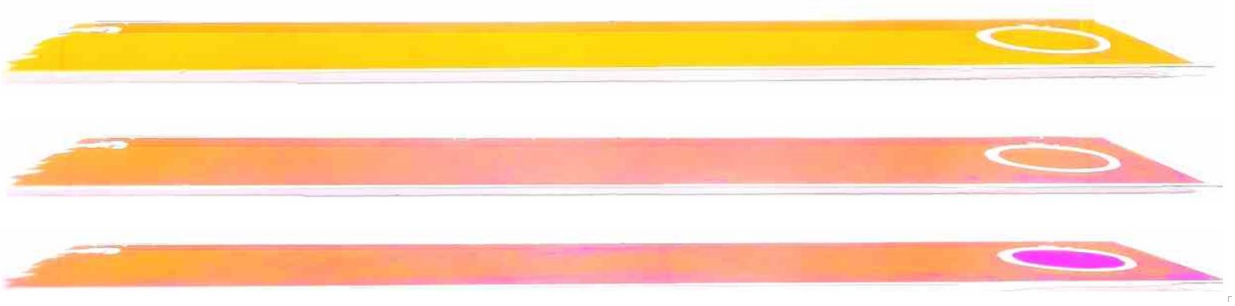


Figure 8.42. Silicon wafer slide (replicate 3) (~ 1.3 cm by ~ 6.2 cm) coated with ~ 200 nm of tantalum and ~ 106 nm of aluminum then anodized at 4 V with no exposure to protein (top), after exposure of entire slide to 532 µL of 1 mg/mL prothrombin for 20 minutes (middle), after subsequent exposure of entire slide to 500 mL of 5 × 10^{-4} mg/mL anti-prothrombin for 20 minutes with continuous stirring at ~ 195 RPM (bottom).

Table 8.7 shows the MSE, Al_2O_3 layer thickness, and EMA% values obtained from ellipsometry for the silicon wafer coated with thin films of tantalum and aluminum, then anodized at 4 V that is shown in Figures 8.37 – 8.42.

Table 8.7. MSE, Al_2O_3 layer thickness, and EMA % of silicon wafer coated with 200 nm of tantalum and 106 nm of aluminum, then anodized at 4 V shown in Figures 8.37 – 8.42.

MSE	18.736
Al_2O_3 layer thickness (nm)	106.01 ± 0.109 nm
EMA%	56.1 ± 0.06

Images were also taken of one of the replicates after 5 minutes of stirring and after 10 minutes of stirring to determine the impact of time. Figures 8.43 and 8.44 show a silicon wafer slide coated with ~ 200 nm of tantalum and ~ 106 nm of aluminum anodized at 4 V after exposure to 500 mL of 5 × 10^{-4} mg/mL anti-prothrombin for 5 and 10 minutes with continuous stirring at ~ 195 RPM, respectively.

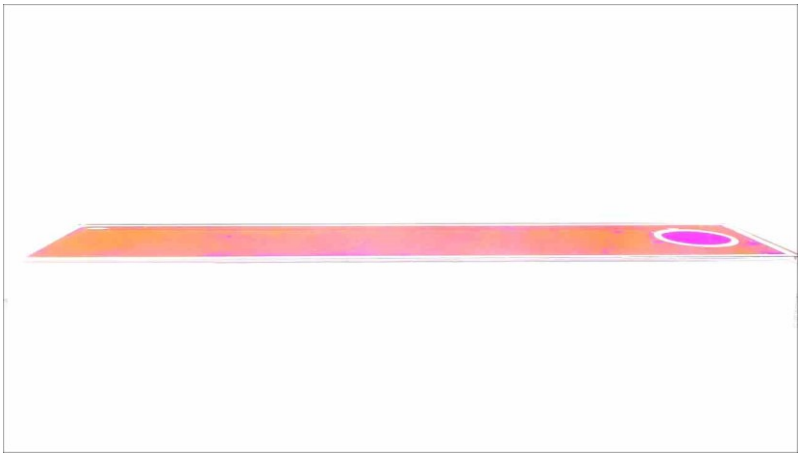


Figure 8.43. Silicon wafer slide (~ 1.3 cm by ~ 6.2 cm) coated with ~ 200 nm of tantalum and ~ 106 nm of aluminum then anodized at 4 V after the entire surface was coated with 532 µL of 1 mg/mL prothrombin for 20 minutes. The hydrophobic circle was subsequently exposed to 20 µL of 0.5 mg/mL anti-prothrombin for 20 minutes. The entire wafer was then exposed to 500 mL of 5 × 10^{-4} mg/mL anti-prothrombin with continuous stirring at ~ 195 RPM for 5 minutes.

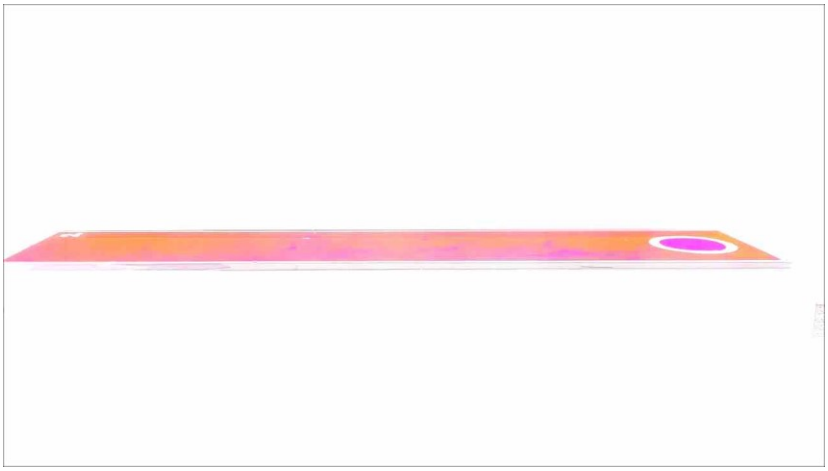


Figure 8.44. Silicon wafer slide (~ 1.3 cm by ~ 6.2 cm) coated with ~ 200 nm of tantalum and ~ 106 nm of aluminum then anodized at 4 V after the entire surface was coated with 532 µL of 1 mg/mL prothrombin for 20 minutes. The hydrophobic circle was subsequently exposed to 20 µL of 0.5 mg/mL anti-prothrombin for 20 minutes. The entire wafer was then exposed to 500 mL of 5 × 10^{-4} mg/mL anti-prothrombin with continuous stirring at ~ 195 RPM for 10 minutes.

Since there was no clear colour shift after exposure to 500 mL of 5×10^{-4} mg/mL anti-prothrombin with continuous stirring for 20 minutes, the same three wafer slides were exposed to 450 mL of 0.005 mg/mL anti-prothrombin for 5 minutes, then another 5 minutes (10 minutes total). Figures 8.45, 8.46 and 8.47 show the three replicate slides after exposure to 450 mL of 0.005 mg/mL anti-prothrombin with continuous stirring at ~ 195 RPM for 5 minutes. Figures 8.48, 8.49 and 8.50 show the three replicate slides after exposure to 450 mL of 0.005 mg/mL anti-prothrombin with continuous stirring at ~ 195 RPM for 10 minutes.



Figure 8.45. Silicon wafer slide (replicate 1) (~ 1.3 cm by ~ 6.2 cm) coated with ~ 200 nm of tantalum and ~ 106 nm of aluminum then anodized at 4 V after the entire surface was coated with 532 µL of 1 mg/mL prothrombin for 20 minutes. The hydrophobic circle was subsequently exposed to 20 µL of 0.5 mg/mL anti-prothrombin for 20 minutes. The entire slide was then exposed to 500 mL of 5×10^{-4} mg/mL anti-prothrombin with continuous stirring at ~ 195 RPM for 20 minutes. The entire slide was then exposed to 450 mL of 0.005 mg/mL anti-prothrombin with continuous stirring at ~ 195 RPM for 5 minutes.

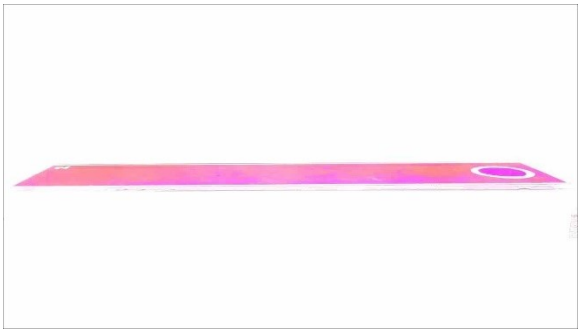


Figure 8.46. Silicon wafer slide (replicate 2) (~ 1.3 cm by ~ 6.2 cm) coated with ~ 200 nm of tantalum and ~ 106 nm of aluminum then anodized at 4 V after the entire surface was coated with 532 µL of 1 mg/mL prothrombin for 20 minutes. The hydrophobic circle was subsequently exposed to 20 µL of 0.5 mg/mL anti-prothrombin for 20 minutes. The entire slide was then exposed to 500 mL of 5 × 10^{-4} mg/mL anti-prothrombin with continuous stirring at for 20 minutes. The entire slide was then exposed to 450 mL of 0.005 mg/mL anti-prothrombin with continuous stirring for 5 minutes.



Figure 8.47. Silicon wafer slide (replicate 3) (~ 1.3 cm by ~ 6.2 cm) coated with ~ 200 nm of tantalum and ~ 106 nm of aluminum then anodized at 4 V after the entire surface was coated with 532 µL of 1 mg/mL prothrombin for 20 minutes. The hydrophobic circle was subsequently exposed to 20 µL of 0.5 mg/mL anti-prothrombin for 20 minutes. The entire slide was then exposed to 500 mL of 5 × 10^{-4} mg/mL anti-prothrombin with continuous stirring for 20 minutes. The entire slide was then exposed to 450 mL of 0.005 mg/mL anti-prothrombin with continuous stirring for 5 minutes.

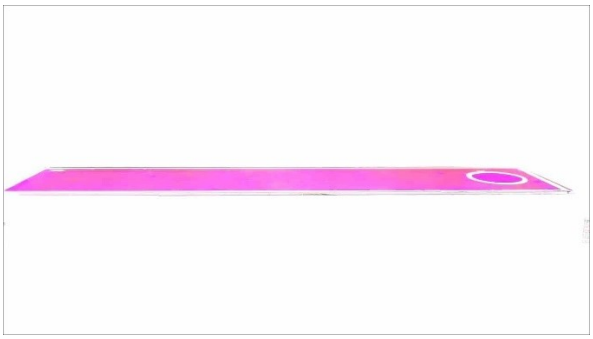


Figure 8.48. Silicon wafer slide (replicate 1) (~ 1.3 cm by ~ 6.2 cm) coated with ~ 200 nm of tantalum and ~ 106 nm of aluminum then anodized at 4 V after the entire surface was coated with 532 μL of 1 mg/mL prothrombin for 20 minutes. The hydrophobic circle was subsequently exposed to 20 μL of 0.5 mg/mL anti-prothrombin for 20 minutes. The entire slide was then exposed to 500 mL of 5 × 10^{-4} mg/mL anti-prothrombin with continuous stirring for 20 minutes. The entire slide was then exposed to 450 mL of 0.005 mg/mL anti-prothrombin with continuous stirring for 10 minutes.



Figure 8.49. Silicon wafer slide (replicate 2) (~ 1.3 cm by ~ 6.2 cm) coated with ~ 200 nm of tantalum and ~ 106 nm of aluminum then anodized at 4 V after the entire surface was coated with 532 μL of 1 mg/mL prothrombin for 20 minutes. The hydrophobic circle was subsequently exposed to 20 μL of 0.5 mg/mL anti-prothrombin for 20 minutes. The entire slide was then exposed to 500 mL of 5 × 10^{-4} mg/mL anti-prothrombin with continuous stirring for 20 minutes. The entire slide was then exposed to 450 mL of 0.005 mg/mL anti-prothrombin with continuous stirring for 10 minutes.

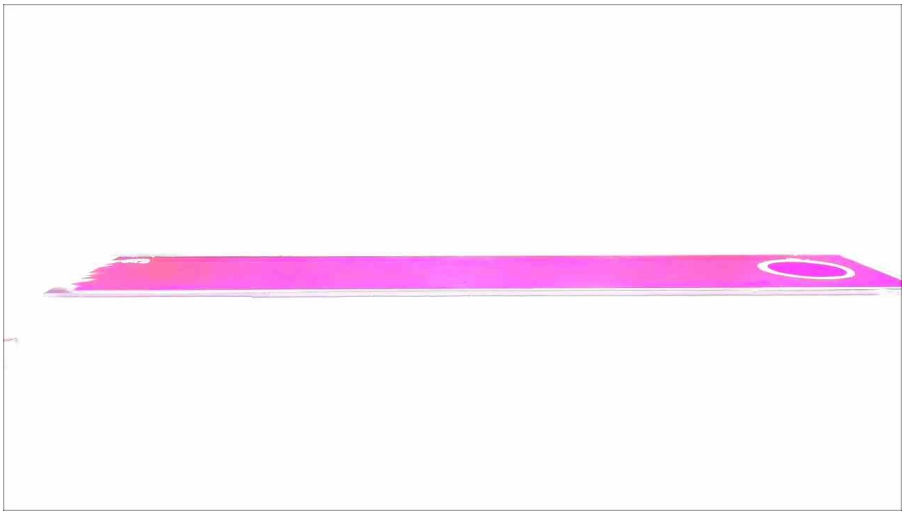


Figure 8.50. Silicon wafer slide (replicate 3) (~ 1.3 cm by ~ 6.2 cm) coated with ~ 200 nm of tantalum and ~ 106 nm of aluminum then anodized at 4 V after the entire surface was coated with 532 µL of 1 mg/mL prothrombin for 20 minutes. The hydrophobic circle was subsequently exposed to 20 µL of 0.5 mg/mL anti-prothrombin for 20 minutes. The entire slide was then exposed to 500 mL of 5 × 10^{-4} mg/mL anti-prothrombin with continuous stirring for 20 minutes. The entire slide was then exposed to 450 mL of 0.005 mg/mL anti-prothrombin with continuous stirring for 10 minutes.

Figures 8.51, 8.52, and 8.53 show the images of the silicon wafer coated with ~ 200 nm of tantalum and ~ 106 nm of aluminum then anodized at 4 V prior to protein work (top), after exposure to 532 µL of 1 mg/mL prothrombin for 20 minutes (middle), and after subsequent exposure to 500 mL of of 5 × 10^{-4} mg/mL anti-prothrombin with continuous stirring at ~ 195 RPM for 20 minutes followed by exposure to 450 mL of 0.005 mg/mL anti-prothrombin for 10 minutes with continuous stirring at ~ 195 RPM (bottom) cropped and lined up to visualize the colour shifts of replicates 1, 2 and 3, respectively. The top and middle images were taken from Figures 8.40, 8.41, and 8.42, while the bottom images were taken from Figures 8.48, 8.49 and 8.50.

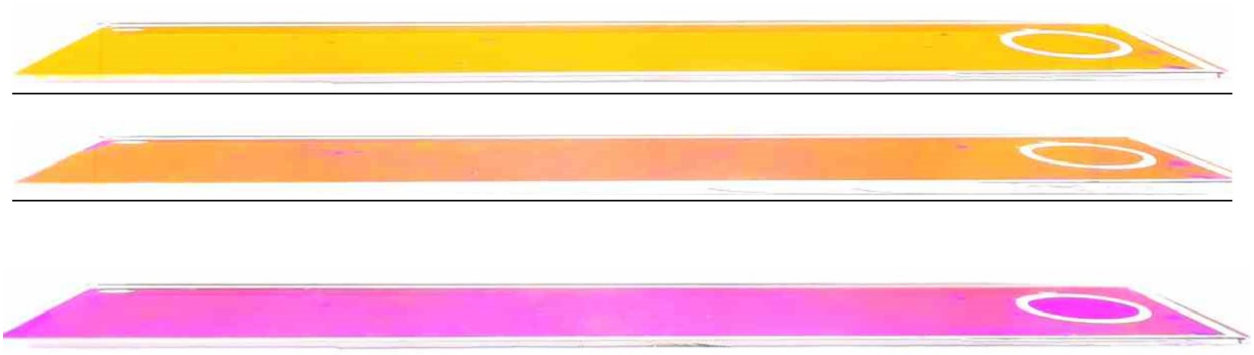


Figure 8.51. Silicon wafer slide (replicate 1) (~ 1.3 cm by ~ 6.2 cm) coated with ~ 200 nm of tantalum and ~ 106 nm of aluminum then anodized at 4 V prior to protein work (top), after the entire surface was coated with 532 µL of 1 mg/mL prothrombin for 20 minutes (middle), and after the entire slide was exposed to 500 mL of 5 × 10^{-4} mg/mL anti-prothrombin with continuous stirring at ~ 195 RPM for 20 minutes and 450 mL of 0.005 mg/mL anti-prothrombin with continuous stirring at ~195 RPM for 10 minutes (bottom).

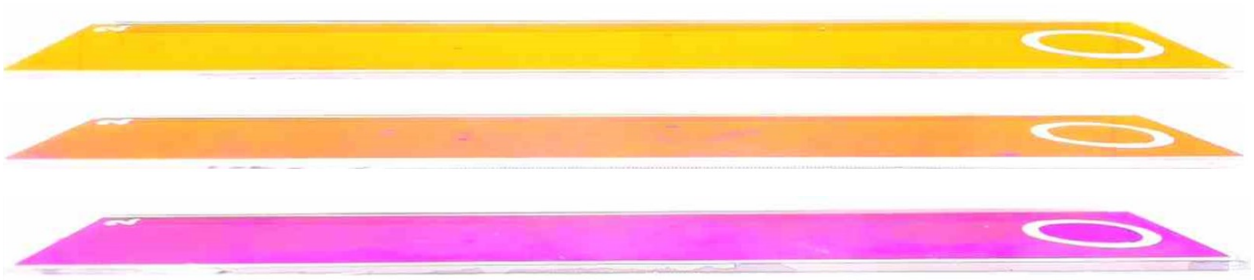


Figure 8.52. Silicon wafer slide (replicate 2) (~ 1.3 cm by ~ 6.2 cm) coated with ~ 200 nm of tantalum and ~ 106 nm of aluminum then anodized at 4 V prior to protein work (top), after the entire surface was coated with 532 µL of 1 mg/mL prothrombin for 20 minutes (middle), and after the entire slide was exposed to 500 mL of 5 × 10^{-4} mg/mL anti-prothrombin with continuous stirring at ~ 195 RPM for 20 minutes and 450 mL of 0.005 mg/mL anti-prothrombin with continuous stirring at ~ 195 RPM for 10 minutes (bottom).

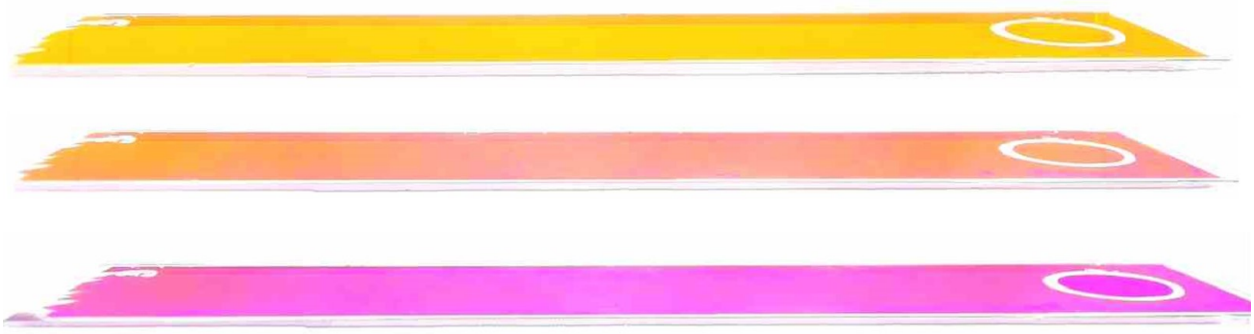


Figure 8.53. Silicon wafer slide (replicate 3) (~ 1.3 cm by ~ 6.2 cm) coated with ~ 200 nm of tantalum and ~ 106 nm of aluminum then anodized at 4 V prior to protein work (top), after the entire surface was coated with 532 µL of 1 mg/mL prothrombin for 20 minutes (middle), and after the entire slide was exposed to 500 mL of 5 × 10^{-4} mg/mL anti-prothrombin with continuous stirring at ~ 195 RPM for 20 minutes and 450 mL of 0.005 mg/mL anti-prothrombin with continuous stirring at ~ 195 RPM for 10 minutes (bottom).

Statistical analysis was conducted on the replicates in Figures 8.51, 8.52 and 8.53 to determine if there was a statistically significant difference in the colour coordinates for the prothrombin only coated slides, and the slides exposed to the larger volumes at an anti-prothrombin concentration of 5 × 10^{-4} mg/mL for 20 minutes with continuous stirring at ~ 195 RPM, followed by a concentration of 0.005 mg/mL with continuous stirring at ~ 195 RPM for 10 minutes. For each replicate, the entire coloured rectangular area was selected and analyzed using ImageJ to determine the RGB coordinates. The average RGB coordinates were taken for each of the three replicates for the prothrombin only slides and for the slides exposed to anti-prothrombin. The RGB coordinates were converted to Yxy colour coordinates using the ColorMine website (http://colormine.org/convert/rgb-to-yxy). The x and y coordinates were analyzed separately using independent T-tests. Table 8.8 shows the results of the statistical analysis on the effect of 500 mL of 5 × 10^{-4} mg/mL anti-prothrombin for 20 minutes followed by

450 mL of 0.005 mg/mL of anti-prothrombin for 10 minutes on the surface colour of the prothrombin-coated wafer based on x and y chromaticity coordinates. The x and y coordinates after exposure to anti-prothrombin (AP) were compared to the prothrombin (II) control, and a p value less than 0.05 indicates statistical significance.

Table 8.8. Results of the independent T-test statistical analysis tests on the effect of 500 mL of 5 × 10^{-4} mg/mL anti-prothrombin for 20 minutes followed by 450 mL of 0.005 mg/mL of anti-prothrombin for 10 minutes with continuous stirring on the surface colour of the prothrombin-coated wafer based on x and y chromaticity coordinates compared to the prothrombin only control. Statistically significant results are in italics. (n = 3).

Prothrombin (II) control	**Vs. II + AP (mg/mL)**	**Difference detectable by eye vs. control?**	**x coordinate + p values**	**y coordinate + p values**
1 mg/mL II control x = 0.44 ± 0.01 y = 0.38 ± 0.02	5 × 10^{-4} (20 minutes) followed by 0.005 (10 minutes) with continuous stirring at ~ 195 RPM	Yes	x = 0.34 ± 0.01 *p < 0.001*	y = 0.21 ± 0.01 *p < 0.001*

By visual detection, a strong colour shift from light orange (prothrombin only) to bright pink (prothrombin + anti-prothrombin) occurred in all three replicates. As the p values were less than 0.05 for both the x coordinate and the y coordinate, the chromaticity coordinates after exposure to 532 µL of 1 mg/mL prothrombin for 20 minutes and subsequent exposure to 500 mL of 5 × 10^{-4} mg/mL anti-prothrombin for 20 minutes followed by 0.005 mg/mL anti-prothrombin for 10 minutes with continuous stirring are statistically different compared to the chromaticity coordinates after exposure to 1 mg/mL of prothrombin only.

The same stirring experiments were completed in triplicate using a fresh anti-prothrombin solution. Silicon wafers were prepared by sputtering ~ 200 nm of tantalum then ~ 106 nm of aluminum and anodizing at 4 V. Ellipsometry data for the three silicon wafers used for anti-prothrombin concentrations of 0.005 mg/mL, 0.0025 mg/mL and 5×10^{-4} mg/mL are shown in Tables 8.9, 8.10 and 8.11, respectively.

Table 8.9. MSE, Al_2O_3 layer thickness, and EMA % from ellipsometry of silicon wafer coated with 200 nm of tantalum and 106 nm of aluminum, then anodized at 4 V used for protein work at an anti-prothrombin concentration of 0.005 mg/mL in following experiments.

MSE	17.090
Al_2O_3 layer thickness (nm)	105.50 ± 0.107 nm
EMA%	61.4 ± 0.06

Table 8.10. MSE, Al_2O_3 layer thickness, and EMA % from ellipsometry of silicon wafer coated with 200 nm of tantalum and 106 nm of aluminum, then anodized at 4 V used for protein work at an anti-prothrombin concentration of 0.0025 mg/mL in following experiments.

MSE	17.719
Al_2O_3 layer thickness (nm)	106.22 ± 0.110 nm
EMA%	60.8 ± 0.06

Table 8.11. MSE, Al_2O_3 layer thickness, and EMA % from ellipsometry of silicon wafer coated with 200 nm of tantalum and 107 nm of aluminum, then anodized at 4 V used for protein work at an anti-prothrombin concentration of 5×10^{-4} mg/mL in following experiments.

MSE	16.788
Al_2O_3 layer thickness (nm)	107.04 ± 0.105 nm
EMA%	60.9 ± 0.06

The wafers were cut into slides using the 3D printed tool and a Sharpie pen was used to draw a hydrophobic outline along the edges of the rectangular slide. The entire rectangular slide was then coated with prothrombin by pipetting 532 μL volume of 1 mg/mL prothrombin onto the surface and spreading it to the edges and was left in a Petri dish with a wet paper towel for 20 minutes. The wafer was then rinsed with deionized water and dried with oil free compressed air. An image was taken of the slide after coating with prothrombin to compare to the wafer with no protein and the wafer after exposure to anti-prothrombin. Next, a 0.7 cm hydrophobic circle was drawn on the wafer and a 20 μL solution of 0.5 mg/mL anti-prothrombin was pipetted into the circle and left in a Petri dish with a wet paper towel for 20 minutes. After 20 minutes, the wafer slide was rinsed with deionized water and dried with oil free compressed air. The wafer slide was then attached to an old tantalum disc using double sided Scotch 3M tape and placed in the bottom of the stirring apparatus. A 500 mL solution of 0.005 mg/mL anti-prothrombin was then placed into the beaker and the impeller was attached and lowered into the beaker. The 500 mL solution of 0.005 mg/mL anti-prothrombin was prepared by adding 250 μL of the 10 mg/mL anti-prothrombin stock solution to 499.75 mL of MilliQ water. The Tech II Railmaster 2400 was turned on and set to an impeller power of ~ 13 – 14, and the solution was stirred for 20 minutes while the wafer slide attached to the tantalum disc remained at the bottom of the beaker. After 20 minutes, the impeller was stopped, and the substrate was removed from the solution. The wafer slide was rinsed with deionized water and dried with oil free compressed air. The experiment was repeated at an anti-prothrombin concentration of 0.0025 mg/mL and an anti-prothrombin concentration of 5×10^{-4} mg/mL. These solutions were prepared by first making a 550 mL solution of 0.005 mg/mL anti-prothrombin by placing 275 μL of the 10 mg/mL anti-prothrombin stock solution to 549.275 mL of MilliQ water. To form the 0.0025 mg/mL anti-prothrombin

solution, 500 mL of the 550 mL 0.005 mg/mL anti-prothrombin solution was placed in 500 mL of MilliQ water and mixed. From this 1 L solution, 500 mL was used for the experiment. To form the 5×10^{-4} mg/mL anti-prothrombin solution, 50 mL of the 550 mL 0.005 mg/mL anti-prothrombin solution was placed in 450 mL of MilliQ water and mixed.

Figures 8.54, 8.55, and 8.56 show the images of the silicon wafer coated with ~ 200 nm of tantalum and ~ 106 nm of aluminum then anodized at 4 V prior to protein work (top), after exposure to 532 µL of 1 mg/mL prothrombin for 20 minutes (middle), and after subsequent exposure to 500 mL of 0.005 mg/mL anti-prothrombin for 20 minutes with continuous stirring at ~ 195 RPM (bottom) cropped and lined up to visualize the colour shifts of replicates 1, 2 and 3, respectively. Figures 8.57, 8.58, and 8.59 show the images of the silicon wafer coated with ~ 200 nm of tantalum and ~ 106 nm of aluminum then anodized at 4 V prior to protein work (top), after exposure to 532 µL of 1 mg/mL prothrombin for 20 minutes (middle), and after subsequent exposure to 500 mL of 0.0025 mg/mL anti-prothrombin for 20 minutes with continuous stirring at ~ 195 RPM (bottom) cropped and lined up to visualize the colour shifts of replicates 1, 2 and 3, respectively. Figures 8.60, 8.61, and 8.62 show the images of the silicon wafer coated with ~ 200 nm of tantalum and ~ 107 nm of aluminum then anodized at 4 V prior to protein work (top), after exposure to 532 µL of 1 mg/mL prothrombin for 20 minutes (middle), and after subsequent exposure to 500 mL of 5×10^{-4} mg/mL anti-prothrombin for 20 minutes with continuous stirring at ~ 195 RPM (bottom) cropped and lined up to visualize the colour shifts of replicates 1, 2 and 3, respectively.



Figure 8.54. Silicon wafer slide (replicate 1) (~ 1.3 cm by ~ 6.2 cm) coated with ~ 200 nm of tantalum and ~ 106 nm of aluminum then anodized at 4 V with no exposure to protein (top), after exposure of entire slide to 532 µL of 1 mg/mL prothrombin for 20 minutes (second from top), after subsequent exposure of hydrophobic circle to 20 µL of 0.5 mg/mL anti-prothrombin for 20 minutes (second from bottom), after subsequent exposure of entire slide to 500 mL of 0.005 mg/mL anti-prothrombin for 20 minutes with continuous stirring at ~ 195 RPM (bottom).

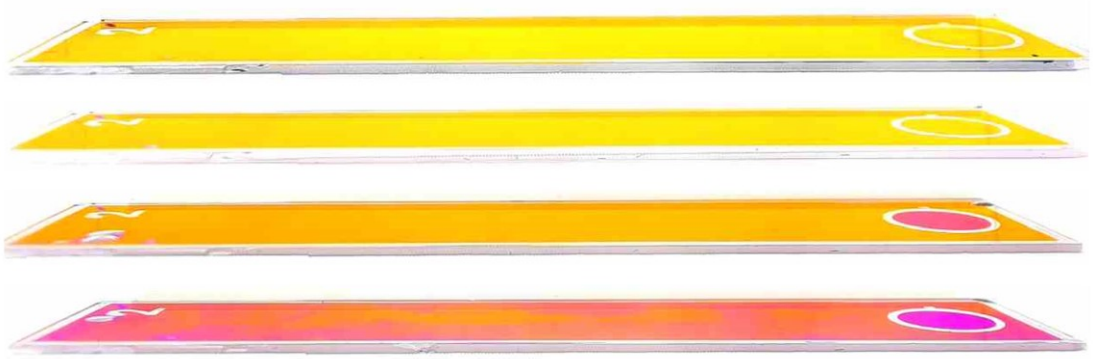


Figure 8.55. Silicon wafer slide (replicate 2) (~ 1.3 cm by ~ 6.2 cm) coated with ~ 200 nm of tantalum and ~ 106 nm of aluminum then anodized at 4 V with no exposure to protein (top), after exposure of entire slide to 532 µL of 1 mg/mL prothrombin for 20 minutes (second from top), after subsequent exposure of hydrophobic circle to 20 µL of 0.5 mg/mL anti-prothrombin for 20 minutes (second from bottom), after subsequent exposure of entire slide to 500 mL of 0.005 mg/mL anti-prothrombin for 20 minutes with continuous stirring at ~ 195 RPM (bottom).

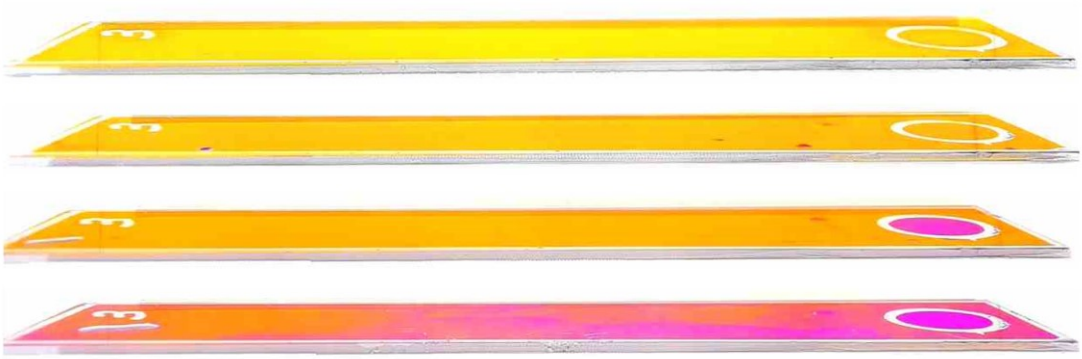


Figure 8.56. Silicon wafer slide (replicate 3) (~ 1.3 cm by ~ 6.2 cm) coated with ~ 200 nm of tantalum and ~ 106 nm of aluminum then anodized at 4 V with no exposure to protein (top), after exposure of entire slide to 532 µL of 1 mg/mL prothrombin for 20 minutes (second from top), after subsequent exposure of hydrophobic circle to 20 µL of 0.5 mg/mL anti-prothrombin for 20 minutes (second from bottom), after subsequent exposure of entire slide to 500 mL of 0.005 mg/mL anti-prothrombin for 20 minutes with continuous stirring at ~ 195 RPM (bottom).



Figure 8.57. Silicon wafer slide (replicate 1) (~ 1.3 cm by ~ 6.2 cm) coated with ~ 200 nm of tantalum and ~ 106 nm of aluminum then anodized at 4 V with no exposure to protein (top), after exposure of entire slide to 532 µL of 1 mg/mL prothrombin for 20 minutes (second from top), after subsequent exposure of hydrophobic circle to 20 µL of 0.5 mg/mL anti-prothrombin for 20 minutes (second from bottom), after subsequent exposure of entire slide to 500 mL of 0.0025 mg/mL anti-prothrombin for 20 minutes with continuous stirring at ~ 195 RPM (bottom).



Figure 8.58. Silicon wafer slide (replicate 2) (~ 1.3 cm by ~ 6.2 cm) coated with ~ 200 nm of tantalum and ~ 106 nm of aluminum then anodized at 4 V with no exposure to protein (top), after exposure of entire slide to 532 µL of 1 mg/mL prothrombin for 20 minutes (second from top), after subsequent exposure of hydrophobic circle to 20 µL of 0.5 mg/mL anti-prothrombin for 20 minutes (second from bottom), after subsequent exposure of entire slide to 500 mL of 0.0025 mg/mL anti-prothrombin for 20 minutes with continuous stirring at ~ 195 RPM (bottom).



Figure 8.59. Silicon wafer slide (replicate 3) (~ 1.3 cm by ~ 6.2 cm) coated with ~ 200 nm of tantalum and ~ 106 nm of aluminum then anodized at 4 V with no exposure to protein (top), after exposure of entire slide to 532 µL of 1 mg/mL prothrombin for 20 minutes (second from top), after subsequent exposure of hydrophobic circle to 20 µL of 0.5 mg/mL anti-prothrombin for 20 minutes (second from bottom), after subsequent exposure of entire slide to 500 mL of 0.0025 mg/mL anti-prothrombin for 20 minutes with continuous stirring at ~ 195 RPM (bottom).

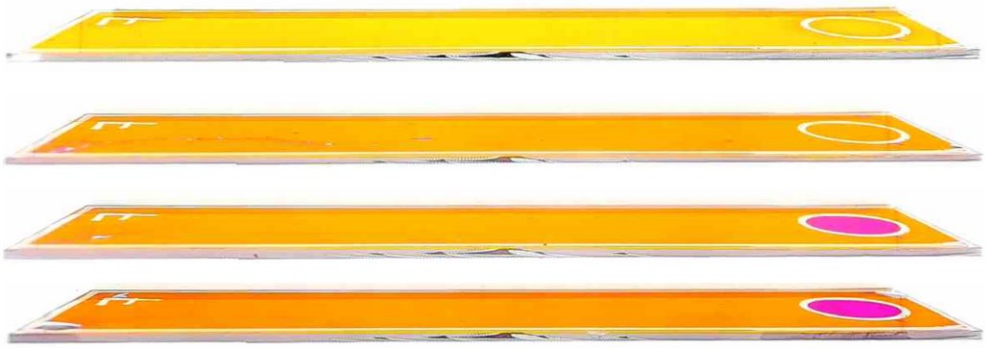


Figure 8.60. Silicon wafer slide (replicate 1) (~ 1.3 cm by ~ 6.2 cm) coated with ~ 200 nm of tantalum and ~ 107 nm of aluminum then anodized at 4 V with no exposure to protein (top), after exposure of entire slide to 532 µL of 1 mg/mL prothrombin for 20 minutes (second from top), after subsequent exposure of hydrophobic circle to 20 µL of 0.5 mg/mL anti-prothrombin for 20 minutes (second from bottom), after subsequent exposure of entire slide to 500 mL of 5 × 10^{-4} mg/mL anti-prothrombin for 20 minutes with continuous stirring at ~ 195 RPM (bottom).

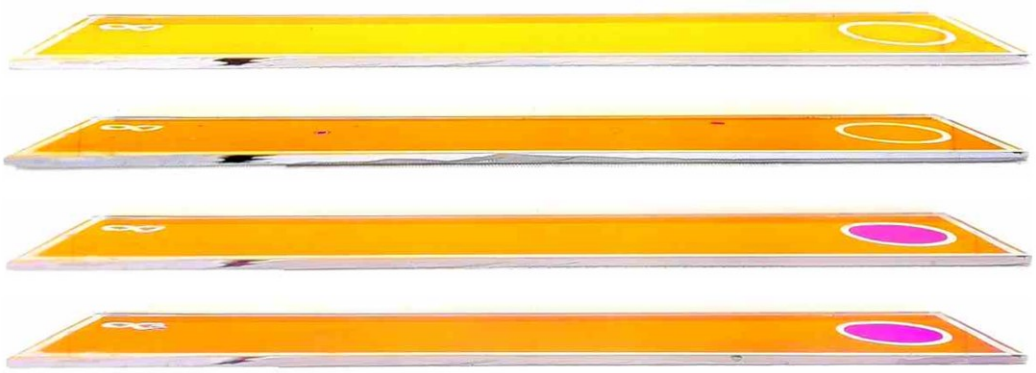


Figure 8.61. Silicon wafer slide (replicate 2) (~ 1.3 cm by ~ 6.2 cm) coated with ~ 200 nm of tantalum and ~ 107 nm of aluminum then anodized at 4 V with no exposure to protein (top), after exposure of entire slide to 532 µL of 1 mg/mL prothrombin for 20 minutes (second from top), after subsequent exposure of hydrophobic circle to 20 µL of 0.5 mg/mL anti-prothrombin for 20 minutes (second from bottom), after subsequent exposure of entire slide to 500 mL of 5 × 10^{-4} mg/mL anti-prothrombin for 20 minutes with continuous stirring at ~ 195 RPM (bottom).

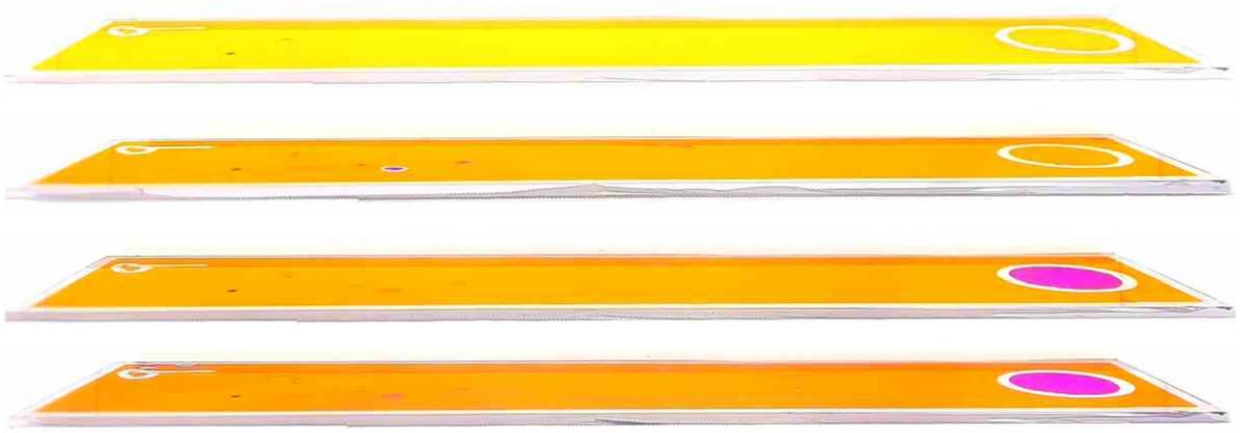


Figure 8.62. Silicon wafer slide (replicate 3) (~ 1.3 cm by ~ 6.2 cm) coated with ~ 200 nm of tantalum and ~ 107 nm of aluminum then anodized at 4 V with no exposure to protein (top), after exposure of entire slide to 532 µL of 1 mg/mL prothrombin for 20 minutes (second from top), after subsequent exposure of hydrophobic circle to 20 µL of 0.5 mg/mL anti-prothrombin for 20 minutes (second from bottom), after subsequent exposure of entire slide to 500 mL of 5 × 10^{-4} mg/mL anti-prothrombin for 20 minutes with continuous stirring at ~ 195 RPM (bottom).

Since the colour appeared non-uniform after exposure to 0.005 mg/mL anti-prothrombin, the RGB colour coordinates were studied on three separate areas of each replicate prior to protein exposure (blank), after exposure to 532 µL of 1 mg/mL prothrombin for 20 minutes, and after exposure to 500 mL of anti-prothrombin. Three areas were selected on each replicate to assess the colour consistency across the slide, as at all concentrations, the colour did not appear uniform on the slide after exposure to anti-prothrombin. Table 8.12 shows the RGB colour coordinates for three areas on each slide for three replicates prior to protein exposure, after exposure to 532 µL of 1 mg/mL prothrombin for 20 minutes, and after subsequent exposure to 500 mL of anti-prothrombin at concentrations of 0.005 mg/mL. The selected areas were between 5,000 and 11,000 pixels and were analyzed using the ImageJ software.

Table 8.12. RGB colour coordinates for three areas on each slide for three replicates prior to protein exposure, after exposure to 532 µL of 1 mg/mL prothrombin for 20 minutes, and after subsequent exposure to 500 mL of 0.005 mg/mL anti-prothrombin (AP) at concentrations.

		No protein exposure	**1 mg/mL prothrombin**	**0.005 mg/mL AP**
Replicate 1	Area 1	R: 253.111 ± 1.760 G: 234.164 ± 3.645 B: 9.257 ± 3.148	R: 253.564 ± 1.247 G: 173.209 ± 3.010 B: 0.669 ± 1.226	R: 253.774 ± 1.676 G: 104.061 ± 10.577 B: 71.556 ± 31.808
	Area 2	R: 253. 425 ± 1.794 G: 245.686 ± 3.047 B: 9.579 ± 3.901	R: 254.078 ± 1.379 G: 186.164 ± 3.632 B: 1.665 ± 2.098	R: 253.483 ± 2.222 G: 116.606 ± 14.687 B: 105.125 ± 39.007
	Area 3	R: 253.960 ± 1.355 G: 242.618 ± 2.800 B: 9.545 ± 4.124	R: 253.712 ± 2.924 G: 183.006 ± 3.435 B: 1.848 ± 3.083	R: 253.726 ± 1.838 G: 91.377 ± 15.793 B: 132.553 ± 43.814
Replicate 2	Area 1	R: 253.484 ± 1.392 G: 234.583 ± 5.266 B: 9.576 ± 4.577	R: 253.920 ± 1.340 G: 178.388 ± 3.618 B: 1.254 ± 1.528	R: 253.849 ± 1.772 G: 117.952 ± 8.925 B: 94.969 ± 24.009
	Area 2	R: 253.600 ± 1.611 G: 246.361 ± 3.869 B: 9.788 ± 3.682	R: 253.937 ± 1.188 G: 190.501 ± 2.774 B: 2.633 ± 2.260	R: 253.601 ± 1.788 G: 147.107 ± 10.769 B: 72.472 ± 30.721
	Area 3	R: 254.395 ± 1.242 G: 244.191 ± 3.303 B: 9.159 ± 3.937	R: 252.620 ± 2.361 G: 191.400 ± 2.361 B: 1.887 ± 2.153	R: 253.881 ± 1.427 G: 130.222 ± 10.112 B: 89.608 ± 23.806
Replicate 3	Area 1	R: 253.818 ± 2.111 G: 233.754 ± 3.174 B: 12.128 ± 7.616	R: 254.537 ± 1.009 G: 181.624 ± 2.835 B: 0.714 ± 1.275	R: 254.100 ± 1.178 G: 145.105 ± 4.164 B: 26.117 ± 9.630
	Area 2	R: 253.445 ± 1.964 G: 242.299 ± 2.810 B: 9.887 ± 4.229	R: 254.224 ± 1.676 G: 185.433 ± 3.492 B: 1.989 ± 2.744	R: 253.395 ± 2.766 G: 121.965 ± 10.367 B: 150.652 ± 25.844
	Area 3	R: 254.077 ± 0.903 G: 241.612 ± 2.236 B: 10.492 ± 3.309	R: 254.086 ± 1.232 G: 179.542 ± 3.339 B: 2.070 ± 2.218	R: 253.659 ± 2.008 G: 93.880 ± 15.996 B: 149.708 ± 35.948

The RGB colour coordinates for the three areas for the prothrombin coated slides are similar to each other for each replicate, suggesting that the 1 mg/mL prothrombin solution produced uniform binding on the surface. The large standard deviations and discrepancies on different areas of the same slide for the RGB colour coordinates on the areas after exposure to

500 mL of 0.005 mg/mL anti-prothrombin with continuous stirring for 20 minutes suggest that the colour on the surface is non uniform for all three replicates. This is likely due to an uneven distribution of anti-prothrombin on the prothrombin coated surface, possibly due to the large surface area of the silicon wafer slides. For a larger surface area, more anti-prothrombin is required to bind to produce a uniform layer compared to a smaller surface area.

Tables 8.13, 8.14 and 8.15 show the results of statistical analysis on the three replicates (n = 3) after exposure to anti-prothrombin at concentrations of 0.005 mg/mL, 0.0025 mg/mL and 5×10^{-4} mg/mL, respectively, to determine if there was a statistically different colour for the prothrombin only coated slides vs. the prothrombin + anti-prothrombin coated slides based on the x and y chromaticity coordinates. For each replicate, the entire coloured rectangular area was selected and analyzed using ImageJ to determine the RGB coordinates. The average RGB coordinates were taken at each of the three replicates for the prothrombin only slides and for the slides exposed to anti-prothrombin. The RGB coordinates were converted to Yxy colour coordinates using the ColorMine website (http://colormine.org/convert/rgb-to-yxy). The x and y coordinates were analyzed using an independent T-test for each concentration. The x and y coordinates after exposure to anti-prothrombin (AP) were compared to the prothrombin (II) control, and a p value less than 0.05 indicates statistical significance.

Table 8.13. Results of the independent T-test statistical analysis tests on the effect of 500 mL of 0.005 mg/mL of anti-prothrombin for 20 minutes with continuous stirring on the surface colour of the prothrombin-coated wafer based on x and y chromaticity coordinates compared to the prothrombin only control. Statistically significant results are in italics. (n = 3).

Prothrombin (II) control	**Vs. II + AP (mg/mL)**	**Difference detectable by eye vs. control?**	**x coordinate + p values**	**y coordinate + p values**
1 mg/mL II control x = 0.48 ± 0.00 y = 0.46 ± 0.00	0.005 (20 minutes with continuous stirring at ~ 195 RPM)	Yes	x = 0.49 ± 0.02 p > 0.4	y = 0.35 ± 0.02 *p < 0.001*

Table 8.14. Results of the independent T-test statistical analysis tests on the effect of 500 mL of 0.0025 mg/mL of anti-prothrombin for 20 minutes with continuous stirring on the surface colour of the prothrombin-coated wafer based on x and y chromaticity coordinates compared to the prothrombin only control. Statistically significant results are in italics. (n = 3).

Prothrombin (II) control	**Vs. II + AP (mg/mL)**	**Difference detectable by eye vs. control?**	**x coordinate + p values**	**y coordinate + p values**
1 mg/mL II control x = 0.49 ± 0.01 y = 0.45 ± 0.01	0.0025 (20 minutes with continuous stirring at ~ 195 RPM)	No	x = 0.53 ± 0.02 *p < 0.05*	y = 0.40 ± 0.01 *p = 0.005*

Table 8.15. Results of the independent T-test statistical analysis tests on the effect of 500 mL of 5 × 10^{-4} mg/mL anti-prothrombin for 20 minutes with continuous stirring on the surface colour of the prothrombin-coated wafer based on x and y chromaticity coordinates compared to the prothrombin only control. Statistically significant results are in italics. (n = 3).

Prothrombin (II) control	**Vs. II + AP (mg/mL)**	**Difference detectable by eye vs. control?**	**x coordinate + p values**	**y coordinate + p values**
1 mg/mL II control x = 0.48 ± 0.00 y = 0.46 ± 0.00	5×10^{-4} (20 minutes with continuous stirring at ~ 195 RPM)	No	x = 0.49 ± 0.02 p > 0.1	y = 0.35 ± 0.02 p > 0.1

Statistical analysis on the chromaticity coordinates for the ~ 1.2 cm by ~ 6.3 cm silicon wafer slides coated with 200 nm of tantalum and ~ 106 nm of aluminum, then anodized at 4 V yielded the following results: For an anti-prothrombin concentration of 0.005 mg/mL, the x chromaticity coordinate is not statistically different compared to the prothrombin only control, while the y chromaticity coordinate is statistically different. For an anti-prothrombin concentration of 0.0025 mg/mL, the x and y chromaticity coordinates both have p values less than 0.05, suggesting the x and y chromaticity coordinates are both statistically different based on the three replicates compared to the prothrombin only control. For an anti-prothrombin concentration of 5×10^{-4} mg/mL, the x and y chromaticity coordinates are not statistically different compared to the prothrombin only control, and no visible colour shift was detected in any of the three replicates.

Since the surface colour did not appear uniform, the experiment was repeated in triplicate at an anti-prothrombin concentration of 0.005 mg/mL. Ellipsometry data for the silicon wafer used in the following experiment is shown in Table 8.16.

Table 8.16. MSE, Al_2O_3 layer thickness, and EMA % from ellipsometry of silicon wafer coated with 200 nm of tantalum and 105 nm of aluminum, then anodized at 4 V used for protein work at an anti-prothrombin concentration of 0.005 mg/mL in following repeat experiments.

MSE	17.718
Al_2O_3 layer thickness (nm)	105.22 ± 0.111 nm
EMA%	61.0 ± 0.06

Figures 8.63, 8.64, and 8.65 show the images of the silicon wafer coated with ~ 200 nm of tantalum and ~ 105 nm of aluminum then anodized at 4 V prior to protein work (top), after exposure to 532 µL of 1 mg/mL prothrombin for 20 minutes (middle), and after subsequent exposure to 500 mL of 0.005 mg/mL anti-prothrombin for 20 minutes with continuous stirring (bottom) cropped and lined up to visualize the colour shifts of replicates 1, 2 and 3, respectively, in the repeated experiments. The silicon wafer slide shown in Figure 8.65 broke after the stirring experiment when removing the tape adhering the slide to the tantalum disc.

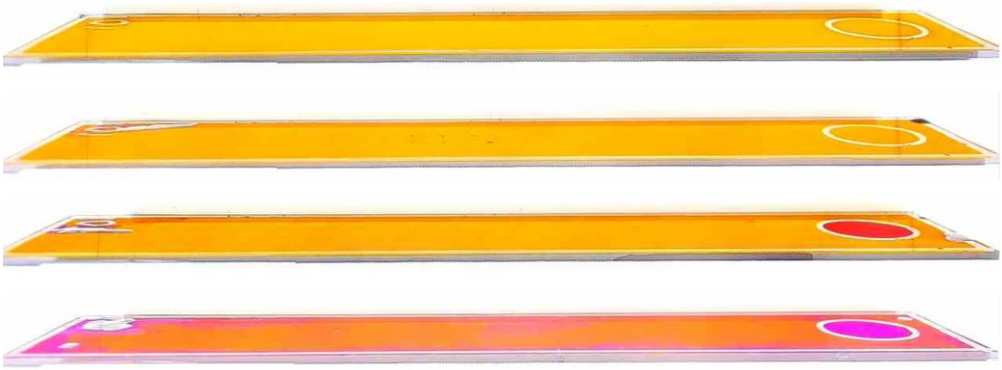


Figure 8.63. Silicon wafer slide (replicate 1) (~ 1.3 cm by ~ 6.2 cm) coated with ~ 200 nm of tantalum and ~ 105 nm of aluminum then anodized at 4 V with no exposure to protein (top), after exposure of entire slide to 532 µL of 1 mg/mL prothrombin for 20 minutes (second from top), after subsequent exposure of hydrophobic circle to 20 µL of 0.5 mg/mL anti-prothrombin for 20 minutes (second from bottom), after subsequent exposure of entire slide to 500 mL of 0.005 mg/mL anti-prothrombin for 20 minutes with continuous stirring at ~ 195 RPM (bottom).

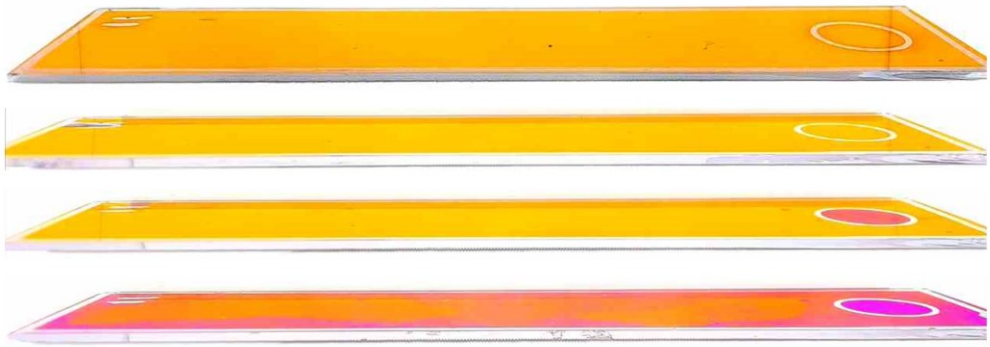


Figure 8.64. Silicon wafer slide (replicate 2) (~ 1.3 cm by ~ 6.2 cm) coated with ~ 200 nm of tantalum and ~ 105 nm of aluminum then anodized at 4 V with no exposure to protein (top), after exposure of entire slide to 532 µL of 1 mg/mL prothrombin for 20 minutes (second from top), after subsequent exposure of hydrophobic circle to 20 µL of 0.5 mg/mL anti-prothrombin for 20 minutes (second from bottom), after subsequent exposure of entire slide to 500 mL of 0.005 mg/mL anti-prothrombin for 20 minutes with continuous stirring at ~ 195 RPM (bottom).

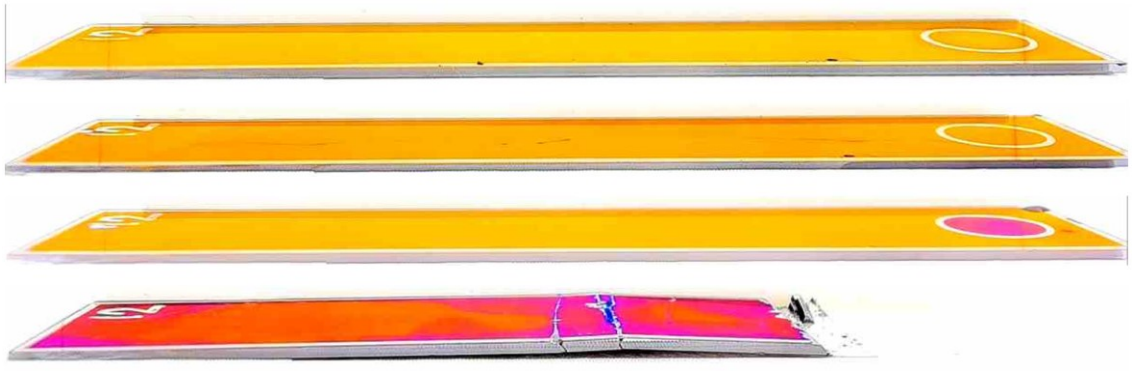


Figure 8.65. Silicon wafer slide (replicate 3) (~ 1.3 cm by ~ 6.2 cm) coated with ~ 200 nm of tantalum and ~ 105 nm of aluminum then anodized at 4 V with no exposure to protein (top), after exposure of entire slide to 532 µL of 1 mg/mL prothrombin for 20 minutes (second from top), after subsequent exposure of hydrophobic circle to 20 µL of 0.5 mg/mL anti-prothrombin for 20 minutes (second from bottom), after subsequent exposure of entire slide to 500 mL of 0.005 mg/mL anti-prothrombin for 20 minutes with continuous stirring at ~ 195 RPM (bottom).

Table 8.17 shows the results of statistical analysis on the three replicates (shown in Figures 8.63 – 8.65) after exposure to anti-prothrombin at a concentration of 0.005 mg/mL in the repeated experiment to determine if there was a statistically different colour for the prothrombin only coated slides vs. the prothrombin + anti-prothrombin coated slides based on the x and y chromaticity coordinates. For each replicate, the entire coloured rectangular area was selected and analyzed using ImageJ to determine the RGB coordinates. RGB coordinates were averaged across the three replicates for the prothrombin only slides and for the slides exposed to anti-prothrombin. The RGB coordinates were converted to Yxy colour coordinates using the ColorMine website (http://colormine.org/convert/rgb-to-yxy). The x and y coordinates were analyzed using an independent T-test for each concentration. The x and y coordinates after exposure to anti-prothrombin (AP) were compared to the prothrombin (II) control, and a p value less than 0.05 indicates statistical significance.

Table 8.17. Results of the independent T-test statistical analysis tests on the effect of 500 mL of 0.005 mg/mL of anti-prothrombin for 20 minutes with continuous stirring on the surface colour of the prothrombin-coated wafer based on x and y chromaticity coordinates compared to the prothrombin only control. Statistically significant results are in italics. (n = 3).

Prothrombin (II) control	**Vs. II + AP (mg/mL)**	**Difference detectable by eye vs. control?**	**x coordinate + p values**	**y coordinate + p values**
1 mg/mL II control x = 0.47 ± 0.01 y = 0.46 ± 0.01	0.005 repeated (20 minutes with continuous stirring at ~ 195 RPM)	Yes	x = 0.53 ± 0.04 p = 0.065	y = 0.39 ± 0.02 *p < 0.005*

For the repeated experiment at an anti-prothrombin concentration of 0.005 mg/mL, the x chromaticity coordinate is not statistically different compared to the prothrombin only control, while the y chromaticity coordinate is statistically different. By visual detection, the colour after exposure to anti-prothrombin appears more pink compared to the prothrombin only surface (orange), however, the colour did not appear uniform across the surface.

It is possible that the non-uniform surface after exposure to anti-prothrombin on the 1.2 cm by 6.3 cm silicon wafer slides could be due to the large surface area, which would require more anti-prothrombin to bind to produce a uniform colour shift. Referring to Section 8.3 – Theoretical Calculations for Anti-prothrombin Limit of Detection, Sweet found the theoretical limit of detection for anti-prothrombin on a prothrombin coated surface in a 1 cm circle (0.7854 cm^2 surface area) to be 2.7 pmol [5]. From this, the theoretical limits of detection were calculated for anti-prothrombin on prothrombin coated surfaces with surface areas of 8.06 cm^2 (silicon

wafer slide with dimensions of 1.3 cm by 6.2 cm) and 1.2 cm^2 (silicon wafer rectangle with dimensions of 1.2 cm by 1 cm) to be 27.7 pmol and 4.13 pmol, respectively. The theoretical limit for the smaller surface area rectangle (4.13 pmols) is much lower than for the entire slide (27.7 pmols), and less anti-prothrombin will be required to bind to produce a uniform colour shift across the entire surface. Using a smaller surface area may potentially improve the sensitivity as fewer pmols of anti-prothrombin from solution are required to bind to the surface, meaning a solution with a lower anti-prothrombin concentration can potentially be used. Experimentally, Sweet determined the limit of detection for anti-prothrombin to bind to a 1 cm diameter circle prothrombin coated surface to be ~ 1.3 pmols of anti-prothrombin, which is lower than the theoretical limit of detection [5]. From Sweet's experimental limit of detection, ~ 13.3 pmols and ~ 2.0 pmols of anti-prothrombin would be required to bind for surface areas of 8.06 cm^2 and 1.2 cm^2, respectively, to produce visible colour shifts.

For the next set of experiments, the silicon wafer slides were cut into smaller pieces with dimensions of ~ 1 cm by ~ 1.2 cm and fresh protein solutions were used for each experiment to ensure that the anti-prothrombin would be uniformly distributed across the surface. The smaller surface areas used in these experiments require less protein in solution for uniform binding to occur over the whole surface and may result in stronger and more uniform colour shifts at lower protein concentrations. In addition to stirred tank experiments, experiments were conducted using stationary volumes of 500 mL with no stirring. The stationary experiments were used to assess the ability of diffusion alone to generate a visible colour shift in a larger volume sample, and confirm the need for well-mixed, turbulent flow. No colour shift was expected to occur in the stationary volume experiments, as it is not expected that diffusion alone would allow for adequate binding to generate a colour shift within 20 minutes. In these experiments, the silicon

wafer substrates were coated with ~ 200 nm of tantalum and ~ 108.30 nm of aluminum then anodized at 4 V and cut using the diamond scribe and the stencil. The silicon wafer slides were then further cut into smaller squares with dimensions of ~ 1 cm by ~ 1.2 cm. A Sharpie was used to trace the edges of the rectangles to contain the protein solutions, and images were taken prior to protein exposure. Then, the surfaces were completely exposed to 1 mg/mL prothrombin for 20 minutes by pipetting a 35 μL solution onto the rectangle and spreading the solution to the edges using a pipette tip. The silicon wafer rectangles were then left in a Petri dish with a wet paper towel for 20 minutes. After exposure to prothrombin, the wafers were rinsed with deionized water and dried with oil free compressed air, and images were taken. The prothrombin coated wafers were then placed in the bottom of a beaker containing 500 mL of anti-prothrombin solution with a concentration of 0.005 mg/mL. In one case, the solution was left for 20 minutes with no stirring (completed in triplicate). In the second case, the silicon wafer rectangles were attached to tantalum discs using double sided tape, and the solution was stirred continuously over the silicon wafer rectangles for 20 minutes, as was done in previous experiments (completed in triplicate). Images were taken of the silicon wafer pieces prior to prothrombin exposure, after exposure to prothrombin, and after exposure to 0.005 mg/mL anti-prothrombin in both the stirring experiments and the no stirring experiments. Figures 8.66 shows the three replicates prior to protein exposure (top), after exposure of each rectangle to 35 μL of 1 mg/mL prothrombin for 20 minutes (middle), and after exposure of each rectangle to 500 mL of 0.005 mg/mL of anti-prothrombin for 20 minutes with no stirring (bottom). Figure 8.67 shows the three replicates prior to protein exposure (top), after exposure of each rectangle to 35 μL of 1 mg/mL prothrombin for 20 minutes (middle), and after exposure of each rectangle to 500 mL of 0.005 mg/mL of anti-prothrombin for 20 minutes with continuous stirring at ~ 195 RPM (bottom).



Figure 8.66. Silicon wafer rectangles (three replicates – ~ 1 cm by ~ 1.2 cm each) coated with ~ 200 nm of tantalum and ~ 108 nm of aluminum then anodized at 4 V with no exposure to protein (top), after exposure of each rectangle to 35 µL of 1 mg/mL prothrombin for 20 minutes (middle), after subsequent exposure of each rectangle to 500 mL of 0.005 mg/mL anti-prothrombin for 20 minutes with no stirring (bottom).

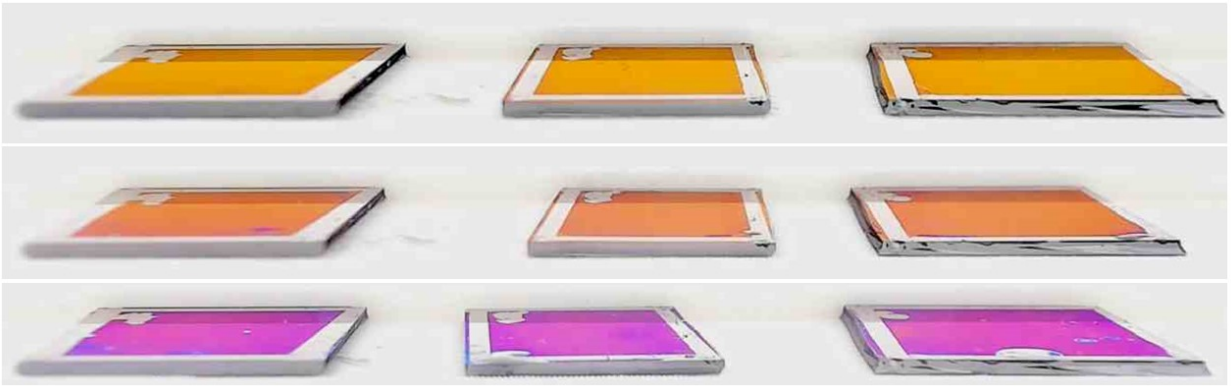


Figure 8.67. Silicon wafer rectangles (three replicates – ~ 1 cm by ~ 1.2 cm each) coated with ~ 200 nm of tantalum and ~ 108 nm of aluminum then anodized at 4 V with no exposure to protein (top), after exposure of each rectangle to 35 µL of 1 mg/mL prothrombin for 20 minutes (middle), after subsequent exposure of each rectangle to 500 mL of 0.005 mg/mL anti-prothrombin for 20 minutes with continuous stirring at ~ 195 RPM (bottom).

As shown in Figures 8.66 and 8.67, the silicon wafer rectangles were a tan/orange colour prior to protein exposure. After exposure of each rectangle to 35 µL of 1 mg/mL prothrombin for 20 minutes, the surface colour shifted to a darker orange. In both the stirred and non-stirred experiments, exposure to 500 mL of 0.005 mg/mL anti-prothrombin for 20 minutes resulted in a strong colour shift to bright pink. Unexpectedly, strong colour shifts occurred in the no stirring experiment. It is likely that less anti-prothrombin in solution was required to bind uniformly to the entire surface, due to the smaller surface area. Theoretically, only 4.13 pmols of anti-prothrombin were required to bind to the surface to generate a visible colour shift, compared to 27.7 pmols required for the 1.2 cm by 6.3 cm silicon wafer slides. In the 500 mL 0.005 mg/mL (33.3 nM) solution, 16.7 nmols of anti-prothrombin are present and available for binding. It is possible that the concentration of anti-prothrombin in solution was large enough to reach the surface and bind due to a combination of convection and diffusion in the system.

Since the smaller silicon wafer rectangles produced such strong colour shifts at an anti-prothrombin concentration of 0.005 mg/mL in both the stirred and non-stirred 500 mL volume experiments, the same experiments were conducted at an anti-prothrombin concentration of 0.0025 mg/mL. Figure 8.68 shows the three replicates prior to protein exposure (top), after exposure of each rectangle to 35 µL of 1 mg/mL prothrombin for 20 minutes (middle), and after exposure of each rectangle to 500 mL of 0.0025 mg/mL of anti-prothrombin for 20 minutes with no stirring (bottom). Figure 8.69 shows the three replicates prior to protein exposure (top), after exposure of each rectangle to 35 µL of 1 mg/mL prothrombin for 20 minutes (middle), and after exposure of each rectangle to 500 mL of 0.0025 mg/mL of anti-prothrombin for 20 minutes with continuous stirring at ~ 195 RPM (bottom).

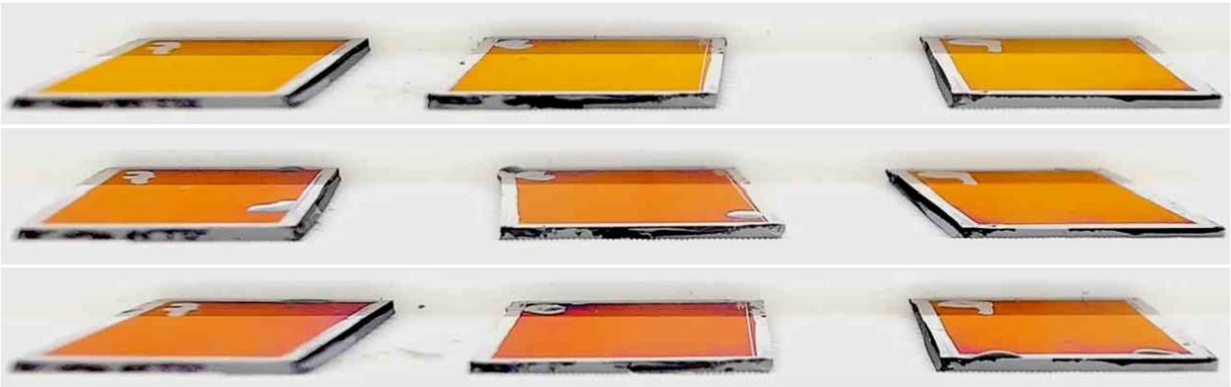


Figure 8.68. Silicon wafer rectangles (three replicates – ~ 1 cm by ~ 1.2 cm each) coated with ~ 200 nm of tantalum and ~ 108 nm of aluminum then anodized at 4 V with no exposure to protein (top), after exposure of each rectangle to 35 µL of 1 mg/mL prothrombin for 20 minutes (middle), after subsequent exposure of each rectangle to 500 mL of 0.0025 mg/mL anti-prothrombin for 20 minutes with no stirring (bottom).



Figure 8.69. Silicon wafer rectangles (three replicates – ~ 1 cm by ~ 1.2 cm each) coated with ~ 200 nm of tantalum and ~ 108 nm of aluminum then anodized at 4 V with no exposure to protein (top), after exposure of each rectangle to 35 µL of 1 mg/mL prothrombin for 20 minutes (middle), after subsequent exposure of each rectangle to 500 mL of 0.0025 mg/mL anti-prothrombin for 20 minutes with continuous stirring at ~ 195 RPM (bottom).

As shown in Figures 8.68 and 8.69, the silicon wafer rectangles were a tan/orange colour prior to protein exposure. After exposure of each rectangle to 35 μL of 1 mg/mL prothrombin for 20 minutes, the surface colour shifted to a darker orange. In the non-stirred experiment (Figure 8.68), no colour shift occurred after exposure to 500 mL of 0.0025 mg/mL anti-prothrombin, and the surface remained a dark orange. In the stirred experiments, a colour shift occurred from dark orange to bright pink after exposure to 500 mL of 0.0025 mg/mL anti-prothrombin with continuous stirring at ~ 195 RPM for 20 minutes. By visual observation, the results of this experiment suggest that an anti-prothrombin concentration of 0.0025 mg/mL is too low to generate a colour shift by only diffusion and convection. The strong colour shift in the stirred experiment suggests that turbulence and mixing are required for a colour shift to occur at an anti-prothrombin concentration of 0.0025 mg/mL.

Tables 8.18 and 8.19 show the results of statistical analysis on the three replicates (n = 3) shown in Figures 8.66 and 8.67, after exposure to 500 mL of anti-prothrombin at a concentration of 0.005 mg/mL with no stirring for 20 minutes and with stirring at ~ 195 RPM for 20 minutes, respectively, to determine if there was a statistical difference in colour for the prothrombin only coated slides vs. the prothrombin + anti-prothrombin coated slides based on the x and y chromaticity coordinates. Tables 8.20 and 8.21 show the results of statistical analysis on the three replicates (n = 3) shown in Figures 8.68 and 8.69, after exposure to 500 mL of anti-prothrombin at a concentration of 0.0025 mg/mL with no stirring for 20 minutes and with stirring for 20 minutes, respectively, to determine if there was a statistical difference in colour for the prothrombin only coated slides vs. the prothrombin + anti-prothrombin coated slides based on the x and y chromaticity coordinates. For each replicate, the entire coloured rectangular area (between 3,000 and 9,000 pixels) was selected and analyzed using the ImageJ software to

determine the RGB coordinates. The average RGB coordinates of each of the three replicates were converted to Yxy colour coordinates using the ColorMine website (http://colormine.org/convert/rgb-to-yxy). The x and y coordinates were analyzed using an independent T-test for each concentration in the no stirring and the stirring experiments. The x and y coordinates after exposure to anti-prothrombin (AP) were compared to the prothrombin (II) control, and a p value less than 0.05 indicates statistical significance.

Table 8.18. Results of the independent T-test statistical analysis tests on the effect of 500 mL of 0.005 mg/mL of anti-prothrombin for 20 minutes with no stirring on the surface colour of the prothrombin-coated wafer based on x and y chromaticity coordinates compared to the prothrombin only control. Statistically significant results are in italics. (n = 3).

Prothrombin (II) control	**Vs. II + AP (mg/mL)**	**Difference detectable by eye vs. control?**	**x coordinate + p values**	**y coordinate + p values**
1 mg/mL II control x = 0.51 ± 0.01 y = 0.41 ± 0.01	0.005 (20 minutes with no stirring)	Yes	x = 0.37 ± 0.01 *p < 0.001*	y = 0.18 ± 0.00 *p < 0.001*

Table 8.19. Results of the independent T-test statistical analysis tests on the effect of 500 mL of 0.005 mg/mL of anti-prothrombin for 20 minutes with continuous stirring at ~ 195 RPM on the surface colour of the prothrombin-coated wafer based on x and y chromaticity coordinates compared to the prothrombin only control. Statistically significant results are in italics. (n = 3).

Prothrombin (II) control	**Vs. II + AP (mg/mL)**	**Difference detectable by eye vs. control?**	**x coordinate + p values**	**y coordinate + p values**
1 mg/mL II control x = 0.48 ± 0.01 y = 0.39 ± 0.00	0.005 (20 minutes with continuous stirring at ~ 195 RPM)	Yes	x = 0.34 ± 0.01 *p < 0.001*	y = 0.21 ± 0.01 *p < 0.001*

Table 8.20. Results of the independent T-test statistical analysis tests on the effect of 500 mL of 0.0025 mg/mL of anti-prothrombin for 20 minutes with no stirring on the surface colour of the prothrombin-coated wafer based on x and y chromaticity coordinates compared to the prothrombin only control. Statistically significant results are in italics. (n = 3).

Prothrombin (II) control	**Vs. II + AP (mg/mL)**	**Difference detectable by eye vs. control?**	**x coordinate + p values**	**y coordinate + p values**
1 mg/mL II control x = 0.51 ± 0.01 y = 0.42 ± 0.01	0.0025 (20 minutes with no stirring)	No	x = 0.52 ± 0.00 p > 0.4	y = 0.41 ± 0.01 p > 0.05

Table 8.21. Results of the independent T-test statistical analysis tests on the effect of 500 mL of 0.0025 mg/mL of anti-prothrombin for 20 minutes with continuous stirring at ~ 195 RPM on the surface colour of the prothrombin-coated wafer based on x and y chromaticity coordinates compared to the prothrombin only control. Statistically significant results are in italics. (n = 3).

Prothrombin (II) control	**Vs. II + AP (mg/mL)**	**Difference detectable by eye vs. control?**	**x coordinate + p values**	**y coordinate + p values**
1 mg/mL II control x = 0.51 ± 0.00 y = 0.41 ± 0.01	0.0025 (20 minutes with continuous stirring at ~ 195 RPM)	Yes	x = 0.43 ± 0.01 *p < 0.001*	y = 0.27 ± 0.03 *p < 0.001*

The results of the statistical analysis indicated that the x and y chromaticity coordinates are statistically different for the prothrombin only surface compared to the prothrombin + anti-prothrombin surface for anti-prothrombin concentrations of 0.005 mg/mL with no stirring, 0.005 mg/mL with continuous stirring, and 0.0025 mg/mL with continuous stirring, all of which produced visibly detectable colour shifts on the surface. For an anti-prothrombin concentration of 0.0025 mg/mL with no stirring, there was no statistical difference in the x and y chromaticity coordinates between the prothrombin coated surface and the prothrombin + anti-prothrombin coated surface, and no visible colour shift occurred.

To assess the effect of sample volume, the same experiments as conducted above were repeated, but images were taken after 5 minutes, 10 minutes, 20 minutes, and 40 minutes of exposure to a 250 mL fluid volume with an anti-prothrombin concentration of 0.0025 mg/mL. In these experiments, the silicon wafer substrates were coated with ~ 200 nm of tantalum and ~

108.30 nm (no stirring) or ~ 111 nm (regular stirring) of aluminum then anodized at 4 V and cut using the diamond scribe and the stencil. The silicon wafer slides were then further cut into smaller squares with dimensions of ~ 1 cm by ~ 1.2 cm. A Sharpie was used to trace the edges of the rectangles to contain the protein solutions. Then, the surfaces were completely exposed to 1 mg/mL prothrombin for 20 minutes by pipetting a 35 μL solution onto the rectangle and spreading the solution to the edges using a pipette tip. The silicon wafer rectangles were then left in a Petri dish with a wet paper towel for 20 minutes. After exposure to prothrombin, the wafers were rinsed with deionized water and dried with oil free compressed air. The prothrombin coated wafers were then placed in the bottom of a 600 mL beaker containing 250 mL of an anti-prothrombin solution with a concentration of 0.0025 mg/mL. The smaller beaker was used for the smaller volume experiments to ensure that the impeller could be fully submerged in the solution for the duration of the experiments. In one experiment, there was no stirring (laminar condition) and in the other experiment, the solution was stirred at the regular impeller power of ~ 13 (turbulent condition). In both experiments, images were taken of the slides after 5 minutes, 10 minutes, 20 minutes, and 40 minutes of exposure to the 250 mL solution (completed in triplicate). Figure 8.70 shows the three replicates prior to protein exposure (row 1), after exposure of each rectangle to 35 μL of 1 mg/mL prothrombin for 20 minutes (row 2), and after exposure of each rectangle to 250 mL of 0.0025 mg/mL of anti-prothrombin with no stirring for 5 minutes, 10 minutes, 20 minutes and 40 minutes (rows 3, 4, 5, 6). In the stirred experiments, the silicon wafer rectangles were attached to tantalum discs using double sided tape, and the solution was stirred continuously over the silicon wafer rectangles at the regular stir speed (~ 195 RPM) that has been used for all experiments thus far (impeller power set to ~ 13). To assess the impact of time, images were taken after 5 minutes, 10 minutes, 20 minutes, and 40 minutes

(completed in triplicate). Figure 8.71 shows the three replicates prior to protein exposure (row 1), after exposure of each rectangle to 35 μL of 1 mg/mL prothrombin for 20 minutes (row 2), and after exposure of each rectangle to 250 mL of 0.0025 mg/mL of anti-prothrombin with continuous stirring at the regular impeller speed of ~ 195 RPM after 5 minutes, 10 minutes, 20 minutes, and 40 minutes (rows 3, 4, 5, 6).



Figure 8.70. Silicon wafer rectangles (three replicates – ~ 1 cm by ~ 1.2 cm each) coated with ~ 200 nm of tantalum and ~ 108 nm of aluminum then anodized at 4 V with no exposure to protein (row 1), after exposure of each rectangle to 35 μL of 1 mg/mL prothrombin for 20 minutes (row 2), after subsequent exposure of each rectangle to 250 mL of 0.0025 mg/mL anti-prothrombin for 5, 10, 20 and 40 minutes with no stirring (rows 3, 4, 5, 6).

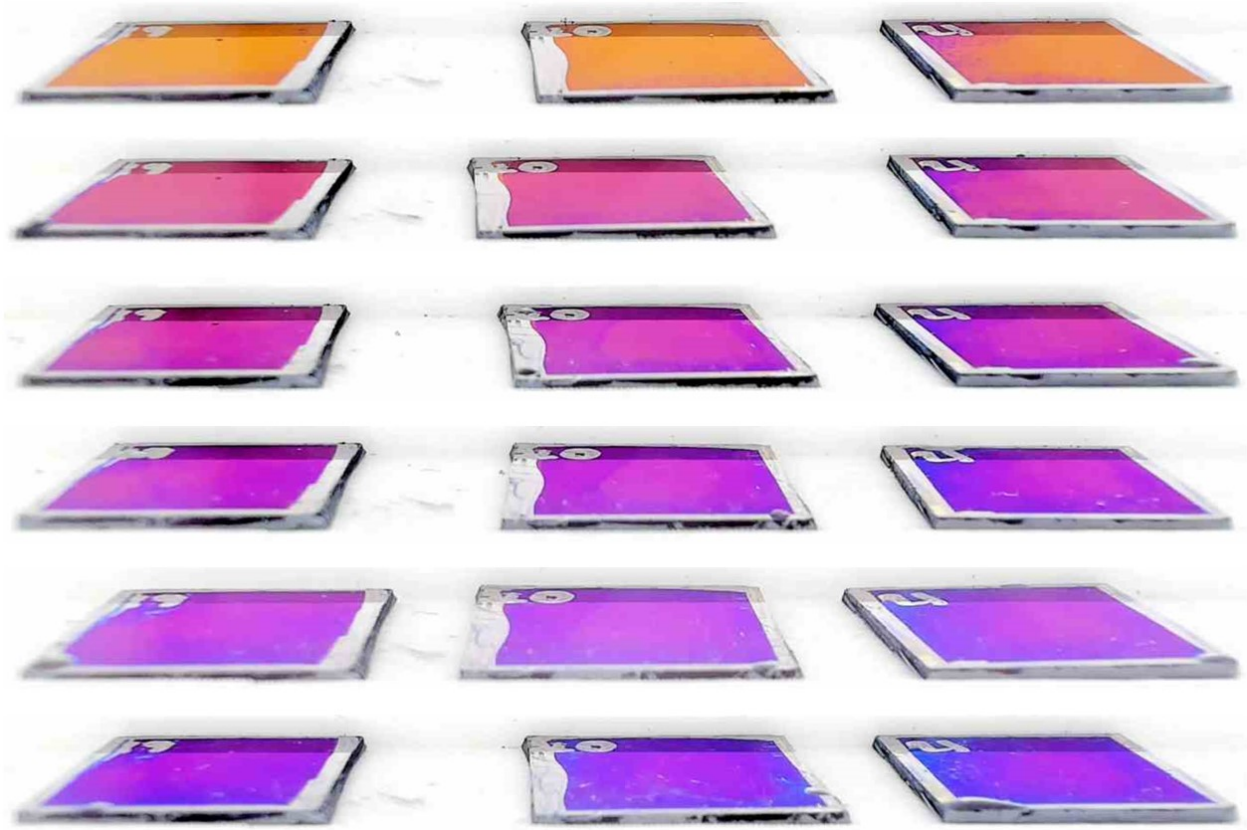


Figure 8.71. Silicon wafer rectangles (three replicates – ~ 1 cm by ~ 1.2 cm each) coated with ~ 200 nm of tantalum and ~ 111 nm of aluminum then anodized at 4 V with no exposure to protein (row 1), after exposure of each rectangle to 35 µL of 1 mg/mL prothrombin for 20 minutes (row 2), after subsequent exposure of each rectangle to 250 mL of 0.0025 mg/mL anti-prothrombin for 5, 10, 20 and 40 minutes with continuous stirring at the regular impeller speed of ~ 195 RPM (rows 3, 4, 5, 6).

Statistical analysis was completed on the three replicates shown in Figure 8.70 (n = 3) and the three replicates shown in Figure 8.71 (n = 3) to determine the effect of various exposure times on the surface colour of the prothrombin coated wafer for a 250 mL anti-prothrombin solution with a concentration of 0.0025 mg/mL with no stirring (laminar condition) and with continuous stirring at the regular impeller speed of ~ 195 RPM (low turbulence condition). For

each time interval, an area in the coloured circle was selected and analyzed using ImageJ to determine the RGB coordinates. The average RGB coordinates were taken for each of the three samples for the prothrombin only circle and for each anti-prothrombin concentration. The RGB coordinates were converted to Yxy colour coordinates using the ColorMine website (http://colormine.org/convert/rgb-to-yxy). The x and y coordinates were analyzed using one-way ANOVA and Tukey post hoc tests. Tables 8.22 and 8.23 shows the results of the statistical analysis on the effect of various exposure times for a 250 mL sample with an anti-prothrombin concentration of 0.0025 mg/mL with no stirring and with continuous stirring (low turbulence) on the surface colour of the prothrombin-coated wafer based on x and y chromaticity coordinates, respetively. The x and y coordinates at each anti-prothrombin (AP) concentration were compared to the prothrombin (II) control, and a p value less than 0.05 indicates statistical significance.

Table 8.22. Results of the ANOVA and Tukey post hoc statistical analysis tests on the effect of various anti-prothrombin exposure times for a 250 mL volume at a concentration of 0.0025 mg/mL with no stirring on the surface colour using x and y chromaticity coordinates compared to the prothrombin only control. Statistically significant results are in italics. (n = 3).

Prothrombin (II) control	**Vs. II + AP 0.0025 mg/mL, no stirring (exposure time)**	**Difference detectable by eye vs. control?**	**x coordinate + p values**	**y coordinate + p values**
1 mg/mL II control x = 0.43 ± 0.02 y = 0.29 ± 0.01	5 minutes	No	x = 0.42 ± 0.03 p > 0.9	y = 0.27 ± 0.01 p > 0.3
	10 minutes	No	x = 0.41 ± 0.01 p > 0.8	y = 0.26 ± 0.00 *p = 0.015*
	20 minutes	Yes	x = 0.39 ± 0.02 p > 0.05	y = 0.23 ± 0.00 *p < 0.001*
	40 minutes	Yes	x = 0.37 ± 0.01 *p = 0.01*	y = 0.21 ± 0.01 *p < 0.001*

Table 8.23. Results of the ANOVA and Tukey post hoc statistical analysis tests on the effect of various anti-prothrombin exposure times for a 250 mL volume at a concentration of 0.0025 mg/mL with continuous stirring at ~ 195 RPM on the surface colour using x and y chromaticity coordinates compared to the prothrombin only control. Statistically significant results are in italics. (n = 3).

Prothrombin (II) control	**Vs. II + AP 0.0025 mg/mL, stirring at ~ 195 RPM (exposure time)**	**Difference detectable by eye vs. control?**	**x coordinate + p values**	**y coordinate + p values**
1 mg/mL II control x = 0.39 ± 0.01 y = 0.25 ± 0.01	5 minutes	Yes	x = 0.35 ± 0.01 *p = 0.001*	y = 0.19 ± 0.01 *p < 0.001*
	10 minutes	Yes	x = 0.30 ± 0.02 *p < 0.001*	y = 0.16 ± 0.01 *p < 0.001*
	20 minutes	Yes	x = 0.28 ± 0.00 *p < 0.001*	y = 0.17 ± 0.00 *p < 0.001*
	40 minutes	Yes	x = 0.24 ± 0.00 *p < 0.001*	y = 0.12 ± 0.00 *p < 0.001*

The results of the statistical analysis for the no stirring experiments (Table 8.22) indicate statistical significance in the x coordinate only after exposure to 250 mL of 0.0025 mg/mL anti-prothrombin for 40 minutes, compared to the prothrombin only control. No statistical significance was observed for the x coordinate after 5, 10 or 20 minutes. For the y coordinate, statistical significance was observed after 10 minutes, 20 minutes and 40 minutes compared to the prothrombin only control. No statistical significance was observed for the y coordinate after 5 minutes. By visual observation, a slight colour shift to a darker pink can be seen on the surface after 20 minutes and 40 minutes compared to the prothrombin only control surface (light pink). No visible colour shift was observed after 5 minutes or 10 minutes.

The results of the statistical analysis for the low turbulence mixing experiments (stirring at ~ 195 RPM) (Table 8.23) indicate statistical significance in both the x and y coordinate after exposure to 250 mL of 0.0025 mg/mL anti-prothrombin for 5, 10, 20 and 40 minutes, compared to the prothrombin only control. By visual observation, a colour shift from light pink to dark pink occurred after exposure to the anti-prothrombin solution for 5 minutes with continuous stirring. After 10, 20 and 40 minutes, a clear colour shift to purple can be seen, indicating formation of the antigen-antibody complex on the surface.

The next set of experiments was conducted to assess several variables on the resulting colour shift: time, sample volume, shear/mixing, and anti-prothrombin concentration. The colour shift after exposure to large volumes of anti-prothrombin solution was assessed after 5 minutes, 10 minutes, 20 minutes, and 40 minutes for each experiment, except for the high turbulence condition with an impeller speed of ~ 360 RPM, as the colour shift was clear after 20 minutes in this case. The sample volumes studied were 100 mL and 500 mL solutions of anti-prothrombin diluted in MilliQ water. Shear/mixing was assessed by varying the impeller speed: the laminar condition was assessed when there was no stirring, the low turbulence condition was assessed when the impeller power was set to ~ 13 (regular stirring ~ 195 RPM), and the high turbulence condition was assessed when the impeller power was set to ~ 18 (increased stirring ~ 360 RPM). Anti-prothrombin concentrations of 0.005 mg/mL, 0.0025 mg/mL, and 0.00125 mg/mL were assessed. The Reynolds number for each stir speed was calculated using the impeller Reynolds number equation (Equation 2-3) shown in Chapter 2. The impeller diameter (D_i) was measured to be 3.5 cm (0.035 m), the density of water at 21°C, 997.9 kg/m^3, was used as the fluid density (ρ), the dynamic viscosity of water at 21°C, 0.000976 Pa·s, was used as the fluid viscosity (μ), and 3.25 RPS (195 RPM) and 6 RPS (360 RPM) were used as the stirrer speeds (N_i) ([10], [11]).

The impeller Reynolds numbers, Re_i, were calculated to be ~ 4071 and ~ 7515 for impeller speeds of 195 RPM (low turbulence) and 360 RPM (high turbulence), respectively. The variables assessed are summarized in Table 8.24, and experiments were conducted for each combination of variables in triplicate.

Table 8.24. Methods table for subsequent experiments to assess impact of anti-prothrombin concentration, exposure time, sample volume, and shear/mixing.

Sample Volume	**Mixing Condition**	**Anti-prothrombin concentration (mg/mL)**	**Time (minutes)**
100 mL	Laminar (no mixing)	0.005	5, 10, 20, 40
		0.0025	5, 10, 20, 40
		0.00125	5, 10, 20, 40
	Low turbulence (mixing at ~ 195 RPM)	0.005	5, 10, 20, 40
		0.0025	5, 10, 20, 40
		0.00125	5, 10, 20, 40
	High turbulence (mixing at ~ 360 RPM)	0.005	5, 10, 20
		0.0025	5, 10, 20
		0.00125	5, 10, 20
500 mL	Laminar (no mixing)	0.005	5, 10, 20, 40
		0.0025	5, 10, 20, 40
		0.00125	5, 10, 20, 40
	Low turbulence (mixing at ~ 195 RPM)	0.005	5, 10, 20, 40
		0.0025	5, 10, 20, 40
		0.00125	5, 10, 20, 40
	High turbulence (mixing at ~ 360 RPM)	0.005	5, 10, 20
		0.0025	5, 10, 20
		0.00125	5, 10, 20

In all experiments, silicon wafer substrates were coated with ~ 200 nm of tantalum and between 107 nm and 111 nm of aluminum then anodized at 4 V and cut using the diamond scribe and the stencil. The silicon wafer slides were then further cut into smaller squares with dimensions of ~ 1 cm by ~ 1.2 cm. A Sharpie was used to trace the edges of the rectangles to contain the protein solutions. Then, the surfaces were completely exposed to 1 mg/mL prothrombin for 20 minutes by pipetting a 35 or 40 μL solution, depending on the size of the rectangle, onto the rectangle and spreading the solution to the edges using a pipette tip. The silicon wafer rectangles were then left in a Petri dish with a wet paper towel for 20 minutes. After exposure to prothrombin, the wafers were rinsed with deionized water and dried with oil free compressed air. The prothrombin coated wafers were then placed in the bottom of a 250 mL beaker (for the 100 mL samples) or a 1 L beaker (for the 500 mL samples). The smaller beaker was used for the smaller volume experiments to ensure that the impeller could be fully submerged in the solution for the duration of the experiments. Three experiments were run for each volume and each anti-prothrombin concentration to assess the impact of time and the impact of impeller speed. In the first experiment, the solution was not stirred (laminar condition) and images were taken of the slides after 5 minutes, 10 minutes, 20 minutes, and 40 minutes (completed in triplicate). Figures 8.72, 8.73 and 8.74 show the three replicates prior to protein exposure (row 1), after exposure of each rectangle to 35 or 40 μL of 1 mg/mL prothrombin for 20 minutes (row 2), and after exposure of each rectangle to 100 mL with no stirring after 5 minutes, 10 minutes, 20 minutes, and 40 minutes (rows 3, 4, 5, 6), at anti-prothrombin concentrations of 0.005 mg/mL, 0.0025 mg/mL and 0.00125 mg/mL, respectively. Figures 8.75, 8.76 and 8.77 show the three replicates prior to protein exposure (row 1), after exposure of each rectangle to 35 or 40 μL of 1 mg/mL prothrombin for 20 minutes (row 2), and after exposure of

each rectangle to 500 mL with no stirring after 5 minutes, 10 minutes, 20 minutes, and 40 minutes (rows 3, 4, 5, 6), at anti-prothrombin concentrations of 0.005 mg/mL, 0.0025 mg/mL and 0.00125 mg/mL, respectively. Statistical analysis was completed on the three replicates for each experiment to determine the effect of various exposure times, volumes, and anti-prothrombin concentrations on the surface colour of the prothrombin coated wafer with no stirring (laminar condition). For each set of wafers, an area in the coloured circle was selected and analyzed using ImageJ to determine the RGB coordinates. The average RGB coordinates were taken for each of the three samples for the prothrombin only circle and for each anti-prothrombin concentration. The RGB coordinates were converted to Yxy colour coordinates using the ColorMine website (http://colormine.org/convert/rgb-to-yxy). To determine if variances were equal between groups, a Levene's homogeneity of variances test was used. The x and y coordinates were analyzed using one-way ANOVA and Tukey post hoc tests when variances were equal, and a Welch's t-test and Games-Howell post hoc test was used when variances were unequal. Tables 8.25, 8.26 and 8.27 shows the results of the statistical analysis on the effect of various exposure times for a 100 mL sample with no stirring at anti-prothrombin concentrations of 0.005 mg/mL, 0.0025 mg/mL and 0.00125 mg/mL on the surface colour of the prothrombin-coated wafer based on x and y chromaticity coordinates, respectively. Tables 8.28, 8.29 and 8.30 show the results of the statistical analysis on the effect of various exposure times for a 500 mL sample with no stirring at anti-prothrombin concentrations of 0.005 mg/mL, 0.0025 mg/mL and 0.00125 mg/mL on the surface colour of the prothrombin-coated wafer based on x and y chromaticity coordinates, respectively. The x and y coordinates at each anti-prothrombin (AP) concentration were compared to the prothrombin (II) control, and a p value less than 0.05 indicates statistical significance.



Figure 8.72. Silicon wafer rectangles (three replicates – ~ 1 cm by ~ 1.2 cm each) coated with ~ 200 nm of tantalum and ~ 108 nm of aluminum then anodized at 4 V with no exposure to protein (row 1), after exposure of each rectangle to 40 μL of 1 mg/mL prothrombin for 20 minutes (row 2), after subsequent exposure of each rectangle to 100 mL of 0.005 mg/mL anti-prothrombin for 5, 10, 20 and 40 minutes with no stirring (rows 3, 4, 5, 6).



Figure 8.73. Silicon wafer rectangles (three replicates – ~ 1 cm by ~ 1.2 cm each) coated with ~ 200 nm of tantalum and ~ 108 nm of aluminum then anodized at 4 V with no exposure to protein (row 1), after exposure of each rectangle to 35 μL of 1 mg/mL prothrombin for 20 minutes (row 2), after subsequent exposure of each rectangle to 100 mL of 0.0025 mg/mL anti-prothrombin for 5, 10, 20 and 40 minutes with no stirring (rows 3, 4, 5, 6).



Figure 8.74. Silicon wafer rectangles (three replicates – ~ 1 cm by ~ 1.2 cm each) coated with ~ 200 nm of tantalum and ~ 107 nm of aluminum then anodized at 4 V with no exposure to protein (row 1), after exposure of each rectangle to 35 μL of 1 mg/mL prothrombin for 20 minutes (row 2), after subsequent exposure of each rectangle to 100 mL of 0.00125 mg/mL anti-prothrombin for 5, 10, 20 and 40 minutes with no stirring (rows 3, 4, 5, 6).

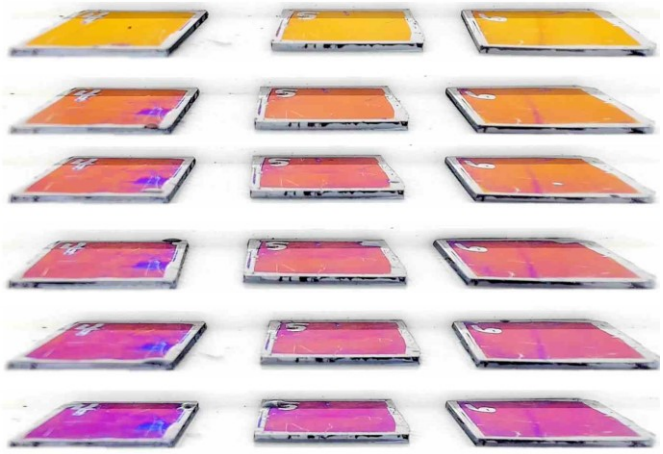


Figure 8.75. Silicon wafer rectangles (three replicates – ~ 1 cm by ~ 1.2 cm each) coated with ~ 200 nm of tantalum and ~ 107 nm of aluminum then anodized at 4 V with no exposure to protein (row 1), after exposure of each rectangle to 35 μL of 1 mg/mL prothrombin for 20 minutes (row 2), after subsequent exposure of each rectangle to 500 mL of 0.005 mg/mL anti-prothrombin for 5, 10, 20 and 40 minutes with no stirring (rows 3, 4, 5, 6).



Figure 8.76. Silicon wafer rectangles (three replicates – ~ 1 cm by ~ 1.2 cm each) coated with ~ 200 nm of tantalum and ~ 108 nm of aluminum then anodized at 4 V with no exposure to protein (row 1), after exposure of each rectangle to 35 μL of 1 mg/mL prothrombin for 20 minutes (row 2), after subsequent exposure of each rectangle to 500 mL of 0.0025 mg/mL anti-prothrombin for 5, 10, 20 and 40 minutes with no stirring (rows 3, 4, 5, 6).



Figure 8.77. Silicon wafer rectangles (three replicates – ~ 1 cm by ~ 1.2 cm each) coated with ~ 200 nm of tantalum and ~ 107 nm of aluminum then anodized at 4 V with no exposure to protein (row 1), after exposure of each rectangle to 35 μL of 1 mg/mL prothrombin for 20 minutes (row 2), after subsequent exposure of each rectangle to 500 mL of 0.00125 mg/mL anti-prothrombin for 5, 10, 20 and 40 minutes with no stirring (rows 3, 4, 5, 6).

Table 8.25. Results of the ANOVA and Tukey post hoc post hoc statistical analysis tests on the effect of various anti-prothrombin exposure times for a 100 mL volume at a concentration of 0.005 mg/mL with no stirring on the surface colour using x and y chromaticity coordinates compared to the prothrombin only control. Statistically significant results are in italics. (n = 3).

Prothrombin (II) control	**Vs. II + AP 0.005 mg/mL, 100 mL sample no stirring (exposure time)**	**Difference detectable by eye vs. control?**	**x coordinate + p values**	**y coordinate + p values**
1 mg/mL II control x = 0.46 ± 0.02 y = 0.33 ± 0.01	5 minutes	No	x = 0.42 ± 0.01 p > 0.05	y = 0.30 ± 0.01 *p = 0.004*
	10 minutes	Yes	x = 0.41 ± 0.01 *p < 0.05*	y = 0.28 ± 0.00 *p < 0.001*
	20 minutes	Yes	x = 0.39 ± 0.01 *p = 0.001*	y = 0.25 ± 0.01 *p < 0.001*
	40 minutes	Yes	x = 0.37 ± 0.00 *p < 0.001*	y = 0.24 ± 0.01 *p < 0.001*

Table 8.26. Results of the ANOVA and Tukey post hoc statistical analysis tests on the effect of various anti-prothrombin exposure times for a 100 mL volume at a concentration of 0.0025 mg/mL with no stirring on the surface colour using x and y chromaticity coordinates compared to the prothrombin only control. Statistically significant results are in italics. (n = 3).

Prothrombin (II) control	**Vs. II + AP 0.0025 mg/mL, 100 mL sample no stirring (exposure time)**	**Difference detectable by eye vs. control?**	**x coordinate + p values**	**y coordinate + p values**
1 mg/mL II control x = 0.43 ± 0.01 y = 0.28 ± 0.01	5 minutes	No	x = 0.43 ± 0.01 p > 0.8	y = 0.28 ± 0.01 p > 0.9
	10 minutes	No	x = 0.41 ± 0.01 p > 0.05	y = 0.25 ± 0.01 *p = 0.005*
	20 minutes	Yes	x = 0.38 ± 0.00 *p < 0.001*	y = 0.22 ± 0.01 *p < 0.001*
	40 minutes	Yes	x = 0.36 ± 0.00 *p < 0.001*	y = 0.21 ± 0.01 *p < 0.001*

Table 8.27. Results of the ANOVA and Tukey post hoc statistical analysis tests on the effect of various anti-prothrombin exposure times for a 100 mL volume at a concentration of 0.00125 mg/mL with no stirring on the surface colour using x and y chromaticity coordinates compared to the prothrombin only control. Statistically significant results are in italics. (n = 3).

Prothrombin (II) control	**Vs. II + AP 0.00125 mg/mL, 100 mL sample no stirring (exposure time)**	**Difference detectable by eye vs. control?**	**x coordinate + p values**	**y coordinate + p values**
1 mg/mL II control x = 0.48 ± 0.01 y = 0.42 ± 0.01	5 minutes	No	x = 0.49 ± 0.02 p > 0.9	y = 0.41 ± 0.00 p > 0.8
	10 minutes	No	x = 0.48 ± 0.01 p > 0.9	y = 0.40 ± 0.01 p > 0.6
	20 minutes	No	x = 0.48 ± 0.01 p > 0.9	y = 0.39 ± 0.02 p > 0.1
	40 minutes	No	x = 0.47 ± 0.01 p > 0.8	y = 0.38 ± 0.02 *p < 0.05*

Table 8.28. Results of the ANOVA and Tukey post hoc statistical analysis tests on the effect of various anti-prothrombin exposure times for a 500 mL volume at a concentration of 0.005 mg/mL with no stirring on the surface colour using x and y chromaticity coordinates compared to the prothrombin only control. Statistically significant results are in italics. (n = 3).

Prothrombin (II) control	**Vs. II + AP 0.005 mg/mL, 500 mL sample no stirring (exposure time)**	**Difference detectable by eye vs. control?**	**x coordinate + p values**	**y coordinate + p values**
1 mg/mL II control x = 0.48 ± 0.01 y = 0.39 ± 0.02	5 minutes	No	x = 0.46 ± 0.02 p > 0.8	y = 0.36 ± 0.03 p > 0.5
	10 minutes	Yes	x = 0.43 ± 0.01 p > 0.05	y = 0.31 ± 0.02 *p < 0.05*
	20 minutes	Yes	x = 0.40 ± 0.01 *p < 0.005*	y = 0.27 ± 0.03 *p < 0.005*
	40 minutes	Yes	x = 0.36 ± 0.03 *p < 0.001*	y = 0.22 ± 0.04 *p < 0.001*

Table 8.29. Results of the ANOVA and Tukey post hoc statistical analysis tests on the effect of various anti-prothrombin exposure times for a 500 mL volume at a concentration of 0.0025 mg/mL with no stirring on the surface colour using x and y chromaticity coordinates compared to the prothrombin only control. Statistically significant results are in italics. (n = 3).

Prothrombin (II) control	**Vs. II + AP 0.0025 mg/mL, 500 mL sample no stirring (exposure time)**	**Difference detectable by eye vs. control?**	**x coordinate + p values**	**y coordinate + p values**
1 mg/mL II control x = 0.43 ± 0.04 y = 0.29 ± 0.01	5 minutes	No	x = 0.41 ± 0.04 p > 0.9	y = 0.26 ± 0.01 p > 0.09
	10 minutes	Yes	x = 0.39 ± 0.03 p > 0.5	y = 0.23 ± 0.01 *p < 0.05*
	20 minutes	Yes	x = 0.37 ± 0.03 p > 0.1	y = 0.21 ± 0.01 *p < 0.001*
	40 minutes	Yes	x = 0.35 ± 0.02 p > 0.05	y = 0.19 ± 0.01 *p < 0.001*

Table 8.30. Results of the ANOVA and Tukey post hoc statistical analysis tests on the effect of various anti-prothrombin exposure times for a 500 mL volume at a concentration of 0.00125 mg/mL with no stirring on the surface colour using x and y chromaticity coordinates compared to the prothrombin only control. Statistically significant results are in italics. (n = 3).

Prothrombin (II) control	**Vs. II + AP 0.00125 mg/mL, 500 mL sample no stirring (exposure time)**	**Difference detectable by eye vs. control?**	**x coordinate + p values**	**y coordinate + p values**
1 mg/mL II control x = 0.48 ± 0.01 y = 0.43 ± 0.04	5 minutes	No	x = 0.48 ± 0.03 p > 0.9	y = 0.41 ± 0.05 p > 0.9
	10 minutes	No	x = 0.47 ± 0.03 p > 0.9	y = 0.39 ± 0.05 p > 0.9
	20 minutes	No	x = 0.46 ± 0.04 p > 0.9	y = 0.38 ± 0.06 p > 0.8
	40 minutes	No	x = 0.46 ± 0.04 p > 0.8	y = 0.37 ± 0.06 p > 0.6

For the 100 mL no stirring (laminar condition) experiments, there was a visible colour shift for an anti-prothrombin concentration of 0.005 mg/mL after 10 minutes, 20 minutes and 40 minutes. The x chromaticity coordinate was statistically significant compared to the prothrombin only control for exposure times of 10 minutes, 20 minutes and 40 minutes, and the y chromaticity coordinate was statistically significant compared to the prothrombin only control for all exposure times (5, 10, 20 and 40 minutes) at a concentration of 0.005 mg/mL. For an anti-prothrombin concentration of 0.0025 mg/mL, there was a visible colour shift after 20 minutes and 40 minutes. Compared to the prothrombin only control, the x chromaticity coordinate was statistically significant after 20 minutes and 40 minutes, and the y chromaticity coordinate was statistically significant after 10, 20 and 40 minutes for a concentration of 0.0025 mg/mL. For an anti-prothrombin concentration of 0.00125 mg/mL, no visible colour shift occurred after any time interval (5, 10, 20 or 40 minutes). No statistical significance was found for the x chromaticity coordinate after any time interval, and the y coordinate was only statistically significant compared to the prothrombin only control after 40 minutes for concentration of 0.00125 mg/mL. For the 500 mL no stirring (laminar condition) experiments, there was a visible colour shift for an anti-prothrombin concentration of 0.005 mg/mL after 10, 20 and 40 minutes. The x chromaticity coordinate was statistically significant after 20 and 40 minutes of exposure, and the y chromaticity coordinate was statistically significant after 10, 20 and 40 minutes compared to the prothrombin only control. For a concentration of 0.0025 mg/mL (500 mL), a visible colour shift occurred after exposure for 20 minutes and 40 minutes. No statistical significance was observed for the x chromaticity coordinate after any time interval, but the y chromaticity coordinate was statistically significant after 10, 20 and 40 minutes of exposure. For a concentration of 0.00125 mg/mL (500 mL), no visible colour shift was detected after any time

interval and neither the x nor y coordinate was statistically significant compared to the prothrombin only control after any time interval.

For the stirred experiments, the silicon wafer rectangles were attached to tantalum discs using double sided tape, and the solution was stirred continuously over the silicon wafer rectangles at the regular stir speed of 195 RPM (impeller power set to ~ 13) to assess the low turbulence condition. To assess the impact of time, images were taken after 5 minutes, 10 minutes, 20 minutes, and 40 minutes (completed in triplicate). Figures 8.78, 8.79 and 8.80 show the three replicates prior to protein exposure (row 1), after exposure of each rectangle to 35 or 40 μL of 1 mg/mL prothrombin for 20 minutes (row 2), and after exposure of each rectangle to 100 mL with continuous stirring at the regular impeller speed of 195 RPM (low turbulence) after 5 minutes, 10 minutes, 20 minutes, and 40 minutes (rows 3, 4, 5, 6), at anti-prothrombin concentrations of 0.005 mg/mL, 0.0025 mg/mL and 0.00125 mg/mL, respectively. Figures 8.81, 8.82 and 8.83 show the three replicates prior to protein exposure (row 1), after exposure of each rectangle to 35 or 40 μL of 1 mg/mL prothrombin for 20 minutes (row 2), and after exposure of each rectangle to 500 mL with continuous stirring at the regular impeller speed of 195 RPM (low turbulence) after 5 minutes, 10 minutes, 20 minutes, and 40 minutes (rows 3, 4, 5, 6), at anti-prothrombin concentrations of 0.005 mg/mL, 0.0025 mg/mL and 0.00125 mg/mL, respectively. Statistical analysis was completed on the three replicates for each experiment to determine the effect of various exposure times, volumes, and anti-prothrombin concentrations on the surface colour of the prothrombin coated wafer with stirring at the regular impeller speed of ~ 195 RPM (low turbulence condition). The x and y coordinates were analyzed using one-way ANOVA and Tukey post hoc tests when variances were equal, and a Welch's t-test and Games-Howell post hoc test when variances were unequal. Tables 8.31, 8.32 and 8.33 shows the results of the

statistical analysis on the effect of various exposure times for a 100 mL sample with stirring at 195 RPM at anti-prothrombin concentrations of 0.005 mg/mL, 0.0025 mg/mL and 0.00125 mg/mL on the surface colour of the prothrombin-coated wafer based on x and y chromaticity coordinates, respectively. Tables 8.34, 8.35 and 8.36 show the results of the statistical analysis on the effect of various exposure times for a 500 mL sample with stirring at 195 RPM at anti-prothrombin concentrations of 0.005 mg/mL, 0.0025 mg/mL and 0.00125 mg/mL on the surface colour of the prothrombin-coated wafer based on x and y chromaticity coordinates, respectively. The x and y coordinates at each anti-prothrombin (AP) concentration were compared to the prothrombin (II) control, and a p value less than 0.05 indicates statistical significance.



Figure 8.78. Silicon wafer rectangles (three replicates – ~ 1 cm by ~ 1.2 cm each) coated with ~ 200 nm of tantalum and ~ 107 nm of aluminum then anodized at 4 V with no exposure to protein (row 1), after exposure of each rectangle to 35 µL of 1 mg/mL prothrombin for 20 minutes (row 2), after subsequent exposure of each rectangle to 100 mL of 0.005 mg/mL anti-prothrombin for 5, 10, 20 and 40 minutes with continuous stirring at the regular impeller speed of 195 RPM (rows 3, 4, 5, 6).



Figure 8.79. Silicon wafer rectangles (three replicates – ~ 1 cm by ~ 1.2 cm each) coated with ~ 200 nm of tantalum and ~ 108 nm of aluminum then anodized at 4 V with no exposure to protein (row 1), after exposure of each rectangle to 35 μL of 1 mg/mL prothrombin for 20 minutes (row 2), after subsequent exposure of each rectangle to 100 mL of 0.0025 mg/mL anti-prothrombin for 5, 10, 20 and 40 minutes with continuous stirring at the regular impeller speed of 195 RPM (rows 3, 4, 5, 6).



Figure 8.80. Silicon wafer rectangles (three replicates – ~ 1 cm by ~ 1.2 cm each) coated with ~ 200 nm of tantalum and ~ 108 nm of aluminum then anodized at 4 V with no exposure to protein (row 1), after exposure of each rectangle to 40 μL of 1 mg/mL prothrombin for 20 minutes (row 2), after subsequent exposure of each rectangle to 100 mL of 0.00125 mg/mL anti-prothrombin for 5, 10, 20 and 40 minutes with continuous stirring at the regular impeller speed of 195 RPM (rows 3, 4, 5, 6).



Figure 8.81. Silicon wafer rectangles (three replicates – ~ 1 cm by ~ 1.2 cm each) coated with ~ 200 nm of tantalum and ~ 111 nm of aluminum then anodized at 4 V with no exposure to protein (row 1), after exposure of each rectangle to 35 μL of 1 mg/mL prothrombin for 20 minutes (row 2), after subsequent exposure of each rectangle to 500 mL of 0.005 mg/mL anti-prothrombin for 5, 10, 20 and 40 minutes with continuous stirring at the regular impeller speed of 195 RPM (rows 3, 4, 5, 6).



Figure 8.82. Silicon wafer rectangles (three replicates – ~ 1 cm by ~ 1.2 cm each) coated with ~ 200 nm of tantalum and ~ 109 nm of aluminum then anodized at 4 V with no exposure to protein (row 1), after exposure of each rectangle to 35 μL of 1 mg/mL prothrombin for 20 minutes (row 2), after subsequent exposure of each rectangle to 500 mL of 0.0025 mg/mL anti-prothrombin for 5, 10, 20 and 40 minutes with continuous stirring at the regular impeller speed of 195 RPM (rows 3, 4, 5, 6).

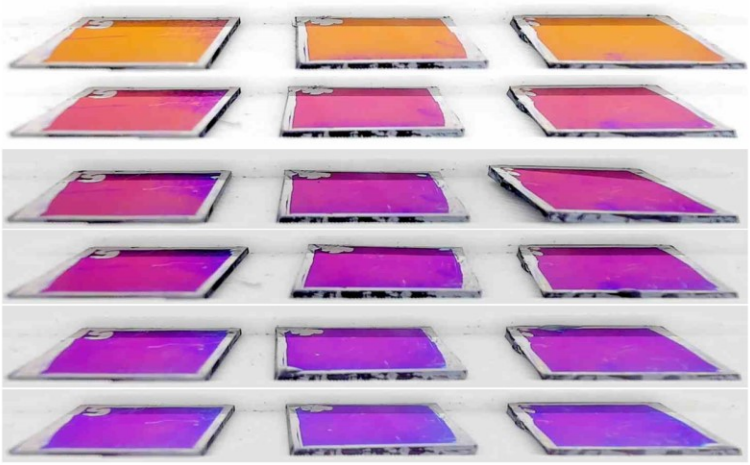


Figure 8.83. Silicon wafer rectangles (three replicates – ~ 1 cm by ~ 1.2 cm each) coated with ~ 200 nm of tantalum and ~ 111 nm of aluminum then anodized at 4 V with no exposure to protein (row 1), after exposure of each rectangle to 40 μL of 1 mg/mL prothrombin for 20 minutes (row 2), after subsequent exposure of each rectangle to 500 mL of 0.00125 mg/mL anti-prothrombin for 5, 10, 20 and 40 minutes with continuous stirring at the regular impeller speed of 195 RPM (rows 3, 4, 5, 6).

Table 8.31. Results of the ANOVA and Tukey post hoc statistical analysis tests on the effect of various anti-prothrombin exposure times for a 100 mL volume at a concentration of 0.005 mg/mL with stirring at 195 RPM on the surface colour using x and y chromaticity coordinates compared to the prothrombin only control. Statistically significant results are in italics. (n = 3).

Prothrombin (II) control	**Vs. II + AP 0.005 mg/mL, 100 mL, 195 RPM (exposure time)**	**Difference detectable by eye vs. control?**	**x coordinate + p values**	**y coordinate + p values**
1 mg/mL II control x = 0.49 ± 0.02 y = 0.40 ± 0.01	5 minutes	Yes	x = 0.44 ± 0.02 p > 0.1	y = 0.32 ± 0.02 *p = 0.06*
	10 minutes	Yes	x = 0.40 ± 0.02 *p < 0.005*	y = 0.26 ± 0.02 *p < 0.001*
	20 minutes	Yes	x = 0.33 ± 0.02 *p < 0.001*	y = 0.19 ± 0.03 *p < 0.001*
	40 minutes	Yes	x = 0.31 ± 0.02 *p < 0.001*	y = 0.18 ± 0.02 *p < 0.001*

Table 8.32. Results of the ANOVA and Tukey post hoc statistical analysis tests on the effect of various anti-prothrombin exposure times for a 100 mL volume at a concentration of 0.0025 mg/mL with stirring at 195 RPM on the surface colour using x and y chromaticity coordinates compared to the prothrombin only control. Statistically significant results are in italics. (n = 3).

Prothrombin (II) control	**Vs. II + AP 0.0025 mg/mL, 100 mL, 195 RPM (exposure time)**	**Difference detectable by eye vs. control?**	**x coordinate + p values**	**y coordinate + p values**
1 mg/mL II control x = 0.43 ± 0.03 y = 0.29 ± 0.01	5 minutes	Yes	x = 0.40 ± 0.02 p > 0.3	y = 0.24 ± 0.01 *p < 0.001*
	10 minutes	Yes	x = 0.37 ± 0.02 *p < 0.05*	y = 0.20 ± 0.01 *p < 0.001*
	20 minutes	Yes	x = 0.33 ± 0.01 *p < 0.001*	y = 0.18 ± 0.01 *p < 0.001*
	40 minutes	Yes	x = 0.31 ± 0.01 *p < 0.001*	y = 0.16 ± 0.00 *p < 0.001*

Table 8.33. Results of the Welch's t-test and Games-Howell post hoc statistical analysis tests on the effect of various anti-prothrombin exposure times for a 100 mL volume at a concentration of 0.00125 mg/mL with stirring at 195 RPM on the surface colour using x and y chromaticity coordinates compared to the prothrombin only control. Statistically significant results are in italics. (n = 3).

Prothrombin (II) control	**Vs. II + AP 0.00125 mg/mL, 100 mL, 195 RPM (exposure time)**	**Difference detectable by eye vs. control?**	**x coordinate + p values**	**y coordinate + p values**
1 mg/mL II control x = 0.47 ± 0.02 y = 0.33 ± 0.02	5 minutes	No	x = 0.45 ± 0.01 p > 0.8	y = 0.31 ± 0.01 p > 0.4
	10 minutes	No	x = 0.44 ± 0.01 p > 0.4	y = 0.30 ± 0.01 p > 0.2
	20 minutes	No	x = 0.43 ± 0.01 p > 0.2	y = 0.29 ± 0.00 p > 0.1
	40 minutes	No	x = 0.43 ± 0.01 p > 0.2	y = 0.29 ± 0.01 p > 0.05

Table 8.34. Results of the ANOVA and Tukey post hoc statistical analysis tests on the effect of various anti-prothrombin exposure times for a 500 mL volume at a concentration of 0.005 mg/mL with stirring at 195 RPM on the surface colour using x and y chromaticity coordinates compared to the prothrombin only control. Statistically significant results are in italics. (n = 3).

Prothrombin (II) control	**Vs. II + AP 0.005 mg/mL, 500 mL, 195 RPM (exposure time)**	**Difference detectable by eye vs. control?**	**x coordinate + p values**	**y coordinate + p values**
1 mg/mL II control x = 0.40 ± 0.02 y = 0.26 ± 0.02	5 minutes	Yes	x = 0.36 ± 0.03 p > 0.1	y = 0.21 ± 0.02 *p < 0.01*
	10 minutes	Yes	x = 0.31 ± 0.02 *p < 0.001*	y = 0.17 ± 0.02 *p < 0.001*
	20 minutes	Yes	x = 0.26 ± 0.00 *p < 0.001*	y = 0.14 ± 0.01 *p < 0.001*
	40 minutes	Yes	x = 0.20 ± 0.01 *p < 0.001*	y = 0.11 ± 0.01 *p < 0.001*

Table 8.35. Results of the ANOVA and Tukey post hoc statistical analysis tests on the effect of various anti-prothrombin exposure times for a 500 mL volume at a concentration of 0.0025 mg/mL with stirring at 195 RPM on the surface colour using x and y chromaticity coordinates compared to the prothrombin only control. Statistically significant results are in italics. (n = 3).

Prothrombin (II) control	**Vs. II + AP 0.0025 mg/mL, 500 mL, 195 RPM (exposure time)**	**Difference detectable by eye vs. control?**	**x coordinate + p values**	**y coordinate + p values**
1 mg/mL II control x = 0.43 ± 0.02 y = 0.27 ± 0.01	5 minutes	Yes	x = 0.39 ± 0.01 *p < 0.05*	y = 0.24 ± 0.02 *p < 0.01*
	10 minutes	Yes	x = 0.35 ± 0.01 *p < 0.001*	y = 0.19 ± 0.00 *p < 0.001*
	20 minutes	Yes	x = 0.31 ± 0.01 *p < 0.001*	y = 0.17 ± 0.00 *p < 0.001*
	40 minutes	Yes	x = 0.28 ± 0.01 *p < 0.001*	y = 0.14 ± 0.00 *p < 0.001*

Table 8.36. Results of the ANOVA and Tukey post hoc statistical analysis tests on the effect of various anti-prothrombin exposure times for a 500 mL volume at a concentration of 0.00125 mg/mL with stirring at 195 RPM on the surface colour using x and y chromaticity coordinates compared to the prothrombin only control. Statistically significant results are in italics. (n = 3).

Prothrombin (II) control	**Vs. II + AP 0.00125 mg/mL, 500 mL, 195 RPM (exposure time)**	**Difference detectable by eye vs. control?**	**x coordinate + p values**	**y coordinate + p values**
1 mg/mL II control x = 0.42 ± 0.03 y = 0.29 ± 0.02	5 minutes	Yes	x = 0.39 ± 0.04 p > 0.4	y = 0.22 ± 0.03 *p = 0.005*
	10 minutes	Yes	x = 0.35 ± 0.03 *p < 0.05*	y = 0.18 ± 0.02 *p < 0.001*
	20 minutes	Yes	x = 0.30 ± 0.01 *p = 0.001*	y = 0.16 ± 0.01 *p < 0.001*
	40 minutes	Yes	x = 0.26 ± 0.01 *p < 0.001*	y = 0.15 ± 0.00 *p < 0.001*

For the 100 mL volume low turbulence condition with stirring at ~ 195 RPM, anti-prothrombin concentrations of 0.005 mg/mL and 0.0025 mg/mL yielded visible colour shifts after 5, 10, 20 and 40 minutes. The x chromaticity coordinate was statistically significant after 10, 20 and 40 minutes, and the y chromaticity coordinate was statistically significant at all time intervals (5, 10, 20, 40 minutes) compared to the prothrombin only control for both concentrations (0.005 mg/mL and 0.0025 mg/mL). For an anti-prothrombin concentration of 0.00125 mg/mL, no visible colour shift was detected at any time interval, and the x and y chromaticity coordinates were not statistically significant compared to the prothrombin only control at any time intervals. For the 500 mL volume low turbulence conditions with stirring at ~ 195 RPM, a visible colour shift was detected after 5, 10, 20 and 40 minutes for an anti-prothrombin concentration of 0.005 mg/mL. The x chromaticity coordinate was statistically significant after 10, 20 and 40 minutes, while the y chromaticity coordinate was statistically

significant after 5, 10, 20 and 40 minutes compared to the prothrombin only control. For a concentration of 0.0025 mg/mL, a visible colour shift was detected at each time interval, and both the x and y chromaticity coordinates were statistically significant at each time interval compared to the prothrombin only control. For a concentration of 0.00125 mg/mL, a visible colour shift was detected at each time interval. The x chromaticity coordinate was statistically significant after 10, 20 and 40 minutes, and the y chromaticity coordinate was statistically significant after each time interval (5, 10, 20, 40 minutes) compared to the prothrombin only control.

To assess the high turbulence condition, silicon wafer rectangles were attached to tantalum discs using double sided tape, and the solution was stirred continuously over the silicon wafer rectangles at an increased stir speed of ~ 360 RPM (impeller power set to ~ 18). To assess the impact of time, images were taken after 5 minutes, 10 minutes, and 20 minutes (completed in triplicate). The impact after 40 minutes was not studied, as it required a significant amount of power and there were clear colour shifts after 20 minutes in each case. Figures 8.84, 8.85 and 8.86 show the three replicates prior to protein exposure (row 1), after exposure of each rectangle to 35 or 40 μL of 1 mg/mL prothrombin for 20 minutes (row 2), and after exposure of each rectangle to 100 mL with continuous stirring at the increased impeller speed of ~ 360 RPM (high turbulence) after 5 minutes, 10 minutes, and 20 minutes, (rows 3, 4, 5), at anti-prothrombin concentrations of 0.005 mg/mL, 0.0025 mg/mL and 0.00125 mg/mL, respectively. Figures 8.87, 8.88 and 8.89 show the three replicates prior to protein exposure (row 1), after exposure of each rectangle to 35 μL of 1 mg/mL prothrombin for 20 minutes (row 2), and after exposure of each rectangle to 500 mL with continuous stirring at the increased impeller speed of ~ 360 RPM (high turbulence) after 5 minutes, 10 minutes, and 20 minutes (rows 3, 4, 5), at anti-prothrombin

concentrations of 0.005 mg/mL, 0.0025 mg/mL and 0.00125 mg/mL, respectively. Statistical analysis was completed on the three replicates for each experiment to determine the effect of various exposure times, volumes, and anti-prothrombin concentrations on the surface colour of the prothrombin coated wafer with stirring at the increased impeller speed of ~ 360 RPM (high turbulence condition). The x and y coordinates were analyzed using one-way ANOVA and Tukey post hoc tests when variances were equal, and a Welch's t-test and Games-Howell post hoc test when variances were unequal. Tables 8.37, 8.38 and 8.39 shows the results of the statistical analysis on the effect of various exposure times for a 100 mL sample with stirring at 360 RPM at anti-prothrombin concentrations of 0.005 mg/mL, 0.0025 mg/mL and 0.00125 mg/mL on the surface colour of the prothrombin-coated wafer based on x and y chromaticity coordinates, respectively. Tables 8.40, 8.41 and 8.42 show the results of the statistical analysis on the effect of various exposure times for a 500 mL sample with stirring at 360 RPM at anti-prothrombin concentrations of 0.005 mg/mL, 0.0025 mg/mL and 0.00125 mg/mL on the surface colour of the prothrombin-coated wafer based on x and y chromaticity coordinates, respectively. The x and y coordinates at each anti-prothrombin (AP) concentration were compared to the prothrombin (II) control, and a p value less than 0.05 indicates statistical significance.



Figure 8.84. Silicon wafer rectangles (three replicates – ~ 1 cm by ~ 1.2 cm each) coated with ~ 200 nm of tantalum and ~ 108 nm of aluminum then anodized at 4 V with no exposure to protein (row 1), after exposure of each rectangle to 40 µL of 1 mg/mL prothrombin for 20 minutes (row 2), after subsequent exposure of each rectangle to 100 mL of 0.005 mg/mL anti-prothrombin for 5, 10, and 20 minutes with continuous stirring at an increased impeller speed of 360 RPM (rows 3, 4, 5).

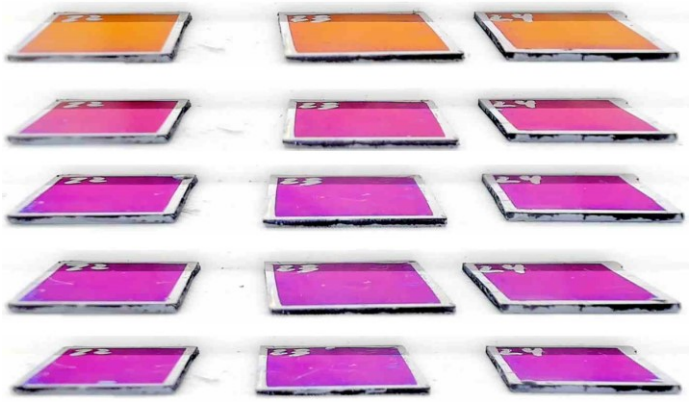


Figure 8.85. Silicon wafer rectangles (three replicates – ~ 1 cm by ~ 1.2 cm each) coated with ~ 200 nm of tantalum and ~ 111 nm of aluminum then anodized at 4 V with no exposure to protein (row 1), after exposure of each rectangle to 35 µL of 1 mg/mL prothrombin for 20 minutes (row 2), after subsequent exposure of each rectangle to 100 mL of 0.0025 mg/mL anti-prothrombin for 5, 10, and 20 minutes with continuous stirring at an increased impeller speed of 360 RPM (rows 3, 4, 5).

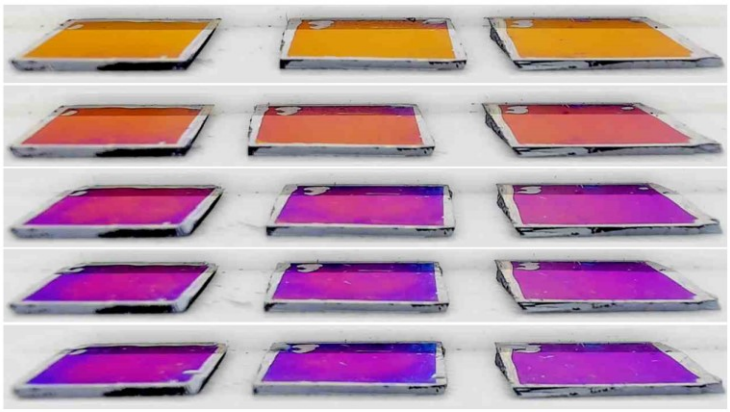


Figure 8.86. Silicon wafer rectangles (three replicates – ~ 1 cm by ~ 1.2 cm each) coated with ~ 200 nm of tantalum and ~ 111 nm of aluminum then anodized at 4 V with no exposure to protein (row 1), after exposure of each rectangle to 40 μL of 1 mg/mL prothrombin for 20 minutes (row 2), after subsequent exposure of each rectangle to 100 mL of 0.00125 mg/mL anti-prothrombin for 5, 10, and 20 minutes with continuous stirring at an increased impeller speed of 360 RPM (rows 3, 4, 5).



Figure 8.87. Silicon wafer rectangles (three replicates – ~ 1 cm by ~ 1.2 cm each) coated with ~ 200 nm of tantalum and ~ 111 nm of aluminum then anodized at 4 V with no exposure to protein (row 1), after exposure of each rectangle to 40 μL of 1 mg/mL prothrombin for 20 minutes (row 2), after subsequent exposure of each rectangle to 500 mL of 0.005 mg/mL anti-prothrombin for 5, 10, and 20 minutes with continuous stirring at an increased impeller speed of 360 RPM (rows 3, 4, 5).



Figure 8.88. Silicon wafer rectangles (three replicates – ~ 1 cm by ~ 1.2 cm each) coated with ~ 200 nm of tantalum and ~ 109 nm of aluminum then anodized at 4 V with no exposure to protein (row 1), after exposure of each rectangle to 35 µL of 1 mg/mL prothrombin for 20 minutes (row 2), after subsequent exposure of each rectangle to 500 mL of 0.0025 mg/mL anti-prothrombin for 5, 10, and 20 minutes with continuous stirring at an increased impeller speed of 360 RPM (rows 3, 4, 5).



Figure 8.89. Silicon wafer rectangles (three replicates – ~ 1 cm by ~ 1.2 cm each) coated with ~ 200 nm of tantalum and ~ 111 nm of aluminum then anodized at 4 V with no exposure to protein (row 1), after exposure of each rectangle to 40 µL of 1 mg/mL prothrombin for 20 minutes (row 2), after subsequent exposure of each rectangle to 500 mL of 0.00125 mg/mL anti-prothrombin for 5, 10, and 20 minutes with continuous stirring at an increased impeller speed of 360 RPM (rows 3, 4, 5).

Table 8.37. Results of the ANOVA and Tukey post hoc statistical analysis tests on the effect of various anti-prothrombin exposure times for a 100 mL volume at a concentration of 0.005 mg/mL with stirring at 360 RPM on the surface colour using x and y chromaticity coordinates compared to the prothrombin only control. Statistically significant results are in italics. (n = 3).

Prothrombin (II) control	**Vs. II + AP 0.005 mg/mL, 100 mL, 360 RPM (exposure time)**	**Difference detectable by eye vs. control?**	**x coordinate + p values**	**y coordinate + p values**
1 mg/mL II control x = 0.49 ± 0.03 y = 0.37 ± 0.03	5 minutes	Yes	x = 0.44 ± 0.04 p > 0.3	y = 0.29 ± 0.03 *p < 0.05*
	10 minutes	Yes	x = 0.39 ± 0.03 *p < 0.05*	y = 0.23 ± 0.02 *p < 0.001*
	20 minutes	Yes	x = 0.36 ± 0.03 *p < 0.01*	y = 0.22 ± 0.02 *p < 0.001*

Table 8.38. Results of the Welch's t-test and Game-Howell post hoc statistical analysis tests on the effect of various anti-prothrombin exposure times for a 100 mL volume at a concentration of 0.0025 mg/mL with stirring at 360 RPM on the surface colour using x and y chromaticity coordinates compared to the prothrombin only control. Statistically significant results are in italics. (n = 3).

Prothrombin (II) control	**Vs. II + AP 0.0025 mg/mL, 100 mL, 360 RPM (exposure time)**	**Difference detectable by eye vs. control?**	**x coordinate + p values**	**y coordinate + p values**
1 mg/mL II control x = 0.40 ± 0.01 y = 0.25 ± 0.01	5 minutes	Yes	x = 0.35 ± 0.01 *p < 0.01*	y = 0.20 ± 0.00 *p < 0.05*
	10 minutes	Yes	x = 0.35 ± 0.01 *p < 0.01*	y = 0.19 ± 0.01 *p < 0.01*
	20 minutes	Yes	x = 0.33 ± 0.01 *p < 0.01*	y = 0.18 ± 0.00 *p < 0.05*

Table 8.39. Results of the ANOVA and Tukey post hoc statistical analysis tests on the effect of various anti-prothrombin exposure times for a 100 mL volume at a concentration of 0.00125 mg/mL with stirring at 360 RPM on the surface colour using x and y chromaticity coordinates compared to the prothrombin only control. Statistically significant results are in italics. (n = 3).

Prothrombin (II) control	**Vs. II + AP 0.00125 mg/mL, 100 mL, 360 RPM (exposure time)**	**Difference detectable by eye vs. control?**	**x coordinate + p values**	**y coordinate + p values**
1 mg/mL II control x = 0.49 ± 0.03 y = 0.36 ± 0.02	5 minutes	Yes	x = 0.39 ± 0.06 *p < 0.05*	y = 0.22 ± 0.03 *p < 0.001*
	10 minutes	Yes	x = 0.34 ± 0.03 *p < 0.005*	y = 0.17 ± 0.01 *p < 0.001*
	20 minutes	Yes	x = 0.30 ± 0.03 *p < 0.001*	y = 0.15 ± 0.01 *p < 0.001*

Table 8.40. Results of the ANOVA and Tukey post hoc statistical analysis tests on the effect of various anti-prothrombin exposure times for a 500 mL volume at a concentration of 0.005 mg/mL with stirring at 360 RPM on the surface colour using x and y chromaticity coordinates compared to the prothrombin only control. Statistically significant results are in italics. (n = 3).

Prothrombin (II) control	**Vs. II + AP 0.005 mg/mL, 500 mL, 360 RPM (exposure time)**	**Difference detectable by eye vs. control?**	**x coordinate + p values**	**y coordinate + p values**
1 mg/mL II control x = 0.42 ± 0.01 y = 0.28 ± 0.01	5 minutes	Yes	x = 0.37 ± 0.01 *p < 0.005*	y = 0.20 ± 0.01 *p < 0.001*
	10 minutes	Yes	x = 0.34 ± 0.01 *p < 0.001*	y = 0.17 ± 0.01 *p < 0.001*
	20 minutes	Yes	x = 0.29 ± 0.00 *p < 0.001*	y = 0.15 ± 0.01 *p < 0.001*

Table 8.41. Results of the ANOVA and Tukey post hoc statistical analysis tests on the effect of various anti-prothrombin exposure times for a 500 mL volume at a concentration of 0.0025 mg/mL with stirring at 360 RPM on the surface colour using x and y chromaticity coordinates compared to the prothrombin only control. Statistically significant results are in italics. (n = 3).

Prothrombin (II) control	**Vs. II + AP 0.0025 mg/mL, 500 mL, 360 RPM (exposure time)**	**Difference detectable by eye vs. control?**	**x coordinate + p values**	**y coordinate + p values**
1 mg/mL II control x = 0.40 ± 0.01 y = 0.26 ± 0.00	5 minutes	Yes	x = 0.35 ± 0.01 *p < 0.001*	y = 0.19 ± 0.01 *p < 0.001*
	10 minutes	Yes	x = 0.33 ± 0.00 *p < 0.001*	y = 0.18 ± 0.01 *p < 0.001*
	20 minutes	Yes	x = 0.30 ± 0.01 *p < 0.001*	y = 0.16 ± 0.01 *p < 0.001*

Table 8.42. Results of the ANOVA and Tukey post hoc statistical analysis tests on the effect of various anti-prothrombin exposure times for a 500 mL volume at a concentration of 0.00125 mg/mL with stirring at 360 RPM on the surface colour using x and y chromaticity coordinates compared to the prothrombin only control. Statistically significant results are in italics. (n = 3).

Prothrombin (II) control	**Vs. II + AP 0.00125 mg/mL, 500 mL, 360 RPM (exposure time)**	**Difference detectable by eye vs. control?**	**x coordinate + p values**	**y coordinate + p values**
1 mg/mL II control x = 0.38 ± 0.01 y = 0.28 ± 0.00	5 minutes	No	x = 0.37 ± 0.01 p > 0.7	y = 0.25 ± 0.00 *p < 0.001*
	10 minutes	Yes	x = 0.36 ± 0.02 p > 0.05	y = 0.21 ± 0.00 *p < 0.001*
	20 minutes	Yes	x = 0.33 ± 0.01 *p < 0.005*	y = 0.19 ± 0.01 *p < 0.001*

For the 100 mL experiments at an increased impeller speed of ~ 360 RPM (high turbulence condition), anti-prothrombin concentrations of 0.005 mg/mL, 0.0025 mg/mL and 0.00125 mg/mL all yielded visible colour shifts after 5, 10 and 20 minutes of exposure to the

solution with continuous stirring. For a concentration of 0.005 mg/mL, the x chromaticity coordinate was statistically significant after 10 and 20 minutes, and the y chromaticity coordinate was statistically significant after 5, 10 and 20 minutes compared to the prothrombin only control. For concentrations of 0.0025 mg/mL and 0.00125 mg/mL, the x and y coordinates were both statistically significant after each time interval (5, 10, 20 minutes) compared to the prothrombin only control. For the 500 mL experiments at an increased impeller speed of ~ 360 RPM, anti-prothrombin concentration of 0.005 mg/mL and 0.0025 mg/mL yielded visible colour shifts after each time interval (5, 10, 20 minutes) and the x and y chromaticity coordinates were statistically significant compared to the prothrombin only control after each time interval. For a concentration of 0.00125 mg/mL, a visible colour shift occurred after 10 and 20 minutes of exposure to the solution. The x chromaticity coordinate was only statistically significant compared to the prothrombin only control after 20 minutes, while the y coordinate was statistically significant compared to the prothrombin only control after 5, 10 and 20 minutes.

The results from the above series of experiments suggest that both 100 mL and 500 mL volumes produced similar results, indicating that both sample volumes are suitable for this application. For both sample volumes, a visible colour shift could be detected at an anti-prothrombin concentration of 0.00125 mg/mL after 10 minutes with continuous stirring at 360 RPM. As the anti-prothrombin concentration is decreased, more time is required to achieve a visible colour shift, indicating that residence time is important to experimental results. For a 500 mL sample at an anti-prothrombin concentration of 0.00125 mg/mL, continuous stirring at 360 RPM did not produce a visible colour shift after 5 minutes but increasing the residence time to 10 minutes allowed for a visible colour shift to occur. Increasing the impeller speed from 195 RPM to 360 RPM allowed for an improvement in sensitivity for a 100 mL volume, as mixing at

195 RPM yielded no visible colour shift after 40 minutes, but mixing at 360 RPM yielded a visible colour shift after only 5 minutes for an anti-prothrombin concentration of 0.00125 mg/mL. For both 100 mL and 500 mL samples with an anti-prothrombin concentration of 0.0025 mg/mL, a visible colour shift was not detected until after 20 minutes in the no stirring (laminar condition experiments), while stirring at 195 RPM yielded a colour shift after only 5 minutes for both volumes. Increasing turbulence in the system by increasing the impeller speed allows for lower concentrations of anti-prothrombin to be detected in both 100 mL and 500 mL samples, and also reduces the residence time required for a visible colour shift to occur on the surface.

As a clear colour shift occurred after exposure to the 100 mL sample at an anti-prothrombin concentration of 0.00125 mg/mL after 20 minutes with increased stirring (360 RPM), the experiments were repeated for 100 mL samples with anti-prothrombin concentrations of 6.25×10^{-4} mg/mL and 5×10^{-4} mg/mL. Figures 8.90, 8.91 and 8.92 show the three replicates prior to protein exposure (row 1), after exposure of each rectangle to 40 µL of 1 mg/mL prothrombin for 20 minutes (row 2), and after exposure of each rectangle to a 100 mL anti-prothrombin solution with a concentration of 6.25×10^{-4} mg/mL after 5 minutes, 10 minutes, 20 minutes, and 40 minutes (rows 3, 4, 5, 6), with no stirring, with stirring at ~ 195 RPM (low turbulence) and with stirring at ~ 360 RPM (high turbulence), respectively. Statistical analysis was completed on the three replicates to determine the effect of various exposure times and impeller mixing speeds on the surface colour of the prothrombin coated wafer. The x and y coordinates were analyzed using one-way ANOVA and Tukey post hoc tests. Tables 8.43, 8.44 and 8.45 show the results of the statistical analysis on the effect of various exposure times for a 100 mL sample with an anti-prothrombin concentration of 6.25×10^{-4} mg/mL with no stirring,

stirring at 195 RPM, and stirring at 360 RPM on the surface colour of the prothrombin-coated wafer based on x and y chromaticity coordinates, respectively.



Figure 8.90. Silicon wafer rectangles (three replicates – ~ 1 cm by ~ 1.2 cm each) coated with ~ 200 nm of tantalum and ~ 106 nm of aluminum then anodized at 4 V with no exposure to protein (row 1), after exposure of each rectangle to 40 µL of 1 mg/mL prothrombin for 20 minutes (row 2), after subsequent exposure of each rectangle to 100 mL of 6.25×10^{-4} mg/mL anti-prothrombin for 5, 10, 20 and 40 minutes with no stirring (rows 3, 4, 5, 6).



Figure 8.91. Silicon wafer rectangles (three replicates – ~ 1 cm by ~ 1.2 cm each) coated with ~ 200 nm of tantalum and ~ 106 nm of aluminum then anodized at 4 V with no exposure to protein (row 1), after exposure of each rectangle to 40 µL of 1 mg/mL prothrombin for 20 minutes (row 2), after subsequent exposure of each rectangle to 100 mL of 6.25×10^{-4} mg/mL anti-prothrombin for 5, 10, 20 and 40 minutes with continuous stirring at the regular impeller speed of 195 RPM (rows 3, 4, 5, 6).



Figure 8.92. Silicon wafer rectangles (three replicates – ~ 1 cm by ~ 1.2 cm each) coated with ~ 200 nm of tantalum and ~ 106 nm of aluminum then anodized at 4 V with no exposure to protein (row 1), after exposure of each rectangle to 40 µL of 1 mg/mL prothrombin for 20 minutes (row 2), after subsequent exposure of each rectangle to 100 mL of 6.25 × 10^{-4} mg/mL anti-prothrombin for 5, 10, and 20 minutes with continuous stirring at an increased impeller speed of 360 RPM (rows 3, 4, 5).

Table 8.43. Results of the ANOVA and Tukey post hoc statistical analysis tests on the effect of various anti-prothrombin exposure times for a 100 mL volume at a concentration of 6.25 × 10^{-4} mg/mL with no stirring on the surface colour using x and y chromaticity coordinates compared to the prothrombin only control. Statistically significant results are in italics. (n = 3).

Prothrombin (II) control	**Vs. II + AP 6.25 × 10^{-4} mg/mL, 100 mL, no stirring (exposure time)**	**Difference detectable by eye vs. control?**	**x coordinate + p values**	**y coordinate + p values**
1 mg/mL II control x = 0.47 ± 0.01 y = 0.32 ± 0.01	5 minutes	No	x = 0.46 ± 0.01 p > 0.9	y = 0.31 ± 0.01 p > 0.7
	10 minutes	No	x = 0.44 ± 0.02 p > 0.1	y = 0.29 ± 0.02 *p < 0.05*
	20 minutes	Yes	x = 0.43 ± 0.01 *p < 0.05*	y = 0.28 ± 0.02 *p < 0.05*
	40 minutes	Yes	x = 0.42 ± 0.01 *p < 0.005*	y = 0.28 ± 0.01 *p < 0.01*

Table 8.44. Results of the ANOVA and Tukey post hoc statistical analysis tests on the effect of various anti-prothrombin exposure times for a 100 mL volume at a concentration of 6.25 × 10^{-4} mg/mL with stirring at 195 RPM on the surface colour using x and y chromaticity coordinates compared to the prothrombin only control. Statistically significant results are in italics. (n = 3).

Prothrombin (II) control	**Vs. II + AP 6.25 × 10^{-4} mg/mL, 100 mL, 195 RPM (exposure time)**	**Difference detectable by eye vs. control?**	**x coordinate + p values**	**y coordinate + p values**
1 mg/mL II control x = 0.44 ± 0.02 y = 0.26 ± 0.01	5 minutes	Yes	x = 0.38 ± 0.02 *p < 0.05*	y = 0.22 ± 0.01 *p < 0.01*
	10 minutes	Yes	x = 0.36 ± 0.03 *p < 0.005*	y = 0.19 ± 0.02 *p < 0.001*
	20 minutes	Yes	x = 0.32 ± 0.01 *p < 0.001*	y = 0.18 ± 0.00 *p < 0.001*
	40 minutes	Yes	x = 0.31 ± 0.01 *p < 0.001*	y = 0.17 ± 0.01 *p < 0.001*

Table 8.45. Results of the ANOVA and Tukey post hoc statistical analysis tests on the effect of various anti-prothrombin exposure times for a 100 mL volume at a concentration of 6.25 × 10^{-4} mg/mL with stirring at 360 RPM on the surface colour using x and y chromaticity coordinates compared to the prothrombin only control. Statistically significant results are in italics. (n = 3).

Prothrombin (II) control	**Vs. II + AP 6.25 × 10^{-4} mg/mL, 100 mL, 360 RPM (exposure time)**	**Difference detectable by eye vs. control?**	**x coordinate + p values**	**y coordinate + p values**
1 mg/mL II control x = 0.48 ± 0.01 y = 0.43 ± 0.00	5 minutes	No	x = 0.47 ± 0.01 p > 0.9	y = 0.42 ± 0.00 p > 0.7
	10 minutes	Yes	x = 0.46 ± 0.01 p > 0.4	y = 0.39 ± 0.01 *p < 0.01*
	20 minutes	Yes	x = 0.45 ± 0.01 p > 0.05	y = 0.35 ± 0.01 *p < 0.001*

Observing Figure 8.90, a strong colour shift did not occur after exposure to the 100 mL solution of 6.25×10^{-4} mg/mL anti-prothrombin with no stirring compared to the prothrombin only control. Observing Figure 8.91, a clear colour shift from light pink to purple can be seen between the prothrombin only control and after 20 minutes of exposure to a 100 mL solution of 6.25×10^{-4} mg/mL anti-prothrombin with continuous stirring at the regular impeller speed of 195 RPM (low turbulence). For the high turbulence condition, shown in Figure 8.92, a slight colour shift from light orange to an orange pink can be seen after 20 minutes of exposure to the 100 mL solution of 6.25×10^{-4} mg/mL anti-prothrombin. A visible colour shift occurred after 20 and 40 minutes of exposure to 100 mL of 6.25×10^{-4} mg/mL anti-prothrombin with no stirring, and statistical analysis indicated that the x chromaticity coordinate was statistically significant after 20 and 40 minutes while the y chromaticity coordinate was statistically significant after 10, 20 and 40 minutes compared to the prothrombin only control. For continuous stirring at 195 RPM at an anti-prothrombin concentration of 6.25×10^{-4} mg/mL, a visible colour shift occurred after each time interval (5, 10, 20 and 40 minutes) and both the x and y chromaticity coordinates were statistically significant compared to the prothrombin only control after each time interval. For stirring at 360 RPM at an anti-prothrombin concentration of 6.25×10^{-4} mg/mL, a visible colour shift occurred after 10 minutes and 20 minutes. The x chromaticity coordinate was not statistically significant after any time interval, and the y chromaticity coordinate was statistically significant after 10 and 20 minutes compared to the prothrombin only control.

As a strong colour shift occurred for an anti-prothrombin concentration of 6.25×10^{-4} mg/mL with continuous stirring after 20 minutes, the experiments were repeated at an anti-prothrombin concentration of 5×10^{-4} mg/mL. Figures 8.93, 8.94 and 8.95 show the three replicates prior to protein exposure (row 1), after exposure of each rectangle to 40 μL of 1

mg/mL prothrombin for 20 minutes (row 2), and after exposure of each rectangle to a 100 mL anti-prothrombin solution with a concentration of 5×10^{-4} mg/mL after 5 minutes, 10 minutes, 20 minutes, and 40 minutes (rows 3, 4, 5, 6), with no stirring, with stirring at ~ 195 RPM (low turbulence) and with stirring at ~ 360 RPM (high turbulence), respectively. Tables 8.46, 8.47 and 8.48 show the results of the statistical analysis on the effect of various exposure times for a 100 mL sample with an anti-prothrombin concentration of 5×10^{-4} mg/mL with no stirring, stirring at 195 RPM, and stirring at 360 RPM on the surface colour of the prothrombin-coated wafer based on x and y chromaticity coordinates, respectively. The x and y coordinates at each anti-prothrombin (AP) concentration were compared to the prothrombin (II) control, and a p value less than 0.05 indicates statistical significance.



Figure 8.93. Silicon wafer rectangles (three replicates – ~ 1 cm by ~ 1.2 cm each) coated with ~ 200 nm of tantalum and ~ 106 nm of aluminum then anodized at 4 V with no exposure to protein (row 1), after exposure of each rectangle to 40 µL of 1 mg/mL prothrombin for 20 minutes (row 2), after subsequent exposure of each rectangle to 100 mL of 5×10^{-4} mg/mL anti-prothrombin for 5, 10, 20 and 40 minutes with no stirring (rows 3, 4, 5, 6).



Figure 8.94. Silicon wafer rectangles (three replicates – ~ 1 cm by ~ 1.2 cm each) coated with ~ 200 nm of tantalum and ~ 106 nm of aluminum then anodized at 4 V with no exposure to protein (row 1), after exposure of each rectangle to 40 μL of 1 mg/mL prothrombin for 20 minutes (row 2), after subsequent exposure of each rectangle to 100 mL of 5 × 10^{-4} mg/mL anti-prothrombin for 5, 10, 20 and 40 minutes with continuous stirring at the regular impeller speed of 195 RPM (rows 3, 4, 5, 6).



Figure 8.95. Silicon wafer rectangles (three replicates – ~ 1 cm by ~ 1.2 cm each) coated with ~ 200 nm of tantalum and ~ 106 nm of aluminum then anodized at 4 V with no exposure to protein (row 1), after exposure of each rectangle to 40 μL of 1 mg/mL prothrombin for 20 minutes (row 2), after subsequent exposure of each rectangle to 100 mL of 5 × 10^{-4} mg/mL anti-prothrombin for 5, 10, and 20 minutes with continuous stirring at an increased impeller speed of 360 RPM (rows 3, 4, 5).

Table 8.46. Results of the ANOVA and Tukey post hoc statistical analysis tests on the effect of various anti-prothrombin exposure times for a 100 mL volume at a concentration of 5 × 10^{-4} mg/mL with no stirring on the surface colour using x and y chromaticity coordinates compared to the prothrombin only control. Statistically significant results are in italics. (n = 3).

Prothrombin (II) control	**Vs. II + AP 5 × 10^{-4} mg/mL, 100 mL, no stirring (exposure time)**	**Difference detectable by eye vs. control?**	**x coordinate + p values**	**y coordinate + p values**
1 mg/mL II control x = 0.48 ± 0.01 y = 0.43 ± 0.00	5 minutes	No	x = 0.48 ± 0.01 p > 0.9	y = 0.43 ± 0.01 p > 0.9
	10 minutes	No	x = 0.48 ± 0.01 p > 0.9	y = 0.43 ± 0.00 p > 0.9
	20 minutes	No	x = 0.47 ± 0.01 p > 0.9	y = 0.43 ± 0.01 p > 0.9
	40 minutes	No	x = 0.47 ± 0.01 p > 0.9	y = 0.42 ± 0.01 p > 0.9

Table 8.47. Results of the ANOVA and Tukey post hoc statistical analysis tests on the effect of various anti-prothrombin exposure times for a 100 mL volume at a concentration of 5 × 10^{-4} mg/mL with stirring at 195 RPM on the surface colour using x and y chromaticity coordinates compared to the prothrombin only control. Statistically significant results are in italics. (n = 3).

Prothrombin (II) control	**Vs. II + AP 5 × 10^{-4} mg/mL, 100 mL, 195 RPM (exposure time)**	**Difference detectable by eye vs. control?**	**x coordinate + p values**	**y coordinate + p values**
1 mg/mL II control x = 0.47 ± 0.01 y = 0.43 ± 0.02	5 minutes	No	x = 0.47 ± 0.01 p > 0.9	y = 0.42 ± 0.02 p > 0.9
	10 minutes	No	x = 0.47 ± 0.01 p > 0.9	y = 0.41 ± 0.02 p > 0.9
	20 minutes	No	x = 0.47 ± 0.01 p > 0.9	y = 0.41 ± 0.02 p > 0.8
	40 minutes	No	x = 0.47 ± 0.02 p > 0.9	y = 0.39 ± 0.03 p > 0.4

Table 8.48. Results of the ANOVA and Tukey post hoc statistical analysis tests on the effect of various anti-prothrombin exposure times for a 100 mL volume at a concentration of 5 × 10^{-4} mg/mL with stirring at 360 RPM on the surface colour using x and y chromaticity coordinates compared to the prothrombin only control. Statistically significant results are in italics. (n = 3).

Prothrombin (II) control	**Vs. II + AP 5 × 10^{-4} mg/mL, 100 mL, 360 RPM (exposure time)**	**Difference detectable by eye vs. control?**	**x coordinate + p values**	**y coordinate + p values**
1 mg/mL II control x = 0.48 ± 0.01 y = 0.43 ± 0.01	5 minutes	No	x = 0.47 ± 0.01 p > 0.9	y = 0.42 ± 0.01 p > 0.9
	10 minutes	Yes	x = 0.46 ± 0.02 p > 0.7	y = 0.38 ± 0.04 p > 0.1
	20 minutes	Yes	x = 0.45 ± 0.03 p > 0.3	y = 0.34 ± 0.04 *p < 0.05*

For an anti-prothrombin concentration of 5 × 10^{-4} mg/mL, no visible colour shift occurred after 40 minutes for the laminar condition (no stirring) and the low turbulence condition (regular stirring at ~ 195 RPM). A slight colour shift from light orange to an orange pink occurred in the high turbulence condition (increased stirring at ~ 360 RPM) after 20 minutes, though the colour shift did not appear uniform on the surface. For the no stirring and stirring at 195 RPM conditions at an anti-prothrombin concentration of 5 × 10^{-4} mg/mL, there was no statistical significance in the x or y chromaticity coordinates after any time interval (5, 10, 20 or 40 minutes) compared to the prothrombin only control. For the high turbulence condition (stirring at 360 RPM), there was no statistical significance in the x chromaticity coordinate after any time interval, and the y chromaticity coordinate was statistically significant after 20 minutes of exposure to the anti-prothrombin solution compared to the prothrombin only control.

The results of the stirred tank experiments indicate that the limit of detection for a 100 mL or 500 mL solution of anti-prothrombin after 20 minutes is 0.0025 mg/mL if no stirring

occurs. By increasing the volume without the addition of stirring, the limit of detection was improved ten times compared to work previously done that indicated the limit of detection for a 20 μL on a stationary surface is 0.025 mg/mL [5]. By introducing mixing into the system by stirring the fluid sample with an impeller at a speed of 195 RPM or 360 RPM, the limit of detection after 20 minutes is an anti-prothrombin concentration of 6.25×10^{-4} mg/mL.

To further assess the importance of residence time, the syringe-filter diagnostic design that uses a tantalum disc substrate was studied. For these experiments, tantalum discs with five holes were coated with ~ 200 nm of tantalum and ~ 110 nm of aluminum, then anodized at 4 V using the horizontal method with the conductive epoxy attachment. A Hydrophobic Sharpie was used to outline the holes and the edges of the tantalum discs to control the protein exposure area. An 80 μL solution of 1 mg/mL prothrombin was then pipetted on to the disc surface and spread to edges and left in a Petri dish with a wet paper towel for 20 minutes. After 20 minutes, the solution was pipetted off the surface and the discs were rinsed with deionized water and dried with oil free compressed air. The tantalum disc was then placed in the 3D printed filter (Fusion 360 design shown in Figure 7.1) without the impeller and the filter was attached to a 60 cc/mL Air-Tite syringe, as shown in Figure 8.96. A 500 mL solution of 0.005 mg/mL anti-prothrombin was prepared, and 50 mL of the solution was taken into the syringe at a time, then the syringe was screwed into the 3D printed filter containing the tantalum disc. The syringe was then pushed at a speed of ~ 1 cm/s and the sample was pushed through the filter and over the tantalum disc surface into a beaker. The process was repeated 10 times at a volume of 50 mL to expose the prothrombin coated disc to a 500 mL sample of 0.005 mg/mL anti-prothrombin. Figures 8.97, 8.98 and 8.99 show the tantalum disc prior to protein exposure (top), after exposure of the entire surface to 80 μL of 1 mg/mL prothrombin for 20 minutes (middle), and after exposure to the 500

mL 0.005 mg/mL anti-prothrombin solution in the syringe-filter device (bottom) without the impeller for three replicates. Statistical analysis was completed on the three replicates to determine if a statistically significant difference in x and y chromaticity coordinates occurred after exposure to the anti-prothrombin solution compared to the prothrombin only control. For each replicate, three areas on the coloured tantalum disc were selected and analyzed using ImageJ to determine the RGB coordinates. The average RGB coordinates were taken at each of the three replicates for the prothrombin only slides and for the slides exposed to anti-prothrombin. The RGB coordinates were converted to Yxy colour coordinates using the ColorMine website (http://colormine.org/convert/rgb-to-yxy). The x and y coordinates were analyzed using an independent T-test for each replicate. The x and y coordinates after exposure to anti-prothrombin (AP) were compared to the prothrombin (II) control, and a p value less than 0.05 indicates statistical significance. Tables 8.49, 8.50 and 8.51 show the results of the statistical analysis for the tantalum disc after exposure to 500 mL of 0.005 mg/mL anti-prothrombin in the syringe-filter device without the impeller for replicates 1, 2 and 3, respectively.



Figure 8.96. 3D printed filter containing tantalum disc attached to 60 cc/mL Air-Tite syringe for filter-syringe experiments.

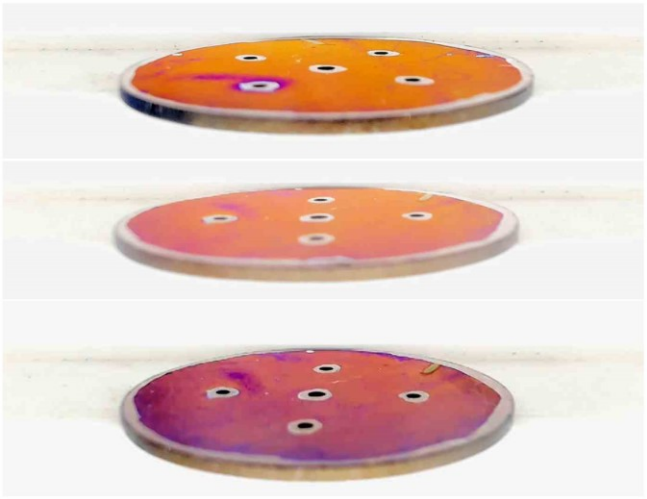


Figure 8.97. Tantalum disc (replicate 1 – 26.6 mm diameter) coated with ~ 200 nm of tantalum and ~ 110 nm of aluminum then anodized at 4 V prior to protein exposure (top), after exposure of entire surface to 80 µL of 1 mg/mL prothrombin for 20 minutes (middle), and after exposure to 500 mL of 0.005 mg/mL anti-prothrombin in the syringe-filter device without impeller (bottom).

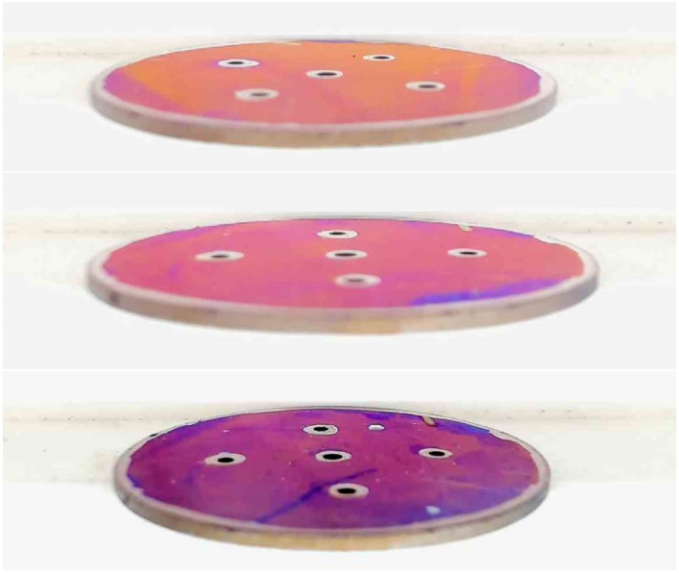


Figure 8.98. Tantalum disc (replicate 2 – 26.6 mm diameter) coated with ~ 200 nm of tantalum and ~ 110 nm of aluminum then anodized at 4 V prior to protein exposure (top), after exposure of entire surface to 80 µL of 1 mg/mL prothrombin for 20 minutes (middle), and after exposure to 500 mL of 0.005 mg/mL anti-prothrombin in the syringe-filter device without impeller (bottom).

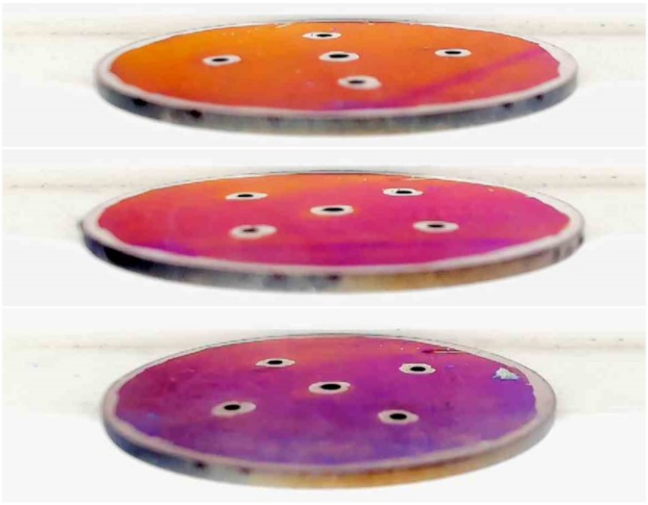


Figure 8.99. Tantalum disc (replicate 3 – 26.6 mm diameter) coated with ~ 200 nm of tantalum and ~ 110 nm of aluminum then anodized at 4 V prior to protein exposure (top), after exposure of entire surface to 80 µL of 1 mg/mL prothrombin for 20 minutes (middle), and after exposure to 500 mL of 0.005 mg/mL anti-prothrombin in the syringe-filter device without impeller (bottom).

Table 8.49. Results of the independent T-test statistical analysis on the effect of 500 mL of 0.005 mg/mL of anti-prothrombin (AP) in the syringe-filter device (replicate 1) without the impeller on the surface colour of the prothrombin-coated tantalum disc based on x and y chromaticity coordinates compared to the prothrombin (II) only control. Statistically significant results are in italics. (n = 3).

Prothrombin (II) control	**Vs. II + AP (mg/mL) (replicate 1)**	**Difference detectable by eye vs. control?**	**x coordinate + p values**	**y coordinate + p values**
1 mg/mL II control x = 0.45 ± 0.01 y = 0.42 ± 0.01	0.005 mg/mL (500 mL) in syringe-filter device without impeller mixing	Yes	x = 0.44 ± 0.03 p > 0.2	y = 0.30 ± 0.02 *p < 0.01*

Table 8.50. Results of the independent T-test statistical analysis on the effect of 500 mL of 0.005 mg/mL of anti-prothrombin (AP) in the syringe-filter device (replicate 2) without the impeller on the surface colour of the prothrombin-coated tantalum disc based on x and y chromaticity coordinates compared to the prothrombin (II) only control. Statistically significant results are in italics. (n = 3).

Prothrombin (II) control	**Vs. II + AP (mg/mL) (replicate 2)**	**Difference detectable by eye vs. control?**	**x coordinate + p values**	**y coordinate + p values**
1 mg/mL II control x = 0.42 ± 0.01 y = 0.29 ± 0.00	0.005 mg/mL (500 mL) in syringe-filter device without impeller mixing	Yes	x = 0.38 ± 0.02 *p < 0.05*	y = 0.23 ± 0.01 *p < 0.001*

Table 8.51. Results of the independent T-test statistical analysis on the effect of 500 mL of 0.005 mg/mL of anti-prothrombin (AP) in the syringe-filter device (replicate 3) without the impeller on the surface colour of the prothrombin-coated tantalum disc based on x and y chromaticity coordinates compared to the prothrombin (II) only control. Statistically significant results are in italics. (n = 3).

Prothrombin (II) control	**Vs. II + AP (mg/mL) (replicate 3)**	**Difference detectable by eye vs. control?**	**x coordinate + p values**	**y coordinate + p values**
1 mg/mL II control x = 0.48 ± 0.03 y = 0.28 ± 0.02	0.005 mg/mL (500 mL) in syringe-filter device without impeller mixing	Yes	x = 0.35 ± 0.03 *p < 0.05*	y = 0.21 ± 0.01 *p < 0.05*

At an anti-prothrombin concentration of 0.005 mg/mL, a visible colour shift occurred on the tantalum disc for all three replicates after exposure to the 500 mL solution in the syringe-filter device without the impeller. For replicate 1, only the y chromaticity coordinate was statistically significant after exposure to the anti-prothrombin solution compared to the prothrombin only control. For replicates 2 and 3, both the x and y chromaticity coordinates were statistically significant after exposure to the anti-prothrombin solution compared to the prothrombin only control. The surfaces did not appear completely uniform, but visible colour shifts did occur on the surface for all three replicates.

As a visible colour shift was detected at an anti-prothrombin concentration of 0.005 mg/mL, the syringe-filter experiments were repeated with a 500 mL solution at an anti-prothrombin concentration of 0.00125 mg/mL. Figures 8.100, 8.101 and 8.102 show the tantalum disc prior to protein exposure (top), after exposure of the entire surface to 80 µL of 1 mg/mL prothrombin for 20 minutes (middle), and after exposure to the 500 mL 0.00125 mg/mL anti-

prothrombin solution in the syringe-filter device (bottom) without the impeller for three replicates. Statistical analysis was completed on the three replicates for each experiment to determine if a statistically significant difference in x and y chromaticity coordinates occurred after exposure to the anti-prothrombin solution compared to the prothrombin only control. For each replicate, three areas on the coloured tantalum disc were selected and analyzed using ImageJ to determine the average RGB coordinates. The x and y coordinates were analyzed using an independent T-test for each replicate. The x and y coordinates after exposure to anti-prothrombin (AP) were compared to the prothrombin (II) control, and a p value less than 0.05 indicates statistical significance. Tables 8.52, 8.53 and 8.54 show the results of the statistical analysis for the tantalum disc after exposure to 500 mL of 0.00125 mg/mL anti-prothrombin in the syringe-filter device without the impeller for replicates 1, 2 and 3, respectively.

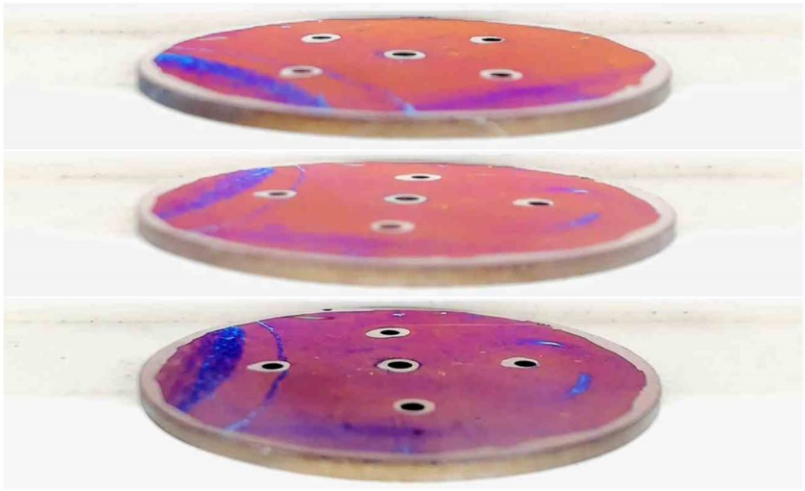


Figure 8.100. Tantalum disc (replicate 1 – 26.6 mm diameter) coated with ~ 200 nm of tantalum and ~ 110 nm of aluminum then anodized at 4 V prior to protein exposure (top), after exposure of entire surface to 80 µL of 1 mg/mL prothrombin for 20 minutes (middle), and after exposure to 500 mL of 0.00125 mg/mL anti-prothrombin in the syringe-filter device without impeller (bottom).

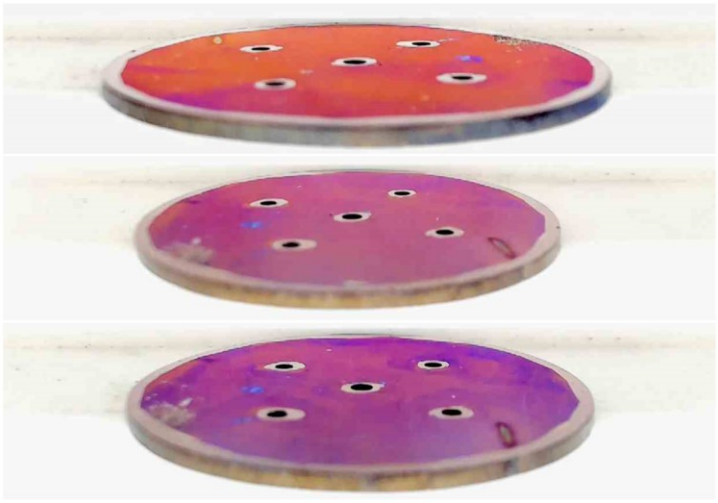


Figure 8.101. Tantalum disc (replicate 2 – 26.6 mm diameter) coated with ~ 200 nm of tantalum and ~ 110 nm of aluminum then anodized at 4 V prior to protein exposure (top), after exposure of entire surface to 80 µL of 1 mg/mL prothrombin for 20 minutes (middle), and after exposure to 500 mL of 0.00125 mg/mL anti-prothrombin in the syringe-filter device without impeller (bottom).

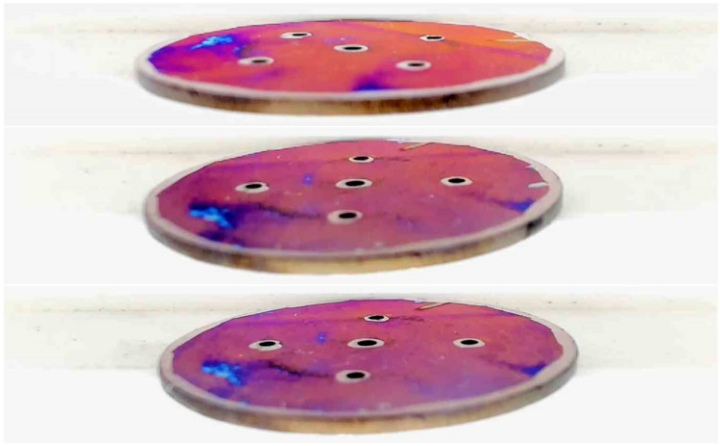


Figure 8.102. Tantalum disc (replicate 3 – 26.6 mm diameter) coated with ~ 200 nm of tantalum and ~ 110 nm of aluminum then anodized at 4 V prior to protein exposure (top), after exposure of entire surface to 80 µL of 1 mg/mL prothrombin for 20 minutes (middle), and after exposure to 500 mL of 0.00125 mg/mL anti-prothrombin in the syringe-filter device without impeller (bottom).

Table 8.52. Results of the independent T-test statistical analysis on the effect of 500 mL of 0.00125 mg/mL of anti-prothrombin (AP) in the syringe-filter device (replicate 1) without the impeller on the surface colour of the prothrombin-coated tantalum disc based on x and y chromaticity coordinates compared to the prothrombin (II) only control. Statistically significant results are in italics. (n = 3).

Prothrombin (II) control	**Vs. II + AP (mg/mL) (replicate 1)**	**Difference detectable by eye vs. control?**	**x coordinate + p values**	**y coordinate + p values**
1 mg/mL II control x = 0.43 ± 0.00 y = 0.32 ± 0.01	0.00125 mg/mL (500 mL) in syringe-filter device without impeller mixing	Yes	x = 0.39 ± 0.02 p > 0.05	y = 0.26 ± 0.01 *p < 0.001*

Table 8.53. Results of the independent T-test statistical analysis on the effect of 500 mL of 0.00125 mg/mL of anti-prothrombin (AP) in the syringe-filter device (replicate 2) without the impeller on the surface colour of the prothrombin-coated tantalum disc based on x and y chromaticity coordinates compared to the prothrombin (II) only control. Statistically significant results are in italics. (n = 3).

Prothrombin (II) control	**Vs. II + AP (mg/mL) (replicate 2)**	**Difference detectable by eye vs. control?**	**x coordinate + p values**	**y coordinate + p values**
1 mg/mL II control x = 0.39 ± 0.00 y = 0.27 ± 0.01	0.00125 mg/mL (500 mL) in syringe-filter device without impeller mixing	Yes	x = 0.35 ± 0.01 *p < 0.01*	y = 0.22 ± 0.01 *p < 0.005*

Table 8.54. Results of the independent T-test statistical analysis on the effect of 500 mL of 0.00125 mg/mL of anti-prothrombin (AP) in the syringe-filter device (replicate 3) without the impeller on the surface colour of the prothrombin-coated tantalum disc based on x and y chromaticity coordinates compared to the prothrombin (II) only control. Statistically significant results are in italics. (n = 3).

Prothrombin (II) control	**Vs. II + AP (mg/mL) (replicate 3)**	**Difference detectable by eye vs. control?**	**x coordinate + p values**	**y coordinate + p values**
1 mg/mL II control x = 0.42 ± 0.02 y = 0.29 ± 0.01	0.00125 mg/mL (500 mL) in syringe-filter device without impeller mixing	No	x = 0.40 ± 0.02 p > 0.2	y = 0.27 ± 0.01 p > 0.2

For a 500 mL sample at an anti-prothrombin concentration of 0.00125 mg/mL in the filter-syringe device, a visible colour shift occurred for replicate 1, a slight colour shift occurred for replicate 2, and no visual colour shift occurred for replicate 3. For all three replicates, the surface and colour shifts did not appear uniform. For the first replicate, only the y chromaticity coordinate was statistically significant after exposure to the anti-prothrombin solution compared to the prothrombin only control. For replicate 2, both the x and y chromaticity coordinates were statistically significant after exposure to the anti-prothrombin solution compared to the prothrombin only control. For replicate 3, there was no statistical significance in either the x or y coordinate after exposure to the anti-prothrombin solution compared to the prothrombin only control. The inconsistent results and poor colour shifts in the syringe-filter device at an anti-prothrombin concentration of 0.00125 mg/mL could be due to the smaller exposure time of the solution to the surface. To push a 50 mL solution through the syringe and past the tantalum disc

at a rate of 1 cm/s, it took approximately 7.4 seconds. As this was done 10 times to expose the surface to a 500 mL sample, the total exposure time of the prothrombin coated discs to the anti-prothrombin solution was ~ 74 seconds. Compared to the stirred tank experiments with a residence time of 20 minutes, the syringe-filter device has a much lower exposure time to the solution. As the stirred tank experiments produced strong, uniform colour shifts at an anti-prothrombin concentration of 0.00125 mg/mL and the filter-syringe device did not, the filter-syringe design was not further considered.

For the stirred tank experiments, the limit of detection was found to be an anti-prothrombin concentration of 6.25×10^{-4} mg/mL when an impeller was used to mix the sample for 20 minutes. Another diagnostic device design containing a graduated cylinder, a draft tube and a bubbler was investigated to see if the sensitivity could be improved even further. The draft tube was drafted in Fusion 360 by Ben Damant, and the Fusion 360 design of the draft tube is shown in Figure 8.103. The inner diameter of the draft tube was 1.4 cm, and the outer diameter was 2 cm. From the bottom of the legs to the top of the tube, the height of the draft tube apparatus was 12.6 cm, with the draft tube portion being 10.8 cm. The draft tube was designed such that the silicon wafer slides were clipped and secured 1 cm below the bottom of the tube to ensure that the coated surface was exposed to as much fluid as possible. The draft tube and silicon wafer holder were 3D printed using poly(lactic acid) (PLA) polymer and a bubbler made up of a brass tube containing 19 holes at the bottom was wrapped around the bottom of the tube and ran past the top outlet of the tube. A Porter Cable compressor was connected to a rotameter to measure the gas flow rate, and then to the bubbler to induce bubbling and mixing in the system. The bubbler and compressor were used to generate mixing and turbulence in the system for the draft tube design instead of the impeller, as impeller mixing at increased speeds generates

heat within the solution. The draft tube design allows for the fluid sample to be continuously directed just above the coated silicon wafer slide and recirculates the solution throughout the device. By directing the flow towards the surface, the sensitivity could potentially be improved compared to the stirred tank apparatus in which the fluid flow was random within the beaker. The draft tube and bubbler were placed into a 1 L graduated cylinder that had been cut around the 600 mL mark to form the final device. After 3D printing, screws were added to the sides of the draft tube to ensure it would stand upright inside the graduated cylinder. The Porter Cable Compressor and the rotameter used to measure the gas flow rate are shown in Figure 8.104. The 3D printed draft tube and the bubbler made of brass tubing are shown in Figure 8.105.

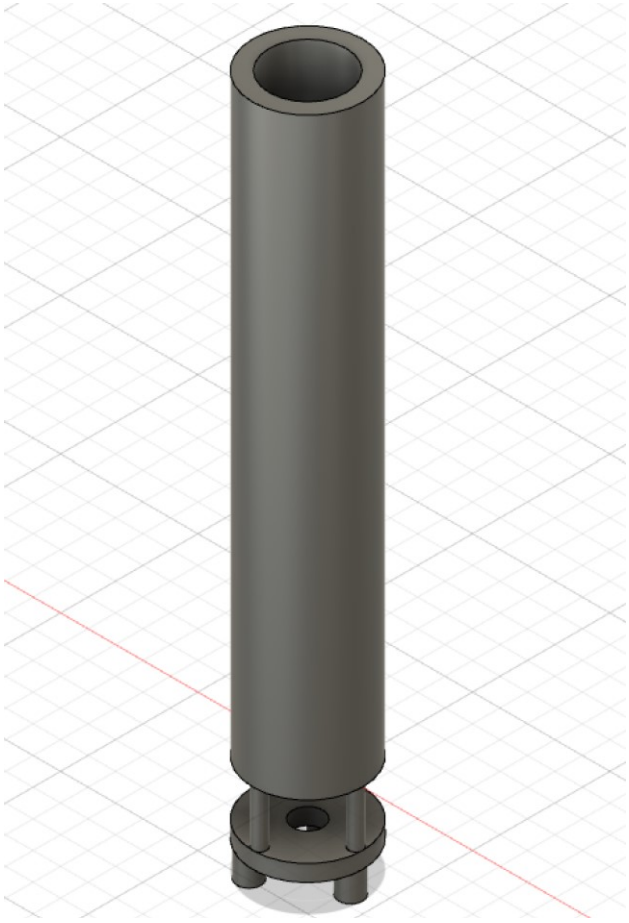


Figure 8.103. Draft tube Fusion 360 design.



Figure 8.104. Porter Cable compressor used to introduce bubbling into the system (left) and rotameter used to measure gas flow rate (right).



Figure 8.105. 3D printed draft tube with screws attached (left), brass tube bubbler (middle), and 3D printed draft tube and bubbler placed in a graduated cylinder to form final draft tube apparatus (right).

The draft tube and bubbler device functions as an airlift bioreactor, in which mixing is induced by bubbling of a gas stream into the system. The draft tube design ensures the fluid is recirculated through the system as it is mixed. The airlift bioreactor design also reduces heat generation in the system compared to the stirred tank impeller set up. As the draft tube was expected to improve the device sensitivity, a 500 mL solution of anti-prothrombin at a concentration of 6.25×10^{-4} mg/mL was tested first in the draft tube device. Silicon wafer substrates were coated with ~ 200 nm of tantalum and ~ 111 nm of aluminum then anodized at 4 V and cut using the diamond scribe and the stencil. The silicon wafer slides were then further cut into smaller squares with dimensions of ~ 1 cm by ~ 1.2 cm. A Sharpie was used to trace the edges of the rectangles to contain the protein solutions. Then, 40 μL of 1 mg/mL prothrombin was placed on the surface and spread to the edges of the rectangle using a pipette tip and was left in a Petri dish with a wet paper towel for 20 minutes. After exposure to prothrombin, the wafers were rinsed with deionized water and dried with oil free compressed air. The prothrombin coated wafers were then placed under the outlet of the 3D printed draft tube and secured using a paperclip, and the draft tube and bubbler apparatus were placed in a 1 L graduated cylinder that had been cut at the 600 mL mark. A 500 mL solution of 6.25×10^{-4} mg/mL anti-prothrombin was placed in the graduated cylinder, and the compressor attached to the bubbler was turned on and set to gas flow rates of either ~ 3.5 lpm and ~ 9.5 lpm, as measured by the rotameter, to assess the effect of gas flow rate. The Reynolds number of the draft tube apparatus was calculated using Equation 2-4, shown in Chapter 2, as the bubble Reynolds number, Re_b. The bubble rising velocity, v_z, was calculated by measuring the time for one bubble to travel 18.3 cm from the entrance point of the bubbles from the sparger to the top of the fluid volume. The bubble equivalent diameter, d_{10}, was found by counting the number of bubbles across the 6 cm

diameter of the graduated cylinder from a top view. Dividing 6 cm by the number of bubbles to cover a 6 cm distance gave the bubble equivalent diameter. The kinematic viscosity of water at 21°C, 9.78×10^{-7} m^2/s, was used as the kinematic viscosity of the liquid phase [11]. For a gas flow rate of ~ 3.5 lpm, the bubble rising velocity was found to be ~ 26.1 cm/s, the bubble equivalent diameter was found to be ~ 0.75 cm, and the Reynolds number was calculated to be ~ 2005 (transition regime). For a gas flow rate of ~ 9.5 lpm, the bubble rising velocity was found to be ~ 39.8 cm/s, the bubble equivalent diameter was found to be ~ 1 cm, and the Reynolds number was calculated to be ~ 4068 (turbulent regime). Images were taken prior to protein exposure, after exposure to prothrombin, and after exposure to the anti-prothrombin solution for 5 and 10 minutes. As a strong colour shift occurred after 5 minutes, longer time intervals were not investigated at an anti-prothrombin concentration of 6.25×10^{-4} mg/mL. Figures 8.106 and 8.107 show the three replicates prior to protein exposure (row 1), after exposure of each rectangle to 40 µL of 1 mg/mL prothrombin for 20 minutes (row 2), and after exposure of each rectangle to a 500 mL anti-prothrombin solution with a concentration of 6.25×10^{-4} mg/mL after 5 minute and 10 minutes (rows 3, 4), in the draft tube apparatus at gas flow rates of ~ 3.5 lpm and ~ 9.5 lpm, respectively. Statistical analysis was completed on the three replicates to determine the effect of various exposure times and gas flow rates on the surface colour of the prothrombin coated wafer. The x and y coordinates were analyzed using one-way ANOVA and Tukey post hoc tests. Tables 8.55 and 8.56 show the results of the statistical analysis on the effect of various exposure times for a 500 mL sample with an anti-prothrombin concentration of 6.25×10^{-4} mg/mL in the draft tube apparatus with gas flow rates of ~ 3.5 lpm and ~ 9.5 lpm on the surface colour of the prothrombin-coated wafer based on x and y chromaticity coordinates, respectively.

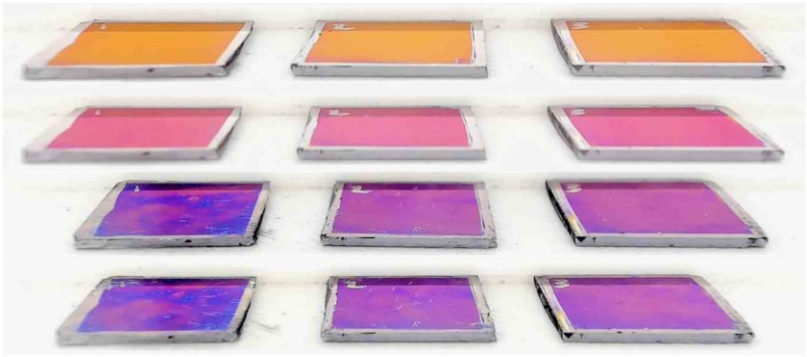


Figure 8.106. Silicon wafer rectangles (three replicates – ~ 1 cm by ~ 1.2 cm each) coated with ~ 200 nm of tantalum and ~ 111 nm of aluminum then anodized at 4 V with no exposure to protein (row 1), after exposure of each rectangle to 40 μL of 1 mg/mL prothrombin for 20 minutes (row 2), after subsequent exposure of each rectangle to 500 mL of 6.25×10^{-4} mg/mL anti-prothrombin for 5 and 10 minutes in the draft tube apparatus at a gas flow rate of ~ 3.5 lpm (rows 3, 4).

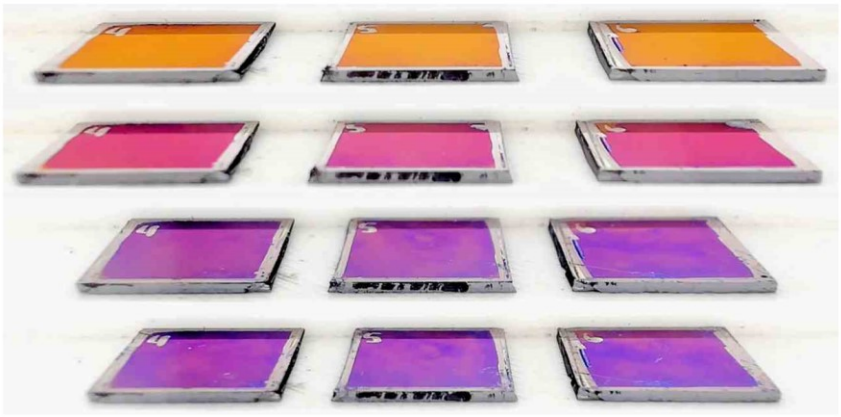


Figure 8.107. Silicon wafer rectangles (three replicates – ~ 1 cm by ~ 1.2 cm each) coated with ~ 200 nm of tantalum and ~ 111 nm of aluminum then anodized at 4 V with no exposure to protein (row 1), after exposure of each rectangle to 40 μL of 1 mg/mL prothrombin for 20 minutes (row 2), after subsequent exposure of each rectangle to 500 mL of 6.25×10^{-4} mg/mL anti-prothrombin for 5 and 10 minutes in the draft tube apparatus at a gas flow rate of ~ 9.5 lpm (rows 3, 4).

Table 8.55. Results of the ANOVA and Tukey post hoc statistical analysis tests on the effect of various anti-prothrombin exposure times for a 500 mL volume at a concentration of 6.25 × 10^{-4} mg/mL in the draft tube apparatus at a gas flow rate of ~ 3.5 lpm on the surface colour using x and y chromaticity coordinates compared to the prothrombin only control. Statistically significant results are in italics. (n = 3).

Prothrombin (II) control	**Vs. II + AP 6.25 × 10^{-4} mg/mL, ~ 3.5 lpm (exposure time)**	**Difference detectable by eye vs. control?**	**x coordinate + p values**	**y coordinate + p values**
1 mg/mL II control x = 0.40 ± 0.01 y = 0.29 ± 0.01	5 minutes	Yes	x = 0.31 ± 0.05 *p < 0.05*	y = 0.20 ± 0.05 *p < 0.05*
	10 minutes	Yes	x = 0.29 ± 0.03 *p < 0.05*	y = 0.19 ± 0.03 *p < 0.05*

Table 8.56. Results of the ANOVA and Tukey post hoc statistical analysis tests on the effect of various anti-prothrombin exposure times for a 500 mL volume at a concentration of 6.25 × 10^{-4} mg/mL in the draft tube apparatus at a gas flow rate of ~ 9.5 lpm on the surface colour using x and y chromaticity coordinates compared to the prothrombin only control. Statistically significant results are in italics. (n = 3).

Prothrombin (II) control	**Vs. II + AP 6.25 × 10^{-4} mg/mL, ~ 9.5 lpm (exposure time)**	**Difference detectable by eye vs. control?**	**x coordinate + p values**	**y coordinate + p values**
1 mg/mL II control x = 0.43 ± 0.02 y = 0.26 ± 0.01	5 minutes	Yes	x = 0.31 ± 0.02 *p < 0.005*	y = 0.20 ± 0.02 *p < 0.005*
	10 minutes	Yes	x = 0.29 ± 0.02 *p < 0.001*	y = 0.18 ± 0.01 *p < 0.001*

For a 500 mL sample at an anti-prothrombin concentration of 6.25 × 10^{-4} mg/mL, a strong visible colour shift from pink (prothrombin only) to purple occurred in the draft tube apparatus after 5 minutes and 10 minutes at both gas flow rates of ~ 3.5 lpm and ~ 9.5 lpm. For

both gas flow rates, both the x and y chromaticity coordinates were statistically significant after exposure to the anti-prothrombin solution for 5 and 10 minutes compared to the prothrombin only control, indicating the formation of an antigen-antibody complex on the surface. Since a strong colour shift occurred on the surface after only 5 minutes in the draft tube apparatus, the experiment was repeated at an anti-prothrombin concentration of 5×10^{-4} mg/mL. Figures 8.108 and 8.109 show the three replicates prior to protein exposure (row 1), after exposure of each rectangle to 40 μL of 1 mg/mL prothrombin for 20 minutes (row 2), and after exposure of each rectangle to a 500 mL anti-prothrombin solution with a concentration of 5×10^{-4} mg/mL after 5 minutes (row 3) in the draft tube apparatus at gas flow rates of ~ 3.5 lpm and ~ 9.5 lpm, respectively. Statistical analysis was completed on the three replicates and the x and y coordinates were analyzed using an independent t-test. Tables 8.57 and 8.58 show the results of the statistical analysis on the effect of exposure to a 500 mL sample with an anti-prothrombin concentration of 5×10^{-4} mg/mL for 5 minutes in the draft tube apparatus with gas flow rates of ~ 3.5 lpm and ~ 9.5 lpm on the surface colour of the prothrombin-coated wafer based on x and y chromaticity coordinates, respectively.

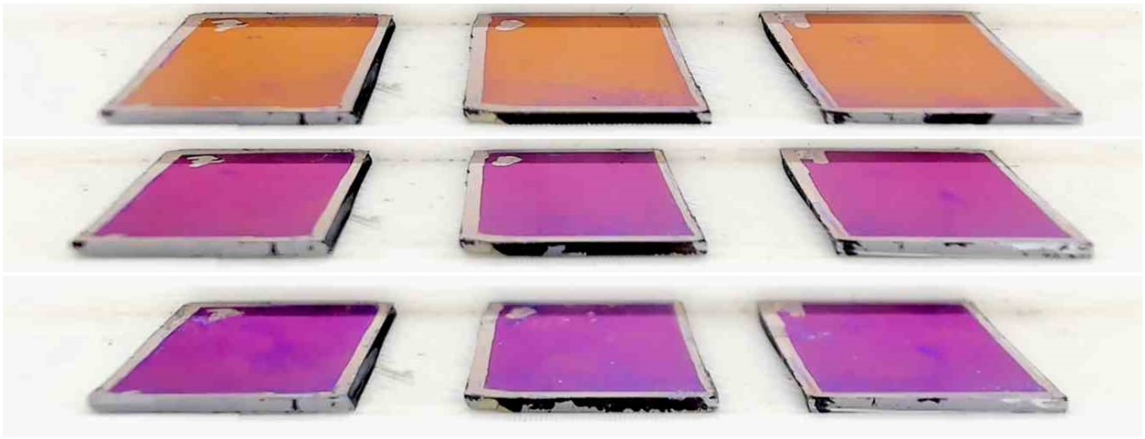


Figure 8.108. Silicon wafer rectangles (three replicates – ~ 1 cm by ~ 1.2 cm each) coated with ~ 200 nm of tantalum and ~ 111 nm of aluminum then anodized at 4 V with no exposure to protein (row 1), after exposure of each rectangle to 40 μL of 1 mg/mL prothrombin for 20 minutes (row 2), after subsequent exposure of each rectangle to 500 mL of 5 × 10^{-4} mg/mL anti-prothrombin for 5 minutes in the draft tube apparatus at a gas flow rate of ~ 3.5 lpm (row 3).

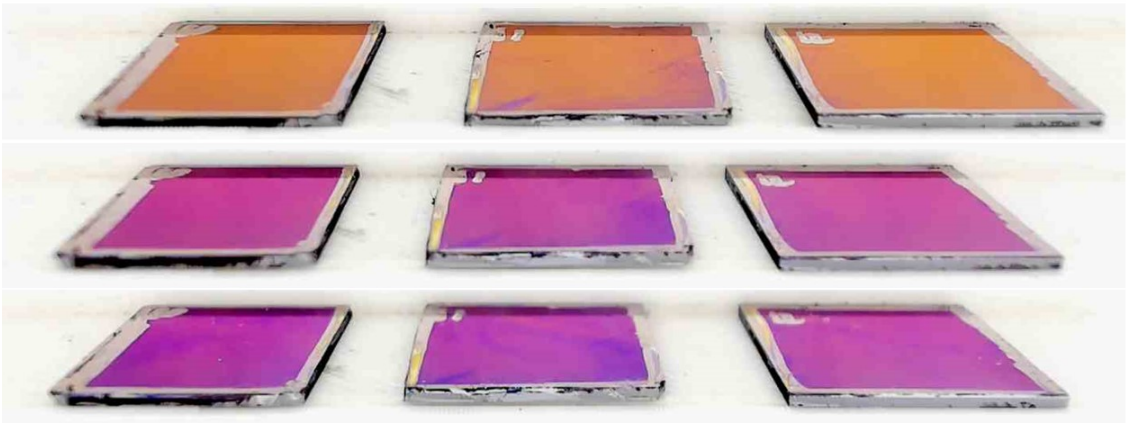


Figure 8.109. Silicon wafer rectangles (three replicates – ~ 1 cm by ~ 1.2 cm each) coated with ~ 200 nm of tantalum and ~ 111 nm of aluminum then anodized at 4 V with no exposure to protein (row 1), after exposure of each rectangle to 40 μL of 1 mg/mL prothrombin for 20 minutes (row 2), after subsequent exposure of each rectangle to 500 mL of 5 × 10^{-4} mg/mL anti-prothrombin for 5 minutes in the draft tube apparatus at a gas flow rate of ~ 9.5 lpm (row 3).

Table 8.57. Results of the independent T-test statistical analysis on the effect of 500 mL of 5 × 10^{-4} mg/mL of anti-prothrombin (AP) in the draft tube apparatus at a gas flow rate of ~ 3.5 lpm on the surface colour based on x and y chromaticity coordinates compared to the prothrombin (II) only control. Statistically significant results are in italics. (n = 3).

Prothrombin (II) control	**Vs. II + AP (mg/mL)**	**Difference detectable by eye vs. control?**	**x coordinate + p values**	**y coordinate + p values**
1 mg/mL II control x = 0.36 ± 0.02 y = 0.23 ± 0.00	5 × 10^{-4} (500 mL) in draft tube apparatus at ~ 3.5 lpm	Yes	x = 0.33 ± 0.01 *p < 0.05*	y = 0.19 ± 0.01 *p < 0.005*

Table 8.58. Results of the independent T-test statistical analysis on the effect of 500 mL of 5 × 10^{-4} mg/mL of anti-prothrombin (AP) in the draft tube apparatus at a gas flow rate of ~ 9.5 lpm on the surface colour based on x and y chromaticity coordinates compared to the prothrombin (II) only control. Statistically significant results are in italics. (n = 3).

Prothrombin (II) control	**Vs. II + AP (mg/mL)**	**Difference detectable by eye vs. control?**	**x coordinate + p values**	**y coordinate + p values**
1 mg/mL II control x = 0.36 ± 0.01 y = 0.22 ± 0.00	5 × 10^{-4} (500 mL) in draft tube apparatus at ~ 9.5 lpm	Yes	x = 0.33 ± 0.01 *p < 0.05*	y = 0.20 ± 0.02 *p < 0.05*

For a 500 mL sample at an anti-prothrombin concentration of 5 × 10^{-4} mg/mL, a visible colour shift from pink (prothrombin only) to purple occurred in the draft tube apparatus after 5 minutes at both gas flow rates of ~ 3.5 lpm and ~ 9.5 lpm. For both gas flow rates, both the x and y chromaticity coordinates were statistically significant after exposure to the anti-prothrombin solution for 5 minutes compared to the prothrombin only control, indicating the formation of an antigen-antibody complex on the surface. Since a colour shift occurred on the surface after only

5 minutes in the draft tube apparatus, the anti-prothrombin concentration was lowered to 6.25×10^{-5} mg/mL and the experiments were repeated. Figures 8.110 and 8.111 show the three replicates prior to protein exposure (row 1), after exposure of each rectangle to 40 μL of 1 mg/mL prothrombin for 20 minutes (row 2), and after exposure of each rectangle to a 500 mL anti-prothrombin solution with a concentration of 6.25×10^{-5} mg/mL after 5 minutes, 10 minutes, 15 minutes and 20 minutes (rows 3, 4, 5, 6) in the draft tube apparatus at gas flow rates of ~ 3.5 lpm and ~ 9.5 lpm, respectively. Statistical analysis was completed on the three replicates to determine the effect of various exposure times and gas flow rates on the surface colour of the prothrombin coated wafer. The x and y coordinates were analyzed using one-way ANOVA and Tukey post hoc tests. Tables 8.59 and 8.60 show the results of the statistical analysis on the effect of various exposure times for a 500 mL sample with an anti-prothrombin concentration of 6.25×10^{-5} mg/mL in the draft tube apparatus with gas flow rates of ~ 3.5 lpm and ~ 9.5 lpm on the surface colour of the prothrombin-coated wafer based on x and y chromaticity coordinates, respectively.

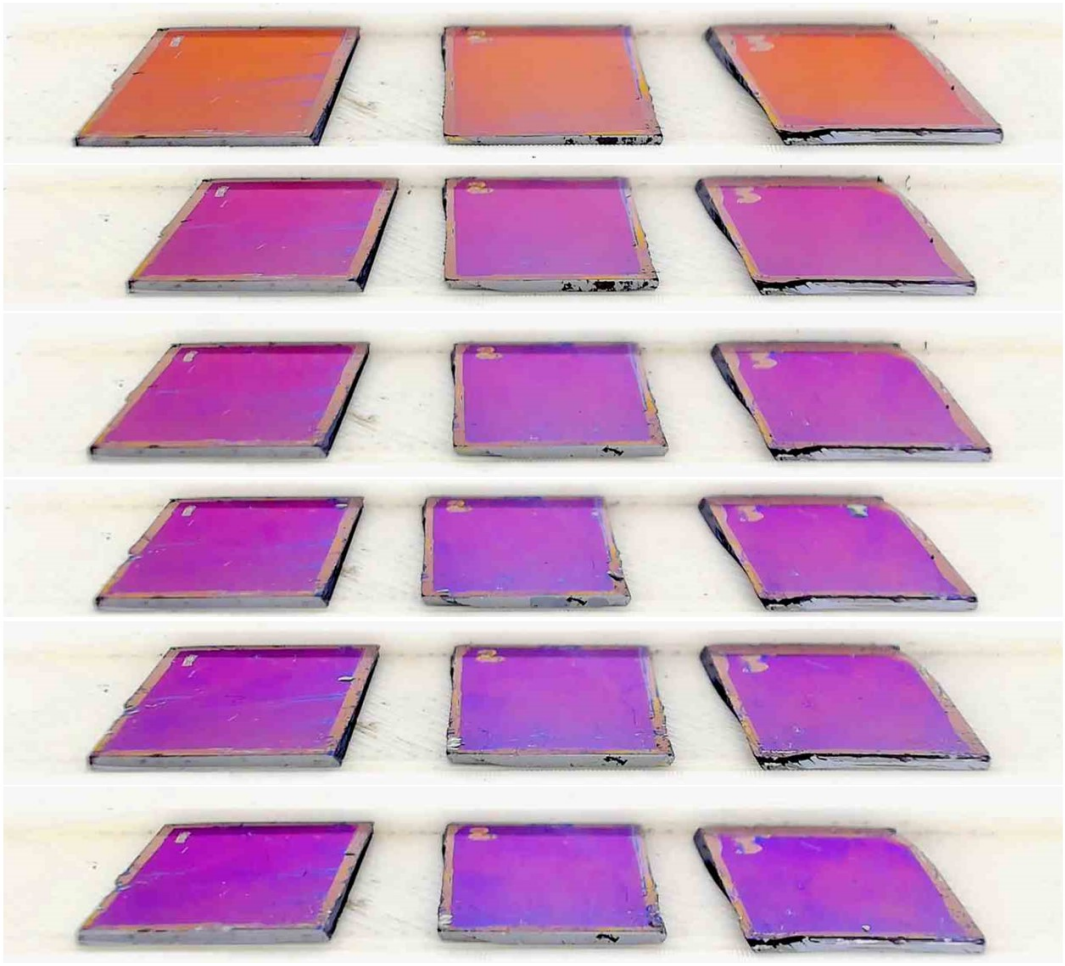


Figure 8.110. Silicon wafer rectangles (three replicates – ~ 1 cm by ~ 1.2 cm each) coated with ~ 200 nm of tantalum and ~ 111 nm of aluminum then anodized at 4 V with no exposure to protein (row 1), after exposure of each rectangle to 40 μL of 1 mg/mL prothrombin for 20 minutes (row 2), after subsequent exposure of each rectangle to 500 mL of 6.25×10^{-5} mg/mL anti-prothrombin for 5, 10, 15 and 20 minutes in the draft tube apparatus at a gas flow rate of ~ 3.5 lpm (rows 3, 4, 5, 6).

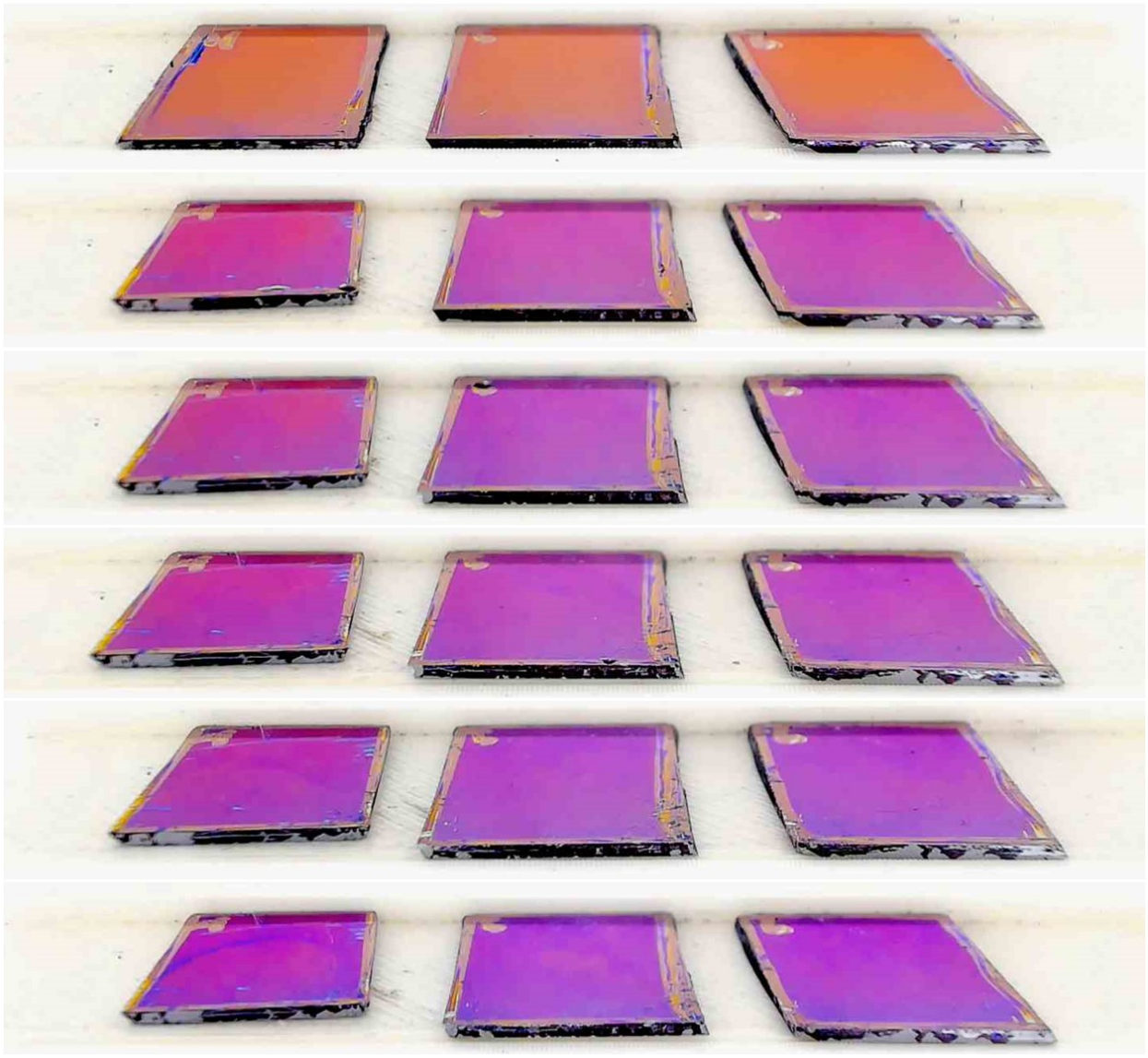


Figure 8.111. Silicon wafer rectangles (three replicates – ~ 1 cm by ~ 1.2 cm each) coated with ~ 200 nm of tantalum and ~ 111 nm of aluminum then anodized at 4 V with no exposure to protein (row 1), after exposure of each rectangle to 40 μL of 1 mg/mL prothrombin for 20 minutes (row 2), after subsequent exposure of each rectangle to 500 mL of 6.25×10^{-5} mg/mL anti-prothrombin for 5, 10, 15 and 20 minutes in the draft tube apparatus at a gas flow rate of ~ 9.5 lpm (rows 3, 4, 5, 6).

Table 8.59. Results of the ANOVA and Tukey post hoc statistical analysis tests on the effect of various anti-prothrombin exposure times for a 500 mL volume at a concentration of 6.25 × 10^{-5} mg/mL in the draft tube apparatus at a gas flow rate of ~ 3.5 lpm on the surface colour using x and y chromaticity coordinates compared to the prothrombin only control. Statistically significant results are in italics. (n = 3).

Prothrombin (II) control	**Vs. II + AP 6.25 × 10^{-5} mg/mL, ~ 3.5 lpm (exposure time)**	**Difference detectable by eye vs. control?**	**x coordinate + p values**	**y coordinate + p values**
1 mg/mL II control x = 0.34 ± 0.01 y = 0.21 ± 0.01	5 minutes	No	x = 0.32 ± 0.01 p > 0.2	y = 0.20 ± 0.01 p > 0.2
	10 minutes	No	x = 0.31 ± 0.01 *p < 0.05*	y = 0.18 ± 0.01 *p < 0.05*
	15 minutes	Yes	x = 0.30 ± 0.01 *p < 0.005*	y = 0.18 ± 0.01 *p < 0.01*
	20 minutes	Yes	x = 0.29 ± 0.01 *p < 0.001*	y = 0.16 ± 0.01 *p < 0.001*

Table 8.60. Results of the ANOVA and Tukey post hoc statistical analysis tests on the effect of various anti-prothrombin exposure times for a 500 mL volume at a concentration of 6.25 × 10^{-5} mg/mL in the draft tube apparatus at a gas flow rate of ~ 9.5 lpm on the surface colour using x and y chromaticity coordinates compared to the prothrombin only control. Statistically significant results are in italics. (n = 3).

Prothrombin (II) control	**Vs. II + AP 6.25 × 10^{-5} mg/mL, ~ 9.5 lpm (exposure time)**	**Difference detectable by eye vs. control?**	**x coordinate + p values**	**y coordinate + p values**
1 mg/mL II control x = 0.36 ± 0.03 y = 0.21 ± 0.01	5 minutes	No	x = 0.33 ± 0.03 p > 0.5	y = 0.20 ± 0.01 p > 0.05
	10 minutes	No	x = 0.33 ± 0.02 p > 0.3	y = 0.19 ± 0.00 *p < 0.01*
	15 minutes	No	x = 0.30 ± 0.01 p > 0.05	y = 0.18 ± 0.01 *p < 0.001*
	20 minutes	Yes	x = 0.29 ± 0.01 *p < 0.05*	y = 0.16 ± 0.00 *p < 0.001*

For an anti-prothrombin concentration of 6.25×10^{-5} mg/mL in the draft tube apparatus, a visible colour shift occurred from pink to purple after 20 minutes at both gas flow rates of ~ 3.5 lpm and ~ 9.5 lpm. For a gas flow rate of ~ 3.5 lpm, both the x and y chromaticity coordinates were statistically significant after 10, 15, and 20 minutes compared to the prothrombin only control. For a gas flow rate of ~ 9.5 lpm, the x chromaticity coordinate was only statistically significant after 20 minutes, and the y chromaticity coordinate was statistically significant after 10, 15, and 20 minutes compared to the prothrombin only control. Since a colour shift occurred on the surface after 20 minutes in the draft tube apparatus at an anti-prothrombin concentration of 6.25×10^{-5} mg/mL, the anti-prothrombin concentration was lowered to 6.25×10^{-6} mg/mL and the experiments were repeated. Figures 8.112 and 8.113 show the three replicates prior to protein exposure (row 1), after exposure of each rectangle to 40 μL of 1 mg/mL prothrombin for 20 minutes (row 2), and after exposure of each rectangle to a 500 mL anti-prothrombin solution with a concentration of 6.25×10^{-6} mg/mL after 20 minutes and 40 minutes (rows 3, 4) in the draft tube apparatus at gas flow rates of ~ 3.5 lpm and ~ 9.5 lpm, respectively. Statistical analysis was completed on the three replicates to determine the effect of various exposure times and gas flow rates on the surface colour of the prothrombin coated wafer. The x and y coordinates were analyzed using one-way ANOVA and Tukey post hoc tests. Tables 8.61 and 8.62 show the results of the statistical analysis on the effect of various exposure times for a 500 mL sample with an anti-prothrombin concentration of 6.25×10^{-6} mg/mL in the draft tube apparatus with gas flow rates of ~ 3.5 lpm and ~ 9.5 lpm on the surface colour of the prothrombin-coated wafer based on x and y chromaticity coordinates, respectively.

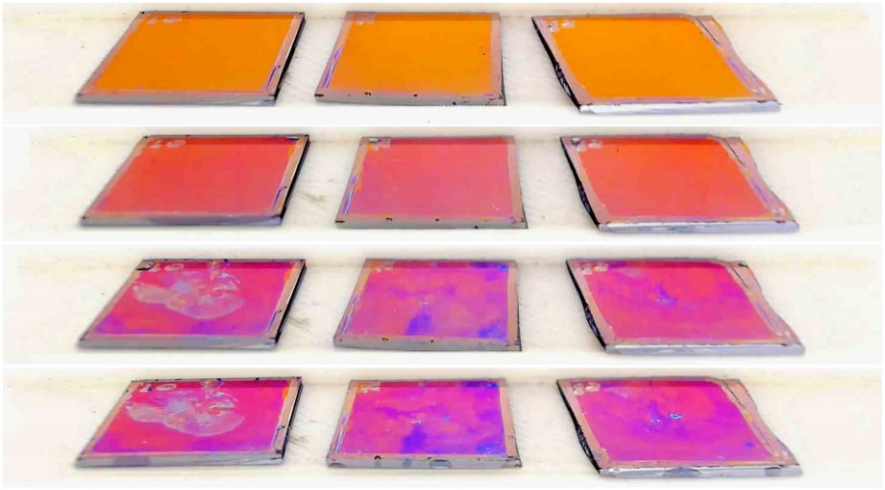


Figure 8.112. Silicon wafer rectangles (three replicates – ~ 1 cm by ~ 1.2 cm each) coated with ~ 200 nm of tantalum and ~ 105 nm of aluminum then anodized at 4 V with no exposure to protein (row 1), after exposure of each rectangle to 40 μL of 1 mg/mL prothrombin for 20 minutes (row 2), after subsequent exposure of each rectangle to 500 mL of 6.25 × 10^{-6} mg/mL anti-prothrombin for 20 and 40 minutes in the draft tube apparatus at a gas flow rate of ~ 3.5 lpm (rows 3, 4).

Table 8.61. Results of the ANOVA and Tukey post hoc statistical analysis tests on the effect of various anti-prothrombin exposure times for a 500 mL volume at a concentration of 6.25 × 10^{-6} mg/mL in the draft tube apparatus at a gas flow rate of ~ 3.5 lpm on the surface colour using x and y chromaticity coordinates compared to the prothrombin only control. Statistically significant results are in italics. (n = 3).

Prothrombin (II) control	**Vs. II + AP 6.25 × 10^{-6} mg/mL, ~ 3.5 lpm (exposure time)**	**Difference detectable by eye vs. control?**	**x coordinate + p values**	**y coordinate + p values**
1 mg/mL II control x = 0.50 ± 0.03 y = 0.33 ± 0.02	20 minutes	Yes	x = 0.43 ± 0.05 p > 0.1	y = 0.26 ± 0.02 *p < 0.02*
	40 minutes	Yes	x = 0.39 ± 0.03 *p < 0.05*	y = 0.22 ± 0.02 *p < 0.001*

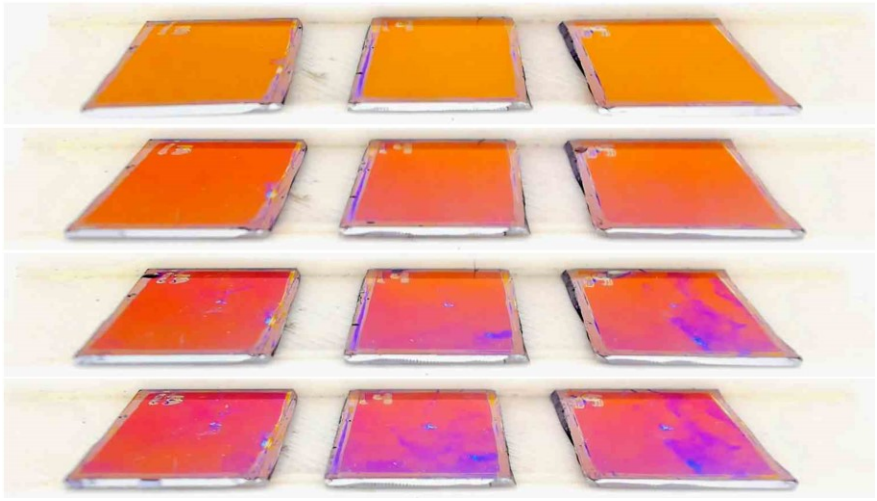


Figure 8.113. Silicon wafer rectangles (three replicates – ~ 1 cm by ~ 1.2 cm each) coated with ~ 200 nm of tantalum and ~ 105 nm of aluminum then anodized at 4 V with no exposure to protein (row 1), after exposure of each rectangle to 40 μL of 1 mg/mL prothrombin for 20 minutes (row 2), after subsequent exposure of each rectangle to 500 mL of 6.25 × 10^{-6} mg/mL anti-prothrombin for 20 and 40 minutes in the draft tube apparatus at a gas flow rate of ~ 9.5 lpm (rows 3, 4).

Table 8.62. Results of the ANOVA and Tukey post hoc statistical analysis tests on the effect of various anti-prothrombin exposure times for a 500 mL volume at a concentration of 6.25 × 10^{-6} mg/mL in the draft tube apparatus at a gas flow rate of ~ 9.5 lpm on the surface colour using x and y chromaticity coordinates compared to the prothrombin only control. Statistically significant results are in italics. (n = 3).

Prothrombin (II) control	**Vs. II + AP 6.25 × 10^{-6} mg/mL, ~ 9.5 lpm (exposure time)**	**Difference detectable by eye vs. control?**	**x coordinate + p values**	**y coordinate + p values**
1 mg/mL II control x = 0.54 ± 0.03 y = 0.36 ± 0.01	20 minutes	No	x = 0.51 ± 0.06 p > 0.7	y = 0.47 ± 0.07 p > 0.2
	40 minutes	Yes	x = 0.32 ± 0.04 p > 0.3	y = 0.28 ± 0.03 *p < 0.05*

For an anti-prothrombin concentration of 6.25×10^{-6} mg/mL in the draft tube apparatus, a visible colour shift from orange (prothrombin only) to pink/purple occurred after 20 minutes at both gas flow rates of ~ 3.5 lpm and ~ 9.5 lpm. For a gas flow rate of ~ 3.5 lpm, only the y chromaticity coordinate was statistically significant after 20 minutes and both the x and y chromaticity coordinates were statistically significant after 40 minutes compared to the prothrombin only control. For a gas flow rate of ~ 9.5 lpm, the x chromaticity coordinate was not statistically significant after 20 or 40 minutes, and the y chromaticity coordinate was only statistically significant after 40 minutes compared to the prothrombin only control. For both gas flow rates, the colour shift appeared uneven and patchy on the surface, likely due to a disruption in the fluid flow by the clip just above the prothrombin coated slides. Although the colour shift did not appear completely uniform, a visible colour shift did occur at an anti-prothrombin concentration of 6.25×10^{-6} mg/mL (41.7 pM), and this concentration was determined to be the limit of detection for the draft tube apparatus at both gas flow rates of ~ 3.5 lpm and ~ 9.5 lpm, with better visual detection at a gas flow rate of ~ 3.5 lpm compared to ~ 9.5 lpm.

To confirm anti-prothrombin binding to the prothrombin coated surface, a secondary antibody, rabbit anti-sheep IgG (H+L)-horseradish peroxidase (HRP), that is expected to bind to anti-prothrombin, was placed on the surface of the slide after exposure to the anti-prothrombin solution in the draft tube apparatus. A 500 mL sample of MilliQ water containing anti-prothrombin at a concentration of 6.25×10^{-4} mg/mL was prepared to assess binding of the secondary antibody. Silicon wafer substrates were coated with ~ 200 nm of tantalum and ~ 107 nm of aluminum then anodized at 4 V and cut using the diamond scribe and the stencil. The silicon wafer slides were then further cut into smaller squares with dimensions of ~ 1 cm by ~ 1.2 cm. A Sharpie was used to trace the edges of the rectangles to contain the protein solutions.

Then, 40 µL of 1 mg/mL prothrombin was placed on the surface and spread to the edges of the rectangle using a pipette tip and was left in a Petri dish with a wet paper towel for 20 minutes. After exposure to prothrombin, the wafers were rinsed with deionized water and dried with oil free compressed air. The prothrombin coated slides were then placed in the draft tube apparatus and a solution containing anti-prothrombin at a concentration of 6.25×10^{-4} mg/mL was added to the graduated cylinder. A gas flow rate of ~ 3.5 lpm was used and the slides were viewed after 10 minutes. After exposure to the anti-prothrombin solution in the draft tube apparatus, 0.7 cm hydrophobic circles were drawn on each slide with a Sharpie marker and 15 µL of rabbit anti-sheep IgG (H+L)-horseradish peroxidase antibody was pipetted and spread to the edges of the circle. The slides were placed on a wet paper towel in a Petri dish for 20 minutes. After 20 minutes, the slides were rinsed with deionized water and dried with oil free compressed air. Figure 8.114 shows the three replicates prior to protein exposure (row 1), after exposure of each rectangle to 40 µL of 1 mg/mL prothrombin for 20 minutes (row 2), after exposure of each rectangle to a 500 mL anti-prothrombin solution with a concentration of 6.25×10^{-4} mg/mL for 10 minutes in the draft tube apparatus at a gas flow rate of ~ 3.5 lpm, and after exposure of the hydrophobic circles to 15 µL of rabbit anti-sheep IgG (H+L)-horseradish peroxidase for 20 minutes (row 4). The x and y coordinates were analyzed using an independent T-test to assess the surface colour after exposure to anti-prothrombin (AP) in the draft tube apparatus and after exposure to the secondary antibody, and a p value less than 0.05 indicates statistical significance. Table 8.63 shows the results of the statistical analysis on the effect of 15 µL of rabbit anti-sheep IgG (H+L)-horseradish peroxidase (HRP) (secondary antibody) in the hydrophobic circles on the surface colour based on x and y chromaticity coordinates compared to the surface colour after

exposure to 500 mL of 6.25×10^{-4} mg/mL anti-prothrombin for 10 minutes in the draft tube apparatus at a gas flow rate of ~ 3.5 lpm based on x and y chromaticity coordinates.

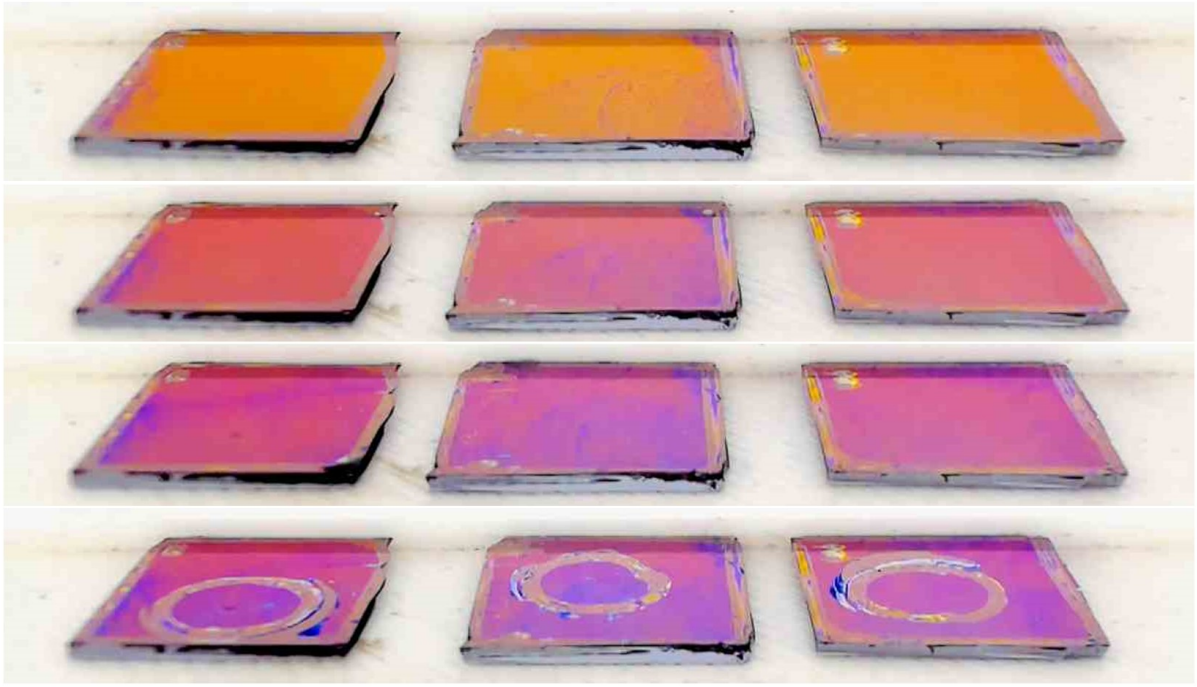


Figure 8.114. Silicon wafer rectangles (three replicates – ~ 1 cm by ~ 1.2 cm each) coated with ~ 200 nm of tantalum and ~ 107 nm of aluminum then anodized at 4 V with no exposure to protein (row 1), after exposure of each rectangle to 40 µL of 1 mg/mL prothrombin for 20 minutes (row 2), after subsequent exposure of each rectangle to 500 mL of 6.25×10^{-4} mg/mL anti-prothrombin for 10 minutes in the draft tube apparatus at a gas flow rate of ~ 3.5 lpm (row 3), after subsequent exposure of hydrophobic circles to 15 µL of rabbit anti-sheep IgG (H+L)-horseradish peroxidase (HRP) conjugate for 20 minutes (row 4).

Table 8.63. Results of the independent T-test statistical analysis on the effect of 15 μL of rabbit anti-sheep IgG (H+L)-horseradish peroxidase (HRP) in the hydrophobic circles on the surface colour based on x and y chromaticity coordinates compared to the surface colour after exposure to 500 mL of 6.25 × 10^{-4} mg/mL anti-prothrombin for 10 minutes in the draft tube apparatus at a gas flow rate of ~ 3.5 lpm. Statistically significant results are in italics. (n = 3).

AP (6.25 × 10^{-4} mg/mL in draft tube apparatus ~ 3.5 lpm)	**Vs. AP + secondary antibody**	**Difference detectable by eye vs. control?**	**x coordinate + p values**	**y coordinate + p values**
x = 0.38 ± 0.05 y = 0.26 ± 0.03	Rabbit anti-sheep IgG (H+L)- (HRP)	Yes	x = 0.30 ± 0.02 p > 0.05	y = 0.20 ± 0.02 *p < 0.05*

A visible colour shift occurred after exposure of the hydrophobic circles to 15 μL of the rabbit anti-sheep IgG (H+L)-horseradish peroxidase (HRP) secondary antibody for 20 minutes, indicating binding of the secondary antibody to bound anti-prothrombin. The y chromaticity coordinate was statistically significant after exposure to the secondary antibody compared to the surface colour after exposure to anti-prothrombin in the draft tube apparatus for 10 minutes, confirming the presence of anti-prothrombin on the prothrombin coated surface.

A negative control experiment was conducted in which 500 mL of MilliQ water containing no anti-prothrombin was placed in the draft tube apparatus at a gas flow rate of ~ 9.5 lpm for 10 minutes, and no colour shift was expected on the surface. Figure 8.115 shows the three replicates prior to protein exposure (row 1), after exposure of each rectangle to 40 μL of 1 mg/mL prothrombin for 20 minutes (row 2), and after exposure of each rectangle to 500 mL of MilliQ water containing no anti-prothrombin in the draft tube apparatus at a gas flow rate of ~ 9.5 lpm for 10 minutes (row 3). The x and y coordinates were analyzed using an independent T-

test to assess the surface colour of the prothrombin only coated slides and after exposure to 500 mL of MilliQ water containing no anti-prothrombin in the draft tube apparatus at a gas flow rate of ~ 9.5 lpm. A p value less than 0.05 indicates statistical significance. Table 8.64 shows the results of the statistical analysis on the effect of 500 mL of MilliQ water containing no anti-prothrombin in the draft tube apparatus at a gas flow rate of ~ 9.5 lpm for 10 minutes on the surface colour based on x and y chromaticity coordinates compared to the prothrombin only control based on x and y chromaticity coordinates.

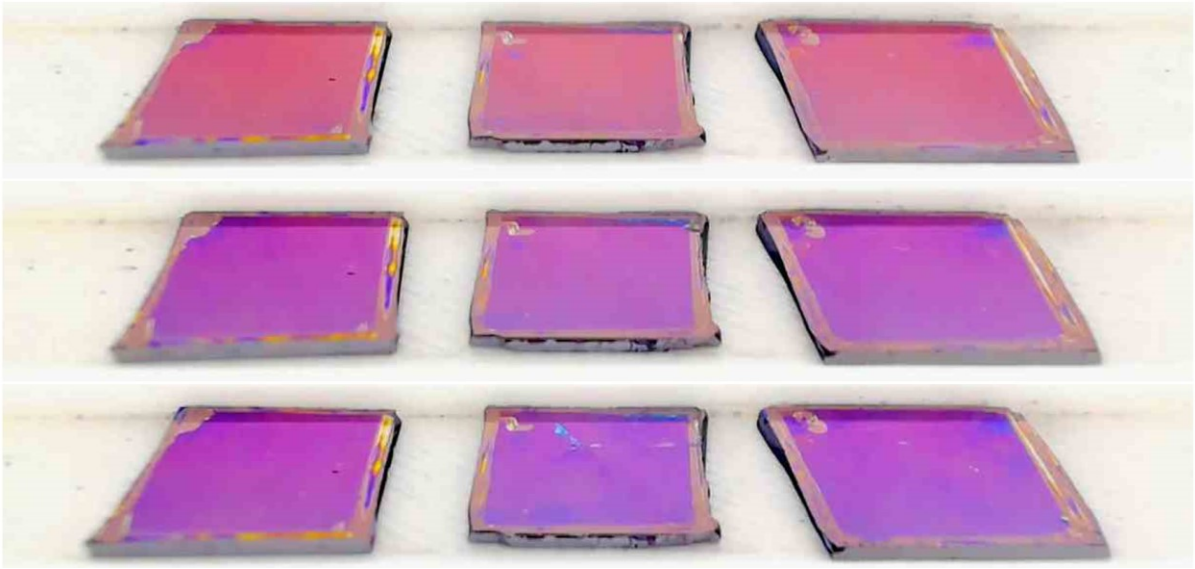


Figure 8.115. Silicon wafer rectangles (three replicates – ~ 1 cm by ~ 1.2 cm each) coated with ~ 200 nm of tantalum and ~ 110 nm of aluminum then anodized at 4 V with no exposure to protein (row 1), after exposure of each rectangle to 40 µL of 1 mg/mL prothrombin for 20 minutes (row 2), and after subsequent exposure of each rectangle to 500 mL of MilliQ water in the draft tube apparatus at a gas flow rate of ~ 9.5 lpm for 10 minutes (row 3).

Table 8.64. Results of the independent T-test statistical analysis on the effect of 500 mL of MilliQ water containing no anti-prothrombin (AP) in the draft tube apparatus at a gas flow rate of ~ 9.5 lpm for 10 minutes on the surface colour based on x and y chromaticity coordinates compared to the prothrombin (II) only control. Statistically significant results are in italics. (n = 3).

Prothrombin (II) control	**Vs. II + MilliQ (MQ) water**	**Difference detectable by eye vs. control?**	**x coordinate + p values**	**y coordinate + p values**
1 mg/mL II control x = 0.31 ± 0.01 y = 0.20 ± 0.01	No AP, 500 mL MQ, draft tube apparatus at ~ 9.5 lpm	No	x = 0.30 ± 0.01 p > 0.3	y = 0.19 ± 0.01 p > 0.05

No visible colour shift occurred on the surface after exposure to 500 mL of MilliQ water in the draft tube apparatus at a gas flow rate of ~ 9.5 lpm, and neither the x or the y chromaticity coordinate was statistically significant after 10 minutes compared to the prothrombin only control. From this experiment, it was determined that the MilliQ water does not induce a colour shift on the prothrombin coated surface, and colour shifts in previous experiments are due to binding of anti-prothrombin to prothrombin on the surface.

To assess the draft tube design on the device sensitivity, a conical shaped draft tube was drafted in Fusion 360 by Ben Damant and 3D printed for use in the draft tube device. The inlet diameter at the top of the conical draft tube was 3.93 cm, and the outlet diameter at the bottom of the draft tube was 1.4 cm. From the base of the slide holder to the top of the tube, the height of the draft tube apparatus was 12.1 cm, with the draft tube portion being 10.8 cm. The draft tube was designed such that the silicon wafer slides were clipped and secured 1 cm below the outlet of the tube. By reducing the cross-sectional area from the inlet at the top of the draft tube to the outlet at the bottom of the draft tube, it was expected that the fluid velocity at the outlet would be

greater, increasing the Reynolds number just above the silicon wafer slides. Figure 8.116 shows the Fusion 360 design of the conical draft tube.



Figure 8.116. Fusion 360 design of conical shaped draft tube.

To calculate the Reynolds number in the downcomer section of the draft tube, the pipe flow Reynolds number equation (Equation 2-1) was used. The density of water at 21°C, 997.9 kg/m^3, was used as the fluid density (ρ), the dynamic viscosity of water at 21°C, 0.000976 Pa·s, was used as the fluid viscosity (μ), the average pipe diameter of 2.665 cm (calculated as the outlet diameter plus the inlet diameter divided by 2) was used as the pipe diameter (D), and the average fluid velocity in the tube was used for the fluid velocity (v). To determine the average fluid velocity in the draft tube, an experiment was conducted in which the time taken for a drop of dye to travel from the top of the tube to the bottom of the tube was measured while bubbling at a gas flow rate of 3.5 lpm. It took 0.47 seconds for the dye to travel the distance of the draft

tube (0.108 m), resulting in the average fluid velocity in the tube of 0.23 m/s. From these values, the Reynolds number in the conical draft tube was calculated to be ~ 6267.

Initially, a 500 mL solution of anti-prothrombin at a concentration of 6.25×10^{-6} mg/mL was tested in the conical draft tube device. Silicon wafer substrates were coated with ~ 200 nm of tantalum and ~ 110 nm of aluminum then anodized at 4 V and cut using the diamond scribe and the stencil. The silicon wafer slides were then further cut into smaller squares with dimensions of ~ 1 cm by ~ 1.2 cm, then subsequently cut in half to produce rectangles with dimensions of ~ 1 cm by ~ 0.6 cm. As these slides had a smaller surface area, fewer molecules would be required to bind to produce a uniform colour shift, potentially improving the device sensitivity. A Sharpie was used to trace the edges of the rectangles to contain the protein solutions. Then, 20 µL of 1 mg/mL prothrombin was placed on the surface and spread to the edges of the rectangle using a pipette tip and was left in a Petri dish with a wet paper towel for 20 minutes. After exposure to prothrombin, the wafers were rinsed with deionized water and dried with oil free compressed air. The prothrombin coated wafers were then placed under the outlet of the 3D printed conical draft tube and secured using a clip, and the draft tube and bubbler apparatus were placed in a 1 L graduated cylinder that had been cut at the 600 mL mark. A 500 mL solution of 6.25×10^{-6} mg/mL anti-prothrombin was placed in the graduated cylinder, and the compressor attached to the bubbler was turned on and set to a gas flow rate of ~ 3.5 lpm, as measured by the rotameter. Figure 8.117 shows the three replicates prior to protein exposure (row 1), after exposure of each rectangle to 20 µL of 1 mg/mL prothrombin for 20 minutes (row 2), and after exposure of each rectangle to a 500 mL anti-prothrombin solution with a concentration of 6.25×10^{-6} mg/mL for 20 minutes in the conical draft tube apparatus at a gas flow rate of ~ 3.5 lpm (row 3). The x and y chromaticity coordinates were analyzed separately

using independent T-tests. Table 8.65 shows the results of the statistical analysis on the effect of 500 mL of 6.25×10^{-6} mg/mL anti-prothrombin for 20 minutes in the conical draft tube apparatus at ~ 3.5 lpm on the surface colour of the prothrombin-coated wafer based on x and y chromaticity coordinates.

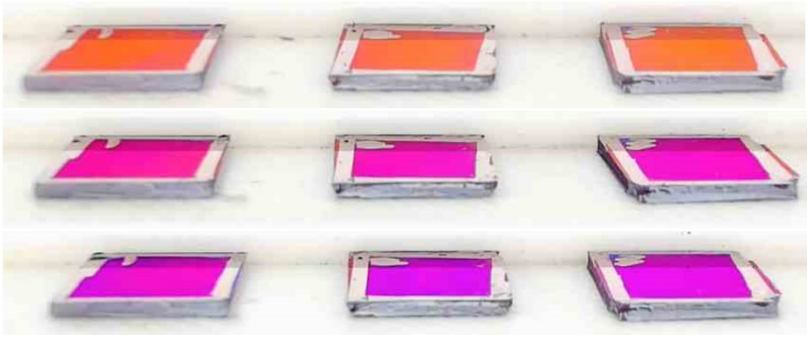


Figure 8.117. Silicon wafer rectangles (three replicates – ~ 1 cm by ~ 0.6 cm each) coated with ~ 200 nm of tantalum and ~ 110 nm of aluminum then anodized at 4 V with no exposure to protein (row 1), after exposure of each rectangle to 20 µL of 1 mg/mL prothrombin for 20 minutes (row 2), and after subsequent exposure of each rectangle to 500 mL of 6.25×10^{-6} mg/mL anti-prothrombin for 20 minutes in the conical draft tube apparatus at a gas flow rate of ~ 3.5 lpm (row 3).

Table 8.65. Results of the independent T-test statistical analysis on the effect of 500 mL of 6.25×10^{-6} mg/mL anti-prothrombin (AP) in the conical draft tube apparatus at a gas flow rate of ~ 3.5 lpm for 20 minutes on the surface colour based on x and y chromaticity coordinates compared to the prothrombin (II) only control. Statistically significant results are in italics. (n = 3).

Prothrombin (II) control	**Vs. II + AP (mg/mL)**	**Difference detectable by eye vs. control?**	**x coordinate + p values**	**y coordinate + p values**
1 mg/mL II control x = 0.40 ± 0.03 y = 0.20 ± 0.02	6.25×10^{-6} (500 mL) in draft tube apparatus, 3.5 lpm, 20 min	Yes	x = 0.33 ± 0.03 *$p < 0.05$*	y = 0.16 ± 0.02 *$p < 0.05$*

For an anti-prothrombin concentration of 6.25×10^{-6} mg/mL in the conical draft tube apparatus, a visible colour shift from pink (prothrombin only) to purple occurred, and both the x and y chromaticity coordinates were significant after 20 minutes at a gas flow rate of ~ 3.5 lpm. The colour shift appeared even and uniform across the surface, suggesting that the conical draft tube improved the uniformity issue faced at an anti-prothrombin concentration of 6.25×10^{-6} mg/mL in the original, straight draft tube. As a strong, uniform colour shift occurred at a concentration of 6.25×10^{-6} mg/mL in the conical draft tube apparatus, the experiments were repeated using slides with dimensions of ~ 1 cm by ~ 0.6 cm at an anti-prothrombin concentration of 6.25×10^{-7} mg/mL. After cutting the slides, a Sharpie was used to trace the edges of the rectangles to contain the protein solutions. Then, 20 µL of 1 mg/mL prothrombin was placed on the surface and spread to the edges of the rectangle using a pipette tip and was left in a Petri dish with a wet paper towel for 20 minutes. After exposure to prothrombin, the wafers were rinsed with deionized water and dried with oil free compressed air. The slides were then exposed to a 500 mL solution of 6.25×10^{-7} mg/mL anti-prothrombin in the conical draft tube apparatus at a gas flow rate of ~ 3.5 lpm for 20 minutes. After 20 minutes, the slides were rinsed with deionized water and dried with oil free compressed air. Hydrophobic circles with a diameter of 0.7 cm were then drawn on the slides, and 15 µL of rabbit anti-sheep IgG (H+L)-horseradish peroxidase (secondary antibody) was placed in the circles for 20 minutes on a wet paper towel in a Petri dish. The secondary antibody solution was removed after 20 minutes, and the slides were rinsed with deionized water and dried with oil free compressed air. The secondary antibody was used to confirm anti-prothrombin binding to the surface, indicated by a colour shift due to the binding of the secondary antibody to the bound anti-prothrombin on the surface. Figure 8.118 shows the three replicates prior to protein exposure (row 1), after exposure of each rectangle to

20 µL of 1 mg/mL prothrombin for 20 minutes (row 2), after exposure of each rectangle to a 500 mL anti-prothrombin solution with a concentration of 6.25×10^{-7} mg/mL for 20 minutes in the conical draft tube apparatus at a gas flow rate of ~ 3.5 lpm (row 3), and after exposure of the hydrophobic circles to 15 µL of rabbit anti-sheep IgG (H+L)-horseradish peroxidase for 20 minutes (row 4). The x and y chromaticity coordinates were analyzed separately using independent T-tests. Table 8.66 shows the results of the statistical analysis on the effect of 500 mL of 6.25×10^{-7} mg/mL anti-prothrombin for 20 minutes in the conical draft tube apparatus at ~ 3.5 lpm on the surface colour of the prothrombin-coated wafer based on x and y chromaticity coordinates.

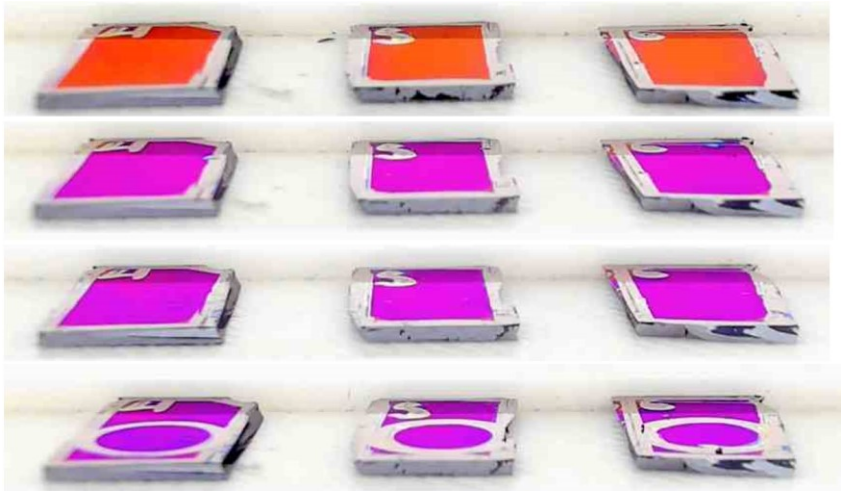


Figure 8.118. Silicon wafer rectangles (three replicates – ~ 1 cm by ~ 0.6 cm each) coated with ~ 200 nm of tantalum and ~ 110 nm of aluminum then anodized at 4 V with no exposure to protein (row 1), after exposure of each rectangle to 20 µL of 1 mg/mL prothrombin for 20 minutes (row 2), after subsequent exposure of each rectangle to 500 mL of 6.25×10^{-7} mg/mL anti-prothrombin for 20 minutes in the conical draft tube apparatus at a gas flow rate of ~ 3.5 lpm (row 3), and after subsequent exposure of hydrophobic circles to 15 µL of rabbit anti-sheep IgG (H+L)-horseradish peroxidase (HRP) conjugate for 20 minutes (row 4).

Table 8.66. Results of the independent T-test statistical analysis on the effect of 500 mL of 6.25 × 10^{-7} mg/mL anti-prothrombin (AP) in the conical draft tube apparatus at a gas flow rate of ~ 3.5 lpm for 20 minutes on the surface colour based on x and y chromaticity coordinates compared to the prothrombin (II) only control. Statistically significant results are in italics. (n = 3).

Prothrombin (II) control	**Vs. II + AP (mg/mL)**	**Difference detectable by eye vs. control?**	**x coordinate + p values**	**y coordinate + p values**
1 mg/mL II control x = 0.34 ± 0.00 y = 0.17 ± 0.00	6.25 × 10^{-7} (500 mL) in conical draft tube, 3.5 lpm, 20 min	Yes	x = 0.31 ± 0.00 *p < 0.01*	y = 0.15 ± 0.00 *p < 0.01*

For a 500 mL sample containing anti-prothrombin at a concentration of 6.25 × 10^{-7} mg/mL, a visible and uniform colour shift from pink (prothrombin only) to light purple occurred on the surface, and both the x and y chromaticity coordinates were statistically significant after 20 minutes in the conical draft tube apparatus at a gas flow rate of ~ 3.5 lpm. Another visible colour shift from light purple to darker purple occurred in the hydrophobic circles after exposure to the secondary antibody, suggesting the secondary antibody was able to bind to anti-prothrombin. To assess binding of the secondary antibody, the x and y coordinates were analyzed using an independent T-test to assess the surface colour after exposure to the anti-prothrombin (AP) solution in the draft tube apparatus and after exposure to the secondary antibody in the hydrophobic circles. Table 8.67 shows the results of the statistical analysis on the effect of 15 µL of rabbit anti-sheep IgG (H+L)-horseradish peroxidase (HRP) (secondary antibody) in the hydrophobic circles on the surface colour based on x and y chromaticity coordinates compared to the surface colour after exposure to 500 mL of 6.25 × 10^{-7} mg/mL anti-prothrombin for 20 minutes in the conical draft tube apparatus at a gas flow rate of ~ 3.5 lpm.

Table 8.67. Results of the independent T-test statistical analysis on the effect of 15 µL of rabbit anti-sheep IgG (H+L)-horseradish peroxidase (HRP) in the hydrophobic circles on the surface colour based on x and y chromaticity coordinates compared to the surface colour after exposure to 500 mL of 6.25 × 10^{-7} mg/mL anti-prothrombin for 20 minutes in the conical draft tube apparatus at a gas flow rate of ~ 3.5 lpm. Statistically significant results are in italics. (n = 3).

AP (6.25 × 10^{-7} mg/mL in draft tube apparatus ~ 3.5 lpm)	**Vs. AP + secondary antibody**	**Difference detectable by eye vs. control?**	**x coordinate + p values**	**y coordinate + p values**
x = 0.31 ± 0.00 y = 0.15 ± 0.00	Rabbit anti-sheep IgG (H+L)- (HRP)	Yes	x = 0.29 ± 0.01 *p < 0.05*	y = 0.14 ± 0.01 *p < 0.05*

A visible colour shift occurred after exposure of the hydrophobic circles to 15 µL of the rabbit anti-sheep IgG (H+L)-horseradish peroxidase (HRP) secondary antibody for 20 minutes, indicating binding of the secondary antibody to bound anti-prothrombin. Both the x and y chromaticity coordinates were statistically significant after exposure to the secondary antibody compared to the surface colour after exposure to anti-prothrombin in the conical draft tube apparatus for 20 minutes, confirming the presence of anti-prothrombin on the prothrombin coated surface. As a strong, visible colour shift occurred on the surface after exposure to a 500 mL sample containing anti-prothrombin at a concentration of 6.25 × 10^{-7} mg/mL for 20 minutes in the conical draft tube at a gas flow rate of ~ 3.5 lpm, the limit of detection for the conical shaped draft tube was determined to be 6.25 × 10^{-7} mg/mL (4.17 pM). Adjusting the design of the draft tube from straight to conical allowed for the draft tube device sensitivity to be improved by a factor of 10 and solved the surface uniformity issue faced at the limit of detection concentration in the straight draft tube (6.25 × 10^{-6} mg/mL).

8.7. Discussion

For the small volume stationary sensitivity tests, a 20 µL volume of 0.05 mg/mL anti-prothrombin on a prothrombin coated surface led to a visible colour shift on the surface after 20 minutes, while an anti-prothrombin concentration of 0.005 mg/mL did not, for a silicon wafer substrate coated with 200 nm of tantalum and ~ 106 nm of aluminum, then anodized at 4 V. This suggests that the limit of detection likely fell somewhere in between these two values, agreeing with previous work done by Sweet, in which the limit of detection for anti-prothrombin on a prothrombin coated surface was found to be 0.025 mg/mL for a 20 µL volume [5]. As the larger volume experiments were expected to improve sensitivity due to turbulence and mixing, an anti-prothrombin concentration of 0.005 mg/mL was tested in a 500 mL volume, with continuous stirring above the coated substrate material. Large volume sensitivity tests were conducted at anti-prothrombin concentration of 0.005 mg/mL, 0.0025 mg/mL, and 5×10^{-4} mg/mL. For silicon wafer slides with dimensions of ~ 1.3 cm by ~ 6.2 cm, uniform colour shifts were not consistently produced, likely due to the large surface area. By cutting the slides into smaller pieces, with dimensions of ~ 1.2 cm by ~ 1 cm, the surface area required to bind anti-prothrombin was reduced and the uniformity of the colour shifts was improved. For the smaller surface areas, increasing the volume of the sample to 100 mL or 500 mL was able to improve the sensitivity, even without mixing and turbulence. Without mixing, the limit of detection for anti-prothrombin in a 100 mL and a 500 mL solution was found to be 0.0025 mg/mL (16.7 nM), as this concentration produced strong colour shifts in the stationary volume. Introducing turbulence into the system by using an impeller to mix the solution above the coated wafers allowed for an improvement in sensitivity, and the limit of detection for a 100 mL volume with continuous stirring at 195 RPM or 360 RPM was found to be 6.25×10^{-4} mg/mL (4.2 nM) of anti-

prothrombin on a silicon wafer with a rectangular area of ~ 1.2 cm^2. The tantalum disc substrate material was investigated to determine the importance of residence time and was able to detect an anti-prothrombin concentration of 0.00125 mg/mL. However, the colour shift appeared uneven and difficult to assess at a concentration of 0.00125 mg/mL, so the tantalum discs and syringe-filter design were not further considered. The sensitivity was even further improved by introducing directed turbulence using the draft tube apparatus. The draft tube apparatus ensured fluid flow was continuously circulated and directed over the prothrombin coated membrane for the duration of the experiment. In the draft tube apparatus, the limit of detection for a 500 mL volume was found to be 6.25×10^{-6} mg/mL (41.7 pM) of anti-prothrombin at a gas flow rate of ~ 3.5 lpm on a silicon wafer with a rectangular area of ~ 1.2 cm^2. Adjusting the design of the draft tube apparatus from straight to conical and cutting the silicon wafer slides in half to have an area of ~ 0.6 cm^2 improved the sensitivity even further. The conical shape draft tube achieved a limit of detection of 6.25×10^{-7} mg/mL (4.17 pM) of anti-prothrombin for a 500 mL sample at a gas flow rate of ~ 3.5 lpm.

From this work, the limit of detection for a 20 µL drop on a silicon wafer coated with prothrombin was found to be 0.05 mg/mL anti-prothrombin. By increasing the sample volume from 20 µL to 100 mL or 500 mL, the sensitivity was improved twenty-fold, and the limit of detection was found to be 0.0025 mg/mL anti-prothrombin, even in the absence of mixing. By introducing directed turbulence and mixing, the device sensitivity improved even further, and the limit of detection for a 500 mL volume was found to be 6.25×10^{-6} mg/mL of anti-prothrombin (an 8,000-fold improvement compared to the 20 µL drop limit of detection of 0.05 mg/mL). Using a stationary large volume sample (100 mL or 500 mL) allowed for a ten-fold improvement in sensitivity (limit of detection: 0.0025 mg/mL) compared to previous work that found the limit

of detection for anti-prothrombin on a prothrombin coated surface to be 0.025 mg/mL [5]. Introducing mixing and turbulence to the system in a stirred tank with an impeller allowed for a 40-fold improvement in sensitivity (limit of detection: 6.25×10^{-4} mg/mL) compared to previous work that found a limit of detection for anti-prothrombin on a prothrombin coated surface to be 0.025 mg/mL [5]. The use of an airlift bioreactor design including a draft tube improved the sensitivity by a factor of 100 compared to the stirred tank set up, as the draft tube ensures the fluid sample is continuously recirculated and directed at the prothrombin coated membrane. In the straight draft tube set up, the limit of detection was found to be 6.25×10^{-6} mg/mL for a gas flow rate of ~ 3.5 lpm. Compared to the 20 μL drop with an experimental limit of detection of 0.05 mg/mL, the airlift bioreactor and draft tube allowed for an 8,000-fold improvement in sensitivity, with a limit of detection of 6.25×10^{-6} mg/mL (41.7 pM) of anti-prothrombin. Compared to previous work that found a limit of detection for anti-prothrombin on a prothrombin coated surface to be 0.025 mg/mL, the draft tube set up improved the sensitivity by a factor of 4,000 [5]. The use of a conical shaped draft tube allowed for a ten-fold improvement in sensitivity compared to the straight draft tube, achieving a limit of detection of 6.25×10^{-7} mg/mL (4.17 pM). Compared to the 20 μL drop with an experimental limit of detection of 0.05 mg/mL, the conical draft tube allowed for an 80,000-fold improvement in sensitivity. Compared to previous work that found a limit of detection for anti-prothrombin on a prothrombin coated surface to be 0.025 mg/mL, the conical draft tube set up improved the sensitivity by a factor of 40,000 [5]. Quinn et al. (2002) found that an enzyme-linked immunosorbent assay (ELISA) for immunoglobulin G (IgG) antibodies to *Bacillus anthracis* protective antigen in human serum had a minimum detection limit of 0.06 μg/mL and it takes between 150 and 180 minutes to complete the test [12]. The use of the conical draft tube apparatus in the diagnostic device achieved a limit

of detection of 6.25×10^{-7} mg/mL (0.000625 µg/mL) in 20 minutes, a 96-fold improvement in sensitivity achieved 7.5 times faster than the ELISA method described by Quinn et al. (2002). Zhang et al. (2014) suggested that the detection limit for a horseradish peroxidase (HRP)/3,3,5,5'-tetramethylbenzidine (TMB)-based ELISA should be around 100 pg/mL (1×10^{-7} mg/mL) [13]. ThermoFisher Scientific states that the Invitrogen ELISA kits have an analytical sensitivity in the range of < 1 pg/mL (1×10^{-9} mg/mL) to < 5 pg/mL (5×10^{-9} mg/mL), depending on the format, and take between 90 minutes and 12 hours to complete the test [14]. Although the draft tube apparatus is not as sensitive as some ELISA tests, it offers other benefits compared to ELISA, such as the ability to conduct the test at the point-of-care, the reduced time required to complete the test and obtain results, and the lower cost. Table 8.68 summarizes the Reynolds numbers, limits of detection and the improvement in sensitivity compared to the small volume (20 µL) static test for each of the device designs investigated and the ELISA tests discussed.

Table 8.68. Summary table for each device design investigated and the discussed ELISA tests including the Reynolds number, limit of detection and the improvement in sensitivity compared to the small volume static test.

Device Design	**Reynolds number**	**Limit of Detection (mg/mL)**	**Improvement in sensitivity compared to small volume static test**
Small volume static	0	0.05	-
Large volume static	0	0.0025	20 times more sensitive
Syringe-filter membrane	~ 2863	0.00125	40 times more sensitive
Stirred tank	~ 4071	6.25×10^{-4}	80 times more sensitive
ELISA (Quinn et al.)	0	6.00×10^{-5} [12]	833 times more sensitive
Draft tube apparatus	~ 2005	6.25×10^{-6}	8,000 times more sensitive
Conical draft tube apparatus	~ 6267	6.25×10^{-7}	80,000 times more sensitive
ELISA (Zhang et al.)	0	1×10^{-7} [13]	500,000 times more sensitive
ELISA (ThermoFisher)	0	1×10^{-9} [14]	50,000,000 times more sensitive

8.8. Conclusions

Using larger fluid volumes allowed for an improvement in sensitivity, as a lower concentration of antibody can be detected in solution by a visible colour shift on the surface, and the addition of stirring and turbulence allowed for an even greater improvement in sensitivity. Increasing the sample volume from 20 µL to 500 mL allowed for a twenty-fold improvement in sensitivity, decreasing the limit of detection for anti-prothrombin in solution on a prothrombin coated surface from 0.05 mg/mL in a 20 µL solution to 0.0025 mg/mL in a 500 mL solution in 20 minutes, in the absence of stirring. Introducing mixing and turbulent flow to the 500 mL fluid sample in the draft tube apparatus allowed for an even greater improvement in sensitivity, reducing the limit of detection to 6.25×10^{-6} mg/mL (41.7 pM) of anti-prothrombin, an 8,000-fold improvement compared to the 20 µL stationary drop, which had a limit of detection of 0.05 mg/mL. The use of a conical shape draft tube achieved a limit of detection of 6.25×10^{-7} mg/mL (4.17 pM) of anti-prothrombin, an 80,000-fold improvement compared to the 20 µL stationary drop. In this work, the limits of detection were determined by visually analyzing the surface colours after exposure to prothrombin and subsequent exposure to anti-prothrombin, and by completing statistical analysis on the chromaticity coordinates of the prothrombin only coated surface compared to the prothrombin and anti-prothrombin coated surface. The experiments in Chapter 8 involved studying anti-prothrombin diluted in MilliQ water, and Chapter 9 will investigate anti-prothrombin diluted in synthetic urine to assess the impact of the sample solution. Further, other large volume mixing tank designs should be investigated in the future to increase turbulence and mixing in the system to potentially improve the device sensitivity even more.

8.9. References

1. Reverberi, R. and L. Reverberi, *Factors affecting the antigen-antibody reaction.* Blood Transfus, 2007. **5**(4): p. 227-40.

2. Jung, Y., J.Y. Jeong, and B.H. Chung, *Recent advances in immobilization methods of antibodies on solid supports.* Analyst, 2008. **133**(6): p. 697-701.

3. Bio-Rad. *ELISA: Results - Quantitative, Qualitative and Sensitivity*. [cited 2022 March 17]; Available from: https://www.bio-rad-antibodies.com/elisa-results-quantitative-semi-qualitative.html?JSESSIONID_STERLING=5934FDBD25D2B6A93E93E6A3FB555367.ecommerce2&evCntryLang=CA-en&cntry=CA&thirdPartyCookieEnabled=true.

4. ThermoFisher Scientific. *Overview of ELISA*. [cited 2022 March 16]; Available from: https://www.thermofisher.com/ca/en/home/life-science/protein-biology/protein-biology-learning-center/protein-biology-resource-library/pierce-protein-methods/overview-elisa.html.

5. Sweet, H.M., *Development of a Nanostructured Thin Film Device and Optics System for Protein Detection*, in *Materials Engineering*. 2018, University of Alberta.

6. Lim, T.K., V.A. Bloomfield, and G.L. Nelsestuen, *Structure of the prothrombin- and blood clotting factor X-membrane complexes.* Biochemistry, 1977. **16**(19): p. 4177-81.

7. Tan, Y.H., et al., *A nanoengineering approach for investigation and regulation of protein immobilization.* ACS Nano, 2008. **2**(11): p. 2374-84.

8. Lee, J.F., G.M. Stovall, and A.D. Ellington, *Aptamer therapeutics advance.* Curr Opin Chem Biol, 2006. **10**(3): p. 282-9.

9. Nickel, M.R., *Physical and Optical Characterization of Anodized Aluminum-Tantalum Thin Films for use in Thin Film Diagnostics*, in *Materials Engineering*. 2018, University of Alberta.

10. Engineering ToolBox. *Water - Density, Specific Weight and Thermal Expansion Coefficients*. 2003 [cited 2022 April 6]; Available from: https://www.engineeringtoolbox.com/water-density-specific-weight-d_595.html.

11. Engineering ToolBox. *Water - Dynamic (Absolute) and Kinematic Viscosity vs. Temperature and Pressure*. 2004 [cited 2022 May]; 22]. Available from: https://www.engineeringtoolbox.com/water-dynamic-kinematic-viscosity-d_596.html.

12. Quinn, C.P., et al., *Specific, sensitive, and quantitative enzyme-linked immunosorbent assay for human immunoglobulin G antibodies to anthrax toxin protective antigen.* Emerging infectious diseases, 2002. **8**(10): p. 1103-1110.

13. Zhang, S., et al., *Predicting detection limits of enzyme-linked immunosorbent assay (ELISA) and bioanalytical techniques in general.* Analyst, 2014. **139**(2): p. 439-445.

14. ThermoFisher Scientific. *ELISA Kits*. [cited 2022 July 26]; Available from: https://www.thermofisher.com/ca/en/home/life-science/antibodies/immunoassays/elisa-kits.html.

Chapter 9 – A Model Urinary Antibody Detection Test Using an Ultrasensitive Thin Film Diagnostic Device

9.1. Introduction

Research has investigated the detection of antibodies in urine as an alternative to serum or blood diagnostic tests as it is less invasive and has higher patient acceptance [1]. Urine samples contain a high enough level of antibodies for detection and avoid risks, such as infection, associated with drawing blood for antibody samples [2]. The concentration of antibodies found in urine is about 1/4,000 to 1/10,000 of the concentration of antibodies found in serum [2], so a highly sensitive diagnostic device is required for detection of antibodies in urine. The normal concentration range for immunoglobulin G (IgG) in adult human serum is 6.0 g/L to 16.0 g/L [3]. As the physiological concentration of IgG in urine can be up to 10,000 times less than plasma, the concentration range for IgG in urine would fall in the range of 6×10^{-4} g/L to 16×10^{-4} g/L (4 nM to 10.7 nM) ([2], [4]). The ultrasensitive diagnostic device is sensitive for the clinically relevant range for IgG levels in urine, as it achieved a limit of detection of 6.25×10^{-7} g/L (4.17 pM) (see Chapter 8 – Anti-Prothrombin Sensitivity on a Prothrombin-Coated Membrane Device). As the diagnostic device achieved a limit of detection lower than the clinically relevant concentration range for IgG in urine, the diagnostic device would be suitable for detecting IgG in urine. Previous work has investigated the use of a urine-based assay for the HIV-1 antibody [1], as well as urine antibody assays with urine for seven parasitic diseases, including strongyloidiasis [2]. Strongyloidiasis is an intestinal infection caused by a roundworm parasite called *Strongyloides sterocoralis* [5]. The use of a urinary IgG assay to screen for strongyloidiasis provides a less invasive and more sensitive diagnostic approach compared to the coprological and serodiagnosis tests typically used [4]. Further, urinary tests have the potential to

improve the detection of bladder cancer at early stages based on biomarkers in a less invasive and less expensive manner than a cystoscopy, which is normally required for detection of bladder cancer [6]. The typical volume of urine passed by an adult in one sitting varies between 250 – 400 mL, which is suitable for testing in the ultrasensitive diagnostic device designed in this work [7]. Urine behaves as a Newtonian fluid, meaning that the viscosity of urine is independent of the shear rate [8]. At 20 °C, the kinematic viscosity of urine is 1.0700 cSt [9]. This chapter investigates the use of the diagnostic device for detection of anti-prothrombin on a prothrombin coated surface in a synthetic urine sample.

9.2. Prothrombin-Anti-Prothrombin Model System

An antigen-antibody prototype consisting of prothrombin and anti-prothrombin has been shown to generate visible colour shifts on a silicon wafer coated with tantalum, tantala, and alumina, and was selected as the model system for this work ([10], [11]). Chapter 8 studied the limit of detection for anti-prothrombin diluted 100 mL, 250 mL and 500 mL volumes of MilliQ water after immobilization of a prothrombin layer on the thin film surface. Visible colour shifts were detected on silicon wafer surfaces coated with ~ 200 nm of tantalum and ~ 105 – 111 nm of aluminum, then anodized at 4 V to form the porous anodic alumina layer. For stirred tank experiments with a volume of 100 mL, the limit of detection for anti-prothrombin in solution on a prothrombin coated wafer was 6.25×10^{-4} mg/mL (4.2 nM). For 500 mL volumes in the straight draft tube apparatus at a gas flow rate of ~ 3.5 lpm, the limit of detection for anti-prothrombin in solution on a prothrombin coated wafer was 6.25×10^{-6} mg/mL (41.7 pM). As the prothrombin-anti-prothrombin model has been proven to show strong visible colour shifts in this work and in previous work ([10], [11]), it was selected as the model system for experiments in synthetic urine.

9.3. Materials and Methods

Detailed materials and methods regarding the adsorption of biologics can be found in Chapter 3 – General Materials and Methods. Thin films of tantalum (~ 200 nm) and aluminum (~ 105 – 111 nm) were sputtered onto the silicon wafers using the Bob and Floyd DC-planar magnetron sputtering systems, respectively, at the University of Alberta nanoFAB. Prior to protein adsorption, the aluminum faces of the substrates were anodized at 4 V to create the porous aluminum oxide layer and the tantala barrier. Further details on sputtering and anodization can be found in Chapter 3 – Materials and Methods. A prothrombin/anti-prothrombin model was used to study protein adsorption and detection. Hyphen BioMed highly purified human prothrombin from citrated human plasma from Aniara was reconstituted in distilled water at a concentration of 1 mg/mL and used for experiments. The antibody used was an affinity purified IgG sheep anti-human prothrombin in a 10 mM 4-(2-hydroxyethyl)-1-piperazineethanesulfonic acid (HEPES), 150 mM NaCL, 50% (v/v) glycerol buffer at a pH of 7.4 from Affinity Biologicals with a concentration of 10 mg/mL prior to dilution in large volume samples. Bovine serum albumin (BSA) in the form of lyophilized powder, $\geq$ 96% (agarose gel electrophoresis) from Sigma Life Science was used and diluted in MilliQ water for the 500 mL volume experiments. Synthetic urine was prepared by dissolving the following ingredients in the order shown in 1 L of distilled water (dH_2O) while stirring with a magnetic stir bar at 250 – 500 rpm: 1.0 g peptone, 0.005 g yeast extract, 0.1 g lactic acid, 0.4 g citric acid, 2.1 g $NaHCO_3$, 10 g urea, 0.07 g uric acid, 0.8 g creatinine, 0.32 g $CaCl_2.2H_2O$, 5.2 g NaCl, 0.99 g $MgSO_4.7H_2O$, 1.19 g Na_2SO_4, 0.95 g KH_2PO_4, 1.5 g $K_2HPO_4.3H_2O$, 1.3 g NH_4Cl, and 1.9 mL at 3.6 mM $FeSO_4.7H_2O$. The pH of the synthetic urine was then adjusted to ~ 7.1 by adding 1 M

hydrochloric acid (HCl) dropwise to the solution. For all experiments in Chapter 9, the straight draft tube device was used.

9.4. Device Preparation

Thin films of tantalum that were ~ 200 nm thick and aluminum thin films with thicknesses between ~ 105 nm and ~ 111 nm were sputtered onto the tantalum discs and the silicon wafers using the Bob and Floyd DC-planar magnetron sputtering systems, respectively, at the University of Alberta nanoFAB. The aluminum faces of the substrates were anodized at 4 V until the end of pore formation to create the porous aluminum oxide layer and the dielectric tantala layer. Further details on sputtering and anodization can be found in Chapter 3 – Materials and Methods. Details of the 3D printed draft tube and brass bubbler apparatus can be found in Chapter 8 – Anti-Prothrombin Sensitivity on a Prothrombin Coated Membrane Device. A Porter Cable compressor was used to induce bubbling in the system and the gas flow rates were measured using a rotameter.

9.5. Results

The limit of detection found in Chapter 8 – Anti-Prothrombin Sensitivity on a Prothrombin Coated Membrane Device in the straight draft tube apparatus was 6.25×10^{-6} mg/mL (41.7 pM) of anti-prothrombin. An anti-prothrombin concentration of 6.25×10^{-5} mg/mL (0.42 nM) was used for the synthetic urine experiments as this concentration achieved a uniform colour shift after 20 minutes, and is beneath the lower limit of the concentration range for IgG in urine (6×10^{-4} g/L or 4 nM) ([2], [3]). Synthetic urine was prepared using the recipe described in Section 9.3. Silicon wafer slides were sputtered with ~ 200 nm of tantalum and ~ 105 nm of aluminum, then anodized at 4 V to produce the porous anodic alumina layer. The silicon wafer slides were cut using the diamond scribe and the stencil, then further cut into smaller squares

with dimensions of ~ 1 cm by ~ 1.2 cm. A Sharpie was used to trace the edges of the rectangles to contain the protein solutions. Then, 40 µL of 1 mg/mL prothrombin was placed on the surface and spread to the edges of the rectangle using a pipette tip and was left in a Petri dish with a wet paper towel for 20 minutes. After exposure to prothrombin, the wafers were rinsed with deionized water and dried with oil free compressed air. A synthetic urine solution containing anti-prothrombin at a concentration of 6.25×10^{-5} mg/mL was prepared by diluting 3.125 µL of 10 mg/mL anti-prothrombin in ~ 500 mL of synthetic urine. The prothrombin coated slides were then placed in the draft tube apparatus and the 500 mL synthetic urine solution with an anti-prothrombin concentration of 6.25×10^{-5} mg/mL was added to the graduated cylinder. A gas flow rate of ~ 3.5 lpm was used in the draft tube apparatus and the slides were viewed after 20 minutes of exposure to the solution. Figure 9.1 shows the three replicates prior to protein exposure (row 1), after exposure of each rectangle to 40 µL of 1 mg/mL prothrombin for 20 minutes (row 2), and after exposure of each rectangle to a 500 mL synthetic urine solution containing anti-prothrombin at a concentration of 6.25×10^{-5} mg/mL after 20 minutes (row 3) in the draft tube apparatus at a gas flow rate of ~ 3.5 lpm. Statistical analysis was completed on the three replicates to determine the effect of synthetic urine containing anti-prothrombin at a concentration of 6.25×10^{-5} mg/mL for 20 minutes on the surface colour of the prothrombin coated wafer. The x and y coordinates were analyzed using an independent t-test. Table 9.1 shows the results of the statistical analysis on the effect of a 500 mL synthetic urine sample with an anti-prothrombin concentration of 6.25×10^{-5} mg/mL in the draft tube apparatus at a gas flow rate of ~ 3.5 lpm for 20 minutes on the surface colour of the prothrombin-coated wafer based on x and y chromaticity coordinates.

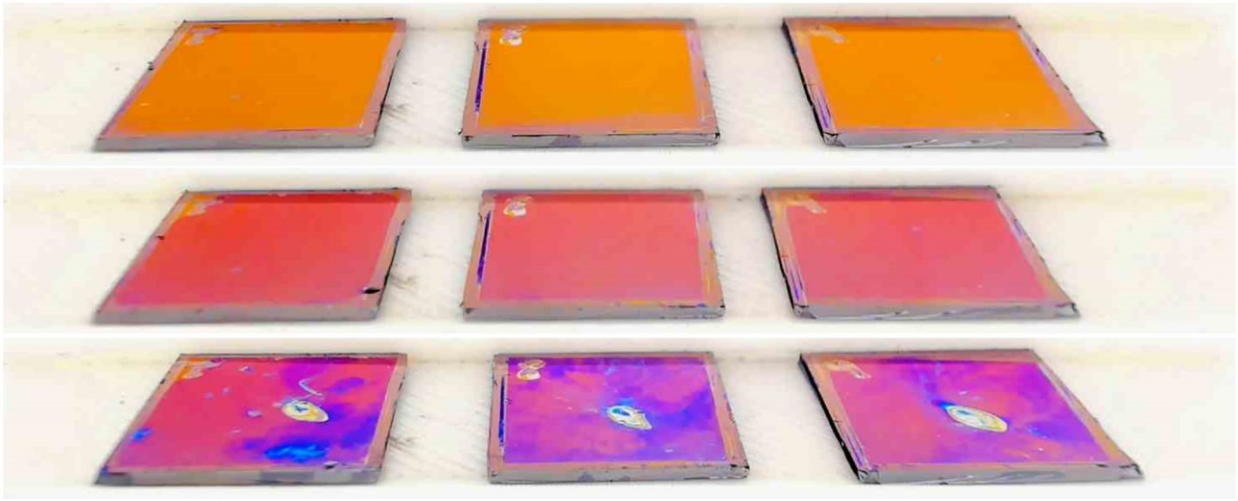


Figure 9.1. Silicon wafer rectangles (three replicates – ~ 1 cm by ~ 1.2 cm each) coated with ~ 200 nm of tantalum and ~ 105 nm of aluminum then anodized at 4 V with no exposure to protein (row 1), after exposure of each rectangle to 40 µL of 1 mg/mL prothrombin for 20 minutes (row 2), after subsequent exposure of each rectangle to 500 mL of synthetic urine containing anti-prothrombin at a concentration of 6.25 × 10^{-5} mg/mL for 20 minutes in the draft tube apparatus at a gas flow rate of ~ 3.5 lpm (row 3).

Table 9.1. Results of the independent T-test statistical analysis on the effect of 500 mL of synthetic urine containing anti-prothrombin (AP) at a concentration of 6.25 × 10^{-5} mg/mL in the draft tube apparatus at a gas flow rate of ~ 3.5 lpm for 20 minutes on the surface colour based on x and y chromaticity coordinates compared to the prothrombin (II) only control. Statistically significant results are in italics. (n = 3).

Prothrombin (II) control	**Vs. II + AP (mg/mL)**	**Difference detectable by eye vs. control?**	**x coordinate + p values**	**y coordinate + p values**
1 mg/mL II control x = 0.49 ± 0.05 y = 0.32 ± 0.01	6.25 × 10^{-5} (500 mL synthetic urine) ~ 3.5 lpm	Yes	x = 0.39 ± 0.04 p > 0.05	y = 0.24 ± 0.03 *p < 0.01*

For an anti-prothrombin concentration of 6.25×10^{-5} mg/mL in synthetic urine, a visible colour shift from orange/pink to pink/purple occurred on the surface and the y chromaticity coordinate was statistically significant after 20 minutes in the draft tube apparatus at a gas flow rate of ~ 3.5 lpm compared to the prothrombin only control. Although the entire slide appeared a different colour after exposure to the synthetic urine and anti-prothrombin solution, the colour shift did not appear uniform and patches of blue appeared on the surface. The uneven colour shift could be a result of a disruption to the fluid flow pattern by the clip just above the coated slide. The clip holds the slide in place in the draft tube, and as a result, the flow just above the surface is slightly redirected around the clip. Although uneven, a strong visible colour shift with statistically significant chromaticity coordinates did occur in the synthetic urine sample at an anti-prothrombin concentration of 6.25×10^{-5} mg/mL. To ensure that the colour shift was due to binding of anti-prothrombin and not to the synthetic urine solution, the experiment was repeated using a 500 mL synthetic urine sample containing no anti-prothrombin as a negative control. Silicon wafer slides were coated with ~ 200 nm of tantalum and ~ 110 nm of aluminum, then anodized at 4 V to produce the porous anodic alumina layer. The silicon wafer slides were cut using the diamond scribe and the stencil, then further cut into smaller squares with dimensions of ~ 1 cm by ~ 1.2 cm. A Sharpie was used to trace the edges of the rectangles to contain the protein solutions. Then, 40 μL of 1 mg/mL prothrombin was placed on the surface and spread to the edges of the rectangle using a pipette tip and was left in a Petri dish with a wet paper towel for 20 minutes. After exposure to prothrombin, the wafers were rinsed with deionized water and dried with oil free compressed air. A synthetic urine solution containing no anti-prothrombin was prepared according to the recipe in Section 9.3. The prothrombin coated slides were then placed in the draft tube apparatus and a 500 mL synthetic urine solution with no anti-prothrombin was

added to the graduated cylinder. A gas flow rate of ~ 3.5 lpm was used in the draft tube apparatus and the slides were rinsed with deionized water, dried with oil free compressed air, and viewed after 10 and 20 minutes of exposure to the solution. After exposure to the synthetic urine solution for 20 minutes, hydrophobic Sharpie circles with a diameter of 0.7 cm were drawn on each slide. To ensure the prothrombin could still bind anti-prothrombin after exposure to synthetic urine, 15 μL of 0.5 mg/mL anti-prothrombin was placed in the hydrophobic circles for 20 minutes, then the slides were rinsed with deionized water and dried with oil free compressed air. Figure 9.2 shows the three replicates prior to protein exposure (row 1), after exposure of each rectangle to 40 μL of 1 mg/mL prothrombin for 20 minutes (row 2), after exposure of each rectangle to a 500 mL synthetic urine solution containing no anti-prothrombin after 10 minutes and 20 minutes (rows 3, 4) in the draft tube apparatus at gas flow rates of ~ 3.5 lpm, and after subsequent exposure of the hydrophobic circles to 15 μL of 0.5 mg/mL anti-prothrombin for 20 minutes (row 5). The x and y coordinates were analyzed using one-way ANOVA and Tukey post hoc tests to assess if a statistically significant colour shift occurred after exposure to the synthetic urine solution containing no anti-prothrombin compared to the prothrombin only control. Table 9.2 shows the results of the statistical analysis on the effect of various exposure times for a 500 mL synthetic urine sample with no anti-prothrombin in the draft tube apparatus at a gas flow rate of ~ 3.5 lpm on the surface colour of the prothrombin-coated wafer based on x and y chromaticity coordinates.

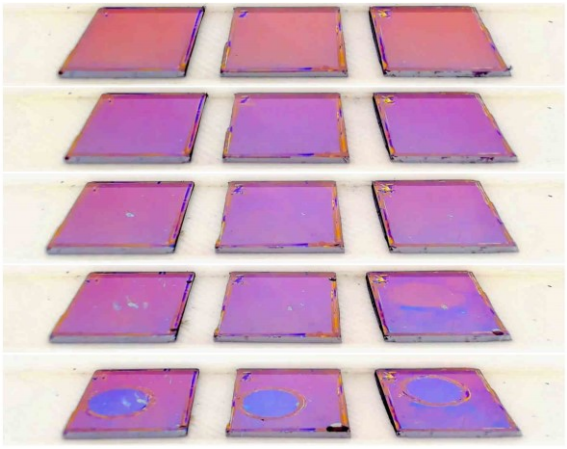


Figure 9.2. Silicon wafer rectangles (three replicates – ~ 1 cm by ~ 1.2 cm each) coated with ~ 200 nm of tantalum and ~ 105 nm of aluminum then anodized at 4 V with no exposure to protein (row 1), after exposure of each rectangle to 40 µL of 1 mg/mL prothrombin for 20 minutes (row 2), after subsequent exposure of each rectangle to 500 mL of synthetic urine containing no anti-prothrombin for 10 and 20 minutes in the draft tube apparatus at a gas flow rate of ~ 3.5 lpm (rows 3, 4), and after exposure of the hydrophobic circles to 15 µL of 0.5 mg/mL anti-prothrombin for 20 minutes (row 5).

Table 9.2. Results of the ANOVA and Tukey post hoc statistical analysis tests on the effect of various synthetic urine exposure times for a 500 mL volume containing no anti-prothrombin (AP) in the draft tube apparatus at a gas flow rate of ~ 3.5 lpm on the surface colour using x and y chromaticity coordinates compared to the prothrombin only control. Statistically significant results are in italics. (n = 3).

Prothrombin (II) control	**Vs. II + 500 mL synthetic urine, no AP ~ 3.5 lpm (exposure time)**	**Difference detectable by eye vs. control?**	**x coordinate + p values**	**y coordinate + p values**
1 mg/mL x = 0.30 ± 0.01 y = 0.22 ± 0.01	10 minutes	No	x = 0.31 ± 0.00 p > 0.9	y = 0.23 ± 0.01 p > 0.09
	20 minutes	No	x = 0.31 ± 0.01 p > 0.5	y = 0.23 ± 0.01 p > 0.2

For a 500 mL synthetic urine sample containing no anti-prothrombin, no visible colour shift occurred on the surface after 10 or 20 minutes in the draft tube apparatus at a gas flow rate of ~ 3.5 lpm and both the x and y chromaticity coordinates were not statistically significant compared to the prothrombin only control. The lack of colour shift in the synthetic urine sample without anti-prothrombin suggests that the colour shift seen in Figure 9.1 is due to anti-prothrombin binding to the prothrombin coated surface, and not to the synthetic urine. Further, a clear colour shift from purple to blue occurred in the hydrophobic circle after exposure of the prothrombin coated surface to 15 µL of 0.5 mg/mL anti-prothrombin after 20 minutes of exposure to synthetic urine in the draft tube apparatus in Figure 9.2, suggesting that the synthetic urine solution has no impact on the ability of prothrombin to bind to anti-prothrombin. Table 9.3 shows the results of the independent T-test statistical analysis on the effect of 15 µL of 0.5 mg/mL anti-prothrombin for 20 minutes in the hydrophobic circle compared to the prothrombin only surface after exposure to 500 mL of synthetic urine in the draft tube apparatus at a gas flow rate of ~ 3.5 lpm for 20 minutes.

Table 9.3. Results of the independent T-test statistical analysis on the effect 15 µL of 0.5 mg/mL anti-prothrombin (AP) for 20 minutes on the surface colour based on x and y chromaticity coordinates compared to the prothrombin (II) only control after exposure to 500 mL of synthetic urine in the draft tube apparatus at a gas flow rate of ~ 3.5 lpm for 20 minutes. Statistically significant results are in italics. (n = 3).

Prothrombin (II) + synthetic urine (20 minutes)	**Vs. II + AP (mg/mL)**	**Difference detectable by eye vs. control?**	**x coordinate + p values**	**y coordinate + p values**
1 mg/mL II control x = 0.31 ± 0.01 y = 0.23 ± 0.01	0.5 (hydrophobic circles)	Yes	x = 0.22 ± 0.01 *p < 0.001*	y = 0.17 ± 0.02 *p < 0.05*

Both the x and y chromaticity coordinates were statistically significant after exposure to 15 μL of 0.5 mg/mL anti-prothrombin in the hydrophobic circles for 20 minutes compared to the prothrombin coated surface after exposure to 500 mL of synthetic urine in the draft tube apparatus at a gas flow rate of ~ 3.5 lpm for 20 minutes.

9.6. Limitations

Increasing the sample volume from 20 μL to 500 mL allows for the device sensitivity to be increased significantly for detection of the analyte of interest. However, increasing the sample volume also increases the chances of non-specific binding of other analytes onto the device surface. Non-specific binding, or non-specific adsorption, occurs when an antibody binds to unintended proteins, receptors, or transporters, and is a persistent challenge faced in the development of biosensors ([12], [13]). Non-specific binding of other analytes in the sample could potentially lead to a colour shift on the surface, leading to background and signals and potentially interfering with the detection of the analyte of interest. To assess non-specific binding in the diagnostic device, a 500 mL sample of bovine serum albumin (BSA) at a concentration of 6.25×10^{-5} mg/mL was prepared by diluting BSA in MilliQ water. Silicon wafer substrates were coated with ~ 200 nm of tantalum and ~ 110 nm of aluminum then anodized at 4 V and cut using the diamond scribe and the stencil. The silicon wafer slides were then further cut into smaller squares with dimensions of ~ 1 cm by ~ 1.2 cm. A Sharpie was used to trace the edges of the rectangles to contain the protein solutions. Then, 40 μL of 1 mg/mL prothrombin was placed on the surface and spread to the edges of the rectangle using a pipette tip and was left in a Petri dish with a wet paper towel for 20 minutes. After exposure to prothrombin, the wafers were rinsed with deionized water and dried with oil free compressed air. The prothrombin coated slides were then placed in the draft tube apparatus and a 500 mL solution containing BSA in MilliQ water at

a concentration of 6.25×10^{-5} mg/mL was added to the graduated cylinder. A gas flow rate of ~ 3.5 lpm was used and the slides were viewed after 10 and 20 minutes of exposure to the solution. After exposure to the BSA solution in the draft tube apparatus, 0.7 cm diameter hydrophobic circles were drawn on each slide using a Sharpie pen, and 15 µL of 0.5 mg/mL anti-prothrombin was placed in the hydrophobic circle and left on a wet paper towel in a Petri dish for 20 minutes. Anti-prothrombin was placed on the surfaces of the slides after exposure to the BSA solution to confirm that the presence of BSA in solution would not block subsequent binding of anti-prothrombin to the prothrombin coated surface. Figure 9.3 shows the three replicates prior to protein exposure (row 1), after exposure of each rectangle to 40 µL of 1 mg/mL prothrombin for 20 minutes (row 2), after exposure of each rectangle to a 500 mL sample containing BSA at a concentration of 6.25×10^{-5} mg/mL after 10 minutes and 20 minutes (rows 3, 4) in the draft tube apparatus at gas flow rates of ~ 3.5 lpm, and after subsequent exposure of the hydrophobic circles to 15 µL of 0.5 mg/mL anti-prothrombin for 20 minutes (row 5). Statistical analysis was completed on the three replicates to determine the effect of various exposure times of the 6.25×10^{-5} mg/mL BSA solution on the surface colour of the prothrombin coated wafer. The x and y coordinates were analyzed using one-way ANOVA and Tukey post hoc tests. Table 9.4 shows the results of the statistical analysis on the effect of various exposure times for a 500 mL sample containing BSA at a concentration of 6.25×10^{-5} mg/mL in the draft tube apparatus with a gas flow rate of ~ 3.5 lpm on the surface colour of the prothrombin-coated wafer based on x and y chromaticity coordinates.

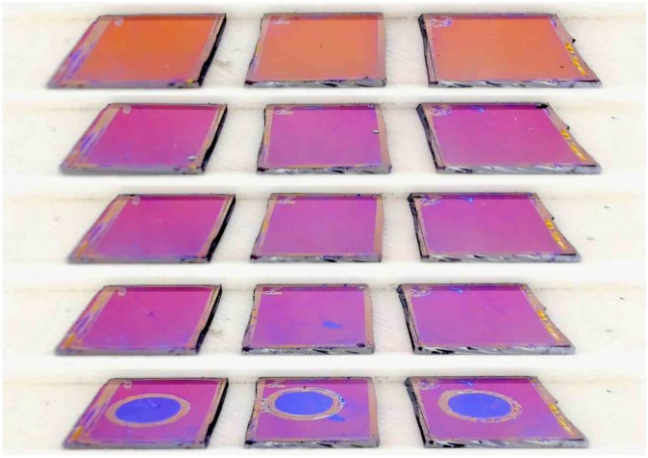


Figure 9.3. Silicon wafer rectangles (three replicates – ~ 1 cm by ~ 1.2 cm each) coated with ~ 200 nm of tantalum and ~ 110 nm of aluminum then anodized at 4 V with no exposure to protein (row 1), after exposure of each rectangle to 40 µL of 1 mg/mL prothrombin for 20 minutes (row 2), after subsequent exposure of each rectangle to 500 mL of 6.25 × 10^{-5} mg/mL lyophilized bovine serum albumin for 10 and 20 minutes in the draft tube apparatus at a gas flow rate of ~ 3.5 lpm (rows 3, 4) and after exposure of the hydrophobic circles to 15 µL of 0.5 mg/mL anti-prothrombin for 20 minutes (row 5).

Table 9.4. Results of the ANOVA and Tukey post hoc statistical analysis tests on the effect of various bovine serum albumin (BSA) exposure times for a 500 mL volume at a concentration of 6.25 × 10^{-5} mg/mL in the draft tube apparatus at a gas flow rate of ~ 3.5 lpm on the surface colour using x and y chromaticity coordinates compared to the prothrombin only control. Statistically significant results are in italics. (n = 3).

Prothrombin (II) control	**Vs. II + BSA 6.25 × 10^{-5} mg/mL, ~ 3.5 lpm (exposure time)**	**Difference detectable by eye vs. control?**	**x coordinate + p values**	**y coordinate + p values**
1 mg/mL II control x = 0.36 ± 0.02 y = 0.24 ± 0.00	10 minutes	No	x = 0.35 ± 0.02 p > 0.6	y = 0.23 ± 0.01 p > 0.4
	20 minutes	No	x = 0.33 ± 0.02 p > 0.2	y = 0.21 ± 0.01 *p < 0.05*

For a bovine serum albumin concentration of 6.25×10^{-5} mg/mL in MilliQ water, no visible colour shift occurred on the surface compared to the prothrombin only control after 10 or 20 minutes. After 10 minutes, neither the x or y chromaticity coordinate was statistically significant, and after 20 minutes, only the y chromaticity coordinate was statistically significant compared to the prothrombin only control. A clear colour shift occurred from purple to blue after placing 15 μL of 0.5 mg/mL anti-prothrombin in the hydrophobic circles for 20 minutes, indicating that exposure to BSA in the draft tube apparatus did not block prothrombin from being able to bind to anti-prothrombin. Although a visible colour shift did not appear on the surface after exposure to 500 mL of MilliQ water containing BSA at a concentration of 6.25×10^{-5} mg/mL, the y chromaticity coordinate was statistically significant after 20 minutes, indicating a slightly different surface colour, potentially due to non-specific binding of BSA to anti-prothrombin or to the alumina surface. Further, the concentration of albumin in urine is greater than 6.25×10^{-5} mg/mL (less than 0.02 mg/mL [14]), and a higher concentration of albumin may lead to increased non-specific binding on the surface. To address non-specific binding, experiments were conducted in which the surface was saturated with BSA prior to exposure to an anti-prothrombin solution in the draft tube apparatus to investigate whether anti-prothrombin was still able to bind to prothrombin and produce a colour shift on the surface. Silicon wafer substrates were coated with ~ 200 nm of tantalum and ~ 110 nm of aluminum then anodized at 4 V and cut using the diamond scribe and the stencil. The silicon wafer slides were then further cut into smaller squares with dimensions of ~ 1 cm by ~ 1.2 cm. A Sharpie was used to trace the edges of the rectangles to contain the protein solutions. Then, 40 μL of 1 mg/mL prothrombin was placed on the surface and spread to the edges of the rectangle using a pipette tip and was left in a Petri dish with a wet paper towel for 20 minutes. After exposure to prothrombin, the wafers

were rinsed with deionized water and dried with oil free compressed air. Then, 40 µL of 1 mg/mL BSA was placed on the surface and spread to the edges of the rectangle using a pipette tip and was left in a Petri dish with a wet paper towel for 20 minutes, and subsequently rinsed with deionized water and dried with oil free compressed air. The prothrombin and BSA coated slides were then placed in the draft tube apparatus and a 500 mL solution containing anti-prothrombin in MilliQ water at a concentration of 6.25×10^{-5} mg/mL was added to the graduated cylinder. A gas flow rate of ~ 3.5 lpm was used and the slides were viewed after 10 and 20 minutes of exposure to the solution. Figure 9.4 shows the three replicates prior to protein exposure (row 1), after exposure of each rectangle to 40 µL of 1 mg/mL prothrombin for 20 minutes (row 2), after exposure of each rectangle to 40 µL of 1 mg/mL BSA for 20 minutes (row 3), and after exposure of each rectangle to a 500 mL sample containing anti-prothrombin at a concentration of 6.25×10^{-5} mg/mL after 10 minutes and 20 minutes (rows 4, 5) in the draft tube apparatus at gas flow rates of ~ 3.5 lpm. Statistical analysis was completed on the three replicates to determine the effect of various exposure times of the 6.25×10^{-5} mg/mL anti-prothrombin solution on the surface colour of the prothrombin and BSA coated wafer. The x and y coordinates were analyzed using one-way ANOVA and Tukey post hoc tests. Table 9.5 shows the results of the statistical analysis on the effect of various exposure times for a 500 mL sample containing anti-prothrombin at a concentration of 6.25×10^{-5} mg/mL in the draft tube apparatus with a gas flow rate of ~ 3.5 lpm on the surface colour of the prothrombin and BSA-coated wafer based on x and y chromaticity coordinates.

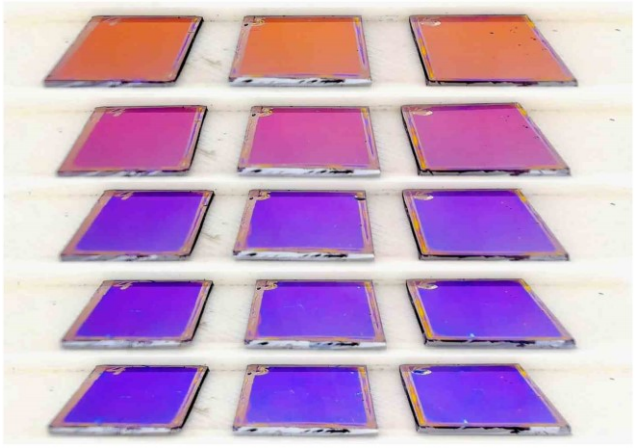


Figure 9.4 Silicon wafer rectangles (three replicates – ~ 1 cm by ~ 1.2 cm each) coated with ~ 200 nm of tantalum and ~ 110 nm of aluminum then anodized at 4 V with no exposure to protein (row 1), after exposure of each rectangle to 40 µL of 1 mg/mL prothrombin for 20 minutes (row 2), after subsequent exposure of each rectangle to 40 µL of 1 mg/mL lyophilized bovine serum albumin for 20 minutes (row 3), and after subsequent exposure of each rectangle to 500 mL of 6.25 × 10^{-5} mg/mL anti-prothrombin for 10 and 20 minutes in the draft tube apparatus at a gas flow rate of ~ 3.5 lpm (rows 4, 5).

Table 9.5. Results of the ANOVA and Tukey post hoc statistical analysis tests on the effect of various anti-prothrombin (AP) exposure times for a 500 mL volume at a concentration of 6.25 × 10^{-5} mg/mL in the draft tube apparatus at a gas flow rate of ~ 3.5 lpm on the surface colour using x and y chromaticity coordinates compared to the prothrombin and bovine serum albumin (BSA) coated surface. Statistically significant results are in italics. (n = 3).

Prothrombin (II) + BSA surface	**Vs. II + BSA + 500 mL AP 6.25 × 10^{-5} mg/mL, ~ 3.5 lpm (exposure time)**	**Difference detectable by eye vs. control?**	**x coordinate + p values**	**y coordinate + p values**
1 mg/mL II + BSA x = 0.23 ± 0.01 y = 0.12 ± 0.01	10 minutes	No	x = 0.21 ± 0.00 *p < 0.05*	y = 0.11 ± 0.01 p > 0.2
	20 minutes	Yes	x = 0.20 ± 0.00 *p < 0.001*	y = 0.10 ± 0.01 p > 0.05

After coating the entire slide with 1 mg/mL BSA, a strong colour shift from pink (prothrombin only) to purple (prothrombin + BSA) occurred, indicating binding of BSA to the prothrombin and alumina coated surface. Subsequent exposure of the prothrombin and BSA coated surface to anti-prothrombin at a concentration of 6.25×10^{-5} mg/mL in the draft tube apparatus at a gas flow rate of ~ 3.5 lpm did not yield a visible colour shift after 10 minutes but yielded a visible colour shift from purple to blue after 20 minutes. The x chromaticity coordinate was statistically significant after 10 and 20 minutes compared to the prothrombin and BSA coated surface, and the y chromaticity coordinate was not statistically significant after 10 or 20 minutes. Although saturating the prothrombin coated surface with BSA yielded a strong colour shift compared to the prothrombin only control, exposure to the anti-prothrombin solution yielded another colour shift, indicating binding of anti-prothrombin to prothrombin. The results of this experiment suggest that although non-specific binding may occur and generate a colour shift on the surface, subsequent exposure of the surface to anti-prothrombin in solution will generate an additional colour shift signal on the surface due to binding of anti-prothrombin. Saturating the device surface with the protein that may potentially non-specifically bind to the surface may lead to a colour shift but will not prevent the detection of anti-prothrombin in solution, as binding of anti-prothrombin would produce an additional colour shift on the surface. One potential method of mitigating colour shifts due to non-specific binding is saturating the surface with the protein that may non-specifically bind prior to exposure to the fluid sample in the draft tube apparatus. Blinding the surface to the non-specific protein in this manner does not impact the device sensitivity, as an additional colour shift can be achieved when the analyte of interest is present in the sample and binds to the surface.

9.7. Discussion

The prothrombin/anti-prothrombin model system was able to generate a visible colour shift in a 500 mL sample of synthetic urine containing anti-prothrombin at a concentration of 6.25×10^{-5} mg/mL in the draft tube apparatus at a gas flow rate of ~ 3.5 lpm on a silicon wafer slide coated with thin films of alumina, tantala, and tantalum. The synthetic urine solution did not interfere with the ability of the prothrombin coated surface to bind to anti-prothrombin statically or in solution. A 500 mL sample of synthetic urine containing no anti-prothrombin did not produce a visible colour shift on the surface and did not impact subsequent detection of anti-prothrombin on the surface. Though the colour shift on the surface after exposure to synthetic urine containing anti-prothrombin at a concentration of 6.25×10^{-5} mg/mL was not completely uniform, the shift was strong and visible. In comparison, a synthetic urine solution with no anti-prothrombin did not produce a visible colour shift. As the normal concentration range for IgG in adult human serum is 6.0 g/L to 16.0 g/L, and the physiological concentration of IgG in urine can be up to 10,000 times less than plasma, the concentration range for IgG in urine would be 6×10^{-4} g/L to 16×10^{-4} g/L (4 nM to 10.7 nM) ([2], [3], [4]). The diagnostic device was able to detect anti-prothrombin in a synthetic urine solution at a concentration of 6.25×10^{-5} g/L (0.42 nM), which is well below the lower limit of the concentration of IgG in urine (4 nM), making the device suitable for detecting IgG at clinically relevant levels in urine.

One limitation of increasing the sample volume is that the chance of non-specific binding occurring also increases, in which an unintended molecule binds to the device surface and potentially interferes with the detection signal for the analyte of interest. One method to address non-specific binding by blinding the surface with the non-specific protein prior to exposure to the fluid sample was investigated in this work. Blinding the prothrombin coated surface with

BSA led to a colour shift compared to the prothrombin only coated slide, but exposure to the anti-prothrombin solution produced an additional and detectable colour shift on the surface due to anti-prothrombin binding to prothrombin without impacting the device sensitivity. In future work, other methods to assess non-specific binding should also be investigated.

9.8. Future Work

Future work should further investigate the device specificity and non-specific binding on the surface by diluting anti-prothrombin in biological samples that contain other proteins and assessing for binding with non-specific proteins. Additional methods of reducing non-specific binding to the device surface should be studied. Future work also involves developing the device for the detection of a specific disease, such as Strongyloides, and testing for a specific urinary biomarker associated with the disease. Another potential application of the device is the detection of lipopolysaccharide (LPS) in urine. LPS is produced by gram negative bacteria and indicates a gram-negative infection [15]. The ability to determine whether a urinary tract infection is caused by gram-negative or gram-positive bacteria within 20 minutes allows for the appropriate antibiotic to be prescribed at the point-of-care, leading to better patient outcomes and combatting the problem of antibiotic resistance due to the misuse of antibiotics. The concentration of LPS in urine ranges between 10 – 350 pg/mL (~ 0.01 – 0.35 pM) for patients with urinary tract infections when the number of bacteria is greater than 10^4 CFU/mL [16]. With a limit of detection of ~ 4.17 pM, the diagnostic device sensitivity is not in the range for detecting LPS in urine, however, the diagnostic device has the potential to be used for such an application if the sensitivity is improved in the future. Future work could investigate other diagnostic device designs to improve circulation and mixing, such as including baffles or by modifying the draft tube apparatus. The device design could also be improved by securing the

slide to the draft tube in a manner that does not involve placing a clip above the slide. Securing the slide in place without covering a portion of the surface with a clip may allow for an improvement in sensitivity, and for more uniform colour shifts to be produced as fluid flow would not be disrupted just above the coated surface. Additionally, optimizing the gas flow rate in the draft tube apparatus and the resulting fluid flow patterns could improve the device sensitivity. In this work, only two gas flow rates were studied, with a gas flow rate of ~ 3.5 lpm producing better results than a gas flow rate of ~ 9.5 lpm at the limit of detection concentration. In the future, other gas flow rates should be studied to determine the optimal gas flow rate for the device.

Further, future work should investigate designing the diagnostic device to be more suitable for point-of-care. In this work, bubbling in the draft tube system was induced by a Porter Cable compressor at gas flow rates of ~ 3.5 lpm and ~ 9.5 lpm. Smaller and more portable systems such as aquarium pumps or negative pressure wound therapy systems can be used to induce gas flow and bubbling in the device. For example, the Pawfly Adjustable Aquarium Air Pump is small and portable with a gas flow rate of 4 lpm and could be used to induce bubbling in the diagnostic device instead of the Porter Cable compressor, making it more suitable for use at the point of care [17].

9.9. Conclusions

In this chapter, the prothrombin/anti-prothrombin model system was tested in a synthetic urine solution, and an anti-prothrombin concentration of 6.25×10^{-5} mg/mL (0.42 nM) in a 500 mL synthetic urine sample was detectable by a visible colour shift on the prothrombin coated slide after 20 minutes in the draft tube apparatus at a gas flow rate of ~ 3.5 lpm. The sensitivity of the diagnostic device is suitable for the detection of IgG in urine, as the device limit of

detection is lower than the lower limit of the concentration range for IgG in urine. In a 500 mL synthetic urine sample, an 800-fold improvement in sensitivity was demonstrated compared to the stationary 20 μL tests in Chapter 8, which had a limit of detection of 0.05 mg/mL. The limit of detection for the conical draft tube diagnostic device was found to be 6.25×10^{-7} mg/mL (4.17 pM) in Chapter 8 and demonstrated an 80,000-fold improvement in sensitivity compared to the stationary 20 μL tests. With slight modifications to the diagnostic device design in the future, such as the use of a smaller and more portable system to induce bubbling, the device is suitable for the detection of specific analytes in a urine sample at the point of care. Future work involves optimizing the test surface area to volume ratio, optimizing fluid flow in the draft tube device, and developing the device for a specific disease, such as Strongyloides. Based on the demonstration of greater than 1,000-fold increase in sensitivity, Pavonis Diagnostics Inc. is assuming the commercialization including prosecuting the patent draft.

9.10. References

1. Urnovitz, H.B., et al., *Urine Antibody Tests: New Insights into the Dynamics of HIV-1 Infection.* Clinical Chemistry, 1999. **45**(9): p. 1602-1613.

2. Nagaoka, F., et al., *Detection of Urinary Antibodies and Its Application in Epidemiological Studies for Parasitic Diseases.* Vaccines, 2021. **9**(7): p. 778.

3. Oxford University Hospitals. *Immunoglobulins*. 2022 [cited 2022 June 4]; Available from: https://www.ouh.nhs.uk/immunology/diagnostic-tests/tests-catalogue/immunoglobulins.aspx.

4. Eamudomkarn, C., et al., *Diagnostic performance of urinary IgG antibody detection: A novel approach for population screening of strongyloidiasis.* PLoS ONE, 2018. **13**(7).

5. WebMD. *What Is Strongyloidiasis?* 2021 [cited 2022 June 4]; Available from: https://www.webmd.com/a-to-z-guides/what-is-strongyloidiasis.

6. Nelson, R. *Simple Urine Test Could Improve Detection of Bladder Cancer*. 2022 [cited 2022 June 4].

7. Continence New Zealand. *Bladder Retraining*. 2022 [cited 2022 April 21]; Available from: https://www.continence.org.nz/pages/Bladder-Retraining/48/#:~:text=What%20is%20a%20normal%20bladder,between%20visits%20to%20the%20toilet.

8. Palagi, S., et al., *Chapter 8 - Micro- and nanorobots in Newtonian and biological viscoelastic fluids*, in *Microbiorobotics (Second Edition)*, M. Kim, A.A. Julius, and U.K. Cheang, Editors. 2017, Elsevier: Boston. p. 133-162.

9. Inman, B.A., et al., *The impact of temperature and urinary constituents on urine viscosity and its relevance to bladder hyperthermia treatment.* Int J Hyperthermia, 2013. **29**(3): p. 206-10.

10. Sweet, H.M., *Development of a Nanostructured Thin Film Device and Optics System for Protein Detection*, in *Materials Engineering*. 2018, University of Alberta.

11. Nickel, M.R., *Physical and Optical Characterization of Anodized Aluminum-Tantalum Thin Films for use in Thin Film Diagnostics*, in *Materials Engineering*. 2018, University of Alberta.

12. Surmodics. *Non-Specific Binding*. 2022 [cited 2022 June 5]; Available from: https://shop.surmodics.com/non-specific-binding#:~:text=Non%2DSpecific%20binding%20(NSB)%20refers%20to%20an%20occurrence%20of,the%20specificity%20of%20the%20antibodies.

13. Lichtenberg, J.Y., Y. Ling, and S. Kim, *Non-Specific Adsorption Reduction Methods in Biosensing.* Sensors (Basel, Switzerland), 2019. **19**(11): p. 2488.

14. Heerspink, H., et al., *Albuminuria Assessed From First-Morning-Void Urine Samples Versus 24-Hour Urine Collections as a Predictor of Cardiovascular Morbidity and Mortality.* American journal of epidemiology, 2008. **168**: p. 897-905.

15. Bertani, B. and N. Ruiz, *Function and Biogenesis of Lipopolysaccharides.* EcoSal Plus, 2018. **8**(1): p. 10.1128/ecosalplus.ESP-0001-2018.

16. Prywer, J. and A. Torzewska, *Aggregation of poorly crystalline and amorphous components of infectious urinary stones is mediated by bacterial lipopolysaccharide.* Scientific Reports, 2019. **9**(1): p. 17061.

17. Pawfly. *Pawfly Adjustable Aquarium Air Pump 4-LPM 2 Outlets with Oxygen Accessories for 10-60 Gallon Fish Tank Pond*. 2022 [cited 2022 June 8]; Available from: https://www.amazon.ca/Pawfly-Adjustable-Aquarium-Outlets-Accessories/dp/B01EBXI7PG.

Bibliography

Chapter 1

1. Chin, C.D., V. Linder, and S.K. Sia, *Commercialization of microfluidic point-of-care diagnostic devices.* LAB ON A CHIP, 2012. **12**(12): p. 2118-2134.

2. Ng, E., et al., *Magneto-nanosensor smartphone platform for the detection of HIV and leukocytosis at point-of-care.* Nanomedicine, 2019. **16**: p. 10-19.

3. Li, D. and M.M. Mielke, *An Update on Blood-Based Markers of Alzheimer's Disease Using the SiMoA Platform.* Neurol Ther, 2019. **8**(Suppl 2): p. 73-82.

4. Malecka, K., D. Pankratov, and E.E. Ferapontova, *Femtomolar electroanalysis of a breast cancer biomarker HER-2/neu protein in human serum by the cellulase-linked sandwich assay on magnetic beads.* Analytica Chimica Acta, 2019. **1077**: p. 140-149.

Chapter 2

1. Alhajj, M. and A. Farhana, *Enzyme Linked Immunosorbent Assay*, in *StatPearls*. 2022: Treasure Island (FL).

2. ThermoFisher Scientific. *Overview of ELISA*. [cited 2022 March 16]; Available from: https://www.thermofisher.com/ca/en/home/life-science/protein-biology/protein-biology-learning-center/protein-biology-resource-library/pierce-protein-methods/overview-elisa.html.

3. Thiha, A. and F. Ibrahim, *A Colorimetric Enzyme-Linked Immunosorbent Assay (ELISA) Detection Platform for a Point-of-Care Dengue Detection System on a Lab-on-Compact-Disc.* Sensors (Basel), 2015. **15**(5): p. 11431-41.

4. Price, C.P., *Point of care testing.* BMJ, 2001. **322**(7297): p. 1285-8.

5. Vashist, S.K., *Point-of-Care Diagnostics: Recent Advances and Trends.* Biosensors (Basel), 2017. **7**(4).

6. Koczula, K.M. and A. Gallotta, *Lateral flow assays.* Essays Biochem, 2016. **60**(1): p. 111-20.

7. Andryukov, B.G., *Six decades of lateral flow immunoassay: from determining metabolic markers to diagnosing COVID-19.* AIMS Microbiol, 2020. **6**(3): p. 280-304.

8. Chin, C.D., V. Linder, and S.K. Sia, *Commercialization of microfluidic point-of-care diagnostic devices.* LAB ON A CHIP, 2012. **12**(12): p. 2118-2134.

9. Breitbach, A. *Milenia HybriDetect – A Universal Lateral Flow Development Platform*. 2021 [cited 2022 March 16]; Available from: https://www.milenia-biotec.com/en/universal-lateral-flow-development-tool/.

10. Nsamela, A. *Microfluidics for point of care diagnostic devices: a review*. 2020 [cited 2022 March 16]; Available from: https://www.elveflow.com/microfluidic-reviews/general-microfluidics/microfluidics-for-point-of-care-diagnostic-devices-a-review/.

11. Mejia-Salazar, J.R., et al., *Microfluidic Point-of-Care Devices: New Trends and Future Prospects for eHealth Diagnostics.* Sensors (Basel), 2020. **20**(7).

12. Campbell, J.M., et al., *Microfluidic and Paper-Based Devices for Disease Detection and Diagnostic Research.* Int J Mol Sci, 2018. **19**(9).

13. Arshavsky-Graham, S. and E. Segal, *Lab-on-a-Chip Devices for Point-of-Care Medical Diagnostics*. Springer Berlin Heidelberg: Berlin, Heidelberg. p. 1-19.

14. Medical Design Briefs. *Biosensors: Bringing Diagnosis to the Point of Care*. 2019 March 16, 2022; Available from: https://www.medicaldesignbriefs.com/component/content/article/mdb/features/articles/33568.

15. Thoren, K. *The Role of Surface Plasmon Resonance in Clinical Laboratories*. 2019 [cited 2022 March 16]; Available from: https://www.aacc.org/cln/articles/2019/may/the-role-of-surface-plasmon-resonance-in-clinical-laboratories.

16. Ng, E., et al., *Magneto-nanosensor smartphone platform for the detection of HIV and leukocytosis at point-of-care.* Nanomedicine, 2019. **16**: p. 10-19.

17. Li, D. and M.M. Mielke, *An Update on Blood-Based Markers of Alzheimer's Disease Using the SiMoA Platform.* Neurol Ther, 2019. **8**(Suppl 2): p. 73-82.

18. Malecka, K., D. Pankratov, and E.E. Ferapontova, *Femtomolar electroanalysis of a breast cancer biomarker HER-2/neu protein in human serum by the cellulase-linked sandwich assay on magnetic beads.* Analytica Chimica Acta, 2019. **1077**: p. 140-149.

19. HyperPhysics. *Oil Film Interference*. [cited 2022 March 16]; Available from: http://hyperphysics.phy-astr.gsu.edu/hbase/phyopt/oilfilm.html.

20. Physics World. *Rainbow on the oil*. [cited 2022 March 16]; Available from: http://www.hk-phy.org/iq/oil_rainbow/oil_rainbow_e.html.

21. Lumen. *Thin Film Interference*. [cited 2022 March 16]; Available from: https://courses.lumenlearning.com/physics/chapter/27-7-thin-film-interference/.

22. National Aeronautics and Space Administration Science Mission Directorate. *Visible Light*. 2010 [cited 2022 March 16]; Available from: http://science.nasa.gov/ems/09_visiblelight.

23. Frey, H., *Cathode Sputtering*, in *Handbook of Thin-Film Technology*, H. Frey and H.R. Khan, Editors. 2015, Springer Berlin Heidelberg: Berlin, Heidelberg. p. 133-165.

24. Macagno, V. and J.W. Schultze, *The growth and properties of thin oxide layers on tantalum electrodes.* Journal of Electroanalytical Chemistry and Interfacial Electrochemistry, 1984. **180**(1): p. 157-170.

25. Charlesby, A. and J.J. Polling, *The Optical Properties of Thin Oxide Films on Tantalum.* Proceedings of the Royal Society of London. Series A, Mathematical and Physical Sciences, 1955. **227**(1171): p. 434-447.

26. Voros, J., *The density and refractive index of adsorbing protein layers.* Biophys J, 2004. **87**(1): p. 553-61.

27. Wypych, G., *Handbook of Fillers (3rd Edition)*. ChemTec Publishing.

28. Engineering ToolBox. *Refractive Index common Liquids, Solids and Gases*. 2008 [cited 2022 April 4]; Available from: https://www.engineeringtoolbox.com/refractive-index-d_1264.html.

29. Ono, S. and N. Masuko, *Evaluation of pore diameter of anodic porous films formed on aluminum.* Surface and Coatings Technology, 2003. **169-170**: p. 139-142.

30. Open Learn. *Interference Colours*. [cited 2022 March 16]; Available from: https://www.open.edu/openlearn/science-maths-technology/introduction-minerals-and-rocks-under-the-microscope/content-section-2.2.5.

31. LEC Expert. *White and LEDs binning*. 2015 [cited 2022 March 16]; Available from: https://www.lec-expert.com/topics/white-and-leds-binning.

32. Sandström, T., M. Stenberg, and H. Nygren, *Visual detection of organic monomolecular films by interference colors.* Applied Optics, 1985. **24**(4): p. 472-479.

33. Shashi Menon, E., *Chapter Five - Fluid Flow in Pipes*, in *Transmission Pipeline Calculations and Simulations Manual*, E. Shashi Menon, Editor. 2015, Gulf Professional Publishing: Boston. p. 149-234.

34. The Editors of Encyclopaedia Britannica. *"laminar flow"*. 2018 [cited 2022 March 16]; Available from: https://www.britannica.com/science/laminar-flow.

35. Engineering ToolBox. *Laminar, Transitional and Turbulent Flow*. 2004 [cited 2022 March 16]; Available from: https://www.engineeringtoolbox.com/laminar-transitional-turbulent-flow-d_577.html.

36. The Editors of Encyclopaedia Britannica. *"turbulent flow"*. 2020 [cited 2022 March 16]; Available from: https://www.britannica.com/science/turbulent-flow

37. SU2. *Transitional Flat Plate*. 2020 [cited 2022 March 16]; Available from: https://su2code.github.io/tutorials/Transitional_Flat_Plate/

38. The Pillars Curriculum. *ITP: Laminar vs Turbulent*. 2008 [cited 2022 March 16]; Available from: http://pillars.che.pitt.edu/student/slide.cgi?course_id=10&slide_id=14.0

39. Kumar, S.S., et al., *Three dimensional flow motions in the viscous sublayer.* Theoretical and Applied Mechanics Letters, 2021. **11**(2): p. 100239.

40. Rapp, B.E., *Chapter 9 - Fluids*, in *Microfluidics: Modelling, Mechanics and Mathematics*, B.E. Rapp, Editor. 2017, Elsevier: Oxford. p. 243-263.

41. Cebeci, T., *Chapter 4 - General Behavior of Turbulent Boundary Layers*, in *Analysis of Turbulent Flows with Computer Programs (Third Edition)*, T. Cebeci, Editor. 2013, Butterworth-Heinemann: Oxford. p. 89-153.

42. Pokrić, B. and Z. Pučar, *The two-cross immunodiffusion technique: Diffusion coefficients and precipitating titers of IgG in human serum and rabbit serum antibodies.* Analytical Biochemistry, 1979. **93**: p. 103-114.

43. Çengel, Y.A. and J.M. Cimbala, *Fluid Mechanics: Fundamentals and Applications*. 1st ed. 2006, New York: McGraw-Hill.

44. Norstone Inc. *Four Main Types of Mixing Blades and Dispersing Impellers*. [cited 2022 March 16]; Available from: https://www.norstoneinc.com/four-main-types-of-mixing-blades-and-dispersing-impellers/#:~:text=There%20are%20four%20main%20impeller,propeller%20blade%2C%20or%20radial%20blade.

45. CFM. *ELTA Axial Airfoil Impellers 16-A150P05*. 2022 [cited 2022 March 16]; Available from: https://select.cfmfans.com/catalog/axial-impellers/elta-axial-airfoil-impellers/16-A150P05.

46. Caframo LabSolutions. *4 Blade Pitched Only*. 2022 [cited 2022 March 16]; Available from: https://www.caframolabsolutions.com/products/impellers-shafts/pitched-turbine-a561/.

47. Mixer Direct. *3 Blade Propeller, LH, Sq, 3" Dia, 3/4" Bore*. 2022 [cited 2022 March 16]; Available from: https://www.mixerdirect.com/products/3-blade-propeller-lh-sq-3-dia-3-4-bore.

48. Indco. *6" Dia. 4-Blade Radial Flow Turbine - Mill Finish*. 2021 [cited 2022 March 16]; Available from: https://www.indco.com/shop/product/rti-6/6-dia-4-blade-radial-flow-turbine-mill-finish.

49. Mirro, R. and K. Voll. *Which Impeller Is Right for Your Cell Line?* 2009 [cited 2022 March 16]; Available from: https://bioprocessintl.com/analytical/cell-line-development/which-impeller-is-right-for-your-cell-line-183538/#:~:text=The%20blades%20on%20pitched%2Dblade,of%20unidirectional%20marine%20blade%20impellers.

50. Rewatkar, V.B. and J.B. Joshi, *EFFECT OF IMPELLER DESIGN ON LIQUID PHASE MIXING IN MECHANICALLY AGITATED REACTORS.* Chemical Engineering Communications, 1991. **102**(1): p. 1-33.

51. Li, X., et al., *Numerical optimization for blades of Intermig impeller in solid–liquid stirred tank.* Chinese Journal of Chemical Engineering, 2021. **29**: p. 57-66.

52. Boonkanokwong, V., et al., *The effect of the number of impeller blades on granular flow in a bladed mixer.* Powder Technology, 2016. **302**: p. 333-349.

53. Djerroud, M., G. Dituba Ngoma, and W. Ghie, *Numerical Identification of Key Design Parameters Enhancing the Centrifugal Pump Performance: Impeller, Impeller-Volute, and Impeller-Diffuser.* ISRN Mechanical Engineering, 2011. **2011**: p. 794341.

54. Doran, P.M., *Chapter 7 - Fluid Flow*, in *Bioprocess Engineering Principles (Second Edition)*, P.M. Doran, Editor. 2013, Academic Press: London. p. 201-254.

55. *Airlift Bioreactors: Hydrodynamics and Rheology Application to Secondary Metabolites Production*. 2013, IntechOpen 2013-07-24.

56. Wang, S.-J. and J.-J. Zhong, *Chapter 6 - Bioreactor Engineering*, in *Bioprocessing for Value-Added Products from Renewable Resources*, S.-T. Yang, Editor. 2007, Elsevier: Amsterdam. p. 131-161.

57. Doran, P.M., *Chapter 14 - Reactor Engineering*, in *Bioprocess Engineering Principles (Second Edition)*, P.M. Doran, Editor. 2013, Academic Press: London. p. 761-852.

58. Zhu, Y., *Chapter 14 - Immobilized Cell Fermentation for Production of Chemicals and Fuels*, in *Bioprocessing for Value-Added Products from Renewable Resources*, S.-T. Yang, Editor. 2007, Elsevier: Amsterdam. p. 373-396.

59. Chisti, Y. and M. Moo-Young, *Bioreactors*, in *Encyclopedia of Physical Science and Technology (Third Edition)*, R.A. Meyers, Editor. 2003, Academic Press: New York. p. 247-271.

60. de Jesus, S.S., et al., *Influence of impeller type on hydrodynamics and gas-liquid mass-transfer in stirred airlift bioreactor.* AIChE Journal, 2015. **61**(10): p. 3159-3171.

61. Khan, S., M. Siddiqui, and K. Osama, *Bioreactors for Hairy Roots Culture: A Review.* 2019.

62. Luo, H.-P. and M.H. Al-Dahhan, *Local characteristics of hydrodynamics in draft tube airlift bioreactor.* Chemical Engineering Science, 2008. **63**(11): p. 3057-3068.

63. Kim, T.D., et al., *Thermal behavior of proteins: Heat-resistant proteins and their heat-induced secondary structural changes.* Biochemistry, 2000. **39**(48): p. 14839-14846.

64. BioReactor Sciences. *Airlift (AL) Bioreactor Systems*. [cited 2022 May 13]; Available from: https://www.bioreactorsciences.com/air-lift-bioreactor-system#:~:text=AirLift%20(or%20GasLift)%20bioreactors%20are,as%20animal%20and%20plant%20cells.

65. Molina Grima, E., Y. Chisti, and M. Moo-Young, *Characterization of shear rates in airlift bioreactors for animal cell culture.* Journal of Biotechnology, 1997. **54**(3): p. 195-210.

66. Mehmia, M.R., et al., *Design and operational aspects of airlift bioreactors for petroleum biodesulfurization.* ENVIRONMENTAL PROGRESS, 2004. **23**(3): p. 206-214.

67. Lübbert, A., *Bubble Columns and Airlift Bioreactors*, in *Encyclopedia of Life Support Systems (EOLSS)*. 2017.

68. Colombet, D., et al., *Experiments and modelling of a draft tube airlift reactor operated at high gas throughputs.* Chemical Engineering Science, 2013. **104**: p. 32-43.

69. Aluminum Anodizers Council. *What is Anodizing?* [cited 2022 March 16]; Available from: https://www.anodizing.org/general/custom.asp?page=what-is-anodizing.

70. Mohamed, A.K., *Growth Mechanism of Porous Anodic Films Formed on Aluminium in Sulphuric Acid*, in *Faculty of Engineering and Physical Sciences* 2010, University of Manchester.

71. Lee, W. and S.-J. Park, *Porous Anodic Aluminum Oxide: Anodization and Templated Synthesis of Functional Nanostructures.* Chemical Reviews, 2014. **114**(15): p. 7487-7556.

72. Sweet, H.M., *Development of a Nanostructured Thin Film Device and Optics System for Protein Detection*, in *Materials Engineering*. 2018, University of Alberta.

73. Aramesh, M. and J. Cervenka, *Surface Modification of Porous Anodic Alumina for Medical and Biological Applications*. 2014. p. 439-467.

74. Kapruwan, P., J. Ferré-Borrull, and L.F. Marsal, *Nanoporous Anodic Alumina Platforms for Drug Delivery Applications: Recent Advances and Perspective.* Advanced Materials Interfaces, 2020. **7**(22): p. 2001133.

75. Porta-i-Batalla, M., et al., *3D Nanoporous Anodic Alumina Structures for Sustained Drug Release.* Nanomaterials, 2017. **7**(8): p. 227.

76. Santos, A., et al., *Photoluminescent Enzymatic Sensor Based on Nanoporous Anodic Alumina.* ACS Applied Materials & Interfaces, 2012. **4**(7): p. 3584-3588.

77. Pol, L., et al., *Real-Time Monitoring of Biotinylated Molecules Detection Dynamics in Nanoporous Anodic Alumina for Bio-Sensing.* Nanomaterials, 2019. **9**(3): p. 478.

78. Davoodi, E., et al., *Nano-porous anodic alumina: fundamentals and applications in tissue engineering.* Journal of Materials Science: Materials in Medicine, 2020. **31**(7): p. 60.

79. Kumeria, T., et al., *Label-free reflectometric interference microchip biosensor based on nanoporous alumina for detection of circulating tumour cells.* Biosens Bioelectron, 2012. **35**(1): p. 167-173.

80. Rajeev, G., et al., *A label-free optical biosensor based on nanoporous anodic alumina for tumour necrosis factor-alpha detection in chronic wounds.* Sensors and Actuators, B: Chemical, 2018. **257**: p. 116-123.

81. de la Escosura-Muñiz, A., et al., *In situ monitoring of PTHLH secretion in neuroblastoma cells cultured onto nanoporous membranes.* Biosensors and Bioelectronics, 2018. **107**: p. 62-68.

82. Amouzadeh Tabrizi, M., J. Ferre-Borrull, and L.F. Marsal, *Advances in Optical Biosensors and Sensors Using Nanoporous Anodic Alumina.* Sensors (Basel), 2020. **20**(18).

83. Liu, Y., et al., *A colorimetric sensor based on anodized aluminum oxide (AAO) substrate for the detection of nitroaromatics.* Sensors and Actuators B: Chemical, 2011. **160**(1): p. 1149-1158.

84. Ayas, S., et al., *Colorimetric detection of ultrathin dielectrics on strong interference coatings.* Optics Letters, 2018. **43**(6): p. 1379-1382.

85. Kasprzyk-Hordern, B., *Chemistry of alumina, reactions in aqueous solution and its application in water treatment.* Adv Colloid Interface Sci, 2004. **110**(1-2): p. 19-48.

86. Nickel, M.R., *Physical and Optical Characterization of Anodized Aluminum-Tantalum Thin Films for use in Thin Film Diagnostics*, in *Materials Engineering*. 2018, University of Alberta.

87. Costa, D., L. Savio, and C.M. Pradier, *Adsorption of Amino Acids and Peptides on Metal and Oxide Surfaces in Water Environment: A Synthetic and Prospective Review.* The Journal of Physical Chemistry B, 2016. **120**(29): p. 7039-7052.

88. van den Brand, J., et al., *Interaction of Anhydride and Carboxylic Acid Compounds with Aluminum Oxide Surfaces Studied Using Infrared Reflection Absorption Spectroscopy.* Langmuir, 2004. **20**(15): p. 6308-6317.

89. Kummert, R. and W. Stumm, *The surface complexation of organic acids on hydrous γ-Al2O3.* Journal of Colloid And Interface Science, 1980. **75**(2): p. 373-385.

90. Evans, H.E. and W.H. Weinberg, *A comparison of the vibrational structures of ethanol, acetic acid, and acetaldehyde adsorbed on alumina.* The Journal of Chemical Physics, 1979. **71**(12): p. 4789-4798.

91. Barron, A.R., *The interaction of carboxylic acids with aluminium oxides: journeying from a basic understanding of alumina nanoparticles to water treatment for industrial*

and humanitarian applications. DALTON TRANSACTIONS, 2014. **43**(22): p. 8127-8143.

92. Karaman, M.E., D.A. Antelmi, and R.M. Pashley, *The production of stable hydrophobic surfaces by the adsorption of hydrocarbon and fluorocarbon carboxylic acids onto alumina substrates.* Colloids and Surfaces A: Physicochemical and Engineering Aspects, 2001. **182**(1-3): p. 285-298.

93. Chinnaraj, M., et al., *Structure of prothrombin in the closed form reveals new details on the mechanism of activation.* Scientific Reports, 2018. **8**(1): p. 2945.

94. Austen, D.E.G., *29 - Clinical Biochemistry of Blood Coagulation*, in *Scientific Foundations of Biochemistry in Clinical Practice (Second Edition)*, D.L. Williams and V. Marks, Editors. 1994, Butterworth-Heinemann. p. 495-513.

95. Lim, T.K., V.A. Bloomfield, and G.L. Nelsestuen, *Structure of the prothrombin- and blood clotting factor X-membrane complexes.* Biochemistry, 1977. **16**(19): p. 4177-81.

96. Pozzi, N., Z. Chen, and E. Di Cera, *How the Linker Connecting the Two Kringles Influences Activation and Conformational Plasticity of Prothrombin.* J Biol Chem, 2016. **291**(12): p. 6071-82.

97. InterPro. *Gamma-carboxyglutamic acid-rich (GLA) domain*. [cited 2022 March 16]; Available from: https://www.ebi.ac.uk/interpro/entry/InterPro/IPR000294/.

98. Walz, D.A., D. Hewett-Emmett, and W.H. Seegers, *Amino Acid Sequence of Human Prothrombin Fragments 1 and 2.* Proceedings of the National Academy of Sciences of the United States of America, 1977. **74**(5): p. 1969-1972.

Chapter 3

1. Sweet, H.M., *Development of a Nanostructured Thin Film Device and Optics System for Protein Detection*, in *Materials Engineering*. 2018, University of Alberta.

2. Nickel, M.R., *Physical and Optical Characterization of Anodized Aluminum-Tantalum Thin Films for use in Thin Film Diagnostics*, in *Materials Engineering*. 2018, University of Alberta.

3. C-therm. *What is Coefficient of Thermal Expansion (CTE)? How Do I Measure It?* 2018 [cited 2022 March 17]; Available from: https://ctherm.com/resources/newsroom/blog/coefficient-of-thermal-expansion/.

4. Engineering ToolBox. *Thermal Expansion - Linear Expansion Coefficients*. 2003 [cited 2022 March 17]; Available from: https://www.engineeringtoolbox.com/linear-expansion-coefficients-d_95.html.

5. GM Quartz. *Quartz Fritted Porous Discs*. [cited March 17 2022]; Available from: https://gm-quartz.com/products/quartz-fritted-discs.

6. MicQuartz. *Custom Quartz Frits Porous Glass Filter Disc Quartz Sand Filter in Different Porosity*. [cited 2022 March 17]; Available from: https://www.micquartz.com/quartz-glass-products/quartz-plates/custom-different-porosity-of-quartz-porous-glass-filter-disc-quartz-sand-filter/.

Chapter 4

1. Huang, P.-c., et al., *The Effect of Sputtering Parameters on the Film Properties of Molybdenum Back Contact for CIGS Solar Cells.* International Journal of Photoenergy, 2013. **2013**: p. 390824.

2. Belwalkar, A., et al., *Effect of Processing Parameters on Pore Structure and Thickness of Anodic Aluminum Oxide (AAO) Tubular Membranes.* J Memb Sci, 2008. **319**(1-2): p. 192-198.

3. Sweet, H.M., *Development of a Nanostructured Thin Film Device and Optics System for Protein Detection*, in *Materials Engineering*. 2018, University of Alberta.

4. Nickel, M.R., *Physical and Optical Characterization of Anodized Aluminum-Tantalum Thin Films for use in Thin Film Diagnostics*, in *Materials Engineering*. 2018, University of Alberta.

5. Rezaee, M., et al., *Quantitative peel test for thin films/layers based on a coupled parametric and statistical study.* Scientific Reports, 2019. **9**(1): p. 19805.

6. ManualsLib. *Jenn-Air JJW9527DDS Manuals*. [cited 2022 March 17]; Available from: https://www.manualslib.com/products/Jenn-Air-Jjw9527dds-2860632.html.

Chapter 5

1. Toccafondi, C., et al., *Biomedical Applications of Anodic Porous Alumina.* Current Nanoscience, 2015. **11**.

2. Sweet, H.M., *Development of a Nanostructured Thin Film Device and Optics System for Protein Detection*, in *Materials Engineering*. 2018, University of Alberta.

3. Nickel, M.R., *Physical and Optical Characterization of Anodized Aluminum-Tantalum Thin Films for use in Thin Film Diagnostics*, in *Materials Engineering*. 2018, University of Alberta.

4. Pozzi, N. and E. Di Cera, *Prothrombin structure: unanticipated features and opportunities.* Expert Rev Proteomics, 2014. **11**(6): p. 653-5.

5. Burrell, R.E., *Aluminum oxide surfaces and interface molecules*. 2019.

Chapter 6

1. Pozzi, N. and E. Di Cera, *Prothrombin structure: unanticipated features and opportunities.* Expert Rev Proteomics, 2014. **11**(6): p. 653-5.

2. Burrell, R.E., *Aluminum oxide surfaces and interface molecules*. 2019.

Chapter 7

1. ThermoFisher Scientific. *Immunoassays*. [cited 2022 March 17]; Available from: 1. ThermoFisher Scientific. *Immunoassays*. [cited 2022 March 17]; Available from: https://www.thermofisher.com/ca/en/home/life-science/antibodies/immunoassays.html.

2. Khan, N.I., et al., *An integrated microfluidic platform for selective and real-time detection of thrombin biomarkers using a graphene FET.* Analyst, 2020. **145**(13): p. 4494-4503.

3. Nickel, M.R., *Physical and Optical Characterization of Anodized Aluminum-Tantalum Thin Films for use in Thin Film Diagnostics*, in *Materials Engineering*. 2018, University of Alberta.

4. Sweet, H.M., *Development of a Nanostructured Thin Film Device and Optics System for Protein Detection*, in *Materials Engineering*. 2018, University of Alberta.

5. Bekard, I.B., et al., *The effects of shear flow on protein structure and function.* Biopolymers, 2011. **95**(11): p. 733-745.

6. Thomas, C.R. and D. Geer, *Effects of shear on proteins in solution.* Biotechnol Lett, 2011. **33**(3): p. 443-56.

7. Stein, P.D. and H.N. Sabbah, *Turbulent blood flow in the ascending aorta of humans with normal and diseased aortic valves.* Circulation Research, 1976. **39**(1): p. 58-65.

8. Maa, Y.-F. and C.C. Hsu, *Effect of high shear on proteins.* Biotechnology and Bioengineering, 1996. **51**(4): p. 458-465.

9. Biddlecombe, J.G., et al., *Factors influencing antibody stability at solid–liquid interfaces in a high shear environment.* Biotechnology Progress, 2009. **25**(5): p. 1499-1507.

10. Kim, M.H., et al., *Surface deactivation of cellulase and its prevention.* Enzyme and Microbial Technology, 1982. **4**(2): p. 99-103.

11. Thomas, C.R., A.W. Nienow, and P. Dunnill, *Action of shear on enzymes: Studies with alcohol dehydrogenase.* Biotechnology and Bioengineering, 1979. **21**(12): p. 2263-2278.

12. Thomas, C.R. and P. Dunnill, *Action of shear on enzymes: Studies with catalase and urease.* Biotechnology and Bioengineering, 1979. **21**(12): p. 2279-2302.

13. Maa, Y.F. and C.C. Hsu, *Protein denaturation by combined effect of shear and air-liquid interface.* Biotechnol Bioeng, 1997. **54**(6): p. 503-12.

14. Sarkar, M. and V. Prabhu, *Basics of cardiopulmonary bypass.* Indian J Anaesth, 2017. **61**(9): p. 760-767.

15. Pruitt, K.M., R.M. Stroud, and J.W. Scott, *Blood Damage in the Heart-Lung Machine.* Proceedings of the Society for Experimental Biology and Medicine, 1971. **137**(2): p. 714-718.

16. *Plasma Protein Denaturation during Cardiopulmonary Bypass and the Influence of the Reticuloendothelial System upon these Changes*. [cited 2022 March 17]; Available from: https://www.osti.gov/opennet/servlets/purl/16011725.pdf.

17. Lumb, A.B., *Chapter 31 - Respiratory Support and Artificial Ventilation*, in *Nunn's Applied Respiratory Physiology (Eighth Edition)*, A.B. Lumb, Editor. 2017, Elsevier. p. 451-478.e3.

18. Brillman, J., *Chapter 185 - Neurologic Complications of Cardiac Surgery*, in *Office Practice of Neurology (Second Edition)*, M.A. Samuels and S.K. Feske, Editors. 2003, Churchill Livingstone: Philadelphia. p. 1188-1195.

19. Mirro, R. and K. Voll. *Which Impeller Is Right for Your Cell Line?* 2009 [cited 2022 March 16]; Available from: https://bioprocessintl.com/analytical/cell-line-development/which-impeller-is-right-for-your-cell-line-183538/#:~:text=The%20blades%20on%20pitched%2Dblade,of%20unidirectional%20marine%20blade%20impellers.

20. Li, X., et al., *Numerical optimization for blades of Intermig impeller in solid–liquid stirred tank.* Chinese Journal of Chemical Engineering, 2021. **29**: p. 57-66.

21. Rewatkar, V.B. and J.B. Joshi, *EFFECT OF IMPELLER DESIGN ON LIQUID PHASE MIXING IN MECHANICALLY AGITATED REACTORS.* Chemical Engineering Communications, 1991. **102**(1): p. 1-33.

22. Hu, H.H., *Chapter 10 - Computational Fluid Dynamics*, in *Fluid Mechanics (Fifth Edition)*, P.K. Kundu, I.M. Cohen, and D.R. Dowling, Editors. 2012, Academic Press: Boston. p. 421-472.

23. ANSYS, I. *ANSYS Innovation Courses: Basics of Turbulent Flows*. 2020 [cited 2022 April 14]; Available from: https://courses.ansys.com/index.php/courses/basics-of-turbulent-flows/.

24. Datawave Marine Solutions. *Practical CFD Modeling: Turbulence*. 2021 [cited 2022 April 14]; Available from: https://dmsonline.us/practical-cfd-modeling-turbulence/.

25. ANSYS, I. *ANSYS Innovation Courses: Governing Equations of Fluid Dynamics*. 2021 [cited 2022 April 27]; Available from: https://courses.ansys.com/index.php/courses/governing-equations-of-fluid-dynamics/.

26. Ferziger, J.H., M. Perić, and R.L. Street, *Computational methods for fluid dynamics*. Fourth edition. ed. 2020: Springer.

27. Roberts, P.J. and D.R. Webster. *TURBULENT DIFFUSION*. 2002.

28. SimScale. *K-Omega and K-Omega SST*. 2021 [cited 2022 April 29]; Available from: https://www.simscale.com/docs/simulation-setup/global-settings/k-omega-sst/.

29. Autodesk. *SST K-Omega Turbulence Models*. 2018 [cited 2022 April 18]; Available from: https://knowledge.autodesk.com/fr/support/cfd/learn-explore/caas/CloudHelp/cloudhelp/2019/FRA/SimCFD-Learning/files/GUID-0F5C4828-9F91-46B6-A16A-2578D72DCFCC-htm.html.

30. *Mesh Convergence*. [cited 2022 April 5]; Available from: https://abaqus-docs.mit.edu/2017/English/SIMACAEGSARefMap/simagsa-c-ctmmeshconverg.htm.

31. Zhao, F., et al., *Optimization design of the impeller based on orthogonal test in an ultra-low specific speed magnetic drive pump.* Energies, 2019. **12**(24).

32. Šškerlavaj, A. and R. Pavlin. *Effect of vortical structures on cavitation on impeller blades in pumps with suction chambers*. 2014. Institute of Physics Publishing.

33. Xu, J., *Fluid machinery and fluid mechanics : 4th International Symposium (4th ISFMFE)*. 2009: Springer.

34. Riquelme, M.C.S., *CFD Modelling of Bioprocesses: Integrating Mechanical Mixing, Aeration and Dynamic Rheology*, in *Chemical and Materials Engineering*. 2021, University of Alberta.

35. Engineering ToolBox. *Water - Density, Specific Weight and Thermal Expansion Coefficients*. 2003 [cited 2022 April 6]; Available from: https://www.engineeringtoolbox.com/water-density-specific-weight-d_595.html.

36. Demartini, L.C., H.A. Vielmo, and S.V. Möller, *Numeric and experimental analysis of the turbulent flow through a channel with baffle plates.* Journal of the Brazilian Society of Mechanical Sciences and Engineering, 2004. **26**(2): p. 153-159.

37. Kamla, Y., et al., *Effect of the Inclination of Baffles on the Power Consumption and Fluid Flows in a Vessel Stirred by a Rushton Turbine.* Chinese Journal of Mechanical Engineering, 2017. **30**(4): p. 1008-1016.

Chapter 8

1. Reverberi, R. and L. Reverberi, *Factors affecting the antigen-antibody reaction.* Blood Transfus, 2007. **5**(4): p. 227-40.

2. Jung, Y., J.Y. Jeong, and B.H. Chung, *Recent advances in immobilization methods of antibodies on solid supports.* Analyst, 2008. **133**(6): p. 697-701.

3. Bio-Rad. *ELISA: Results - Quantitative, Qualitative and Sensitivity*. [cited 2022 March 17]; Available from: https://www.bio-rad-antibodies.com/elisa-results-quantitative-semi-qualitative.html?JSESSIONID_STERLING=5934FDBD25D2B6A93E93E6A3FB555367.ecommerce2&evCntryLang=CA-en&cntry=CA&thirdPartyCookieEnabled=true.

4. ThermoFisher Scientific. *Overview of ELISA*. [cited 2022 March 16]; Available from: https://www.thermofisher.com/ca/en/home/life-science/protein-biology/protein-biology-learning-center/protein-biology-resource-library/pierce-protein-methods/overview-elisa.html.

5. Sweet, H.M., *Development of a Nanostructured Thin Film Device and Optics System for Protein Detection*, in *Materials Engineering*. 2018, University of Alberta.

6. Lim, T.K., V.A. Bloomfield, and G.L. Nelsestuen, *Structure of the prothrombin- and blood clotting factor X-membrane complexes.* Biochemistry, 1977. **16**(19): p. 4177-81.

7. Tan, Y.H., et al., *A nanoengineering approach for investigation and regulation of protein immobilization.* ACS Nano, 2008. **2**(11): p. 2374-84.

8. Lee, J.F., G.M. Stovall, and A.D. Ellington, *Aptamer therapeutics advance.* Curr Opin Chem Biol, 2006. **10**(3): p. 282-9.

9. Nickel, M.R., *Physical and Optical Characterization of Anodized Aluminum-Tantalum Thin Films for use in Thin Film Diagnostics*, in *Materials Engineering*. 2018, University of Alberta.

10. Engineering ToolBox. *Water - Density, Specific Weight and Thermal Expansion Coefficients*. 2003 [cited 2022 April 6]; Available from: https://www.engineeringtoolbox.com/water-density-specific-weight-d_595.html.

11. Engineering ToolBox. *Water - Dynamic (Absolute) and Kinematic Viscosity vs. Temperature and Pressure*. 2004 [cited 2022 May]; 22]. Available from: https://www.engineeringtoolbox.com/water-dynamic-kinematic-viscosity-d_596.html.

12. Quinn, C.P., et al., *Specific, sensitive, and quantitative enzyme-linked immunosorbent assay for human immunoglobulin G antibodies to anthrax toxin protective antigen.* Emerging infectious diseases, 2002. **8**(10): p. 1103-1110.

13. Zhang, S., et al., *Predicting detection limits of enzyme-linked immunosorbent assay (ELISA) and bioanalytical techniques in general.* Analyst, 2014. **139**(2): p. 439-445.

14. ThermoFisher Scientific. *ELISA Kits*. [cited 2022 July 26]; Available from: https://www.thermofisher.com/ca/en/home/life-science/antibodies/immunoassays/elisa-kits.html.

Chapter 9

1. Urnovitz, H.B., et al., *Urine Antibody Tests: New Insights into the Dynamics of HIV-1 Infection.* Clinical Chemistry, 1999. **45**(9): p. 1602-1613.

2. Nagaoka, F., et al., *Detection of Urinary Antibodies and Its Application in Epidemiological Studies for Parasitic Diseases.* Vaccines, 2021. **9**(7): p. 778.

3. Oxford University Hospitals. *Immunoglobulins*. 2022 [cited 2022 June 4]; Available from: https://www.ouh.nhs.uk/immunology/diagnostic-tests/tests-catalogue/immunoglobulins.aspx.

4. Eamudomkarn, C., et al., *Diagnostic performance of urinary IgG antibody detection: A novel approach for population screening of strongyloidiasis.* PLoS ONE, 2018. **13**(7).

5. WebMD. *What Is Strongyloidiasis?* 2021 [cited 2022 June 4]; Available from: https://www.webmd.com/a-to-z-guides/what-is-strongyloidiasis.

6. Nelson, R. *Simple Urine Test Could Improve Detection of Bladder Cancer*. 2022 [cited 2022 June 4].

7. Continence New Zealand. *Bladder Retraining*. 2022 [cited 2022 April 21]; Available from: https://www.continence.org.nz/pages/Bladder-Retraining/48/#:~:text=What%20is%20a%20normal%20bladder,between%20visits%20to%20the%20toilet.

8. Palagi, S., et al., *Chapter 8 - Micro- and nanorobots in Newtonian and biological viscoelastic fluids*, in *Microbiorobotics (Second Edition)*, M. Kim, A.A. Julius, and U.K. Cheang, Editors. 2017, Elsevier: Boston. p. 133-162.

9. Inman, B.A., et al., *The impact of temperature and urinary constituents on urine viscosity and its relevance to bladder hyperthermia treatment.* Int J Hyperthermia, 2013. **29**(3): p. 206-10.

10. Sweet, H.M., *Development of a Nanostructured Thin Film Device and Optics System for Protein Detection*, in *Materials Engineering*. 2018, University of Alberta.

11. Nickel, M.R., *Physical and Optical Characterization of Anodized Aluminum-Tantalum Thin Films for use in Thin Film Diagnostics*, in *Materials Engineering*. 2018, University of Alberta.

12. Surmodics. *Non-Specific Binding*. 2022 [cited 2022 June 5]; Available from: https://shop.surmodics.com/non-specific-

binding#:~:text=Non%2DSpecific%20binding%20(NSB)%20refers%20to%20an%20occurrence%20of,the%20specificity%20of%20the%20antibodies.

13. Lichtenberg, J.Y., Y. Ling, and S. Kim, *Non-Specific Adsorption Reduction Methods in Biosensing.* Sensors (Basel, Switzerland), 2019. **19**(11): p. 2488.

14. Heerspink, H., et al., *Albuminuria Assessed From First-Morning-Void Urine Samples Versus 24-Hour Urine Collections as a Predictor of Cardiovascular Morbidity and Mortality.* American journal of epidemiology, 2008. **168**: p. 897-905.

15. Bertani, B. and N. Ruiz, *Function and Biogenesis of Lipopolysaccharides.* EcoSal Plus, 2018. **8**(1): p. 10.1128/ecosalplus.ESP-0001-2018.

16. Prywer, J. and A. Torzewska, *Aggregation of poorly crystalline and amorphous components of infectious urinary stones is mediated by bacterial lipopolysaccharide.* Scientific Reports, 2019. **9**(1): p. 17061.

17. Pawfly. *Pawfly Adjustable Aquarium Air Pump 4-LPM 2 Outlets with Oxygen Accessories for 10-60 Gallon Fish Tank Pond*. 2022 [cited 2022 June 8]; Available from: https://www.amazon.ca/Pawfly-Adjustable-Aquarium-Outlets-Accessories/dp/B01EBXI7PG.

Appendix 1 – Standard Operating Procedures (SOPs)

1.1. Bob Sputtering System SOP

THE nanoFAB
Fabrication | Characterization | Expertise

W1-60 ECERF Building Edmonton, AB, CANADA T6G 2V4
p: 780.492.0167 f: 780.492.1811 www.nanofab.ualberta.ca

BOB SPUTTERING TOOL

August 06 2014



Location: 10K PVD area
Primary Trainer: Les Schowalter (587-879-1516), les.schowalter@ualberta.ca)
Secondary Trainer:

OVERVIEW
A planar magnetron sputter system with three sources. The gun/substrate configuration is designed for sequential sputtering. The third source can be used for magnetic materials.

SAFETY PRECAUTIONS
When using the hoist to close the system take care that your fingers are not between the chamber lid and body. Some materials are not compatible with a vacuum system; if you aren't sure of your material please see the primary trainer.

If you are bringing any new materials into the NanoFab for use in your process, it is necessary to fill out a chemical import form (available on our website, http://www.nanofab.ualberta.ca) and supply an MSDS data sheet to Stephanie Bozic.

OPERATING INSTRUCTIONS

Opening & Loading

W1-60 ECERF Building Edmonton, AB, CANADA T6G 2V4
p: 780.492.0167 f: 780.492.1811 **www.nanofab.ualberta.ca**

1.0 Press "**emis**" on the multi gauge controller to turn off the ion gauge then press "**channel**" until TC1 is shown and nothing on the bottom right.
2.0 Turn the Baratron valve clockwise until closed.
3.0 Close the cryopump valve clockwise until closed; there should be a solid click sound when closed. Also note the cryopump temperature, if it's not below 20K please inform nanoFAB staff.
4.0 Flip the chamber vent switch up. When the pressure readout is at 760 Torr the chamber should be at atmosphere and the chamber vent switch must be closed.
5.0 Lift the lever on the back of the chamber lid.
6.0 Press the up button on the hoist and raise the top of the chamber until the substrate holder is clear of the main chamber, and then move the chamber top away.
7.0 Please put gloves on for the next steps.
8.0 Check the inside of the chamber for flaking and other debris; vacuum as required.
9.0 If the glass view port is coated with metal, pull out and replace glass. Please use IPA to clean all six sides of glass before installing.
10.0 Change targets as required, check to see if the proper target is in the chamber or in the correct container. Sputtering the wrong material may set your project back.
11.0 Make sure the dark space shield has adequate spacing. Most targets are ¼" thick and the dark space shield shouldn't be on any notch, Targets such as Au and Pt are thinner and should go onto the smallest notch. Check spacing with the voltmeter, you should have an open circuit.
12.0 Close the shutters. Remove any particles around the main o-ring using a cleanroom wipe and IPA.
13.0 Load your substrate(s) and move the top over the chamber; move the lever down and press the lower button on the hoist. Make sure you hold onto the top section as it wants to move to the right. When the top meets the chamber stop pressing the lower button, it can't lower any further!

Pump down

1.0 Open the chamber roughing valve about one full turn and observe if the chamber pressure is dropping. If the pressure doesn't change, check to see if the lid is properly seated onto the chamber. If pressure still doesn't drop close roughing valve and find nano**FAB** staff to look into the issue.
2.0 Rough to about 350 Torr then open the roughing valve all the way then close about a half turn. Rough out to $3.0X10^{-1}$ (about five minutes depending on which roughing pump is used.) then close roughing valve.
3.0 Slowly open the cryo valve all the way by turning counterclockwise.
4.0 Open the Baratron valve by turning it counterclockwise.
5.0: Press "**channel**" on the multi gauge controller until BA1 is shown in the lower right of the display, then press "**emis**".
6.0 Pumpdown takes about one hour to reach the low -6 Torr.
7.0 Write your deposition parameters in the logbook, and put the sputter system in use sign up.

Deposition

W1-60 ECERF Building Edmonton, AB, CANADA T6G 2V4
p: 780.492.0167 f: 780.492.1811 **www.nanofab.ualberta.ca**

1. Press "**emis**" on the multi gauge to turn off the filament, then press "**channel**" until aux1 is shown in the lower section of the display.
2.0 Pull and lift the power switch on the MKS controller, then lift switch 1 for Ar gas, close the cryo gate valve about four turns until the Multi gauge controller reads $7X10^{-3}$ Torr.
3.0 Put target selector switch to the desired target. Switch on the power on the back of the MDX 500 power supply; adjust the power setting required for the material you are depositing. Remember the power supply should only be used in power mode.
4.0 Set substrate rotation to the desired speed, three to four is normal. Press the rotation switch.
5.0 Set a timer for the deposition time plus preconditioning. Target conditioning is usually three minutes except for Pt and Au which is one minute.
6.0 Press start on the power supply to condition the target. Look in the chamber to make sure the shutter is closed.
7.0 After the target conditioning step is over gently open the shutter and deposit for the desired time. Remember to write the voltage in the logbook. Press stop on the power supply when the desired time is reached.
8.0 Close the shutter and repeat steps three to six if another metal is required.
9.0 After the deposition is completed, turn off MDX 500 power supply (switch at the back).
10.0 Stop substrate rotation.
11.0 Turn target selector switch to off.
12.0 Turn off Argon switch, and MKS master power.
13.0 Press "**channel"** on the multi gauge controller until TC1 is shown and nothing else in the lower right section of the display.
14.0 Close the Baratron valve.
15.0 Close the cryo gate valve.
16.0 Flick the chamber vent switch to put a few Torr of N_2 in the chamber then wait five minutes before venting.
17.0 After venting, open chamber using the same instructions as opening and loading starting at step #5. Put gloves on after moving the chamber top, remove substrate(s) and inspect chamber for flaking. If flaking is discovered please vacuum.
18.0 If you used a Pt target, please remove it from the system.
19.0 Follow steps from pumpdown section. Please note that you don't have to start with slow pump down.

TROUBLESHOOTING
If you can't get a plasma do the following:
Close the cryo gate valve to the point of causing resistance.
Change power setting to 50 watts.
If you still can't get a plasma find the trainer for the tool or other nanoFAB staff to look into the issue.

W1-60 ECERF Building Edmonton, AB, CANADA T6G 2V4
p: 780.492.0167 f: 780.492.1811 **www.nanofab.ualberta.ca**

If you encounter an unexpected error or require assistance please contact the primary or secondary trainer listed above. Should they not be available, please contact any staff member for assistance.

APPROVAL

Qualified Trainer: Les Schowalter
Training Coordinator: Stephanie Bozic

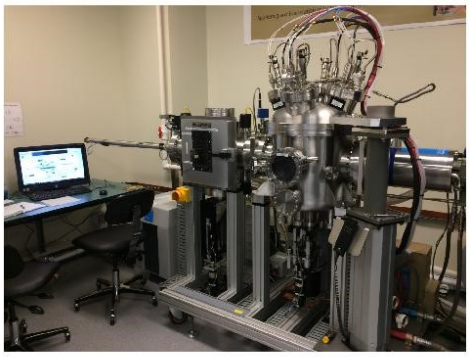
1.2. Floyd Sputtering System SOP

THE nanoFAB UNIVERSITY OF ALBERTA
Fabrication | Characterization | Expertise

W1-60 ECERF Building Edmonton, AB, CANADA T6G 2V4
p: 780.492.0167 www.nanofab.ualberta.ca

Sputtering System #3 (Floyd)

2016-11-11



Location: 10k Deposition Area

Primary Trainer: Les Schowalter
587.879.1516
les.schowalter@ualberta.ca

Secondary Trainer: Aaron Hryciw
780.940.7938
ahryciw@ualberta.ca

OVERVIEW

Sputtering System #3 (Floyd) is an automated planar DC magnetron sputtering system with four sputter guns. The system load lock contains six shelves, each of which can accommodate substrates from small pieces up to 150 mm diameter wafers, in a sputter-down configuration. The transfer of shelves to/from the process chamber, as well as the deposition itself, is computer controlled. The system is also equipped with a power supply for RF etchback, primarily used for resist descum prior to deposition for lift-off.

SAFETY PRECAUTIONS

Do not put any pressure on the load lock door: this can put it out of alignment, compromising the load lock chamber vacuum.

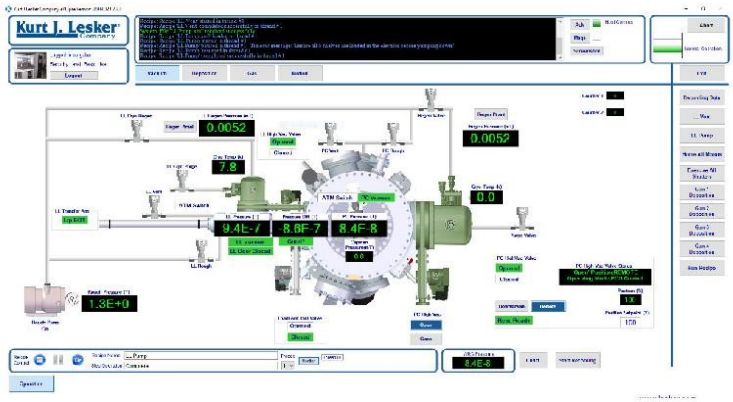
Before bringing any new materials into the nanoFAB for processing, it is necessary to fill out a new chemical import request on LMACS.

W1-60 ECERF Building Edmonton, AB, CANADA T6G 2V4
p: 780.492.0167 **www.nanofab.ualberta.ca**

OPERATING PROCEDURE

1. On LMACS, login to tool *Sputtering System #3 (Floyd)*; Location: *10k Deposition Area*.
2. The system control software, eKLipse, should be running. If not, start it by clicking the eKLipse icon on the desktop.



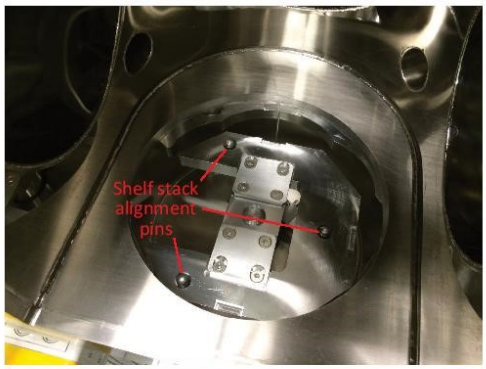


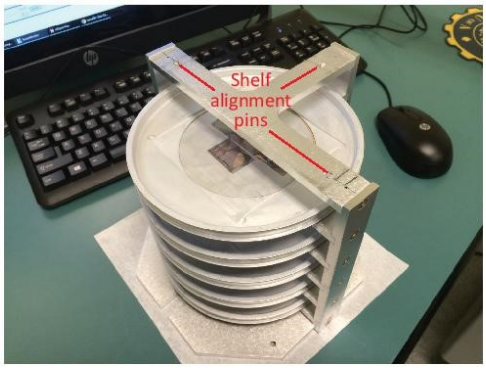
3. Login to eKLipse: click the **Login** button in the upper-left corner and enter your username and password. All users receive their own unique login information once signed off on Floyd.
4. Click **LL Vent** on the right side of the screen. Wait for venting to finish: the Recipe Name field of the *RecipeMonitor* window should read LL Vent Recipe Complete, and the load lock atmosphere indicator should be green: ATM Switch.
5. Open the load lock door and load your specimens.
   - If you only require one shelf, place specimen(s) on the top shelf (Shelf 6); in this case, it is not necessary to remove the shelf or shelf stack from the load lock.
   - If you require more than one shelf, remove the six-shelf stack and place it on a cleanroom wipe on the table. Load each individual shelf with your samples. It is important that the top shelf has notches cut out of the left and right sides, and that all shelves have their flat edges aligned to the right side of the stack (see following image). Ensure each shelf is securely seated on its three pins: failure to do this will cause a loading failure and possible damage to the loading arm. Return the six-shelf stack to the load lock, fitting it securely to the three pins in the load lock.

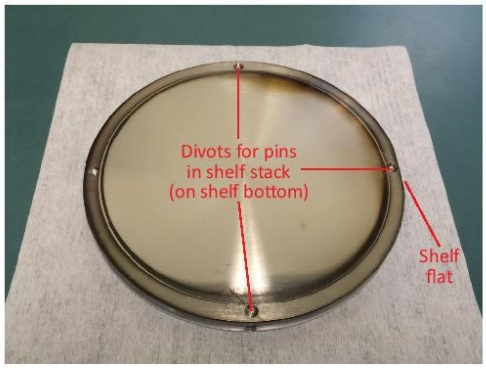
     N.B. Ensure that the shelf stack is full (i.e., has six shelves loaded) and that the top shelf has the appropriate notches before continuing.

W1-60 ECERF Building Edmonton, AB, CANADA T6G 2V4
p: 780.492.0167 www.nanofab.ualberta.ca









6. Click **LL Pump**. Do not load any shelves into the process chamber until the load lock pressure drops below 5e-6 Torr; this may be a few minutes after the recipe completes.

7. While waiting for the load lock to pump down, exercise the gun shutters: click **Exercise All Shutters**. It is recommended to do this twice to ensure all shutters open and close smoothly.

8. Load the desired shelf into the process chamber: click **Run Recipe** to open the *RecipeSelector* window, and select the appropriate "S[N] to PC" recipe, where [N] is the number of the shelf you wish to load. Remember that the shelves are numbered from 6 to 1, top to bottom. Click the **Run Recipe** button in the *RecipeSelector* window to start the shelf transfer.

9. After the shelf load recipe is finished, you may run a deposition or RF etchback process. To deposit a film, click the appropriate **Gun [N] Deposition**, where [N] is the gun containing the material you wish to deposit (e.g., **Gun 4 Deposition** to deposit Al); the current gun configuration is posted on the wall above the computer monitor. In the resulting *Parameter Passing Recipe* window, adjust the parameters in the *Value* column as required. The default parameters usually do not need to be changed, except for deposition time and possibly burn-in time. The default burn-in time of 30 s is generally sufficient unless a lot of material (different from the material you wish to sputter) has

been deposited immediately before (consult the logbook to verify); in this case, a burn-in time of 60 s is recommended. Next, enter your required deposition time in seconds; a table of deposition rates for different materials and powers is posted on the power supply rack. Click **Continue Load**.

N.B. It is also possible to run process recipes by clicking the **Run Recipe** button and choosing from the list in the *RecipeSelector* window. The four **Gun [N] Deposition** recipes can be run this way, as well as **Cr/Au Deposition** (a shortcut to deposit two common films back to back) and **RF Etchback**.

10. After the recipe is complete, repeat Step 9 to perform further deposition/etchback processes on the loaded shelf, if required.
11. Unload the shelf from the process chamber: click **Run Recipe** to open the *RecipeSelector* window, and select the appropriate "PC to S[N]" recipe. Click the **Run Recipe** button in the RecipeSelector window to start the shelf transfer back to the load lock.
12. After the shelf unload recipe is complete, repeat Steps 8–11 to process additional shelves, if required.
13. Vent the load lock by clicking the **LL Vent** button.
14. When the recipe is complete you can safely open the door and remove the shelf stack and/or remove your specimens from the shelves. Return all shelves to the shelf stack (ensuring that each one is properly seated on its three pins in the shelf stack), and return the shelf stack to the load lock (properly seated on the three load lock pins).
15. Click **LL Pump**.
16. Logout from eKLipse: click the **Logout** button in the upper-left corner.
17. Logout from tool *Sputtering System #3 (Floyd)*; on LMACS.

TROUBLESHOOTING

If there are any problems or questions regarding use of the tool, do not hesitate to contact the primary or secondary trainers.

APPROVAL

Qualified Trainer: Les Schowalter

Fabrication Group Manager: Aaron Hryciw

Version history
Les Schowalter, 2016-11-08 (*Floyd SOP.docx*)

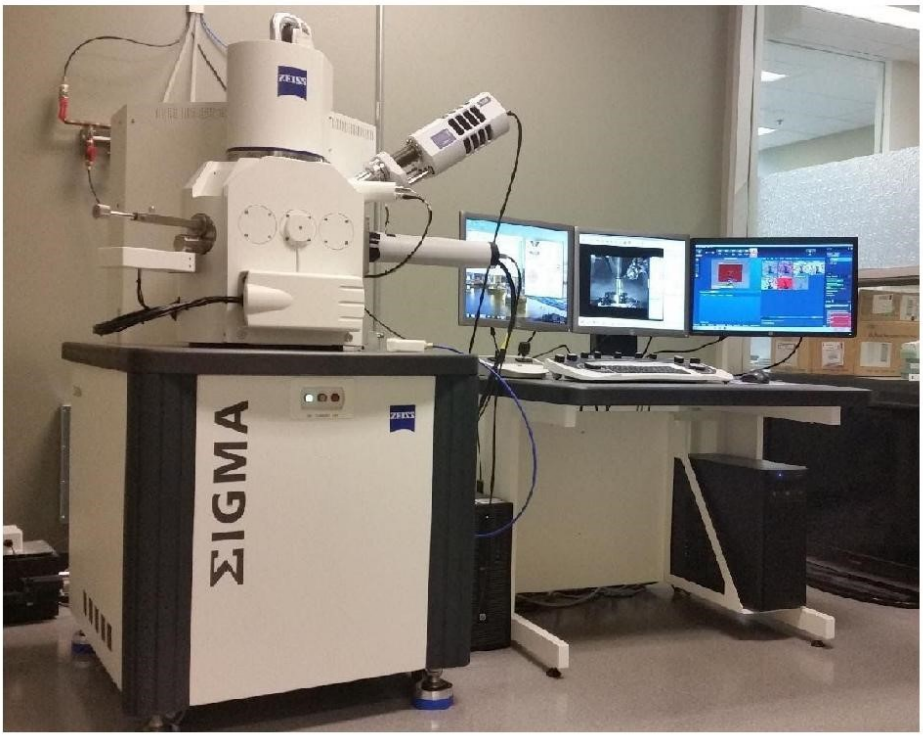
1.3. Zeiss Sigma Field Emission Scanning Electron Microscope SOP

THE nanoFAB
Fabrication | Characterization | Expertise

W1-60 ECERF Building Edmonton, AB, CANADA T6G 2V4
p: 780.492.0167 f: 780.492.1811 www.nanofab.ualberta.ca

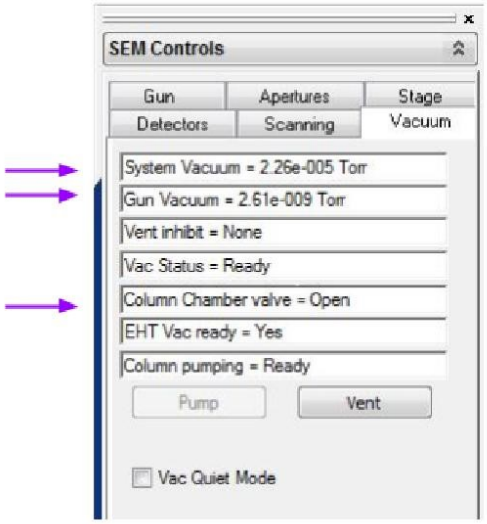
2020-10-22

Zeiss Sigma (Gemie) Field Emission Scanning Electron Microscope (FE-SEM) with EDX/EBSD



Location:	**ECERF W1-060A**	
Primary trainer:	Shiau-Yin Wu	(780-289-4700, shiauyin@ualberta.ca)
Secondary trainer:	Shihong Xu	(780-918-0523, shihongx@ualberta.ca)
	Emmett (Haoyang) Yu	(Hy1@ualberta.ca)
	Peng Li	(780-918-2094, Peng.Li@ualberta.ca)

1. Preparation
   a. Log in on the LMACS system:
      i. **"Zeiss Sigma FESEM - imaging"** for SEM imaging only
      ii. **"Zeiss Sigma FESEM w/EDX&EBSD"** for SEM/EDX or SEM/EBSD analysis
   b. The **Smart SEM** GUI program should be running all the time. If the software happens to be closed, find the SmartSEM icon on the desktop and double click to start the software.
      Username: **trainee**
      Password: **trainee**
   c. Measure your sample thickness. Enter it on the Stage navigation/specimen **height**.

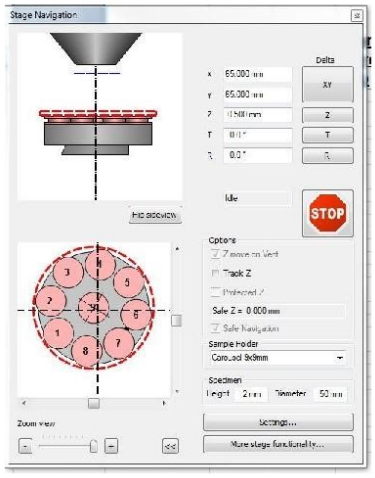


   d. Check the Vacuum (Gun Colum Vacuum and System Column) and enter the data on the Sigma daily log.
   e. Check the stage position. The default stage position before loading any sample should be (X, Y) = (65,65), Z = 0 or 0.5 mm and T (tilt) = 0

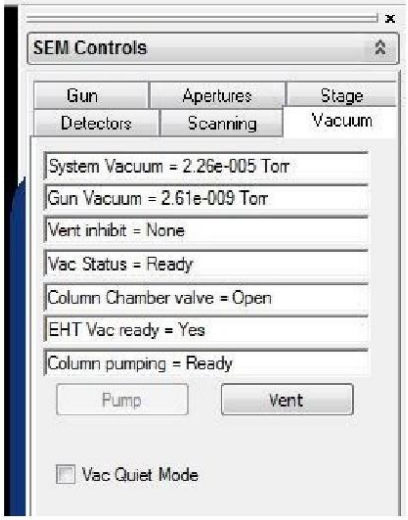
2. Sample loading process
   a. Check and record system vacuum parameters on the Daily-Log Excel sheet.
   b. System vacuum should be ready, Column/Chamber Isolation valve should be Open, Gun should be on and EHT should be off. Chamber camera should be off.



c. Before venting the system, you need to record the system vacuum and gun column vacuum when the valve is open.
d. After you vent the system, you need to record the gun column vacuum. At this time, the valve is closed.
e. At the end of your session, you need to record the system vacuum, gun column vacuum, EHT, WD, aperture and detectors used.
f. Load your sample on the stage.
    i. The Maximum sample height is 17.5mm for imaging and 13.5mm for EDX.
    ii. Sample holders are stored in a dry box on the sample preparation table
    iii. Make sure you wear a pair of gloves whenever you need to handle your samples/stubs, holders and inside the chamber.
    iv. **All samples need to be mounted on the SEM stub first**. Do not mount the sample directly on the stage. The standard stage can load upto 9 samples. Each position is labelled with a number. If you have more than one sample, make sure you record the stub location numbers before loading. Please make sure you don't completely loosen any or over-tighten any screws when mounting/unmounting samples.
g. If the stage is not at the default setting, change it. On the Stage Navigation window, Make sure X, Y, Z is (65, 65, 0) and the T and R are also (0, 0).



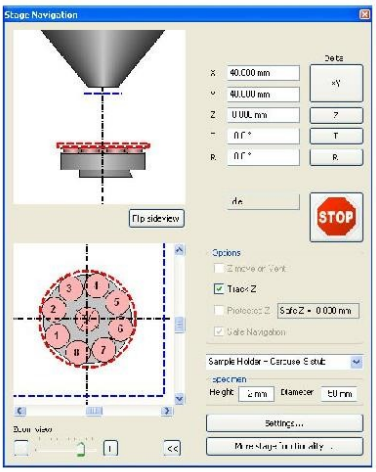
h. Vent the system.
   i. Go to the SmartSEM control window/Vacuum tab and click Vent.



   ii. It will take ~90s to be fully vented; wait until the chamber door can be opened easily. Do not attempt to force the door open.

i. Turn on chamber scope/TV. Open the chamber door, and load the holder. Make sure the orientation of the stage is correct before closing the chamber door. The chamber door should only be open when loading and unloading the holder.
j. Close the chamber door.
k. Go to the software. Find the SEM control/Vacuum and click pump. It will take at least 7-10 minutes to reach the desired pressure (< 2.0e-5 torr).
l. During the pumping down, go to the stage navigation window. Under the option/specimen, enter the tallest sample height in **Specimen Height.** This will limit how much you can raise the stage. This is extremely important. The operator should always check the sample height setting before raising the stage.

W1-60 ECERF Building Edmonton, AB, CANADA T6G 2V4
p: 780.492.0167 f: 780.492.1811 www.nanofab.ualberta.ca



m. If tilting of the stage is required, first ensure the Z height = 0. Tilting with a high Z height may result in physical collision.
   i. Make sure the camera is on.
   ii. Make sure the stage is at the lowest (z=0).
   iii. Rotate that sample to 6 oclock position using the proper joystick.
   iv. On the navigation window, change the T (tilt) to the angle that you want. At the time, the sample stage will tilt.
   v. Using the proper joystick to move the stage up to proper height.

3. Alignment and Imaging

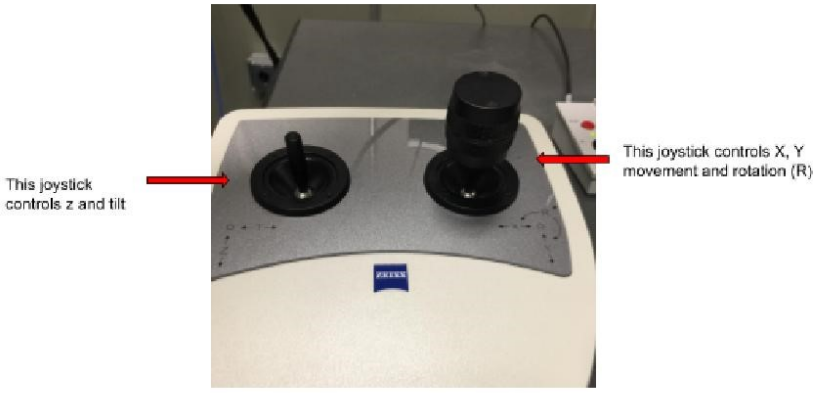
a. Once the vacuum reaches the minimum requirement (<2e-5 torr), you can turn on EHT.
   i. **EHT** is the acceleration voltage of the primary electron beam. Higher EHT results in higher spatial resolution, but increases penetration depth, thus images are not as surface sensitive as low voltages. Higher EHT also increases potential charging and sample damages. Typical EHT for imaging is between 5-10 kV.

b. Choose a proper aperture for your sample. Default is 30 micron.

c. Choose the proper detector.

W1-60 ECERF Building Edmonton, AB, CANADA T6G 2V4
p: 780.492.0167 f: 780.492.1811 www.nanofab.ualberta.ca





d. In TV mode, move the sample to the center of the stage either by using the joystick or double click the sample number on the stage under stage navigation.
e. Move the stage to the proper height by using the joystick. Typical WDs are: 4 - 6 mm for inlens detector, 7 - 12 mm for SE detector and 8.5 mm for EDX.
f. Change to imaging mode, adjust Brightness and Contrast to see an image or proper signal level on the screen. At low magnification (~50X), adjust the focus knob on the keyboard to ensure the image is well focused. Then you can increase the magnification and readjust the focus knob. Repeat this process whenever it is needed.
g. Adjust the stigmation. Begin by adjusting the Stigmator X dial and attempt to achieve the best image possible, and repeat with the Stigmator Y dial. Repeat until the best image is obtained.
h. Adjust the wobble (aperture alignment).

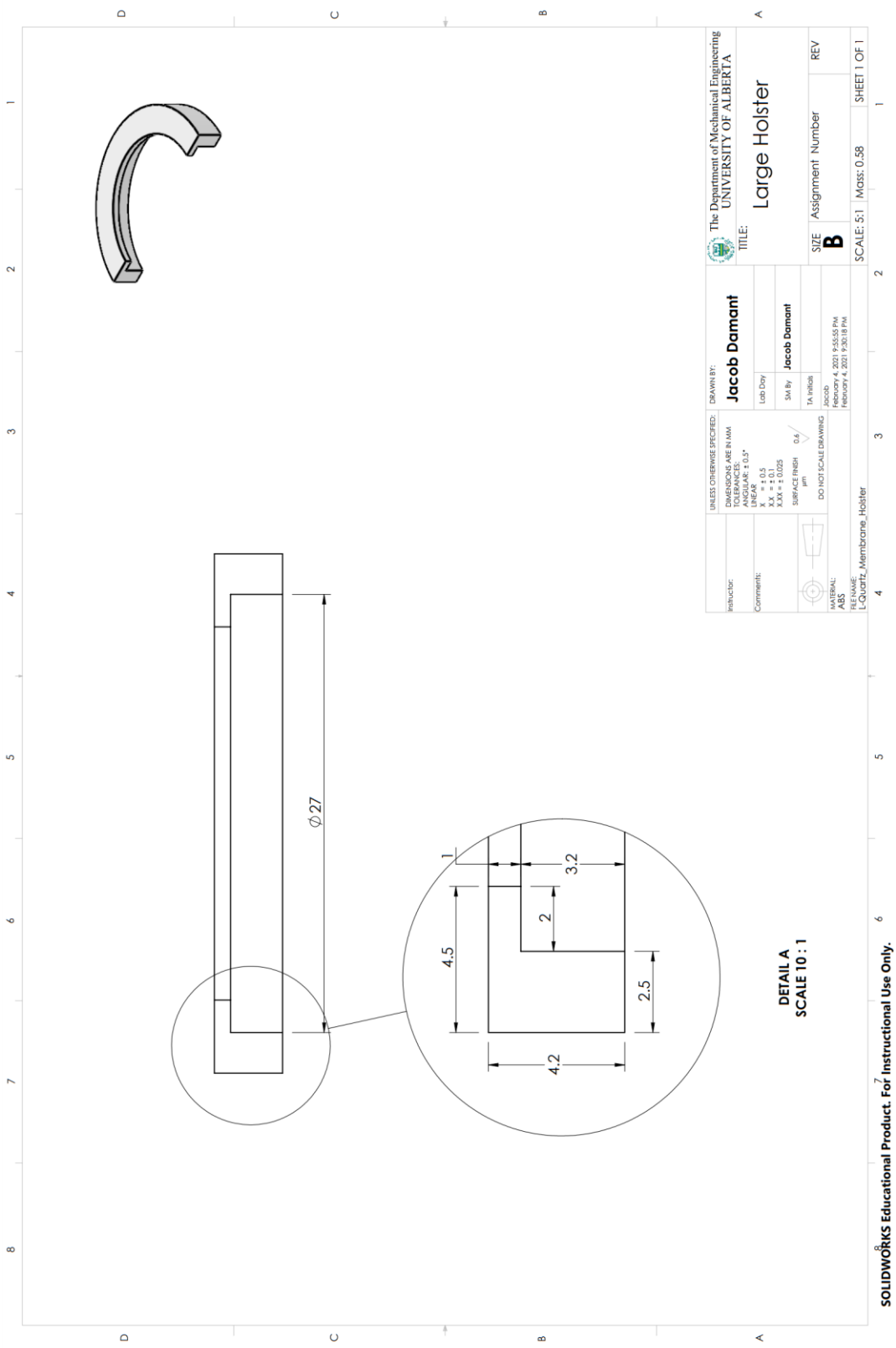
i. Press the Wobble button on the keyboard to open the reduced window and begin the scanning. The SEM will scan through a range of focal points, with the feature coming in and out of focus.
ii. Adjust Aperture X and Y to eliminate or minimize any lateral imaging shift.

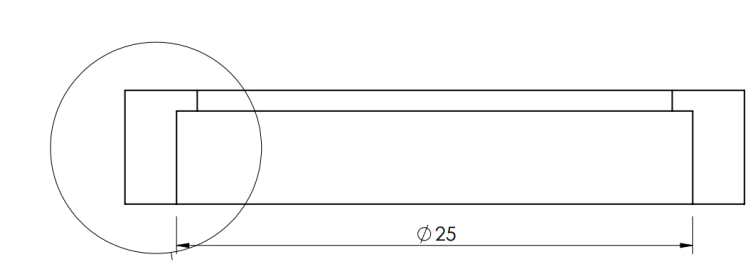
i. Adjust Brightness and Contrast
j. Capture an image. Higher scan speed means scan slower but less noise. Use noise reduction whenever it is needed. Change the scan speed (7-9) and noise reduction to line average (increase N to what you need) to improve the image quality.
k. Save the image to your own folder. File/save images. Please make sure you select the proper directory.
l. Transfer files using winSCP.

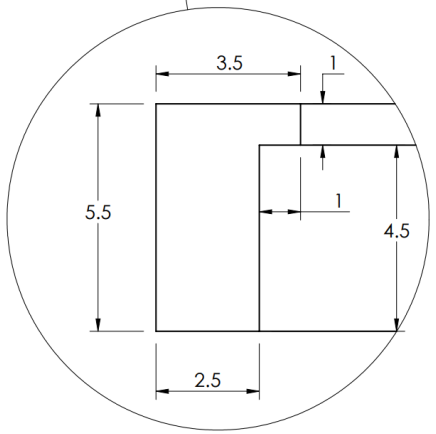
4. Shut down process

a. Adjust the magnification to the lowest setting.
b. Reset the scan rate to 3 and Noise reduction to pixel average.
c. Lower the stage Z to 0. Tilt the stage back tilt T to 0.
d. Move the stage to the initial coordinate (X,Y) = (65, 65) (or double click on the position 9 on stage navigation windows).
e. Return the brightness to contrast to a reasonable setting
f. Adjust the focus to a reasonable level. Users should be able to see a clear image of the stage.
g. Turn off the EHT.
h. Vent the chamber and remove samples.
i. Return the stage holder back to the desiccator and pump it down.
j. Turn off TV mode/chamber scope.
k. Wait until the vacuum is ready.
l. Log off.

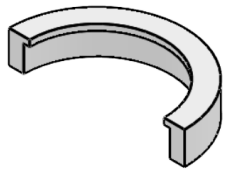
Appendix 2 – Quartz Frits Disc Holster Designs







DETAIL D
SCALE 10 : 1



Instructor:	UNLESS OTHERWISE SPECIFIED: DIMENSIONS ARE IN MM TOLERANCES: ANGULAR: ± 0.5° LINEAR X = ± 0.5 X.X = ± 0.1 X.XX = ± 0.025 SURFACE FINISH 0.6 µm DO NOT SCALE DRAWING	DRAWN BY: **Jacob Damant**	The Department of Mechanical Engineering UNIVERSITY OF ALBERTA
Comments:		Lab Day	TITLE: Small Holster
		SM By **Jacob Damant**	
		TA Initials	SIZE **B** Assignment Number REV
MATERIAL: ABS		Jacob February 4, 2021 9:27:24 PM February 4, 2021 8:54:07 PM	SCALE: 5:1 Mass: 0.64 SHEET 1 OF 1
FILE NAME: S-Quartz_Membrane_Holster			

SOLIDWORKS Educational Product. For Instructional Use Only.

Appendix 3 – Fusion 360 Impeller, Membrane Disc and Membrane Reinforcement Designs

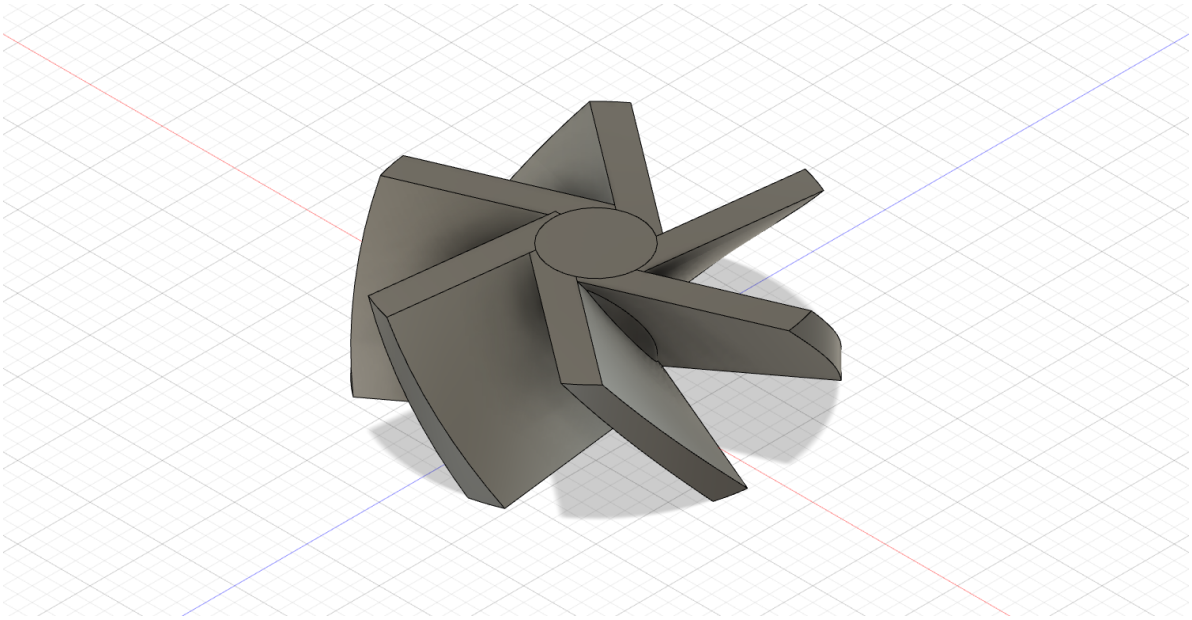


Figure A3.1. Fusion 360 impeller design.

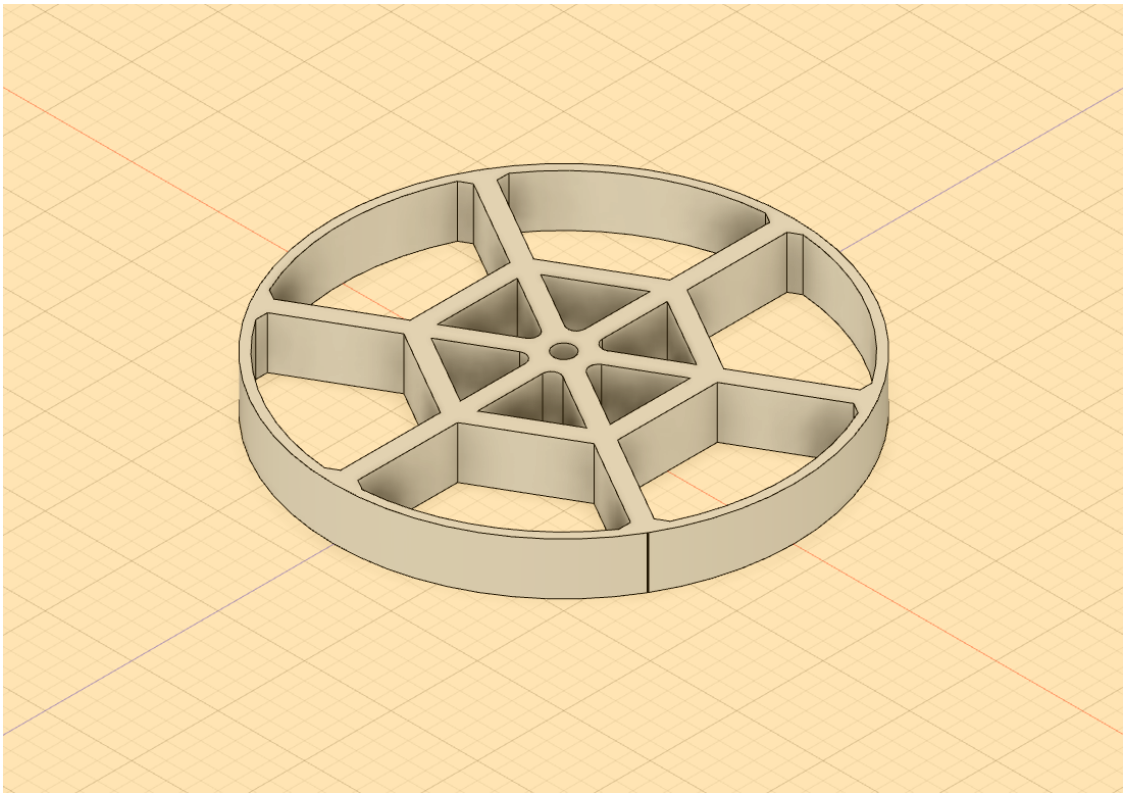


Figure A3.2. Fusion 360 membrane reinforcement design.

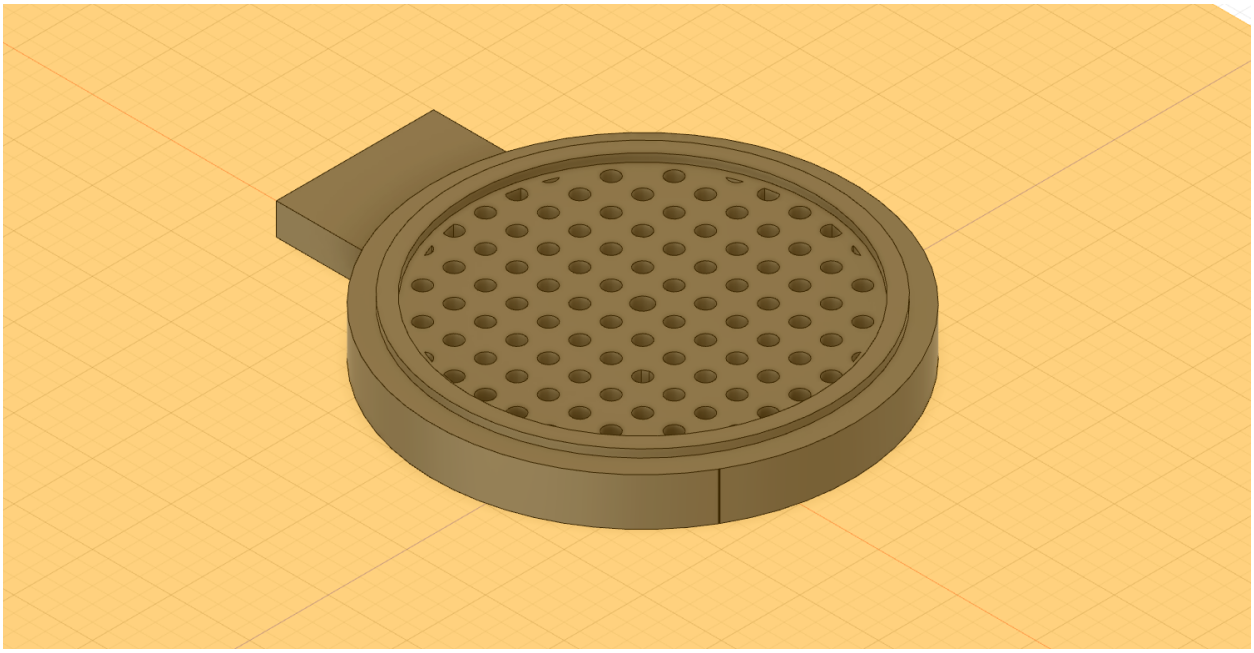


Figure A3.3. Fusion 360 membrane design.

Appendix 4 – Anodization Data

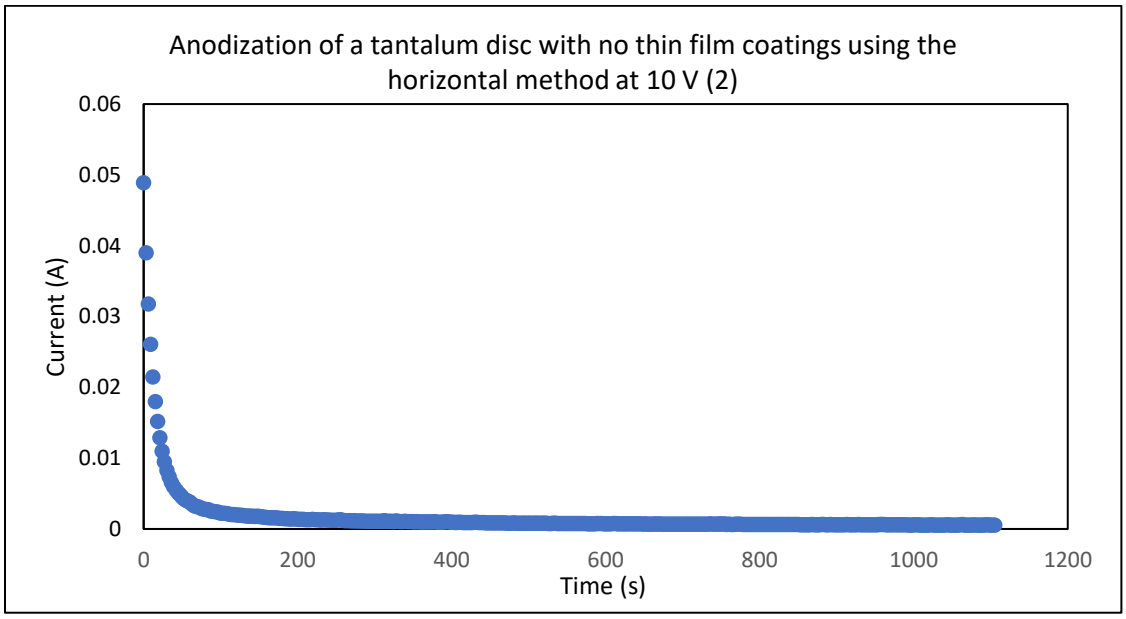


Figure A4.1. Current vs. time anodization plot for a tantalum disc (2) with no coatings using the horizontal anodization method at 10 V.

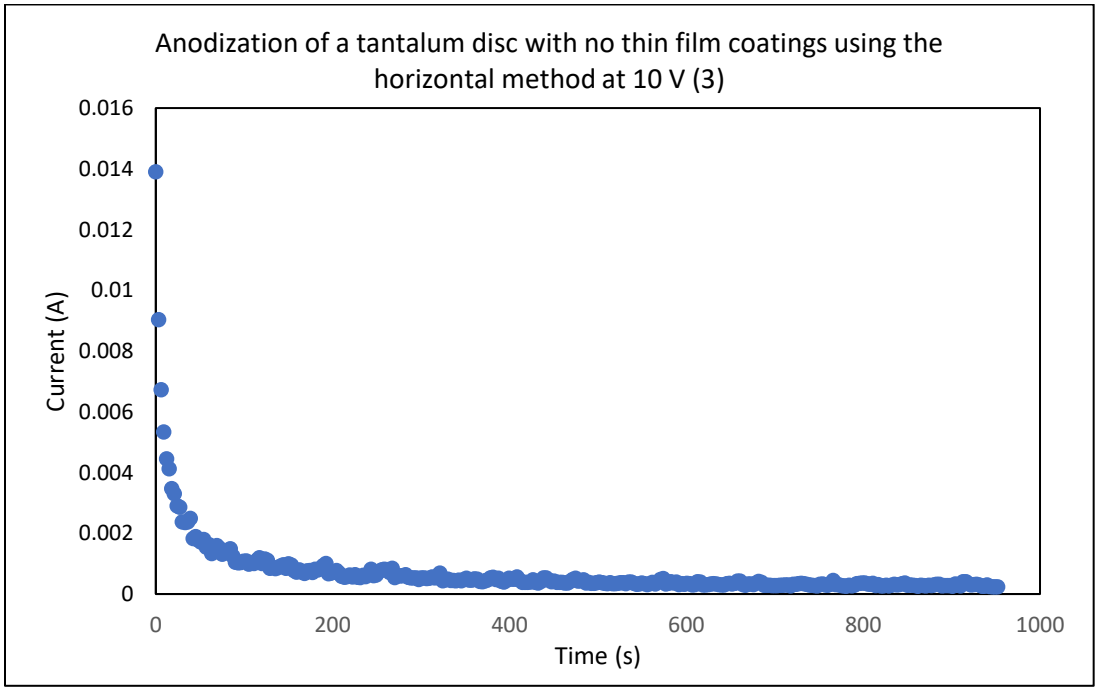


Figure A4.2. Current vs. time anodization plot for a tantalum disc (3) with no coatings using the horizontal anodization method at 10 V.

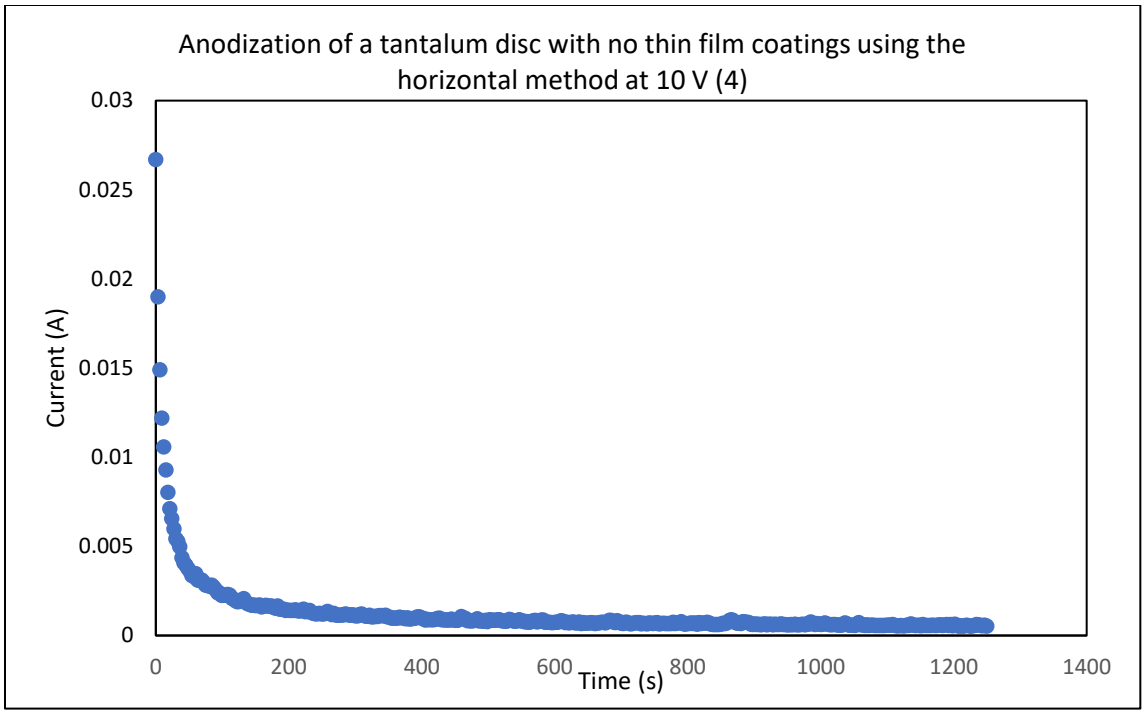


Figure A4.3. Current vs. time anodization plot for a tantalum disc (4) with no coatings using the horizontal anodization method at 10 V.

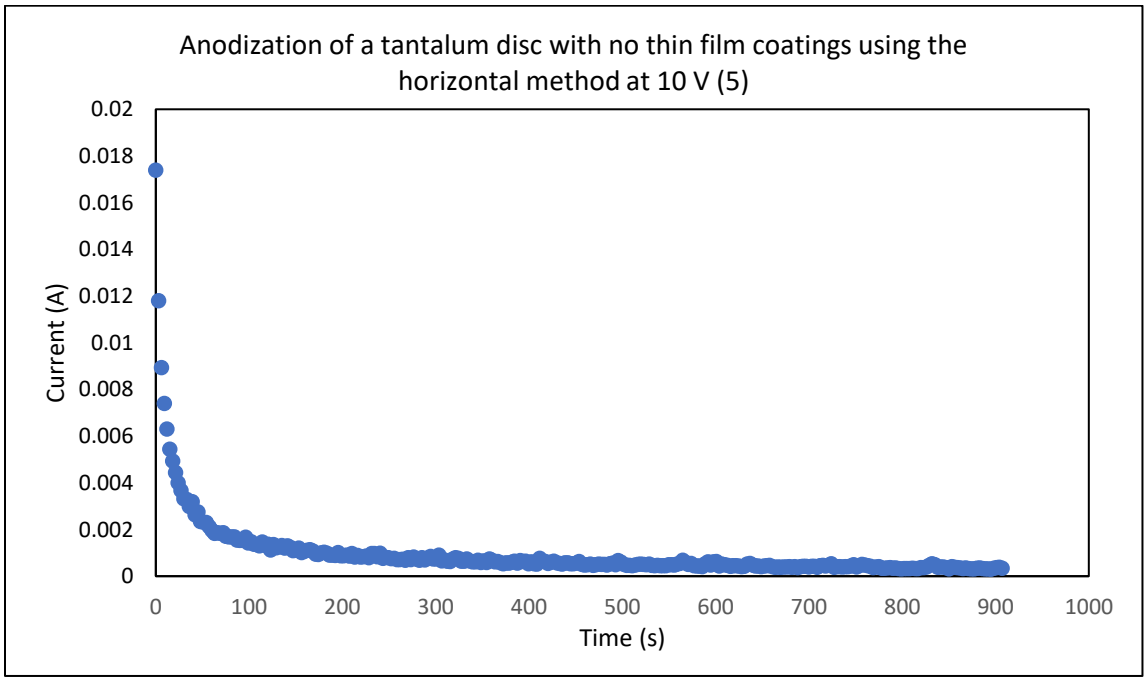


Figure A4.4. Current vs. time anodization plot for a tantalum disc (5) with no coatings using the horizontal anodization method at 10 V.

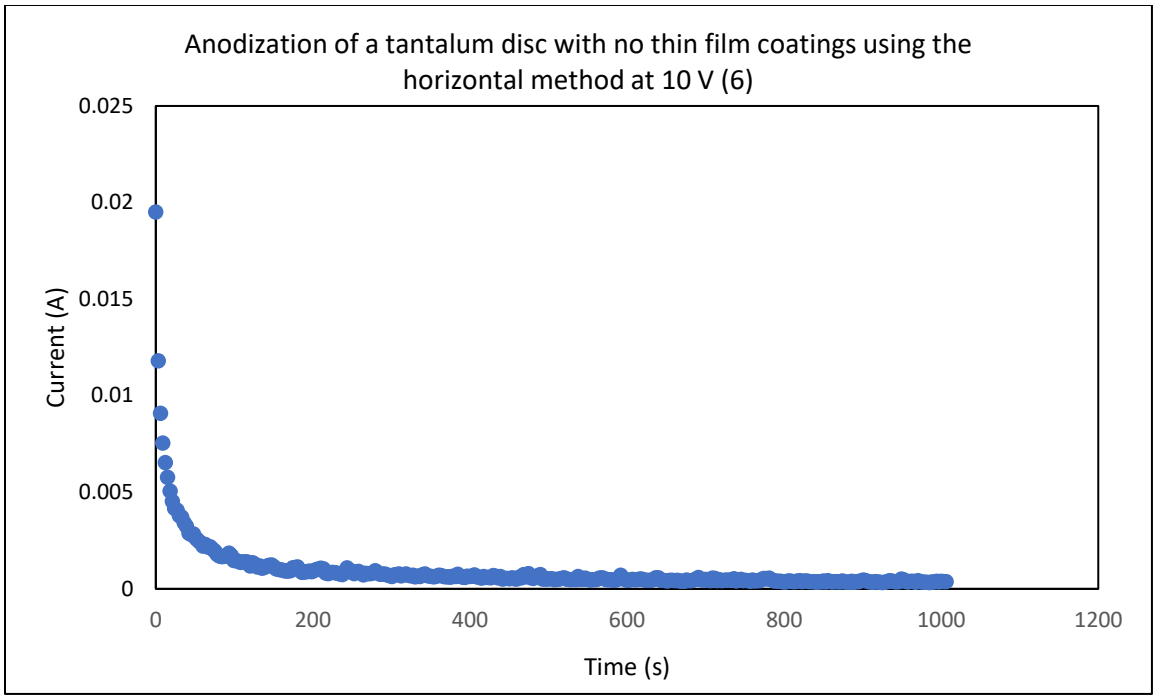


Figure A4.5. Current vs. time anodization plot for a tantalum disc (6) with no coatings using the horizontal anodization method at 10 V.

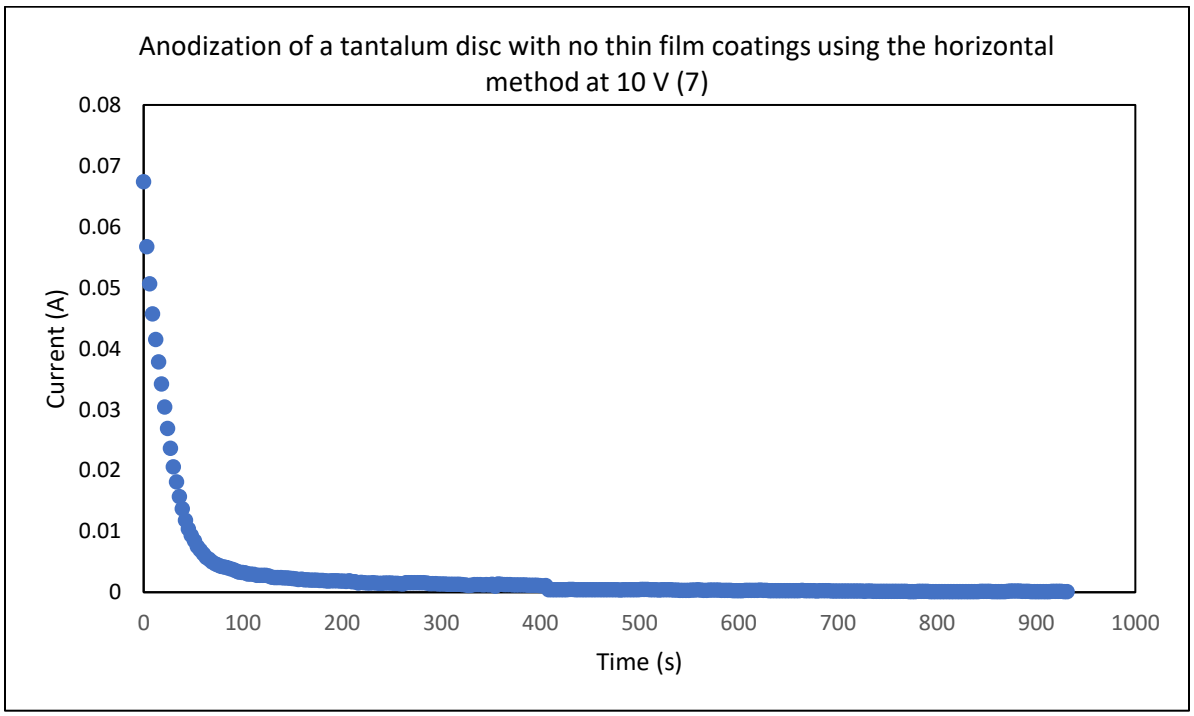


Figure A4.6. Current vs. time anodization plot for a tantalum disc (7) with no coatings using the horizontal anodization method at 10 V.

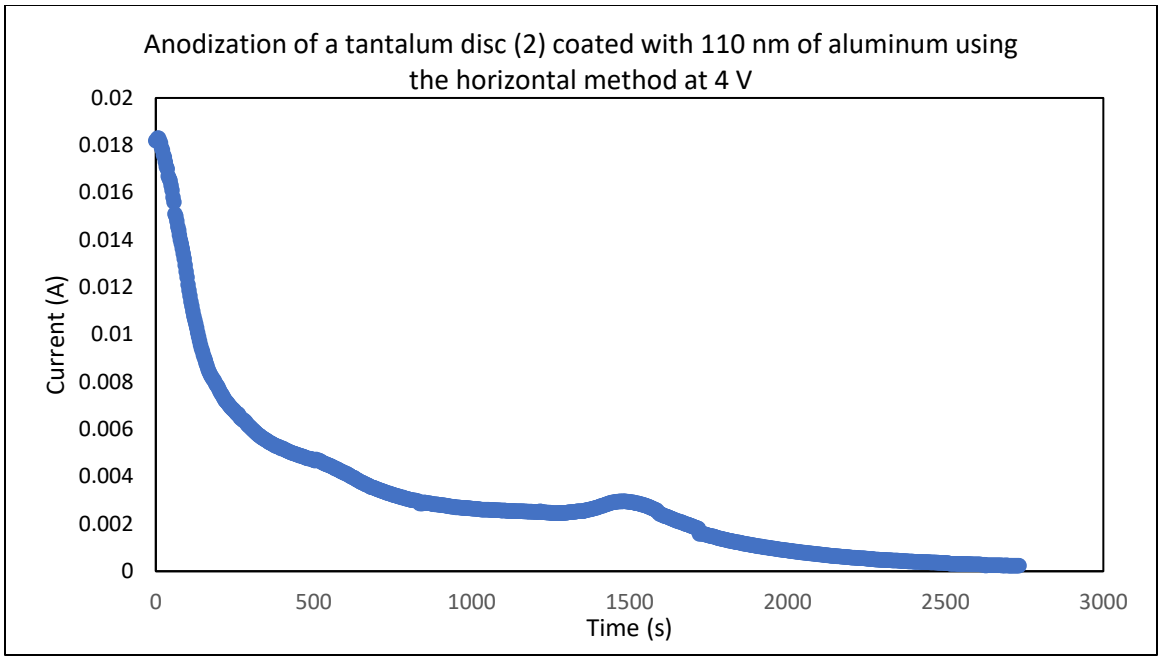


Figure A4.7. Current vs. time anodization plot for a tantalum disc (2) coated with 110 nm of aluminum using the horizontal anodization method to anodize the aluminum face at 4 V.

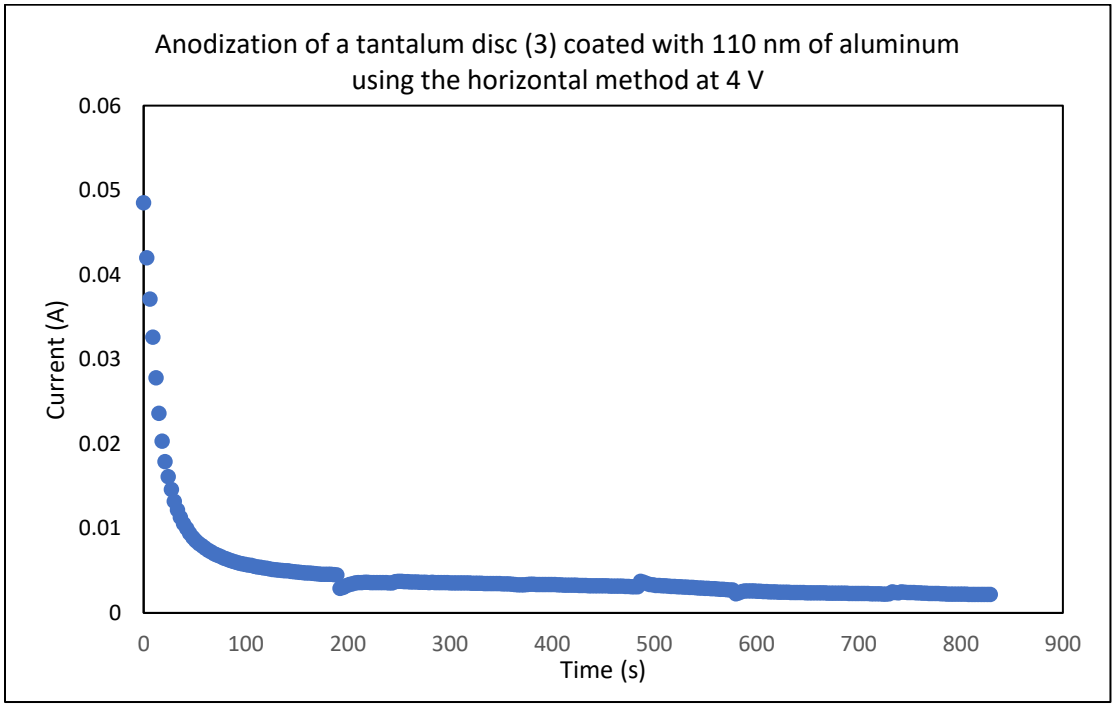


Figure A4.8. Current vs. time anodization plot for a tantalum disc (3) coated with 110 nm of aluminum using the horizontal anodization method to anodize the aluminum face at 4 V.

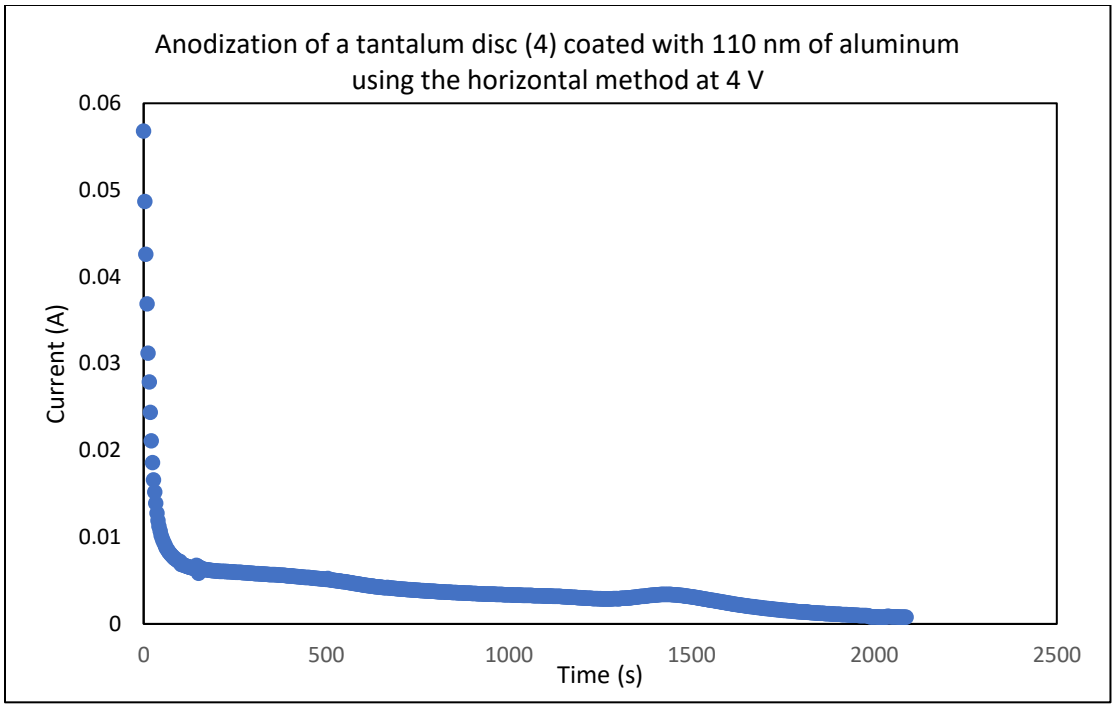


Figure A4.9. Current vs. time anodization plot for a tantalum disc (4) coated with 110 nm of aluminum using the horizontal anodization method to anodize the aluminum face at 4 V.

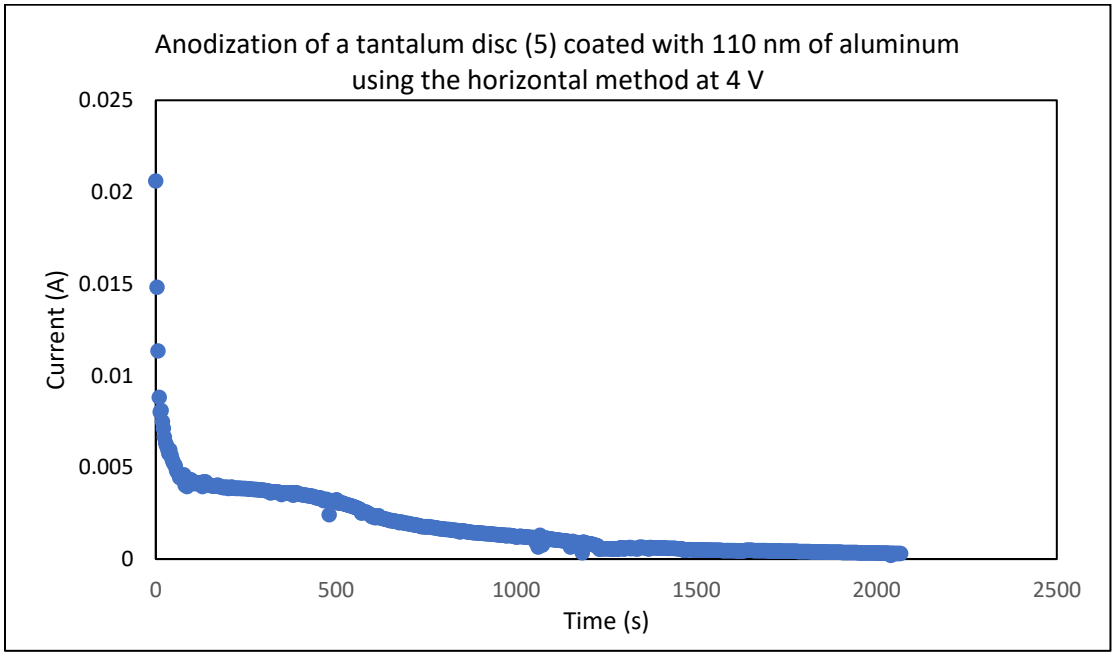


Figure A4.10. Current vs. time anodization plot for a tantalum disc (5) coated with 110 nm of aluminum using the horizontal anodization method to anodize the aluminum face at 4 V.

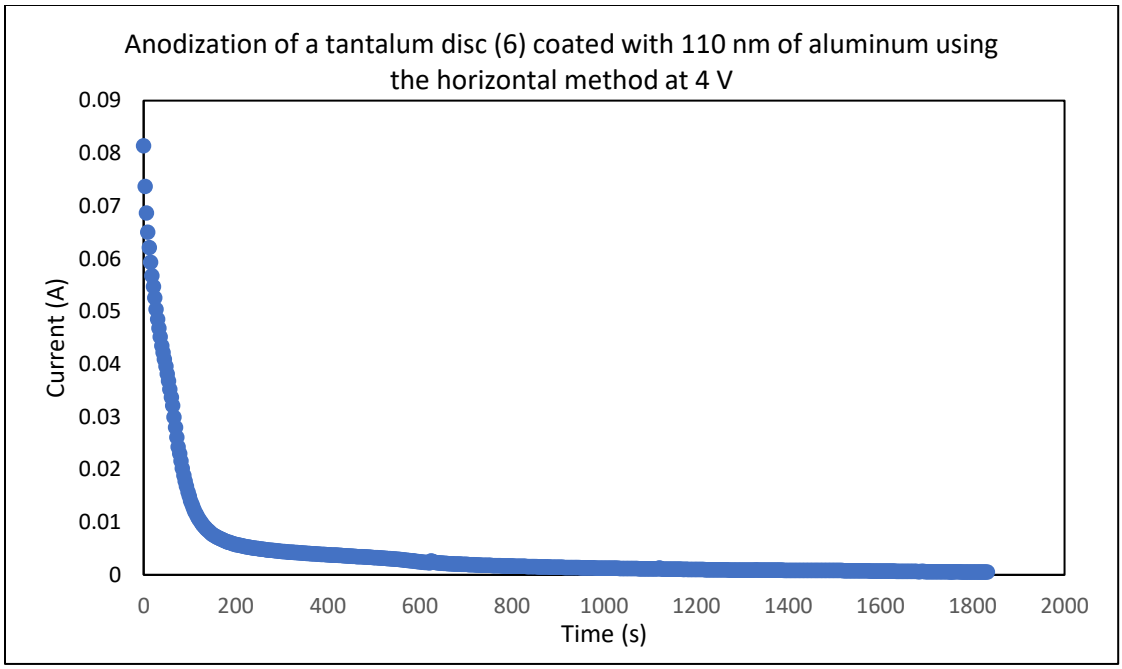


Figure A4.11. Current vs. time anodization plot for a tantalum disc (6) coated with 110 nm of aluminum using the horizontal anodization method to anodize the aluminum face at 4 V.

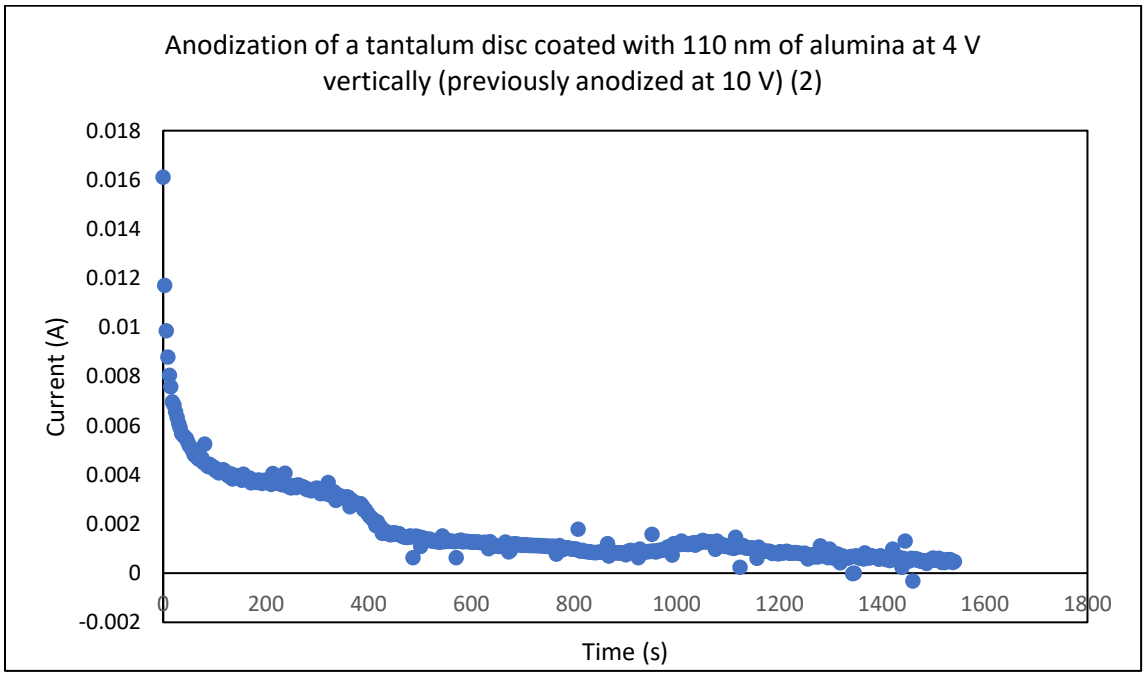


Figure A4.12. Current vs. time anodization plot for a tantalum disc coated with 110 nm of aluminum at 4 V (vertical) with previous anodization of tantalum face at 10 V (2).

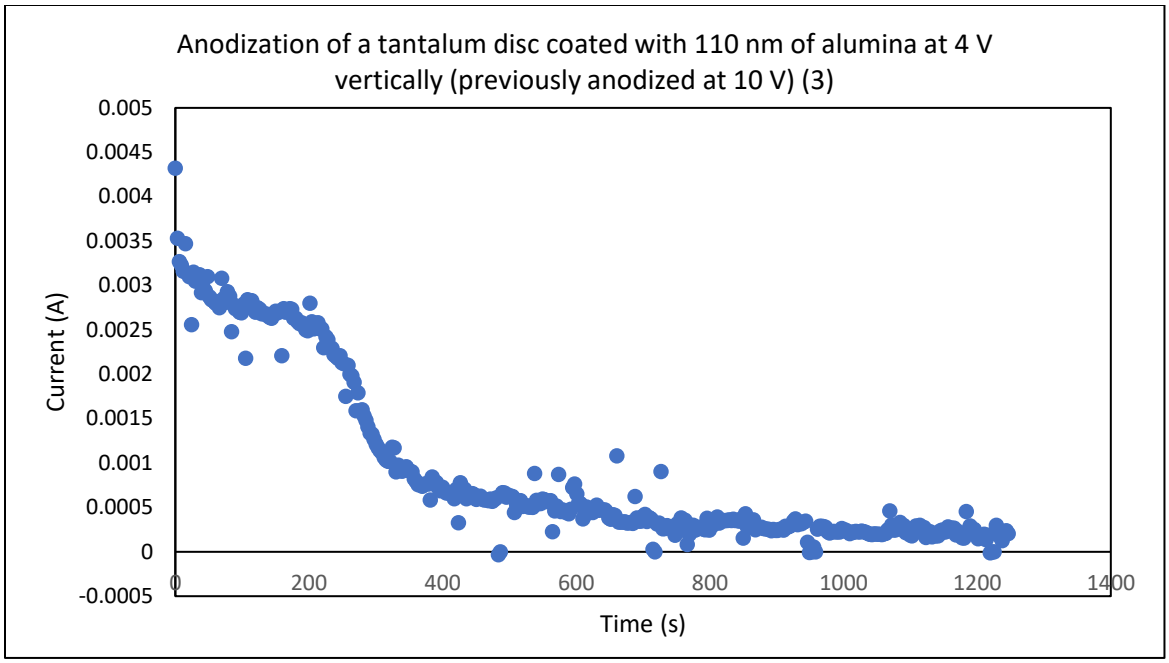


Figure A4.13. Current vs. time anodization plot for a tantalum disc coated with 110 nm of aluminum at 4 V (vertical) with previous anodization of tantalum face at 10 V (3).

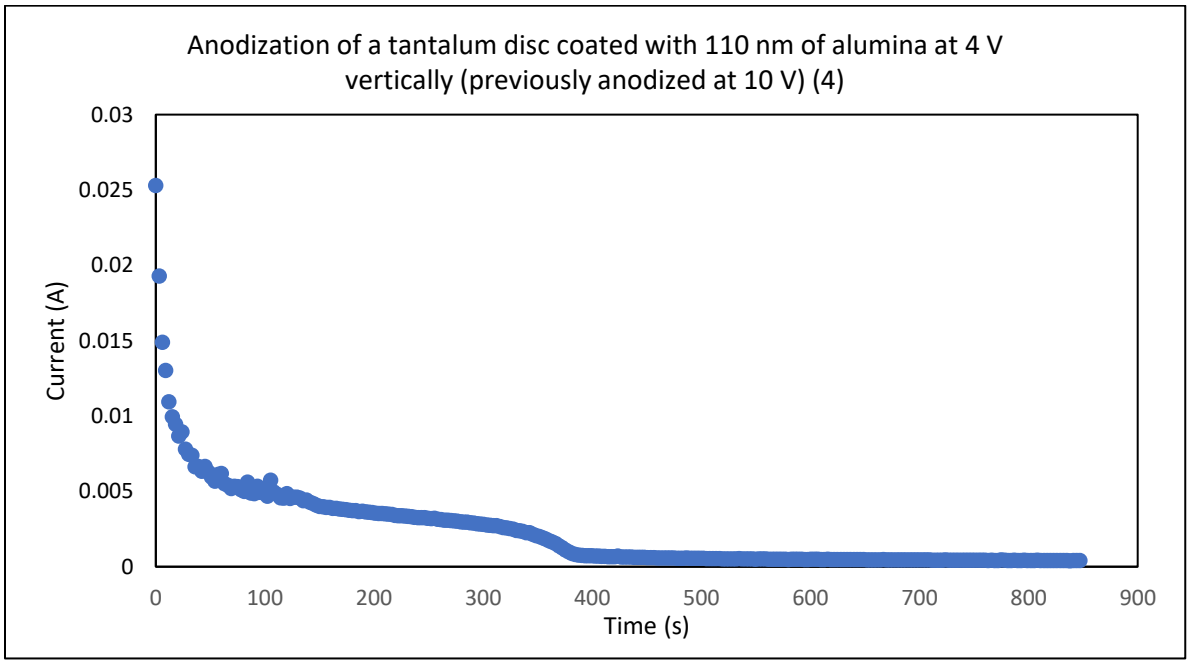


Figure A4.14. Current vs. time anodization plot for a tantalum disc coated with 110 nm of aluminum at 4 V (vertical) with previous anodization of tantalum face at 10 V (4).

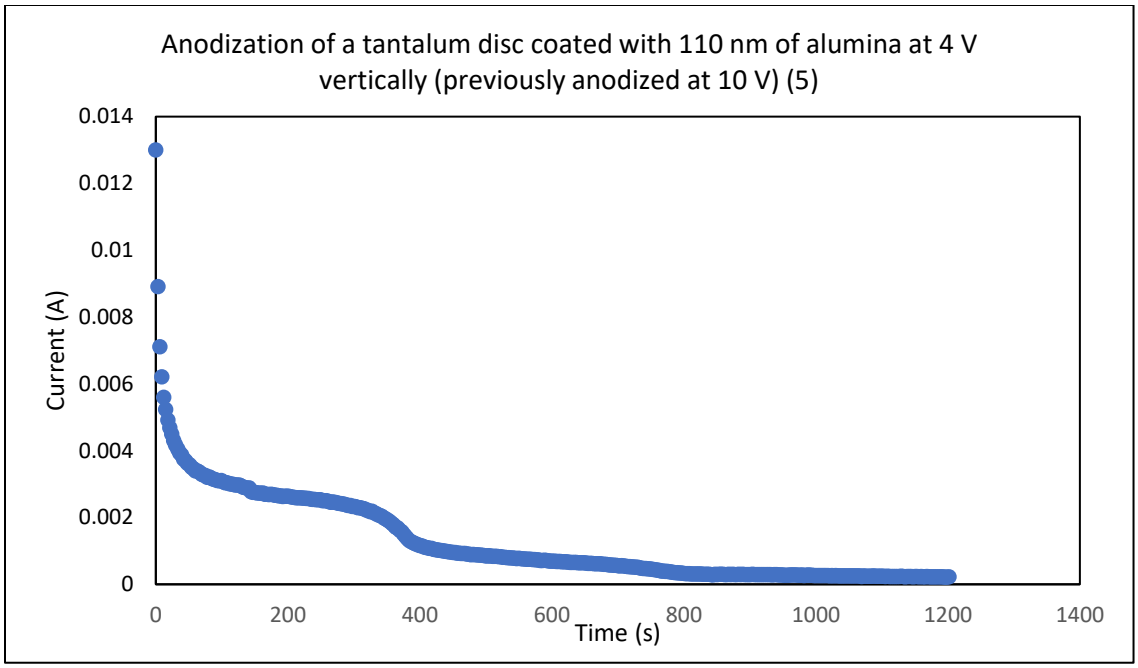


Figure A4.15. Current vs. time anodization plot for a tantalum disc coated with 110 nm of aluminum at 4 V (vertical) with previous anodization of tantalum face at 10 V (5).

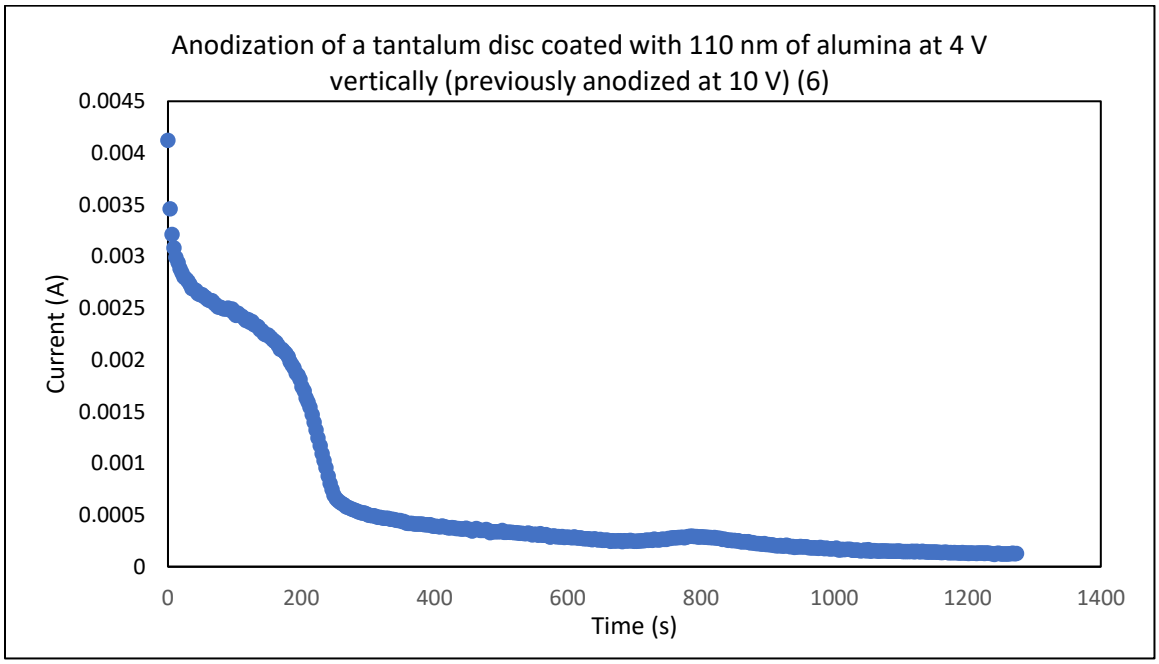


Figure A4.16. Current vs. time anodization plot for a tantalum disc coated with 110 nm of aluminum at 4 V (vertical) with previous anodization of tantalum face at 10 V (6).

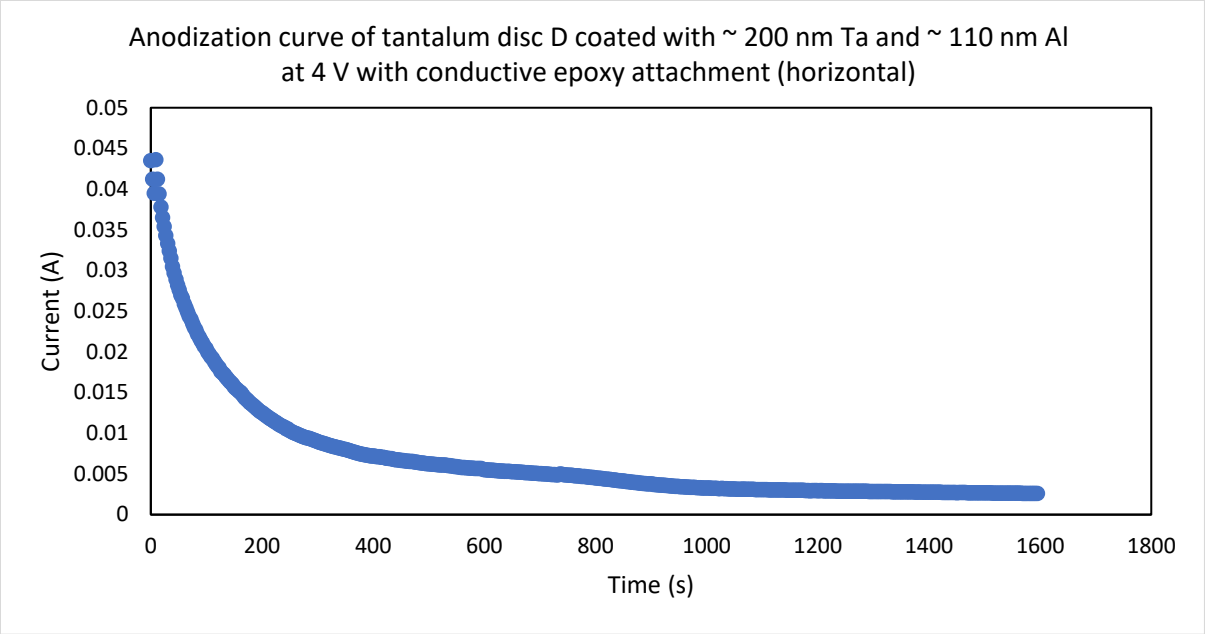


Figure A4.17. Current vs. time anodization plot for tantalum disc D coated with 200 nm of tantalum and 110 nm of aluminum at 4 V (horizontal with conductive epoxy attachment).

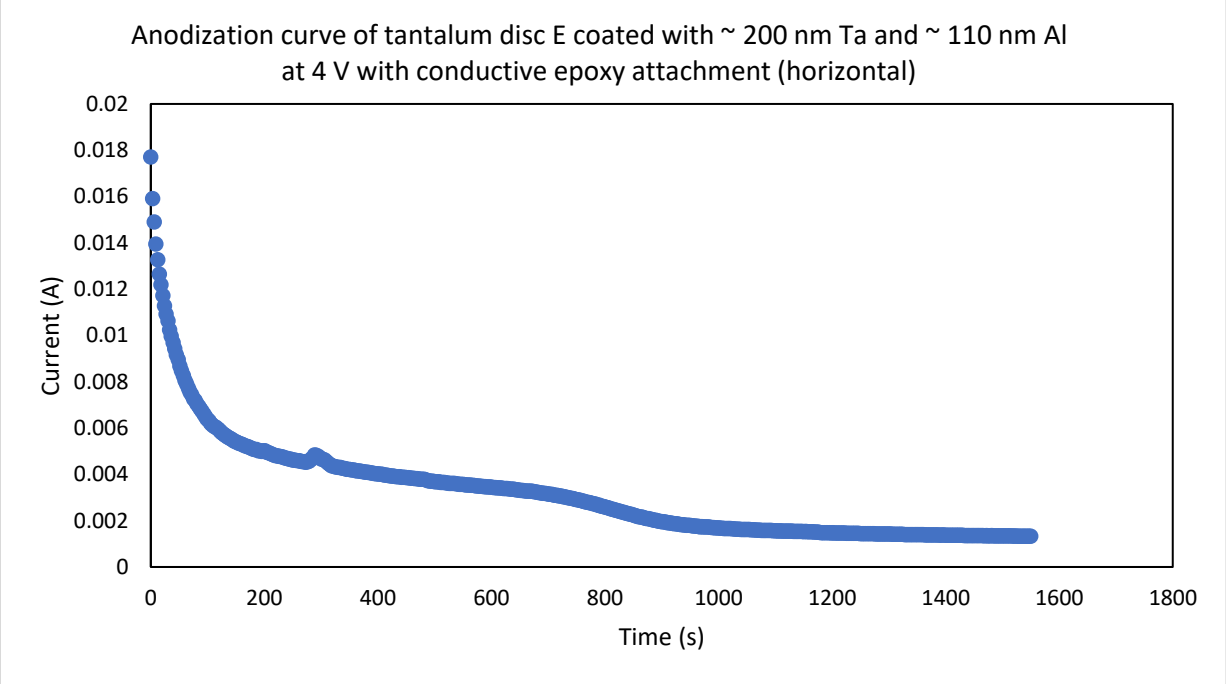


Figure A4.18. Current vs. time anodization plot for tantalum disc E coated with 200 nm of tantalum and 110 nm of aluminum at 4 V (horizontal with conductive epoxy attachment).

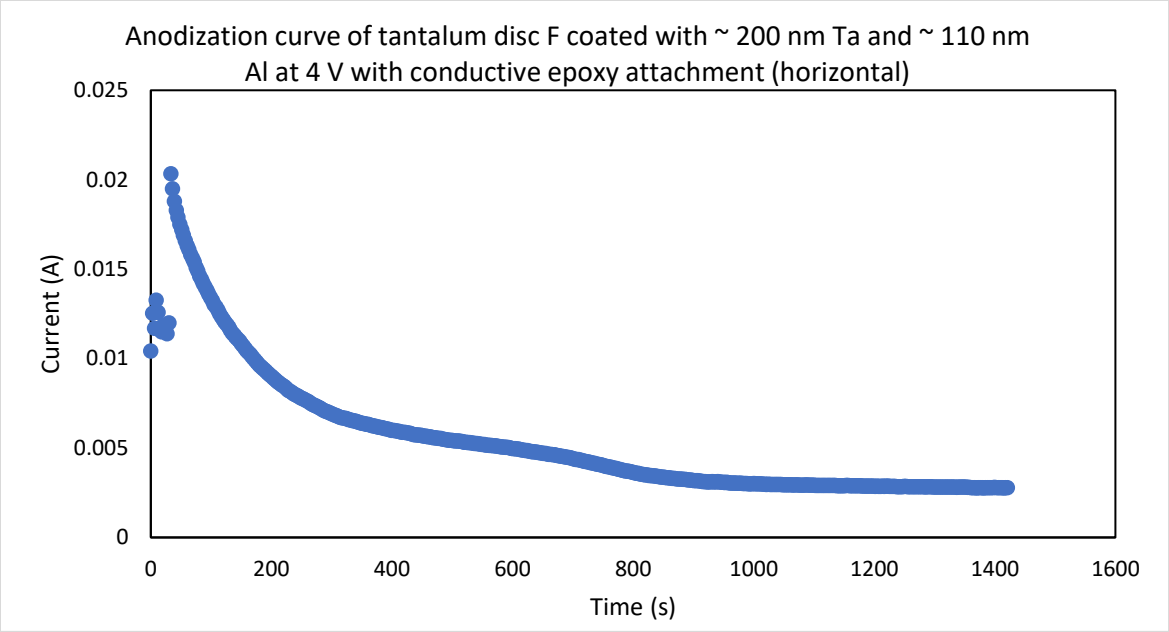


Figure A4.19. Current vs. time anodization plot for tantalum disc F coated with 200 nm of tantalum and 110 nm of aluminum at 4 V (horizontal with conductive epoxy attachment).

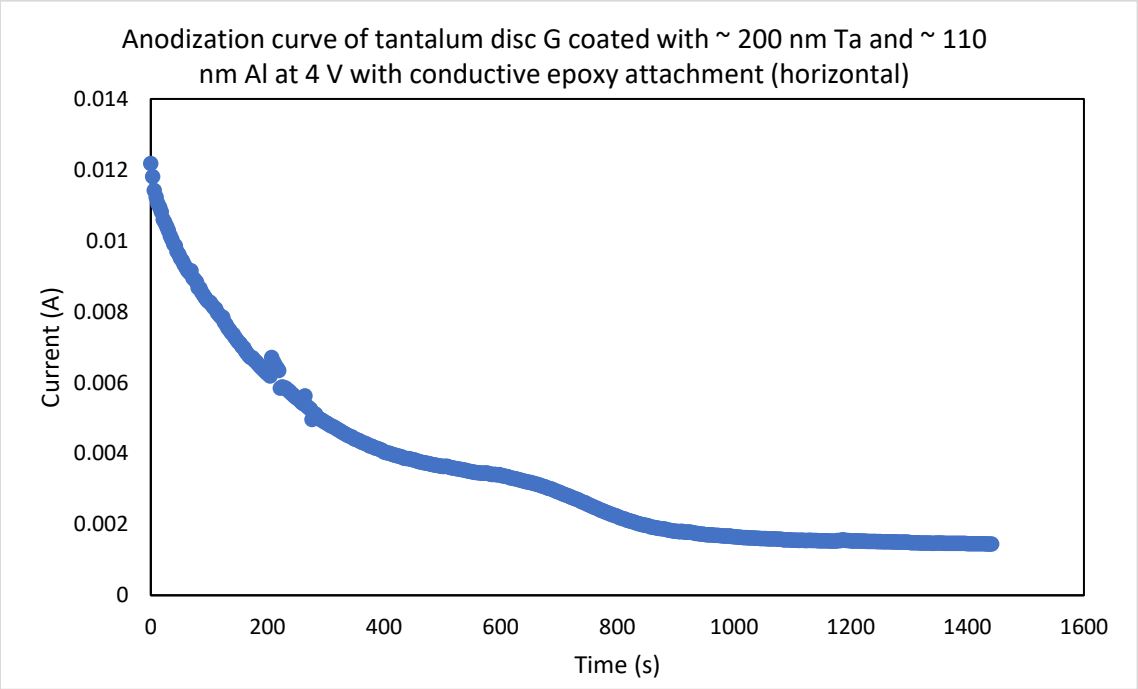


Figure A4.20. Current vs. time anodization plot for tantalum disc G coated with 200 nm of tantalum and 110 nm of aluminum at 4 V (horizontal with conductive epoxy attachment).